National Technical University of Athens
School of Chemical Engineering
Department II: Process Analysis and Plant Design
Thermodynamics and Transport Phenomena Laboratory

Development of a group – contribution equation of state for the thermodynamic modelling of associating mixtures.

Ph.D. Thesis

Eirini G. Petropoulou

Supervisor: Epaminondas C. Voutsas, Assoc. Professor

Athens, November 2018

Development of a group – contribution equation of state for the thermodynamic modelling of associating mixtures

A dissertation presented

by

Eirini G. Petropoulou

to

the School of Chemical Engineering

in partial fulfillment of the requirements for the degree of

Doctor of Philosophy

in

Chemical Engineering

National Technical University of Athens

Athens, Greece

November 2018

Η έγκριση της διδακτορικής διατριβής από την Ανωτάτη Σχολή Χημικών Μηχανικών του Εθνικού Μετσόβιου Πολυτεχνείου δεν υποδηλώνει αποδοχή των απόψεων του συγγραφέα (Ν. 5343/1932 Άρθρο 202 § 2).

The approval of this Ph.D. dissertation by the School of Chemical Engineering of the National Technical University of Athens does not imply the acceptance of the author's opinions (Law 5343/1932 Article 202 § 2).

Το Πρώτο Σκαλί

Εις τον Θεόκριτο παραπονιούνταν
μια μέρα ο νέος ποιητής Ευμένης·
«Τώρα δυο χρόνια πέρασαν που γράφω
κ' ένα ειδύλλιο έκαμα μονάχα.
Το μόνον άρτιόν μου έργον είναι.
Αλλοίμονον, είν' υψηλή το βλέπω,
πολύ υψηλή της Ποιήσεως η σκάλα·
κι απ' το σκαλί το πρώτο εδώ που είμαι
ποτέ δεν θ' ανεβώ ο δυστυχισμένος.»
Είπ' ο Θεόκριτος· «Αυτά τα λόγια
ανάρμοστα και βλασφημίες είναι.
Κι αν είσαι στο σκαλί το πρώτο, πρέπει
νάσαι υπερήφανος κ' ευτυχισμένος.
Εδώ που έφθασες, λίγο δεν είναι·
τόσο που έκαμες, μεγάλη δόξα.
Κι αυτό ακόμη το σκαλί το πρώτο
πολύ από τον κοινό τον κόσμο απέχει.
Εις το σκαλί για να πατήσεις τούτο
πρέπει με το δικαίωμά σου νάσαι
πολίτης εις των ιδεών την πόλι.
Και δύσκολο στην πόλι εκείνην είναι
και σπάνιο να σε πολιτογραφήσουν.
Στην αγορά της βρίσκεις Νομοθέτας
που δεν γελά κανένας τυχοδιώκτης.
Εδώ που έφθασες, λίγο δεν είναι·
τόσο που έκαμες, μεγάλη δόξα.»

Κωνσταντίνος Π. Καβάφης

(Από τα *Ποιήματα* 1897-1933, Ίκαρος 1984)

The First Step

The young poet Evmenis
complained one day to Theocritos:
«I've been writing for two years now
and I've composed only one idyll.
It's my single completed work.
I see, sadly, that the ladder
of Poetry is tall, extremely tall;
and from this first step I'm standing on now
I'll never climb any higher.»
Theocritos retorted: «Words like that
are improper, blasphemous.
Just to be on the first step
should make you happy and proud.
To have reached this point is no small achievement:
what you've done already is a wonderful thing.
Even this first step
is a long way above the ordinary world.
To stand on this step
you must be in your own right
a member of the city of ideas.
And it's a hard, unusual thing
to be enrolled as a citizen of that city.
Its councils are full of Legislators
no charlatan can fool.
To have reached this point is no small achievement:
what you've done already is a wonderful thing.»

Constantine P. Cavafy

Πρόλογος

Ολοκληρώνοντας το κείμενο της διατριβής κανείς συνειδητοποιεί ότι αυτό δεν είναι παρά μόνο η αρχή για το επόμενο κεφάλαιο, όπου η σελίδα είναι ακόμη κενή… Έτσι, η τελευταία λέξη δεν αποτελεί παρά την αρχή για το επόμενο ταξίδι στη θερμοδυναμική, στην επιστήμη, στην έρευνα, στη ζωή θέτοντας το λιθαράκι για να ανέβει κανείς στο σκαλοπάτι στην προσπάθεια να προσεγγίσει «των Ιδεών την πόλι».

Αυτό όμως δεν είναι κάτι που μπορεί να το επιτελέσει κανείς – εκτός από απειροελάχιστες εξαιρέσεις – μονάχος του, αλλά βασίζεται στη συσσωρευμένη γνώση και εμπειρία των ατόμων που έχει κοντά του. Δε θα μπορούσα λοιπόν παρά να ξεκινήσω ευχαριστώντας τον επιβλέποντα μου, αναπ. καθηγητή κ. Επαμεινώνδα Βουτσά, που με εισήγαγε στον κόσμο της θερμοδυναμικής και μου εμπιστεύθηκε την εκπόνηση ενός θέματος που από μία άποψη παντρεύει δύο από τα μοντέλα του εργαστηρίου, τα πνευματικά του παιδιά. Το πάθος του για τη θερμοδυναμική αποτελεί μοχλό κίνησης για όλα τα μέλη του εργαστηρίου να στοχεύουν όλο και πιο ψηλά, χωρίς όμως να χάνει την αμεσότητα και την απλότητά του. Θέλω επίσης να ευχαριστήσω τα υπόλοιπα μέλη της τριμελούς συμβουλευτικής επιτροπής και συγκεκριμένα τον καθηγητή κ. Κωστή Μαγουλά για το ενδιαφέρον και την υποστήριξη που έδειξε καθ' όλη τη διάρκεια των σπουδών μου καθώς και τον καθηγητή κ. Ανδρέα Μπουντουβή, που αν και δεν βρισκόμασταν σε καθημερινή επικοινωνία οι συζητήσεις μας προσέφεραν μία διαφορετική οπτική γωνία. Επίσης, θα ήθελα να ευχαριστήσω τον Ομότιμο καθηγητή, κ. Δημήτριο Τασιό για τις εύστοχες παρατηρήσεις του ιδιαίτερα κατά την αρχή της διατριβής. Πέρα όμως από τα επιστημονικά θέματα, η εμπειρία και οι ιστορίες του αποτελούν πηγή έμπνευσης, όχι μόνο για εμένα προσωπικά αλλά και για όλα τα μέλη του εργαστηρίου.

Στο σημείο αυτό θα ήθελα να ευχαριστήσω τον Ειδικό Λογαριασμό Κονδυλίων Έρευνας του Εθνικού Μετσόβιου Πολυτεχνείου, για τη χρηματική υποστήριξη της διατριβής μέσω Υποτροφίας κατά το χρονικό διάστημα 2012 – 2016. Επιπλέον, θα ήθελα να ευχαριστήσω το ευρωπαϊκό πρόγραμμα ECCSEL, μέρος του προγράμματος Horizon 2020 (αρ. προγράμματος 675206), που μου έδωσε τη δυνατότητα να μεταβώ στις εγκαταστάσεις της SINTEF Energi Research (Τροντχάιμ, Νορβηγία) για την πραγματοποίηση των πειραματικών μετρήσεων ισορροπίας φάσεων. Εδώ θα ήθελα επίσης να ευχαριστήσω την νορβηγική εταιρεία Equinor (τέως Statoil) για τις πολύτιμες συμβουλές και παρατηρήσεις σχετικές με τις διεργασίες επεξεργασίας και μεταφοράς φυσικού αερίου.

Παίρνοντας έναυσμα από αυτό, θα ήθελα να ευχαριστήσω τα μέλη της SINTEF Energi Research για την υποδοχή τους και το ωραίο κλίμα που υπήρχε κατά τη συνεργασία μας. Ιδιαίτερα θα ήθελα να εκφράσω τις ευχαριστίες μου στον Dr. Snorre Foss Westman για την πολύτιμη βοήθειά του καθ' όλη την παραμονή μου, την προθυμία και τη διάθεσή του να μεταλαμπαδεύσει την εμπειρία του, αλλά επίσης για την καλή του διάθεση και αίσθηση του χιούμορ που έκαναν ωραίες τις ώρες αναμονής για την αποκατάσταση της ισορροπίας. Ένα μεγάλο ευχαριστώ οφείλω στον Dr. Anders Austegard που με εκπαίδευσε στη μεθοδολογία του υπολογισμό της ανασφάλειας των πειραματικών μετρήσεων αλλά και για την εύρεση κατάλληλης συνάρτησης για την ακριβέστερη αποτύπωση της "ουράς" του διοξειδίου στο χρωματογράφημα. Θα ήθελα να ευχαριστήσω επίσης τον Dr. Jacob Stang για τις πολύτιμες συμβουλές του καθώς και για την παρουσία του στο εργαστήριο ακόμη και σε ημέρες αργίας ώστε να εξασφαλιστεί η απρόσκοπτη διεξαγωγή των μετρήσεων και φυσικά τον Dr. Sigurd

Løvseth για την εμπιστοσύνη και τη συνεργασία του. Η ζωή όμως στο Τροντχάιμ δε θα ήταν ίδια χωρίς την πολύτιμη φιλία, τις συμβουλές και τη στήριξη της Δρ. Ελένης Παντελή, την οποία και ευχαριστώ ιδιαίτερα.

Επιστρέφοντας στα πάτρια εδάφη, θα ήθελα να ευχαριστήσω όλα τα μέλη του Εργαστηρίου Θερμοδυναμικής και Φαινομένων Μεταφοράς που ο καθένας με τον δικό του τρόπο συνέβαλε στην περάτωση αυτού του έργου. Πιο συγκεκριμένα, θα ήθελα να εκφράσω ένα μεγάλο ευχαριστώ στις Δρ. Βίκη Λούλη και Δρ. Γεωργία Παππά για την αμέριστη στήριξη και συμπαράσταση τόσο στα επιστημονικά αλλά όσο και σε οργανωτικά και πρακτικά θέματα. Πρόκειται για δύο καταξιωμένους επιστήμονες μα πάνω από όλα ανθρώπους που με μύησαν στον κόσμο της έρευνας και ήταν πάντα εκεί να συμπαρασταθούν στις απογοητεύσεις και στις δύσκολες στιγμές, με τη φρεσκάδα και τον διαφορετικό τρόπο αντιμετώπισης να προτείνουν λύσεις που αλλιώς θα ήταν δύσκολο να διακρίνει κανείς. Είναι όμως και όλα αυτά που δεν περιγράφονται σε λίγες γραμμές, οι απλές καθημερινές στιγμές, τα γέλια, οι γκρίνιες που έχουν αντιμετωπίσει υπομονετικά και έχουν κερδίσει έτσι ξεχωριστή θέση στην καρδιά μου.

Φυσικά δε γίνεται σε αυτό τον πρόλογο να μην αναφερθώ στους συνοδοιπόρους σε αυτό το ταξίδι, υποψήφιους διδάκτορες. Θα ξεκινήσω με τη - Δρ. πλέον - Έφη Αλεβίζου, που αν και στη τελευταία φάση της διατριβής της όταν τη γνώρισα, δημιούργησε ένα κλίμα παρεΐστικο στο εργαστήριο, με το γέλιο και τα έξυπνα σχόλιά της να βγάζει ένα φωτεινό χαμόγελο σε όποια κατάσταση. Ιδιαίτερα όμως ευχαριστώ την Νεφέλη Νόβακ για την έμπρακτη στήριξη σε πολλαπλά αλγοριθμικά θέματα και την Ελένη Μπόλη που με καθοδήγησε στη λειτουργία των πειραματικών διατάξεων. Καθώς αυτόν τον δρόμο τον διασχίζουμε μαζί, δεν μπορώ παρά να θυμηθώ τις φιλοσοφικές (αλλά και τις πολύ απλές) συζητήσεις, τις κοινές εμπειρίες, τους προβληματισμούς, τα ταξίδια, τις κοινές εξόδους που δημιούργησαν ένα ωραίο κλίμα συνεργασίας και άμιλλας και έδιναν έναν ευχάριστο τόνο στην κάθε ημέρα. Εδώ θέλω να ευχαριστήσω την επόμενη γενιά του εργαστηρίου που παίρνει τη σκυτάλλη μετά από εμάς, την Ανθή Πλακιά και τον Βασίλη Κουλοχέρη, που έφεραν έναν τόνο ανανέωσης με τις ιδέες και τη φιλική τους διάθεση.

Μέσα σε αυτό το διάστημα έχουν περάσει πολλά άτομα, για μικρότερο ή μεγαλύτερο διάστημα, δημιουργώντας ένα ξεχωριστό κλίμα και διαφοροποιώντας το χρόνο από το χρόνο. Ανάμεσά τους θα ξεχωρίσω τη Νέλλη Μυλωνά, με την αισιοδοξία και το χαμόγελό της, την προθυμία στο να μάθει πράγματα, τις εύστοχες προτάσεις και ιδέες της, καθώς και τον Δρ. Χρήστο Τσάνα, που αν και άλλαξε θερμοδυναμική οικογένεια, με παρότρυνε στο να στοχεύω όλο και ψηλότερα και με έκανε να αντιμετωπίσω την έννοια του διδακτορικού διαφορετικά. Επίσης, τη Cristina Carollo, η οποία αφιέρωσε πολύ χρόνο στην παραμετρική ανάλυση των προσομοιώσεων στα πλαίσια της διπλωματικής της εργασίας αλλά και με έφερε σε επαφή με την κουλτούρα και τον πολιτισμό της όμορρης χώρας.

Τέλος, θα ήθελα να ευχαριστήσω την οικογένειά μου για την αμέριστη στήριξη και κατανόηση όλα αυτά τα χρόνια καθώς και τους φίλους μου που προσέφεραν ένα διαφορετικό είδος association.

Κι αν η διάθεση μοιάζει μελαγχολική, δεν είναι παρά γιατί ένα μεγάλο και ωραίο κεφάλαιο τελειώνει. Ας στοχεύουμε στο επόμενο Σκαλί…

Ειρήνη

Αθήνα, 2018

Preface

The last line of the thesis is not anything different but the beginning of a new journey in thermodynamics, science, life in general. It is just the first step towards the "city of Ideas".

This path of devotion and solitarism, cannot be followed without the guidance and help of other people; either co-workers or friends. I am grateful to my supervisor, Assoc. Prof. Epaminondas Voutsas, who entrusted me with this topic and has been an unending source of inspiration. I would also like to express my gratitude to the rest of the supervising committee members, Prof. Kostis Magoulas and Prof. Andreas Boudouvis, for their support throughout this project. I would also like to express my appreciation to Emeritus Prof. Dimitrios Tassios for his fruitful comments and the prolonged discussions especially in the early days of this study.

This research has been financial supported in the form of Grant by ELKE NTUA (2012 – 2016). Also, I would like to express my gratitude to the European programme, ECCSEL (Project No. 675206) which granted me access to the SINTEF Energi facilities (Trondheim, Norway) to conduct the experimental equilibrium measurements. I would like to acknowledge also the invaluable advice from Equinor (former Statoil) concerning natural gas processing and transportation.

I am very grateful to the researchers at SINTEF Energi for their warm welcome and collaboration. Special thanks to Dr. Snorre Foss Westman for his support and experience through the project, to Dr. Anders Austegard who trained me on the uncertainty analysis and his help with the gas chromatograph calibration. Also, I would like to thank Dr. Jacob Stang and Dr. Sigurd Løvseth for their valuable advice. However, the Trondheim experience would not have been as enjoyable if not for Dr. Eleni Panteli whose friendship I cherish. Our prolonged discussions renewed my determination and motivation at a time it was most needed.

I am grateful to my colleagues at Thermodynamics and Transport Phenomena Laboratory who each in their unique way had an impact on me. I am deeply indebt to Dr. Vicky Louli and Dr. Georgia Pappa for their invaluable support during my studies. From our long discussions on scientific matters to trivial everyday situations.

Of course, I would like to thank my fellow PhD students, along with we shared all the spectra of experiences. Although in the final chapters of her dissertation when I first met her, Dr. Efi Alevizou guided me to the world of research. A special thanks is towards Nefeli Novak for her invaluable help with algorithmic issues and Eleni Boli who trained me in the use of several experimental apparati. But mostly, it is the moments we shared and the unending discussions that created such inspirational and friendly environment. Also, the new members of the group, Anthi Plakia and Vassilis Koulocheris, brought an air of change and refresh.

During this time several collaborations or diploma students have passed – and surpassed – each of whom marked with his/her presence each time period, differencing it from another. Among them, I would like to refer to Nelly Mylona and Dr. Christos Tsanas, who kept giving motivation and showed me a different perspective. Also, I would like to thank Cristina Carollo for striving with the sensitivity analysis of the simulations during her master thesis.

Last but not least, I would like to thank my family and friends for all their support and patience.

And if the mood seems rather melancholic, it is because a big and unique chapter is ending. Let us move towards the next Step…

Eirini

Athens, 2018

Abstract

The purpose of the present thesis is the development of a group – contribution model able to accurately describe the phase equilibria of mixtures comprising of associating compounds. Modelling of phase equilibrium in mixtures involving hydrocarbons, such as those comprising natural gas, water and alcohols or glycols is a very challenging task for the gas industry. The accurate modelling of such mixtures is vital for the safe and optimum operation and design of natural gas transportation pipelines and unit operations. Classic thermodynamic models, such as cubic equations of state (EoS), usually used in industrial practice, fail to accurately describe the phase behavior of strongly polar or hydrogen bonding mixtures. As such, the development of an appropriate thermodynamic framework to describe the phase behavior of such mixtures is deemed necessary.

In the first part of the thesis, new experimental vapor – liquid equilibrium (VLE) measurements of the CO_2/methane binary are conducted close to the critical temperature of CO_2, in order to extend the applicability of the models in a wider temperature range. The obtained data are of high accuracy (3 mK in temperature, 0.02 bar in pressure and 0.0008 in composition) and are successfully validated against literature values. Emphasis is given in the determination of the critical point of the mixture through a scaling law based on statistical mechanics. Moreover, the obtained data are correlated with different EoS of various complexity. Actually, two cubic EoS are used, Peng – Robinson (PR) and Soave – Redlich – Kwong (SRK) and the obtained results are compared with those of two more advanced models; the UMR-PRU which belongs to the EoS/G^E class and combines the PR EoS with the UNIFAC activity coefficient model through advanced mixing rules and the Perturbed – Chain Statistical Associating Fluid Theory (PC-SAFT) EoS which is one of the most successful versions of SAFT. All models correlated satisfactorily the experimental data. UMR-PRU yields overall the lowest deviations both away from the critical region, as well as in the prediction of the critical point.

In the second part, the UMR-PRU model is extended to mixtures of natural gas components and strongly polar compounds. Very satisfactory correlation of the VLE and liquid – liquid equilibrium (LLE) is obtained for the examined systems. The performance of the model is also evaluated against that of another model belonging to the same class, TST/NRTL, which is suggested by the commercial Aspen HYSYS© (Hysys) process simulator for use in natural gas dehydration applications with glycols. It is shown that in most cases UMR-PRU yields superior results, despite its group – contribution nature, while TST/NRTL systematically fails to predict well the solubility of heavier hydrocarbons (HCs) in the aqueous phase. Both models yield good results in the prediction of multicomponent mixtures containing methane, aromatic hydrocarbons, triethylene glycol (TEG) and water, at conditions similar with those

used in natural gas dehydration units, which suggests that both models can satisfactorily predict the aromatic components distribution.

After the evaluation in the phase equilibrium of binary and multicomponent mixtures, UMR-PRU is implemented in commercial process simulators, Hysys and Honeywell UniSim© (Unisim), through the CAPE–Open protocol. As expected, identical results are obtained in both simulators. Two cases are examined and the results are compared with those of TST/NRTL; *Case I* represents a simple absorber, while *Case II* a simplified offshore dehydration process. In *Case I*, UMR-PRU yields the same level of dehydration as TST/NRTL, while in *Case II* it is shown that UMR-PRU and TST/NRTL calculate similar stripping gas rate, TEG purity and circulation rate for achieving the same dry gas water content. Nevertheless, the two models differ in the calculated TEG loss, where UMR-PRU is considered to be closer to the real case than TST/NRTL. UMR-PRU also predicts lower duties in the reboiler, condenser and heat exchangers compared to TST/NRTL, which is considered more realistic due to better prediction of the aqueous TEG heat capacities. Furthermore, a sensitivity analysis of several operating parameters, such as stripping gas rate, operating temperature and pressure of the columns, is conducted. The qualitative comparisons for several properties predicted in *Case II* are consistent with what is theoretically expected.

Based on the observations of the sensitivity analysis, an optimization of the process parameters in terms of operating cost is performed with the UMR-PRU model, along with a preliminary economic evaluation for the base and optimized conditions through the Aspen ICARUS® (Icarus) software and with literature correlations. A relatively low plant capacity (360 SMcm/y) is considered where it is shown that the optimized process conditions do not actually affect the fixed capital cost. The calculated capital cost is in relative good agreement with literature values. For the operating cost, a 6 % decrease is obtained, which corresponds to a cost reduction of about 37 €/SMcm of treated wet gas.

In the third part of the thesis, the effect of the mixing rules used in an EoS and the direct accounting for the hydrogen bonding forces, by application of Wertheim's first order perturbation theory on the phase equilibria of natural gas mixtures with associating compounds is examined. To this end, three versions of the Peng – Robinson equation of state are evaluated in the prediction of the VLE of ternary and multicomponent natural gas mixtures that contain water and methanol or MEG. These are, the cubic Peng – Robinson with conventional van der Waals one fluid (vdW1f) mixing rules, the UMR-PRU model, which combines PR with UNIFAC through the Universal Mixing Rules, and the Cubic Plus Association Peng – Robinson (CPA-PR), which incorporates the Wertheim's term of statistical mechanics in the PR EoS. It is shown that both UMR-PRU and CPA-PR provide significant improvement over PR EoS in the prediction of multicomponent phase equilibrium. Moreover, UMR-PRU and CPA-PR are able to predict satisfactorily the dew points of natural gas mixtures containing water and methanol, yielding much better results compared to PR. CPA-PR yields the best overall results suggesting that the incorporation of the associating term

is necessary to obtain better prediction of hydrogen bonding mixtures. On the other hand, the selection of advanced mixing rules for the attractive and co-volume parameters, also improves the prediction of phase equilibria of complex mixtures containing natural gas components, water and hydrogen bonding compounds such as methanol and MEG, yielding satisfactory results.

Based on this observation, a new model, the so-called UMR-CPAPRU, is proposed which combines the advantages of EoS/G^E models with the increased accuracy of the perturbation theory. It is first validated in the prediction of two ternary mixtures consisting of methane, water and a hydrate inhibitor (methanol or MEG) and it yields improved results compared to those of UMR-PRU and CPA-PR. This is more pronounced for the methane solubility in liquid phase, where the associating effects are more severe. Very satisfactory correlation results are obtained in the VLE of binary mixtures, where the model improves the UMR-PRU performance both qualitatively and quantitatively. For example, UMR-CPAPRU correlates very well the azeotrope formation in the VLE of hydrocarbons (HC) with methanol yielding substantial improvement over the UMR-PRU predictions. Also, the new model yields better results in the LLE of HC/water and HC/methanol mixtures than UMR-PRU. Then, the model is evaluated in the prediction of the LLE of ternary mixtures, where it yields better qualitative and quantitative results compared to UMR-PRU. Finally, the UMR-CPAPRU improves the performance of UMR-PRU in the dew point prediction of synthetic natural gas mixtures with water and methanol.

Σύνοψη

Αντικείμενο της παρούσας διατριβής αποτελεί η ανάπτυξη ενός μοντέλου συνεισφοράς ομάδων με στόχο την ακριβή πρόβλεψη της θερμοδυναμικής συμπεριφοράς μιγμάτων που περιέχουν ενώσεις που μπορούν να σχηματίσουν δεσμούς υδρογόνου. Η μοντελοποίηση τέτοιων μιγμάτων, όπως τα υδατικά μίγματα υδρογονανθράκων, αποτελούν πρόκληση για τους μελετητές καθώς εμφανίζουν ελάχιστη αναμιξιμότητα, είναι όμως απαραίτητη ώστε να διασφαλιστεί η ασφαλής και αποδοτική λειτουργία διαφόρων διεργασιών στην αλυσίδα αξίας του φυσικού αερίου. Το νερό αποτελεί ένα από τα συστατικά του φυσικού αερίου, η παρουσία του οποίου σε συνδυασμό με τα μικρά μόρια, όπως διοξείδιο του άνθρακα, υδρόθειο, μεθάνιο κ.α. μπορεί να οδηγήσει στο σχηματισμό υδριτών. Οι τελευταίοι δύνανται να παρεμποδίσουν τη ροή ή και σε έντονες συνθήκες να φράξουν πλήρως τον αγωγό. Για το σκοπό αυτό, πολικά μόρια που ταπεινώνουν τη θερμοκρασία σχηματισμού υδριτών, λειτουργώντας ως παρεμποδιστές, προστίθενται σε κατάλληλη ποσότητα στη ροή του φυσικού αερίου. Επιπρόσθετα, η επιτρεπόμενη ποσότητα του νερού στο αέριο ρυθμίζεται μέσω μίας διεργασίας αφυδάτωσης. Στην πλειονότητα των υπεράκτιων πλατφόρμων επεξεργασίας αερίου αυτό επιτυγχάνεται με φυσική απορρόφηση σε υδατικό διάλυμα γλυκόλης, συνήθως τριαιθυλενογλυκόλης (TEG). Συνεπώς, η ακριβής θερμοδυναμική μοντελοποίηση είναι ιδιαίτερα σημαντική σε όλα τα στάδια της παραγωγής, μεταφοράς και επεξεργασίας φυσικού αερίου. Τα κλασσικά θερμοδυναμικά μοντέλα, όπως είναι οι κυβικές καταστατικές εξισώσεις, που χρησιμοποιούνται κατά κόρον από τη βιομηχανία αποτυγχάνουν να περιγράψουν με ικανοποιητική ακρίβεια την ισορροπία φάσεων έντονα πολικών ενώσεων ή ενώσεων που μπορούν να σχηματίσουν δεσμούς υδρογόνου και συνεπώς η ανάπτυξη ενός κατάλληλου θερμοδυναμικού φορμαλισμού για την περιγραφή τέτοιων μιγμάτων είναι απαραίτητη.

Το πρώτο μέρος της διατριβής επικεντρώνεται, λοιπόν, στην πειραματική μέτρηση της ισορροπίας φάσεων ατμών – υγρού για το δυαδικό μίγμα διοξειδίου του άνθρακα/ μεθανίου σε θερμοκρασίες που προσεγγίζουν την κρίσιμη θερμοκρασία του διοξειδίου. Νέα πειραματικά δεδομένα υψηλής ακρίβειας (3 mK στη θερμοκρασία, 0.02 bar στην πίεση και 0.0008 στη συγκέντρωση, στην υποκρίσιμη περιοχή) μετρήθηκαν σε τρεις ισόθερμες, διευρύνοντας έτσι το θερμοκρασιακό εύρος στο οποίο μπορούν να εφαρμοστούν τα θερμοδυναμικά μοντέλα. Έμφαση δόθηκε στην εκτίμηση του κρίσιμου σημείου του μίγματος το οποίο προσδιορίστηκε μέσω του νόμου κλιμάκωσης ο οποίος διέπεται από τις αρχές της στατιστικής μηχανικής. Τα δεδομένα που μετρήθηκαν αξιολογήθηκαν σε σύγκριση με άλλα δεδομένα που ήταν διαθέσιμα στη βιβλιογραφία για την ισόθερμη των 293 K οπότε βρέθηκε ικανοποιητική συμφωνία στην υποκρίσιμη περιοχή. Στη συνέχεια, τα πειραματικά δεδομένα συσχετίστηκαν με τέσσερα θερμοδυναμικά μοντέλα, τα οποία διέπονται από διαφορετικές αρχές. Πρόκειται για δύο κυβικές καταστατικές εξισώσεις με κανόνες ανάμιξης του ενός ρευστού, όπως

προτάθηκαν από τον van der Waals και συγκεκριμένα τις εξισώσεις Peng – Robinson (PR) και Soave – Redlich – Kwong (SRK). Επιπλέον, προσαρμόστηκαν οι παράμετροι του μοντέλου (UMR-PRU) που ανήκει στην κατηγορία των EoS/G^E, δηλαδή εξισώνει την περίσσεια της ελεύθερης ενέργειας Gibbs, όπως αυτή υπολογίζεται μέσω μίας καταστατικής εξίσωσης και συγκεκριμένα την PR, με αυτή που υπολογίζεται από ένα μοντέλο τοπικής σύστασης και εν προκειμένω το μοντέλο συνεισφοράς ομάδων UNIFAC, οδηγώντας σε νέους κανόνες ανάμειξης, τους λεγόμενους UMR. Τέλος, επιλέχθηκε μία καταστατική εξίσωση, ανώτερης τάξης ως προς τον όγκο, η οποία διέπεται από αρχές της στατιστικής θερμοδυναμικής, δηλαδή η καταστατική εξίσωση PC-SAFT. Όλες οι υπό μελέτη εξισώσεις συσχέτισαν με πολύ καλή ακρίβεια τα πειραματικά δεδομένα, ιδίως στην υποκρίσιμη περιοχή, ενώ το μοντέλο UMR-PRU οδήγησε στις συνολικά μικρότερες αποκλίσεις και στις δύο φάσεις, καθώς και καλύτερη πρόβλεψη του κρίσιμου σημείου.

Στο δεύτερο μέρος της διατριβής πραγματοποιείται η επέκταση του θερμοδυναμικού μοντέλου UMR-PRU σε μίγματα φυσικού αερίου με ενώσεις που μπορούν να σχηματίσουν δεσμούς υδρογόνου. Πολύ καλά αποτελέσματα συσχέτισης αποκτήθηκαν για τα εξεταζόμενα δυαδικά μίγματα τόσο στην ισορροπία ατμών – υγρού, όσο και στην ισορροπία υγρού – υγρού που εμφανίζεται στα υδατικά μίγματα υδρογονανθράκων. Τα αποτελέσματα του μοντέλου συγκρίθηκαν με επιτυχία με αυτά ενός μοντέλου που ανήκει στην ίδια κατηγορία (EoS/G^E) και προτείνεται από τον εμπορικό προσομοιωτή Aspen HYSYS© (Hysys) για τη χρήση σε διεργασίες φυσικού αερίου που περιλαμβάνουν πολικά συστατικά, όπως είναι οι γλυκόλες. Μάλιστα, αποδείχθηκε ότι στις περισσότερες περιπτώσεις το μοντέλο UMR-PRU δίνει καλύτερα αποτελέσματα στην περίπτωση των πολικών συστατικών τόσο ως προς την ισορροπία φάσεων, ιδιαίτερα όσον αφορά στη διαλυτότητα των βαρύτερων υδρογονανθράκων στην υδατική φάση. Τα μοντέλα αξιολογήθηκαν επίσης στην πρόρρηση της ισορροπίας φάσεων πολυσυστατικών μιγμάτων μεθανίου, αρωματικών υδρογονανθράκων, νερού και τρι-αιθυλενογλυκόλης (TEG) σε συνθήκες παρόμοιες με αυτές που επικρατούν στη διεργασία αφυδάτωσης, οδηγώντας σε πολύ καλά αποτελέσματα ως προς τις κατανομές των συστατικών.

Εν συνεχεία, το μοντέλο UMR-PRU εισήχθη σε εμπορικούς προσομοιωτές μέσω του πρωτοκόλλου CAPE–Open 1.1 και συγκεκριμένα στους Hysys και Honeywell© UniSim (Unisim), με στόχο την προσομοίωση διεργασιών αφυδάτωσης φυσικού αερίου με απορρόφηση σε γλυκόλη. Όπως ήταν αναμενόμενο, το μοντέλο κατέληξε σε πανομοιότυπα αποτελέσματα και στους δύο προσομοιωτές. Τα αποτελέσματα συγκρίθηκαν, επιπλέον, με αυτά που προκύπτουν με χρήση του μοντέλου TST/NRTL που ανήκει στην ίδια κλάση και προτείνεται για χρήση σε διεργασίες αφυδάτωσης φυσικού αερίου με γλυκόλες από τον εμπορικό προσομοιωτή Hysys. Δύο περιπτώσεις μελετήθηκαν. Η πρώτη αφορά σε μία απλή στήλη απορρόφησης, ενώ η δεύτερη στην προσομοίωση μίας απλοποιημένης μονάδας αφυδάτωσης φυσικού αερίου με απορρόφηση σε TEG. Αποδεικνύεται ότι στην περίπτωση της απλής στήλης απορρόφησης, όπου είναι συγκεκριμένη και ίδια η τροφοδοσία σε αέριο και διαλύτη, και τα δύο μοντέλα οδηγούν σε παρόμοιο ποσοστό αφυδάτωσης, ενώ στη δεύτερη και

πιο σύνθετη περίπτωση, τα δύο μοντέλα καταλήγουν σε παρόμοια ροή αερίου απογύμνωσης, παρόμοια ανακυκλοφορία και καθαρότητα γλυκόλης για να πετύχουν μία συγκεκριμένη προδιαγραφή. Ωστόσο, διαφέρουν ως προς την εκτίμηση των απωλειών σε TEG και υδρογονάνθρακες, όπου το UMR-PRU συστηματικά υπολογίζει υψηλότερα επίπεδα συγκρινόμενα με το TST/NRTL. Δυστυχώς δεν υπάρχουν διαθέσιμα πειραματικά δεδομένα για την άμεση αξιολόγηση των μοντέλων, ωστόσο θεωρείται ότι τα αποτελέσματα του UMR-PRU είναι κοντινότερα σε αυτά που συναντώνται στην πράξη, καθώς περιγράφει με καλύτερη ακρίβεια τις διαλυτότητες στα αντίστοιχα δυαδικά μίγματα. Επιπρόσθετα, το UMR-PRU συστηματικά υπολογίζει χαμηλότερες ενεργειακές απαιτήσεις σε σχέση με αυτές του TST/NRTL. Και σε αυτή την περίπτωση, εκτιμάται ότι τα αποτελέσματα του UMR-PRU προσεγγίζουν καλύτερα την πραγματικότητα, δεδομένου ότι το τελευταίο περιγράφει με μεγαλύτερη ακρίβεια την ειδική θερμοχωρητικότητα υδατικών διαλυμάτων TEG σε σχέση με το TST/NRTL, καθώς η τελευταία αποτελεί την ιδιότητα – κλειδί για τον υπολογισμό των ενεργειακών απαιτήσεων.

Έπειτα από τη μεταξύ τους αξιολόγηση, πραγματοποιήθηκε μία ανάλυση ευαισθησίας ως προς διάφορες λειτουργικές παραμέτρους και με τα δύο μοντέλα οπότε προτάθηκαν αριστοποιημένες συνθήκες λειτουργίας με στόχο την εξοικονόμηση ενέργειας. Πραγματοποιήθηκε, επιπλέον, μία προκαταρκτική οικονομική ανάλυση της διεργασίας, τόσο απευθείας μέσω του λογισμικού Aspen ICARUS® (Icarus), όσο και με γενικευμένες συσχετίσεις που προτείνονται από τη βιβλιογραφία. Και οι δύο μεθοδολογίες οδηγούν σε παρόμοιο πάγιο κόστος, που είναι συγκρίσιμο με βιβλιογραφικές τιμές για μία μονάδα σχετικά χαμηλής δυναμικότητας (360 SMcm/y). Αποδείχθηκε, επίσης, ότι η επιλογή αριστοποιημένων συνθηκών λειτουργίας δεν επηρεάζει σημαντικά το πάγιο κόστος. Εν αντιθέσει, η τελευταία οδηγεί σε μία μείωση κατά περίπου 6 % του λειτουργικού κόστους σε ετήσια βάση, το οποίο αντιστοιχεί σε εξοικονόμηση περίπου 37 €/SMcm αερίου υπό επεξεργασία.

Στο τελευταίο μέρος της διατριβής, μελετήθηκε η επίδραση της επιλογής κανόνων ανάμιξης και του άμεσου υπολογισμού των δυνάμεων δεσμών υδρογόνου όπως αυτοί υπολογίζονται με τη βοήθεια της θεωρίας των διαταραχών πρώτης τάξης που προτάθηκε από τον Wertheim, στην ισορροπία φάσεων μιγμάτων φυσικού αερίου που περιέχουν πολικά συστατικά. Για το σκοπό αυτό επιλέχθηκε η καταστατική εξίσωση Peng – Robinson και μελετήθηκε σε τρεις διαφορετικές εκδοχές. Ως βάση, επιλέχθηκε η κλασσική κυβική έκφραση με τους κανόνες ανάμιξης ενός ρευστού του van der Waals, ενώ η επίδραση εναλλακτικών κανόνων ανάμιξης μελετήθηκε μέσω του μοντέλου UMR-PRU, το οποίο συνδέει την PR με το μοντέλο τοπικής σύστασης, UNIFAC. Τέλος, εξετάστηκε η συμπεριφορά της καταστατικής εξίσωσης CPA-PR, η οποία συνδυάζει την έκφραση της PR για τον φυσικό όρο των αλληλεπιδράσεων, ενώ εμπεριέχει έναν επιπρόσθετο όρο που προέρχεται από τη θεωρία των διαταραχών και χρησιμοποιείται για τον απευθείας υπολογισμό των αλληλεπιδράσεων δεσμού υδρογόνου μεταξύ κατάλληλων δεσμικών κέντρων των μορίων. Αποδεικνύεται ότι τόσο η επιλογή προηγμένων κανόνων ανάμιξης (UMR-PRU) όσο και η καταστατική εξίσωση CPA-PR βελτιώνουν σημαντικά την πρόρρηση της ισορροπίας φάσεων πολυσυστατικών

μιγμάτων φυσικού αερίου με νερό και αλκοόλη ή γλυκόλη, ξεκινώντας από παρόμοια συμπεριφορά στα δυαδικά μίγματα. Επιπρόσθετα, τόσο το UMR-PRU όσο και η CPA-PR προβλέπουν ικανοποιητικά τα σημεία δρόσου μιγμάτων φυσικού αερίου που περιέχουν νερό και μεθανόλη, οδηγώντας σε σημαντική βελτίωση της πρόρρησης της PR. Η CPA-PR οδηγεί στα καλύτερα συνολικά αποτελέσματα αναδεικνύοντας έτσι τη σημαντικότητα του απευθείας υπολογισμού των αλληλεπιδράσεων δεσμών υδρογόνου. Ωστόσο, η επιλογή προηγμένων κανόνων ανάμιξης βελτιώνει τα αποτελέσματα της PR οδηγώντας ακόμη και σε εφάμιλλα αποτελέσματα με αυτά ενός μοντέλου που απευθείας υπολογίζει αυτές τις αλληλεπιδράσεις. Συνεπώς, τόσο οι κανόνες ανάμιξης όσο και η προσθήκη του όρου των δεσμικών αλληλεπιδράσεων βελτιώνουν σημαντικά τη συμπεριφορά των καταστατικών εξισώσεων σε μίγματα φυσικού αερίου με νερό και έντονα πολικές ενώσεις.

Με γνώμονα τα παραπάνω, προτείνεται ένα νέο θερμοδυναμικό μοντέλο, το UMR-CPAPRU, το οποίο συνδυάζει τη χρήση προηγμένων κανόνων ανάμιξης για τον φυσικό όρο με τον όρο δεσμικών αλληλεπιδράσεων που προέρχεται από τη θεωρία των διαταραχών της στατιστικής μηχανικής. Το προτεινόμενο μοντέλο αρχικά αξιολογείται στην πρόρρηση της ισορροπίας φάσεων δύο τριαδικών μιγμάτων, αποτελούμενων από μεθάνιο, νερό και παρεμποδιστή υδριτών (μεθανόλη ή MEG), οπότε αποδεικνύεται ότι δίνει βελτιωμένα αποτελέσματα σε σύγκριση με το μοντέλο UMR-PRU αλλά και τη CPA-PR κυρίως ως προς τη διαλυτότητα του μεθανίου στην υγρή φάση, όπου οι αλληλεπιδράσεις δεσμού υδρογόνου είναι πιο ισχυρές. Το μοντέλο UMR-CPAPRU οδηγεί σε πολύ καλά αποτελέσματα συσχέτισης της ισορροπίας φάσεων ατμών – υγρού οπού βελτιώνει σημαντικά τόσο ποιοτικά όσο και ποσοτικά την πρόρρηση του UMR-PRU μοντέλου. Αυτό γίνεται ιδιαίτερα εμφανές στην περίπτωση της ισορροπίας φάσεων ατμών – υγρού δυαδικών μιγμάτων μεθανόλης με υδρογονάνθρακες όπου αναμένεται ο σχηματισμός αζεοτρόπου, καθώς και σε ακόμη καλύτερα αποτελέσματα στην ισορροπία υγρού – υγρού υδατικών μιγμάτων υδρογονανθράκων. Πολύ καλά αποτελέσματα πρόρρησης και βελτιωμένα σε σχέση με το UMR-PRU λαμβάνονται στην ισορροπία υγρού – υγρού τριαδικών μιγμάτων υδρογονάνθρακα με μεθανόλη και νερό. Τέλος, πραγματοποιείται πρόρρηση των σημείων δρόσου μιγμάτων φυσικού αερίου με νερό και μεθανόλη, όπου το UMR-CPAPRU βελτιώνει την πρόβλεψη του UMR-PRU.

Table of Contents

Πρόλογος vi
Preface viii
Abstract x
Σύνοψη xiv
Table of Contents xviii
List of Tables xxiv
List of Figures xxviii
Abbreviations xxxviii
Chapter 1: Scope 1
Chapter 2: Elements of NG processing 5
2.1. Overview of the world energy consumption 6
2.2. A brief history of Natural Gas 7
2.3. Natural gas value chain 7
2.4. Natural Gas Components and Important Impurities 9
2.5. Pipeline specifications 10
2.6. Problems encountered due to the presence of water 12
2.7. Natural gas moisture control techniques 13
2.7.1. Inhibitor injection 13
2.7.2. MEG loop 14
2.7.3. Natural Gas dehydration 15
References 19
Chapter 3: Hydrogen bonding interactions 21
3.1. Introduction 22
3.2. Physical Interactions 23
3.2.1. Attractive forces 24
3.2.2. Repulsive forces 26
3.3. Chemical interactions: hydrogen bond 27
3.3.1. Hydrogen Bonds 28
3.3.2. Electron donors – electron acceptors 30
3.3.3. An example: the anomalous properties of water 30

List of Symbols 34
Latin Characters 34
Greek Characters 34
Superscripts and Subscripts 34
References 35
Chapter 4: Phase Equilibrium calculations 37
4.1. Thermodynamic equilibrium and phase rule 38
4.2. Phase equilibrium at low pressure 40
4.2.1. Vapor – liquid equilibrium 40
4.2.2. Liquid – Liquid Equilibrium 40
4.3. Phase equilibrium with an Equation of State 42
4.4. Phase equilibrium algorithms 42
4.4.1. Bubble point calculation 43
4.4.2. Dew point calculation 44
4.4.3. Isothermal Flash calculation 44
List of Symbols 46
Latin Characters 46
Greek Characters 46
Superscripts and Subscripts 46
References 48
Chapter 5: Thermodynamic Models 49
5.1. Introduction 50
5.2. Cubic EoS with classic mixing rules 51
5.3. Advanced Mixing Rules 54
5.3.1. UMR-PRU 55
5.3.2. TST/NRTL model 58
5.4. Models directly accounting for association 60
5.4.1. Cubic Plus Association (CPA-PR) EoS 60
5.4.2. Perturbed – Chain Statistical Associating Fluid Theory (PC-SAFT) 66
5.5. The GERG-2008 model 69
List of Symbols 71
Latin Characters 71

Greek Characters 72
Superscripts and Subscripts 73
References 75
Chapter 6: Experimental Measurement of the Vapor – Liquid Equilibrium (VLE) of the carbon dioxide/methane mixture at three isotherms 79
6.1. Introduction 80
6.2. Experimental Section 82
6.2.1. Experimental Apparatus 82
6.2.2. Calibration 86
6.2.3. Experimental Procedure 87
6.2.4. Uncertainty Analysis 89
6.2.5. Data Reduction 99
6.3. VLE Experimental Results 101
6.3.1. Summary and Analysis of Uncertainty Estimates 109
6.3.2. Critical Point Estimation 109
6.3.3. Comparison with literature data and GERG-2008 prediction 113
6.4. Model Fitting 114
6.5. Conclusions 118
List of Symbols 119
Latin Characters 119
Greek Characters 120
Superscripts and Subscripts 121
References 122
Chapter 7: Extension of UMR-PRU to natural gas mixtures containing polar components 125
7.1. Introduction 126
7.2. Pure component parameters 127
7.3. Binary mixtures 130
7.3.1. Vapor – Liquid Equilibrium 130
7.3.2. Liquid – Liquid Equilibrium 143
7.4. Multicomponent Mixtures 149
7.4.1. Ternary mixtures 149
7.4.2. Multicomponent mixtures containing BTEX components 153

7.4.3. Phase envelope of wet natural gases 155
7.5. Conclusions 156
List of Symbols 157
Latin Characters 157
Greek Characters 157
Superscripts and Subscripts 157
References 158
Chapter 8: Simulation of a natural gas TEG dehydration unit 165
8.1. Introduction 166
8.2. Literature Review 166
8.3. Process description 169
8.3.1. Glycol purity enhancing alternatives 172
8.4. Incorporation of the UMR-PRU in process simulators 174
8.5. Simulation Results 175
8.5.1. *Case I*: the simple absorber 175
8.5.2. *Case II*: Simplified TEG dehydration unit 178
8.6. Sensitivity Analysis 185
8.6.1. Effect of the stripping gas rate 186
8.6.2. Effect of the reboiler temperature 187
8.6.3. Effect of the Regenerator pressure 188
8.6.4. Effect of the feed temperature in the regenerator 189
8.6.5. Effect of the flash tank temperature 190
8.6.6. Effect of the contactor temperature 191
8.6.7. Effect of the contactor pressure 193
8.7. Process Optimization 194
8.8. Economic Evaluation 195
8.8.1. Capital Cost 195
8.8.2. Operating cost 199
8.9. Conclusions 200
List of Symbols 201
Latin Characters 201
Greek Characters 201

Superscripts and Subscripts 201
References 202
Chapter 9: Impact of the advanced mixing rules and explicit calculation of association at natural gas mixtures with hydrogen bonding compounds 205
9.1. Introduction 206
9.2. Literature review 206
9.3. Investigation of the associating schemes of CPA-PR 207
9.3.1. Associating schemes for MEG and glycols 207
9.3.2. Selection of associating scheme for CO_2 208
9.4. Binary phase equilibrium results 210
9.5. Multicomponent mixtures prediction results 215
9.5.1. Ternary Mixtures 215
9.5.2. Dew point prediction of SNG mixtures 219
9.6. Conclusions 224
List of Symbols 224
Latin Characters 224
Superscripts and Subscripts 224
References 225
Chapter 10: Development of a new group – contribution EoS for the modelling of hydrogen bonding mixtures 229
10.1. Introduction 230
10.2. Model development 230
10.3. Pure Component Parameters 233
10.4. Evaluation of the UMR-CPAPRU model in two ternary mixtures and their respective binaries 236
10.5. Development of a group-contribution EoS for associating mixtures 244
10.6. Prediction results 253
10.6.1. Ternary mixtures prediction results 253
10.6.2. Dew point prediction of SNG mixtures 255
10.7. Conclusions 259
List of Symbols 260
Latin Characters 260
Greek Characters 261

Superscripts and Subscripts 261
References 262
Chapter 11: Concluding remarks 267
11.1. Conclusions 268
11.2. Future work 271
Appendix A 273
Literature Cited 279
Appendix B 283
Appendix C 287
Literature Cited 295
Appendix D 301
Appendix E 303
Appendix F 307
F.1. Paper I 308
F.2. Paper II 309
F.3. Paper III 310
F.4. Contribution in a peer-reviewed book chapter 311
F.5. Communications in National and International Scientific Conferences 313

List of Tables

Table 2.1: Typical natural gas compositions (% molar)[8] 9
Table 3.1: Phase change properties for water and methane[5]..... 29
Table 4.1: Equilibrium criteria for a closed system. 38
Table 4.2: Different type of equilibrium calculations along with the defined and calculated variables of each case..... 42
Table 5.1: Cubic EoS parameters for the SRK and PR used in eq. 5.3 - eq. 5.5.[35]..... 52
Table 5.2: Critical properties and acentric factors for cubic EoS. MC parameters for PR are also given. Deviation from DIPPR with ΔT step equal to 5 K.....53
Table 5.3: UNIFAC structural van der Waals volume (R_i) and area (Q_i) parameters for group i, used in the UMR-PRU model. 56
Table 5.4: UNIFAC group interaction parameters for UMR-PRU following the temperature dependency of eq. 5.19..... 57
Table 5.5: Pure component parameters for CPA-PR. The deviation is defined from DIPPR correlation with a temperature step equal to 5 K..... 63
Table 5.6: Association schemes used in this work based on the terminology of Huang and Randosz[18]. 65
Table 6.1: Characteristics of pure chemicals used.....86
Table 6.2: Molar masses of atomic elements and compounds with uncertainties 94
Table 6.3: CO_2/CH_4 calibration gas mixtures: CO_2 mol fractions and corresponding standard uncertainties. 97
Table 6.4: Fitted parameters for the vapor and liquid relation between the GC response and the number of moles, along with the standard uncertainty of composition analysis. 98
Table 6.5: liquid phase: Experimental VLE data for CO_2 and CH_4 at mean temperature, T_f, mean pressure, p_f, and mean liquid phase mol fraction, x_{CO_2}..... 103
Table 6.6: Vapor phase: Experimental VLE data for CO_2 and CH_4 at mean temperature, T_f, mean pressure, p_f, and mean vapor phase mol fraction, y_{CO_2} 106
Table 6.7: Parameters of the scaling law (eq. 6.32) fitted to critical region data from this work for the three different average temperatures. 111
Table 6.8: Pure component parameters for PC-SAFT EoS.....114
Table 6.9: Binary interaction parameters for SRK, PR, PC-SAFT and UMR-PRU fitted to the experimental data of this work, through eq. 6.35, for each isotherm.....115
Table 6.10: Deviations of the UMR-PRU model from the estimated by the scaling law critical point data. 117
Table 7.1: TEG pure component properties and vapor pressure constants (DIPPR-101)[1] from different versions of DIPPR.....128
Table 7.2: VLE binary BPP correlation results with UMR-PRU. Prediction with TST/NRTL for comparison purposes.....131

Table 7.3: VLE binary flash prediction results with the UMR-PRU and TST/NRTL models. 139
Table 7.4: Prediction results of aqueous TEG heat capacity with UMR-PRU and TST/NRTL. Experimental data by Li et al.[16] 142
Table 7.5: Temperature effect of decompression valve with the UMR-PRU and TST/NRTL models. Experimental data by Satyro et al.[75] 142
Table 7.6: LLE binary prediction results with the UMR-PRU and TST/NRTL models. 144
Table 7.7: VLE ternary mixtures prediction results with UMR-PRU and TST/NRTL. 150
Table 8.1: Glycol decomposition temperature and corresponding lean glycol concentration calculated through Campbell's correlations[1]. 171
Table 8.2: Compound specific properties and properties calculated through the CAPE OPEN standard. 174
Table 8.3: Simulation Results for Case I with UMR-PRU model in two different simulators (Hysys, Unisim) and TST/NRTL model in Hysys 177
Table 8.4: Simulation results in Hysys for the streams connected to the Contactor of Case II with UMR-PRU and TST/NRTL. 180
Table 8.5: Specifications for the columns used in Case II. 181
Table 8.6: Simulation Results in Hysys for the streams connected to the Regenerator of Case II with UMR-PRU and TST/NRTL. 182
Table 8.7: Simulation Results in Hysys for the streams connected to the flash tank for Case II with UMR-PRU and TST/NRTL. 183
Table 8.8: Simulation results in Hysys for Case II, with UMR-PRU and TST/NRTL. 183
Table 8.9: Simulation Results in Hysys concerning the Energy Requirements of Case II, with UMR-PRU and TST/NRTL. 185
Table 8.10: Operating parameters for base and optimized simulation 194
Table 8.11: Simulation results for base and optimized conditions with UMR-PRU .. 194
Table 8.12: Simulation results in Hysys concerning the Energy Requirements of the optimized simulation, with UMR-PRU and TST/NRTL and comparison with the base case scenario. 195
Table 8.13: Cost parameters for the calculation of the equipment costs for the major pieces of equipment (eq. 8.2) and the hand factor for eq. 8.1. 196
Table 8.14: Total equipment and fixed capital costs calculated with UMR-PRU for base and optimized conditions based on Aspen Icarus and literature correlations. 197
Table 8.15: Economic evaluation results of base and optimized case[a] with UMR-PRU with Aspen Icarus software and based on empirical correlations 198
Table 8.16: Operating cost for base and optimized process with UMR-PRU. 199
Table 8.17: Calculated required rates in terms of utilities and electricity by Hysys for base and optimized process with UMR-PRU. 199
Table 9.1: Database of experimental data used for fitting the EoS parameters 210
Table 9.2: Binary group interaction parameters of UMR-PRU determined in this study. 211
Table 9.3: Binary interaction parameters for PR and CPA-PR. 211

Table 9.4: Binary interaction parameters for PR, UMR-PRU and CPA-PR regressed from experimental data at 313 K. 211
Table 9.5: VLE correlation results with PR, UMR-PRU and CPA-PR. 212
Table 9.6: VLE prediction results for the ternary methane (1) / hydrate inhibitor (2) / water (3) with PR, UMR-PRU and CPA-PR. 218
Table 9.7: Composition of the Dry Synthetic Natural Gas Mixtures (% molar). 219
Table 9.8: Dew point temperature prediction of SNGs and their mixtures with water and methanol, with PR, UMR-PRU and CPA-PR. 220
Table 10.1: Pure component parameters for UMR-CPAPRU EoS. The deviation refers to that from DIPPR correlation. 235
Table 10.2: Temperature – specific interaction parameters for UMR-CPAPRU for the isotherms of 298.15 K and 313.15 K. 236
Table 10.3: VLE correlation results per isotherm for the mixtures of interest with UMR-PRU, CPA-PR and UMR-CPAPRU. 237
Table 10.4: VLE ternary prediction results for mixtures containing methane (1), hydrate inhibitor (2) and water (3) with UMR-PRU, CPA-PR and UMR-CPAPRU. . 240
Table 10.5: Binary interaction parameters for the UMR-CPAPRU model. 245
Table 10.6: VLE binary correlation results with the UMR-CPAPRU model. Comparison with UMR-PRU is given 246
Table 10.7: LLE results with the UMR-PRU and the UMR-CPAPRU. 250
Table 10.8: Dew point temperature (DPT) predictions of SNGs and their mixtures with water and methanol, with UMR-CPAPRU, UMR-PRU and CPA-PR. 256
Table A.1: Database of experimental binary VLE data used for the regression of UNIFAC group IPs for UMR-PRU. 274
Table A.2: Database of experimental binary LLE data used for the regression of UNIFAC group IPs for UMR-PRU. 278
Table B.1: Cashflow parameters as used in the Aspen Icarus software for the economic evaluation of a natural gas TEG dehydration plant 284
Table B.2: Summary of the project parameters used for the evaluation of the capital cost and the time period in Aspen Icarus Software. 285
Table B.3: Equipment type used for the mapping and costing of the equipment cost in Aspen Icarus software. 285
Table B.4: Summary of the utility types and rate used by Aspen Icarus software for the estimation of the operating cost 285
Table C.1: Database of experimental binary VLEdata used for the regression of UNIFAC group IPs for UMR-CPAPRU. 288
Table C.2: Database of experimental binary LLE data used for the regression of UNIFAC group IPs for UMR-CPAPRU. 294
Table D.1: UNIFAC group interaction parameters for the UMR-PR-fit model following the temperature dependency of eq. 5.19, used for the interactions between the non-associating components for UMR-CPAPRU. 302

List of Figures

Figure 2.1: Total energy consumption by fuel type. *(a)* in EU for 1990-2014[1], *(b)* worldwide; from 1990 projection to 2040.[3] 6
Figure 2.2: Natural gas value chain[6] 8
Figure 2.3: Natural gas use by sector in the USA for the year 2011.[7] 8
Figure 2.4: Phase behavior of natural gas with traces (40 ppm) of water. Composition (% molar) on dry basis *(a)*. 85 C1, 10 C2, 4 C3, 0.5 iC4, 0.5 nC4 and *(b)* 7 N_2, 0.5 CO_2, 88 C1, 3 C2, 0.9 C3, 0.2 iC4, 0.3 nC4, 0.09 iC5, 0.09 nC5, 0.12 nC6, 0.03 nC7 and 0.02 nC8. 11
Figure 2.5: Gas hydrate structures. Image taken from the Institute of Petroleum Engineering.[13] 12
Figure 2.6: A composite diagram showing the phase boundary of methane hydrate formation as a function of temperature and pressure. The black lines show the phase boundary line shifting to the left on the addition of increasing methanol concentration. On the right: the blue region is that where hydrate crystals are not formed and superimposed over this is a pipeline of about 45 miles in length containing natural gas.[15] 13
Figure 2.7: Full reclamation scheme that removes all the salts to prevent scaling in the pipelines[18] 14
Figure 2.8: Simplified flowchart of a glycol dehydration plant[19] 15
Figure 2.9: Simplified flow diagram of dehydration unit by adsorption.[20] 17
Figure 2.10: Typical flowchart of a refrigeration process. 18
Figure 3.1: Orientation of two dipoles.[1] 24
Figure 3.2: Difference between the different kinds of linear moments appearing at electric neutral molecules. 24
Figure 3.3: Cluster formation between two water molecules. The normal intramolecular covalent bond is depicted with solid line while the hydrogen bond between the hydrogen of the one molecule and the oxygen of the other is depicted with dashed line. 28
Figure 3.4: Difference in the properties of water due to hydrogen bonding, in comparison with those of the other hydrogen chalcogenides. For comparison, the same properties for hydrogen halides and metal tetrahydrides are also depicted. Dashed line indicates the expected temperature if a linear approximation of the melting or boiling points of the rest components is assumed *(a)* melting points, *(b)* normal boiling points. 31
Figure 3.5: Liquid (left) vs solid (right) water structure.[10] 31
Figure 3.6: *(a)* Liquid density of water at 1 bar.[5] *(b)* Schematic effect of water temperature at the bottom of a lake for two different seasons.[11] 32
Figure 4.1: Flowchart of a bubble point calculation algorithm 43
Figure 4.2: Flowchart of a dew point calculation algorithm. 44
Figure 4.3: Isothermal (TP) flash algorithm flowchart. 45

Figure 6.1: Experimental VLE data of CO_2/CH_4 mixture at *(a)* 270.15 K[8-12], *(b)* at 283.15 K[4, 5, 7], *(c)* at 288.15 K[6, 7, 13, 14] and *(d)* at 293.15 K[5-7]. 81
Figure 6.2: VLE of the CO_2/CH_4 at two isotherms and prediction with the SRK EoS with k_{ij} equal to 0.0956 as suggested by Perez et al.[16]. *(a)* at 223 K. Experimental data by Donelly et al.[18], Knapp et al.[19] and Joffe et al.[20] and *(b)* at 301 K. Experimental data by Bian et al.[15]. 82
Figure 6.3: Principal diagram of cell and ancillary apparatus. LS,VS: Liquid and vapor phase Rolsi™ samplers, respectively. SM: Rolsi™ controller. M: Gear for rotating permanent magnet below cell, which rotates stirrer inside cell. Gear connected to electric motor outside bath. T_{04}: Top flange SPRT. T_{05}: Bottom flange SPRT. (reproduced from Westman et al.[22]) 83
Figure 6.4: Borescope picture of liquid and vapor interface for 303.15 K and 73.5 bar. 88
Figure 6.5: Schematic depiction of the pressure measurement system, where the different contributions affecting the overall pressure are shown.[17] 90
Figure 6.6: *(a)* Pressure standard uncertainty relative to the measured pressure for the VLE measurements performed, expressed as $100 \cdot \bar{u}_c(\bar{p})/\bar{p}_f$. $\bar{p}_f$ stands for the measured pressure and $\bar{u}_c(\bar{p})$ for the standard uncertainty. *(b)*. Temperature deviations for each VLE measurement from isotherm mean temperature, and temperature standard uncertainty, expressed together as $\bar{T}_f \pm \bar{u}_c(\bar{T}) - isotherm\ mean\ temp.$, versus the VLE experimental pressure $\bar{p}_f$. $\bar{T}_f$ stands for the VLE experimental mean temperature and $\bar{u}_c(\bar{T})$ for the standard uncertainty in temperature. Blue colour indicates the isotherm at the mean temperature of 293.130 K, red colour indicates the isotherm at the mean temperature of 298.142 K and green colour indicates the isotherm at the mean temperature of 303.145 K. 93
Figure 6.7: Error between actual compositions in Table 6.3 and the composition determined by the GC using the fit of eq. 6.20 - eq. 6.22. Composition analysis uncertainty $u(x_{CO_2}) = u(y_{CO_2}) = s(e)$ as reported in Table 6.4. 99
Figure 6.8: VLE pressure – composition diagram for the CO_2/CH_4 for the different isotherms measured in this work. Blue colour indicates the liquid phase and red colour the vapor one. (x) indicates the experimental data measured in this work along with the estimated uncertainties (black uncertainty bars). (◇) Indicates the critical point of the mixture as estimated by the fitting of the Scaling Law (eq. 6.32). The solid line is the prediction of GERG-2008. *(a)*. Mean temperature 293.130 K. (○) indicates the data by Xu et al.[6], (Δ) indicates the data by Nasir et al.[5] and (□) indicates the data by Devlikamov et al.[7] *(b)*. Mean temperature 298.142 K. (□) indicates the data by Devlikamov et al.[7] *(c)*. Mean temperature 303.145 K. Please note that the scaling in *(c)* is very narrow due to the proximity in CO_2 critical temperature. 102
Figure 6.9: Pressure – composition phase behavior in the critical region estimated by the scaling law model in eq. 6.32. (+) indicates the points used for the fitting of the scaling law (see Table 6.7), (x) indicates the points not used in the fitting of scaling law and solid line indicates the scaling law correlation. Dashed line indicates a second set of the scaling law parameters to show the effect of the appropriate selection of data points used for the fitting of the parameters. Blue colour indicates the liquid phase and

red colour the vapor one. Please note that the scales of the graphs are very different from each other. *(a)* 293.13 K, *(b)* 298.14 K and *(c)* 303.15 K. 112
Figure 6.10: Phase diagram of pure CO_2 with PC-SAFT using two sets of pure component parameters. Exp. data are taken from NIST[39]. 114
Figure 6.11: Binary VLE correlation results for the CO_2/CH_4 mixture at *(a)* 293.13 K, *(b)* 298.14 K and *(c)* 303.15 K, with the: PR (blue solid line), SRK (green long dashed line), PC-SAFT (grey dotted line) and UMR-PRU (black solid line). (○) denotes the experimental data of this work as presented in Table 6.5 and Table 6.6. Note that the critical point estimated through the scaling law from the experimental data is marked as a green (◇) while the predicted critical point of the models as a (★) of the same coloring as the respective model. 116
Figure 7.1: VLE prediction of the n-hexane/water mixture with UMR-PRU using two sets of IPs. Dashed line indicates the VLE 2 coeff. IPs of the original UNIFAC while solid line the IPs fitted to hydrocarbon/water LLE data. Experimental data by Tsonopoulos et al.[4]. 126
Figure 7.2: Vapor pressure of pure TEG. *(a)* Comparison of three DIPPR correlations against raw experimental data and model predictions: Experimental data (□) by Wise et al.[11], (○) by Steele et al.[12] and (Δ) by Stull et al.[13]. DIPPR-1981 with black dotted line, DIPPR-1987 with black dashed line, DIPPR-2001 with black long dash, dotted line, UMR-PRU with black solid line and TST/NRTL with grey dashed line; *(b)* focus at low temperatures. 128
Figure 7.3: Prediction of heat capacity at constant pressure for pure components. Solid line denotes the UMR-PRU prediction and dashed line the TST/NRTL one. *(a)* Saturated water heat capacity. Circles denote experimental data by NIST.[14] *(b)* TEG heat capacity at 1 bar. Circles denote experimental points by Stephens et al.[15], diamonds by Steele et al.[12] and triangles by Li et al.[16].....129
Figure 7.4: MEG/water VLE at 323.15 K with UMR-PRU using two different sets of interaction parameters. Solid line presents the fitted IPs and dotted line the prediction using the UNIFAC VLE 2 coeff. Experimental data by Gonzales et al.[32] 133
Figure 7.5: VLE correlation results with UMR-PRU (solid) line for methane with polar chemicals. Prediction results with TST/NRTL are also given (dashed line). *(a)* methane/water; black colour denotes 274.15 K, red 298.15 K and green 313.15 K[24-27, 30] *(b)* methane/methanol; blue colour denotes 273.15 K, red 298.15 K and green 313.15 K[25, 30, 36, 53] *(c)* liquid phase of methane/MEG; black colour denotes 298.15 K, red 323.15 K, green 373.15 K and blue 398.15 K[44, 48] and *(d)* methane/TEG (liquid phase); black colour denotes 298.15 K, red 323.15 K and blue 373.15 K[49, 50]. 134
Figure 7.6: VLE of CO_2 with water and polar chemicals with UMR-PRU (solid line) and TST/NRTL (dashed line). *(a)* CO_2/H_2O (liquid phase). Exp. data by [18, 23], *(b)* CO_2/H_2O (vapor phase). Exp. data by [18, 54, 55], *(c)* CO_2/methanol. Exp. data by [34], *(d)* CO_2/MEG. Exp. data by [45, 48, 56], *(e)* CO_2/TEG (liquid phase). Exp. data by [49] and *(f)* CO_2/TEG (vapor phase). Exp. data by [57]. Colouring corresponds to the same temperature with the experimental points. 135
Figure 7.7: Binary VLE results for mixtures of light gases with water with UMR-PRU (solid line) and TST/NRTL (dashed line). *(a)* Vapor phase composition predictions for

the methane/water mixture. Experimental data by Sage et Lacey[58]. (○) at 310.93 K, (+) at 344.26 K, (Δ) at 377.59 K, (★) at 410.93 K, (□) at 444.26 K and (◇) at 477.59 K. *(b)*. Vapor phase composition predictions for the ethane/water mixture. Experimental data by Yarrison et al.[59]. (○) at 314.8 K, (Δ) at 366.5 K, (□) at 422 K and (◇) at 466.5 K.. 136
Figure 7.8: VLE of light gases and hydrocarbons with TEG with UMR-PRU (solid line) and TST/NRTL (dashed line). *(a)* Methane/TEG (liquid phase). (Δ) Experimental data by Wilson et al.[50] at 298.15 K, (○) by Jou et al.[49] at 323.15 K and (◇) by Jou et al.[49] at 373.15 K. *(b)* Vapor phase of the methane/TEG. Experimental data by Jerinic et al.[60]. (○) at 298.15 K and (◇) at 316.75 K. *(c)* Ethane/TEG. Experimental data by Jou et al.[49]. (Δ) at 298.15 K, (○) at 323.15 K and (◇) at 373.15 K. *(d)* Propane/TEG. Experimental data by Jou et al.[49]. (Δ) at 298.15 K, (○) at 323.15 K, (◇) at 373.15 K and (□) at 398.15 K. *(e)* Benzene/TEG at 1.01325 bar. (◇) Experimental points by Gupta et al.[52] and *(f)* Toluene/TEG mixture at 1.01325 bar. (◇) Experimental points by Gupta et al.[52]. 137
Figure 7.9: TEG/water mixture results with UMR-PRU (solid line) and TST/NRTL (dashed line). *(a)* VLE at 0.85 bar. (◇) Exp. data by Mostafazadeh et al.[33], *(b)* VLE at constant pressure. Exp. data by Piemonte et al.[66], (○) at 0.07 bar, (Δ) at 0.13 bar, (□) at 0.27 bar and (◇) at 0.54 bar. *(c)* Water activity coefficients. Experimental data by Herskowitz et al.[73] (○) at 297.6 K and (◇) at 332.6 K. *(d)*. Water infinite dilution activity coefficients. Experimental data (○) by Parrish et al.[71] and (◇) by Bestani et al.[70], *(e)* Excess Enthalpies (◇) Experimental data by Hamam et al.[74] and *(f)* Heat capacity at constant pressure. Experimental data by Li et al.[16]. (○) x_{TEG} = 0.2, (★) x_{TEG} = 0.4, (◇) x_{TEG} = 0.5, (□) x_{TEG} = 0.6 and (Δ) x_{TEG} = 0.8. 141
Figure 7.10: LLE prediction results of hydrocarbons with water with UMR-PRU (solid line) and TST/NRTL (dashed line). Blue circles denote experimental points in the aqueous phase (I), black diamonds in the HC-rich phase (II), and red triangles in the vapor phase. *(a)* Propane/H_2O. Exp. data by Kobayashi et al.[76], *(b)* n-hexane/H_2O. Exp. data by Tsonopoulos et al.[4], *(c)* n-decane/H_2O. Exp. data by Revellame et al.[92], Ng et al.[91] and Economou et al.[90], *(d)*. cyclohexane/H_2O. Exp. data by Burd et al.[89], Guseva et al.[95], Pereda et al.[96], Marche et al.[82], Pierotti et al.[97], Goldman et al.[94] and Tsonopoulos et al.[4], *(e)* Benzene/H_2O. Exp. data by Tsonopoulos et al.[4] and *(f)* p-xylene/H_2O. Experimental data by Chen et al.[103] and Jou et al.[98]. 147
Figure 7.11: LLE prediction results of hydrocarbons with TEG with UMR-PRU (solid line) and TST/NRTL (dashed line). Red circles denote experimental points in the polar phase (I) and black colour (triangles and diamonds) in the HC-rich phase (II). *(a)* n-heptane/TEG. Exp. data by Derawi et al.[99] and Rawat et al.[100]. *(b)* Benzene/TEG. Exp. data by Folas et al.[101]. *(c)* Toluene/TEG. Exp. data by Folas et al.[101] and Hughes et al.[102]. 148
Figure 7.12: VLE bubble point temperature prediction results for the TEG/water/ toluene mixture with UMR-PRU (solid line) and TST/NRTL (dashed line). Experimental data by Mostafazadeh et al.[33]. Black circles denote experimental solubility data of toluene in liquid phase, red diamonds the solubility of TEG in vapor phase and blue triangles the water solubility in vapor phase; *(a)*, *(b)* indicate different tielines. 149

Figure 7.13: VLE prediction results for the CO_2/TEG/water mixture with UMR-PRU (solid line) and TST/NRTL (dashed line). (✶) 0 % wt. water, (□) 3.5 % wt. water, (+) 7 % wt. water, (○) 10 % wt. water, (Δ) 40 % wt. water and (◇) 60 % wt. water. *(a)* Experimental data at 297.04 K by Kaminishi et al.[106], at 298.15 K by Wise et al.[69] and Jou et al.[49]. *(b)* Experimental data by Kaminishi et al.[106] at 322.04 K. *(c)*. Experimental data by Wise et al.[69] at 343.15 K. 151
Figure 7.14: VLE prediction results for ternary mixtures containing methane, an aromatic hydrocarbon and TEG with UMR-PRU (solid line) and TST/NRTL (dashed line). Black circles denote experimental partition coefficients of methane and red diamonds partition coefficients of the respective aromatic hydrocarbon. Experimental data by Ng et al.[105]; *(a)* methane/benzene/TEG at 348.15 K, *(b)* methane/ethylbenzene/ TEG at 348.15 K, *(c)* methane/toluene/TEG at 348.15 K and *(d)* methane/toluene/TEG at 398.15 K. 152
Figure 7.15: VLE prediction results for mixtures containing methane, BTEX, water and TEG at different conditions relative to dehydration process. Experimental data by Ng et al.[107]. Modelling results (○) with UMR-PRU (in black) and (Δ) with TST/NRTL (in red); *(a)* Flash drum conditions on dry basis, at 348.1 K and 6.89 bar, *(b)* Flash tank conditions with 5 % wt. water, at 348.1 K and 6.89 bar, *(c)* Regenerator conditions on dry basis, at 477.6 K and 1.38 bar, *(d)* Regenerator conditions with 1 % wt. water, at 477.6 K and 1.62 bar, *(e)* Contactor conditions on dry basis, at 298.1 K and 68.95 bar and *(f)* Contactor conditions with 1 % wt. water, at 298.1 K and 68.95 bar. 154
Figure 7.16: Dew point prediction on dry and wet basis with UMR-PRU (solid line) and TST/NRTL (dashed line). *(a)* Exp. data by Avila et al.[108]. Composition (molar) on dry basis: N_2: 0.31, CO_2: 0.20, CH_4: 90.42, C2: 8.04, C3: 0.80, iC4: 0.08, nC4: 0.12, iC5: 0.01, nC5: 0.01, nC6: 0.005 and nC7: 0.001 and *(b)* Exp. data by Jarne et al.[109]. Composition (molar) on dry basis: N_2: 0.77, CO_2: 1.70, CH_4: 84.45, C2: 8.68, C3: 3.3, iC4: 0.29, nC4: 0.59, iC5: 0.08, nC5: 0.09 and nC6: 0.05. 155
Figure 8.1: Typical TEG dehydration unit[1] 170
Figure 8.2: Typical stripping gas unit structure.[1] 172
Figure 8.3: Alternative methods of glycol enrichment: *(a)* the DRIZO® process, *(b)* the coldfinger® process 173
Figure 8.4: Process flowchart of Case I, as constructed in the Hysys environment. . 176
Figure 8.5: Simulation results for Case I with UMR-PRU implemented in Hysys and Unisim and TST/NRTL. UMR-PRU in Hysys is given with solid black fill, TST/NRTL is given in solid blue fill and UMR-PRU in Unisim is given with stripped patterned black color in green background; *(a)* TEG and water composition in the dry gas, *(b)* Natural gas components composition in the dry gas, *(c)* TEG and water composition in the Rich TEG stream and *(d)* Natural gas components composition in the Rich TEG stream. 176
Figure 8.6: Process flowchart of Case II, as constructed in the Hysys environment. 179
Figure 8.7: Simulation results for the Contactor of Case II with UMR-PRU (solid black fill) and TST/NRTL (solid blue fill). *(a)* NG Component distribution in the dry gas stream and *(b)* TEG and water distribution in the Rich and Lean TEG streams. 184
Figure 8.8: Simulation results for the Regenerator of Case II with UMR-PRU (solid black fill) and TST/NRTL (solid blue fill). *(a)* Vapor stream and *(b)* Reflux stream. . 184

Figure 8.9: Effect of stripping gas rate in *(a)* lean TEG purity, *(b)* dry gas water content, *(c)* TEG loss and *(d)* Reboiler duty. 186
Figure 8.10: Effect of the reboiler operating temperature in *(a)* lean TEG purity, *(b)* dry gas water content, *(c)* TEG loss and *(d)* Reboiler duty. 187
Figure 8.11: Effect of the regenerator pressure in *(a)* Reboiler duty, *(b)* TEG loss and *(c)* lean TEG purity 188
Figure 8.12: Effect of the temperature of the feed stream to the regenerator (S5) in *(a)* lean TEG purity, *(b)* dry gas water content, *(c)* reboiler duty, *(d)* cooler duty and *(e)* TEG loss. 189
Figure 8.13: Effect of the flash tank temperature on *(a)* lean TEG purity, *(b)* dry gas water content, *(c)* TEG loss, *(d)* flash gas hydrocarbon content and *(e)* reboiler duty. 190
Figure 8.14: Effect of the contactor operating temperature at *(a)* lean TEG purity, *(b)* dry gas water content, *(c)* TEG loss and *(d)* rich TEG hydrocarbon content. 192
Figure 8.15: Effect of the contactor operating temperature at *(a)* reboiler duty and *(b)* cooler duty. 192
Figure 8.16: Effect of the contactor operating pressure at *(a)* lean TEG purity, *(b)* dry gas water content, *(c)* TEG loss and *(d)* rich TEG hydrocarbon content. 193
Figure 8.17: Capital cost of a TEG dehydration plant for year 2008 as a function of the capacity of the plant.[33] 197
Figure 9.1: LLE prediction of the n-heptane/MEG mixture with CPA-PR using the 2B and 4C associating scheme. Experimental data by Derawi et al.[20] 208
Figure 9.2: Dew point prediction results with CPA-PR for two SNGs, with the CO_2 assigned as a 4C-sites component (solid black line) and as inert one (gray dashed line). Diamonds denote experimental data by Jarne et al.[18] SNG composition (% molar): *(a)* N_2: 1.56, CO_2: 15.91 , CH_4: 69.11, C2: 2.62 , C3:0.42 , iC4: 0.11 , nC4: 0.10, iC5: 0.03, nC5: 0.02, nC6: 0.11 and *(b)* N_2: 0.77, CO_2: 1.70, CH_4: 84.45, C2: 8.68, C3: 3.3, iC4: 0.29, nC4: 0.59, iC5: 0.08, nC5: 0.09 and nC6: 0.05. 209
Figure 9.3: VLE correlation results with PR (dashed line), UMR-PRU (solid line) and CPA-PR (dotted line) for: *(a)* methane (1)/water (2) at 298.15 K, *(b)* methane (1)/water (2) at 313.15 K, *(c)* methane (1)/methanol (2) at 298.15 K, *(d)* methane (1)/methanol (2) at 313.15 K, and *(e)* methane (1)/MEG (2) at 298.15 K. Triangles denote data by Frost et al.[7], circles by Yarym – Agaev et al.[27], crosses by Chapoy et al.[11], squares by Kim et al.[26], ex (x) by Jou et al.[41] and diamonds by Folas et al.[1]. Blue colour for the liquid phase and red for the vapor one. 213
Figure 9.4: Binary VLE and LLE results with PR (dashed line), UMR-PRU (solid line) and CPA-PR (dotted line) for the mixtures *(a)* CO_2 (1)/water (2) at 288 K, *(b)* n-pentane (1)/methanol (2) at 372.7 K and *(c)* n-hexane (1)/water (2). Circles denote experimental data by Valtz et al.[25], triangles by King et al.[24], diamonds by Wilsak et al.[39]; blue colour for liquid phase and red for the vapor one. For *(c)* experimental are by Tsonopoulos et al.[31]; blue colour for aqueous phase and black for the HC-rich one. 214
Figure 9.5: VLE prediction results for the ternary mixture methane/methanol/water at (i) 298.15 K and (ii) 313.15 K, for three concentrations (% wt.) of methanol in feed: *(a)* 42.7 %, *(b)* 50.2 % and *(c)* 75.6 %, with PR (dashed line), UMR-PRU (solid line) and

CPA-PR (dotted line). Experimental data by Sinyavskaya et al.[42] and Frost et al. [7]. Black circles denote the solubility of methane in liquid phase, red triangles the solubility of methanol in vapor phase, and blue diamonds the solubility of water in vapor phase. 216
Figure 9.6: VLE prediction results for the ternary mixture methane/MEG/water at 298.15 K (44.6 % wt. MEG in feed) with: PR (dashed line), UMR-PRU (solid line) and CPA-PR (dotted line). Experimental data by Folas et al.[1]. Black circles denote methane solubility in liquid phase, red triangles MEG solubility in vapor phase and blue diamonds water solubility in vapor phase. 217
Figure 9.7: Dew point prediction results of synthetic natural gases and their mixtures with water and methanol, with PR (dashed line), UMR-PRU (solid line) and CPA-PR (dotted line). Experimental data by Avila et al.[14-17] and Jarne et al.[18]. 222
Figure 10.1: Phase diagram of pure components calculated with the parameters determined in this study with UMR-CPAPRU. Experimental vapor pressure data are taken from DIPPR[13] while the density ones are from NIST[14] *(a)* water and *(b)* methanol. 234
Figure 10.2: VLE correlation results at 298.15 K with UMR-PRU (dashed line), CPA-PR (dotted line) and UMR-CPAPRU (solid line). *(a)* methane/water, *(b)* methane/ methanol and *(c)* methane/MEG. In *(a)* and *(b)* circles denote experimental data by Yarym – Agaev et al.[23], triangles by Kim et al.[24], squares by Chapoy et al.[28] and triangles by Frost et al.[26]. In *(c)* circles denote exp. data by Jou et al.[22], triangles by Folas et al.[29] and squares by Abdi et al.[30]. 238
Figure 10.3: VLE correlation results at 313.15 K with UMR-PRU (dashed line), CPA-PR (dotted line) and UMR-CPAPRU (solid line). *(a)* methane/water, *(b)* methane/methanol and *(d)* methane/MEG. Circles denote experimental data by Yarym – Agaev et al.[23], squares by Chapoy et al.[28] and diamonds by Frost et al.[26]..... 239
Figure 10.4: VLE prediction results for the methane/methanol/water mixture at 298.15 K with different concentrations of methanol in feed (% wt.) with UMR-PRU (dashed line), CPA-PR (dotted line) and UMR-CPAPRU (solid line). *(a)* 26 % methanol in liquid, *(b)* 42 % methanol in liquid, *(c)* 50 % methanol in liquid and *(d)* 75 % methanol in liquid. Exp. data by Sinyavskaya et al.[31] and Frost et al.[26]. Black circles denote methane solubility in liquid, red diamonds methanol in the vapor phase and blue triangles water in the vapor phase. 241
Figure 10.5: VLE prediction results for the methane solubility in liquid phase of the methane/methanol/water mixture at 298.15 K, at different methanol concentrations in feed (% wt.) with UMR-PRU (dashed line), CPA-PR (dotted line) and UMR-CPAPRU (solid line). Exp. data by Sinyavskaya et al.[31]. Blue circles denote 26 % methanol, red ex (x) 50 % methanol and black stars 75 % methanol in feed..... 242
Figure 10.6: VLE prediction results for the methane/methanol/water mixture at 313.15 K with different concentrations of methanol in feed (% wt.) with UMR-PRU (dashed line), CPA-PR (dotted line) and UMR-CPAPRU (solid line). *(a)* 26 % methanol in liquid, *(b)* 42 % methanol in liquid, *(c)* 50 % methanol in liquid and *(d)* 75 % methanol in liquid. Exp. data by Sinyavskaya et al.[31] and Frost et al.[26]. Black circles

denote methane solubility in liquid, red diamonds methanol in the vapor phase and blue triangles water in the vapor phase. 243
Figure 10.7: VLE prediction results for the methane/MEG/water mixture at 298.15 K. with UMR-PRU (dashed line), CPA-PR (dotted line) and UMR-CPAPRU (solid line) at different concentrations of MEG in the feed (% molar). Blue circles denote methane solubility in liquid phase, red diamonds MEG solubility in vapor phase and blue triangles water solubility in vapor phase. *(a)* 19 % MEG, Experimental data by Folas et al.[29], *(b)* 46 %, *(c)* 47 % and *(d)* 56 %. Exp. data by Kruger et al.[32]. 244
Figure 10.8: VLE correlation results with UMR-CPAPRU (solid line). Prediction with UMR-PRU model using the UNIFAC VLE 2 coeff. parameters is also presented (dashed line). *(a)* methanol/water. Black circles denote exp. data by Koner et al.[20] at 298 K, red squares at 323 K by McGlashan et al.[33] and blue diamonds at 338 K by McGlashan et al.[33] and *(b)* ethanol/water. Red diamonds denote exp. data by Niesen et al.[34] and Barr – David et al.[35] at 373 K, blue diamonds at 523.2 K, yellow stars at 548.2 K, green circles at 573.2 K, purple ex at 598.2 K and black cross at 623.2 K. Exp. data by Barr – David et al.[35] 248
Figure 10.9: VLE correlation results with UMR-CPAPRU model (solid line). Prediction with UMR-PRU (dashed line) is also presented. *(a)* n-pentane/methanol. Experimental data by Wilsak et al.[36] black circles denote 373 K, red diamonds 398 K, *(b)* benzene/methanol. Black circles denote exp. data by Goetschel et al.[37] at 288 K, red triangles by Iguchi et al.[38] at 298 K and blue diamonds by Kolodziej et al.[39] at 308 K. and *(c)* CO_2/methanol. Experimental data by Hong et al.[40], Black triangles denote 230 K, green ex 250 K, red circles 273 K and blue stars 290 K. 249
Figure 10.10: LLE prediction results of HCs with water with the UMR-CPAPRU and the UMR-PRU. Blue circles denote HC solubility in aqueous phase, black diamonds water solubility in HC-rich phase and red diamonds water solubility in vapor phase. *(a)* propane/water, exp. data by Kobayashi et al.[43]. *(b)* n-pentane/water, exp. data by Black et al.[44] , Polak et al.[45] *(c)* n-hexane/water, exp. data by Tsonopoulos et al.[46], *(d)* n-decane/water, exp. data by Revellame et al.[47], Ng et al.[48] and Economou et al.[49], *(e)* cyclohexane/water, exp. data by Burd et al.[50], Guseva et al.[51], Pereda et al.[52], Marche et al.[53], Pierotti et al.[54], Goldman et al.[55] and Tsonopoulos et al.[46], *(f)* i-pentane/water, exp data by Black et al. [76], Polak et al. [79] and Pavlova et al. [93], *(g)* benzene/water, exp. data by Tsonopoulos et al.[46] and *(h)* toluene/water, exp data by Marche et al.[53], Ng et al.[48] and Jou et al.[56] 251
Figure 10.11: LLE prediction results of HCs with methanol with UMR-CPAPRU (solid line) and UMR-PRU (dashed line). red circles denote the polar phase while black diamonds the HC-rich one. *(a)* n-hexane/methanol, exp. data by Higashiuchi et al.[57] and *(b)* n-heptane/methanol, exp. data by Higashiuchi et al.[58]. 252
Figure 10.12: LLE prediction results for the propane/water/methanol mixture with UMR-PRU (dashed line) and UMR-CPAPRU (solid line) at *(a)* 273.15 K and *(b)* 293.15 K. Red colour indicates the polar phase while black the HC-rich one. (*i*) solubility and (*ii*) methanol partition coefficient. Exp. data by Noda et al.[59].....253
Figure 10.13: LLE prediction results for the n-butane/water/methanol mixture with UMR-PRU (dashed line) and UMR-CPAPRU (solid line) at *(a)* 273.15 K and *(b)*

293.15 K. Red colour indicates the polar phase while black the HC-rich one. (i) solubility and (ii) methanol partition coefficient. Exp. data by Noda et al.[59] 254
Figure 10.14: LLE prediction results for benzene/water/methanol mixture at 303.15 K with UMR-PRU (dashed line) and UMR-CPAPRU (solid line). Red colour indicates the polar phase while black the HC-rich one. *(a)* solubility and *(b)* methanol partition coefficient. Exp. data by Udovenko et al.[60] 255
Figure 10.15: Dew point prediction results of synthetic natural gases and their mixtures with water and methanol, with UMR-CPAPRU (solid line), UMR-PRU (dashed line) and CPA-PR (dotted line). Experimental data by Avila et al.[61-64] and Jarne et al.[65] 257

Abbreviations

AAD	Absolute Average Deviation, $AAD = 100 \cdot \frac{1}{n_p}\sum_{i=1}^{n_p}\left\| x^{exp} - x^{calc}\right\|$, where n_p is the number of points, exponent *exp* indicates the experimental value of the size x and exponent *calc* indicates the calculated value of the size x by the respective thermodynamic model
AARD	Absolute Average Relative Deviation, $\%AARD = 100 \cdot \frac{1}{n_p}\sum_{i=1}^{n_p}\frac{\left\| x^{exp} - x^{calc}\right\|}{x^{exp}}$, where n_p is the number of points, exponent *exp* indicates the experimental value of the size x and exponent *calc* indicates the calculated value of the size x by the respective thermodynamic model
BP	British Petroleum
BPP	Bubble point pressure (bar)
BPT	Bubble point temperature (K)
BTEX	Benzene, toluene, ethyl-benzene, and xylene compounds
CAPE	Computer Aided Process Engineering
CCS	Carbon capture and storage
CN	Carbon number
Cond.	Condenser of the TEG Regenerator
CPA	Cubic Plus Association EoS
DEG	Diethylene glycol
DIPPR	Design Institute for Physical Properties
DPP	Dew point pressure (bar)
DPT	Dew point temperature (K)
eCPA	electrolyte Cubic Plus Association EoS
EoS	Equation of State
etOH	ethanol
EU	European Union
Eurostat	Statistical Office of the EU

GC	Gas Chromatograph
GC	Glycol cooler
GERG	Group Européen de la Researche Gazière
GPA	Gas Processing Association
GUM	ISO Guide for the estimation of Uncertainty in Measurement
HC	Hydrocarbons
HE-i	Glycol/Glycol Heat Exchanger, where i stands for 1,2
HV	Huron-Vidal mixing rules
Hysys	Aspen HYSYS©
Icarus	Aspen ICARUS©
IP	Interaction parameters
ITS-90	International Temperature Scale of 1990
IUPAC	International Union of Pure and Applied Chemistry
JT	Joule-Thomson
LLE	Liquid – Liquid Equilibrium
LNG	Liquefied natural gas
LS	Liquid sampler
MC	Mathias-Copeman expression for the alpha function (eq. 5.7)
MEG	(Mono) Ethylene Glycol
meOH	methanol
MHV2	modified Michelsen – HV mixing rule
NIST	National Institute of Standards and Technology
NG	Natural gas
NGL	Natural gas liquids
NMR	Nuclear magnetic resonance
NRTL	Non-random two liquid activity coefficient model
P-i	Glycol Pump, where i stands for 1, 2
PC-SAFT	Perturbed Chain – Statistical Associating Fluid Theory

PR	Peng – Robinson EoS
qCPA	quadrupole Cubic Plus Association EoS
Reb.	Reboiler of the TEG Regenerator
Rolsi	Rapid On Line Sampler Injector
SAFT	Statistical Associating Fluid Theory
Si	Stream of the dehydration process, where i stands for 1-12
SG	Stripping Gas
SNG	Synthetic natural gas
SPRT	Standard platinum resistance thermometer
SRK	Soave-Redlich-Kwong EoS
SW	Span-Wagner EoS for CO_2
TCD	Thermal conductivity detector in GC
TeEG	Tetraethylene glycol
TEG	Triethylene glycol
TST	Twu – Sim – Tassone EoS
TST/NRTL	EoS/A^E mixing rule combining the TST EoS with NRTL activity coefficient model
UMR-PRU	Universal Mixing Rule combined with PR and UNIFAC
UNIFAC	UNIQUAC Functional-Group Activity Coefficients
Unisim	Honeywell UniSim©
vdW1f	van der Waals one fluid mixing rules
VLE	Vapor – liquid equilibrium
VLLE	Vapor – liquid – liquid equilibrium
VOCs	Volatile Organic Compounds
VP	Vacuum pump
VS	Vapor sampler
W	water
WS	Wong – Saddler mixing rule

Chapter 1: Scope

This Chapter states the scope of this thesis and it briefly describes the context per Chapter so that the reader can have an overview of the work presented.

One of the most challenging issues of the 21st century is the increased emissions of CO_2 due to anthropogenic activities that lead to greenhouse effect and severe climate change. Consequently, there is an increasing demand for alternative fuels such as renewable energy sources, but still fossil fuels play a significant role in the energy mix. Among the fossil fuels, natural gas is considered more environmentally friendly since it is a low-emission fuel, as compared to other fossil fuels such as coal and oil, and it does not contain other heavy oil derivatives, such as mercaptanes, which can cause severe problems to environment and human life.

Natural gas (NG) consists mostly of light hydrocarbons, but it contains also some impurities. Among them, water is considered a significant one, since it is highly immiscible with hydrocarbons and given the appropriate conditions it can lead to the formation of a separate, aqueous, phase. This can cause slug flow e.g. in transportation pipelines which are designed for single – phase flow. Additionally, at low temperature and high pressure conditions the presence of water in adequate quantity along with that of small molecules, as is methane or CO_2, can lead to the formation of gas hydrates which can cause operational problems or plug the pipeline. To prevent hydrate formation polar chemicals, such as alcohols or glycols, are added to the gas flow. Also, to ensure process and product quality the water content is controlled and kept under specified limits. Usually, offshore, this is handled by physical absorption of water in a glycol desiccant. Furthermore, to meet the demand the oil and gas industry invests in new types of reservoirs which operate at demanding conditions and most times the assistance of several chemicals, which are or contain high amounts of polar molecules, is needed.

For the design and optimum operation of natural gas facilities, an adequate thermodynamic framework is therefore necessary. Molecules such as water which form hydrogen bonds, exhibit strong attractive interactions which have significant effect on the mixture properties. Such interactions are difficult to be described with the simple semi-empirical equations of state which are commonly used by the oil and gas industry for the monitoring of the processes, while they are difficult to predict even with more sophisticated models based on molecular simulation. The demand of accurate knowledge of the components distribution, to comply with the environmental legislation, as well as the need for process optimization gives birth to the seeking of new, more accurate thermodynamic models for the description of natural gas mixtures with associating compounds. The purpose of the thesis is three – fold. First, is to evaluate the applicability of the existent thermodynamic models, classic and more advanced, in handling of complex mixtures of natural gas with associating molecules. Second and uttermost aim of this dissertation is the development of a group – contribution equation of state, which can improve the existent ones, so that it can accurately describe the phase equilibria of hydrogen bonding compounds. The advantage of the proposed model compared to those already existing in literature for the accurate description of polar and associating mixtures is the use of the group – contribution approach. This way it is possible to predict the phase equilibria of several mixtures, by fitting interaction parameters only in a limited database of experimental

data. To validate the models accurate experimental data are required. Therefore, the third purpose of this thesis is to perform new experimental measurements for systems of interest to the oil and gas industry, where the literature data are scarce or not available, in order to extend the applicability of the models in a wider temperature range.

The structure of the thesis is as follows.

The first part of the dissertation is an introductory one. It consists of a brief description of the global energy mix as it is shaped the latest years along with the basic characteristics of natural gas (Chapter 2). The impurities of interest are presented along with the processes used for their handling. The basic terminology which is used in the dissertation is also given there. The second part of the introduction (Chapter 3) focuses on the intermolecular forces encountered in the physical systems, with special emphasis given in the hydrogen bonding interactions. Then, Chapter 4 deals with the fundamental theoretical background of phase equilibrium calculations, while the existent in literature thermodynamic models, along with the parametrization used in this work are presented in Chapter 5.

Following the theoretical discussion, Chapter 6 consists the experimental section of this dissertation that is the vapor – liquid equilibrium measurements of the CO_2/ methane mixture at three isotherms. The obtained data are validated against literature values as well as with the predictions of a state – of – the – art model for natural gas mixtures. Then, the measured data are used to fit the interaction parameters of several thermodynamic models, from simple ones that is cubic equations of state, to sophisticated models involving advanced mixing rules (UMR-PRU) and based on the statistical association fluid theory (SAFT).

In Chapter 7 the UMR-PRU thermodynamic model which has been developed in the Thermodynamics and Transport Phenomena Laboratory of National Technical University of Athens and combines the Peng – Robinson equation of state with the UNIFAC activity coefficient model is extended in the modelling of natural gas components with associating compounds. The parametrization of the model is based solely on binary phase equilibrium data and its predictive performance is evaluated in multicomponent mixtures comprising natural gas components, water and alcohols or glycols. The model is compared with another model which belongs to the same class, TST/NRTL, which is proposed by one of the most popular commercial process simulators for use in the simulation of natural gas dehydration process with glycols. Then, in Chapter 8, such a process is simulated. Actually, water absorption in triethylene glycol is considered and the predictions of UMR-PRU are evaluated against those of TST/NRTL. Furthermore, a sensitivity analysis of the operating parameters of the process is realized, which finally leads to the minimization of operating cost. The latter is based on a preliminary economic evaluation.

The good performance of models belonging to the EoS/G^E class, such as UMR-PRU and TST/NRTL, generates the following question, "*Is it really necessary to use complex*

theories based on statistical mechanics to directly calculate the hydrogen bonding interactions, or simpler models that are easier to apply are adequate for the modelling of natural gas mixtures with polar compounds?" Chapter 9 deals with this question by the investigation of the effect of advanced mixing rules and the direct incorporation of the associating term deriving from Wertheim's first order perturbation theory. To that end, two ternary mixtures comprising of methane, which is the main natural gas component, water and a hydrate inhibitor are thoroughly studied with different versions of the Peng – Robinson equation of state. To fairly examine the performance of the models, a specific database of binary mixtures is used for fitting the parameters of the models, and then their performance is examined in the prediction of multicomponent mixtures containing natural gas components, water and methanol or MEG. Based on the results of this analysis, a new group – contribution model which combines the advantages of the application of advanced mixing rules and the associating term is suggested for the accurate modelling of natural gas components with associating mixtures (Chapter 10). The performance of the proposed model is evaluated by comparing the obtained results in the phase equilibria of ternary mixtures with the results of models already existing in literature. Then, its database of group – interaction parameters is extended to handling components of interest to natural gas industry and is then evaluated in the prediction of phase equilibria of multicomponent mixtures.

Finally, the thesis closes with a brief presentation of the main conclusions. Suggestions that can be future challenges for further study are also discussed (Chapter 11).

Chapter 2: Elements of NG processing

The main focus of this chapter is the introduction to the nature and processing of natural gas. For this reason, typical properties and composition of natural gas coming from the reservoir are discussed, as well as problems encountered due to the presence of water. Naturally, the techniques used to prevent hydrate formation or water removal, especially involving alcohols or glycols, are also discussed.

2.1. Overview of the world energy consumption

Introduction of fossil fuels, such as oil and gas, in the energy mix has been the revolution in the energy sector especially at the second half of the twentieth century. The depletion of easily – recoverable oil fields as well as the rising concern for the environment and therefore the enforcement of more environmentally friendly policies leads to a change in the energy mix with the introduction of renewable energy sources, especially after 2010. Furthermore, the increasing development of Asian or African economies, such as India or China, leads to an increasing global energy demand. In Europe, on the other hand, between 2005 and 2014, primary energy consumption decreased by 12 %, due to energy efficiency improvements, the economic recession and fear of climate warming. Figure 2.1*a* shows the primary energy consumption in European Union (EU), as it is provided by the Statistical Office of the European Union (Eurostat)[1]. It is worthy to note that despite the EU target for decreasing use of non-renewable energy sources, fossil fuels continue to dominate as primary energy source. Yet, as a proportion of the total primary energy consumption, they fell from 77.8 % in 2005 to 71.6 % in 2014. On the same time, the proportion of renewable energy sources has been almost doubled over the same period, from 7.1 % in 2005 to 13.4 % in 2014, at an average annual increase rate of about 5.8 % between 2005 and 2014.[1, 2]

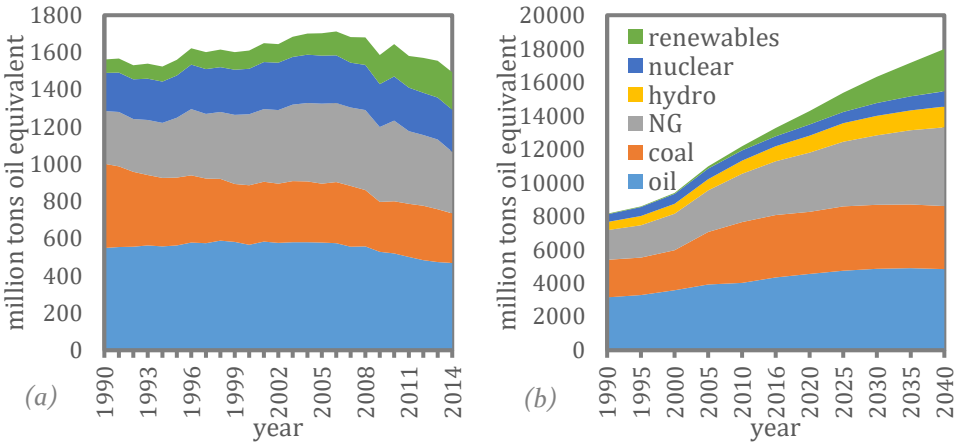

Figure 2.1: Total energy consumption by fuel type. (a) in EU for 1990-2014[1], (b) worldwide; from 1990 projection to 2040.[3]

According to British Petroleum (BP) statistical review of world energy[2], the natural gas consumption worldwide grew by 1.5 % in 2016 while the projections of natural gas consumption are increasing (Figure 2.1*b*). This increasing trend of natural gas portion is due to the fact that it is the cleanest of the fossil fuels, producing only water and carbon dioxide after combustion[4]. At the same time, the advances in technology and crude oil prices made economically feasible the drilling of more unconventional natural gas sources, such as deep – water reservoirs or shale gas, increasing, thus, the proved natural gas reserves.

2.2. A brief history of Natural Gas

The nature of natural gas makes it difficult to handle. As a result, although natural gas sources have been discovered since ancestry, its use has not been widespread until the late 1930s. The first mention of the use of natural gas is at about 940 B.C. in China. The gas piped through hollow bamboo poles has been used to boil ocean water and collect salt. In other civilizations, temples have been built to honor the "*eternal fire*" occurring when natural gas escaped from the ground. In the early 1800s, manufactured gas produced from coal replaced the scarce and expensive whale oil used for lightning purposes, transforming, thus, the way of living. The invention of electrical bulb by Thomas Edison made its use obsolete but the foundations for the use of natural gas had already been established.

During drilling for water or brine natural gas has been produced accidentally, but it was regarded as nuisance and only small attempts had been made to use it. It was only in 1821 when William Hart drilled the first US natural gas well. The produced gas was transported to nearby residences via wooden pipes. In the following years, a few other wells had been drilled, but soon were disregarded due to the discovery of oil. The reason was the much easier transportation of oil in barrels compared to the handling of natural gas. Gas fields discovered at that time had been uncontrolled and were allowed to leak or were burned out. Gradually, the increase in the amounts of discovered gases and the improvements in pipeline technology set the basis for the industry to begin to grow. The introduction of seamless steel pipe in 1920 made possible the long – range transportation of natural gas. Its strength allowed the use of higher pressure and consequently higher quantities, increasing thus the profit margin. The long – distance transmission of gas, lowered its cost and made it more competitive with other fuels leading to its gradual introduction to the energy mix.[4]

2.3. Natural gas value chain

The natural gas value chain includes a variety of facilities and systems from exploration and production, to the final consumer and it basically consists of three parts; upstream, midstream and downstream. Exploration involves all the activities, such as seismic tests, drilling tests etc. which take place before the construction of an oil or gas production field. Upstream production usually refers to the facilities and processes required for production and stabilization of oil and gas. Midstream refers to gas treatment, liquefied natural gas (LNG) production & regasification plants and pipeline systems. The tip of the midstream affinities is the refining sector, where the major processing occurs. At the onshore refinery, oil and condensates are fractionized to marketable products following the required specifications. Furthermore, the produced gas is processed to meet the downstream, sales gas and pipeline specifications. Finally, downstream includes the final products and their transportation to the final consumer.[5] A simplified scheme of a typical natural gas value chain is depicted in Figure 2.2.

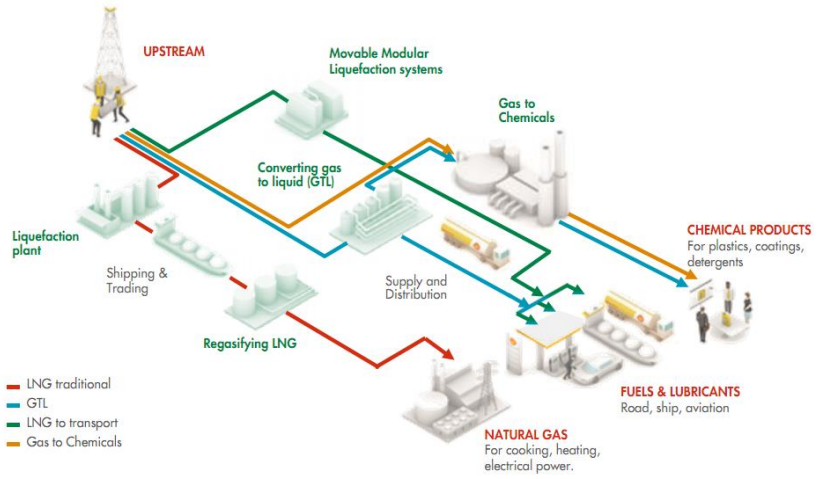

Figure 2.2: Natural gas value chain[6]

Natural gas has several uses nowadays but the foremost one, due to its simplicity and efficiency, is as a fuel. Due to its lower calorific value compared to other fossil fuels, it is usually intended for heating purposes. The end users can be divided in three main sectors, residential, commercial and industrial while the later years significant increase has been noted in the transportation and electrical power generation. According to the statistics provided by the international energy agency[7] the use of gas by sector is generally stable since 1995. It is interesting to note that at the same time, the use of natural gas for electric power generation showed significant increase. Figure 2.3 presents the natural gas consumption by sector in US for 2011.

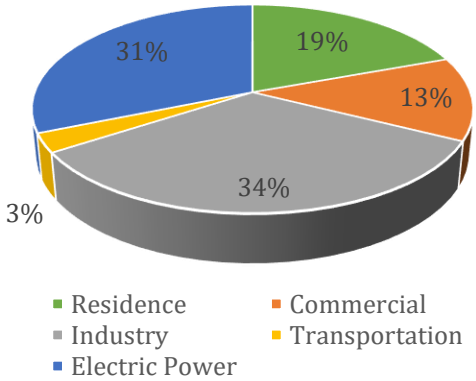

Figure 2.3: Natural gas use by sector in the USA for the year 2011.[7]

Note that apart from the industrial use, where a significant part contributes to heating purposes, a significant percentage (31 %) is attributed to power generation. Of course,

residential use maintains a significant portion of the pie, with 19 % of the total gas consumption. Finally, although the use of natural gas as a fuel is more convenient, in the prospect of a "*cleaner energy*", the use of natural gas as raw material for the production of more complex and additive value products shows an increasing trend and it is expected to gain a higher part of the share of natural gas uses in the near future.

2.4. Natural Gas Components and Important Impurities

As the natural gas is a product of a series of reactions which depend on the raw materials, the depth and the conditions of the reservoir, its composition differs substantially from field to field. Some difference in the composition is also expected depending on its characterization as an associated gas field or an independent natural gas reservoir. In a typical natural gas reservoir the main component is methane, while other gases and heavier hydrocarbons are always present. Apart from the hydrocarbon components, there usually exist non-hydrocarbon gases and water. Their composition can vary from a few ppm up to 60 or 70 % of the composition. Such a case is for example the Natuna gas field in Indonesia. Table 2.1 presents some typical gas compositions of fields worldwide, where the diversity of the compositions is apparent.

Table 2.1: Typical natural gas compositions (% molar)[8]

	Alberta (Canada)	Western Colorado	Southwest Kansas	Bach Ho Field[a] (Vietnam)	Miskar Field (Tunisia)	Rio Arriba County (New Mexico)	Cliffside Hill, Amarillo (Texas)
He	0	0	0.45	0	0	0	1.8
N_2	3.2	26.1	14.65	0.21	16.903	0.68	25.6
CO_2	1.7	42.66	0	0.06	13.588	0.82	0
H_2S	3.3	0	0	0	0.092	0	0
CH_4	77.1	29.98	72.89	70.85	63.901	96.91	65.8
C2	6.6	0.55	6.27	13.41	3.349	1.33	3.8
C3	3.1	0.28	3.74	7.5	0.960	0.19	1.7
C4	2	0.21	1.38	4.02	0.544	0.05	0.8
C5+	3	0.25	0.62	2.64	0.630	0.02	0.5

[a] The % mol data are in a wet basis (1.3 % molar water)

The diversity either in methane composition, heavier ends or impurities is apparent. Some reservoirs that contain much amount of heavier components are characterized as condensate reservoirs. Apart from the above, the gas may include trace pollutants, such as mercury and chlorides, while apart from hydrogen sulfide, some mercaptans, such as methanethiol or ethanethiol can be also present.[9] Water is the most common impurity in natural gas, usually in the range of 8000 - 10000 ppmv and it is almost always present at wellhead conditions.[8, 9]

Depending on the content of these compounds, the natural gas can be characterized in several ways. The most common terms encountered in the natural gas industry and which will be used in the next chapters are the following:

- *Wet gas* is the natural gas saturated with water, as it comes out of the wellhead.
- *Dry gas* is raw or treated gas which has been dehydrated up to the specification of the pipeline. For midstream pipeline transportation in North Europe, this is about 30 ppm molar.
- *Acid gas* is a gas which contains high quantity of acidic gases, such as carbon dioxide or hydrogen sulfide. The pipeline specification is typically less than 2 % molar.
- *Condensates* are a mixture of hydrocarbons, usually of higher molecular weight, and other natural gas components. Because of the higher quantity of heavier components, they exist in gaseous form in the well, but they condense as liquid during the production process, due to the more moderate temperature and pressure conditions.

Apart from the water that naturally coexists in the reservoir, alternative sources of water can be several processes in the gas chain which use it as a solvent. A typical such example is the natural gas sweetening, where a mixture of amines and water is used to remove carbon dioxide and hydrogen sulfide to the specified concentration.

2.5. Pipeline specifications

The natural gas specifications are a product of mutual agreement between the producer and the pipeline companies, or the final purchaser. They can also depend on the geographical altitude, e.g. different specifications of water content are required in Northern and Southern Europe. Usually, the following specifications are taken under consideration:

- minimum, maximum and nominal delivery pressure
- water dew point or water content
- maximum condensable hydrocarbon content, or hydrocarbon dew point
- minimum heating value
- contaminants
- maximum delivery temperature.

The above specifications determine the required processes, as well as the operating conditions.[10] To meet the pipeline specifications, several procedures much precede midstream or downstream transportation. Offshore, such procedures are the minimum necessary to satisfy secure transportation and involve sweetening, mercury removal, natural gas liquids (NGL) recovery, hydrocarbon dew point control and dehydration.

Before the further discussion of the processes, is deemed necessary to define the terminology related with gas processing. Due to the nature of the specific thesis which

has an interest in associating compounds, emphasis is given in the water – related processes.

- *Phase envelope* for the two-phase region is the boundary of the region where vapor and liquid coexist in equilibrium. Outside this envelope, the fluid exists in single phase (vapor, liquid or dense fluid).
- *HC dew point* is the temperature, in a specified pressure, where the first drop of liquid condenses, for a gas of specific composition under cooling.
- *water dew point* is the temperature, at a specified pressure, where the first drop of water spontaneously condenses, for a wet gas of specific composition and water content under cooling.
- *aqueous dew point* is the highest temperature at a specified pressure where a solution of water and trace chemicals (e.g. methanol, ethylene glycol (MEG) etc.) can spontaneously condense from the natural gas.
- *frost point* is the highest temperature, at a specified pressure, where ice can spontaneously precipitate from natural gas.
- *hydrate point temperature* is the highest temperature, at a specified pressure, where natural gas hydrate can spontaneously form in a gas mixture.[11]

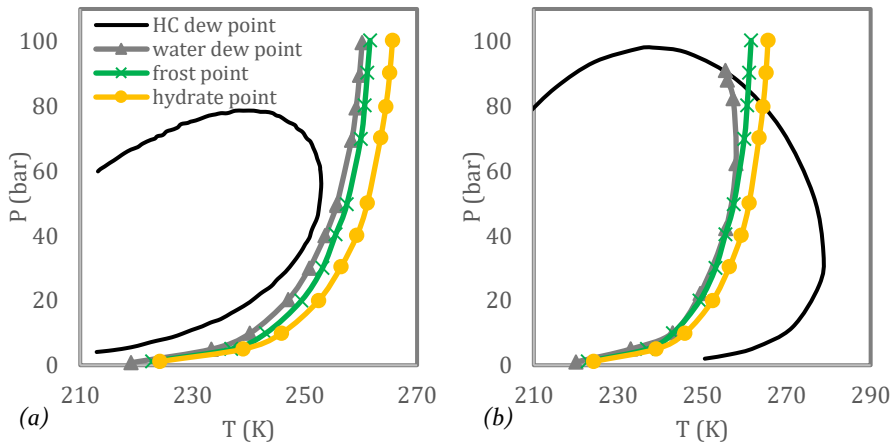

Figure 2.4: Phase behavior of natural gas with traces (40 ppm) of water. Composition (% molar) on dry basis (a). 85 C1, 10 C2, 4 C3, 0.5 iC4, 0.5 nC4 and (b) 7 N_2, 0.5 CO_2, 88 C1, 3 C2, 0.9 C3, 0.2 iC4, 0.3 nC4, 0.09 iC5, 0.09 nC5, 0.12 nC6, 0.03 nC7 and 0.02 nC8.

Figure 2.4 presents a typical phase behavior of a natural gas, where the different predicted values of some points of interest as determined above are given. Specifically, the black line illustrates the hydrocarbon dew point curve, grey line is the water dew point curve, the green line presents the frost points, where water in the form of ice may precipitate and the yellow line is the hydrate point line. Two different compositions in dry basis have been considered, namely a lighter (Figure 2.4*a*) and a heavier one (Figure 2.4*b*). It is shown that in the case of the lighter gas, hydrates, water or ice may precipitate before the hydrocarbons. Instead, for the heavier one, hydrocarbons are the first to condense. Yet, if the temperature and pressure conditions are appropriate, instead of hydrocarbons, hydrate or water may start to precipitate.

For that reason, water and its derivatives, must be monitored and controlled during all stages of the natural gas value chain.

2.6. Problems encountered due to the presence of water

The principal reasons for water treatment or water removal from the natural gas is the operational or process problems encountered due to the presence of water. In low temperature and high pressure conditions, such as those that occur on subsea transportation pipelines hydrates may form causing flow disruption or even pipeline blockage. Hydrates are stable structures caused by van der Waals forces, created between water, which acts like a host molecule and a small molecule, such as CO_2 or methane, which is encapsulated in the water lattice. The hydrate crystals have complex, three-dimensional structures in which the water molecules form a cage, where the guest molecules are entrapped.[12] The type of gas hydrate depends on the entrapped molecule, while the most common types encountered in the NG processing are presented in Figure 2.5.

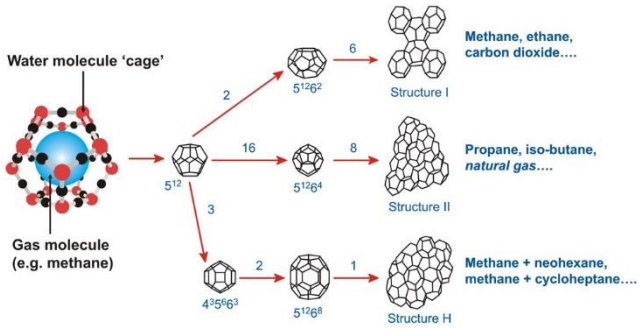

Figure 2.5: Gas hydrate structures. Image taken from the Institute of Petroleum Engineering.[13]

Apart from the plugging problems encountered in the case of hydrate formation, if sufficient water exists in natural gas, at appropriate temperature and pressure conditions, it may condense, forming a free-water phase. Usually, the long-distance high – pressure midstream pipelines are designed to operate at one-phase flow. The presence of the free-water phase disrupts the normal operation of the pipeline causing plugging problems. Additionally, it can lead to corrosive conditions, especially in the case of acid gases. That is because hydrogen sulfide and CO_2, in lesser grade, act like weak acids, reacting with water. Furthermore, the presence of water vapor in natural gas increases its volume while it decreases the heating value of the gas. The first leads to reduced gas capacity of the pipeline, while the latter can cause the final product to be outside of the required specifications.[14]

2.7. Natural gas moisture control techniques

2.7.1. Inhibitor injection

As it has been mentioned in the previous sections, water is omnipresent from the early stages of natural gas production. Depending on the process, or the affinity of the stage, such as upstream, midstream or downstream, different solutions of water treatment are selected. In the current section, the most commonly industrially used methods for water control are presented. Emphasis is given in the methods which use a polar component such as alcohol or glycol to achieve the water content control due to their relativity with the current thesis. Instead, methods such as adsorption on solids, are only briefly referenced. In general, there are two different ways to prevent the negative effects of the presence of water in the natural gas. In the first case, which is usually applied in upstream processes, some hydrate inhibitor, such as methanol or MEG, is introduced in the pipeline, in order to affect the hydrate formation temperature. Polar solvents, such as alcohols, glycols and ionic salts are known to inhibit the formation of gas hydrates. The inhibition mechanism is based on the reduction of the temperature or the increase of pressure at which a hydrate will form, shifting thus its phase equilibrium. For that reason, this type of hydrate inhibitors are called *thermodynamic*. To obtain this effect, the inhibitor must be present in some minimum concentration. For example, for the pipeline considered in Figure 2.6 the minimum concentration of methanol required to avoid hydrate formation is about 30 %.

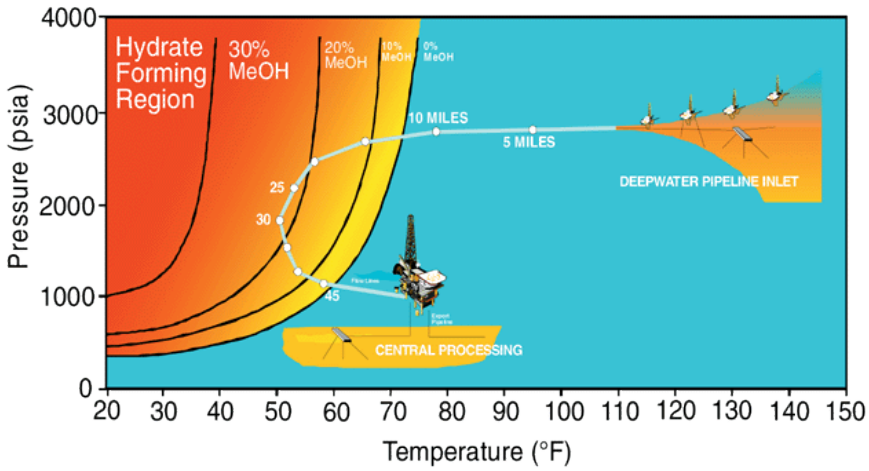

Figure 2.6: A composite diagram showing the phase boundary of methane hydrate formation as a function of temperature and pressure. The black lines show the phase boundary line shifting to the left on the addition of increasing methanol concentration. On the right: the blue region is that where hydrate crystals are not formed and superimposed over this is a pipeline of about 45 miles in length containing natural gas.[15]

Generally, salts are the most effective as hydrate inhibitors. They require significantly lower concentration, to prevent the hydrate formation. For example, to obtain the

same effect on hydrate inhibition, a solution 5 % in salt is required, compared to a 20 % solution of methanol.[16] Similarly, methanol performs better compared to glycols. Their inhibiting effect reduces with the increase in molecular weight (MEG>DEG>TEG> TeEG). Despite the better inhibiting effects of methanol, the latest years its use is depleted and it is replaced usually by MEG. This occurs due to the significantly lower vapor pressure of glycols compared to that of methanol, which leads in lower solvent loss. Furthermore, methanol is highly soluble in water and eventually the methanol lost in the hydrocarbon streams ends up in the sea, leading to increased environmental concerns.[12]

2.7.2. MEG loop

In condensate reservoirs, MEG is usually injected in the wellhead to prevent hydrate formation and enhance flow assurance by removing the salts. A closed loop procedure which involves MEG injection in the wellhead and then treatment of the generated MEG/water and salt mixture occurs. The procedure is referred as MEG loop and it involves a pre-treatment where the rich MEG containing some gas and hydrocarbon liquids passes through a three-phase flash separator. There, the gas is flashed and the recovered liquids are send to separator, while the rich MEG stream is routed to a flash separator under vacuum conditions. The MEG and water contents of the stream are flashed out from the top of separator where they are sent to the MEG vacuum distillation column for further separation. The salt components of the stream precipitate in the separator. The salt-free lean MEG is pumped to storage for reuse, while the water is condensed and collected in the flash drum. The salt crystals precipitated at the separator, are separated by gravity and transferred to the salt tank, where they are concentrated before their removal at a hydrocyclone.[17] A typical MEG loop is depicted on Figure 2.7.

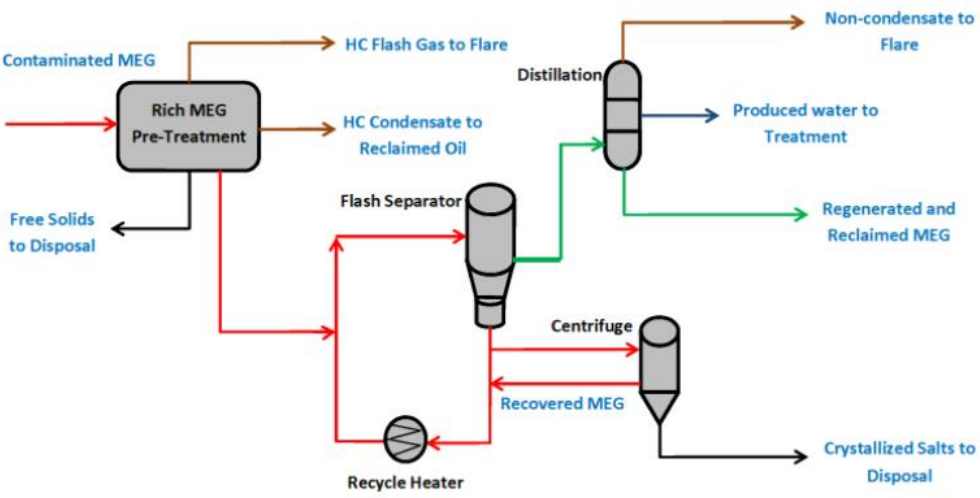

Figure 2.7: Full reclamation scheme that removes all the salts to prevent scaling in the pipelines[18]

2.7.3. Natural Gas dehydration

2.7.3.a. *Absorption in a glycol desiccant*

The typical procedure to meet the pipeline specification for midstream transportation is the dehydration by absorption, using some glycol desiccant. In this process, the wet gas is contacted with a lean solvent, usually triethylene glycol (TEG), producing a rich solvent stream and a dry gas. The criteria for the selection of the appropriate desiccant are the following:

- The solvent must have a strong affinity for water.
- The hydrocarbon components of natural gas should have a low solubility in the solvent to minimize hydrocarbon loss.
- The desiccant should be easily separated from water, usually by heat application, in order to be regenerated in high concentration.
- It should have a low vapor pressure, to avoid natural gas contamination with the solvent, as well as solvent loss.
- It should exhibit thermal stability, particularly in the high temperatures encountered in the regenerator.
- It should not solidify in the temperature range of dehydration and it should have a proper viscosity to enable unhindered flow.
- The liquids must be non-corrosive and non-reactive with the natural gas components.[12]

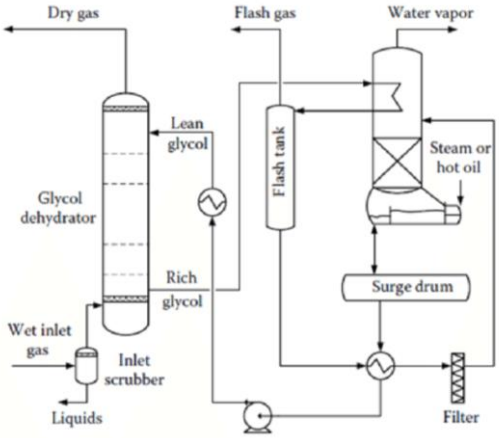

Figure 2.8: Simplified flowchart of a glycol dehydration plant[19]

Most glycols meet the abovementioned criteria, such as diethylene glycol (DEG), triethylene glycol (TEG) and tetraethylene glycol (TeEG), due to their low vapor pressure and higher boiling point compared to that of water. They are also highly hygroscopic and they do not form precipitates with gas constituents. Furthermore, they are essentially non-soluble in liquid hydrocarbons and are relatively stable in the presence of hydrogen sulfide and carbon dioxide. Despite this fact, in most applications TEG is used since it yields the most convenient results in terms of a

technoeconomic approach. DEG is usually cheaper and for this reason it is preferred in some units. However, after its initial installation, there is no any further significant gain. Instead, compared to TEG, DEG has a higher carry-over, offers lower water dewpoint depression and its regeneration to high concentrations is more difficult. TeEG on the other hand is more viscous and expensive, but it offers significantly lower vapor pressure which minimize the glycol loss. Its use is justified in cases where the wet gas temperature exceeds 323 K.[20]

Basically, the glycol dehydration process follows two steps, as shown in Figure 2.8. In the first, the water is absorbed from the gas, usually in a structured packing column (Contactor), at relatively low temperature and high – pressure conditions. Then, the rich glycol obtained at the bottom of the Contactor is regenerated in a still column and is then routed back to the contactor to absorb the water, in a closed loop process. The process is discussed in detail in Chapter 8, so no further description is given here.

2.7.3.b. *Dehydration by adsorption*

In onshore processing, where lower water content is required, less than 1 ppm, the absorption process is not adequate to achieve this level of dehydration and some physical adsorption process is usually preferred. In this process, the water vapor in the gas adheres to the solid surface of a solid due to surface forces. This requires the use of a material with the following properties:

- it should have large surface area to ensure high capacity
- it should have high affinity for water
- its mass transfer rate should be high
- it should be easily and economically regenerated
- it should have good activity retention with time
- it should have small resistance to gas flow
- it should have high mechanical strength to resist crushing and dust formation
- it should be fairly cheap, non-corrosive, non-toxic, chemically inert and it should possess a high bulk density
- it should show no considerable volume change during adsorption and desorption and it should retain its strength during its *wet* state.

The commercial adsorbents have a total surface area of 500 - 800 $m^2 \cdot g^{-1}$, which is achieved by producing a material with large interior surface resulting from capillaries or a crystalline–type lattice, while their exterior surface is almost negligible. The materials which meet the above criteria and are used for dehydration can be categorized in four groups.

- Bauxite, which is a naturally occurring mineral composed primarily of Al_2O_3.
- Alumina, a manufactured version of bauxite.
- Gels, which are manufactured by chemical reaction and they are composed largely of SiO_2 or alumina gel.
- Molecular sieves, which are calcium – sodium alumino – silicates (zeolites).

Molecular sieves, are the most expensive of the above – listed materials, but they possess desirable characteristics, most important of which is their capacity, that justify the extra cost.[20] In order to reduce the size of the molecular sieve unit, a glycol dehydration unit can be used to obtain a first level of dehydration and then the adsorption process is used for further decreasing the water content.[12] Yet, if this procedure is used, the gas can be contaminated by traces of glycol, which does not occur in the case of dehydration by adsorption.[11]

In the molecular sieve process, the wet gas enters a bed of adsorbent material where the water adsorbs onto it, producing dry gas. The process is a batched one; once the bed is saturated with water, it must be regenerated by heating. A hot steam passes through the bed to strip the water, regenerating thus the bed. Therefore, at least two beds are required, as it is presented in a simplified flowchart in Figure 2.9.

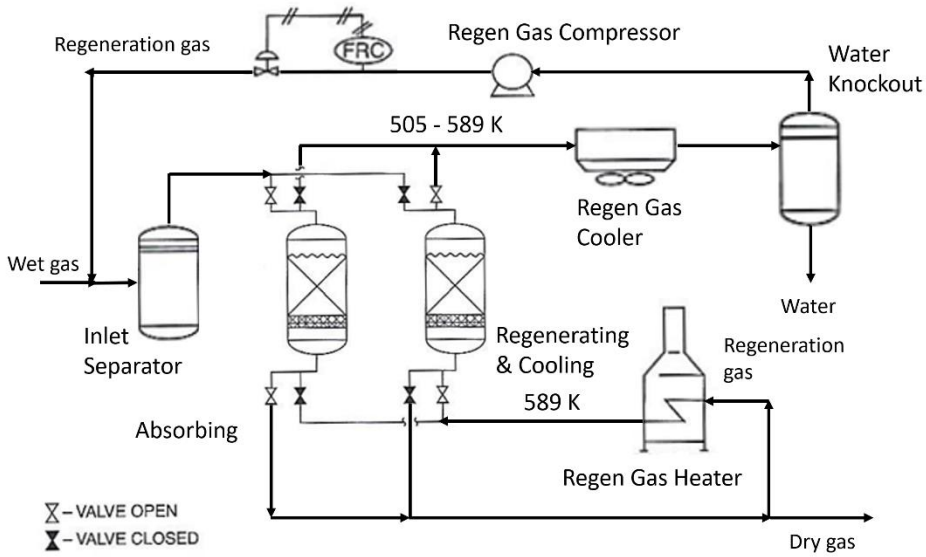

Figure 2.9: Simplified flow diagram of dehydration unit by adsorption.[20]

2.7.3.c. *Dehydration by refrigeration*

Another method used for dehydration is refrigeration, which occurs due to the different solubility of the water in gas at lower temperature. The usual purpose of the refrigeration plant is to remove heavy hydrocarbons from the stream, in order to meet the hydrocarbon dew point specification. In order to prevent the formation of ice or hydrates, the cold gas is mixed with a polar solvent, usually MEG, because it has better low-temperature properties compared to other glycols. A typical refrigeration process can reduce the water content of a gas stream to 1 lb/MMcf.

A simplified flow chart of the refrigeration process is given in Figure 2.10. The gas enters a gas/gas heat exchanger where it is precooled, while further cooling is achieved through refrigeration. The gas enters the reboiler (*chiller*) of a refrigeration unit, where

the refrigerant is boiled and the process steam is cooled. In order to prevent freezing and to pick up condensing water, a glycol is sprayed in both the gas/gas heat exchanger and the chiller. The mixture enters a low temperature three – phase separator, where the gas comes out off the top, the liquid hydrocarbon from the middle and a mixture of glycol and water from the bottom. The hydrocarbon liquids are sent for further treatment, while the glycol/water mixture is sent to a still column, to regenerate the glycol in order to be reused. The sales gas outing the top of the three – phase separator has very low temperature and therefore it is routed to the gas/gas heat exchanger to precool the feed.

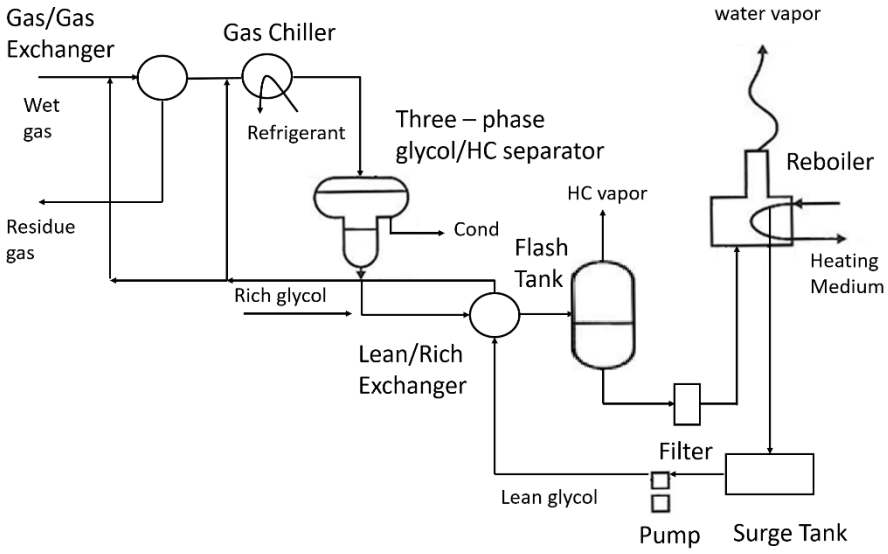

Figure 2.10: Typical flowchart of a refrigeration process.

2.7.3.d. *Novel approaches*

Apart from the conventional dehydration methods, as those discussed in the above, new techniques have been developed in the latest years following other approaches. These include the use of membranes[21, 22] or ionic liquids for hydrate inhibition[23, 24].

References

(1) Barbu A.-D., *Primary energy consumption by fuel*; European Environmental Agency: Copenhagen, 2017.
(2) Dudley B., BP statistical review of world energy. 2016. In 66 ed.; BP Global: 2017.
(3) https://www.statista.com/statistics/222066/projected-global-energy-consumption-by-source/, accessed on 17/05/2018.
(4) Busby R.L., *Natural gas in nontechnical language*. PennWell: Institute of Gas Technology, 1999.
(5) Devold H., Oil and Gas Production Handbook An Introduction to Oil and Gas Production, Transport, Refining and Petrochemical Industry. *ABB, 3rd* **2013**.
(6) natural gas value chain, http://members.igu.org/old/about-igu/images/shell_gas_integrated_value_chain.png, accessed on 21/05/2018.
(7) US energy information administration, https://www.eia.gov/energyexplained/index.php?page=natural_gas_use, accessed on 23/05/2018.
(8) Kidnay A.J., Parrish W.R., *Fundamentals of natural gas processing*. CRC Press, Taylor and Francis: Colombus, Ohaio, 2006.
(9) Devold H., Oil and gas production handbook. *ABB ATPA Oil and Gas* **2006**.
(10) Lyons W.C., *Standard handbook of petroleum & natural gas engineering*. Gulf Professional Publishing: 1996, *Vol. 1*.
(11) Løkken T.V., Bersås A., Christensen K.O., Nygaard C.F.,Solbraa E., In *Water content of high pressure natural gas: data, prediction and experience from field*, presented on IGRC (International Gas Union Research Conference), **2008**
(12) Carroll J., *Natural Gas Hydrates: A Guide for Engineers*. Gulf Professional Publishing, Elsevier: USA, 2003.
(13) What are gas hydrates?, http://www.pet.hw.ac.uk/research/hydrate/hydrates_what.cfm, accessed on 31/05/2018.
(14) Ikoku C.U., *Natural gas production engineering*. Wiley: 1984.
(15) Koh C.A., Towards a fundamental understanding of natural gas hydrates. *Chemical Society Reviews* **2002,** *31*, (3), 157-167.
(16) Haghighi H. Phase equilibria modelling of petroleum reservoir fluids containing water, Hydrate Inhibitors and Electrolyte Solutions. Heriot-Watt University, *2009*.
(17) AlHarooni K., Gubner R., Iglauer S., Pack D., Barifcani A., Influence of Regenerated Monoethylene Glycol on Natural Gas Hydrate Formation. *Energy & Fuels* **2017,** *31*, (11), 12914-12931.
(18) Lehmann M., Bowman C., Mok W., Nguyen H., Salasi M., Lamm A., Gubner R., *Corrosion Inhibitor and Oxygen Scavenger for use as MEG Additives in the Inhibition of Wet Gas Pipelines*. 2014, *Vol. 4*.
(19) Mezni M., *LPG Recovery Unit Optimization*. 2015.
(20) Campbell J.M., Maddox R.N., *Gas conditioning and processing*. Campbell Petroleum Series: 1970, *Vol. 2*.
(21) Karimi A., Abdi M.A., Selective dehydration of high-pressure natural gas using supersonic nozzles. *Chemical Engineering and Processing: Process Intensification* **2009,** *48*, (1), 560-568.
(22) Netusil M., Ditl P., Comparison of three methods for natural gas dehydration. *Journal of Natural Gas Chemistry* **2011,** *20*, (5), 471-476.

(23) Tariq M., Rooney D., Othman E., Aparicio S., Atilhan M., Khraisheh M., Gas Hydrate Inhibition: A Review of the Role of Ionic Liquids. *Industrial & engineering chemistry research* **2014,** *53*, (46), 17855-17868.
(24) Yu G., Dai C., Wu L., Lei Z., Natural Gas Dehydration with Ionic Liquids. *Energy & Fuels* **2017,** *31*, (2), 1429-1439.

Chapter 3: Hydrogen bonding interactions

In the present chapter, the intermolecular forces are briefly described with emphasis given in the hydrogen bonding interactions. The understanding of the intermolecular forces leads to the development of adequate theories to describe the interactions and thus the properties of pure components or their mixtures. Since the current work deals with polar and associating components, the nature of the hydrogen bonds is theoretically stated, as well as the contradictory water nature.

3.1. Introduction

Intermolecular forces are present everywhere. When a molecule is in the proximity of another, forces of attraction and repulsion influence its behavior. If it was not for the attractive forces to hold the molecules together, there would be no solids and liquids; the kinetic energy of the molecules would spread them all over the available space and everything would be in the gaseous state. And if it were not for the repulsive forces, solids and liquids would not resist to compression. Actually, thermodynamic properties of any pure substance are determined by intermolecular forces between the molecules of the specific substance. When a mixture is considered, the intermolecular forces between the molecules of the same substance and those of the different substances in the mixture should be taken into consideration. To interpret the thermodynamic properties of mixtures, it is therefore necessary to have an understanding of the nature of the *intra-* and *inter-* molecular forces. The configurational properties of matter can be considered as a compromise between those forces that join molecules together and those which set them apart. Not all kind of properties depend to the same extend to the intermolecular forces. Some molecular properties, such as the specific heat of a gas at low pressure, depend only on the characteristics of the specific molecule. On the other hand, properties such as the enthalpy of vaporization of a liquid, are strongly affected by the intermolecular forces.[1]

Several considerations and classifications occur in the literature. In the current work, the classification of attractive forces proposed by Tassios[2] is followed; that is grouping the interactions to less intense, characterized as *physical*, and to stronger, classified as *chemical*. In the first category, belong actually the electrostatic forces between charged particles (ions) and permanent dipoles, quadrupoles or multipoles, as well as the induction forces between a permanent dipole and an induced dipole, and the dispersion forces between non-polar molecules. Instead, as chemical, are classified the specific forces leading to associating or solvating effects. As the name suggests, *quasi-*chemical forces are manifested as strong attractive interactions, in which participating species combine to form new chemical entities[3]. That is for example the formation of loose chemical bonds, hydrogen bonds or charge – transfer complexes.

Molecules have kinetic energy because of their velocities relative to some fixed reference state and potential energy due to their positions relative to one with another. If two simple, spherical symmetric molecules are considered, at a distance, r, then the potential energy, Γ, between them is a function of this distance. As such, the force, F, between the molecules is related to the potential energy by eq. 3.1.

$$F = -\frac{d\Gamma}{dr} \qquad \text{eq. 3.1}$$

The negative of the potential energy is the work required to separate two molecules from the intermolecular distance, r, to infinite separation. These forces are usually expressed in terms of potential energy functions. The common convention is that a force of attraction is negative and one of repulsion is positive.

Intermolecular forces of non-spherical molecules depend not only on the center – to – center distance, but also on the relative orientation of the molecules. The effect of the molecular shape is most significant at low temperatures and when the intermolecular distances are small, as in the condensed state. Such an example is the difference in the boiling points of isomeric alkanes which have the same carbon number; the branched one always has lower boiling point compared to the straight one. The same effect is observed in other chemical families as well. This is attributed to the fact that with branching, the shape of the molecule tends to reach that of a sphere, reducing, thus, its surface area. Therefore, the intermolecular attraction per pair of molecules becomes weaker and lower kinetic energy is sufficient. Similarly to the boiling point reduction, other thermodynamic properties are also affected by branching.[1]

3.2. Physical Interactions

Electrostatic forces are based on the Coulomb's law between two point electric charges of magnitudes q_i and q_j, at a distance r, as per eq. 3.2,

$$F = \frac{q_i q_j}{4\pi\varepsilon_0 r^2} \qquad \text{eq. 3.2}$$

where F, is the electrostatic force and $\varepsilon_0 = 8.85419 \cdot 10^{-12} C^2 \cdot J^{-1} \cdot m^{-1}$ the dielectric permittivity at vacuum.

Compared to other physical intermolecular energies, the magnitude of the electrostatic energy is relatively large, while it can be characterized as a long – ranged interaction. If electrostatic forces between ions are considered, those are inversely proportional to the square of the separation and therefore they have a much longer range. These forces make the dominant contribution to the configurational energy of salt crystals causing, thus, the very high melting points of salts. Apart from the forces between ions, electrostatic forces can also arise between particles which do not have a net electric charge. If a particle having two electric charges of the same magnitude, e, but opposite sign held at a distance, d, is considered, then it has a permanent dipole moment, μ, defined through eq. 3.3.

$$\mu = e \cdot d \qquad \text{eq. 3.3}$$

Asymmetric molecules possess permanent dipoles resulting from an uneven spatial distribution of electronic charges around the positively charged nuclei. Symmetric molecules, such as methane or CO_2, have zero dipole moment, while those which show little asymmetry have generally rather small dipole moments.[1] The common unit for the dipole moment is the Debye = 10^{-18} esu·cm. All asymmetric non-hydrocarbon molecules such as ketones, alcohols, ethers, etc. are dipoles since the centers of the positive and negative charges – because of their asymmetry – do not coincide. Such molecules are referred to as *polar,* while those that do not have a dipole moment, as *non-polar*. As it has been stated in the previous section, in terms of strength, the

electrostatic forces can be divided to physical, which are weaker and chemical ones. The most typical example of the latter are the hydrogen bonding interactions.[2]

3.2.1. Attractive forces

3.2.1.a. *Dipole – Dipole*

In an assembly of polar molecules, their relative orientations depend on the interplay of two factors; the presence of an electric field set up by the polar molecules which tends to line up the dipoles and the kinetic energy of the molecules which has the tension to toss them about in a random manner. Therefore, with the increase of temperature, the orientations become more random until the average potential energy due to polarity becomes very small, in the limit of very high temperature[1].

The potential energy of two permanent dipoles *i* and *j* is obtained by considering the coulombic forces between the four charges. The energy of interaction depends on the distance between the dipole centers and on the relative orientations of the dipoles, as shown schematically in Figure 3.1.

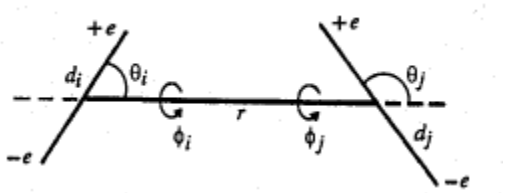

Figure 3.1: Orientation of two dipoles.[1]

If the distance between the dipoles, *r*, is large as compared to their respective diameters, d_i and d_j, the potential energy is calculated through, eq. 3.4,

$$\Gamma_{ij} = -\frac{\mu_i \mu_j}{4\pi\varepsilon_0 r^3}\left(2cos\theta_i cos\theta_j - sin\theta_i sin\theta_j cos(\varphi_i - \varphi_j)\right) \qquad \text{eq. 3.4}$$

where θ and φ are the angles of the dipole axis, as illustrated in Figure 3.1.

In addition to dipole moment, it is possible for molecules to have quadrupole moments due to the concentration of electric charge at four separate points in the molecule. This is depicted schematically in Figure 3.2.

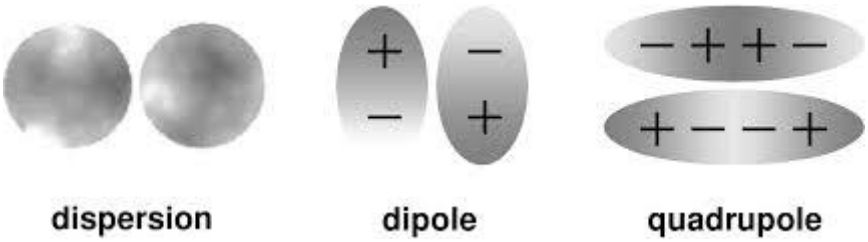

Figure 3.2: Difference between the different kinds of linear moments appearing at electric neutral molecules.

Carbon dioxide is a characteristic example of molecule which does not have a dipole moment, due to its symmetrical structure, but whose quadrupole moment is sufficiently strong to affect its thermodynamic properties. That way, the observed properties of CO_2 are substantially different from those of other non-polar molecules of similar size and molecular weight. For the simple case, where a linear molecule is considered, the quadrupole moment, Q, is defined by the summation of the second moment of charges as per eq. 3.5,

$$Q = \sum_i e_i d_i^2 \qquad \text{eq. 3.5}$$

where the charge e_i is located at a point distance d_i away from some arbitrary origin, where all charges are on the same straight line. Quadrupole moment is independent of the position of the origin provided that the molecule has no net charge and dipole moment. For non-linear quadrupoles or for molecules having permanent dipoles more complicated expressions are required[1].

3.2.1.b. *Induced dipoles*

A non-polar molecule, such as methane, has no permanent dipole moment. Yet, as it is subjected to an electric field, its electrons are displaced from their original position and an induced dipole is created. In fields of moderate strength the induced dipole moment, μ^i, is proportional to the field strength E as per eq. 3.6,

$$\mu^i = \alpha \cdot E \qquad \text{eq. 3.6}$$

where the proportionality factor, α, is a fundamental property of the substance, the *polarizability*. Polarizability, actually, expresses how easily the electrons of a molecule can be displaced by an electric field and can be calculated through the dielectric properties of the substance and from index of refraction data. For asymmetric molecules, it is not constant, but it is a function of the orientation of the molecule relative to the direction of the field.

When a non-polar molecule, *i*, is situated in an electric field set up by the presence of a polar molecule, *j*, the resulting force between the permanent dipole and the induced dipole is always attractive. The mean potential energy is given by eq. 3.7, as proposed by Debye.

$$\bar{\Gamma}_{ij} = -\frac{\alpha_i \mu_j^2}{(4\pi\varepsilon_0)^2 r^6} \qquad \text{eq. 3.7}$$

Polar as well as non-polar molecules can have induced dipoles in an electric field. The general Debye formula for the mean potential energy due to induction by permanent dipoles is given by eq. 3.8.

$$\bar{\Gamma}_{ij} = -\frac{(\alpha_i \mu_j^2 + \alpha_j \mu_i^2)}{(4\pi\varepsilon_0)^2 r^6} \qquad \text{eq. 3.8}$$

At the same consideration with the above, an electric field can also be induced by a quadrupole. In that case, the induced energy is as well always attractive but is rather small compared to that of an induced dipole.

3.2.1.c. *Intermolecular forces between non-polar components*

The concept of polarity has been known for a long time. London in 1930s showed that a non-polar molecule, such as methane, can show deviations from the ideal gas law at moderate pressure. If an instantaneous photograph of such a molecule is taken, at a given instant, the oscillations of the electrons about the nucleus is an arrangement sufficient to produce temporary dipole moment. This dipole moment, rapidly changing its magnitude and direction (Figure 3.2), averages zero over a short period of time. However, these quickly varying dipoles produce an electric field which induces dipoles in the surrounding molecules, resulting in an attractive force called the induced dipole – induced dipole force. London showed, using quantum mechanics, that the potential energy between two simple, spherically symmetrically molecules i and j at large distance is given by eq. 3.9,

$$\bar{\Gamma}_{ij} = -\frac{3}{2}\frac{\alpha_i \alpha_j}{(4\pi\varepsilon_0)^2 r^6}\left(\frac{h\nu_{0,i} h\nu_{0_j}}{h\nu_{0,i} + h\nu_{0,j}}\right) \qquad \text{eq. 3.9}$$

where h is the Plank's constant and ν_o is the characteristic electronic frequency for each molecule in its unexcited state. This is related to the variation of the index of refraction n with light frequency, ν, through eq. 3.10,

$$n - 1 = \frac{c}{\nu_o^2 - \nu^2} \qquad \text{eq. 3.10}$$

with c being a constant. It is a relationship between the index of refraction and the characteristic frequency that is responsible for the name dispersion for the attractive force between non-polar molecules. For a molecule i, the product $h\nu_{o_i}$ is almost equal to its first ionization potential, I_i. Thus, the potential energy between non-polar molecules is independent of the temperature and varies inversely as the sixth power of their distance. This sharp decline in attractive force as distance increases explains why it is easier to melt or vaporize a non-polar substance than an ionic one.

3.2.2. Repulsive forces

If the distance r between two molecules i and j becomes very small, their electron clouds start to overlap leading to strong repulsive forces. Such forces are not well understood and, while theoretical considerations suggest that the repulsive potential should be an exponential function of the intermolecular distance[4], the following expression is typically used:

$$\Gamma = \frac{A}{r^n} \qquad \text{eq. 3.11}$$

where A is a positive constant and n an exponent deriving from London's theory.[2] The value of n usually takes a value in the range of 8 up to 16[1].

3.3. Chemical interactions: hydrogen bond

Numerous types of specific chemical effects are of importance in the thermodynamics of solutions. Their main difference from the physical forces relies on the criterion of saturation; chemical forces are saturated while physical ones are not. The saturated nature of the chemical forces is connected with the theory of the covalent bond and the law of multiple proportions. The latter suggests that the ratio of atoms in a molecule is a small, integral number. If, for example, two hydrogen atoms meet, they have a strong tendency to form a hydrogen molecule, H_2. After the formation of the stable H_2 molecule, the atoms have no further tendency to form a H_3 molecule. The stable H_2 molecule is thus *saturated*. Such a criterion does not exist between the physical forces, e.g. due to coulombic interactions; two hydrogen atoms would be attracted to each other with the same force regardless of their tendency to attract a third atom. In gaseous state, doublets are more probable than triplets but that is because in the dilute state a two-body collision is more probable than a three-body one.

Chemical effects are classified to the categories of *association* and *solvation*. The first indicates the tendency of some molecules to form polymers. Such a characteristic example is the formation of acetic acid dimers due to hydrogen bonding. The term solvation, on the other hand, indicates the tendency of molecules of different species to form complexes. For example, a solution of sulfur dioxide in water shows strong solvation by formation of sulfuric acid. This is an intense example, while in most cases weaker forces are observed, as is the case of acetone with chloroform. Actually, chloroform has the tendency to solvate with acetone due to the hydrogen bond formation between the primary hydrogen of the chloroform and the carbonyl oxygen of the acetone. Yet, this has a profound effect in the properties of the solution, such as the negative deviations from Raoult's law. In case of larger molecules, steric hindrance effects can weaken the effects of solvation, as for example in the case of chloroform with di-isobutyl-ketone.

Solvation has a profound effect on the thermodynamic properties of the solution, while the association effects are not always as marked. This is due to the fact that the extend of association is a strong function of composition, especially in the range of dilution with respect to the associating component. Such an example is the case of methanol, which, as a pure component, exists primarily as dimer, trimer or tetramer, but when it is a component of a mixture, it exists primarily as a monomer, as is the case for methanol diluted in large excess of n-hexane. As the methanol concentration rises, more polymers are formed and thus the fraction of molecules that exist in associating form is strongly dependent on the number of methanol molecules present per unit of solution. Thus, the fugacity of the associating component, in this case, methanol, is a highly a non-linear function of its mol fraction.

The ability of a molecule to solvate or associate is related to its electronic structure. When a molecule has, in the classic formulation of electronic layers, its outer octet of

electrons completed, then its chemical forces are saturated and therefore has no tension to associate or solvate. Instead, if the octet is not complete, the molecule has the tendency to complete the octet either by acting as an electron donor or acceptor.

3.3.1. Hydrogen Bonds

The most common chemical effect encountered in the thermodynamics of solutions is that due to chemical bonding. While the *"normal"* valence of hydrogen is unity, many hydrogen – bonding compounds behave as hydrogen is bivalent. Thus, two sufficiently negative atoms *X* and *Y* (either of the same compound or different ones) may be united through hydrogen bond of the form $X-H-Y$ under suitable circumstances. Consequently, molecules containing hydrogen connected to an electronegative atom, such as oxygen, nitrogen or chlorine show strong tendencies to associate with each other and solvate with other molecules containing accessible electronegative atoms. Molecules, thus, containing a hydrogen atom linked to an electronegative one, such as acids, alcohols, amines and glycols, have a strong tendency to form aggregates with each other or with other molecules containing accessible electronegative atoms. A characteristic example of hydrogen bonding is shown in Figure 3.3, where the cluster formations of water are depicted.

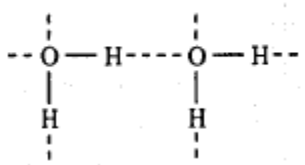

Figure 3.3: Cluster formation between two water molecules. The normal intramolecular covalent bond is depicted with solid line while the hydrogen bond between the hydrogen of the one molecule and the oxygen of the other is depicted with dashed line.

The major difference between a hydrogen bond and a covalent bond is actually their strength. Hydrogen bonds, although they are stronger as compared to physical intermolecular interactions, are rather weak as compared to the covalent bond. As such, there is no creation of a new compound with the former but rather the formation of cluster-like formations. Quantitatively, the bond strength of hydrogen bonds lies in the region of 8 to 40 $kJ \cdot mol^{-1}$, while the energy of the covalent bond is of the range of 200 - 400 $kJ \cdot mol^{-1}$. Therefore, hydrogen bonds break relatively easily, especially at high temperatures where the kinetic energy of molecules is sufficient to overcome the one of the bonds.

The impact of hydrogen bonding is also experimentally observed, as shown by the following characteristics. That is that the distances between the atoms of two hydrogen bonds are substantially smaller compared to the respective van der Waals radius. Furthermore, the covalent bonds stretching modes are shifted towards lower frequencies upon hydrogen bond formation, while their polarities increase. The latter often leads to the formation of complexes whose dipole moment is larger than those

expected from vectorial addition. During nuclear magnetic resonance testing (NMR), the chemical shift of protons in hydrogen bonds is substantially smaller compared to the corresponding isolated molecules. This is in accordance with the reduced electron densities observed at protons participating in hydrogen bonding. The above effects are less pronounced in isolated hydrogen bonding dimers than there are in hydrogen bonding liquids or crystals, indicating thus, the importance of long – range interactions.[1]

The formation of hydrogen bonds consequently affects the properties of the compounds. This influence is more apparent when comparing the properties of a self-associating substance, such as water, with a non-associating one of the same molecular weight, such as methane, as observed in Table 3.1. Methane and water are the first components of their respective homologous series and very close in molecular weight, so one would expect them to have similar properties. Yet, methane is in gaseous state at ambient conditions, while water is in liquid form, as it is indicated by their difference in normal boiling points which is higher than 100 K. Apart from that, the entropy and enthalpy required to vaporize one mol of water at its normal boiling point is substantially larger compared to that of methane. This is because of the strength of the hydrogen bonds; a part of the required energy of vaporization is used to break the hydrogen bond, so it needs to overcome the energy of the bond, as stated above.

Table 3.1: Phase change properties for water and methane[5].

Property	Water	Methane
Molecular weight ($kg \cdot kmol^{-1}$)	18.0153	16.0425
Normal boiling point (K)	373.17	111.00
Enthalpy of vaporization ($kJ \cdot mol^{-1}$)[a]	40.66	8.17 [6]
Entropy of vaporization ($J \cdot mol^{-1} \cdot K^{-1}$)[a]	109.02	88.58 [7]

[a] The enthalpy and entropy of vaporization correspond to the normal boiling point temperature of each substance.

As well, the effect of hydrogen bonding can be observed by studying the thermodynamic properties of a solution of a self-associating molecule diluted in an inert solute, such as a hydrocarbon. Such an example can be an alcohol, such as methanol, diluted in n-hexane. In this case, the hydrogen bonds of methanol are broken and in the limiting case of infinite dilution, all the methanol molecules exist as monomers rather than aggregates. This is a result of the law of mass action. If we consider the equilibrium reaction for the formation of aggregates as in eq. 3.12, where $n \neq 1$ is the order of the aggregate, the fraction of monomers, A, increases with the lowering of the concentration of A molecules. The latter is valid whether the A molecules are in monomer or polymerized form. As the total concentration of A in the solution approaches zero, the fraction of all A molecules that are monomers approaches unity.[1]

$$nA \Leftrightarrow A_n \qquad \text{eq. 3.12}$$

3.3.2. Electron donors – electron acceptors

Chemical forces can occur for other reasons apart from hydrogen bonding. That is other bonding forces which may lead to the formation of loose complexes between electron donors and electron acceptors. These weaker interactions have been experimentally observed through several methods, either directly or by depending on the development of an accurate method to determine the concentration of the complexes. Characteristic examples of this type of interactions are the aromatic hydrocarbons, such as benzene, which can act as electron donors due to the π-valence electrons, in the presence of a molecule which can act as an electron acceptor, such as a polar solvent. The complex stability increases with the number of methyl groups in the benzene ring, which indicates that the π-electrons are easier displaced with the number of methyl group, and depend on the nature of the molecule which acts as electron acceptor. Instead, for saturated hydrocarbons, such as paraffins, Weimer[8] found no such complex formation. As a result, the mixture properties of the same polar solvent with a paraffinic or naphthenic hydrocarbon are expected to be substantially different from that of an aromatic one.[1] This explains the higher solubility of aromatic hydrocarbons in water, alcohols and glycols compared to that of paraffins where the polar components are actually immiscible. In other cases, such as in the mixture of tetrahydrofuran with aromatic hydrocarbons the chemical and physical intermolecular forces are of the same order of magnitude and therefore the sequence of the enthalpy effects does not necessarily follow the complex stability.

3.3.3. An example: the anomalous properties of water

Water covers 71 % of Earth and about 70 % of human body consists of water. The climate and season changing, as well as subsea life, could not occur if it were not for the anomalous properties of water, which are a result of the strong hydrogen bonding interactions of its molecules. Although by experience everybody is very familiar with water and its properties, so that they may not seem obscure, water actually behaves substantially different compared to other compounds of similar structure. To begin with, it differs from the other hydrogen chalcogenides, which are compounds with the chemical formula H_2X where X represents any chalcogen (O, S, Se, Te), in the aspect of being essential for life as we know it, while the rest of the homologous series are toxic and harmful to humans even in small quantities. Water is odorless, while the rest have strong unpleasant smells, such as the characteristic smell resembling that of rotten eggs in the case of hydrogen sulfide.[9]

As it has been stated in Section 3.3.1, the water boiling point is about 100 K higher than the one of other hydrogen chalcogenides. This is illustrated in Figure 3.4, where the melting and normal boiling points of hydrogen halides, hydrogen chalcogenides and metal tetrahydrides of group 14 of the periodic table are presented. The melting points of hydrogen chalcogenides increase linearly with the period number of X component, starting from hydrogen sulfide. The same is observed in the case of hydrogen halides, with the exception of HF. Both water and HF show significantly higher melting points compared to the expected ones based on a linear approximation of the melting points

of the rest of the components in the homologous series, which is about 98 K for water and 64 K for HF. It is thus showed that although HF, due to the higher electronegativity of F compared to that of O, is expected to have stronger hydrogen bonding effects, the association of water has more intense effect. That is due to the ability of the water molecule to act both as an electron donor and acceptor.

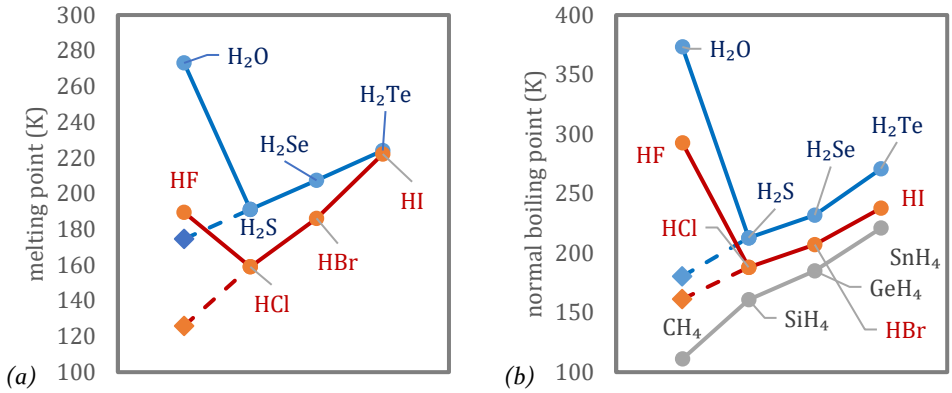

Figure 3.4: Difference in the properties of water due to hydrogen bonding, in comparison with those of the other hydrogen chalcogenides. For comparison, the same properties for hydrogen halides and metal tetrahydrides are also depicted. Dashed line indicates the expected temperature if a linear approximation of the melting or boiling points of the rest components is assumed (a) melting points, (b) normal boiling points.

The same observation is made for their melting points. For comparison purposes, the boiling points of tetrahydrides, which are compounds of the chemical formula XH_4, with X representing any compound of the carbon group, namely C, Si, Ge, Sn etc. In the case of tetrahydrides which are non-polar molecules due to their pyramidal structure, a steady increase in the boiling points is observed. Instead, the boiling points of water and HF are substantially large compared to those of the other compounds of their respective series, even with those belonging in higher periods. The rest of the compounds, although polar, follow the pattern of steady increase of the normal boiling point, proving that the hydrogen bond formation is the dominating one. In this case, an increase of about 193 K for water and 131 K for HF is observed compared to the expected one, if the molecules followed a similar pattern as that of the rest of the compounds in their respective series. So, if it were not for the hydrogen bonding forces, water would have been in the vapor phase at ambient conditions. The latter would thus have a huge impact to life as we know it.

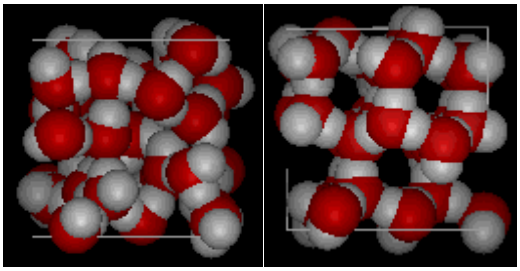

Figure 3.5: Liquid (left) vs solid (right) water structure.[10]

Another strange property of water which is attributed to the structure of its bonds is that it expands upon freezing, in contrast to the other substances, even the hydrogen bonding ones. Additionally, ice, which is the solid state of water is less dense compared to its liquid density. Figure 3.5 shows that at liquid phase, the water molecules are in closer distances to each other. Instead, when ice is formed, the distance in the crystalline structure increases creating some *empty spaces* among the molecules. Thus, the volume occupied by the ice molecules is higher compared to that of water in liquid state, for example, when water freezes under atmospheric pressure, its volume increases by about 9 %. That is the very reason why ice floats in water. The obscure behavior of water density is also expressed in Figure 3.6*a*, where the characteristic maximum of the water density at 4 °C is observed. This property of water permits a constant temperature of about 4 °C to be kept at the seabed all year long, allowing thus the smooth cycle of aqueous life, as depicted schematically in Figure 3.6*b*.

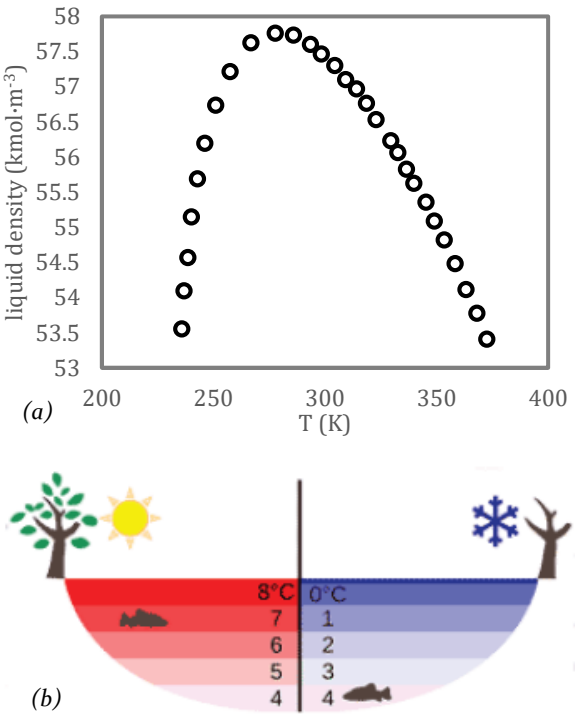

Figure 3.6: (a) Liquid density of water at 1 bar.[5] (b) Schematic effect of water temperature at the bottom of a lake for two different seasons.[11]

The high density of liquid water is mainly due to the cohesive nature of the hydrogen – bonding network, with each water molecule capable of forming four hydrogen bonds. This reduces the free volume and ensures a relatively high density, partially compensating for the open nature of the hydrogen bonding network. The normal phenomenon for liquids is to expand when heated, at all temperatures. Instead, the anomalous density behavior of water can be explained by the opposing effects of

increasing temperature, causing both structural collapse that increases density and thermal expansion that lowers it. Counter – intuitively, the distance between the water molecules decreases as the density decreases as the supercooling temperature is lowered. The decrease in density is primarily due to the reduction of its nearest neighbors and the loss of *interstitial* water. The change between different cluster formations as the temperature rises is accompanied by positive changes in both entropy and enthalpy due to the less ordered structure and greater hydrogen bond bending, respectively.

Furthermore, water has the highest surface tension of any liquid with the exception of mercury and a quite large viscosity. Most importantly, water has a high heat capacity. That is attributed to the fact that it takes quite a lot of energy to break the hydrogen bonds between the water molecules and therefore water has the capacity to store large amounts of energy. As a result, sufficiently enough energy in the forms of heat is required to interfere with the association forces and then increase the water temperature. This ability of water permits the ocean to act as a thermal reservoir, ensuring a smooth season change. Finally, water is considered as the global solvent since it can dilute most polar components, even those salts that are insoluble in other liquids.[9]

List of Symbols

Latin Characters

A, c	constants
d	distance between two electric charges of the same magnitude but opposite polarity
e	elementary charge of the electron ($e = 1.60218 \cdot 10^{-19} C$)
E	field strength
F	the force between the molecules due to intermolecular interactions
h	Plank's constant ($h = 6.62607004 \cdot 10^{-34} \cdot m^2 \cdot kg \cdot s^{-1}$)
I	ionization potential
n	refraction index
r	the distance between the nuclei of two molecules
q	electric change *(c)*
Q	quadrupole moment (Debye)
ν	light frequency
ν_o	characteristic electronic frequency of a molecule in its unexcited state
z	ionic valence

Greek Characters

α	polarizability
Γ	potential energy
$\bar{\Gamma}$	dipole – induced dipole potential energy
ε_o	dielectric permittivity at vacuum ($\varepsilon_0 = 8.85419 \cdot 10^{-12}\ C^2 \cdot J^{-1} \cdot m^{-1}$)
θ, φ	coordinates of the relevant position of the molecules in space (rad)
μ	dipole moment (Debye)

Superscripts and Subscripts

i, j	molecule
n	exponent defined by London's theory

References

(1) Prausnitz J.M., Lichtenthaler R.N., de Azevedo E.G., *Molecular thermodynamics of fluid-phase equilibria*. Pearson Education: 1998.
(2) Tassios D.P., *Applied chemical engineering thermodynamics*. Springer: 1993.
(3) Abbott M., Smith J., Van Ness H., *Introduction to chemical engineering thermodynamics*. McGraw-Hill: 2001.
(4) Reed T.M., Gubbins K.E., Applied statistical mechanics. **1973**.
(5) NIST Thermophysical Properties of Fluid Systems, http://webbook.nist.gov/chemistry/fluid/, accessed on 01/09/2017.
(6) Majer V., Svoboda V., Kehiaian H.V., Enthalpies of vaporization of organic compounds: a critical review and data compilation. **1985**.
(7) Vogt G.J., Pitzer K.S., Entropy and heat capacity of methane; spin-species conversion. *The Journal of Chemical Thermodynamics* **1976,** *8*, (11), 1011-1031.
(8) Weimer R.F., Prausnitz J.M., Ultraviolet spectra and complex formation in mixtures of polar organic solvents and aromatic hydrocarbons. *Spectrochimica Acta* **1966,** *22*, (1), 77-80.
(9) Properties of liquids, http://chemed.chem.purdue.edu/genchem/topicreview/bp/ch14/property.php, accessed on 11/07/2018.
(10) Water and Ice, https://www.nyu.edu/pages/mathmol/textbook/info_water .html, accessed on 11/07/2018.
(11) Chaplin M., Water structure and science, http://www1.lsbu.ac.uk/water/density_anomalies.html#density, accessed on 11/07/2018.

Chapter 4: Phase Equilibrium calculations

To simulate the properties of a system two approaches can be followed. The traditional one is the steady – state approach which is based on the assumption of established equilibrium, while the more contemporary one is the rate – based calculations which derive from transport phenomena. In the context of this work, the equilibrium approach is followed, where the driving force is the thermodynamics of the system. To this purpose, in this chapter the essences of the phase equilibrium calculations are briefly discussed. Basic equilibrium calculations are given and two different methodologies are discussed; the activity coefficient models' approach and the equation of state approach. Finally, the algorithms to perform phase equilibria calculations are briefly discussed.

4.1. Thermodynamic equilibrium and phase rule

As stated by the steady – state approach, equilibrium is a condition where no changes occur in the macroscopic properties of a system with time. This implies a balance of all potentials that may cause change. The thermodynamic equilibrium is rather a dynamic one, in microscopic level, in the essence that molecules of the substances are constantly changing phases. For example, at vapor – liquid equilibrium if we consider *n* moles of liquid phase that have sufficiently high velocity to leave the interface and turn into vapor, the same number of (different) moles, *n*, will condense from the vapor into liquid state. However, the average rate of transition of molecules is the same in both directions, and no net interphase transfer of material occurs, leaving the system thus in equilibrium.[1]

As a consequence of the second law of thermodynamics, an isolated system approaches equilibrium by increasing its entropy and the equilibrium state is reached when the change of entropy is at its maximum.[2] According to the Duhem's theorem, the number of independent variables in a system at equilibrium is defined by the difference between the total number of variables that characterize the intensive state of the system and the number of independent equations that can be written connecting the variables. It is also deprived that for any close system initially formed from given masses, the equilibrium state is completely determined when any two independent variables are fixed.[1] Depending on the selection of the independent variables, different state function has to be at a minimum (or maximum, in case of entropy) so that the equilibrium criteria are satisfied. The corresponding pairs of independent variables and state functions are given in Table 4.1.[2]

Table 4.1: Equilibrium criteria for a closed system.

Independent variables	State function to be minimized
S, v, n	*U*
U, S, n or *A, T, n*	*v*
S, P, n	*H*
T, P, n	*G*
T, v, n	*A*
H, P, n or U, v, n	*-S*

In the common industrial practice, it is easier to control temperature and pressure and therefore they are usually selected as independent variables. Following this specification, the Gibbs' free energy should be at a minimum, for the equilibrium conditions to be satisfied, as it is derived from the 2nd law of the thermodynamics through the relationship of eq. 4.1,

$$\frac{dG}{dt} = -T\frac{dS_g}{dt} \qquad \text{eq. 4.1}$$

where G is the Gibbs free energy and S_g the generated entropy.

This indicates that as the system is driven through equilibrium, its Gibbs' energy continuously decreases until it reaches a minimum value, where no more change is possible. The formalization of Gibbs' energy as the driving force to the equilibrium is given by its derivatives, as per

eq. 4.2.[3]

$$\left(\frac{\partial \Delta_{mix} G}{\partial x}\right)_{T,P} = 0$$
$$\left(\frac{\partial^2 \Delta_{mix} G}{\partial x^2}\right)_{T,P} > 0 \qquad \text{eq. 4.2}$$

The requirement of the minimization of the Gibbs' free energy at equilibrium, of a non-reacting system between two phases, *I* and *II*, when temperature and pressure are the independent variables, results in the equality of the chemical potentials, μ, in the two phases for each component of the mixture. Although, the chemical potential is a fundamental criterion for the establishing of phase equilibrium, it is inconvenient for direct use in calculations, since it is related with internal energy and entropy, for which absolute values are unknown. Thus, the application of equilibrium criteria is facilitated by the introduction of *fugacity*, *f*, which is a quantity that takes the place of the chemical potential but avoids the uncertainties associated with the latter. Actually, fugacity is introduced as the isothermal change in the chemical potential for any compound in a mixture, as per eq. 4.3,

$$\mu_2 - \mu_1 = \mu(P_2, T) - \mu(P_1, T) = RTln\left(\frac{f_2}{f_1}\right) \qquad \text{eq. 4.3}$$

where *R* is the ideal gas constant and *T* the mixture temperature.

The ratio of the fugacity of a pure compound at pressure *P*, divided by the same pressure, *P*, is defined as the *fugacity coefficient* (eq. 4.4) which is actually the value used in the equilibrium calculations.[3]

$$\varphi = \frac{f}{P} \qquad \text{eq. 4.4}$$

Therefore, the phase equilibrium of a mixture between two phases, *I* and *II*, is satisfied from the equifugacity criterion for each component, *i*, of the mixture (eq. 4.5).

$$f_i^I = f_i^{II} \qquad \text{eq. 4.5}$$

The calculation of the fugacity usually occurs through the calculation of the fugacity coefficient and although more practical compared to chemical potential, still several approaches exist. The fugacity coefficient is related to the excess Gibbs' energy through eq. 4.6,

$$G_i^{res} = G_i - G_i^{IG} = RTln\varphi_i \qquad \text{eq. 4.6}$$

where the exponent *res* refers to the residual Gibbs' energy and *IG* to that of the ideal gas at the same conditions.

In the current thesis, only vapor – liquid and liquid – liquid equilibrium are considered. As such, two classic approaches are presented for the calculation of the fugacity. The first one traditionally corresponds to calculations at low pressures and it is obtained by the use of activity coefficient models, while the latter is through equations of state.

4.2. Phase equilibrium at low pressure

This approach is traditionally used at the low – pressure area, to describe the phase equilibria of polar mixtures, such as the separation of ethanol/water, in combination with an activity coefficient model. That is due to the fact that cubic equations of state (EoS) fail to accurately describe the phase equilibria of such mixtures. The examination of this approach is separated in two categories. The first involves the vapor – liquid equilibrium (VLE), the so-called γ-ϕ approach, while the second refers to the liquid – liquid equilibrium (LLE), referred as γ-γ approach.

4.2.1. Vapor – liquid equilibrium

Starting from the equifugacity criterion of eq. 4.5, the vapor phase fugacity is expressed through eq. 4.7,

$$f_i^v = y_i \cdot P \cdot \varphi_i^v \qquad \text{eq. 4.7}$$

where y_i is the vapor phase solubility of the component i, P the pressure and φ_i^v the fugacity coefficient at the vapor phase. The latter can be calculated with sufficient accuracy by some equation of state, such as the virial.

The liquid phase fugacity is calculated through the standard state approach (f_i^o), as per eq. 4.8,

$$f_i^l = x_i \cdot \gamma_i \cdot f_i^o = x_i \cdot \gamma_i \cdot P_i^s \cdot \varphi_i^s \cdot exp\left(\frac{v_i \cdot (P - P_i^s)}{RT}\right) \qquad \text{eq. 4.8}$$

where γ_i is the activity coefficient, x_i the liquid phase composition of the component i, φ_i^s the fugacity coefficient of the saturated pure liquid at temperature T, v_i the average molar volume of the pure liquid i at temperature T from its vapor pressure (P_i^s) to the system pressure P, and R the ideal gas constant. The exponential term is the Poynting effect (Pe_i) and expresses the effect of the pressure in the volume of the system.

Traditionally, the activity coefficient can be calculated with sufficient accuracy by an activity coefficient model, such as Non – Random Two Liquids[4] (NRTL) or UNIQUAC[5]. The vapor pressure can be calculated through the Antoine expression or any sufficient correlation, such those proposed by the Design Institute for Physical Properties (DIPPR).[3]

4.2.2. Liquid – Liquid Equilibrium

Generally, the effect of pressure in liquids is rather small compared to its effect in the vapor phase. Yet, the increase of pressure increases the two – phase region and thus is

unfavorable for the miscibility of two liquids. The criterion for establishing the equilibrium is again the molar Gibbs' energy of mixing, $\Delta_{mix}G$. For the system to reach equilibrium, the latter at constant temperature, T, and pressure should satisfy the relations of eq. 4.2 for all concentrations x.

Because $\Delta_{mix}G$ is a function of pressure, under certain conditions a change in the latter may produce immiscibility in an otherwise miscible system, or the inverse phenomenon. This effect of pressure in a binary liquid mixture is closely connected to the volume change at mixing.[6] When two liquids are immiscible, they ultimately reach a state where they exist under equilibrium. The conditions to satisfy the equilibrium are the same of eq. 4.5, with the difference that in this case *I* and *II* correspond to the two immiscible liquid phases. Such an example commonly known from experience is the liquid – liquid equilibrium of water and oil.

The fugacity of each component in each phase is calculated through eq. 4.8. If each pure component can exist in the liquid phase at the corresponding temperature and pressure condition, then $f_i^I = f_i^{II}$ and as such the equifugacity criterion is simplified into eq. 4.9.[1]

$$x_i^I \cdot \gamma_i^I = x_i^{II} \cdot \gamma_i^{II} \qquad \text{eq. 4.9}$$

Again, the activity coefficient can be calculated through an appropriate activity coefficient model.

If a binary mixture at two – phase LLE is considered, in the limiting case of infinite dilution, e.g. if *I* is the phase rich in component 1, then $\lim_{x_1 \to 1} \gamma_1^I = 1$ and therefore eq. 4.9 is reduced to the following.

$$\gamma_2^{II} = \frac{1}{x_2^{II}} \qquad \text{eq. 4.10}$$

This can be used to calculate *experimentally* the infinite dilution activity coefficient.

4.3. Phase equilibrium with an Equation of State

In contrast with the previous approach, where the fugacity is implicitly estimated, equations of state are tools with which the fugacity coefficient is directly calculated. The fugacity coefficient, φ, for the vapor or the liquid phase of a component i in a mixture, is calculated through eq. 4.11, with the appropriate substitution of each EoS relationships.

$$ln\varphi_i = \frac{1}{RT}\int_0^P \left(\bar{v}_i - \frac{RT}{P}\right) dP \qquad \text{eq. 4.11}$$

where $\bar{v}_i$ is the partial molar volume of the component i in the mixture.[3] Then from the equifugacity criterion, it is yield that:

$$z_i^I \cdot \varphi_i^I = z_i^{II} \cdot \varphi_i^{II} \qquad \text{eq. 4.12}$$

where phases *I* and *II* can either correspond to liquid or vapor.

If the case of VLE is considered, then $x_i \cdot \varphi_i^l = y_i \cdot \varphi_i^v$. Then, the partition coefficient (K-factor) of the component i is defined as per eq. 4.13.

$$K_i = \frac{\varphi_i^l}{\varphi_i^v} \qquad \text{eq. 4.13}$$

The calculation of phase equilibrium is similarly performed for LLE as well. The difference exists in the initialization of the calculations and in the selection of the corresponding liquid volume, instead of the vapor one.

4.4. Phase equilibrium algorithms

Three different types of calculation exist for the calculation of the phase equilibria of a mixture, namely bubble point, dew point and flash calculation. If T is the temperature, P the pressure, x the liquid phase composition and y the vapor phase composition at equilibrium, then Table 4.2, summarizes the different types of calculations along with the known and calculated properties.[3]

Table 4.2: Different type of equilibrium calculations along with the defined and calculated variables of each case.

calculation	known variables	unknown (calculated) variables
Bubble point pressure (BPP)	*T, x*	*P, y*
Bubble point temperature (BPT)	*P, x*	*T, y*
Dew point pressure (DPP)	*T, y*	*P, x*
Dew point temperature (DPT)	*P, y*	*T, x*
flash	*T, P*	*x, y*

4.4.1. Bubble point calculation

In a bubble point calculation the composition of the liquid phase is known along with the temperature or pressure. For easier description of the algorithm, a BPP calculation is assumed, while a similar procedure is followed in the BPT one. An iterative approach is used, where the first step is to estimate an initial pressure and vapor phase composition, either by using an experimental one or by some general initialization method, such as that of Wilson[7]. The latter actually calculates an estimated *K*-factor and thus an initialization of the phase split. Then, with all the variables known, the fugacity coefficients of each component are calculated in both phases and if they are equal under a specified accuracy, then these are the corresponding values at equilibrium. Otherwise, a new value of pressure is calculated through a Newton step as per eq. 4.14 and the procedure is repeated until the equifugacity criterion is satisfied.[2, 3]

$$P^{new} = P^{old} - \frac{g}{\partial g / \partial P} \qquad \text{eq. 4.14}$$

The flowchart of the BP algorithm is illustrated in Figure 4.1.

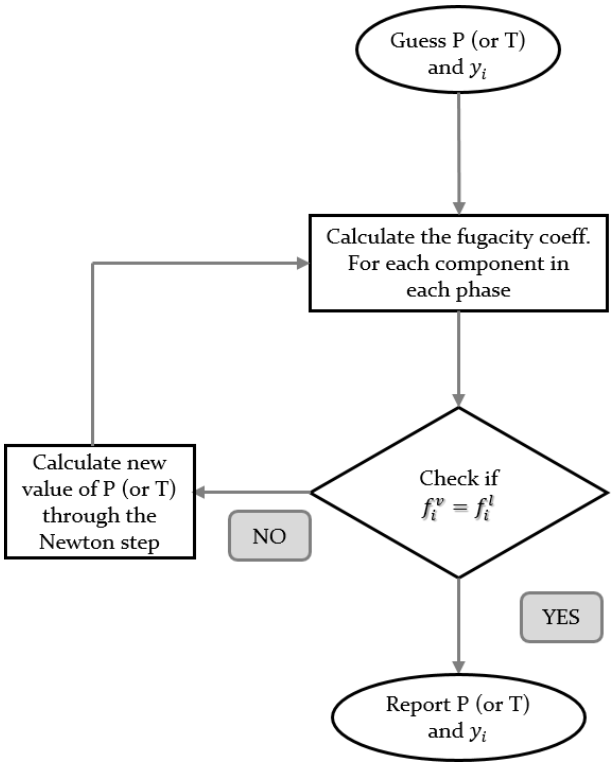

Figure 4.1: Flowchart of a bubble point calculation algorithm

4.4.2. Dew point calculation

The dew point calculation, although similar in principle is more complex compared to the bubble point one and usually requires more iterations. The algorithm is developed as in the case of bubble point calculation, with the difference that the vapor phase composition is known. The flowchart is presented in Figure 4.2.[3]

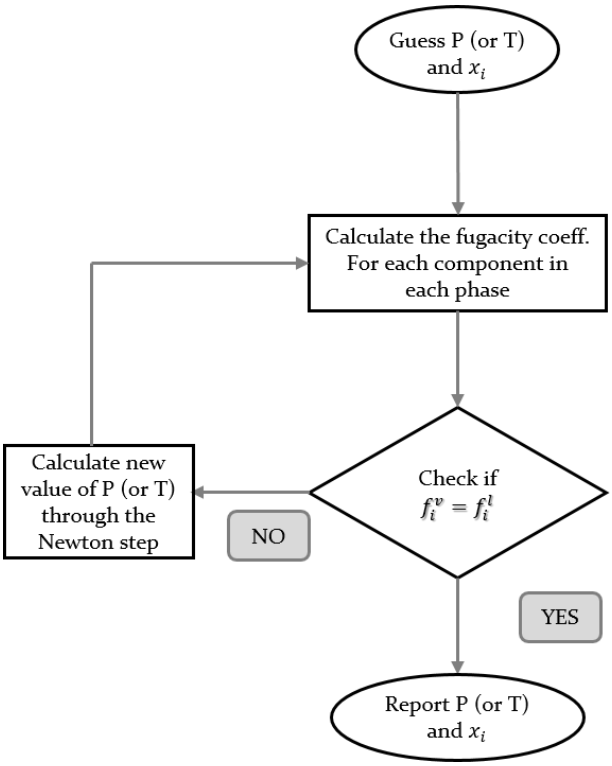

Figure 4.2: Flowchart of a dew point calculation algorithm.

4.4.3. Isothermal Flash calculation

If a mixture of F moles with a feed composition z_i in the two-phase region at temperature T and pressure P is considered, then with the isothermal flash the liquid and vapor phase flows (L and V respectively) and compositions, x_i, y_i are calculated. In this type of calculation both the material balance (eq. 4.15) and the equilibrium equations should be satisfied.

$$F \cdot z_i = L \cdot x_i + V \cdot y_i \qquad \text{eq. 4.15}$$

The Rachford – Rice[8] equation is solved to provide the phase split (eq. 4.16), since it provides a negative derivative, ensuring rapid convergence in the Newton's step.

$$Q = \sum \frac{F \cdot z_i(K_i - 1)}{F + \mathrm{V} \cdot (K_i - 1)} = 0 \qquad \text{eq. 4.16}$$

For the first iteration, an additional step is required, that is estimation of K_i-factors, through e.g. some empirical method and therefore the calculation of the respective fugacity coefficients. Then the Rachford – Rice equation is solved again, until convergence occurs.[2, 3]

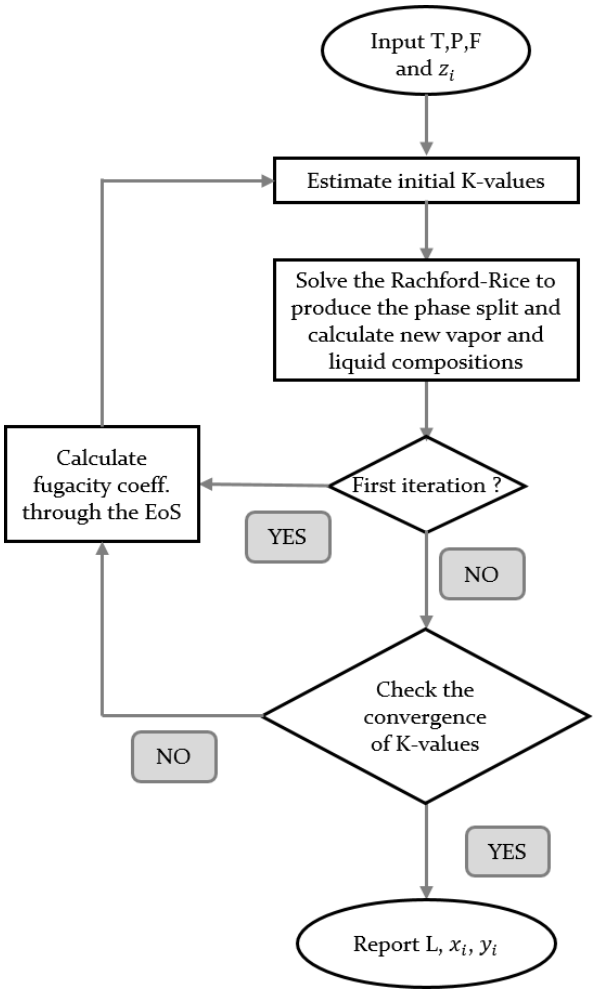

Figure 4.3: Isothermal (TP) flash algorithm flowchart.

List of Symbols

Latin Characters

A	Helmoltz free energy ($J \cdot mol^{-1}$)
f	fugacity (bar)
F	feed molar rate of a flash ($kmol \cdot h^{-1}$)
g	function used for the estimation of new pressure value
G	molar Gibbs free energy ($J \cdot mol^{-1}$)
H	molar enthalpy ($J \cdot kmol^{-1}$)
K_i	partition coefficient of a component *i* between the two phases in equilibrium
n	quantity of matter (mol)
P	pressure (bar)
R	universal ideal gas constant (83.14 $bar \cdot cm^3 \cdot mol^{-1} \cdot K^{-1}$)
S	molar entropy ($J \cdot kmol^{-1} \cdot K^{-1}$)
T	absolute temperature (K)
U	internal energy ($J \cdot kmol^{-1}$)
v	molar volume ($cm^3 \cdot mol^{-1}$)
V	liquid molar flow of a flash ($kmol \cdot h^{-1}$)
x_i	liquid mol fraction of component *i*
y_i	vapor mol fraction of component *i*
z_i	feed mol fraction of component *i*

Greek Characters

μ	chemical potential ($J \cdot mol^{-1}$)
φ	fugacity coefficient

Superscripts and Subscripts

g	generated
i	component in a mixture
I, II	phases at equilibrium

IG	ideal gas
l	liquid
mix	property of mixing
res	residual
s	saturated property
v	vapor
$\bar{\ }$	partial property

References

(1) Abbott M., Smith J., Van Ness H., *Introduction to chemical engineering thermodynamics*. McGraw-Hill: 2001.
(2) Michelsen M.L., Mollerup J., *Thermodynamic Models: Fundamentals and Computational Aspects*. 2nd ed., Tie-Line Publications: 2007.
(3) Tassios D.P., *Applied chemical engineering thermodynamics*. Springer: 1993.
(4) Renon H., Prausnitz J.M., Local compositions in thermodynamic excess functions for liquid mixtures. *AIChE Journal* **1968,** *14*, (1), 135-144.
(5) Abrams D.S., Prausnitz J.M., Statistical thermodynamics of liquid mixtures: A new expression for the excess Gibbs energy of partly or completely miscible systems. *AIChE Journal* **1975,** *21*, (1), 116-128.
(6) Prausnitz J.M., Lichtenthaler R.N.,de Azevedo E.G., *Molecular thermodynamics of fluid-phase equilibria*. Pearson Education: 1998.
(7) Wilson G., In *A modified Redlich–Kwong EoS, Application to General Physical Data Calculations, Paper No. 15C*, presented on AIChE 65th National Meeting, Cleveland, Ohio, 4-7 May **1969.**
(8) Rachford H.H., Jr., Rice J.D., Procedure for Use of Electronic Digital Computers in Calculating Flash Vaporization Hydrocarbon Equilibrium. *Petroleum Transactions, AIME* **1952,** *195*, 327-328.

Chapter 5: Thermodynamic Models

In the present Chapter, the thermodynamic models examined in this work are described. Emphasis is given in the different approaches for the description of the associating fluids, categorizing thus the models in three fundamental groups. That is the cubic equations of state with conventional mixing rules, the cubic EoS combined with an activity coefficient model through advanced mixing rules and the models directly accounting for the hydrogen bonding forces. Finally, an ISO standard model for the description of natural gas mixtures is presented.

5.1. Introduction

Mixtures of natural gas components with water and other polar components, such as alcohols and glycols, are challenging from the thermodynamic modelling aspect. Cubic equations of state are widely used for the calculation of thermodynamic properties and, especially, phase equilibrium, of pure components and mixtures both in industry and academia. Nevertheless, it is well – known that they fail to accurately describe these complex systems, due to the strong associating forces encountered. This is because such strong forces cannot be captured by the attractive term of a cubic EoS, especially if the latter is combined with the van der Waals one fluid mixing rules (vdW1f) for the extension to mixtures.[1]

Accurate description of phase equilibrium of such mixtures requires the use of more sophisticated approaches. Several methods have been proposed in the literature along the years, with varying success. For systems at low pressure, where the non-ideality of the vapor phase can be neglected without significant cost in the obtained accuracy, activity coefficient models, such as UNIQUAC[2], NRTL[3] etc., correlate satisfactorily the phase equilibrium. In case of natural gas mixtures, high pressure is usually encountered rendering those models rather inappropriate. Another traditional approach for the description of associating mixtures is the chemical theory, where the hydrogen bonds are considered to be new species created in the system as a result of chemical reactions.[4-6] Although these approaches yield satisfactory results, they are not easily applied to multicomponent mixtures. Instead, equations of state are rather attractive, since apart from the phase equilibrium calculations, they are able to predict directly other properties and they are also applicable to the whole range of conditions encountered in industrial practice.

An easy way to extend the applicability of a cubic EoS to polar mixtures, while keeping its cubic character, is to use advanced mixing rules. Such an elegant approach is based on the idea of Huron and Vidal[7] to match the excess Gibbs free energy (G^E) of the mixture as calculated by the EoS with the one calculated by a Gibbs free energy (or equivalently activity coefficient) model at the system temperature and composition but at infinite pressure. In this way, if the G^E at infinite pressure has finite value, this corresponds to the co-volume of the EoS. Mollerup[8] and later Michelsen[9, 10], suggested the matching of the excess Gibbs energy of an EoS to that of an activity coefficient model at zero pressure. They obtained, thus, the direct applicability of the existing databases of activity coefficient models fitted at low – pressure data without the need to refit the interaction parameters (IP) of the model. These so-called EoS/G^E mixing rules allow the incorporation of an expression for the activity coefficient inside the EoS, permitting thus a cubic EoS to be applicable to polar compounds at high pressures as well. Several models of this class have been suggested in the literature with varying degrees of success.[10-13]

A more sophisticated approach, which albeit violates its cubic character, is the development of an EoS that accounts explicitly for strongly polar and hydrogen

bonding interactions. The essence of this progress is to use statistical mechanical methods, such as Wertheim's first order perturbation theory.[14-17] Using a first order perturbation theory with a potential function that mimics hydrogen bonding, Wertheim, proposed a statistical mechanical model for systems with a repulsive core and multiple hydrogen bonding sites. Based on this theory, a variety of models has been proposed in the literature for the modelling of associating compounds, such as the statistical associating fluid theory (SAFT)[18, 19], the perturbed chain SAFT (PC-SAFT)[20, 21] and the cubic plus association (CPA)[22].

To overcome the weaknesses and limitations of existing equations of state used in the natural gas industry, a wide – range EoS for natural gases and other mixtures has been developed by Group Européen de Recherché Gazière (GERG). The GERG-2008 EoS, as it is referred, has been adopted as a standard international reference equation suitable for all natural gas applications where thermodynamic properties are required and it has been also adopted as an ISO Standard (ISO 20765-2/3) for natural gases.[23, 24]

Since the scope of this work is to develop an EoS adequate for the description of associating compounds, with emphasis given in the mixtures of natural gas components with water and alcohols or glycols, in the present chapter, the models which are already proposed in the literature are presented. Furthermore, extension of the examined models to mixtures containing natural gas components and polar molecules, where necessary, is also described.

5.2. Cubic EoS with classic mixing rules

The cubic EoS are based on the innovative idea of van der Waals[25] who proposed a semi-empirical approach to relate the volumetric behavior of real fluids with the temperature and the pressure. In this essence, a family of cubic equations of state has been proposed ever since. Among them, the Soave – Redlich – Kwong[26, 27] (SRK) and the Peng – Robinson[28, 29] (PR), are two of the most successful EoS and are still widely used in the oil & gas industry due to the fast calculations and the quite accurate representation of low and high pressure VLE of hydrocarbons and hydrocarbons with gases.[30]

In a generalized form, the cubic EoS are given in eq. 5.1 - eq. 5.5, with the universal constant r_1 equal to zero in the case of SRK and 1 in that of the PR. The corresponding values of the constants for each equation are given in Table 5.1. The temperature dependency of the attractive term parameter for non-polar compounds is given from the Soave[27] expression as described in eq. 5.2 – eq. 5.3, where T_c, P_c and ω are the critical properties of each substance which for the compounds of interest are presented in Table 5.2. Actually, the acentric factor is related to the critical properties of the fluid as suggested by Pitzer[31] through eq. 5.6. For the temperature dependency of the alpha function of the polar components, the Matthias – Copeman[32, 33] (MC) expression (eq. 5.7) is utilized since the Soave expression yields poor results.[11, 34]

The MC parameters considered for the PR EoS have been fitted to vapor pressure data and are either taken from literature or calculated in this work and they are presented in Table 5.2 along with the corresponding deviations in vapor pressure and liquid density.

Table 5.1: Cubic EoS parameters for the SRK and PR used in eq. 5.3 - eq. 5.5.[35]

	d_0	d_1	d_2	d_3	d_4
SRK	0.48508	1.55171	−0.15613	0.42748	0.08664
PR	0.37464	1.54226	−0.26992	0.45724	0.07780

The extension to mixtures requires the use of mixing rules. One methodology which is widely employed and is especially successful for hydrocarbon mixtures is the van der Waals one fluid mixing rules[25], which satisfy the quadratic mixing rule for the second virial coefficient (eq. 5.8). They are usually accompanied by classical combining rules which involve a geometric mean rule for the cross-energy parameter that derives from London theory under specific assumptions (eq. 5.10). That is the assumption of spherical molecules, under infinite distance. For the cross co-volume parameter, an arithmetic mean rule is considered. To account for the non-idealities between the molecules, an interaction parameter, k_{ij} or l_{ij}, is introduced. In the usual case, when the l_{ij} parameter equals zero, as in the present thesis, the cross co-volume parameter is simplified to linear dependency, as per eq. 5.9.

$$P = \frac{RT}{v-b} - \frac{a_c \mathrm{a}(T)}{v(v+b) + r_1 b(v-b)} \qquad \text{eq. 5.1}$$

$$\mathrm{a}(T) = \left(1 + m(1 - T_r^{0.5})\right)^2 \qquad \text{eq. 5.2}$$

$$m = d_0 + d_1\omega + d_2\omega^2 \qquad \text{eq. 5.3}$$

$$a_c = d_3 \frac{(RT_c)^2}{P_c} \qquad \text{eq. 5.4}$$

$$b = d_4 \frac{RT_c}{P_c} \qquad \text{eq. 5.5}$$

$$\omega = -\log P_r^{sat}|_{T_r=0.7} - 1 \qquad \text{eq. 5.6}$$

$$\mathrm{a(T)} = [1 + c_1(1 - T_r^{0.5}) + c_2(1 - T_r^{0.5})^2 + c_3(1 - T_r^{0.5})^3]^2 \quad \text{for} \quad T \le T_r$$

$$\mathrm{a}(T) = [1 + c_1(1 - T_r^{0.5})]^2 \quad \text{for} \quad T > T_r \qquad \text{eq. 5.7}$$

Table 5.2: Critical properties and acentric factors for cubic EoS. MC parameters for PR are also given. Deviation from DIPPR with ΔT step equal to 5 K.

Comp.	Ref.	T_r range	T_c (K)	P_c (bar)	ω	c_1	c_2	c_3	%AARD [a] in P^s	%AARD [a] in v_l
N_2	[36]	0.53 - 0.99	126.10	33.95	0.0403	-	-	-	0.74	8.60
CO_2	[36]	0.72 - 0.98	304.19	73.82	0.2276	-	-	-	0.99	3.86
CH_4	[36]	0.53 - 0.99	190.56	45.99	0.0115	-	-	-	0.79	8.02
C2	[36]	0.41 - 0.99	305.32	48.72	0.0995	-	-	-	1.28	6.47
C3	[36]	0.33 - 0.98	369.83	42.48	0.1523	-	-	-	4.73	4.90
i-C4	[36]	0.45 - 0.99	408.14	36.48	0.1770	-	-	-	2.71	5.34
n-C4	[36]	0.32 - 0.99	425.12	37.96	0.2002	-	-	-	5.75	4.31
i-C5	[36]	0.45 - 0.99	460.43	33.81	0.2275	-	-	-	1.13	4.63
n-C5	[36]	0.40 - 0.99	469.70	33.70	0.2515	-	-	-	2.47	3.47
n-C6	[36]	0.40 - 0.99	507.60	30.25	0.3013	-	-	-	5.19	2.94
n-C7	[36]	0.51 - 0.95	540.20	27.40	0.3495	-	-	-	1.14	2.62
water	[11]	0.55 - 0.90	647.13	220.55	0.3449	0.92366	-0.37937	0.44243	0.10	34.40
meOH	[11]	0.55 - 0.90	512.64	80.97	0.5640	1.22400	-0.27350	-0.39823	0.10	18.72
MEG	This work	0.45 - 0.96	720.00	82.00	0.5068	0.91003	1.34996	-1.89002	3.63	12.52
TEG	This work	0.42 - 0.90	769.50	33.20	0.7587	1.550.76	-0.77780	0.31779	3.09	15.41

[a] $\%\,AARD = \frac{100}{n_p} \cdot \sum_i^{n_p} \frac{abs(X_i^{calc} - X_i^{exp})}{X_i^{exp}}$, where X stands for P^s or v_l and n_p for the number of experimental data points

$$a = \sum_{i}^{n} \sum_{j}^{n} x_i x_j a_{ij} (1 - k_{ij}) \qquad \text{eq. 5.8}$$

$$b = \sum_{i}^{n} x_i b_i \qquad \text{eq. 5.9}$$

$$a_{ij} = (a_i a_j)^{1/2} \qquad \text{eq. 5.10}$$

5.3. Advanced Mixing Rules

As already mentioned, usually cubic EoS fail to satisfactorily predict the phase equilibria of mixtures containing polar compounds. Instead, activity coefficient models correlate satisfactorily the VLE of polar mixtures that exhibit high non-ideality in the liquid phase, but they are limited to low pressure and cannot be extended to the calculation of other properties. To combine the positive characteristics of both considerations, Huron and Vidal[7] matched the excess Gibbs energy calculated from an EoS to that of an activity coefficient model at infinite pressure and then solved for the van der Waals attractive parameter, a, as per eq. 5.11.

$$\left(\frac{G^E}{RT}\right)_{T,P_{ref},x}^{EoS} = \left(\frac{G^E}{RT}\right)_{T,P_{ref},x}^{act.\ coeff.\ model} \qquad \text{eq. 5.11}$$

This equality is valid at a specific pressure, P_{ref}, which is called the reference pressure and it usually corresponds to infinite or zero pressure. Based on this idea, several models have been proposed, with the most successful to be based on the modified Huron – Vidal mixing rules (MHV1) suggested by Michelsen.[9, 10] In this way, an activity coefficient model can be employed to higher pressures. Among them, the models which are coupled with UNIFAC are of special interest, because they can be used as a predictive tool for a variety of mixtures.[11, 37, 38] In the context of this work, two models based on this philosophy, the so-called EoS/G^E, have been considered: the Universal Mixing Rules Peng – Robinson UNIFAC (UMR-PRU) and the Twu – Sim – Tassone Non Random Two Liquid (TST/NRTL).

5.3.1. UMR-PRU

The UMR-PRU model[39, 40] belongs to the EoS/G^E class and is actually based on the MHV1 mixing rules suggested by Michelsen.[9, 10] It combines the Peng – Robinson EoS as it is presented in Section 5.2, with the UNIFAC activity coefficient model through the universal mixing rules (UMR) proposed by Voutsas et al.[40] (eq. 5.12 - eq. 5.13).

$$a = \frac{1}{-0.53}\frac{G_{AC}^{E,SG}+G_{AC}^{E,res}}{RT} + \sum_i x_i \frac{a_i}{b_i RT} \qquad \text{eq. 5.12}$$

$$b = \sum_i \sum_j x_i x_j b_{ij} \text{ with } b_{ij} = \left(\frac{b_i^{1/2} + b_j^{1/2}}{2}\right)^2 \qquad \text{eq. 5.13}$$

The dimensionless quantity a at eq. 5.12 is the cubic EoS cohesion parameter, which is defined as $a = \frac{a}{bRT}$, where a and b are the mixture attractive and co-volume parameters of the EoS, respectively; R is the ideal gas constant; and T is the temperature. Similarly, for the pure component i, the relationship is $a_i = \frac{a_i}{b_i RT}$. The Flory – Huggins term of the UNIFAC combinatorial term is omitted since it results in poor performance in asymmetric systems.[41]

The Staverman – Guggenheim term of the combinatorial part ($G_{AC}^{E,SG}$) and the residual part ($G_{AC}^{E,res}$) of the excess Gibbs energy (G^E) respectively, are calculated from eq. 5.14 - eq. 5.18,

$$\frac{G_{AC}^{E,SG}}{RT} = 5\sum_i x_i q_i \ln\frac{\theta_i}{\varphi_i}, \quad \frac{G_{AC}^{E,res}}{RT} = \sum_{i=1}^{NC} x_i v_k^i \left(\ln\Gamma_k - \ln\Gamma_k^i\right) \qquad \text{eq. 5.14}$$

$$\ln\Gamma_k = Q_k\left[1 - \ln\left(\sum_m \theta_m \Psi_{mk}\right) - \sum_m \frac{\theta_m \Psi_{mk}}{\sum_n \theta_n \Psi_{nm}}\right] \qquad \text{eq. 5.15}$$

For compound i: $\varphi_i = \frac{x_i r_i}{\sum_j x_j r_j}, \quad \theta_i = \frac{x_i q_i}{\sum_j x_j q_j}$ eq. 5.16

$$r_i = \sum_{k=1}^{NG} v_k^i R_k, \quad q_i = \sum_{k=1}^{NG} v_k^i Q_k \qquad \text{eq. 5.17}$$

For group m: $\theta_m = \frac{X_m Q_m}{\sum_n X_n Q_n}, \; X_m = \frac{\sum_j v_m^j x_j}{\sum_j \sum_n v_n^j x_j},$ eq. 5.18

where m, n, k are referred to UNIFAC groups, NC is the number of components in the mixture, NG the number of the UNIFAC groups comprising a component, v_k^i is the number of group k in molecule i, x_i the mol fraction of compound i, R_k the van der

Waals volume parameter of group k, Q_k the surface parameter of group k, φ_i the volume fraction of component i and θ_i the surface fraction of component i.

The interaction parameter Ψ_{mk} between groups m and k is a function of temperature, and it is calculated through eq. 5.19,

$$\Psi_{mk} = exp\left[-\frac{A_{mk} + B_{mk}(T - 298.15) + C_{mk}(T - 298.15)^2}{T}\right] \qquad \text{eq. 5.19}$$

where A_{mk}, B_{mk} and C_{mk} are binary adjustable interaction parameters. The zero pressure reference approach permits the use of the already existent UNIFAC tables. In this work the UNIFAC IPs of Hansen et al.[42] are implemented, while the for the gaseous components, such as methane, ethane etc. the parameters of Louli et al.[43] are utilized.

The UNIFAC structural surface area and volume parameters (R_i, Q_i) used in UMR-PRU are summarized in Table 5.3.

Table 5.3: UNIFAC structural van der Waals volume (R_i) and area (Q_i) parameters for group i, used in the UMR-PRU model.

Group	R_i	Q_i
CO_2	1.2960	1.2610
N_2	0.9340	0.9850
CH_4	1.1290	1.1240
C_2H_6	1.8022	1.6960
CH_3	0.9011	0.8480
CH_2	0.6744	0.5400
CH	0.4469	0.2280
C	0.2195	0.0000
ACH	0.5313	0.4000
AC	0.3652	0.1200
$ACCH_3$	1.2663	0.9680
$ACCH_2$	1.0396	0.6600
ACCH	0.8121	0.3480
H_2O	0.9200	1.4000
CH_3OH	1.4311	1.4320
etOH	2.1054	1.9720
MEG	2.4088	2.2480
TEG	5.5942	4.8800
OH	1.0000	1.2000

For the polar components with the gaseous groups (CO_2, N_2, CH_4, C_2H_6), the UMR-PRU IPs have been fitted in this work by correlating binary phase equilibrium data. The analytic procedure and details, such as the database for fitting the IPs, are presented in Section 7.3 and Appendix A. In order to better describe the liquid – liquid equilibria of hydrocarbons with water, the UNIFAC parameters between the groups of hydrocarbons and water are re-estimated. Table 5.4 presents the temperature dependent IPs of the UMR-PRU model used in this work.

Table 5.4: UNIFAC group interaction parameters for UMR-PRU following the temperature dependency of eq. 5.19.

n	*m*	A_{nm} (K)	B_{nm} (-)	C_{nm} (K^{-1})	A_{mn} (K)	B_{mn} (-)	C_{mn} (K^{-1})
CO_2	CH_2	68.56	-0.8739	-0.000080	90.68	-0.5714	0.005770
CO_2	ACH	16.20	-2.2538	0.001050	94.49	1.5570	0.007850
CO_2	ACCH	-102.70	-3.0502	0.012000	274.36	15.5931	0.012930
CO_2	C_2H_6	92.20	-0.6847	0	110.50	-0.3805	0
N_2	CH_4	-141.07	-0.8494	0	192.06	0.7909	0
N_2	C_2H_6	-157.17	-0.9411	0	308.97	1.0030	0
N_2	CO_2	-128.17	-1.6650	0	366.62	1.5300	0
N_2	CH_2	833.27	-2.5383	0.036193	-190.64	-0.9754	-0.001980
N_2	ACH	363.68	1.8010	-0.006569	37.23	-1.2050	-0.001061
N_2	ACCH	264.19	-3.6140	0.015020	122.55	0.5598	-0.003968
CH_4	CO_2	85.80	-0.1959	0	126.21	-0.4439	0
CH_4	C_2H_6	79.06	0.2497	0	-56.01	-0.1798	0
CH_4	CH_2	555.48	2.8287	-0.010592	-268.42	-1.2346	0.001094
CH_4	ACH	108.99	1.6950	0.000509	-63.53	-1.3050	0.002178
CH_4	ACCH	169.99	-3.1420	0.010180	-88.33	1.3930	-0.008429
C_2H_6	CH_2	-73.88	-0.4092	0.000065	61.45	0.1126	0.000955
C_2H_6	ACH	-104.18	0.1872	0	171.39	-0.7241	0
C_2H_6	ACCH	-240.46	-1.2151	-0.000086	674.59	2.5318	0.051615
H_2O	CH_4	642.84	5.1182	-0.013506	1439.17	-6.87672	0.018497
H_2O	C_2H_6	549.86	3.0874	-0.007000	1490.90	-3.0931	-0.005000
H_2O	CO_2	238.53	2.5382	0.001723	794.50	-4.6872	0.003950
H_2O	N_2	807.57	6.0191	-0.019880	3000.00	0	0
H_2O	CH_2	425.51	2.3347	-0.010620	1303.83	-4.3634	0.006676
H_2O	ACH	261.18	1.0780	-0.005283	820.93	-2.9670	0.002283
H_2O	ACCH	219.27	3.2111	-0.015400	1131.26	-6.6481	0.026300
H_2O	CH_3OH	28.66	4.096	0	-34.07	-2.069	0
H_2O	MEG	-188.03	0.0	0	66.72	0	0
H_2O	TEG	472.57	-1.4976	0	-362.51	0.3311	0
CH_3OH	CO_2	-81.43	0.7278	0.005110	438.59	-1.0752	0.096718
CH_3OH	N_2	157.38	-0.3731	0.000391	583.38	3.9399	0.000500
CH_3OH	CH_4	-18.94	1.0329	0.012878	839.66	-6.7000	-0.006070
CH_3OH	C_2H_6	156.75	1.5900	0.004300	173.38	-0.9464	0.000100
CH_3OH	CH_2	28.03	-1.1030	0	617.00	3.838	0
CH_3OH	ACH	-44.29	0.2903	0	594.40	-1.204	0

Table 5.4 (continued)

n	*m*	A_{nm} (K)	B_{nm} (-)	C_{nm} (K^{-1})	A_{mn} (K)	B_{mn} (-)	C_{mn} (K^{-1})
CH_3OH	ACCH	217.80	-4.0190	0	548.80	19.55	0
CH_3OH	MEG	221.00	-4.4310	0	-168.70	6.0080	0
MEG	CO_2	218.39	-5.6585	0.030200	135.72	8.4768	0.143800
MEG	N_2	500.41	3.9826	0	635.01	-6.7326	0
MEG	CH_4	286.83	0.9565	-0.009268	1279.79	-2.5213	-0.005195
MEG	C_2H_6	257.33	1.3800	0.004300	525.04	-4.3369	0.008900
MEG	CH_2	-79.67	2.1360	0	1425.00	11.500	0
MEG	ACH	155.60	-0.5324	0	266.70	1.057	0
MEG	ACCH	2127.00	-11.9000	0	1714.00	4.024	0
TEG	CO_2	-103.95	1.5947	0.004961	372.26	-4.2923	0.007164
TEG	N_2	592.37	-1.3372	0	347.58	2.6335	0
TEG	CH_4	225.27	-3.9421	0.011400	194.03	6.0149	0.037400
TEG	C_2H_6	4.06	-0.9091	0.001700	1164.88	-3.6733	0.000200
TEG	CH_2	103.84	-0.6775	0.000500	291.99	1.1706	-0.008300
TEG	ACH	-13.11	-0.8810	0	158.47	1.3927	0
TEG	ACCH	-120.77	1.9055	0	966.73	-5.4262	0

5.3.2. TST/NRTL model

Twu et al.[44, 45] developed a cubic EoS/A^E mixing rule by combining the Twu – Sim – Tassone (TST) EoS with the NRTL[3] model through zero – pressure mixing rules.[46] In this essence, they describe the non-ideal binaries, such as the TEG/water through the advanced mixing rules, while for the traditional components, e.g. hydrocarbons, the model reverts to the TST EoS. eq. 5.20 - eq. 5.24 present the TST EoS, where T_c and P_c are the compound critical temperature and pressure. The alpha function of the attractive term is the one proposed by Twu et al.[47] as described in eq. 5.23, where *L*, *M* and *N* are compound specific pure component parameters determined by fitting vapor pressure data.

$$P = \frac{RT}{v-b} - \frac{a}{(v+3\cdot b)(v-0.5\cdot b)} \qquad \text{eq. 5.20}$$

$$a = a_c \cdot \mathrm{a(T)} \qquad \text{eq. 5.21}$$

$$a_c = 0.470507\frac{(RT_c)^2}{P_c} \qquad \text{eq. 5.22}$$

$$\mathrm{a}(T) = T_r^{N(M-1)} e^{L(1-T_r^{NM})} \qquad \text{eq. 5.23}$$

$$b = 0.0740740\frac{RT_c}{P_c} \qquad \text{eq. 5.24}$$

The zero pressure mixing rules are expressed by eq. 5.25 - eq. 5.30. The TST zero – pressure mixing rules assume that the excess Helmholtz energy of the van der Waals fluid at zero pressure, $A^E_{0,vdw}$, can be approximated by the excess Helmholtz energy of the van der Waals fluid at infinite pressure, $A^E_{\infty,vdw}$, as per eq. 5.28.

$$a^* = b^* \left[\frac{a^*_{vdw}}{b^*_{vdw}} + \frac{1}{-0.518850}\left(\frac{A^E_0}{RT} - \frac{A^E_{0,vdw}}{RT}\right)\right] \quad \text{eq. 5.25}$$

$$a^* = \frac{Pa}{(RT)^2} \quad \text{eq. 5.26}$$

$$b^* = \frac{Pb}{RT} \quad \text{eq. 5.27}$$

$$\frac{A^E_{0,vdw}}{RT} = \frac{A^E_{\infty,vdw}}{RT} = -0.59413 \cdot \left[\frac{a^*_{vdw}}{b^*_{vdw}} + \sum_i x_i \frac{a^*_i}{b^*_i}\right] \quad \text{eq. 5.28}$$

$$b = b_{vdw} = \sum_i \sum_j x_i x_j\, b_{ij} \ \text{ with } \ b_{ij} = \frac{b_i + b_j}{2} \quad \text{eq. 5.29}$$

$$a_{vdw} = \sum_i \sum_j x_i x_j a_{ij} \ \ with \ \ a_{ij} = \sqrt{a_i a_j}(1 - k_{ij}) \quad \text{eq. 5.30}$$

Since A^E_o in eq. 5.25 is at zero – pressure, its value is identical to the excess Gibbs free energy G^E at zero – pressure. Twu et al.[46] proposed a multicomponent equation for G^E that has the same structural form with the NRTL activity coefficient model, as shown in eq. 5.31 - eq. 5.33,

$$\frac{G^E}{RT} = \sum_i^n x_j \frac{\sum_j^n x_j \tau_{ji} G_{ji}}{\sum_k^n x_k G_{ki}} \quad \text{eq. 5.31}$$

$$\tau_{ji} = \frac{A_{ji}}{T} + B_{ji} \quad \text{eq. 5.32}$$

$$G_{ji} = \exp(-\alpha_{ji}\tau_{ji}) \quad \text{eq. 5.33}$$

where A_{ji}, B_{ji} and α_{ji} are the NRTL interaction parameters. The pure component and binary interaction parameters for the TEG/water binary mixture are taken from Twu et al.[46], while for the rest from the Aspen HYSYS® (Hysys) vs 8.8 database.

5.4. Models directly accounting for association

It is well known that the cubic EoS in their classical approach do not yield very satisfactory results in the modelling of the vapor – liquid – liquid equilibrium (VLLE) of hydrocarbons with polar components, such as water, alcohols and glycols. Although their combination with activity coefficient models as it has been shown in Section 5.3 results in adequate modelling of such systems, in case of mixtures which have intense hydrogen bonding character they often fail to describe well the multiphase, multicomponent equilibria. The need for more accurate calculations, especially for the highly immiscible systems, gave birth to the need of developing models that directly account for the associating forces. The basis of those models is Wertheim's first order theory of perturbation[14-17], as taken from statistical mechanics, where specific associating sites are assigned to each component, based on its structure. Two models are considered in this thesis, the cubic plus association (CPA-PR) EoS[22, 48] and a more complex EoS belonging to the SAFT family, the perturbed – chain statistical associating fluid theory (PC-SAFT).

5.4.1. Cubic Plus Association (CPA-PR) EoS

CPA-PR EoS combines the simplicity of a cubic equation of state (in this case the Peng – Robinson) and the association term derived from Wertheim's first order perturbation theory, as it is applied in the SAFT formulation. The PR EoS accounts for the physical interactions between the molecules, while the association term takes into account the specific site – site interactions due to associating forces between like molecules (self-association) and unlike molecules (cross-association or solvation). The SAFT formulation proposed by Chapman[49] is also adopted in the CPA. To that end, the activity of each bonding site is assumed independent of the other bonding sites on the same molecule. Therefore, steric hindrance effects, if not implicitly introduced, are neglected. Furthermore, no site on the same molecule can bond simultaneously two different sites of another molecule, and double bonding between molecules is not allowed. Hence, ring–like bonding structures are neglected and only tree–like formations are included. The latter are considered in Wertheim's second and third order theory[50]. Several versions of CPA have been proposed in the literature to explicitly account for other forces, such as the quadrupole CPA[51] (qCPA) which accounts for the quadrupole moment of molecules such as CO_2, or the electrolyte CPA[52, 53] (eCPA) which specifically considers the electrolytic interactions. In this work, no such interactions are explicitly accounted for, while the CPA-PR as it is introduced by Perakis et al.[54] is employed. Actually, the concept is the same with that of the original CPA proposed by Kontogeorgis et al.[22] where for the physical term the PR EoS is considered in contrast to the SRK, as per eq. 5.34,

$$P = \frac{RT}{v-b} - \frac{a}{v(v+b)+b(v-b)} - \frac{1}{2\rho RT}\left(1+\rho\frac{\partial lng}{\partial \rho}\right)\sum_i\sum_{Ai} x_i\,[d(Ai)](1-X_{Ai})$$

eq. 5.34

where R is the ideal gas constant, T the temperature, P the pressure, $\rho = 1 / v$ the molar density, g the radial distribution function, x_i is the analytical mol fraction of the component i in the mixture and $d(A_i)$ is the number of association sites of type A in molecule i.

The attractive parameter, a, required for the physical term is calculated by eq. 5.35. The temperature dependency of the attractive parameter of Boston and Mathias[55] and Mathias et al.[55], as it is proposed by Perakis et al.[54] is utilized as per eq. 5.36 - eq. 5.38.

$$a = a_c \, \mathrm{a(T)} \qquad \text{eq. 5.35}$$

$$\mathrm{a}(T) = [1 + m(1 - T_r^{0.5}) - p(1 - T_r)(0.7 - T_r)]^2, T_r \leq 1$$
$$\mathrm{a}(T) = [exp((1 - 1/d)(1 - T_r^d))]^2, \qquad T_r > 1 \qquad \text{eq. 5.36}$$

$$m = 0.37464 + 1.54226\omega - 0.26992\omega^2 \qquad \text{eq. 5.37}$$

$$d = 1 + \frac{m}{2} + 0.3p \qquad \text{eq. 5.38}$$

The parameter, p, is set to zero since the acentric factor has been fitted to experimental vapor pressure and liquid density data.

Additionally, X^{A_i} in eq. 5.34 is the mol fraction of the molecule i not bonded at site A, which is calculated by eq. 5.39.

$$X_{Ai} = \left(1 + \rho \sum_i \sum_{Bj} x_j X^{Bj} \Delta^{AiBj}\right)^{-1} \qquad \text{eq. 5.39}$$

The associating strength $\Delta^{A_iB_j}$ between the associating sites A and B in the components i and j respectively, is calculated by eq. 5.40,

$$\Delta^{A_iB_j} = g\left[exp\left(\frac{\varepsilon^{A_iB_j}}{RT}\right) - 1\right] \mathrm{b}\beta^{A_iB_j} \qquad \text{eq. 5.40}$$

where g is the radial distribution function which derives from the SAFT formulation, b the co-volume of the EoS, $\varepsilon^{A_iB_j}$ the association energy and $\beta^{A_iB_j}$ the associating volume between the associating sites A and B in the components i and j.

The radial distribution function, g, in CPA is defined analogically to the SAFT formulation as that of a hard – sphere fluid, through the Carnahan – Starling EoS[56] as in eq. 5.41,

$$g = \frac{(1 - y/2)}{(1 - y)^3} \qquad \text{eq. 5.41}$$

where $y = \frac{b\rho}{4}$ is the reduced packing factor. As discussed in the original CPA publication[22], this approximation is considered in order to use a molecular–based formulation instead of a segment–based one.

In the original CPA formulation three pure component parameters (b, a_0 and c_1) are required for the non-associating compounds. However, the critical temperature (T_c) is also needed, increasing thus by one the number of parameters required. In this work, the approach suggested by Perakis et al.[54] for the attractive term parameters is utilized, which is the use of three parameters, namely T_c', P_c' and ω_c' for the non-associating compounds. These correspond to the critical properties of the compounds, where the *prime* (') states that they are not equal to the experimental values, but they are fitted to experimental vapor pressure and liquid density data of the pure substance. This way, the number of the pure component parameters is reduced to three. For the associating components two additional parameters, connected to the hydrogen bond forces are required, namely the association energy, $\varepsilon^{\mathrm{AB}}$, and the associating volume, β^{AB}, between the associating sites *A* and *B* of the molecule. The pure component parameters of the compounds involved in this work are presented on Table 5.5, along with the corresponding deviation in vapor pressure and liquid density.

Table 5.5: Pure component parameters for CPA-PR. The deviation is defined from DIPPR correlation with a temperature step equal to 5 K.

Comp.	Ref.	T_r range	T_c' (K)	P_c' (bar)	ω'	$\varepsilon^{A_iB_j}/R$ (K)	$\beta^{A_iB_j}$	As. S.	%AARD[a] in P^s	%AARD[a] in v_l
N_2	This work	0.53 - 0.99	125.49	32.74	0.0449	-	-	n.a.[b]	0.4	7.3
CO_2	This work	0.72 - 0.98	304.78	74.63	0.2154	-	-	n.a.	0.3	3.8
CO_2	[57]	0.72 - 0.98	259.44	58.42	0.1290	481.1	0.0457	4C	0.3	0.3
CH_4	[57]	0.53 - 0.99	190.80	45.80	0.0092	-	-	n.a	0.4	7.8
C2	[57]	0.41 - 0.99	306.10	48.70	0.0937	-	-	n.a	2.1	6.3
C3	[57]	0.33 - 0.98	371.00	42.50	0.1524	-	-	n.a	2.2	4.1
i-C4	[57]	0.45 - 0.99	405.12	36.17	0.2244	-	-	n.a	5.8	7.8
n-C4	[58]	0.32 - 0.99	425.40	38.10	0.2106	-	-	n.a	2.9	4.4
i-C5	[57]	0.45 - 0.99	458.57	33.70	0.2498	-	-	n.a	2.7	6.3
n-C5	[57]	0.40 - 0.99	470.54	34.59	0.2786	-	-	n.a	1.7	3.3
n-C6	[57]	0.40 - 0.99	508.20	31.10	0.3244	-	-	n.a	3.2	3.7
n-C7	[57]	0.51 - 0.95	542.50	28.70	0.3745	-	-	n.a	0.9	2.2
water	[57]	0.43 - 0.99	305.40	135.62	0.1609	1811.2	0.1062	4C	1.5	0.7
meOH	[57]	0.50 - 0.95	346.61	72.57	0.0640	2771.2	0.0265	2B	1.2	2.0
MEG	This work	0.60 - 0.70	459.40	65.05	0.4805	3218.1	0.1291	2B	1.5	1.2
MEG	This work	0.45 - 0.96	567.36	70.16	0.1104	2371.8	0.0126	4C	0.8	1.6

[a] $\%AARD = \frac{100}{n_p} \cdot \sum_i^{n_p} \frac{abs(X_i^{calc} - X_i^{exp})}{X_i^{exp}}$, where X stands for P^s or v_l and n_p for the number of experimental data points

[b] *n.a. indicates a non-associating compound*

5.4.1.a. *Extension of CPA-PR to mixtures*

When CPA-PR is applied to mixtures, the vdW1f mixing rules are used for the attractive and co-volume parameters of the physical term, as it is described for the cubic EoS through eq. 5.8 - eq. 5.10. The associating term is explicitly extended to mixtures, without the need of any mixing rules.

When cross-associating interactions between the components are present, e.g. for alcohols or glycols with water, combining rules for the associating term are required in order to calculate the value of the association strength in eq. 5.40. As it has been shown in the literature[30], the appropriate selection of combining rules can lead to various results in the phase equilibrium calculations. Following the results of Voutsas et al.[48, 57] the following combining rules are applied where necessary, as they are described in eq. 5.42 - eq. 5.43,

$$\varepsilon^{A_iB_j} = (1 - l_{ij})\frac{\varepsilon^{A_iB_i} + \varepsilon^{A_jB_j}}{2} \qquad \text{eq. 5.42}$$

$$\beta^{A_iB_j} = \sqrt{\beta^{A_iB_i}\beta^{A_jB_j}} \qquad \text{eq. 5.43}$$

where l_{ij} is an adjustable interaction parameter. Actually, its value is set to zero in all cases except of the mixtures of CO_2 with water and methanol, as proposed by Perakis et al.[54].

5.4.1.b. *Association sites*

The association term of CPA-PR and thus its application to phase equilibria calculations depends on the choice of an appropriate association scheme. That is actually the type, e.g. electron donor, electron acceptor, dimer, and the number of association sites assigned to each associating molecule. In this work, the terminology of Huang and Randosz[18] is followed, while the different associating schemes assigned to water, alcohols and glycols are presented in Table 5.6.

Apart from alcohols, water and glycols which are conventional associating components, in Table 5.6 it is observed that the 4C associating scheme has been assigned to CO_2. This approach is based on the results of Pappa et al.[59] and Voutsas et al.[58], where it is shown that the assigning of the 4C associating scheme to CO_2 yields improved results for the CO_2/water mixture. The latter is attributed to the quadrupole moment of the CO_2 molecule, which cannot be accurately described using only the physical term of a cubic EoS. Based on the above, the 4C association scheme is assigned to water, where the bonding symmetry means that all non-bonded fractions are equal. The 2B scheme, i.e. one electron donor and electron acceptor site has been attributed to alcohols. Although the 3B formalism of Huang and Randosz[18] is in better accordance with the structural form of alcohols, it has been shown that the 2B scheme, where the two lone – pair oxygens are considered to be a single site, better describes the phase equilibria.[18, 30] In Section 9.3, a short investigation of the association schemes for

glycols occurs. Based on the work of Derawi et al.[60, 61] the 2B and 4C associating schemes are examined. According to their investigation, although based on their molecular structure at least six association sites are expected, due to steric hindrance and intramolecular hydrogen bonding effects, less associating sites should be considered.

In all examined cases the fraction of monomers (X_l) is equal to the product of the fractions of all non-bonded sites. Due to the symmetrical approach for the 2B and 4C sites considered in this work, the fraction of non-bonded sites is assumed to be equal for all site types, as it is shown in Table 5.6.

Table 5.6: Association schemes used in this work based on the terminology of Huang and Randosz[18].

Species	Formula	Type	Site fractions (X)
alcohols	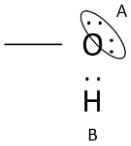	2B	$X^A = X^B$ $X_1 = X^A X^B$
glycols	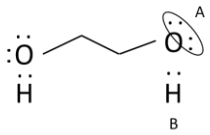	2B	$X^A = X^B$ $X_1 = X^A X^B$
	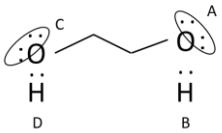	4C	$X^A = X^B = X^C = X^D$ $X_1 = X^A X^B X^C X^D$
water	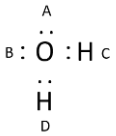	4C	$X^A = X^B = X^C = X^D$ $X_1 = X^A X^B X^C X^D$
CO_2	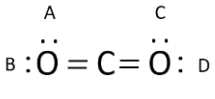	4C	$X^A = X^B = X^C = X^D$ $X_1 = X^A X^B X^C X^D$

5.4.2. Perturbed – Chain Statistical Associating Fluid Theory (PC-SAFT)

One of the most successful attempts to correct the weaknesses of cubic equations of state is the Statistical Associating Fluid Theory (SAFT) family of equations of state, which is rooted on the perturbation theory of Wertheim[14, 15] and has been originally developed by Chapman et al.[49]. In perturbation theory, the potential energy of a relatively complex molecular fluid is described as a summation of the potential energy of a simple reference fluid and a perturbation or correction term. The first term is, usually, accurately known, while the description of the perturbation term is quite challenging. In this essence, if a suitable perturbation term is developed, all the remaining thermodynamic properties can be explicitly calculated using standard thermodynamic expressions. Thus, SAFT–based EoS are written as summations of the residual Helmholtz free energy terms, A^{res}, which occur due to different types of molecular interactions in the system. The residual Helmholtz free energy is equal to the Helmholtz free energy minus that of the ideal gas at the same temperature, T, and density, ρ, as per eq. 5.44. This term is usually a function of temperature, density or pressure, and composition.

$$A^{\mathrm{res}}(\mathrm{T,v,n}) = \mathrm{A}(\mathrm{T,v,n}) - \mathrm{A}^{\mathrm{ideal}}(\mathrm{T,v,n}) = A^{\mathrm{hc}}\left(m,\sigma,\frac{\varepsilon}{k}\right) + A^{\mathrm{disp}} + A^{\mathrm{assoc}} \qquad \text{eq. 5.44}$$

where v is the molar volume and m, σ and $\frac{\varepsilon}{k}$ pure component properties. Exponents hc, $disp$ and $assoc$ denote the hard – chain, dispersion and association contributions to the Helmholtz energy, respectively.

One of the most successful modifications of SAFT, is the Perturbed – Chain SAFT, developed by Gross and Sadowski[20, 21, 62]. The main difference between original SAFT and PC-SAFT is the reference fluid used. Specifically, PC-SAFT uses the hard – chain reference fluid to account for the dispersion interactions unlike SAFT that uses the hard – sphere reference fluid. In the PC-SAFT equation, for non-associating compounds, the residual Helmholtz energy $A^{res}(T,v,n)$ is given as the summation of two terms, the hard – chain (A^{hc}) and the dispersion (A^{disp}), each one representing contributions from the corresponding kind of intermolecular forces. When, associating components are involved, an extra term is considered, A^{assoc}.

The hard – chain term (A^{hc}) is given by eq. 5.45,

$$\frac{A^{hc}}{RT} = \bar{m}\frac{A^{hs}}{RT} - \sum_i x_i(m_i - 1)ln g_{ii}^{hs}(\sigma_{ii}) \qquad \text{eq. 5.45}$$

where m_i is the number of segments in a chain of component I and $\bar{m}$ is the mean segment number in the mixture ($\bar{m} = \sum_i x_i m_i$).

The hard – sphere contribution (A^{hs}) is given by eq. 5.46 - eq. 5.48,

$$\frac{A^{hs}}{RT} = \frac{1}{\zeta_0}\left[\frac{3\zeta_1\zeta_2}{1-\zeta_3} + \frac{{\zeta_2}^3}{\zeta_3(1-\zeta_3)^2} + \left(\frac{{\zeta_2}^3}{{\zeta_3}^2} - \zeta_0\right) ln(1-\zeta_3)\right] \qquad \text{eq. 5.46}$$

$$\zeta_n = \frac{\pi}{6}\rho \sum_i x_i m_i\, d_i^n \qquad \text{eq. 5.47}$$

$$d_i = \sigma_i\left[1 - 0.12exp\left(-3\frac{\varepsilon_i}{kT}\right)\right] \qquad \text{eq. 5.48}$$

where σ_i is the segment diameter, and ε_i is the depth of the potential for the component i. The radial distribution function of the hard sphere fluid (g_{ii}^{hs}) is calculated from eq. 5.49, where the integrals I_1 and I_2 and the compressibility expression C_1 are functions of $\overline{m}$ and the packing fraction n (or ζ_3), while η is the reduced density (eq. 5.50) and, N_{Av}, the Avogadro number.

$$\frac{A^{disp}}{RT} = -2\pi\rho I_1(\eta,\overline{m})\overline{m^2\varepsilon\sigma^3} - \pi\rho\overline{m}C_1(\eta,\overline{m})I_2(\eta,\overline{m})\overline{m^2\varepsilon^2\sigma^3} \qquad \text{eq. 5.49}$$

$$\eta = \frac{\pi N_{Av}}{6}\rho d^3 m \qquad \text{eq. 5.50}$$

The dispersion term is extended to mixtures by assuming the van der Waals one fluid theory approximation, as presented in eq. 5.51 - eq. 5.52.

$$\overline{m^2\varepsilon\sigma^3} = \sum_i\sum_j x_i x_j m_i m_j \left(\frac{\varepsilon_{ij}}{kT}\right)\sigma_{ij}^3 \qquad \text{eq. 5.51}$$

$$\overline{m^2\varepsilon^2\sigma^3} = \sum_i\sum_j x_i x_j m_i m_j \left(\frac{\varepsilon_{ij}}{kT}\right)^2\sigma_{ij}^3 \qquad \text{eq. 5.52}$$

The parameters for a pair of unlike segments are obtained by the conventional Berthelot – Lorentz combining rules, as given in eq. 5.53 - eq. 5.54.

$$\sigma_{ij} = \frac{1}{2}(\sigma_i + \sigma_j) \qquad \text{eq. 5.53}$$

$$\varepsilon_{ij} = \sqrt{\varepsilon_i\varepsilon_j}(1 - k_{ij}) \qquad \text{eq. 5.54}$$

The binary interaction parameter, k_{ij}, is introduced to correct the segment – segment interactions of unlike chains. Actually, it is a binary adjustable parameter that is determined by fitting binary phase equilibrium data, similarly to that of cubic EoS.

The associating term is calculated similarly to that of CPA (eq. 5.55),

$$\frac{A^{assoc}}{RT} = \sum_i X_i \left[\sum_{A_i} lnX^{A_i} - \frac{X^{A_i}}{2} \right] + \frac{1}{2} M_i \qquad \text{eq. 5.55}$$

where X^{A_i} is the fraction of molecules i not bonded at site A, which is a function of density and is calculated through eq. 5.56, as a summation on all association sites over all components and, M, the number of association sites on each molecule.

$$X_{Ai} = \left(1 + N_{AV} \sum_i \sum_{Bj} \rho_j X^{Bj} \Delta^{AiBj} \right)^{-1} \qquad \text{eq. 5.56}$$

The association strength, Δ^{AiBj}, is calculated by eq. 5.57,

$$\Delta^{A_iB_j} = d_{ij}^3 g(d_{ij}) \kappa^{A_iB_j} \left[exp\left(\frac{\varepsilon^{A_iB_j}}{kT} \right) - 1 \right] \qquad \text{eq. 5.57}$$

where $d_{ij} = (d_{ii} + d_{jj})/2$ is the hard sphere diameter, g, the radial distribution function, $\frac{\varepsilon^{A_iB_j}}{k}$, the association energy and $\kappa^{A_iB_j}$, the bonding volume.

The radial distribution function for hard spheres, is calculated through the Carnahan – Starling EoS[56] as in eq. 5.58.

$$g = \frac{(2 - \eta)}{2 \cdot (1 - \eta)^3} \qquad \text{eq. 5.58}$$

The extension of the associating term to mixtures is straightforward and no mixing rules are required; yet, for the cross-associating compounds the following combining rules proposed by Wolbach and Sandler[63] are used, as per eq. 5.59 - eq. 5.60.

$$\varepsilon^{A_iB_j} = \frac{1}{2}\left(\varepsilon^{A_iB_i} + \varepsilon^{A_jB_j}\right) \qquad \text{eq. 5.59}$$

$$\kappa^{A_iB_j} = \sqrt{\kappa^{A_iB_i}\kappa^{A_jB_j}} \left(\frac{\sqrt{\sigma_{ii}\sigma_{jj}}}{\frac{1}{2}\left(\sigma_{ii} + \sigma_{jj}\right)} \right)^3 \qquad \text{eq. 5.60}$$

The associating schemes considered in PC-SAFT follow the formalism of Huang and Radosz[18], as proposed in the original PC-SAFT publication[21].

5.5. The GERG-2008 model

Recent equations of state for mixtures are based on multi – fluid approximations and are explicit in the Helmholtz free energy. In this essence, Kunz et al.[23, 24] developed the GERG model, acronym of Group Européen de la Researche Gazière. This model uses equations of state in the form of fundamental equations for each component of the mixture along with further correlation equations to take into account the residual mixture behavior, enabling thus the accurate description of the thermodynamic properties of mixtures in the entire fluid region (i.e., in the homogeneous gas, liquid, and supercritical regions and for vapor – liquid equilibrium states) over wide ranges of temperature, pressure, and composition. For a pure component, it is reduced to the fundamental equation used for the respective substance. The independent mixture variables are the density, ρ, temperature, T, and the vector of the molar composition, $\bar{x}$. The function $\alpha(\rho,T,\bar{x})$ is split into two terms; the first, α^o, represents the properties of ideal gas mixtures, while the second, α^r, accounts for the residual mixture behavior as per eq. 5.61.

$$a(\rho,\mathrm{T},\bar{x}) = \alpha^o(\rho,\mathrm{T},\bar{x}) + \alpha^r(\rho,\mathrm{T},\bar{x}) \qquad \text{eq. 5.61}$$

The dimensionless form of the Helmholtz free energy for the ideal-gas mixture α_o is given by eq. 5.62,

$$\alpha^o(\rho,\mathrm{T},\bar{x}) = \sum_{i=1}^{N} x_i[\alpha_{oi}^0(\rho,T) + lnx_i] \qquad \text{eq. 5.62}$$

where N is the number of components in the mixture and α_{oi}^0 the dimensionless form of the Helmholtz free energy in the ideal-gas state of component i calculated through eq. 5.63.

$$\alpha^o(\rho,\mathrm{T}) = ln\left(\frac{\rho}{\rho_{c,i}}\right) + \frac{R^*}{R} + [n_{oi,1}^o + n_{oi,2}^o\frac{T_{c,i}}{T} + n_{oi,3}^o ln\left(\frac{T_{c,i}}{T}\right) + \sum_{k=4,6} n_{oi,k}^o ln\left|sinh(\theta_{oi,k}^o)\frac{T_{c,i}}{T}\right| - \sum_{k=5,7} n_{o,k}^o ln\left|cosh(\theta_{oi,k}^o)\frac{T_{c,i}}{T}\right|] \qquad \text{eq. 5.63}$$

where $T_{c,i}$ and $\rho_{c,i}$ are the critical properties of the pure components and R the ideal gas constant. The values of the coefficients $n_{o,k}^o$ and the parameters $\theta_{oi,k}^o$ are listed in Table A1 of Appendix A in Kunz and Wagner[23].

The residual part of the Helmholtz free energy of the component i, is given by

$$a_{oi}^r(\delta,\mathrm{T}) = \sum_{k=1}^{K_{PoI,i}} n_{oi,k}^o \delta^{d_{io,k}} \tau^{t_{oi,k}} + \sum_{k=K_{PoI,i}+1}^{K_{PoI,i}+K_{exp,i}} n_{oi,k}^o \delta^{d_{io,k}} \tau^{t_{oi,k}} e^{-\delta^{c_{oi,k}}} \qquad \text{eq. 5.64}$$

where δ is the reduced mixture density and τ is the inverse reduced mixture temperature. The respective values for the coefficients $n_{oi,k}^o$ and the exponents $\delta^{d_{io,k}}$, $\tau^{t_{oi,k}}$, and $c_{oi,k}$ for all considered components are given in Tables A2 to A4 of Appendix

A in Kunz and Wagner[23] and the critical parameters are listed in Table A5 of the same work.

The GERG-2008 EoS covers 18 natural gas components, namely methane, nitrogen, carbon dioxide, ethane, propane, n-butane, isobutane, n-pentane, isopentane, n-hexane, n-heptane, n-octane, hydrogen, oxygen, carbon monoxide, water, helium, and argon and is appropriate for various natural gas applications. The EoS satisfies the demands on the accuracy in the calculation of thermodynamic properties over the entire fluid region and is has been also adopted as an ISO Standard (ISO 20765-2/3) for natural gases.

List of Symbols

Latin Characters

a	attractive term parameter of a cubic EoS (bar·cm^6·mol^{-2})
a_c	constant term of the attractive parameter of a cubic EoS
$a(T)$	term that express the temperature dependency of the attractive parameter of a cubic EoS
A	residual Helmholtz free energy (J·mol^{-1})
A_{ji}	NRTL binary interaction parameters between components i and j (K)
A_{nm}, B_{nm}, C_{nm}	UNIFAC binary interaction parameter between groups n and m
b	co-volume parameter of a cubic EoS (cm^3·mol^{-1})
B_{ji}	NRTL binary interaction parameters between components i and j
c_1, c_2, c_3	Mathias – Copeman parameters
C_1	compressibility expression
d	parameter for the Boston – Mathias expression for the attractive term of an EoS (eq. 5.38)
d_{A_i}	number of associating sites of type A in molecule i
d_i	constants for PR and SRK expressions (i = 0...4)
d_{ii}	hard sphere diameter
g	radial distribution function
G	molar Gibbs free energy (J·mol^{-1})
G_{ij}	NRTL energy parameter between the components i and j
H	molar enthalpy (J·kmol^{-1})
I_1, I_2	integrals
k	a proportion constant connected to the association energy of PC-SAFT
k_{ij}, l_{ij}	binary interaction parameters
L, M, N	Twu alpha function pure component parameters (eq. 5.23)
m	Soave parameter for the expression of the temperature dependency of the attractive term of an EoS

$\overline{m}$	mean segment number in a mixture
m_i	number of segments in a chain of component i
M_i	number of associating sites in molecule i
N_{AV}	Avogadro's number ($N_{AV} = 6.0221409 \cdot 10^{23}$ molecules)
NC	total number of components in a mixture
NG	total number of groups in a component
p	parameter for the Boston – Mathias expression for the attractive term of an EoS (eq. 5.38)
P	pressure (bar)
P^s	vapor pressure (bar)
q_i	relative van der Waals surface area of component i
Q_i	relative van der Waals surface area of group i
R	universal ideal gas constant (83.14 bar·cm^3·mol^{-1}·K^{-1})
r_i	relative van der Waals volume of component i
R_i	relative van der Waals volume of group i
T	absolute temperature (K)
v	molar volume (cm^3·mol^{-1})
v_l	saturated liquid volume (cm^3·mol^{-1})
ν_k^i	the number of group k in molecule i,
X_{A_i}	the fraction of moles of molecule i not bonded at site A (eq. 5.39)
$\bar{x}$	vector of molar composition
x_i	liquid mol fraction of component i
y	the reduced packing factor ($y = b\rho/4$)
y_i	vapor mol fraction of component i

Greek Characters

α_{ji}	NRTL binary interaction parameter between the components i and j
β^{AiBj}	association volume parameter between site A of component i and site B of component j

γ	activity coefficient
$\Gamma_n^{(i)}$	activity of an isolated UNIFAC group *n* in a solution consisting only of molecules of type *i*
Δ^{AiBj}	associating strength between the sites of types *A* and *B* of components *i* and *j* (eq. 5.40)
ε^{AiBj}	association energy parameter between site *A* of component *i* and site *B* of component *j* ($bar \cdot cm^3 \cdot mol^{-1}$)
ε_i	depth of segment of component *i*
η	reduced density (eq. 5.50)
θ_i	UNIFAC surface fraction of component *i*
κ^{AiBj}	bonding volume between site *A* of component *i* and site *B* of component *j*
ρ	molar density ($mol \cdot m^{-3}$)
σ_i	segment diameter of component *i* (Å)
τ_{ji}	NRTL energy parameter between the components *i and j*
φ_i	UNIFAC volume fraction of component *i*
Ψ_{mk}	binary interaction parameter between the UNIFAC groups *m*, *k* for the UMR-PRU model
ω	acentric factor

Superscripts and Subscripts

assoc	association
c	critical property
Calc	Calculated value
disp	dispersion
E	excess
Exp	Experimental value
hc	hard chain
hs	hard sphere
i, j	component in a mixture
k,m,n	UNIFAC groups

l	liquid
o	properties of ideal gas mixture
p	points
r	ideal mixture behavior
r	reduced value of temperature $(T_r = T / T_c)$
ref	reference
res	residual term of the G^E calculated through UNIFAC
s	saturation
SG	Staverman – Guggenheim contribution of the combinatorial term of UNIFAC
vdw	van der Waals
0	zero pressure
∞	infinite pressure
*	reduced property
‘	states that the property is not the experimentally measured one

References

(1) Economou I.G., Tsonopoulos C., Associating models and mixing rules in equations of state for water/hydrocarbon mixtures. *Chemical Engineering Science* **1997,** *52*, (4), 511-525.
(2) Abrams D.S., Prausnitz J.M., Statistical thermodynamics of liquid mixtures: A new expression for the excess Gibbs energy of partly or completely miscible systems. *AIChE Journal* **1975,** *21*, (1), 116-128.
(3) Renon H., Prausnitz J.M., Local compositions in thermodynamic excess functions for liquid mixtures. *AIChE Journal* **1968,** *14*, (1), 135-144.
(4) Anderko A., Phase equilibria in aqueous systems from an equation of state based on the chemical approach. *Fluid Phase Equilibria* **1991,** *65*, (0), 89-110.
(5) Heidemann R.A., Prausnitz J.M., A van der Waals-type equation of state for fluids with associating molecules. *Proceedings of the National Academy of Sciences* **1976,** *73*, (6), 1773-1776.
(6) Ikonomou G.D., Donohue M.D., Thermodynamics of hydrogen-bonded molecules: The associated perturbed anisotropic chain theory. *AIChE Journal* **1986,** *32*, (10), 1716-1725.
(7) Huron M.-J., Vidal J., New mixing rules in simple equations of state for representing vapour-liquid equilibria of strongly non-ideal mixtures. *Fluid Phase Equilibria* **1979,** *3*, (4), 255-271.
(8) Mollerup J., A note on the derivation of mixing rules from excess Gibbs energy models. *Fluid Phase Equilibria* **1986,** *25*, (3), 323-327.
(9) Michelsen M.L., A method for incorporating excess Gibbs energy models in equations of state. *Fluid Phase Equilibria* **1990,** *60*, (1–2), 47-58.
(10) Michelsen M.L., A modified Huron-Vidal mixing rule for cubic equations of state. *Fluid Phase Equilibria* **1990,** *60*, (1–2), 213-219.
(11) Boukouvalas C., Spiliotis N., Coutsikos P., Tzouvaras N., Tassios D., Prediction of vapor-liquid equilibrium with the LCVM model: a linear combination of the Vidal and Michelsen mixing rules coupled with the original UNIFAC and the t-mPR equation of state. *Fluid Phase Equilibria* **1994,** *92*, 75-106.
(12) Holderbaum T., Gmehling J., PSRK: A Group Contribution Equation of State Based on UNIFAC. *Fluid Phase Equilibria* **1991,** *70*, (2–3), 251-265.
(13) Wong D.S.H., Sandler S.I., A theoretically correct mixing rule for cubic equations of state. *AIChE Journal* **1992,** *38*, (5), 671-680.
(14) Wertheim M., Fluids with highly directional attractive forces. II. Thermodynamic perturbation theory and integral equations. *Journal of statistical physics* **1984,** *35*, (1-2), 35-47.
(15) Wertheim M., Fluids with highly directional attractive forces. I. Statistical thermodynamics. *Journal of statistical physics* **1984,** *35*, (1-2), 19-34.
(16) Wertheim M., Fluids with highly directional attractive forces. III. Multiple attraction sites. *Journal of statistical physics* **1986,** *42*, (3-4), 459-476.
(17) Wertheim M., Fluids with highly directional attractive forces. IV. Equilibrium polymerization. *Journal of statistical physics* **1986,** *42*, (3-4), 477-492.
(18) Huang S.H., Radosz M., Equation of state for small, large, polydisperse, and associating molecules. *Industrial & engineering chemistry research* **1990,** *29*, (11), 2284-2294.

(19) Huang S.H., Radosz M., Equation of state for small, large, polydisperse, and associating molecules: extension to fluid mixtures. *Industrial & engineering chemistry research* **1991,** *30*, (8), 1994-2005.
(20) Gross J., Sadowski G., Application of perturbation theory to a hard-chain reference fluid: an equation of state for square-well chains. *Fluid Phase Equilibria* **2000,** *168*, (2), 183-199.
(21) Gross J., Sadowski G., Application of the perturbed-chain SAFT equation of state to associating systems. *Industrial & engineering chemistry research* **2002,** *41*, (22), 5510-5515.
(22) Kontogeorgis G.M., Voutsas E.C., Yakoumis I.V., Tassios D.P., An Equation of State for Associating Fluids. *Industrial & engineering chemistry research* **1996,** *35*, (11), 4310-4318.
(23) Kunz O., Wagner W., The GERG-2008 wide-range equation of state for natural gases and other mixtures: an expansion of GERG-2004. *Journal of Chemical & Engineering Data* **2012,** *57*, (11), 3032-3091.
(24) Kunz O., Klimeck R., Wagner W., Jaeschke M., *The GERG-2004 Wide-Range Equation of State for Natural Gases and Other Mixtures GERG TM15 2007 TECHNICAL MONOGRAPH*. VDI Verlag GmbH 2007.
(25) van der Waals J.D., *Over de Continuiteit van den Gas-en Vloeistoftoestand*. Sijthoff: 1873, *Vol. 1*.
(26) Redlich O., Kwong J., On the Thermodynamics of Solutions. V. An Equation of State. Fugacities of Gaseous Solutions. *Chemical Reviews* **1949,** *44*, (1), 233-244.
(27) Soave G., Equilibrium constants from a modified Redlich-Kwong equation of state. *Chemical Engineering Science* **1972,** *27*, (6), 1197-1203.
(28) Peng D.-Y., Robinson D.B., A new two-constant equation of state. *Industrial & Engineering Chemistry Fundamentals* **1976,** *15*, (1), 59-64.
(29) Peng D.-Y., Robinson D.B., Two and three phase equilibrium calculations for systems containing water. *The Canadian Journal of Chemical Engineering* **1976,** *54*, (5), 595-599.
(30) Kontogeorgis G.M., Folas G.K., *Thermodynamic models for industrial applications: from classical and advanced mixing rules to association theories*. John Wiley & Sons: 2009.
(31) Pitzer K.S., Lippmann D.Z., Curl R.F., Huggins C.M., Petersen D.E., The Volumetric and Thermodynamic Properties of Fluids. II. Compressibility Factor, Vapor Pressure and Entropy of Vaporization1. *Journal of the American Chemical Society* **1955,** *77*, (13), 3433-3440.
(32) Mathias P.M., A versatile phase equilibrium equation of state. *Industrial & Engineering Chemistry Process Design and Development* **1983,** *22*, (3), 385-391.
(33) Mathias P.M., Copeman T.W., Extension of the Peng-Robinson equation of state to complex mixtures: Evaluation of the various forms of the local composition concept. *Fluid Phase Equilibria* **1983,** *13*, (0), 91-108.
(34) Pedersen K.S., Michelsen M.L., Fredheim A.O., Phase equilibrium calculations for unprocessed well streams containing hydrate inhibitors. *Fluid Phase Equilibria* **1996,** *126*, (1), 13-28.
(35) Tassios D.P., *Applied chemical engineering thermodynamics*. Springer: 1993.
(36) Daubert T.E., Danner R.P., Sibul H.,Stebbins C., *Physical and thermodynamic properties of pure chemicals: data compilation*. Hemisphere: New York, 1989.

(37) Dahl S., Fredenslund A., Rasmussen P., The MHV2 model: a UNIFAC-based equation of state model for prediction of gas solubility and vapor-liquid equilibria at low and high pressures. *Industrial & engineering chemistry research* **1991,** *30*, (8), 1936-1945.
(38) Orbey H., Sandler S.I., Wong D.S.H., Accurate equation of state predictions at high temperatures and pressures using the existing UNIFAC model. *Fluid Phase Equilibria* **1993,** *85*, 41-54.
(39) Voutsas E., Louli V., Boukouvalas C., Magoulas K., Tassios D., Thermodynamic property calculations with the universal mixing rule for EoS/GE models: Results with the Peng–Robinson EoS and a UNIFAC model. *Fluid Phase Equilibria* **2006,** *241*, (1–2), 216-228.
40) Voutsas E., Magoulas K., Tassios D., Universal Mixing Rule for Cubic Equations of State Applicable to Symmetric and Asymmetric Systems: Results with the Peng –Robinson Equation of State. *Industrial & engineering chemistry research* **2004,** *43*, (19), 6238-6246.
(41) Voutsas E.C., Tassios D.P., Prediction of Infinite-Dilution Activity Coefficients in Binary Mixtures with UNIFAC. A Critical Evaluation. *Industrial & engineering chemistry research* **1996,** *35*, (4), 1438-1445.
(42) Hansen H.K., Rasmussen P., Fredenslund A., Schiller M.,Gmehling J., Vapor-liquid equilibria by UNIFAC group contribution. 5. Revision and extension. *Industrial & engineering chemistry research* **1991,** *30*, (10), 2352-2355.
(43) Louli V., Pappa G., Boukouvalas C., Skouras S., Solbraa E., Christensen K.O., Voutsas E., Measurement and prediction of dew point curves of natural gas mixtures. *Fluid Phase Equilibria* **2012,** *334*, 1-9.
(44) Twu C.H., Sim W.D., Tassone V., Liquid activity coefficient model for CEOS/AE mixing rules. *Fluid Phase Equilibria* **2001,** *183–184*, 65-74.
(45) Twu C.H., Sim W.D., Tassone V., A versatile liquid activity model for SRK, PR and a new cubic equation-of-state TST. *Fluid Phase Equilibria* **2002,** *194–197*, 385-399.
(46) Twu C.H., Tassone V., Sim W.D., Watanasiri S., Advanced equation of state method for modeling TEG–water for glycol gas dehydration. *Fluid Phase Equilibria* **2005,** *228–229*, (0), 213-221.
(47) Twu C.H., Bluck D., Cunningham J.R., Coon J.E., A cubic equation of state with a new alpha function and a new mixing rule. *Fluid Phase Equilibria* **1991,** *69*, 33-50.
(48) Voutsas E.C., Yakoumis I.V., Tassios D.P., Prediction of phase equilibria in water/alcohol/alkane systems. *Fluid Phase Equilibria* **1999,** *158–160*, (0), 151-163.
(49) Chapman W.G., Gubbins K.E., Jackson G., Radosz M., New reference equation of state for associating liquids. *Industrial & engineering chemistry research* **1990,** *29*, (8), 1709-1721.
(50) Zmpitas W., Gross J., A new equation of state for linear hard chains: Analysis of a third-order expansion of Wertheim's Thermodynamic Perturbation Theory. *Fluid Phase Equilibria* **2016,** *416*, 18-26.
(51) Bjørner M.G., Kontogeorgis G.M., Modeling derivative properties and binary mixtures with CO_2 using the CPA and the quadrupolar CPA equations of state. *Fluid Phase Equilibria* **2016,** *408*, 151-169.
(52) Courtial X., Ferrando N., de Hemptinne J.-C., Mougin P., Electrolyte CPA equation of state for very high temperature and pressure reservoir and basin applications. *Geochimica et Cosmochimica Acta* **2014,** *142*, 1-14.

(53) Maribo-Mogensen B., Thomsen K., Kontogeorgis G.M., An electrolyte CPA equation of state for mixed solvent electrolytes. *AIChE Journal* **2015,** *61*, (9), 2933-2950.
(54) Perakis C., Voutsas E., Magoulas K., Tassios D., Thermodynamic modeling of the vapor–liquid equilibrium of the water/ethanol/CO_2 system. *Fluid Phase Equilibria* **2006,** *243*, (1–2), 142-150.
(55) Boston J., Mathias P., In presented on Second International Conference on Phase Equilib. Fluid Properties Chem. Process Ind., Berlin, March 17–21, **1980**
(56) Carnahan F.N., Starling K.E., Equation of State for Nonattracting Rigid Spheres. *J. Chem. Phys.* **1969,** *51*, 635.
(57) Voutsas E., Perakis C., Pappa G.,Tassios D., An evaluation of the performance of the Cubic-Plus-Association equation of state in mixtures of non-polar, polar and associating compounds: Towards a single model for non-polymeric systems. *Fluid Phase Equilibria* **2007,** *261*, (1–2), 343-350.
(58) Voutsas E.C., Pappa G.D., Magoulas K., Tassios D.P., Vapor liquid equilibrium modeling of alkane systems with Equations of State: "Simplicity versus complexity". *Fluid Phase Equilibria* **2006,** *240*, (2), 127-139.
(59) Pappa G.D., Perakis C., Tsimpanogiannis I.N., Voutsas E.C., Thermodynamic modeling of the vapor–liquid equilibrium of the CO_2/H_2O mixture. *Fluid Phase Equilibria* **2009,** *284*, (1), 56-63.
(60) Derawi S.O., Kontogeorgis G.M., Michelsen M.L.,Stenby E.H., Extension of the Cubic-Plus-Association Equation of State to Glycol–Water Cross-Associating Systems. *Industrial & engineering chemistry research* **2003,** *42*, (7), 1470-1477.
(61) Derawi S.O., Michelsen M.L., Kontogeorgis G.M., Stenby E.H., Application of the CPA equation of state to glycol/hydrocarbons liquid–liquid equilibria. *Fluid Phase Equilibria* **2003,** *209*, (2), 163-184.
(62) Gross J., Sadowski G., Perturbed-Chain SAFT: An Equation of State Based on a Perturbation Theory for Chain Molecules. *Industrial & engineering chemistry research* **2001,** *40*, (4), 1244-1260.
(63) Wolbach J.P., Sandler S.I., Using Molecular Orbital Calculations To Describe the Phase Behavior of Cross-associating Mixtures. *Industrial & engineering chemistry research* **1998,** *37*, (8), 2917-2928.

Chapter 6: Experimental Measurement of the Vapor – Liquid Equilibrium (VLE) of the carbon dioxide/methane mixture at three isotherms

Methane is the major natural gas component, while CO_2 consists one of its major impurities and have to be kept under certain limits. To this purpose, the accurate knowledge of the phase equilibria of CO_2/methane is of utmost interest to the gas industry. In the present Chapter, new VLE experimental data for the CO_2/CH_4 mixture are presented for three isotherms close to the CO_2 critical temperature, namely 293.13 K and 298.14 K and 303.15 K. The experimental data obtained in this study are validated against the existing literature data where available, as well as against the prediction of a state – of – the – art model for natural gas mixtures, GERG-2008. The results and analysis are presented in accordance to the International Union of Pure and Applied Chemistry (IUPAC) guidelines for reporting phase equilibrium measurements, by performing estimation of the standard uncertainty as described in the Guide for the estimation of the Uncertainty in Measurements ("GUM"). The measured data have been correlated using models that belong to different classes. Two cubic equations of state are examined since they are commonly used in industrial practice, SRK and PR combined with the van der Waals one fluid mixing rules. Furthermore, due to the ambiguous nature of CO_2, two more sophisticated approaches are examined, the UMR-PRU model and PC-SAFT.

6.1. Introduction

The knowledge of vapor – liquid equilibrium of binary mixtures is very important for validating thermodynamic models and tuning model parameters, rendering possible the accurate process design and safe operation. Methane is the major natural gas component and while the NG composition at reservoir differs from region to region, in most cases CO_2 consists an important impurity. The typical concentration of CO_2 in NG reservoirs ranges, depending on the field, from 2 % up to 30 %[1]. The latter can be also considered as CO_2 fields, but in several cases, such as at the Netuna field in Indonesia, natural gas production occurs. Moreover, the accurate knowledge of the phase equilibria of this mixture is important for carbon capture and storage (CCS), in which case, methane can be found as an impurity in CO_2 captured from natural gas sweetening process, as well as from pre-combustion carbon capture in power plants[2].

Due to its importance for the natural gas industry the specific mixture has been studied since the 1970s and according to National Institute of Standards and Technology (NIST) literature report[3], twenty three publications of VLE data are available, covering a temperature range from close to the triple point up to the critical point of CO_2, i.e. from 153 K to 301 K, and pressures from 0.27 up to 87.4 bar. Especially the region from 210 K up to 273.15 K is considered well – covered with measurements over the whole phase boundary. In this region, all the phase envelope area is covered and data from different sources are generally in good agreement, as it is presented in Figure 6.1*a* for the isotherm of 270 K, which is a representative one. Lower temperatures basically concern solid – liquid equilibrium, while at higher than about 270 K, several inconsistencies are observed among the experimental data. This deviation among the different data sources is more apparent in the vapor phase solubility. According to Li et al.[2], the most recent publications should be more accurate due to the use of more advanced techniques. Furthermore, in many cases, especially as approaching the critical temperature area, only one source for each available isotherm exists, making, thus, their validation difficult. The only trustworthy means of validation relies to the comparison with the prediction of a sufficiently accurate thermodynamic model.

The data situation per isotherm is discussed in the following. Experimental data covering both liquid and vapor phases are reported in the work of Kaminishi et al.[4] for 283.15 K, without covering the critical mixture area and Nasir et al.[5] who reported several VLE measurements along the bubble and dew point lines. Much scattering is observed (Figure 6.1*b*) between the available publications. At the isotherm of 288.15 K, four data sources are available which are in very good agreement with each other, especially in the area away from the critical point (Figure 6.1*c*). Xu et al.[6] also reported data for the isotherm of 293.15 K, covering the whole phase boundary, which are in fairly good agreement with the recent data of Nasir et al.[5]. Instead, the data of Devlikamov et al.[7] present a higher CO_2 concentration in liquid phase compared to the other sources (Figure 6.1*d*).

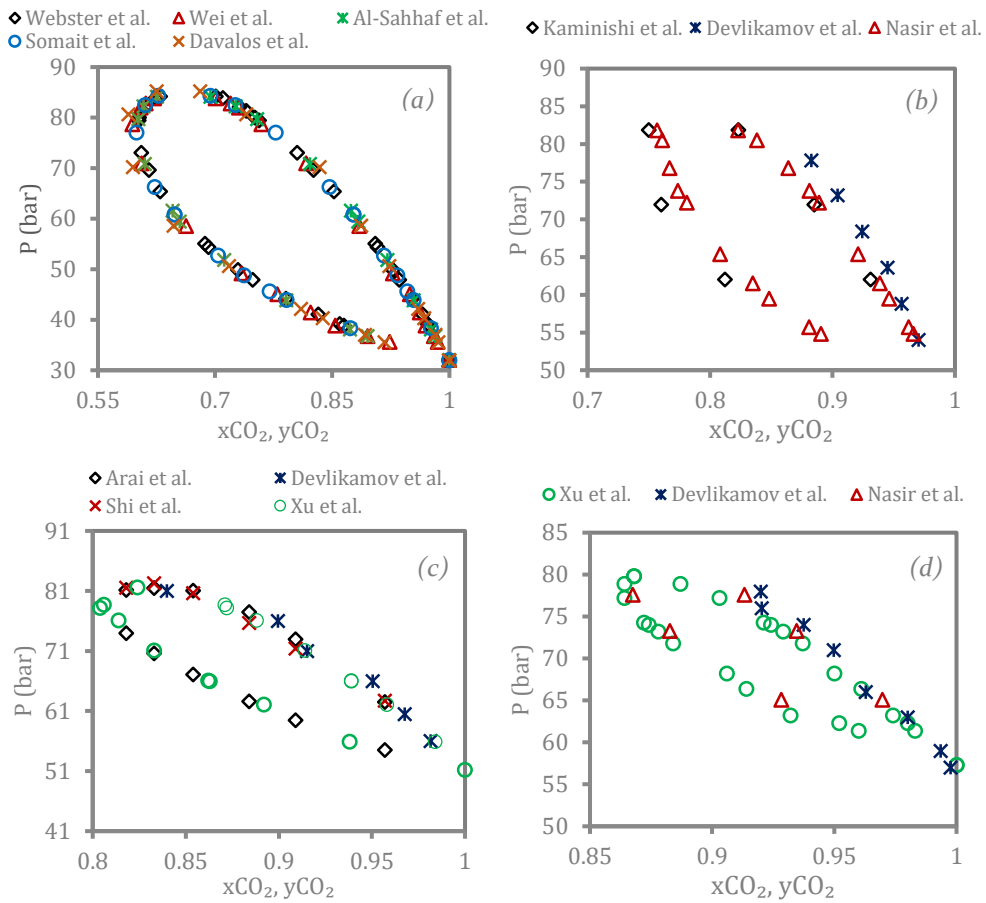

Figure 6.1: Experimental VLE data of CO_2/CH_4 mixture at (a) 270.15 K[8-12], (b) at 283.15 K[4, 5, 7], (c) at 288.15 K[6, 7, 13, 14] and (d) at 293.15 K[5-7].

Recently, Nasir et al.[5] reported the VLE of the CO_2/CH_4 binary for several isotherms ranging from 240 K up to 293 K. Yet, in their work only few data have been reported above 287 K. Meanwhile, the critical mixture area is not sufficiently covered in those isotherms. Finally, Bian et al.[15] measured the VLE close to the critical temperature of CO_2, at 301 K, but away of the critical mixture area. Unfortunately, this is the only isotherm reported by the authors for that mixture, while no further data are available at these conditions. As it is presented in Figure 6.2, the prediction of the SRK EoS with an optimum k_{ij} value equal to 0.0956, as suggested by Perez et al.[16] does not agree with the reported data. Instead, at the isotherm of 223 K, its prediction is in fairly good agreement with most experimental points. Furthermore, the experimental data of the same authors for the N_2/CO_2 mixture are not in good agreement by those of other sources, as it has been shown by Westman et al.[17]. Apart from the publications covering both phases, Devlikamov et al.[7] reported the bubble points of CO_2/CH_4 mixture at four isotherms, which are stated at 278.15 K, 283.15 K, 293.15 K and 298.15 K. Yet, as it has been shown previously, they systematically deviate from the other data sources. As a

result, the highest temperature at which the VLE data of the CO_2/CH_4 mixture are quite accurate is that of 293.15 K.

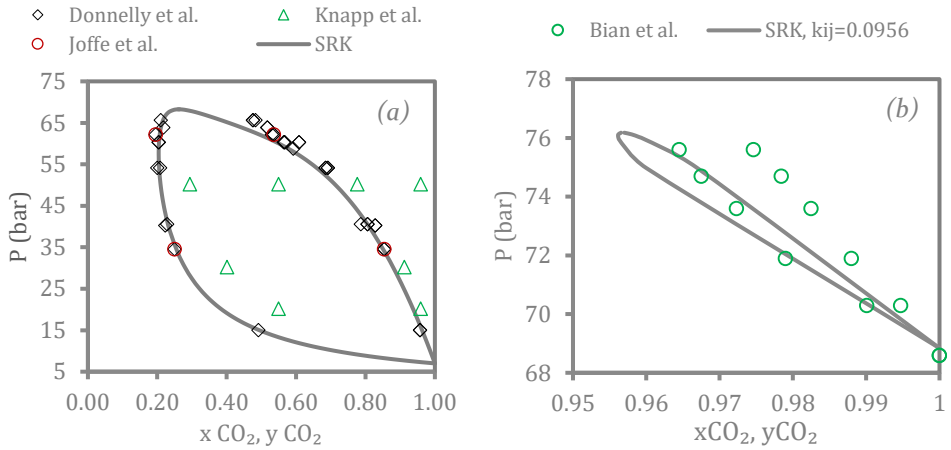

Figure 6.2: VLE of the CO_2/CH_4 at two isotherms and prediction with the SRK EoS with k_{ij} equal to 0.0956 as suggested by Perez et al.[16]. (a) at 223 K. Experimental data by Donelly et al.[18], Knapp et al.[19] and Joffe et al.[20] and (b) at 301 K. Experimental data by Bian et al.[15].

According to Li et al.[2], CCS capture typically involves temperatures above 298.15 K, while the operating window for pipeline transportation is from 273.15 K to 317.15 K[21]. Therefore, new experimental data are required to cover the gaps in the higher temperature area. This can also lead to an extension of the applicability of the thermodynamic models in a higher temperature range. To that purpose VLE data for the CO_2/CH_4 mixture have been measured at three isotherms, namely 293.13 K, 298.14 K and 303.15 K. Emphasis is given in capturing the mixture behavior in the critical region.

6.2. Experimental Section

The vapor – liquid equilibrium measurements were carried out using a static method at the SINTEF Energi facilities, using the apparatus described in Ref.[17] without further modification. A brief description of the apparatus, as well as detailed description of the experimental procedure are given in the following subsections (6.2.1 - 6.2.3). The measurements have been performed using an isothermal analytical method with a variable – volume cell.

6.2.1. Experimental Apparatus

A simplified diagram of the cell and apparatus used to carry out the measurements is presented in Figure 6.3.

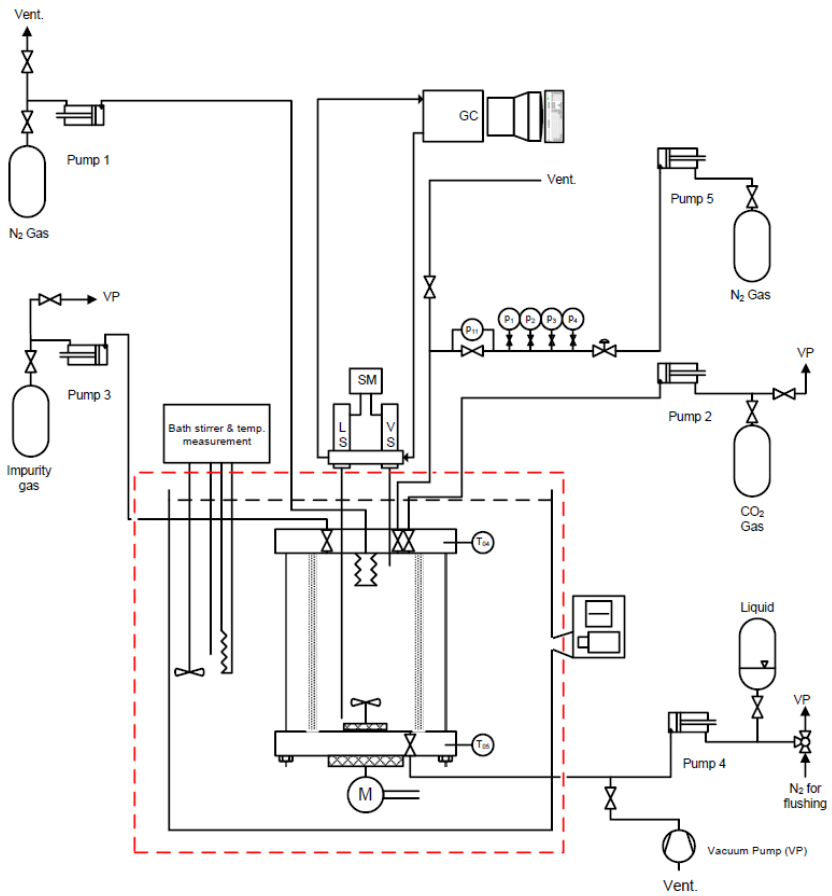

Figure 6.3: Principal diagram of cell and ancillary apparatus. LS,VS: Liquid and vapor phase Rolsi™ samplers, respectively. SM: Rolsi™ controller. M: Gear for rotating permanent magnet below cell, which rotates stirrer inside cell. Gear connected to electric motor outside bath. T_{04}: Top flange SPRT. T_{05}: Bottom flange SPRT. (reproduced from Westman et al.[22])

According to Gibbs' phase rule, for a system of two components with two co-existing phases, only two intensive variables can be independent, in this case the temperature and the pressure. The equilibrium cell, kept at constant temperature using the thermostatic bath, has been filled with both CO_2 and CH_4 so that the two – phase region is reached. Then the composition of both the liquid and vapor phases is determined through an analytical method.

The cell consists of a transparent sapphire cylinder tube placed between two titanium flanges. The internal volume of the cell is approximately 100 ml. To keep the temperature constant, the cell is placed in a thermostatic bath kept at the desired temperature (Fluke Hart Scientific model 6020 with external cooling water for temperatures above ambient). The temperature of the cell is monitored by two Fluke model 5686 glass capsule standard platinum resistance thermometers (SPRT) placed inside the top (T_{04}) and bottom (T_{05}) flanges.

The cell pressure is indirectly measured through a Rosemount 1199 diaphragm connected by an oil-filled circuit to a Rosemount 3051 differential pressure transmitter with an array of four absolute pressure sensors p_i, where i = 1, 2, 3, 4, (Keller model PAA-33X) with full scales of 10, 30, 100 and 200 bar respectively, on the other side. The absolute pressure sensor circuit is filled with nitrogen and is maintained at a pressure such that the differential pressure between this circuit and the cell circuit is close to zero, using syringe Pump 5 (TOP Industrie, model PMHP 100-500).

CO_2 and methane are injected separately into the cell using syringe pumps. Pump 2 is dedicated to the CO_2 injection (model PMHP 100-500) while Pump 3 (model PMHP 200-200) is used for the CH_4 injection. The surface of the parts of the pump and the tubing in contact with the fluid has been sulfinert treated in order to minimize adsorption. Pump 4 (model PMHP 100-500) is out of operation for the specific measurements since it is objected to injection of fluids in liquid state, such as water. All three pumps described above could be evacuated through a connection to a vacuum pump (VP) (Trivac® E 2 from Leybold).

These pumps are connected via tubing to valves integrated in the cell flanges. Integrated valves have been used in order to minimize the dead volume inside the cell. An additional integrated valve can be opened to ventilation for the reduction of the cell pressure. The vacuum pump is connected to an integrated valve, enabling, thus, the evacuation of the cell before its filling with the gases. A magnetic stirrer (M), with a maximum rotation speed of 800 rpm, is placed at the bottom of the cell in order to reduce the time needed to reach equilibrium. A borescope is used for the inspection of the content of the cell through the transparent sapphire cylinder, to ensure that the two-phase region is established and that the liquid level is appropriate.

A custom – made National Instruments LabVIEW program is used for data acquisition of the measured pressure and temperature values, which have been logged every second. The resistance of the two SPRTs is measured one at a time through an ASL SB148 switchbox which change between the two SPRTs, connected to an ASL F650AC thermometry bridge. A resistance measurement point of one resistor is obtained once every 20 s when the ASL bridge is set to obtain the most accurate ratio value. The ASL bridge measured ratio values are obtained by the logging program through a USB connection. The update rates of the four pressure sensors p_i are 400 Hz, and the dead time of the differential pressure sensor p_{11} is approximately 45 ms. The measured pressure values of p_i are obtained by the logging program using the digital output of the sensors through a RS485 serial connection. The values of p_{11} are obtained using a conversion of the analog 4-20 mA DC current output of the sensor to a digital output read through a RS485 serial connection by the logging program.

When equilibrium is established, the compositions of the vapor and liquid phases can be measured by extracting a sample from each phase using a pneumatic version of Rolsi™ (Rapid On Line Sampler – Injector) electromagnetic samplers[23]. The vapor phase sampling capillary inlet is placed close to the top flange inside the cell, while the liquid phase capillary inlet can be moved vertically inside the cell so that it is located

at an appropriate position for the liquid phase sampling. The electromagnetically controlled valves of the Rolsi™ samplers are opened for a specified time period, through the LabVIEW software, to let a sample of appropriate size to flow out of the cell. The sample is routed through the capillaries into a heated gas chromatograph (GC) helium carrier gas circuit at close to atmospheric pressure. The low – pressure side of the Rolsi™ valves and piping between the valves and GC are also heated above the critical temperature of CO_2 (actually at 313.15 K) ensuring, thus, that both the vapor and liquid samples are in gaseous state. The sample is swept by the carrier gas into the GC (Agilent 7890A) equipped with a Supelco Carboxen-1010 PLOT Capillary GC Column (from Sigma – Aldrich, with a column length of 30 m and an internal diameter 0.53 mm) where the CO_2 and CH_4 are separated. Downstream of the column, a thermal conductivity detector (TCD) measures the difference in voltage needed to keep the gas passing the detector at a constant temperature. The detector response is monitored as a function of time at 5 Hz, resulting in two separate peaks corresponding to CH_4 and CO_2. During the sampling, the logging of the detector response is started automatically through the Agilent OpenLAB CDS EZChrom GC data acquisition and control software.

When a sample is extracted, Pump 1 is used to apply an increased N_2 overpressure, from the auxiliary circuit, compared to the cell pressure on a plate bellows inside the cell, to expand the bellows and thereby decrease the cell volume. This way a decrease in cell pressure after the extraction of each sample is prevented. When the bellows are fully expanded, they can cause an approximate volume decrease in the cell of maximum 1 cm^3.

The internal diameter of the Rolsi™ capillaries is 150 mm, and the length of the liquid and vapor phase capillaries are 0.4 and 0.3, respectively. The internal volumes of the liquid and vapor capillaries correspond to approximately 0.007 and 0.005 % of the cell volume, respectively. The upper part of both the liquid and the vapor capillaries are outside the thermostatic bath, and are heated to 313 K to avoid condensation.

As the liquid in the heated upper part of the liquid capillary can boil off, too small samples can only consist of the boil-off gas with a composition that is not representative of the liquid phase in the cell. In order to be sure that the true liquid composition is measured, the number of moles of each liquid sample should at least be as large as the volume of the whole liquid capillary, at the same density and composition as the liquid phase inside the cell. As some of the volume of the liquid sampler is occupied by a vapor phase with lower density than the liquid one, the calculated liquid sample size is probably an overestimate, but it helps to ensure the thorough flushing of the liquid capillary for each sample. Because the sample size should be sufficient to flush the capillaries, the expansion of the bellows is necessary to prevent a significant change in the cell pressure. For the vapor samples, the first sample of a series at a pressure/temperature point is of a sufficient size to flush the vapor capillary. Consecutive sample sizes are set large enough to give a good repeatability in the composition measurements. The repeatability as a function of

sample size is determined from the calibration of the GC using the calibration gas mixtures. Practically, this is translated to an estimation of the sample volumes from the GC traces. The liquid phase density and composition are calculated using the GERG-2008 EoS at the cell pressure and temperature. An estimate of the number of moles in a sample as a function of the peak areas of each component in the GC traces has been established by injecting each of the components into the GC through a sample loop with a known volume, kept at ambient temperature and slightly higher than atmospheric pressure. The densities of the pure components are calculated using the Span – Wagner[24] EoS, which yields very accurately the CO_2 one, since at the examined conditions mostly CO_2 is expected in the mixture.

6.2.2. Calibration

The calibration of the temperature and pressure sensors performed by Westman et al.[17] has been used to perform the experiments and it has been performed in-house. The temperature sensors have been calibrated against fixed point cells according to the International Temperature Scale of 1990 (ITS-90), while the pressure sensors against a recently calibrated dead weight tester. Details concerning the estimated temperature and pressure measurement uncertainties are discussed in Section 6.2.4. The GC has been calibrated against calibration gas mixtures prepared in-house using a custom – built apparatus for the gravimetric preparation of the mixtures. The manufacturer's specifications of the purities of these samples are given in Table 6.1, while no further analysis of the specified purities has been performed. However, as the vapor pressure measurements of CO_2 have been performed at the different temperatures, it is asserted that the vapor pressures are in agreement with the calculated vapor pressures from Span – Wagner EoS, within the combined uncertainty of the pressure measurements and the EoS calculations.

Table 6.1: Characteristics of pure chemicals used.

Chemical Name	Cas No	Source	Initial mol fraction purity	Purification method	Final mol fraction purity	Analysis method
CO_2[a]	124-38-9	AGA	0.999992	None	0.999992	None
CH_4[b]	74-82-8	AGA	0.999995	None	0.999995	None
He[c]	7440-59-7	AGA	0.999999	None	0.999999	None

[a] Maximum specified impurity content by volume is less than 3 ppm H_2O, 1 ppm O_2, 2 ppm N_2, 1 ppm and hydrocarbons C_nH_m.

[b] Maximum specified impurity content by volume is less than 2 ppm H_2O, 0.5 ppm O_2, 4 ppm N_2, 1 ppm other hydrocarbons C_nH_m and 0.1 ppm H_2.

[c] GC carrier gas.

6.2.3. Experimental Procedure

Two different procedures are followed; the first is for the region away of the critical mixture area, while the second is used in order to estimate the critical point of the mixture.

6.2.3.a. *Away from the critical region*

The measurements are performed using an isothermal analytical method with a variable volume cell with the temperature and the pressure as independent variables, as described above. The equilibrium cell is kept at constant temperature using a thermostat bath and is filled with CO_2 and a mixture of CO_2/CH_4 until the target pressure is obtained. The use of the latter as input is justified in order to avoid the input of pure methane, which is explosive. Instead, in lower concentration that 40 % molar in its mixture with CO_2, it is not considered as explosive and thus no further certification of the apparatus is required. The coexistence of the two phases is confirmed visually through a borescope, which is directly connected to a monitor. The experimental procedure is briefly described in the following. Before the start of a VLE experiment, the whole system is evacuated through the vacuum pump to ensure no contamination of the pipelines, the pumps or the equilibrium cell. Specifically, the CO_2 pump (Pump 2), the impurity mixture pump (Pump 3) and their respective lines are evacuated once and then are flushed with their respective gas. The flushing and evacuation procedure is repeated five times in total to remove any impurities remaining in the cell. After the final flushing and evacuation, the gases are filled to their respective lines and pumps and remain at a pressure of at least 5 bar to prevent any contamination. Then, the same procedure is repeated for the equilibrium cell. After setting the required temperature of the thermostatic bath, the cell is filled with CO_2 until the liquid level is about 40 % of the cell volume. The stirrer runs until the temperature and the pressure are stabilized. If the measured vapor pressure is within the uncertainty limits of the Span – Wagner EoS, the setting of the bath is deemed appropriate.

After the CO_2 vapor pressure measurements, methane, in the form of a CO_2/CH_4 mixture, is injected to the cell through Pump 3, until the specified pressure is obtained. The liquid level of the cell is adjusted either by injecting more CO_2 or by venting out some liquid from the bottom of the cell. A representative picture taken through the borescope showing the vapor – liquid interface between the two phases before the stabilization of equilibrium, is depicted in Figure 6.4. The mixture is stirred to equilibrium (600 rpm) and when the temperature and the pressure indications are stabilized for about thirty minutes, the stirrer is turned off and the mixture is left to settle before the start of the sampling. The settling time ranges from thirty minutes to three hours, depending on the proximity to the critical region. Specifically, where the density difference between the vapor and the liquid phase is significant, that is away from the critical region, the settling time is set to thirty minutes, while when approaching the critical region the settling time is increased to one hour. During the settling time, the borescope is inserted into the bath to check the liquid level and then

is quickly removed to ensure that no additional heat transfer affects the equilibrium. When the settling period has been completed, the sampling of both phases starts, beginning with the liquid phase and continuing with the vapor one, by taking six samples from the liquid phase and seven from the vapor, respectively. The samples are withdrawn from the cell every 32 minutes, which is sufficient time to capture the whole CO_2 peak in the chromatogram, as well as for the two phases to settle after the restoration of equilibrium. During sampling, nitrogen in overpressure from the auxiliary circuit is injected through Pump 1 to the bellows plate in the cell to compensate for the decrease in pressure caused from the removal of the sample volume. This procedure is not followed during the VLE measurements at the isotherm of 303.15 K, since the use of the bellows seems to have no significant effect. This is probably due to the high CO_2 concentration, as well as the small differences in density between the two phases. Hence, the bellows' pressure control system does not work and the bellows are not used in the measurements. The first sample of each phase is discarded as flushing sample, while no specific ascending or descending trend has been observed in the series of the remaining samples, which indicates that there is sufficient settling time between each sample.

Figure 6.4: Borescope picture of liquid and vapor interface for 303.15 K and 73.5 bar.

The pressure readings are retrieved from the sensors every second and the resistance values of the temperature sensors are recorded approximately every 20 seconds. The temperature and pressure measurements from the stable period before the withdrawal of the first sample until the end of sampling are used to calculate the VLE data set, following a procedure which is discussed in detail in Section 6.2.5.

6.2.3.b. *Critical Region*

A special procedure is followed for pressures close to the critical point of the mixture for each isotherm, which permits the accurate capturing of the critical area and thus the overall shape of the phase boundary. In this case, the pressure is first increased conventionally, by injecting the CO_2/CH_4 mixture into the cell using Pump 3. The proximity to the critical point is established by a step – by – step increase of the pressure up to the point that the supercritical region is temporarily reached and the mixture reverts to the two – phase region upon reaching the equilibrium. This way, the

critical pressure is identified within a narrow interval, of the order of 0.1 bar. Having established the two-phase region at a point close to the critical one, the stirrer runs from 45 minutes to about one hour and then the mixture is left to settle for 2 - 3 hours. The increased settling time is justified because of the proximity to the critical region, where the densities of both phases are very similar and thus the mass transfer coefficient is lower. After the settling period, five or six samples are taken from the liquid phase, and seven samples are taken from the vapor phase with a 32 minutes period between the opening of the Rolsi™ samplers. During sampling, the bellow plate system is used to compensate for the pressure decrease, with the exception of the isotherm of 303.15 K where this procedure is not necessary as discussed above. After the completion of the VLE measurement, the pressure is slightly decreased by taking samples from the vapor and the liquid phase without using the bellows. The same procedure, that is stirring to the new equilibrium VLE point, waiting for the two phases to settle and finally sampling of the liquid and vapor phase, is repeated until the critical region is sufficiently captured.

6.2.4. Uncertainty Analysis

Special care has been taken to present the results and analysis in accordance with the IUPAC Guidelines for reporting of phase equilibrium measurements given in the work by Chirico et al.[25]. In particular, a thorough estimation of the standard uncertainties, as specified in the ISO Guide for the Estimation of Uncertainty in Measurement, commonly referred to as "GUM"[26], is performed.

6.2.4.a. *Definitions*

The terms and the definitions of the "GUM"[26] are used in the uncertainty analysis. The uncertainty components are evaluated as standard uncertainties, with symbol $u(y)$, where y is the estimate of the measurand, Y, that is the measurement result. $s(y)$ is the standard deviation calculated from the samples of y, and is the estimate for minimum contribution to standard uncertainty from random errors in y. The propagation of the standard uncertainties in the input quantities, X_i, to the standard uncertainty in the final measurand, Y, is expressed through the combined standard uncertainty, $u_c(y)$.

6.2.4.b. *Temperature and Pressure*

The uncertainty analysis for the pressure and the temperature measurements has been given in detail by Westman et al.[17] and they are only briefly discussed here. When the contributions cannot be assumed to be independent, the most conservative estimate is assumed.

As mentioned in the equipment description (Section 6.2.1), the equilibrium pressure at the vapor – liquid interface, p, is measured indirectly. The setup, along with the respective regions of interest is shown in Figure 6.5.

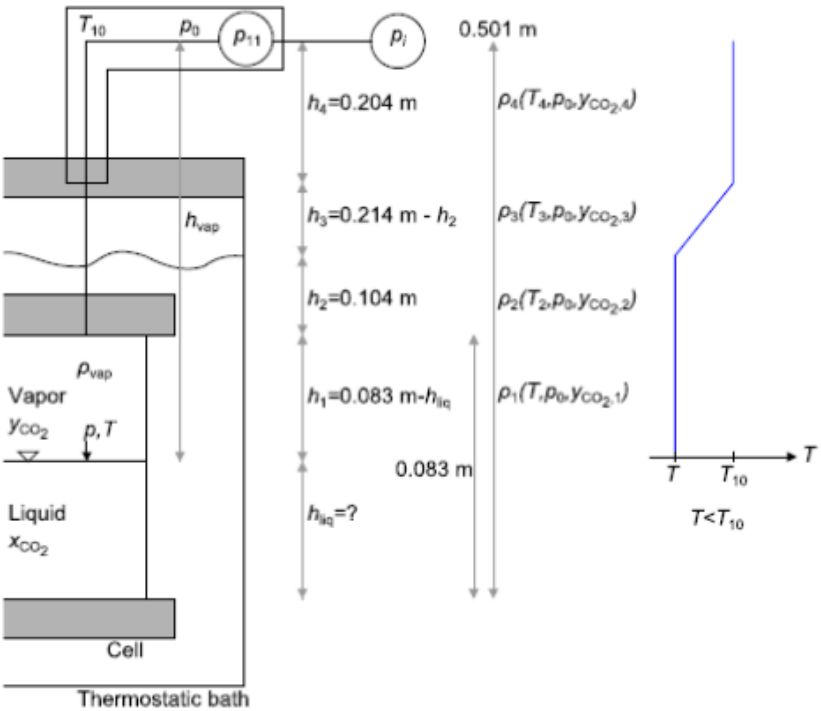

Figure 6.5: Schematic depiction of the pressure measurement system, where the different contributions affecting the overall pressure are shown.[17]

The absolute pressure sensor in use for a given experiment is designated as p_i, where the index i = 1, 2, 3, 4 corresponds to the sensor in use, in this case sensor 3, with increasing full – scale pressure for increasing indices. The differential pressure transducer, designated p_{11}, is placed at the same elevation as the p_i sensors, to avoid a pressure difference due to a hydrostatic pressure. The differential pressure sensor and the tubing going down to the cell are heated to a temperature T_{10} above the cell temperature, to avoid condensation of the vapor phase in the tubing. Using these definitions, the pressure on the cell circuit side of the differential pressure sensor can be stated as $p_0 = p_i + p_{11}$. When equilibrium is reached, the pressure at the vapor – liquid interface, p, is equal to p_0 plus the hydrostatic pressure of the fluid in the vertical distance between the position where p_0 is measured and the vapor – liquid interface. This hydrostatic pressure is designated as p_{hs}. The pressure at the vapor – liquid interface can be then stated as per eq. 6.1.

$$p = p_i + p_{11} + p_{hs} \qquad \text{eq. 6.1}$$

As the hydrostatic pressure, p_{hs}, is a function of the absolute pressure, p_i, and p_{11} changes with the change in p_i, the three terms can not be deemed as independent. The details for the calculation of each uncertainty component are given in detail by Westman et al.[17] where it is shown that the uncertainty is dominated by the uncertainty caused by the A/D conversion in pressure p_{11}. The uncertainty components

contributing to the standard uncertainty for the measured pressure are of the order of 10^{-3} - 10^{-2} bar. In the pressure range of the measurements carried out, the PT-3 sensor is used, with a corresponding uncertainty equal to $7.64 \cdot 10^{-3}$ bar. Thus, the combined standard uncertainty in the cell pressure is calculated through eq. 6.2.

$$u_c(p) = \left|\frac{\partial p}{\partial p_i}\right| |u(p_i)| + \left|\frac{\partial p}{\partial p_{11}}\right| |u(p_{11})| + \left|\frac{\partial p}{\partial p_{hs}}\right| |u(p_{hs})| = |u(p_i)| + |u(p_{11})| + |u(p_{hs})| \qquad \text{eq. 6.2}$$

For the temperature the combined uncertainty, $u_c(\bar{T})$, is given by eq. 6.3

$$u_c(\bar{T}) = \sqrt{s^2(\bar{T}) + u^2(\bar{T})} \qquad \text{eq. 6.3}$$

where $s(\bar{T})$ is the standard deviation of a series of samples and $u(\bar{T})$, the total uncertainty in temperature.

The sensors T_{04} and T_{05} are standard platinum resistance thermometers, whose temperature is calculated by measuring the resistance of the SPRT at the unknown temperature and comparing this resistance to the measured resistance at other known temperatures. The framework used for doing this comparison is the International Temperature Scale of 1990 (ITS-90)[27]. As the VLE measurements are carried out in the temperature range of 293.14 K - 303.15 K, the ITS-90 calibrations are performed in the subrange defined by the triple point of mercury ($T_{90} \equiv 234.3156$ K), the triple point of water ($T_{90} \equiv 273.16$ K) and the melting point of gallium ($T_{90} \equiv 302.9146$ K). The ITS-90 deviation function for this subrange is used together with the ITS-90 reference functions to calculate the ITS-90 temperatures, T_{90}. The extrapolation of this deviation function to 303.15 K, 0.23 K above the gallium melting point, is assumed to give negligible contribution to the temperature uncertainty. The resistance of the SPRT at a certain temperature is measured using an ASL F650AC Thermometry Bridge, together with an external Tinsley 5685A resistance normal placed inside a Tinsley 5648 temperature – controlled enclosure as reference. The measured input quantity was the bridge ratio, defined by eq. 6.4,

$$W_b = \frac{R(T_{90})}{R(T_{ref})} \qquad \text{eq. 6.4}$$

where $R(T_{90})$ is the resistance of the SPRT at the unknown ITS-90 temperature T_{90}, and R_{ref} is the resistance of the Tinsley resistance normal. The resistance normal has been calibrated inside the temperature – controlled enclosure by the Norwegian national metrology service Justervesenet on 2012-04-12. The calibration certificate stated that R_{ref} equals 24.998982 Ω, with a standard uncertainty $u(R_{ref},1) = 6 \cdot 10^{-6}$ Ω. Taking into account the temperature stability of the enclosure and its effect on the resistance of the resistance normal and the long term stability of the resistance, the total standard uncertainty at the time of use is estimated to be $u(R_{ref}) = 8.5 \cdot 10^{-6}$ Ω. The uncertainty $u(T_{90})$ in the calculated temperature, T_{90}, can be stated as per eq. 6.5.

$$u(T_{90}) = \left| u(W_r(T_{90})) \cdot \frac{\partial T_{90}}{\partial W_r(T_{90})} \right| \qquad \text{eq. 6.5}$$

When the contents of the cell are at VLE, the temperature at the vapor – liquid interface, designated T, should be somewhere between the temperatures in the top flange, T_{04}, and that of the bottom flange, T_{05}. This is a reasonable assumption if the temperature of the thermostatic bath fluid is sufficiently uniform and stable in the heat transfer regions between the cell and the bath fluid. The uniformity and stability of the heat transfer in this area can be investigated by measuring the temperature around the perimeter of the cell seen from above and at different vertical positions ranging from the position of the top flange to the bottom flange. For that reason, given that the uniformity and stability in these regions are sufficient, the VLE temperature can be approximated using the arithmetic mean of the two measured temperatures (eq. 6.6).

$$T = \frac{T_{04} + T_{05}}{2} \qquad \text{eq. 6.6}$$

Since T_{04} and T_{05} can not be assumed as independent, the uncertainty in T is expressed through eq. 6.7.

$$u(T) = \left| u(T_{04}) \frac{\partial(T)}{\partial(T_{04})} \right| + \left| u(T_{05}) \frac{\partial(T)}{\partial(T_{05})} \right| = \left| \frac{u(T_{04})}{2} \right| + \left| \frac{u(T_{05})}{2} \right| \qquad \text{eq. 6.7}$$

The calculation of the uncertainty for each of the SPRTs used for the temperature measurement is based on the combined uncertainties of the resistance measurements and the calibration points. Additionally, an uncertainty component, *u(T,diff)*, is taken into account, which is the uncertainty caused by the SPRT being at a temperature other than the one we want to measure, and this is usually the largest contribution to the total uncertainty in a temperature measurement. At an unknown temperature during the VLE experiments, this uncertainty is assumed to be equal to the difference between the measured temperatures of the two SPRTs and is modeled using a rectangular distribution, as per eq. 6.8.

$$(T, diff) = \frac{|T_{04} - T_{05}|}{\sqrt{3}} \qquad \text{eq. 6.8}$$

The uncertainty in the resistance is of the order of 10^{-6} - 10^{-5} Ω which corresponds to $u(T_{H_2O})$ = 0.51 mK and $u(T_{Ga})$ = 0.85 mK.

The detailed uncertainty results for the mean temperature and pressure values are reported along with their respective VLE measurements, in Section 6.3. The resulted standard uncertainties in the pressure measurement are illustrated in Figure 6.6*a* and in temperature in Figure 6.6*b*. As it is observed, the standard uncertainty in pressure is estimated to be below 0.03 % of the measured pressure. Similarly, from the reported

values, the maximum uncertainty in pressure is 0.02 bar while in temperature the maximum uncertainty is 3 mK.

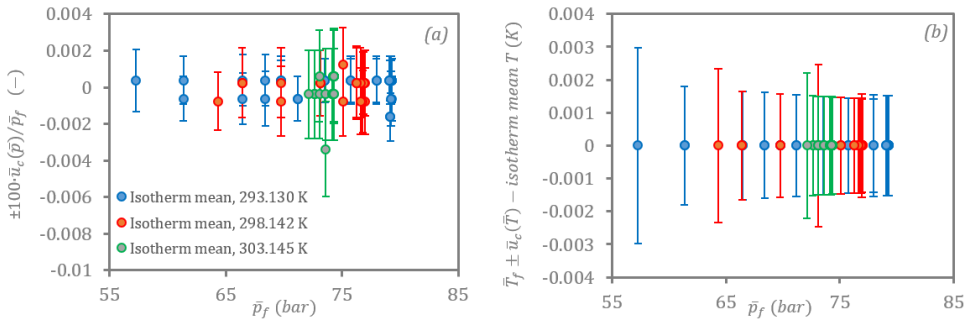

Figure 6.6: (a) Pressure standard uncertainty relative to the measured pressure for the VLE measurements performed, expressed as $100 \cdot \bar{u}_c(\bar{p})/\bar{p}_f$. $\bar{p}_f$ stands for the measured pressure and $\bar{u}_c(\bar{p})$ for the standard uncertainty. (b). Temperature deviations for each VLE measurement from isotherm mean temperature, and temperature standard uncertainty, expressed together as $\bar{T}_f \pm \bar{u}_c(\bar{T})$ − isotherm mean temperature, versus the VLE experimental pressure $\bar{p}_f$. $\bar{T}_f$ stands for the VLE experimental mean temperature and $\bar{u}_c(\bar{T})$ for the standard uncertainty in temperature. Blue colour indicates the isotherm at the mean temperature of 293.130 K, red colour indicates the isotherm at the mean temperature of 298.142 K and green colour indicates the isotherm at the mean temperature of 303.145 K.

6.2.4.c. *Composition*

The VLE composition analysis is performed using a GC, which has been calibrated using gas mixtures with composition known to high accuracy. The calibration mixtures have been gravimetrically prepared using a custom – built rig at the NTNU and SINTEF Energy Research Laboratories, with adherence to the ISO standard[28]. The uncertainty of the VLE composition analysis has contributions from a range of sources, including the impurities of the gases used to prepare the calibration mixtures, the uncertainty in the molar masses, inaccuracies in the weighed masses, adsorption, repeatability, uncertainties of the sampling and GC analysis, and finally the consistency between the GC calibration function and data.

Each calibration gas is filled into the cell using Pump 3, just like when filling the cell with methane. The cell, pump and lines leading to the cell are kept at 313 K, to ensure that the calibration gas is in single phase. Using the same procedure with the one for filling the cell with the respective gases, as described in Section 6.2.3, the pumps and lines have been first evacuated and then are filled with the calibration gas mixture. The evacuation and flushing procedure, is repeated five times in total. After the final evacuation, the calibration gas is filled into Pump 3 and its connected lines, and is maintained at a pressure of at least 5 bar, to prevent contamination of the gas. The cell is flushed with the calibration gas and then is evacuated. This procedure is repeated 5 times to remove most of the remaining impurities in the cell. After the final evacuation of the cell, it is flushed with the calibration gas once more, to minimize the effects of surface adsorption of the components in the calibration gas. The cell has been filled at

different pressures in the range of 60 - 80 bar, which is the expected pressure range for the isotherms of interest, based on the prediction of the GERG-2008 model. Samples of varying sizes have been withdrawn from the cell at various pressures in order to form the basis for the calibration of the composition analysis. That way, a relation between the CO_2 mol fractions of the calibration gas mixtures and the GC detector response is obtained.

6.2.4.c.i. Source gas composition and molar mass

The composition and the corresponding uncertainty of the calibration gas mixtures are results of the purity and the molar mass of the source gases used for its preparation. The molar masses of CO_2 and CH_4 are calculated along with their respective uncertainties from the molar masses of the monoatomic carbon, C, oxygen, O, and hydrogen, H, as given by Wieser et al.[29, 30] and are reported in Table 6.2.

Table 6.2: Molar masses of atomic elements and compounds with uncertainties

Component *i*	M_i	$u(M_i)$	Unit
C[a]	0.0120108	0.0000003	kg·mol^{-1}
C[b]	0.0120108	0.0000001	kg·mol^{-1}
O	0.0159994	0.0000001	kg·mol^{-1}
CO_2	0.0440096	0.0000003	kg·mol^{-1}
CH_4	0.0160427	0.0000002	kg·mol^{-1}
$CO_2 + imp$	0.0440095		kg·mol^{-1}
$CH_4 + imp$	0.0160427		kg·mol^{-1}
$CO_{2,eff}$	0.0440096		kg·mol^{-1}
$CH_{4,eff}$	0.0160428		kg·mol^{-1}

[a] in CO_2 molecule
[b] in CH_4 molecule

The minimum certified purities of the source gases are given in Table 6.1, along with their specifications for certain impurities. Since the source gases are not entirely pure, estimates for their molar masses, M_{CO_2+imp} and M_{CH_4+imp}, are calculated, by assuming the hydrocarbon impurity to be formed entirely from methane, in the case of CO_2 and ethane for CH_4. Since the composition of the source gases, CO_2 and CH_4, is not accurately known, it is assumed that completely pure gases and maximum impurity are equally probable. Specifically, it is assumed that the standard uncertainty of the purity of the source gases equals half the maximum certified impurity fraction and it is estimated that the actual purity level is the minimum purity plus this standard uncertainty. Furthermore, it is assumed that the concentration of each impurity component is proportional to its maximum fraction provided in the gas specifications. Since the mol fractions of the different components have been set, the molar mass of the sample of component *i*, either CO_2 or CH_4, can be estimated through eq. 6.9.

$$M_{i+imp} = y_{i,in\ sample} \cdot M_i + \sum_j y_{j,in\ sample} \cdot M_j \qquad \text{eq. 6.9}$$

The molar mass M_j of each impurity j is calculated using the data of Wieser et al.[29, 30], as discussed above. The calculated molar masses of $CO_2 + imp$ and $CH_4 + imp$ of the gas samples are given in Table 6.2. The effective molar mass of each component i, either CO_2 or CH_4, is given on the same table and it is calculated through eq. 6.10 - eq. 6.11.

$$M_{i,eff} = \frac{M_{i+imp}}{y_{i,in\ sample}} = M_i + \frac{(1 - y_{i,in\ sample}) \cdot M_{imp}}{y_{i,in\ sample}} \qquad \text{eq. 6.10}$$

$$M_{imp} = \frac{\sum_j y_{j,in\ sample} \cdot M_j}{1 - y_{i,in\ sample}} \qquad \text{eq. 6.11}$$

6.2.4.c.ii. Gravimetric Preparation

The calibration gas mixtures are prepared by injecting CO_2 and CH_4 consecutively into the calibration gas cylinder and weighing the cylinder accurately using a comparator with certified weights before and after each gas injection. The resulting masses of each component i with impurities, are converted into moles excluding impurities, as per eq. 6.12.

$$n_i = \frac{m_{i+imp}}{M_{i,eff}} \qquad \text{eq. 6.12}$$

where n_i is mol fraction of component i.

Both the numerator and denominator in eq. 6.12 contribute to the calculated uncertainty. The uncertainty in mass, m_{i+imp}, is a function of a range of factors, including the repeatability of the ABBA mass comparisons, the uncertainty in the buoyancy correction, the uncertainty in the OIML masses, where the repeatability is the dominating contributor. Using the fact that $y_{CO_2,\ in\ sample}$ is close to unity, it can be shown that the uncertainty term from the effective molar mass, $M_{i,eff}$, to the first order can be estimated by eq. 6.13.

$$u(n_i, M_{i,eff}) = n_i \cdot \frac{\sqrt{4u^2(y_{i,in\ sample})M_{imp}^2 + u^2(M_i)}}{M_i} \qquad \text{eq. 6.13}$$

where $u(y_{i,in\ sample}) = 1 - y_{i,in\ sample}$.

6.2.4.c.iii. Composition calibration procedure and estimated composition uncertainty

Each of the two prepared calibration gas mixtures is filled into the cell to calibrate the GC. The cell is kept at 313.15 K to ensure that the contents of the cell are in a uniform supercritical state. Samples are extracted from the VLE cell using both the liquid and vapor Rolsi™ samplers with different opening times to get samples which span the expected sample size during the VLE experiments. Then, samples of varying sizes are extracted from the cell in two different pressures, 60 bar and 80 bar respectively, which are the ranges of the expected pressures at VLE in the isotherms of interest. Seven samples are taken for each selected combination of calibration gas mixture, sampler, and sampler opening time. The first two samples are discarded as flushing samples, leaving thus five valid samples. These samples form the basis for the calibration of the composition analysis, giving a relation between the CO_2 mol fraction of the calibration gas mixtures and the GC detector response.

The uncertainty contribution from the calibration mixture reaching the GC can be calculated from eq. 6.14.

$$u_c(y_{CO_2,cal}) = \sqrt{u^2(y_{CO_2,cal}, m) + u^2(y_{CO_2,cal}, M_{eff}) + u^2(y_{CO_2,cal}, ads)} \qquad \text{eq. 6.14}$$

where $u(y_{CO_2,cal}, m)$ and $u(y_{CO_2,cal}, M_{eff})$ are the contributing uncertainties in the masses of CO_2 and CH_4 in the gas mixture and in the effective molar masses (eq. 6.15 - eq. 6.16).

$$u(y_{CO_2,cal}, m) = \frac{u(n_{CO_2}, m) \cdot n_{CO_2} + u(n_{CH_4}, m) \cdot n_{CH_4}}{(n_{CO_2} + n_{CH_4})^2} \qquad \text{eq. 6.15}$$

$$u(y_{CO_2,cal}, M_{eff}) = \frac{\sqrt{u^2(n_{CO_2}, M_{eff}) \cdot n_{CO_2}^2 + u^2(n_{CH_4}, M_{eff}) \cdot n_{CH_4}^2}}{(n_{CO_2} + n_{CH_4})^2} \qquad \text{eq. 6.16}$$

The term $u(y_{CO_2,cal}, ads)$ is the uncertainty contribution from adsorption and is calculated by assuming higher adsorption of CO_2 compared to that of methane. This is based on the work of Leuenberger et al.[31] who performed experiments with mixtures including CO_2 on commercial steel and aluminum gas cylinders, applying no polishing. Their measurements indicate that CO_2 forms at most a molecular monolayer on steel bottles using a model ignoring surface roughness. To minimize the adsorption effects, the pumps and most of the piping have been sulfinert treated. Also, the cell is expected to have little adsorption. Nevertheless, to consider the worst – case scenario, it is assumed monolayer adsorption in both the cylinders where the calibration mixtures have been prepared and in the cell, and the maximum estimated adsorption of CO_2 in the gas cylinder and cell is calculated through eq. 6.17.

$$\Delta n_{CO_2,max.ads.cyl} = \frac{A_{cyl}}{A_{CO_2} \cdot N_A} \qquad \text{eq. 6.17}$$

$$\Delta n_{CO_2,max.ads.cell} = \frac{A_{cell}}{A_{CO_2} \cdot N_A} \qquad \text{eq. 6.18}$$

In eq. 6.17 and eq. 6.18, $A_{CO_2} \cdot N_A$ denotes the surface area of a monolayer of one mol of CO_2. A_{cyl} and A_{cell}, respectively, are the inner surface areas of the gas cylinder and the cell. The adsorption varies depending on unknown experimental conditions, in particular the unknown surface roughness of the gas cylinder. For simplicity, the uncertainty has been estimated based on the adsorption level provided by eq. 6.19.

$$u(y_{CO_2,cal}, ads) = \frac{\Delta n_{CO_2,max.ads.cyl} \cdot n_{CO_2,cyl}}{(n_{CO_2,cyl} + n_{CH_4,cyl})^2} + \frac{\Delta n_{CO_2,max.ads.cell} \cdot n_{CO_2,cell}}{(n_{CO_2,cell} + n_{CH_4,cell})^2} \qquad \text{eq. 6.19}$$

The mol values in the cell are calculated using the GERG-2008 at a pressure equal to 5 bar. As it is observed from Table 6.3, where the uncertainty terms of the calibration mixtures are presented, the different uncertainty contributions are of the same order of magnitude. The uncertainty contribution, $u(y_{CO_2,cal}, M_{eff})$, dominates the combined total uncertainty, $u_c(y_{CO_2,cal})$, but still it is an order of magnitude lower compared to the uncertainty derived from the calibration function error. Furthermore, the adsorption contribution should have been order of magnitudes larger to be of significance to the final VLE data.

Table 6.3: CO_2/CH_4 calibration gas mixtures: CO_2 mol fractions and corresponding standard uncertainties.

$y_{CO_2,cal}$	$u(y_{CO_2,cal}, m)$	$u(y_{CO_2,cal}, M_{eff})$	$u(y_{CO_2,cal}, ads)$	$u_c(y_{CO_2,cal})$
0.850481	$3.4 \cdot 10^{-6}$	$6.3 \cdot 10^{-6}$	$2.5 \cdot 10^{-6}$	$7.6 \cdot 10^{-6}$
0.943293	$3.9 \cdot 10^{-6}$	$7.8 \cdot 10^{-6}$	$2.8 \cdot 10^{-6}$	$9.1 \cdot 10^{-6}$

6.2.4.c.iv. GC integration and calibration function

The GC column, method and detector are the ones described in Section 6.2.1 using helium as carrier gas with the supplier specifications given in Table 6.1. The CO_2 and CH_4 peaks in the GC chromatogram using this setup are very distinct, leading to very good separation. The areas under the CO_2 and CH_4 GC peaks, A_{CO_2} and A_{CH_4} respectively, are obtained for each sample after numerical integration. The GC thermal conductivity detector response is non-linear with respect to the number of moles of CO_2 and CH_4 that pass through it. The following calibration function correlates the area of each component to the mol number passed through the detector.

$$\hat{n}_{CO_2} \cdot k = A_{CO_2} + c_1 \cdot {A_{CO_2}}^{c_2} \qquad \text{eq. 6.20}$$

$$\hat{n}_{CH_4} \cdot k = c_3 \cdot A_{CH_4} + c_4 \cdot {A_{CH_4}}^{c_5} \qquad \text{eq. 6.21}$$

$$\hat{y}_{CO_2,cal} = \frac{\hat{n}_{CO_2}}{\hat{n}_{CO_2} + \hat{n}_{CH_4}} \qquad \text{eq. 6.22}$$

where $\hat{y}_{CO_2,cal}$ is the estimator of the CO_2 mol fraction of a calibration gas mixture given the corresponding integrated peak areas from the GC chromatogram of a specific sample and k is a constant factor relating the areas to the number of moles. The value of k is not of interest since it is eliminated when the mol fraction is calculated, as per eq. 6.22.

The parameters c_i, with i taking values from 1 up to 5 have been fitted per phase by performing a weighted least squares minimization of the objective function S, as it is described by eq. 6.23.

$$minS(c_i) = \frac{y_{CO_2.cal} - \hat{y}_{CO_2.cal}}{\sqrt{u_c^2(y_{CO_2.cal}) + s^2(y_{CO_2.cal})}} \qquad \text{eq. 6.23}$$

The mean value, $\hat{y}_{CO_2,cal}$, of the estimators calculated for each of the 26 series of 5 valid samples is fitted to the calibration mixture mol fractions, $y_{CO_2,cal}$, and the results along with the standard deviation are presented in Table 6.4. The need for fitting different values of the parameters for the liquid and the vapor phase is justified due to the fact that the liquid sampler extracts helium at a slower rate than the vapor sampler. Thus, the use of the same opening times yields slightly different sample concentration in the column for the two samplers. As it can be observed from Figure 6.7, the errors between the calibration gas CO_2 mol fraction and the mol fraction measured by the GC, $e = y_{CO_2,cal} - \hat{y}_{CO_2,cal}$, are randomly scattered around zero for the two values of $y_{CO_2,cal}$, which indicates that the fit is reasonable. It should be noted, that due to the small number of calibration gas mixtures, a linear correlation had been initially tested, but it failed to accurately describe the relation between the areas and the molar composition of the mixtures, probably due to the high difference in the TCD detector response of CO_2 and CH_4. $s(e)$ is about 10 times higher than $u_c(y_{CO_2,cal})$, and hence the former completely dominates the total systematic uncertainty of the composition measurements.

Table 6.4: Fitted parameters for the vapor and liquid relation between the GC response and the number of moles, along with the standard uncertainty of composition analysis.

Variable	L Rolsi	V Rolsi
$10^3 \cdot c_1$	0.00546	0.00334
c_2	2.13036	2.22570
c_3	1.49009	1.48217
$10^3 \cdot c_4$	0.18510	0.22991
c_5	1.95232	1.94099
$u(x_{CO_2}) = u(y_{CO_2}) = s(e)$	$89.41 \cdot 10^{-6}$	$89.41 \cdot 10^{-6}$
n	13	13

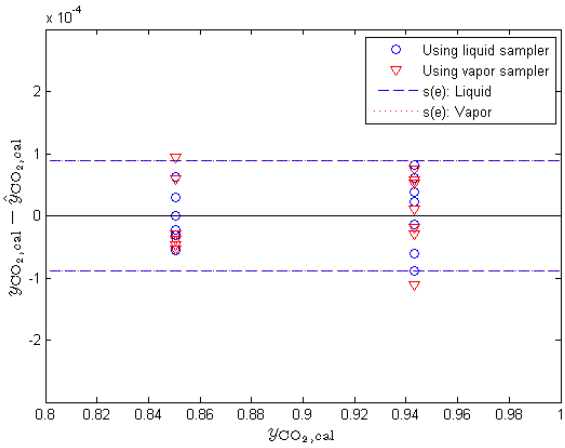

Figure 6.7: Error between actual compositions in Table 6.3 and the composition determined by the GC using the fit of eq. 6.20 - eq. 6.22. Composition analysis uncertainty $u(x_{CO_2}) = u(y_{CO_2}) = s(e)$ as reported in Table 6.4.

6.2.4.c.v. Total uncertainty in liquid and vapor mol fractions

For a set of VLE measurements, the uncertainty in the measurement of temperature, T, and pressure, p, contributes to the total uncertainty in composition at T and p, so that the final total uncertainty in composition is given by eq. 6.24,

$$u_{tot}(z_{CO_2}) = \sqrt{u^2(z_{CO_2}) + \left(u_c(\bar{T})\frac{\partial z_{CO_2}}{\partial T}\right)^2 + \left(u_c(\bar{p})\frac{\partial z_{CO_2}}{\partial p}\right)^2} \qquad \text{eq. 6.24}$$

where z_{CO_2} stands for the composition either for the liquid, x_{CO_2}, or the vapor phase, y_{CO_2}, and $u_c(\bar{T})$ and $u_c(\bar{p})$ are the temperature and pressure uncertainties respectively.

The derivatives of the composition with regard to temperature and pressure, $\frac{\partial z_{CO_2}}{\partial T}$ and $\frac{\partial z_{CO_2}}{\partial p}$, have been calculated numerically from the UMR-PRU thermodynamic model fitted to the data of each isotherm. For data close to the critical region, the calculation of the derivatives with respect to pressure, $\frac{\partial z_{CO_2}}{\partial p}$, is calculated analytically from the fitted scaling law, since the latter better describes the experimental data in this particular region.

6.2.5. Data Reduction

As mentioned in the description of the experimental procedure, there is a small pressure drop after each sample withdrawal from the cell. So, a pressure compensation is used by increasing the volume of the bellow inside the cell. The latter is not required for the isotherm of 303.15 K. Thus, for the isotherms of 293.13 K and 298.14 K, the bellows restore and stabilize the pressure 1 to 3 minutes after the extraction of the sample. For the isotherm of 303.15 K, where the use of the bellows is not required, the pressure returns to its original value after 1 - 3 minutes, probably due to the high

concentration of CO_2. After the return to its original value, the pressure remains stable for 25 to 27 minutes, until the withdrawal of the next sample. In each series of consecutive liquid or vapor composition samples, x_{CO_2} or y_{CO_2}, at a nominal temperature and pressure, it is assumed that each composition sample has the equilibrium composition at the temperature, T, and pressure, p, just before the sample has been extracted.

For each sample, the equilibrium pressure and temperature are assumed to be represented by the pressure and temperature measurements averaged over a time period equal to 75 % of the sampling period ending just before the sample extraction starts, denoted $\bar{p}$ and $\bar{T}$, respectively. During this time period, no systematic trends in pressure and temperature are observed.

The standard systematic uncertainty of these mean values, $u(p)$ and $u(T)$, are assumed to be equal to the arithmetic mean values of the standard systematic uncertainties of the p_i and T_i measurements, $u_c(p)$ and $u_c(T)$ used to calculate the mean pressure and temperature, as per eq. 6.2 and eq. 6.7. The combined standard uncertainty of the mean values $\bar{p}$ and $\bar{T}$ is given as per eq. 6.25 - eq. 6.26.

$$u_c(\bar{p}) = \sqrt{s^2(\bar{p}) + u^2(\bar{p})} \qquad \text{eq. 6.25}$$

$$u_c(\bar{T}) = \sqrt{s^2(\bar{T}) + u^2(\bar{T})} \qquad \text{eq. 6.26}$$

For each of these series of samples, the average mean values of the temperature and pressure and the trimmed mean values for the liquid and vapor phase compositions are calculated, denoted as $\bar{T}_f$, $\bar{p}_f$, $\bar{x}_{CO_2}$, and $\bar{y}_{CO_2}$, respectively. The subscript f is used to differentiate between the temperature and pressure values associated with each composition sample, x_{CO_2} or y_{CO_2}, and of those associated with the average compositions, $\bar{x}_{CO_2}$ or $\bar{y}_{CO_2}$. Thus, $\bar{u}_c(\bar{p})$, $\bar{u}_c(\bar{T})$, $\bar{u}_{tot}(x_{CO_2})$ and $\bar{u}_{tot}(y_{CO_2})$ are calculated as the mean and trimmed mean values of $u_c(\bar{p})$, $u_c(\bar{T})$, $u_{tot}(x_{CO_2})$ and $u_{tot}(y_{CO_2})$ in each series, respectively. The propagation of uncertainty is calculated as per eq. 6.27 - eq. 6.30, with $s(\bar{p}_f)$, $s(\bar{T}_f)$, $s(\bar{x}_{CO_2})$ and $s(\bar{y}_{CO_2})$ calculated as per eq. 6.31,

$$u_c(\bar{p}_f) = \sqrt{s^2(\bar{p}_f) + \bar{u}_c^2(\bar{p})} \qquad \text{eq. 6.27}$$

$$u_c(\bar{T}_f) = \sqrt{s^2(\bar{T}_f) + \bar{u}_c^2(\bar{T})} \qquad \text{eq. 6.28}$$

$$u_c(\bar{x}_{CO_2}) = \sqrt{s^2(\bar{x}_{CO_2}) + \bar{u}_{tot}^2(x_{CO_2})} \qquad \text{eq. 6.29}$$

$$u_c(\bar{y}_{CO_2}) = \sqrt{s^2(\bar{y}_{CO_2}) + \bar{u}_{tot}^2(y_{CO_2})} \qquad \text{eq. 6.30}$$

$$s(z) = \sqrt{\sum_{i=1}^{n_p} \frac{(z_i - \bar{z})^2}{n_p - 1}} \qquad \text{eq. 6.31}$$

where z corresponds to each of the previously referred measurants.

6.3. VLE Experimental Results

VLE measurements at three isotherms of the CO_2/CH_4 binary system at the average temperature of 293.13 K, 298.14 K and 303.15 K have been conducted. Both the dew point and bubble point curves are mapped, starting from CO_2 vapor pressure up to the critical point of the mixture.

The data for each series of samples are given in terms of mean temperature, $\bar{T}_f$, mean pressure, $\bar{p}_f$, and mean mol fractions for the liquid phase, $\bar{x}_{CO_2}$, or the vapor phase, $\bar{y}_{CO_2}$, in Table 6.5 and Table 6.6, respectively. These averaged VLE data are plotted in Figure 6.8 along with the other available experimental data close in temperature, where available, and the predictions of the GERG-2008 model.

The temperature, $\bar{T}$, pressure, $\bar{p}$, and mol fractions for the liquid phase, x_{CO_2}, and the vapor phase, y_{CO_2}, for each individual sample are given in Tables S.1 and S.2 in the Supplementary Material of the respective publication (Appendix F.2), together with their uncertainty estimates. The composition derivatives with respect to pressure, $\frac{\partial x_{CO_2}}{\partial p}$ and $\frac{\partial y_{CO_2}}{\partial p}$, along with the total standard uncertainties in the composition of the samples, $u_{tot}(x_{CO_2})$ and $u_{tot}(y_{CO_2})$, are also reported there.

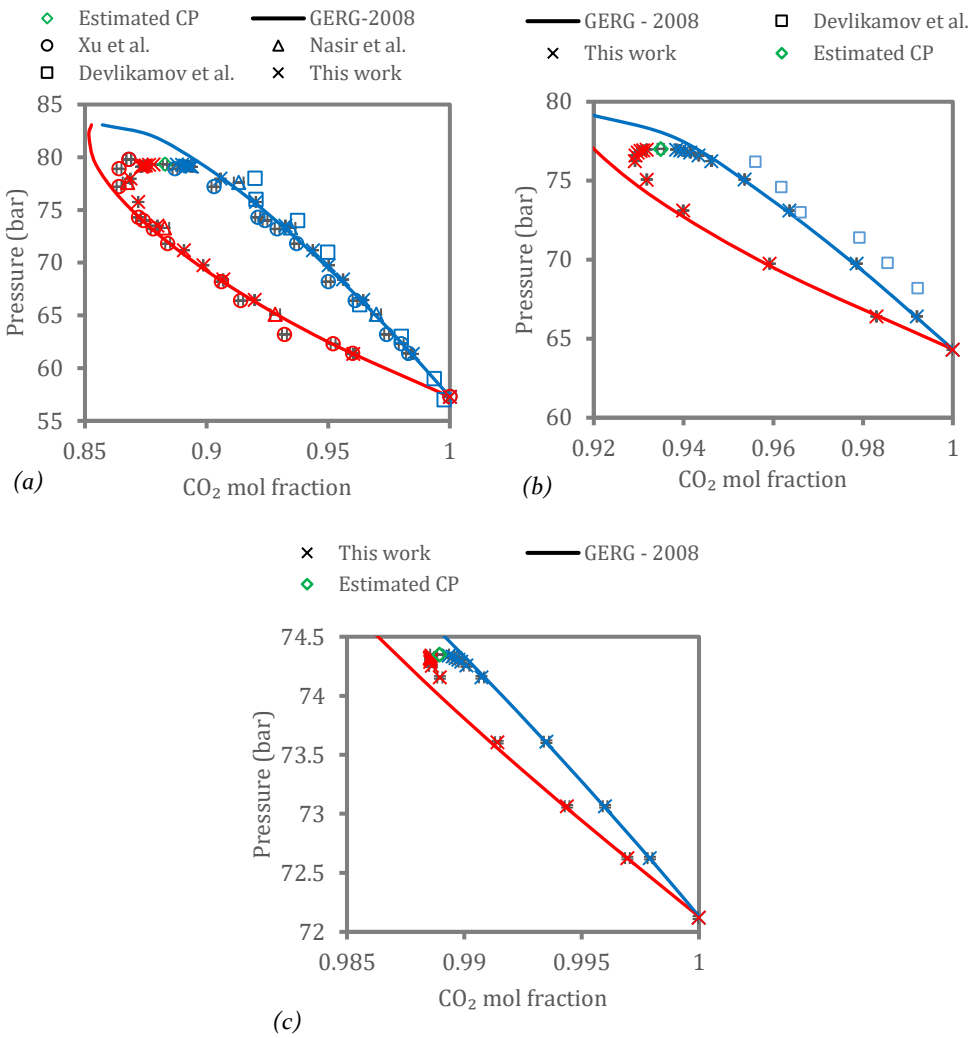

Figure 6.8: VLE pressure – composition diagram for the CO_2/CH_4 for the different isotherms measured in this work. Blue colour indicates the liquid phase and red colour the vapor one. (x) indicates the experimental data measured in this work along with the estimated uncertainties (black uncertainty bars). (◇) Indicates the critical point of the mixture as estimated by the fitting of the Scaling Law (eq. 6.32)*. The solid line is the prediction of GERG-2008. (a). Mean temperature 293.130 K. (○) indicates the data by Xu et al.[6], (Δ) indicates the data by Nasir et al.[5] and (□) indicates the data by Devlikamov et al.[7] (b). Mean temperature 298.142 K. (□) indicates the data by Devlikamov et al.[7] (c). Mean temperature 303.145 K. Please note that the scaling in (c) is very narrow due to the proximity in CO_2 critical temperature.*

Table 6.5: liquid phase: Experimental VLE data for CO_2 and CH_4 at mean temperature, $\bar{T}_f$, mean pressure, $\bar{p}_f$, and mean liquid phase mol fraction, $\bar{x}_{CO_2}$.

ID	Data			Temperature (K)			Pressure (bar)			Composition			
	$\bar{T}_f$ (K)	$\bar{p}_f$ (bar)	$\bar{x}_{CO_2}$ (-)	$s(\bar{T}_f)$	$\bar{u}_c(\bar{T})$	$\bar{u}_c(\bar{T}_f)$	$s(\bar{p}_f)$	$\bar{u}_c(\bar{p})$	$\bar{u}_c(\bar{p}_f)$	$s(\bar{x}_{CO_2})$	$\bar{u}_{tot}(\bar{x}_{CO_2})$	$\bar{u}_c(\bar{x}_{CO_2})$	$\bar{x}_{CO_2,calc}$
P1	293.130	57.273	0.99999	1.3 e-3	1.1 e-3	1.7 e-3	1.3 e-2	1.7 e-2	1.2 e-2				
L1	293.130	61.348	0.98472	6.8 e-4	1.1 e-3	1.3 e-3	3.1 e-4	1.1 e-2	1.1 e-2	3.3 e-6	9.9 e-5	9.9 e-5	0.98537
L2	293.129	66.459	0.96439	1.6 e-4	1.4 e-3	1.4 e-3	2.1 e-4	1.1 e-2	1.1 e-2	5.2 e-6	1.0 e-4	1.0 e-4	0.96486
L3	293.130	68.401	0.95611	3.2 e-4	1.3 e-3	1.4 e-3	8.0 e-5	1.1 e-2	1.1 e-2	1.2 e-5	1.0 e-4	1.0 e-4	0.95629
L4	293.130	69.756	0.95018	5.9 e-4	1.1 e-3	1.3 e-3	1.1 e-4	1.1 e-2	1.1 e-2	1.2 e-5	1.0 e-4	1.0 e-4	0.9500
L5	293.129	71.183	0.94364	2.5 e-4	1.2 e-3	1.2 e-3	1.5 e-4	1.1 e-2	1.1 e-2	8.1 e-6	1.1 e-4	1.1 e-4	0.94307
L6	293.130	73.508	0.93240	2.0 e-4	1.2 e-3	1.2 e-3	7.5 e-5	1.1 e-2	1.1 e-2	1.5 e-5	1.1 e-4	1.1 e-4	0.93096
L7	293.130	75.758	0.92024	7.2 e-5	1.3 e-3	1.3 e-3	1.1 e-4	1.1 e-2	1.1 e-2	5.3 e-6	1.1 e-4	1.1 e-4	0.91800
L8	293.130	77.962	0.90568	2.1 e-4	1.3 e-3	1.3 e-3	2.4 e-4	1.2 e-2	1.2 e-2	9.4 e-6	1.2 e-4	1.2 e-4	0.90350
L9	293.130	79.091	0.89394	4.4 e-4	1.2 e-3	1.3 e-3	1.4 e-4	1.2 e-2	1.2 e-2	4.7 e-6	2.1 e-4+	2.1 e-4+	0.89390
L10	293.130	79.135	0.89309	8.9 e-5	1.1 e-3	1.1 e-3	2.3 e-4	1.2 e-2	1.2 e-2	2.5 e-5	2.5 e-4+	2.5 e-4+	0.89311
L11	293.128	79.179	0.89220	5.9 e-5	1.3 e-3	1.3 e-3	9.6 e-5	1.2 e-2	1.2 e-2	2.5 e-5	2.7 e-4+	2.7 e-4+	0.89223
L12	293.129	79.219	0.89123	8.3 e-4	1.2 e-3	1.5 e-3	1.7 e-4	1.2 e-2	1.2 e-2	2.2 e-5	3.2 e-4+	3.2 e-4+	0.89127
L13	293.130	79.266	0.88982	7.6 e-5	1.1 e-3	1.1 e-3	9.1 e-5	1.2 e-2	1.2 e-2	2.2 e-5	5.1 e-4+	5.1 e-4+	0.88982

Table 6.5 (continued)

ID	Data			Temperature (K)			Pressure (bar)			Composition			
	$\bar{T}_f$ (K)	$\bar{p}_f$ (bar)	$\bar{x}_{CO_2}$ (-)	$s(\bar{T}_f)$	$\bar{u}_c(\bar{T})$	$\bar{u}_c(\bar{T}_f)$	$s(\bar{p}_f)$	$\bar{u}_c(\bar{p})$	$\bar{u}_c(\bar{p}_f)$	$s(\bar{x}_{CO_2})$	$\bar{u}_{tot}(\bar{x}_{CO_2})$	$\bar{u}_c(\bar{x}_{CO_2})$	$\bar{x}_{CO_2,calc}$
L14	293.129	79.308	0.88782	3.4 e-4	1.2 e-3	1.2 e-3	5.9 e-5	1.2 e-2	1.2 e-2	2.00E-5	8.3e-4[+]	8.3 e-4[+]	0.88778
P2	298.141	64.316[c]	0.99999	6.7 e-4	1.4 e-3	1.6 e-3	1.0 e-2	1.5 e-2	1.1 e-2				
L15	298.142	66.411	0.99200	1.9 e-4	1.9 e-3	1.9 e-3	1.0 e-4	1.1 e-2	1.1 e-2	8.2 e-7	9.9 e-5	9.9 e-5	0.99271
L16	298.142	69.755	0.97855	1.5 e-4	1.9 e-3	1.9 e-3	1.4 e-4	1.1 e-2	1.1 e-2	1.7 e-6	1.0 e-4	1.0 e-4	0.97936
L17	298.142	73.114	0.96361	1.1 e-4	1.8 e-3	1.8 e-3	9.8 e-5	1.1 e-2	1.1 e-2	9.2 e-6	1.1 e-4	1.1 e-4	0.96361
L18	298.141	75.079	0.95359	5.2 e-4	1.8 e-3	1.9 e-3	1.8 e-4	1.1 e-2	1.1 e-2	5.0 e-6	1.1 e-4	1.1 e-4	0.95277
L19	298.142	76.25	0.94622	1.5 e-4	2.0 e-3	2.0 e-3	7.5 e-5	1.1 e-2	1.1 e-2	1.9 e-5	1.4 e-4	1.4 e-4	0.94594
L20	298.141	76.599	0.94337	3.6 e-4	1.8 e-3	1.8 e-3	5.7 e-4	1.1 e-2	1.1 e-2	6.10 e-6	1.3 e-4	1.3 e-4	0.94328
L21	298.141	76.783	0.94150	1.5 e-4	1.7 e-3	1.7 e-3	1.0 e-4	1.1 e-2	1.1 e-2	7.5 e-6	1.6 e-4[+]	1.6 e-4[+]	0.94149
L22	298.142	76.886	0.94016	3.0 e-4	1.8 e-3	1.8 e-3	3.3 e-5	1.1 e-2	1.1 e-2	1.4 e-5	1.9 e-4[+]	1.9 e-4[+]	0.94017
L23	298.142	76.938	0.93924	7.9 e-5	1.8 e-3	1.8 e-3	1.5 e-4	1.1 e-2	1.1 e-2	1.7 e-5	1.3 e-4[+]	1.3 e-4[+]	0.94046
L24	298.141	76.978	0.93835	3.3 e-4	1.8 e-3	1.8 e-3	1.4 e-4	1.1 e-2	1.1 e-2	5.4 e-6	1.3e-4[+]	1.3 e-4[+]	0.94015
L25	303.144	72.625	0.99791	2.4 e-4	2.3 e-3	2.4 e-3	3.2 e-4	1.1 e-2	1.1 e-2	1.9 e-6	1.0 e-4	1.0 e-4	0.99778
L26	303.145	73.064	0.99600	6.0 e-4	2.4 e-3	2.5 e-3	8.7 e-4	1.1 e-2	1.1 e-2	2.1 e-6	1.0 e-4	1.0 e-4	0.99589

Table 6.5 (continued)

ID	Data			Temperature (K)			Pressure (bar)			Composition			
	$\bar{T}_f$ (K)	$\bar{p}_f$ (bar)	$\bar{x}_{CO_2}$ (-)	$s(\bar{T}_f)$	$\bar{u}_c(\bar{T})$	$\bar{u}_c(\bar{T}_f)$	$s(\bar{p}_f)$	$\bar{u}_c(\bar{p})$	$\bar{u}_c(\bar{p}_f)$	$s(\bar{x}_{CO_2})$	$\bar{u}_{tot}(\bar{x}_{CO_2})$	$\bar{u}_c(\bar{x}_{CO_2})$	$\bar{x}_{CO_2,calc}$
L27	303.144	73.611	0.99350	4.3 e-4	2.4 e-3	2.5 e-3	4.60e-4	1.1 e-2	1.1 e-2	1.3 e-6	1.1 e-4	1.1 e-4	0.99337
L28	303.144	74.156	0.99073	4.3 e-4	2.5 e-3	2.5 e-3	2.70e-4	1.1 e-2	1.1 e-2	2.4 e-6	1.1 e-4	1.1 e-4	0.99068
L29	303.145	74.256	0.99009	4.4 e-5	2.5 e-3	2.5 e-3	2.90e-4	1.1 e-2	1.1 e-2	1.7 e-5	1.2 e-4[+]	1.2 e-4[+]	0.9901
L29	303.145	74.256	0.99009	4.4 e-5	2.5 e-3	2.5 e-3	2.90e-4	1.1 e-2	1.1 e-2	1.7 e-5	1.2 e-4[+]	1.2 e-4[+]	0.9901
L30	303.145	74.289	0.98988	6.6 e-5	2.6 e-3	2.6 e-3	3.40e-4	1.1 e-2	1.1 e-2	2.8 e-6	1.2 e-4[+]	1.2 e-4[+]	0.98987
L31	303.145	74.306	0.98975	6.9 e-5	2.6 e-3	2.6 e-3	2.10e-4	1.1 e-2	1.1 e-2	4.2 e-6	1.3 e-4[+]	1.3 e-4[+]	0.98974
L32	303.145	74.318	0.98963	1.9 e-4	2.5 e-3	2.5 e-3	4.00e-4	1.1 e-2	1.1 e-2	4.7 e-6	1.4 e-4[+]	1.4 e-4[+]	0.98963
L33	303.145	74.331	0.98950	1.6 e-4	2.6 e-3	2.6 e-3	1.70e-4	1.1 e-2	1.1 e-2	5.6 e-6	1.7 e-4[+]	1.7 e-4[+]	0.98949
L34	303.144	74.341	0.98934	1.2 e-4	2.5 e-3	2.5 e-3	4.20e-4	1.1 e-2	1.1 e-2	1.1 e-5	2.3 e-4[+]	2.3 e-4[+]	0.98934

[+] The derivatives $\frac{\partial x_{CO_2}}{\partial p}$ used in eq. 6.24 to obtain $\bar{u}_{tot}$ are calculated using the scaling law (eq. 6.32) with the parameters in Table 6.7.

[a] Sample standard deviation of the mean of the temperatures, $s(\bar{T}_f)$, mean of the standard systematic uncertainty of the temperature, $\bar{u}_c(\bar{T})$, total standard uncertainty of the temperature, $\bar{u}_c(\bar{T}_f)$, sample standard deviation of the mean of the pressures, $s(\bar{p}_f)$, mean of the standard systematic uncertainty of the pressures, $\bar{u}_c(\bar{p})$, total standard uncertainty of the pressure, $\bar{u}_c(\bar{p}_f)$, sample standard deviation of the mean mol fractions, $s(\bar{x}_{CO_2})$, mean of the total standard uncertainty of the mol fractions, $\bar{u}_{tot}(\bar{x}_{CO_2})$, the combined uncertainties of the mean mol fractions, $\bar{u}_c(\bar{x}_{CO_2})$, and UMR-PRU calculated mol fraction, $\bar{x}_{CO_2,calc}$.

[b] Span-Wagner CO_2 vapor pressure is 57.256 ± 0.017 bar.

[c] Span-Wagner CO_2 vapor pressure is 64.317 ± 0.019 bar.

[d] Span-Wagner CO_2 vapor pressure is 72.131 ± 0.021 bar.

Table 6.6: Vapor phase: Experimental VLE data for CO_2 and CH_4 at mean temperature, $\bar{T}_f$, mean pressure, $\bar{p}_f$, and mean vapor phase mol fraction, $\bar{y}_{CO_2}$

ID	Data			Temperature (K)			Pressure (bar)			Composition			
	$\bar{T}_f$ (K)	$\bar{p}_f$ (bar)	$\bar{x}_{CO_2}$ (-)	$s(\bar{T}_f)$	$\bar{u}_c(\bar{T})$	$\bar{u}_c(\bar{T}_f)$	$s(\bar{p}_f)$	$\bar{u}_c(\bar{p})$	$\bar{u}_c(\bar{p}_f)$	$s(\bar{y}_{CO_2})$	$\bar{u}_{tot}(\bar{y}_{CO_2})$	$\bar{u}_c(\bar{y}_{CO_2})$	$\bar{y}_{CO_2,calc}$
P1	293.130	57.273	0.99999	1.3 e-3	1.1 e-3	1.7 e-3	1.3 e-2	1.7 e-2	1.2 e-2				
V1	293.129	61.346	0.96030	3.3 e-4	1.2 e-3	1.2 e-3	4.7 e-4	1.1 e-2	1.1 e-2	3.6 e-5	1.4 e-4	1.4 e-4	0.96186
V2	293.130	66.458	0.91971	2.8 e-4	1.4 e-3	1.4 e-3	1.5 e-4	1.1 e-2	1.1 e-2	7.5 e-6	1.2 e-4	1.2 e-4	0.92147
V3	293.129	68.401	0.90679	4.1 e-4	1.5 e-3	1.5 e-3	5.3 e-5	1.1 e-2	1.1 e-2	5.9 e-6	1.2 e-4	1.2 e-4	0.90827
V4	293.130	69.755	0.89863	1.4 e-4	1.1 e-3	1.1 e-3	9.1 e-5	1.1 e-2	1.1 e-2	2.0 e-5	1.1 e-4	1.1 e-4	0.89981
V5	293.129	71.183	0.89070	2.4 e-4	1.2 e-3	1.2 e-3	2.2 e-4	1.1 e-2	1.1 e-2	2.6 e-5	1.1 e-4	1.1 e-4	0.89150
V6	293.130	73.508	0.87979	3.3 e-4	1.2 e-3	1.2 e-3	9.9 e-5	1.1 e-2	1.1 e-2	2.7 e-5	1.1 e-4	1.1 e-4	0.87947
V7	293.130	75.758	0.87189	1.5 e-4	1.2 e-3	1.2 e-3	6.4 e-5	1.1 e-2	1.1 e-2	2.2 e-5	1.0 e-4	1.0 e-4	0.86978
V8	293.130	77.961	0.86866	1.0 e-4	1.1 e-3	1.2 e-3	5.7 e-5	1.1 e-2	1.1 e-2	7.4 e-6	9.5 e-5	9.5 e-5	0.86268
V9	293.130	79.091	0.87303	1.1 e-4	1.1 e-3	1.1 e-3	9.2 e-5	1.2 e-2	1.2 e-2	9.3 e-6	1.8e-4[+]	1.8 e-4[+]	0.87301
V10	293.130	79.135	0.87361	1.1 e-4	1.1 e-3	1.1 e-3	7.3 e-5	1.2 e-2	1.2 e-2	6.6 e-6	1.9 e-4[+]	1.9 e-4[+]	0.87358
V11	293.128	79.179	0.87424	2.9 e-4	1.3 e-3	1.3 e-3	8.7 e-5	1.2 e-2	1.2 e-2	9.0 e-6	2.2 e-4[+]	2.2 e-4[+]	0.87427
V12	293.130	79.219	0.87499	5.9 e-4	1.2 e-3	1.3 e-3	7.8 e-5	1.2 e-2	1.2 e-2	9.3 e-6	2.7 e-4[+]	2.7 e-4[+]	0.87504
V13	293.130	79.266	0.87626	9.8 e-5	1.1 e-3	1.1 e-3	6.5 e-5	1.2 e-2	1.2 e-2	4.4 e-6	3.8 e-4[+]	3.8 e-4[+]	0.87626

Table 6.6 (continued)

ID	Data			Temperature (K)			Pressure (bar)			Composition			
	$\bar{T}_f$ (K)	$\bar{p}_f$ (bar)	$\bar{x}_{CO_2}$ (-)	$s(\bar{T}_f)$	$\bar{u}_c(\bar{T})$	$\bar{u}_c(\bar{T}_f)$	$s(\bar{p}_f)$	$\bar{u}_c(\bar{p})$	$\bar{u}_c(\bar{p}_f)$	$s(\bar{y}_{CO_2})$	$\bar{u}_{tot}(\bar{y}_{CO_2})$	$\bar{u}_c(\bar{y}_{CO_2})$	$\bar{y}_{CO_2,calc}$
VI4	293.13	79.308	0.87817	1.5 e-4	1.2 e-3	1.2 e-3	7.2 e-5	1.2 e-2	1.2 e-2	1.50E-5	7.9e-4[+]	7.9e-4[+]	0.87813
P2	298.141	64.316[c]	0.99999	6.7 e-4	1.4 e-3	1.6 e-3	1.0 e-2	1.5 e-2	1.1 e-2				
VI5	298.142	66.410	0.98297	1.6 e-4	1.9 e-3	1.9 e-3	1.7 e-4	1.1 e-2	1.1 e-2	3.7 e-6	1.2 e-4	1.2 e-4	0.98448
VI6	298.141	69.754	0.95917	2.8 e-4	1.8 e-3	1.9 e-3	1.9 e-4	1.1 e-2	1.1 e-2	2.4 e-6	1.2 e-4	1.2 e-4	0.96113
VI7	298.142	73.114	0.93993	1.1 e-4	1.8 e-3	1.8 e-3	8.4 e-3	1.8 e-2	1.6 e-2	9.1 e-6	1.3 e-4	1.3 e-4	0.94114
VI8	298.143	75.078	0.93180	5.3 e-5	2.0 e-3	2.0 e-3	1.1 e-4	1.1 e-2	1.1 e-2	9.1 e-6	1.1 e-4	1.1 e-4	0.93141
VI9	298.142	76.250	0.92917	2.2 e-4	1.9 e-3	1.9 e-3	8.0 e-5	1.1 e-2	1.1 e-2	1.6 e-5	9.8 e-5	9.9 e-5	0.92867
V20	298.142	76.599	0.92928	1.5 e-4	1.9 e-3	1.9 e-3	7.5 e-5	1.1 e-2	1.1 e-2	9.7 e-6	1.1 e-4	1.1 e-4	0.92914
V21	298.142	76.783	0.92979	2.6 e-4	1.7 e-3	1.7 e-3	7.0 e-5	1.1 e-2	1.1 e-2	1.6 e-5	1.1 e-4[+]	1.1e-4[+]	0.92978
V22	298.142	76.886	0.93044	7.7 e-5	1.7 e-3	1.7 e-3	7.1 e-5	1.1 e-2	1.1 e-2	1.3 e-5	2.4 e-4[+]	2.4 e-4[+]	0.93046
V23	298.142	76.938	0.93103	8.0 e-5	1.8 e-3	1.8 e-3	4.4 e-3	1.2 e-2	1.2 e-2	1.7 e-4	2.0 e-4[+]	2.6 e-4[+]	0.92451
V24	298.142	76.977	0.93175	5.2 e-5	1.8 e-3	1.8 e-3	1.7 e-4	1.1 e-2	1.1 e-2	1.6 e-5	9.8 e-5[+]	9.9 e-5[+]	0.92441
P3	303.144	72.121[d]	0.99999	4.2 e-4	2.4 e-3	2.4 e-3	1.1 e-2	1.6 e-2	1.2 e-2				
V25	303.144	72.625	0.99695	1.9 e-4	2.4 e-3	2.4 e-3	1.3 e-4	1.1 e-2	1.1 e-2	2.5 e-6	1.1 e-4	1.1 e-4	0.99697
V26	303.144	73.064	0.99438	2.1 e-4	2.4 e-3	2.4 e-3	1.2 e-4	1.1 e-2	1.1 e-2	2.3 e-6	1.1 e-4	1.1 e-4	0.99455

Table 6.6 (continued)

ID	Data			Temperature (K)			Pressure (bar)			Composition			
	$\bar{T}_f$ (K)	$\bar{p}_f$ (bar)	$\bar{x}_{CO_2}$ (-)	$s(\bar{T}_f)$	$\bar{u}_c(\bar{T})$	$\bar{u}_c(\bar{T}_f)$	$s(\bar{p}_f)$	$\bar{u}_c(\bar{p})$	$\bar{u}_c(\bar{p}_f)$	$s(\bar{y}_{CO_2})$	$\bar{u}_{tot}(\bar{y}_{CO_2})$	$\bar{u}_c(\bar{y}_{CO_2})$	$\bar{y}_{CO_2,calc}$
V27	303.141	73.607	0.99142	9.2 e-4	2.4 e-3	2.6 e-3	9.0 e-5	1.1 e-2	1.1 e-2	5.8 e-6	1.10 e-4	1.1 e-4	0.99164
V28	303.144	74.155	0.98896	2.0 e-4	2.5 e-3	2.5 e-3	2.3 e-4	1.1 e-2	1.1 e-2	4.3 e-6	1.10 e-4	1.1 e-4	0.98894
V29	303.145	74.253	0.98862	7.9 e-5	2.5 e-3	2.5 e-3	3.9 e-4	1.1 e-2	1.1 e-2	2.7 e-6	9.6 e-5[+]	9.6 e-5[+]	0.98863
V30	303.145	74.287	0.98855	1.1 e-4	2.5 e-3	2.5 e-3	2.6 e-4	1.1 e-2	1.1 e-2	7.7 e-6	1.0 e-4[+]	1.0 e-4[+]	0.98855
V31	303.145	74.304	0.98856	2.4 e-4	2.6 e-3	2.6 e-3	2.5 e-4	1.1 e-2	1.1 e-2	9.2 e-6	9.8 e-5[+]	9.8 e-5[+]	0.98853
V32	303.145	74.316	0.98854	9.7 e-5	2.5 e-3	2.5 e-3	3.0 e-4	1.1 e-2	1.1 e-2	7.4 e-6	1.0 e-4[+]	1.0 e-4[+]	0.98853
V33	303.145	74.328	0.98855	2.2 e-4	2.5 e-3	2.5 e-3	1.7 e-4	1.1 e-2	1.1 e-2	6.0 e-6	9.5 e-5[+]	9.5 e-5[+]	0.98855
V34	303.144	74.341	0.98861	1.1 e-4	2.5 e-3	2.5 e-3	1.4 e-4	1.1 e-2	1.1 e-2	2.4 e-6	1.5 e-4[+]	1.5 e-4[+]	0.98862

[+] The derivatives $\frac{\partial y_{CO_2}}{\partial p}$ used in eq. 6.24 to obtain $\bar{u}_{tot}(y_{CO_2})$ were calculated using the scaling law in *eq. 6.32* with the parameters in Table 6.7.

[a] Sample standard deviation of the mean of the temperatures, $s(\bar{T}_f)$, mean of the standard systematic uncertainty of the temperature, $\bar{u}_c(\bar{T})$, total standard uncertainty of the temperature, $\bar{u}_c(\bar{T}_f)$, sample standard deviation of the mean of the pressures, $s(\bar{p}_f)$, mean of the standard systematic uncertainty of the pressure, $\bar{u}_c(\bar{p})$, total standard uncertainty of the pressure, $\bar{u}_c(\bar{p}_f)$, sample standard deviation of the mean of the mol fractions, $s(\bar{x}_{CO_2})$, mean of the total standard uncertainty of the mol fractions, $\bar{u}_{tot}(\bar{y}_{CO_2})$, mean of the total combined uncertainties of the mol fractions, $\bar{u}_c(\bar{y}_{CO_2})$, and UMR-PRU calculated mol fraction, $\bar{y}_{CO_2,calc}$.

[b] Span-Wagner CO_2 vapor pressure is 57.256 ± 0.017 bar.

[c] Span-Wagner CO_2 vapor pressure is 64.317 ± 0.019 bar.

[d] Span-Wagner CO_2 vapor pressure is 72.131 ± 0.021 bar.

6.3.1. Summary and Analysis of Uncertainty Estimates

As it can be retrieved from Table 6.5, the maximum and average standard deviation of the measurements in terms of CO_2 composition in the liquid phase is $2.5 \cdot 10^{-5}$ and $9.6 \cdot 10^{-6}$, respectively. For the vapor phase, as it can be extracted from Table 6.6, the maximum and average standard deviation is $1.7 \cdot 10^{-4}$ and $1.5 \cdot 10^{-5}$, which indicates that there is higher dispersion in the vapor phase compared to the liquid one. Except for the maximum values, the estimated standard deviation in the mean mol fractions is significantly lower than the systematic uncertainty of the composition measurement. It is also apparent from Figure 6.8, that the relative uncertainty in composition is low for the isotherms of 293.13 K and 298.14 K, while it is higher for the isotherm of 303.15 K, where the CH_4 solubility in CO_2 is extremely low. Still, even if we take into account the uncertainty estimates, the data provide a very good description of the phase boundary.

The estimated standard uncertainty of the VLE measurement in terms of mol fractions, $u_{tot}(\bar{x}_{CO_2})$ and $u_{tot}(\bar{y}_{CO_2})$, shows an increasing trend with pressure in general for each isotherm. The maximum of $u_{tot}(\bar{x}_{CO_2})$ is $8.2 \cdot 10^{-4}$ for the series in the critical region, and approximately $1.2 \cdot 10^{-4}$ for the series outside the critical region. $u_{tot}(\bar{y}_{CO_2})$, has a maximum value of $7.9 \cdot 10^{-4}$ in the critical region, and approximately $1.4 \cdot 10^{-4}$ for the series outside the critical region.

The combined standard uncertainty of the measured pressure, $u_c(\bar{p})$, has an average value of 0.011 bar, with a maximum value equal to 0.012 bar. This corresponds to approximately 0.02 % for the lowest measured pressure and 0.01 % for the highest one.

6.3.2. Critical Point Estimation

For binary mixtures the critical point in terms of pressure and temperature is dependent on the composition. For a given temperature, the composition, if any, where the critical point is attained, is denoted as $z_{CO_2,C}$. The critical composition and pressure, p_c, are identified as the maximum pressure point in closed isothermal pressure – composition phase envelopes of binary mixtures. The thermodynamic behavior around critical points in a range of different systems, including VLE, has been estimated using scaling laws from statistical mechanics[32-34]. For binary mixtures, the following scaling law, proposed by Lachet et al.[35] can be applied, as per eq. 6.32.

$$z_{CO_2} = \hat{z}_{CO_2,C} + \left(\lambda_1 + \varepsilon \frac{\lambda_2}{2}\right)(\hat{p}_c - p) + \varepsilon \frac{\mu}{2}(\hat{p}_c - p)^{\beta} \qquad \text{eq. 6.32}$$

Here, ε equals 1 for bubble points and -1 for dew points, z_{CO_2} is the bubble point or dew point composition at pressure p measured in an area close to the critical point, $\hat{z}_{CO_2,C}$ is the estimated composition in the critical point, $\hat{p}_c$ the estimated critical point pressure and λ_1, λ_2, μ and β the scaling law parameters.

According to Sengers et al.[36] a constant value of β equal to 0.325 is appropriate, leaving three parameters, λ_1, λ_2 and μ to be fitted to the data of each isotherm. The regression has been performed to the VLE data indicated in Table 6.7, along with the estimated results, using the ordinary unweighted least squares method.

The uncertainty in the estimated critical composition and pressure, $u(\hat{z}_{CO_2,C})$ and $u(\hat{p}_c)$ respectively, are calculated according to eq. 6.33 - eq. 6.34 and it is based on the uncertainties in the composition and pressure of the VLE data used for the fitting, as well as the standard errors of regression for the critical pressure and composition, $S_E(\hat{p}_C)$ and $S_E(\hat{z}_{CO_2,C})$. These uncertainty estimates are considered conservative in the essence that it is assumed that the measurement errors are systematic, while the uncertainty estimates of the critical points do not fully take into account possible model errors.

$$\mathrm{u}(\hat{z}_{CO_2,c}) = \sqrt{S_E^2(\hat{z}_{CO_2,c}) + \left[\frac{1}{n_p}\sum_{i=1}^{n_p} u_c(\bar{z}_{i,CO_2})\right]^2} \qquad \text{eq. 6.33}$$

$$\mathrm{u}(\hat{\mathrm{p}}_c) = \sqrt{S_E^2(\hat{p}_c) + \left[\frac{1}{n_p}\sum_{i=1}^{n_p} u_c(\bar{p}_{i,f})\right]^2} \qquad \text{eq. 6.34}$$

The total uncertainty in the composition is calculated, as mentioned beforehands, using the derivatives of the composition with respect to pressure, which are calculated numerically by utilizing the scaling law.

The estimated critical point pressure and composition are given along with their respective uncertainties in Table 6.7 and are presented graphically in Figure 6.9.

Although the fitting of the scaling law is straightforward, one parameter of importance is the selection of the experimental points close to the critical area to be included in the fitting. Although different sets of scaling law parameters have been tested for the estimation of the critical point, all VLE measurements close to the critical area are included in order to better attain the trend of the experimental data. As shown in Figure 6.9*c*, only a single vapor phase point has been excluded from the fitting, since it appears to be somewhat of an outlier. The deviations obtained are within the observed uncertainty.

Table 6.7: Parameters of the scaling law (eq. 6.32) fitted to critical region data from this work for the three different average temperatures.

T (K)	Used points	n_p	$10^3 \cdot \hat{\lambda}_1$ (bar^{-1})	$10^2 \cdot \hat{\lambda}_2$ (bar^{-1})	$10^4 \cdot \hat{\mu}$ (bar$^{-\beta}$)	$\hat{z}_{CO_2,c}$	$\hat{p}_c$ (bar)	$S_E(\hat{z}_{CO_2,c})$	$u(\hat{z}_{CO_2,c})$	$S_E(\hat{p}_c)$ (bar)	$u(\hat{p}_c)$ (bar)
293.130	L9-L14, V9-V14	12	2.3192	3.2924	7.8298	0.8829	79.33	8.60E-4	0.00086	0.01	0.0101
298.142	L21-L24, V21-V24	8	3.1311	1.8708	1.3064	0.9349	77.02	6.60E-4	0.00067	0.01	0.0101
303.145	L29-L34, V29, V30, V32-V34	11	4.4845	0.3604	-19.381	0.9889	74.35	3.60E-4	0.00037	0.01	0.0101

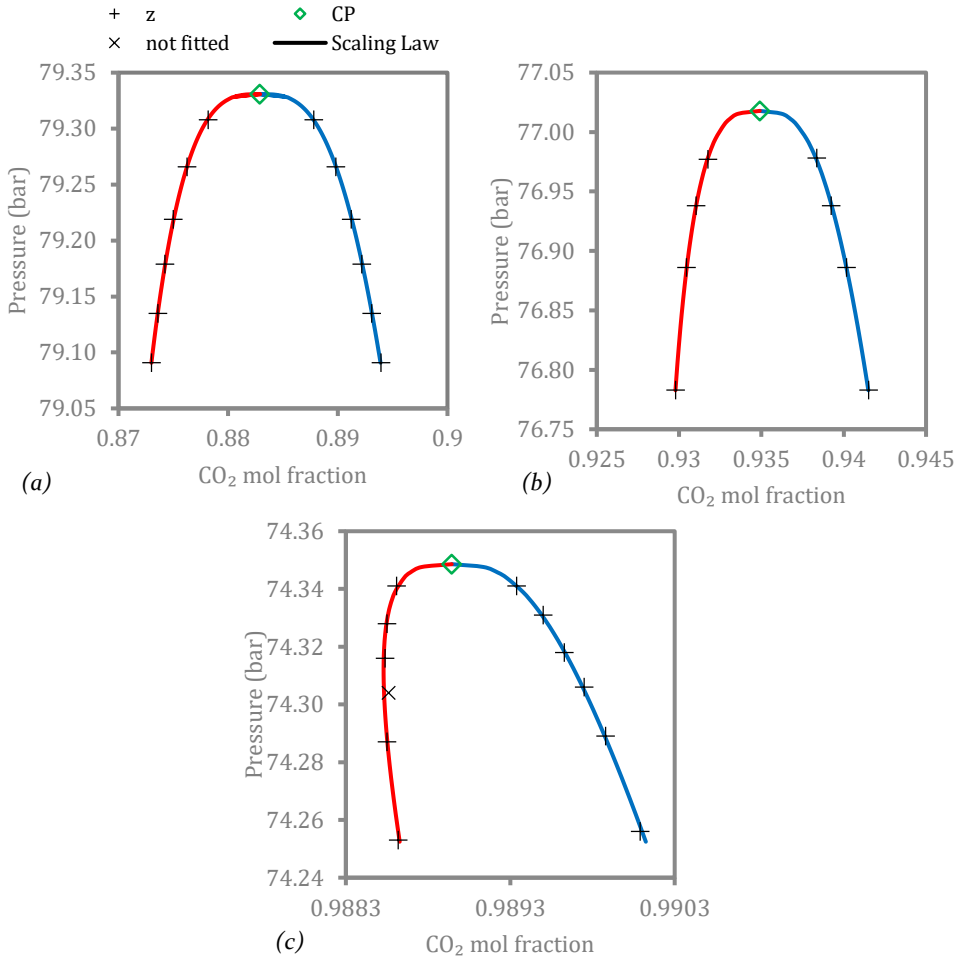

Figure 6.9: Pressure – composition phase behavior in the critical region estimated by the scaling law model in eq. 6.32. (+) indicates the points used for the fitting of the scaling law (see Table 6.7), (x) indicates the points not used in the fitting of scaling law and solid line indicates the scaling law correlation. Dashed line indicates a second set of the scaling law parameters to show the effect of the appropriate selection of data points used for the fitting of the parameters. Blue colour indicates the liquid phase and red colour the vapor one. Please note that the scales of the graphs are very different from each other. (a) 293.13 K, (b) 298.14 K and (c) 303.15 K.

6.3.3. Comparison with literature data and GERG-2008 prediction

As it is has been stated in the above, very few and mostly inconsistent experimental data are available at the temperatures of interest. The isotherm of 293.15 K, where three data sets, namely those of Xu et al.[6], Nasir et al.[5] and Devlikamov et al.[7], are available is used to validate the obtained measurements. To that purpose, they are plotted along with the measurements of this work in Figure 6.8*a*. In general, fairly good agreement is observed between the data of Xu et al.[6] and our measurements, especially in the vapor phase, in the areas away of the critical. It should be noted that the uncertainties reported by Xu et al.[6] are an order of magnitude higher than those in this work, namely, 0.01 K in temperature, 0.2 bar in pressure and 0.001 in the composition. Furthermore, much scattering is observed especially for the vapor phase measurements, indicating that at those points the uncertainty is much higher. For the liquid phase, although there is generally good agreement between the datasets, Xu et al.[6] systematically report slightly lower CO_2 mol fraction in the liquid phase compared to this work. The most distinctive differences are reported in the vicinity of the critical area, where Xu et al.[6] report significantly lower CO_2 mol fraction. Maybe this can be attributed to the difference in the purity between the source chemicals used; that is 99.95 % for methane and 99.97 % for CO_2, compared to 99.9995 % for methane and 99.9992 % for CO_2 used in this work. This difference in the pure chemicals may cause this shift of the phase boundary to lower CO_2 concentrations in both phases due to the existence of higher molecular weight compounds, rendering the VLE data measured in this work more accurate. Nasir et al.[5] recently reported three VLE measurements at the isotherm of 293.65 K. As it is observed in Figure 6.8*a*, our data are in agreement with the reported measurements of Nasir et al.[5] in both phases. Furthermore, the data by Devlikamov et al.[7] for pressure higher than 70 bar, show significantly lower methane content in the liquid phase as compared to the data by Xu et al.[6], Nasir et al.[5], the data measured in this work, as well as the predictions of the GERG-2008 model. Similar behavior is observed at the isotherm of 283.15 K for the bubble point measurements of Devlikamov et al.[7], where they present lower methane solubility compared to the data measured by Kaminishi et al.[4] and Nasir et al.[5] (Figure 6.1*b*). For the above mentioned reasons, the data by Devlikamov et al.[7] are considered inaccurate. Finally, for the non-critical area, the experimental data obtained in this work are in good agreement with the predictions of the GERG-2008 model.

At the mean temperature of 298.14 K, only the data by Devlikamov et al.[7] for the liquid phase exist, which, as discussed above, are generally considered inaccurate and thus cannot be used to evaluate the data obtained in our work. Therefore, the only comparison of value can occur with the prediction of an accurate thermodynamic model. As it is presented in Figure 6.8*b*, the obtained data are in good agreement with the prediction of GERG-2008 and thus are considered to be of reasonable accuracy.

VLE data at 303.15 K for the CO_2/CH_4 mixture have not been presented in the literature and thus, the comparison of the data obtained in this work is limited to the prediction of the GERG-2008 model. As it is observed in Figure 6.8*c*, the GERG-2008 prediction

for both phases is within the limits of the experimental accuracy away from the critical region. Nevertheless, it overpredicts significantly the pressure at the critical region, as well as the composition at the critical point.

6.4. Model Fitting

Due to the deficiency of GERG-2008 model to accurately describe the mixture behavior close to the critical area, isotherm specific parameters are fitted for other thermodynamic models. Since equations of state are usually used for the design and control of process simulations, the SRK and the PR EoSs, the latter with the vdW1f and with advanced mixing rules (UMR-PRU), as well as the PC-SAFT EoS are used to correlate the experimental data of each isotherm. The critical properties (T_c, p_c, ω) required for the pure components for the cubic EoSs and the UMR-PRU model are those of Table 5.2. It should be noted that although there are various versions of PC-SAFT documented in the literature, in this work, the original PC-SAFT proposed by Gross and Sadowski[37] is considered, treating CO_2 as a non-associating compound, as documented in Chapter 5. As illustrated in Figure 6.10, using this consideration PC-SAFT cannot capture accurately the critical point of CO_2 and as such, its pure component parameters had to be refitted to vapor pressure and liquid density data taken from DIPPR[38], with enforced critical temperature and pressure. The new pure component parameters obtained for the PC-SAFT EoS through the fitting procedure are presented in Table 6.8, while their performance is shown graphically in Figure 6.10.

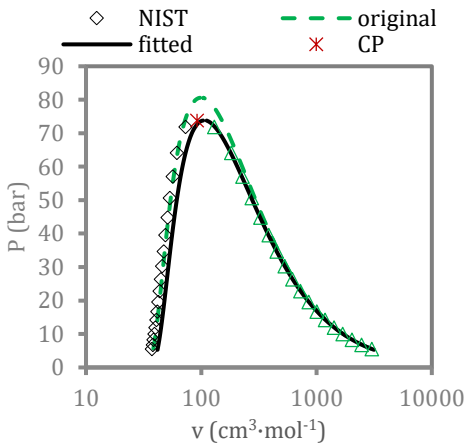

Figure 6.10: Phase diagram of pure CO_2 with PC-SAFT using two sets of pure component parameters. Exp. data are taken from NIST[39].

Table 6.8: Pure component parameters for PC-SAFT EoS.

Component	Ref.	m	ε/k (K)	σ (Å)
CO_2	This work[a]	2.6246	148.39	2.6264
Methane	37	1.0000	150.03	3.7039

[a] PC-SAFT parameters were determined by fitting vapor pressure data and liquid density data[40] in the T_r-range of 0.71 to 0.999, with an average absolute error of 0.03 % in vapor pressure, 14 % in saturated liquid molar volume, ΔT_c = -2.0·10^{-5} K and Δp_c = -1.7·10^{-4} bar, where, $\Delta T_c = T_c^{calc} - T_c^{exp}$ and $\Delta p_c = p_c^{calc} - p_c^{exp}$.

Table 6.9: Binary interaction parameters for SRK, PR, PC-SAFT and UMR-PRU fitted to the experimental data of this work, through eq. 6.35, *for each isotherm.*

$\bar{T}$ (K)	n_p	k_{ij}			UMR-PRU		$\%\Delta p^a$				$100\cdot\Delta y_{CO_2}{}^b$			
		PR	SRK	PC-SAFT	$u_{nm}{}^c$	$u_{mn}{}^c$	PR	SRK	PC-SAFT	UMR-PRU	PR	SRK	PC-SAFT	UMR-PRU
293.130	12	0.1236	0.1319	0.0876	439.69	-136.68	0.62	0.60	0.75	0.29	0.98	1.15	1.01	0.82
298.142	8	0.1251	0.1604	0.0933	635.80	-226.23	0.27	0.44	0.31	0.16	0.43	0.51	0.47	0.34
303.145	11	0.1603	0.1774	0.1200	830.36	-305.00	0.04	0.03	0.09	0.06	0.04	0.04	0.05	0.04
Overall	37	-	-	-	-	-	0.34	0.38	0.42	0.18	0.55	0.58	0.52	0.43

[a] $\%\Delta p = 100\cdot\frac{1}{n_p}\sum_{i=1}^{n_p}\frac{|\bar{p}_f{}^{exp}-\mathrm{p}^{calc}|}{\bar{p}_f{}^{exp}}$, where $\bar{p}_f{}^{exp}$ is the experimental bubble point pressure and p^{calc} the calculated bubble point pressure for each model.

[b] $\%\Delta y_{CO_2} = 100\cdot\frac{1}{n_p}\cdot\sum_{i=1}^{n_p}\frac{|\bar{y}_{CO_2}^{exp}-y_{CO_2}^{calc}|}{\bar{y}_{CO_2}^{exp}}$, where $y_{CO_2}^{exp}$ and $y_{CO_2}^{calc}$ are the experimental and calculated CO_2 concentration in vapor phase at pressure $\bar{p}_f$.

[c] n, m: UNIFAC groups of the UMR-PRU model, where n represents CO_2 and m represents CH_4.

The binary interaction parameters of the models have been determined by fitting the bubble point pressure experimental data presented in Table 6.5, using the objective function of eq. 6.35. The respective results for each isotherm along with the absolute average deviation are tabulated in Table 6.9.

$$S = \frac{1}{n_p}\sum_{i=1}^{n_p} 100\frac{abs(p_i^{exp} - p_i^{calc})}{p_i^{exp}} \qquad \text{eq. 6.35}$$

where S is the objective function to be minimized, n_p the number of experimental data points used for the fitting of the parameters, p_i^{exp}, the experimental pressure of a VLE point, as determined in Table 6.5 and p_i^{calc} the bubble point pressure calculated from the thermodynamic model.

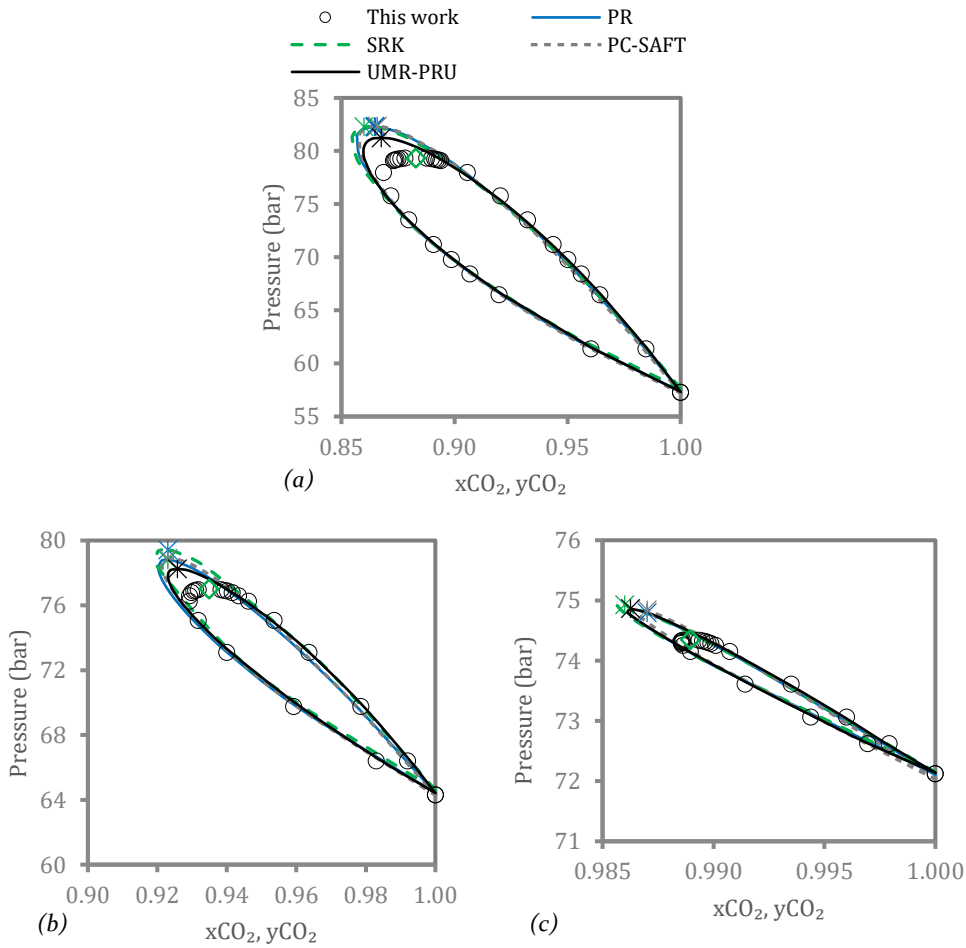

Figure 6.11: Binary VLE correlation results for the CO_2/CH_4 mixture at (a) 293.13 K, (b) 298.14 K and (c) 303.15 K, with the: PR (blue solid line), SRK (green long dashed line), PC-SAFT (grey dotted line) and UMR-PRU (black solid line). (○) denotes the experimental data of this work as presented in Table 6.5 and Table 6.6. Note that the critical point estimated through the scaling law from the experimental data is marked as a green (◇) while the predicted critical point of the models as a (✶) of the same coloring as the respective model.

As it can be observed from the results presented in Table 6.9 and Figure 6.11, all models describe accurately the bubble point pressure even at 303.15 K, which is close to the critical temperature of pure CO_2. The more theoretically strong PC-SAFT equation of state does not pose any advantage compared to the cubic EoSs. Instead, it requires refitting of the pure component parameters in order to be able to describe accurately the CO_2 vapor pressure in the critical area. This can be attributed to the fact that the potential and reference fluid used in PC-SAFT had been initially developed for polymers and thus it is more accurate for larger, chain-like molecules, while both CO_2 and CH_4 deviate from this consideration. SRK and PR combined with the vdW1f mixing rules, on the other hand, result in an overall absolute average relative deviation (AARD) equal to 0.34 % and 0.38 % respectively, which is lower than the one expressed by PC-SAFT EoS, namely 0.42 %. It should be noted that although the vapor phase has been not included in the fitting of the models' parameters, very satisfactory results are obtained for all the examined models. Finally, UMR-PRU yields the best correlation results especially with reference to the critical point estimation. This can be attributed to the fact that UMR-PRU has two adjustable parameters, u_{nm} and u_{mn}, due to the local composition nature of UNIFAC, which provides more flexibility as compared to the one k_{ij} value required for the cubic EoSs and PC-SAFT. Table 6.10 presents the deviations of the UMR-PRU model, which provides the most accurate results with respect to the critical point, against the critical pressure and composition values estimated with the scaling law. The maximum deviation in critical pressure obtained with the UMR-PRU model is 2.37 % and in the critical point composition 1.73 %. Since the UMR-PRU model yields the lower deviation compared to the experimental data, it is used for the calculation of the derivative of the composition with respect to temperature and pressure in order to calculate the total uncertainty in composition.

Table 6.10: Deviations of the UMR-PRU model from the estimated by the scaling law critical point data.

	293.13 K		298.14 K		303.15 K	
	p_c (bar)	$z_{CO_2,c}$	p_c (bar)	$z_{CO_2,c}$	p_c (bar)	$z_{CO_2,c}$
Exp.	79.33	0.8829	77.02	0.9350	74.35	0.98895
UMR-PRU	81.21	0.8676	78.24	0.9258	74.86	0.98625
% AARD[a]	2.37	1.73	1.59	0.97	0.69	0.27

[a] *% AARD* $= 100 \cdot \frac{1}{n_p}\sum_{i=1}^{n_p}\frac{|x^{exp}-x^{calc}|}{x^{exp}}$, *where x represents the critical point pressure,* p_c, *or the composition at the critical point,* $z_{CO_2,c}$.

6.5. Conclusions

Vapor – liquid equilibrium data for the CO_2/CH_4 binary mixture have been measured at the mean temperatures of 293.13 K, 298.14 K and 303.15 K. The reported data map both the bubble point and dew point curves for each isotherm, ranging from the CO_2 vapor pressure up to the critical point of the mixture, with emphasis given to the critical region. The critical point of the mixture has been estimated for each isotherm by fitting the scaling law to the VLE data obtained in the proximity of the critical area. The vapor pressure of the pure CO_2 is consistent with the values calculated with the Span – Wagner equation of state, which is a reference EoS for CO_2 properties. Due to the lack of experimental data in the measured isotherms, comparison with other data available in literature has been only possible for the isotherm of 293.13 K. It is shown that the performed measurements are in fairly good agreement with the reported literature data. Very good agreement between the GERG-2008 predictions and the measurements of this work in the vapor and liquid phase for the non-critical area is also observed.

New binary interaction parameters have been fitted to the experimental data of each isotherm for four models; the cubic EoSs SRK and PR combined with the classic vdWlf mixing rules, the PC-SAFT EoS and the UMR-PRU model. Very satisfactory correlation results have been obtained for all models outside the critical region. In the bubble point pressure, PR yields an overall deviation at the three examined isotherms equal to 0.34 %, the corresponding number for SRK is 0.38 %, PC-SAFT yields slightly higher deviation equal to 0.42 %, while UMR-PRU results in a 0.18 % deviation. In the prediction of the vapor phase composition, all examined models yield satisfactory and similar results. Specifically, PR yields a deviation equal to 0.55 %, SRK 0.58 %, PC-SAFT 0.52 %, while again UMR-PRU gives the lowest deviation equal to 0.43 %. Finally, the accuracy of the models has been also evaluated in the prediction of the critical point of the mixture, where PR, SRK and PC-SAFT yield similar results, while UMR-PRU predicts slightly better the critical point both in terms of critical point pressure and composition with an overall deviation equal to 1.15 % and 0.99 % respectively.

As a concluding remark, the obtained data improve the data situation for the CO_2/CH_4 mixture at temperatures of interest to natural gas applications, and can be also used as a basis for extending the applicability of several thermodynamic models.

List of Symbols

Latin Characters

A_i	area covered in the GC chromatogram for the component *i*, derived after numerical integration
c_i	fitted parameters to relate the area covered in the GC chromatogram to number of moles passed through the detector, $i = 1$ to 5
e	error between the calibration gas CO_2 mol fraction and the mol fraction calculated through the GC adaptation
h	height (m)
k	constant factor relating the areas to the number of moles in eq. 6.20 - eq. 6.21
k_{ij}	binary interaction parameter between the components *i* and *j* for the attractive term of SRK and PR EoS and the segment – segment interaction of unlike chains in the Berthelot – Lorentz mixing rules in PC-SAFT EoS.
M	magnetic stirrer
M_i	molar mass of component *i* ($kg \cdot kmol^{-1}$)
m_i	PC-SAFT segment number of component *i*
n	number of data series used to relate the area covered in the GC chromatogram to number of moles passed through the detector
n_p	number of data points used for the fitting of model parameters used in eq. 6.35
p	pressure at VLE (bar)
p_c	estimated critical pressure (bar)
$\bar{p}$	pressure at VLE: mean pressure before one composition sample (bar)
p_i	absolute pressure sensors ($i = 1$ to 4)
$\bar{p}_f$	pressure at VLE: mean of the pressures $\bar{p}$ for a series of composition samples in Table 6.5 and Table 6.6 (bar)
Q_i	relative van der Waals surface area of group *i*
R	universal ideal gas constant (83.14 bar cm^3 mol^{-1} K^{-1})
R	resistance (Ω)
R_i	relative van der Waals volume of group *i*

$s(z)$	sample standard deviation of variable z
$s(\bar{z})$	sample standard deviation of the mean of variable z
S	model fitting objective function to be minimized.
S_E	standard error of regression.
$\bar{T}$	ITS-90 temperature at VLE: mean temperature before one composition sample (K)
$\bar{T}_f$	ITS-90 temperature at VLE: mean of the temperatures $\bar{T}$ for a series of composition samples in Table 6.5 and Table 6.6 (K)
$u(z)$	standard uncertainty of variable z
$u_c(z)$	combined standard uncertainty of variable z
u_{nm}	UNIFAC binary interaction parameter between groups n and m
$u_{tot}(z)$	total standard uncertainty of variable z = x_{CO_2} or y_{CO_2}
W_b	bridge ratio (eq. 6.4)
x_{CO_2}	liquid phase CO_2 mol fraction at VLE given in Table S.1 in the Supplementary Material.
$\bar{x}_{CO_2}$	liquid phase CO_2 mol fraction at VLE: mean mol fraction for a series of composition samples in Table 6.5.
$x_{CO_2,calc}$	liquid phase CO_2 mol fraction at VLE, calculated from the fitted UMR-PRU.
y_{CO_2}	vapor phase CO_2 mol fraction at VLE.
$\bar{y}_{CO_2}$	vapor phase CO_2 mol fraction at VLE: mean mol fraction for a series of composition samples in Table 6.6.
$\bar{y}_{CO_2,calc}$	vapor phase CO_2 mol fraction at VLE, calculated from the fitted UMR-PRU
z_{CO_2}	liquid or vapor phase CO_2 mol fraction
$z_{CO_2,c}$	estimated critical composition in terms of CO_2 mol fraction.

Greek Characters

β	universal critical exponent of scaling law in eq. 6.32
ε	scaling law parameter in eq. 6.32
ε_i/k	PC-SAFT segment energy parameter of component *i (K)*

λ_i	scaling law parameter in eq. 6.32, $i = 1$ to 2 (bar^{-1})
μ	scaling law parameter in eq. 6.32 ($bar^{-\beta}$)
σ_i	PC-SAFT segment diameter of component i (Å)

Superscripts and Subscripts

ads	adsorption
c	critical property
c	combined
Calc	calculated
cyl	cylinder
eff	effective
Exp	experimental
f	subscript to denote the average mean value of temperature and pressure for a VLE measurement
hs	hydrostatic
imp	impurity
max	maximum
m, n	UNIFAC groups
p	points
r	reduced property
ref	reference
res	residual

References

(1) Pedersen K.S., Christensen P.L., Shaikh J.A., *Phase behavior of petroleum reservoir fluids*. CRC press: 2014.
(2) Li H., Jakobsen J.P., Wilhelmsen Ø.,Yan J., PVTxy properties of CO_2 mixtures relevant for CO2 capture, transport and storage: Review of available experimental data and theoretical models. *Applied Energy* **2011,** *88*, (11), 3567-3579.
(3) http://trc.nist.gov/thermolit/main/home.html#home, accessed on 07/17/2017.
(4) Kaminishi G.-I., Arai Y., Saito S., Maeda S., Vapor-liquid equilibria for binary and ternary systems containing carbon dioxide. *J. Chem. Eng. Jpn.* **1968,** *1*, (2), 109-116.
(5) Nasir Q., Sabil K.M., Lau K.K., Measurement of isothermal (vapor + liquid) equilibria, (VLE) for binary (CH_4 + CO_2) from T = (240.35 to 293.15) K and CO_2 rich synthetic natural gas systems from T = (248.15 to 279.15) K. *Journal of Natural Gas Science and Engineering* **2015,** *27, Part 1*, 158-167.
(6) Xu N.D., Wang, Y., Shi, J., High pressure vapor liquid equilibria at 293 K for systems containing nitrogen, methane and carbon dioxide. *Fluid Phase Equilibria* **1992,** *81*, 175-186.
(7) Devlikamov V.V., Semenova L.V., Repin N.N., Solubility of methane in liquid carbon dioxide. *Izv. Vyssh. Uchebn. Zaved.* **1982,** *8*, 42-44.
(8) Al-Sahhaf T.A., Kidnay A.J., Sloan E.D., Liquid+ vapor equilibriums in the nitrogen+ carbon dioxide+ methane system. *Industrial & Engineering Chemistry Fundamentals* **1983,** *22*, (4), 372-380.
(9) Davalos J.A., W. R., Phelps E., Kidnay, A. J., Liquid-Vapor Equilibria at 150.00K for Systems Containing Methane, Ethane and Carbon Dioxide. *J. Chem. Eng. Data* **1976,** *21*.
(10) Somait F.A.K., A.J., Liquid-Vapor Equilibria at 270.00 K for Systems Containing Nitrogen, Methane, and Carbon Dioxide. *J. Chem. Eng. Data* **1978**.
(11) Webster L.A., Kidnay A.J., Vapor–Liquid Equilibria for the Methane–Propane–Carbon Dioxide Systems at 230 K and 270 K. *Journal of Chemical & Engineering Data* **2001,** *46*, (3), 759-764.
(12) Wei M.S.W., Brown T.S., Kidnay A.J., Sloan E.D., Vapor + Liquid Equilibria for the Ternary System Methane + Ethane + Carbon Dioxide at 230 K and Its Constituent Binaries at Temperatures from 207 to 270 K. *Journal of Chemical & Engineering Data* **1995,** *40*, (4), 726-731.
(13) Arai Y., Kaminishi G.-I., Saito S., The experimental determination of the p-v-t-x (pressure-volume-temperature-composition) relations for the carbon dioxide - nitrogen and the carbon dioxide-methane systems. *J. Chem. Eng. Jpn.* **1971,** *4*, (2), 113-122.
(14) Shi M., Wei M., Zhang J., Wang L., Simple and speedy measurement of bubble point and dew point for VLE binary system under pressure. *Chemical Engineering (China)* **1984,** *6*, 51-54.
(15) Bian B., Wang Y., Shi J., Zhao E., Lu B.C.Y., Simultaneous determination of vapor-liquid equilibrium and molar volumes for coexisting phases up to the critical temperature with a static method. *Fluid Phase Equilibria* **1993,** *90*, (1), 177-187.
(16) Perez A.G., Coquelet C., Paricaud P., Chapoy A., Comparative study of vapour-liquid equilibrium and density modelling of mixtures related to carbon capture and storage with the SRK, PR, PC-SAFT and SAFT-VR Mie equations of state for industrial uses. *Fluid Phase Equilibria* **2017,** *440*, 19-35.

(17) Westman S.F., Stang H.G.J., Løvseth S.W., Austegard A., Snustad I., Størset S.Ø., Ertesvåg I.S., Vapor–liquid equilibrium data for the carbon dioxide and nitrogen ($CO_2 + N_2$) system at the temperatures 223, 270, 298 and 303 K and pressures up to 18 MPa. *Fluid Phase Equilibria* **2016,** *409*, 207-241.
(18) Donnelly H.G., Katz D.L., Phase Equilibria in the Carbon Dioxide–Methane System. *Industrial & Engineering Chemistry* **1954,** *46*, (3), 511-517.
(19) Knapp H., Yang X., Zhang Z., Vapor—liquid equilibria in ternary mixtures containing nitrogen, methane, ethane and carbondioxide at low temperatures and high pressures. *Fluid Phase Equilibria* **1990,** *54*, 1-18.
(20) Joffe J., Vapor-liquid equilibria by the pseudocritical method. *Industrial & Engineering Chemistry Fundamentals* **1976,** *15*, (4), 298-303.
(21) Serpa J., Morbee J., Tzimas E., *Technical and Economic Characteristics of a CO2 Transmission Pipeline Infrastructure* Luxembourg: Publications Office of the European Union 2011.
(22) Westman S.F., Stang H.G.J., Løvseth S.W., Austegard A., Snustad I., Ertesvåg I.S., Vapor-liquid equilibrium data for the carbon dioxide and oxygen (CO2 + O2) system at the temperatures 218, 233, 253, 273, 288 and 298 K and pressures up to 14 MPa. *Fluid Phase Equilibria* **2016,** *421*, 67-87.
(23) Guilbot P., Valtz A., Legendre H., Richon D., Rapid on-line sampler-injector: a reliable tool for HT-HP sampling and on-line GC analysis. *Analusis* **2000,** *28*, (5), 426-431.
(24) Span R.,Wagner W., A New Equation of State for Carbon Dioxide Covering the Fluid Region from the Triple-Point Temperature to 1100 K at Pressures up to 800 MPa. *Journal of Physical and Chemical Reference Data* **1996,** *25*, (6), 1509-1596.
(25) Chirico R.D., de Loos T.W., Gmehling J., Goodwin A.R.H., Gupta S., Haynes W.M., Marsh K.N., Rives V., Olson J.D., Spencer C., Brennecke J.F., Trusler J.P.M., Guidelines for reporting of phase equilibrium measurements (IUPAC Recommendations 2012). In *Pure and Applied Chemistry*, 2012; *Vol. 84*, p 1785.
(26) BIPM I., IFCC I.,ISO I., Iupap and oiml 2008. *Evaluation of Measurement Data - Guide to the Expression of Uncertainty in Measurement* **2008**.
(27) Preston-Thomas H., The international temperature scale of 1990 (ITS-90). *metrologia* **1990,** *27*, (1), 3.
(28) Milton M.J.T., Vargha G.M., Brown A.S., Gravimetric methods for the preparation of standard gas mixtures. *metrologia* **2011,** *48*, (5), R1.
(29) Wieser M.E., Holden N., Coplen T.B., Böhlke J.K., Berglund M., Brand W.A., De Bièvre P., Gröning M., Loss R.D., Meija J., Atomic weights of the elements 2011 (IUPAC Technical Report). *Pure and Applied Chemistry* **2013,** *85*, (5), 1047-1078.
(30) Wieser M.E.,Coplen T.B., Atomic weights of the elements 2009 (IUPAC Technical Report). In *Pure and Applied Chemistry*, 2010; *Vol. 83*, p 359.
(31) Leuenberger M., Schibig M., Nyfeler P., Gas adsorption and desorption effects on cylinders and their importance for long-term gas records. *Atmospheric Chemistry and Physics Discussions* **2014,** *14*, (13), 19293-19314.
(32) Fisher M.E., The theory of equilibrium critical phenomena. *Reports on progress in physics* **1967,** *30*, (2), 615.
(33) Green M.S., Vicentini-Missoni M., Sengers J.L., Scaling-law equation of state for gases in the critical region. *Physical Review Letters* **1967,** *18*, (25), 1113.

(34) Kadanoff L.P., Götze W., Hamblen D., Hecht R., Lewis E., Palciauskas V.V., Rayl M., Swift J., Aspnes D., Kane J., Static phenomena near critical points: theory and experiment. *Reviews of Modern Physics* **1967,** *39*, (2), 395.
(35) Lachet V., de Bruin T., Ungerer P., Coquelet C., Valtz A., Hasanov V., Lockwood F.,Richon D., Thermodynamic behavior of the CO2+SO2 mixture: Experimental and Monte Carlo simulation studies. *Energy Procedia* **2009,** *1*, (1), 1641-1647.
(36) Sengers J.V., Levelt Sengers J.M.H., A universal representation of the thermodynamic properties of fluids in the critical region. *International journal of thermophysics* **1984,** *5*, (2), 195-208.
(37) Gross J., Sadowski G., Perturbed-Chain SAFT: An Equation of State Based on a Perturbation Theory for Chain Molecules. *Industrial & engineering chemistry research* **2001,** *40*, (4), 1244-1260.
(38) Daubert T.E., Danner R.P., Sibul H., Stebbins C., *Physical and thermodynamic properties of pure chemicals: data compilation*. Hemisphere: New York, 1989.
(39) NIST Thermophysical Properties of Fluid Systems, http://webbook.nist.gov/chemistry/fluid/, accessed on 01/09/2017.
(40) Daubert T.E., Danner R.P., *Physical and Thermodynamic Properties of Pure Chemicals: Data Compilation*. Hemisphere: New York, 2003.

Chapter 7: Extension of UMR-PRU to natural gas mixtures containing polar components

In this Chapter, the extension of the UMR-PRU model to mixtures of natural gas components with hydrogen bonding compounds is presented. This extension is necessary due to the fact that UNIFAC has been initially developed for condensable fluids and no interaction parameters are available for components usually encountered in gaseous state. To that end, new binary interaction parameters between light gases, water, methanol and glycols (ethylene glycol, triethylene glycol) are developed and are tested in the prediction of multicomponent mixtures.

7.1. Introduction

The major advantage of UMR-PRU is its attractive ability to predict the phase equilibria of various mixtures due to the group – contribution nature of UNIFAC. However, in the case of natural gas mixtures, where components which are in gaseous phase at ambient conditions such as methane are encountered, there are no available UNIFAC interaction parameters. The latter is due to the fact that UNIFAC, as an activity coefficient model, is developed for compounds existing in the liquid phase. So, in order to extend the applicability of the UMR-PRU model for natural gas mixtures with polar components, new interaction parameters are required. Several approaches exist to this purpose, depending on the application of interest, since in general, it is well – known that thermodynamic models cannot describe with sufficient accuracy all kind of properties using the same interaction parameters. For example, parameters fitted only to vapor – liquid equilibrium data usually are not adequate enough to capture the liquid – liquid equilibria of the same mixture.[1] Following this consideration, since the objective of this work is to develop a thermodynamic framework for the accurate description of natural gas mixtures, while keeping as much as possible the predictive nature of the model, the interaction parameters are fitted only to binary phase equilibria data, in a temperature and pressure range appropriate for handling natural gas processing and transportation.

Emphasis is given in the phase equilibria of water, where the existing CH_2 – H_2O UNIFAC IPs are re-estimated. This is due to the fact that these IPs have been actually fitted to alcohol/water mixtures, which exhibit very different phase equilibria behavior compared to the highly immiscible water/hydrocarbon ones.[2] This becomes apparent in Figure 7.1 where the LLE of the n-hexane/water mixture is presented, using two sets of interaction parameters; the VLE 2 coeff. as exist in the UNIFAC tables of Hansen et al.[3] and the parameters obtained in this work fitted to alkane/water data.

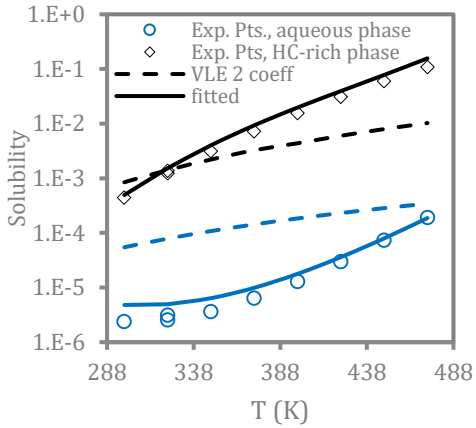

Figure 7.1: VLE prediction of the n-hexane/water mixture with UMR-PRU using two sets of IPs. Dashed line indicates the VLE 2 coeff. IPs of the original UNIFAC while solid line the IPs fitted to hydrocarbon/water LLE data. Experimental data by Tsonopoulos et al.[4].

It is apparent that the first fails to predict the hydrocarbon or water solubility in the aqueous or hydrocarbon – rich phase respectively, while the latter presents a very accurate prediction. This due to the fact that the UNIFAC IPs are fitted to mixtures with compounds miscible in water, such as alcohols and ketones, while HCs and water are highly immiscible and therefore they split in two different liquid phases.

Apart from water, which is a natural gas component, the model is extended to polar chemicals used for the processing and transportation of natural gas. Most of them are involved with the water dew point control and hydrate formation control as it is has been discussed in Chapter 2. Methanol is traditionally used for this purpose, while the last decades it has been replaced by ethylene glycol (MEG). Those chemicals are mostly injected in the natural gas pipelines to depress the hydrate formation temperature and thus avoid operational problems during transportation in the offshore network. On the other hand, triethylene glycol (TEG), is the chemical most commonly used as absorbent during the process of dehydration by physical absorption. The latter is applied in most offshore platforms to satisfy the water dew point specification. To this purpose, the UMR-PRU model is extended to natural gas components with water, methanol and glycols (MEG, TEG).

7.2. Pure component parameters

As it has been stated in the model description in Section 5.3.1, for the temperature dependency of the attractive term parameter UMR-PRU uses the Soave[5] expression, as in the original PR EoS. For non-polar components this consideration is very satisfactory, as shown for example in Louli et al.[6]. When polar components are involved, the Soave's expression for the attractive term parameter is inadequate.[7] This is more apparent in the case of glycols, which have very high critical temperature compared to the temperatures involved in natural gas processing. To better describe the vapor pressure of polar components the Mathias – Copeman expression is used (eq. 5.7). For water and methanol MC parameters are obtained from Boukouvalas et al.[8] where they have been fitted to vapor pressure data. Although, as suggested by Le Guennec et al.[9] the MC parameters can be simultaneously fitted to several properties, such as enthalpies of vaporization and heat capacities, apart from the vapor pressure, in order to improve the performance of the model in those derivative properties, in this work the standard approach is used. That is selected in order to be consistent with the methodology used for fitting the parameters for water and alcohols and also to use as less information in the fitting as possible, so that the predictive nature of the model is somehow kept. The objective function used for the fitting of the MC parameters is that of eq. 7.1.

$$S = \frac{1}{n_p}\sum_{i=1}^{n_p} 100\frac{abs(P_i^{s,exp} - P_i^{s,calc})}{P_i^{s,exp}} \qquad \text{eq. 7.1}$$

where P_i^s is the vapor pressure. Exponent *exp* denotes pseudoexperimental data produced by DIPPR correlations and *calc* the vapor pressure calculated with the EoS.

n_p is the number of the experimental data used for the fitting, which is actually calculated by the reduced temperature range along with the temperature step, as it is denoted in Table 5.2. For ethylene glycol the procedure is straight – forward. Following the conclusion of Derawi et al.[10] the DIPPR-2001 correlation is used which better describes the raw experimental data points for the fitting of the IPs, yielding satisfactory results. For TEG, on the other hand, further investigation is required. Although a liquid chemical, TEG does not exist in the original UNIFAC tables. Since in the latter MEG and DEG are treated as independent groups, in this work TEG is considered to comprise a separate UNIFAC group. Furthermore, even its properties are rather difficult to be measured with high accuracy. As presented in Figure 7.2, different versions of DIPPR correlations for vapor pressure estimation substantially differ, especially in the low temperature area.

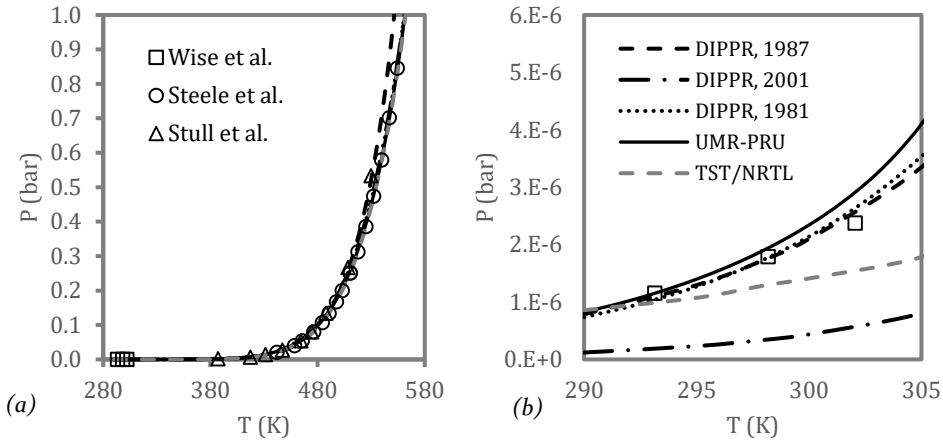

Figure 7.2: Vapor pressure of pure TEG. (a) Comparison of three DIPPR correlations against raw experimental data and model predictions: Experimental data (□) by Wise et al.[11], (○) by Steele et al.[12] and (Δ) by Stull et al.[13]. DIPPR-1981 with black dotted line, DIPPR-1987 with black dashed line, DIPPR-2001 with black long dash, dotted line, UMR-PRU with black solid line and TST/NRTL with grey dashed line; (b) focus at low temperatures.

Apart from the vapor pressure, the DIPPR database provides different values for the critical properties, as presented in Table 7.1.

Table 7.1: TEG pure component properties and vapor pressure constants (DIPPR-101)[1] from different versions of DIPPR

DIPPR	T_c (K)	P_c (bar)	ω	T_b (K)	a	b	c	d	e
1981	769.5	33.2	0.75871	561.5	84.3	-11685	-8.21	2.5E-18	6
1987	700.0	33.2	1.38633	551.0	35.6	-8839	-1.39	2.3E-6	2
2001	769.5	33.2	0.75871	561.5	152.5	-16449	-17.67	6.5E-18	6

[1] Parameters a – e correspond to the constants of the DIPPR-101 equation for the vapor pressure: $P^s = exp\left(a + \frac{b}{T} + clnT + dT^e\right)$ given in Pa, with T the corresponding temperature in K.

DIPPR-1981 shows lower deviation from the raw experimental vapor pressures than the more recent DIPPR-2001 for the low temperatures, which is the region of interest for the design of the absorber in a TEG dehydration unit. On the other hand, similar vapor pressures with DIPPR-2001 are calculated for the higher temperatures, as shown in Figure 7.2*a*. DIPPR-1987 correlation although performs well at the low temperature area, deviates from the majority of the experimental data and from DIPPR-2001 at the higher temperatures. For these reasons, in this work, the MC parameters have been fitted to the vapor pressure data generated by the DIPPR-1981 correlation. It is noted that the temperature range for the fitting of the MC parameters is 323.15 – 692.15 K, in order to avoid the high uncertainty encountered due to the very low vapor pressure at the lower temperatures. Apart from the DIPPR correlations, the vapor pressure calculated with UMR-PRU and TST/NRTL models is also presented. It is observed that UMR-PRU yields better results than TST/NRTL at the lower *T*-range, which are actually extrapolated, while similar ones are obtained by the two models at the higher temperatures. The overall deviation in the examined temperature range is 3.0 % for UMR-PRU while for TST/NRTL is 6.5 %.

Apart from the vapor pressure and liquid density, another significant property for simulation purposes is the heat capacity, since it determines the required heat duty in equipment where heat exchange takes place, such as the reboiler or heat exchangers. The isobaric heat capacity is calculated from eq. 7.2,

$$c_p = \left(\frac{\partial H}{\partial T}\right)_{P,n} \qquad \text{eq. 7.2}$$

where *H* stands for the molar enthalpy, *T* for the temperature, *P* for the pressure and *n* for the number of moles. Since it will be of interest in Chapter 8 the prediction of the heat capacity of water and TEG is depicted in Figure 7.3 and is compared with experimental data taken from the literature and the prediction of TST/NRTL model.

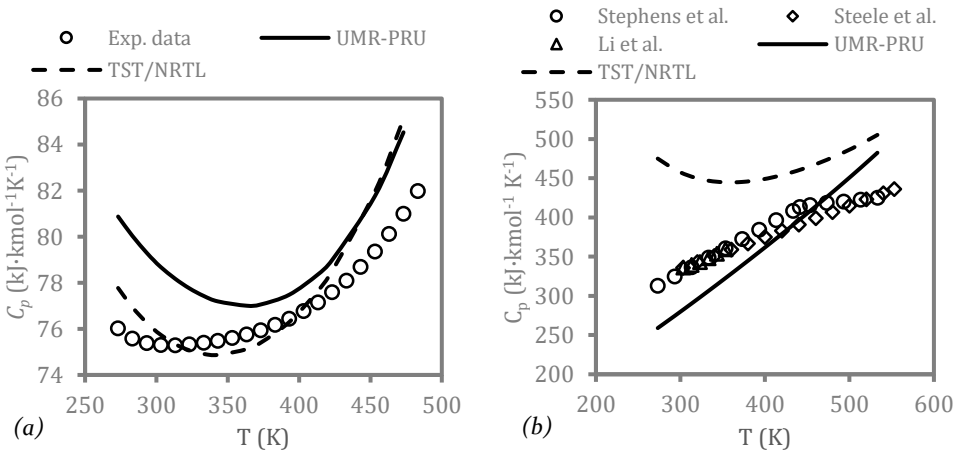

Figure 7.3: Prediction of heat capacity at constant pressure for pure components. Solid line denotes the UMR-PRU prediction and dashed line the TST/NRTL one. (a) Saturated water heat capacity. Circles denote experimental data by NIST.[14] (b) TEG heat capacity at 1 bar. Circles denote experimental points by Stephens et al.[15], diamonds by Steele et al.[12] and triangles by Li et al.[16].

UMR-PRU yields an overall AARD in TEG heat capacity equal to 9.4 %, while TST/NRTL 23.1 %. TST/NRTL systematically overestimates the c_p of TEG, erroneously predicting a minimum at 353 K. UMR-PRU satisfactorily predicts the experimental data both qualitatively and quantitatively, although it gives a relatively higher effect of temperature on c_p. Especially for the temperature range of 373.15 K – 473.15 K where the reboiler of the still column of a dehydration unit operates, and determines more than 25 % of the overall energy requirements of the dehydration unit, the AARD is 5 % for the UMR-PRU while it is over 14 % for the TST/NRTL model. For water, both models yield good results with TST/NRTL to be superior to UMR-PRU. Specifically, the corresponding errors are 3.5 % for UMR-PRU and 1.7 % for TST/NRTL.

7.3. Binary mixtures

The presentation of the binary phase equilibrium results is separated in two categories. The first involves the VLE of light gases with polar components while the second deals with the LLE of hydrocarbons with water.

7.3.1. Vapor – Liquid Equilibrium

7.3.1.a. *Correlation results*

The UNIFAC interaction parameters for the light gases with water, methanol, MEG and TEG, as well as for the HC groups with TEG which are required for the UMR-PRU model, have been fitted to experimental binary VLE data taken from the literature. The detailed list of the references of the experimental data is given in Appendix A. The objective function (S) that has been minimized is given by eq. 7.3, where X corresponds to bubble point pressure, P, or bubble point temperature, T, depending on the type of calculation.

$$S = \frac{1}{n_p}\sum_{i=1}^{n_p} 100 \cdot \frac{abs(X_i^{exp} - X_i^{calc})}{X_i^{exp}} \qquad \text{eq. 7.3}$$

In eq. 7.3 exponent *exp* refers to the experimental measured T or P, while *calc* refers to the values calculated with the UMR-PRU model and n_p is the number of experimental data points used for parameter fitting. The detailed binary VLE correlation results for the UMR-PRU model are presented in Table 7.2, where for comparison purposes prediction with TST/NRTL is also given. For the latter, the default IPs of Aspen Hysys vs 8.8 are utilized.

Table 7.2: VLE binary BPP correlation results with UMR-PRU. Prediction with TST/NRTL for comparison purposes.

System	ref.	n_p	T range (K)	P range (bar)	x_1 range	y_1 range	% AARD[a]		100·AAD[b]	
							UMR-PRU	TST/NRTL	UMR-PRU	TST/NRTL
Water (2) with										
N_2	17	34	298.2 - 513.2	25.0 - 1013.0	0.0002 - 0.0051	-	4.7	14.6	-	-
CO_2	18-23	160	278.2 - 598.2	3.3 - 1500.0	0.0005 - 0.2500	0.0800 - 0.9993	22.4	31.7	5.5	3.2
CH_4	24-30	116	274.2 - 588.7	5.67 - 980.7	0.0002 - 0.0151	0.1678 - 0.9998	10.3	12.1	2.1	1.4
C_2H_6	17, 26, 31	65	274.3 - 444.3	3.7 - 137.89	0.0001 - 0.0017	-	10.9	52.2	-	-
MEG	32	23	323.2	0.0 - 0.1	0.8500 - 1.0000	-	2.2	21.1	-	-
TEG[c]	33	18	371.6 - 421.3	0.85	0.0454 - 0.8830	0.0001 - 0.0220	2.2	2.2	0.2	0.1
Methanol (2) with										
N_2	17	21	273.2 - 343.2	49.0 - 295.0	0.0109 – 0.0687	-	1.1	31.2	-	-
CO_2	34, 35	45	213.12 - 313.2	1.0 - 80.6	0.0246 – 0.9002	0.9363 – 0.9931	3.3	11.0	0.2	0.2
CH_4	25, 36-39	105	273.2 - 373.2	10.5 - 80.6	0.0095 – 0.5648	0.6942 – 0.9991	10.1	21.1	0.5	1.2
C_2H_6	40-43	123	240.0 - 373.2	4.0 - 67.7	0.0027 – 1.0000	0.6870 – 1.0000	7.7	43.3	2.4	2.3

[a] $\%\,AARD = 100 \cdot \frac{abs(X - X^{calc})}{X^{exp}}$, *where X stands for bubble point pressure (BPP) or bubble point temperature (BPT).*
[b] $100 \cdot AAD = 1000 \cdot abs(y_1^{exp} - y_1^{calc})$, where y_1 stands for the vapor phase solubility of component 1.
[c] corresponds to BPT calculation

Table 7.2 (continued)

System	ref.	n_p	T range (K)	P range (bar)	x_1 range	y_1 range	% AARD[a]		1000·AAD[b]	
							UMR-PRU	TST/NRTL	UMR-PRU	TST/NRTL
MEG (2) with										
N_2	44	31	323.2 - 398.2	0.0 - 396.0	0.0002 - 0.0190	-	9.4	12.2	-	-
CO_2	45-47	135	288.2 - 398.2	0.3 - 384.0	0.0007 - 0.1724	-	7.8	61.6	-	-
CH_4	44, 48	63	298.2 - 398.2	0.0 - 396.2	0.0002 - 0.0421	-	4.4	3572.3 [d]	-	-
C_2H_6	48	34	298.2 - 398.2	0.0 - 203.4	0.0003 - 0.0308	-	3.3	-[e]	-	-
TEG (2) with										
CO_2	49	40	298.2 – 398.2	0.0 – 202.5	0.0046 - 0.4848	-	5.7	3.5	-	-
CH_4	49	67	273.2 – 398.2	1.1 – 202.0	0.0006 - 0.0840	-	4.5	6.6	-	-
C_2H_6	49	59	298.2 – 398.2	1.1 – 204.8	0.0016 - 0.1482	-	10.6	3.4	-	-
nC3	50	40	298.2 – 398.2	0.2 – 64.5	0.0007 - 0.1043	-	13.5	11.3	-	-
cyC6	51	19	343.0 – 473.0	0.1 – 13.7	0.0 - 1.0	0.0 - 1.0	10.4	5.4	2.31	2.15
benzene	52	11	354.7 – 428.8	1.0	0.0680 - 0.8849	0.0 - 0.9999	0.2	0.2	0.05	0.04
toluene	52	10	385.2 – 442.5	1.0	0.0815 - 0.9353	0.0 - 0.9995	0.1	0.1	0.05	0.04

[d] *the model erroneously predicts LLE*
[e] *the model fails to calculate BPP, due to lack of appropriate IPs*

As it is apparent from the above, the MEG/water IPs are also re-estimated. This is because the IPs from the UNIFAC tables fail to capture well the VLE of the mixture, especially in the low temperature area which is of special interest to the natural gas industry. This is better illustrated in Figure 7.4, where the original IPs of UNIFAC are compared to the fitted ones. Actually, the first result in negative deviation from Raoult's law, while experimentally an almost ideal behavior is observed.

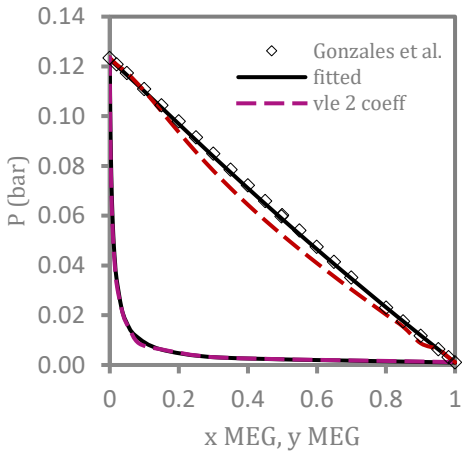

Figure 7.4: MEG/water VLE at 323.15 K with UMR-PRU using two different sets of interaction parameters. Solid line presents the fitted IPs and dotted line the prediction using the UNIFAC VLE 2 coeff. Experimental data by Gonzales et al.[32]

The correlation results are very satisfactory, while a very good prediction of the solubility in vapor phase is obtained, with parameters fitted only in liquid phase experimental data. For comparison purposes, the results with TST/NRTL model, which is suggested by Hysys for the modelling of dehydration processes are also presented. The results are of special interest for the mixtures with water and TEG, for which the parameters of the model are fitted to accurately simulate such a process. Instead, in mixtures with e.g. methanol the TST/NRTL model under circumstances fails to even accurately predict the phase split. For example, in the methane/methanol mixture it predicts LLE instead of the experimentally observed VLE, while in the ethane/ methanol it yields only single – phase region where two phases are experimentally observed. Nevertheless, the prediction of the model is presented for completeness.

Some representative VLE results for the liquid phase of methane with polar chemicals are given in Figure 7.5. It is observed that apart from the very good deviation in terms of AARD and AAD, UMR-PRU correlates very satisfactorily both qualitatively and quantitatively the VLE of methane with water and polar chemicals. Another observation is that TST/NRTL yields very good results for the mixtures of methane with water and TEG but fails to predict even qualitative its VLE with methanol and MEG.

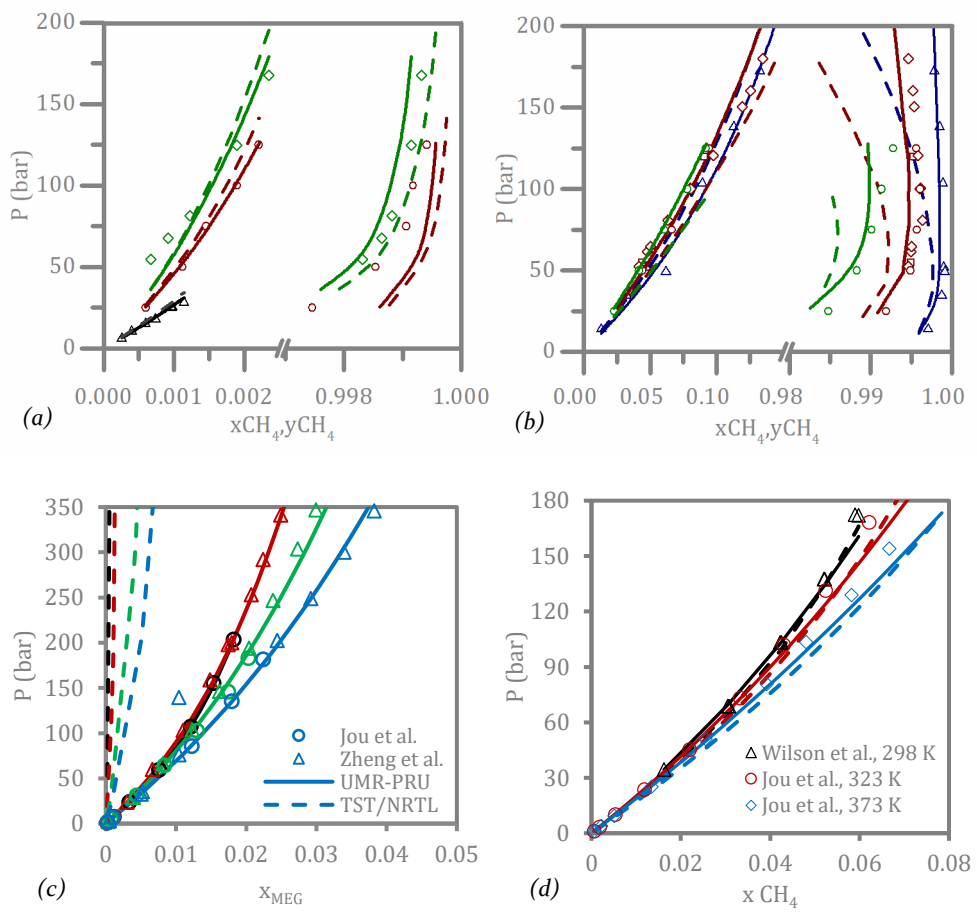

Figure 7.5: VLE correlation results with UMR-PRU (solid) line for methane with polar chemicals. Prediction results with TST/NRTL are also given (dashed line). (a) methane/water; black colour denotes 274.15 K, red 298.15 K and green 313.15 K[24-27, 30] (b) methane/methanol; blue colour denotes 273.15 K, red 298.15 K and green 313.15 K[25, 30, 36, 53] (c) liquid phase of methane/MEG; black colour denotes 298.15 K, red 323.15 K, green 373.15 K and blue 398.15 K[44, 48] and (d) methane/TEG (liquid phase); black colour denotes 298.15 K, red 323.15 K and blue 373.15 K[49, 50].

Another mixture of interest, not only for the natural gas industry but also for carbon capture and storage is the CO_2/water, which is very difficult to handle even with more advanced models. This is due to the obscure behavior of the water solubility in vapor phase, where with the increase of pressure a minimum in the solubility is observed due to the encountered minimum of the water density. Figure 7.6 shows that UMR-PRU predicts very accurately the minimum of the water solubility in CO_2-rich phase, in a wide range of temperature and pressure. The interactions attributed to hydrogen bonds leading to this effect are absorbed in the fitting of the interaction parameters.

In that mixture, TST/NRTL yields also very good results, which are actually better for the vapor phase. Instead, in the liquid one it yields almost double AARD compared to UMR-PRU.

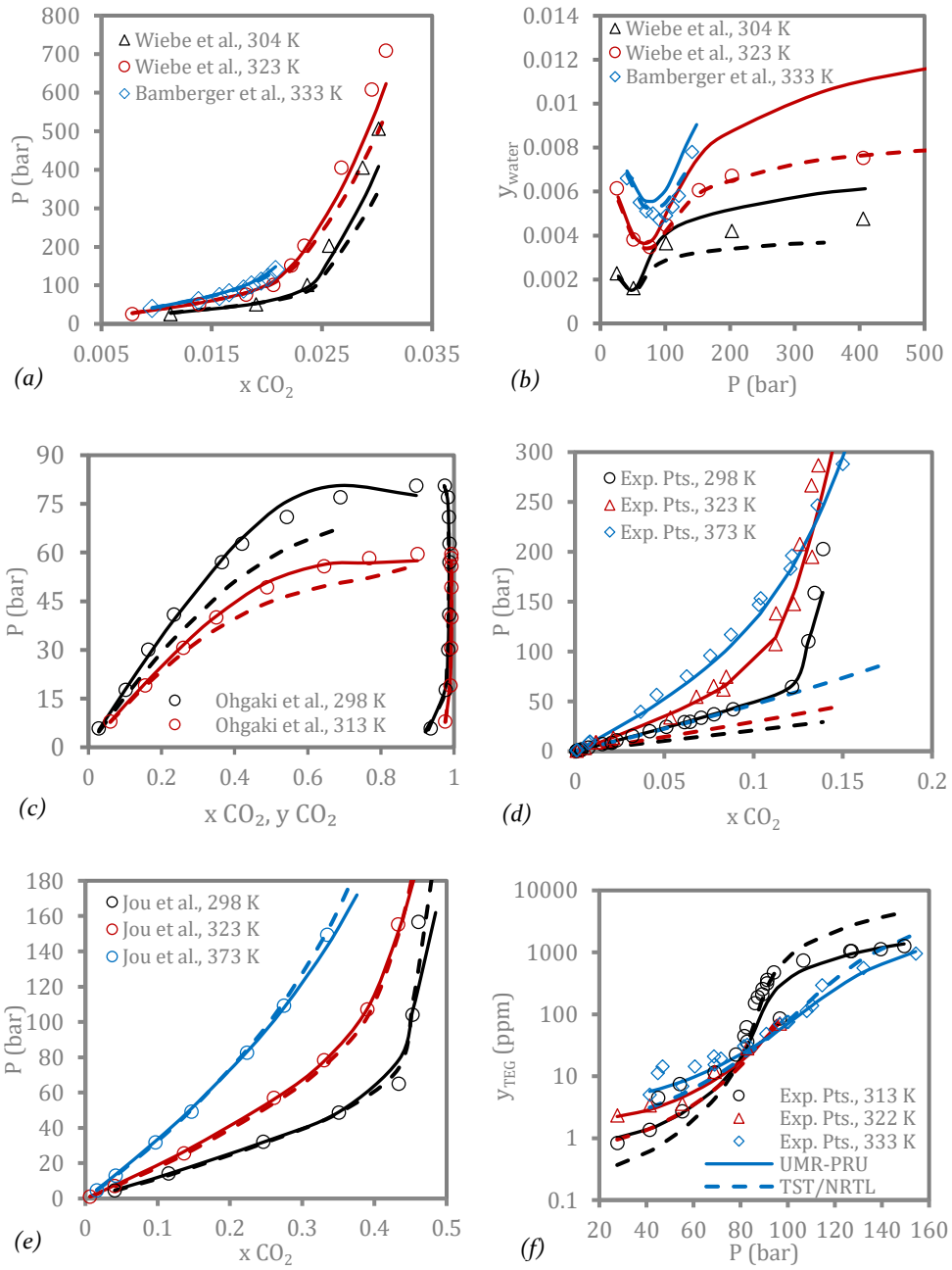

Figure 7.6: VLE of CO_2 with water and polar chemicals with UMR-PRU (solid line) and TST/NRTL (dashed line). (a) CO_2/H_2O (liquid phase). Exp. data by [18, 23], (b) CO_2/H_2O (vapor phase). Exp. data by [18, 54, 55], (c) CO_2/methanol. Exp. data by [34], (d) CO_2/MEG. Exp. data by [45, 48, 56], (e) CO_2/TEG (liquid phase). Exp. data by [49] and (f) CO_2/TEG (vapor phase). Exp. data by [57]. Colouring corresponds to the same temperature with the experimental points.

The same is true for the mixtures with TEG, for which the IPs with the hydrocarbon groups are also estimated. The latter are fitted only to binary VLE data, while their performance in heavier hydrocarbons, where LLE is observed, is examined in Section 7.3.2. Both models yield very good results in both liquid and vapor phase (Figure 7.6 *e* and *f*) and they are able to capture the cross of the solubility with the temperature. It should also be noted that the solubility of glycols in vapor, and especially that of TEG is very low and thus high uncertainty is encountered even at the available experimental data. Again, as expected, at the mixtures of CO_2 with methanol and MEG, TST/NRTL yields poor results, by predicting a narrower two – phase region. UMR-PRU on the other hand correlates satisfactorily both mixtures.

Since the solubility of water in natural gas is what defines the natural gas water content and therefore the appropriate way to handle it, Figure 7.7 emphasizes the prediction of the water solubility in methane and ethane, which are the major natural gas components.

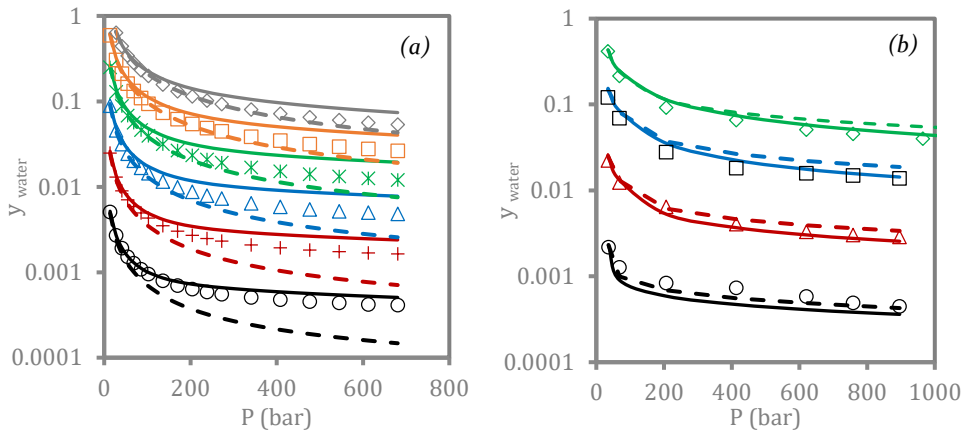

Figure 7.7: Binary VLE results for mixtures of light gases with water with UMR-PRU (solid line) and TST/NRTL (dashed line). (a) Vapor phase composition predictions for the methane/water mixture. Experimental data by Sage et Lacey[58]. (○) at 310.93 K, (+) at 344.26 K, (Δ) at 377.59 K, (✶) at 410.93 K, (□) at 444.26 K and (◇) at 477.59 K. (b). Vapor phase composition predictions for the ethane/water mixture. Experimental data by Yarrison et al.[59]. (○) at 314.8 K, (Δ) at 366.5 K, (□) at 422 K and (◇) at 466.5 K.

UMR-PRU describes very well the bubble point pressure of light gases with water, yielding better results than TST/NRTL especially for the ethane/water binary. As shown in Figure 7.7*a* UMR-PRU predicts satisfactorily the water vapor phase compositions of methane/water, while TST/NRTL systematically underestimates them especially at the lower temperatures. As a result, since methane is the major natural gas component, TST/NRTL predicts lower water content in the saturated gas. UMR-PRU and TST/NRTL perform well in the case of ethane/water mixture as presented in Figure 7.7*b*.

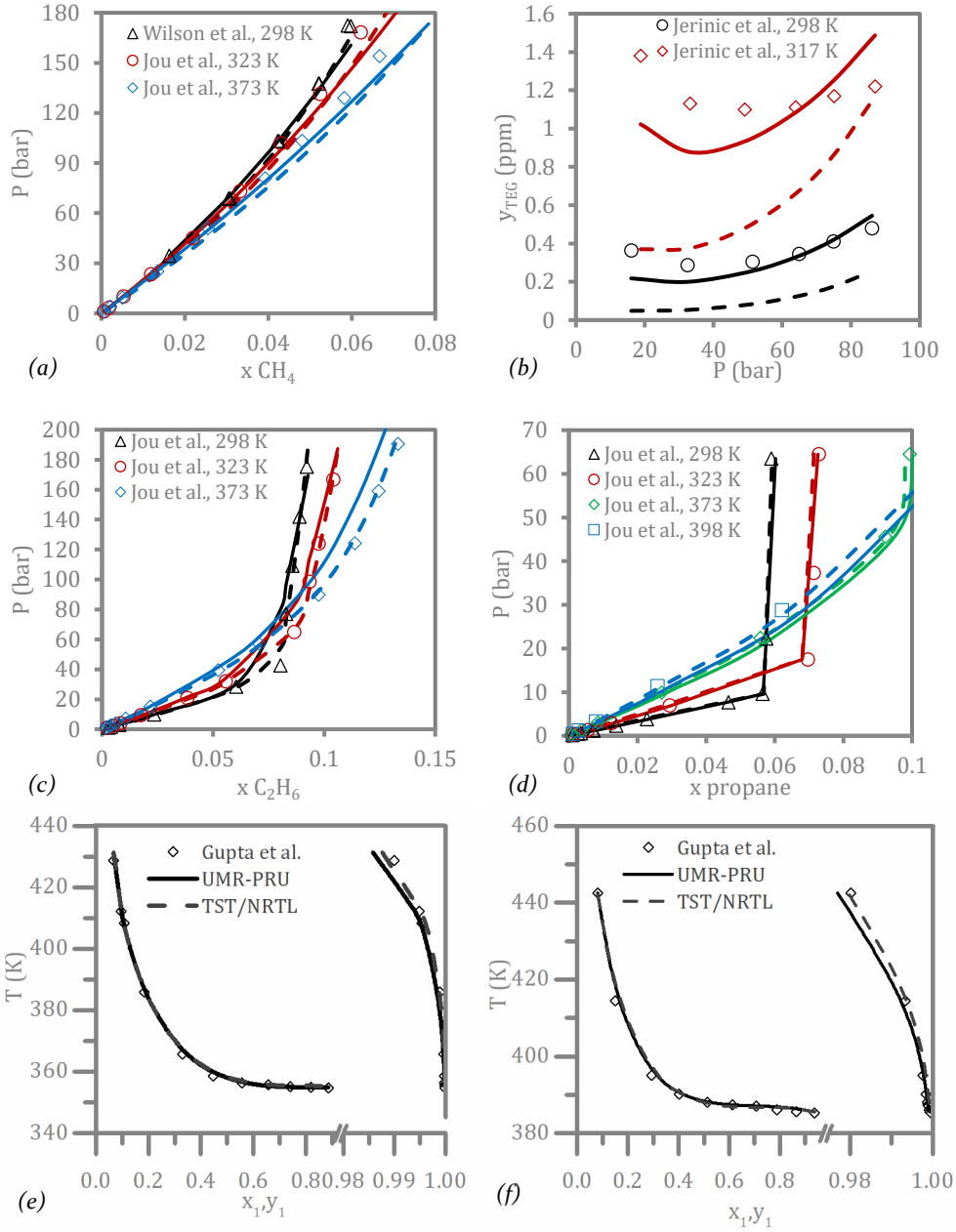

Figure 7.8: VLE of light gases and hydrocarbons with TEG with UMR-PRU (solid line) and TST/NRTL (dashed line). (a) Methane/TEG (liquid phase). (Δ) Experimental data by Wilson et al.[50] at 298.15 K, (○) by Jou et al.[49] at 323.15 K and (◇) by Jou et al.[49] at 373.15 K. (b) Vapor phase of the methane/TEG. Experimental data by Jerinic et al.[60]. (○) at 298.15 K and (◇) at 316.75 K. (c) Ethane/TEG. Experimental data by Jou et al.[49]. (Δ) at 298.15 K, (○) at 323.15 K and (◇) at 373.15 K. (d) Propane/TEG. Experimental data by Jou et al.[49]. (Δ) at 298.15 K, (○) at 323.15 K, (◇) at 373.15 K and (□) at 398.15 K. (e) Benzene/TEG at 1.01325 bar. (◇) Experimental points by Gupta et al.[52] and (f) Toluene/TEG mixture at 1.01325 bar. (◇) Experimental points by Gupta et al.[52].

Very good VLE results are obtained by UMR-PRU and TST/NRTL for the binary mixtures with TEG (Table 7.2 and Figure 7.8). Both models are able to capture the cross of the solubility lines of light gases with increasing temperature at the liquid phase, Figure 7.8*c* and *d*. UMR-PRU and TST/NRTL describe also very well the VLE of heavier hydrocarbons with TEG (Figure 7.8 *e* and *f*). Overall, the results in the VLE of binary mixtures with TEG are comparable with those calculated with the CPA EoS[61] that explicitly accounts for the association effects.

7.3.1.b. *Prediction results*

To verify the good performance of the model, prediction of the VLE in different data than the ones included in the database used for parameter fitting has been performed. The detailed results are presented in Table 7.3 and in some cases they also include extrapolation of the temperature range outside the one used for the correlation.

It is shown that very good results are obtained with both models in the mixtures with TEG and water. In the case of methanol, the results with UMR-PRU seem rather disappointing if the overall range is examined. That is because the higher temperatures have been excluded from the database of the parameter fitting and actually correspond to wrong prediction of the critical point of the mixture. If the extrapolation results are omitted, then the deviation decreases and is overall similar with the one encountered for the correlation results. Furthermore, TST/NRTL yields 13 rejected points, due to wrong calculation of the phase split.

Table 7.3: VLE binary flash prediction results with the UMR-PRU and TST/NRTL models.

System	ref.	n_p	T range (K)	P range (bar)	x_1 range	y_1 range	% AARD[a]		1000·AAD[b]	
							UMR-PRU	TST/NRTL	UMR-PRU	TST/NRTL
Water (2) with										
CH_4	58, 59, 62, 63	192	253.2 - 510.9	13.0 - 1103.0	–	0.1900 - 1.0	–	–	9.2	3.8
C_2H_6	31, 58, 59, 64, 65	248	278.1 - 510.9	3.0 - 1103.0	–	0.2000 - 0.9998	–	–	7.9	8.2
TEG[c]	66	68	317.3 - 534.0	0.1 - 0.6	0.2000 - 1.0	-	5.4	7.4	–	–
Methanol (2) with										
CO_2[d, e]	53, 67, 68	151	230.0 - 477.6	4.4 - 165.0	0.0087 - 0.9865	0.1283 - 0.9998	34.1	14.4	60.0	19.6
TEG (2) with										
CO_2	69	28	273.2 - 343.2	4.2 - 374.0	0.0260 - 0.5060	–	6.9	5.5	–	–
	50, 51	48	313.2 - 333.2	27.6 - 154.3	–	0.9990 - 1.0	–	–	0.0500	0.2500
CH_4	60	12	298.2 - 316.8	16.1 - 87.0	–	0.9990 - 1.0	–	–	0.0001	0.0004

[a] *% AARD is defined as:* $\%AARD = 100 \cdot \frac{abs(X_i^{exp} - X_i^{calc})}{X_i^{exp}}$, *where X stands for liquid phase solubility of component 1. In case of BPP or BPT calculation, it corresponds to the bubble point P* or *T*, respectively.
[b] 1000·AAD is defined as: $1000 \cdot AAD = 1000 \cdot abs(y_1^{exp} - y_1^{calc})$, where y_1 stands for the vapor phase solubility of component 1.
[c] corresponds to BPT calculation
[d] corresponds to BPP calculation
[e] the corresponding results in the temperature range 230 – 313 K is 8.5 for UMR-PRU and 9.8 for TST/NRTL in the BPP, while 3.1 for UMR-PRU and 2.2 for TST/NRTL in the vapor phase solubility.

7.3.1.c. *The TEG/water binary*

A mixture of utmost importance when dehydration of natural gas in considered is the TEG/water binary, since TEG is the most commonly used glycol desiccant. To this purpose and with respect to the simulation of a natural gas dehydration process using TEG in Chapter 8, other properties apart from VLE are examined for this mixture. As with the other examined mixtures, the TEG/H_2O binary interaction parameters for the UMR-PRU have been fitted to bubble point temperature (BPT) experimental data[33]. The correlation results are very satisfactory, with an AARD in BPT equal to 2.2 % and an AAD in vapor phase composition equal to 2.3. The deviations with TST/NRTL are similar to those obtained with UMR-PRU as shown in Table 7.2 and graphically in Figure 7.9*a*. Furthermore, as illustrated in Figure 7.9*b* both models perform similarly also in the prediction of the bubble point temperature against the experimental data of Piemonte et al.[66], which have not been included in the database used for the fitting of the UMR-PRU IPs. For these data, UMR-PRU yields an AARD equal to 5.4 % and TST/NRTL 7.4 %. Both models are able to capture well the effect of pressure in the bubble point temperature, while they better predict the richer in water compositions.

In Figure 7.9*c*, it is shown that UMR-PRU better describes the activity coefficients of water, where it gives an AARD in water activity coefficient equal to 1.5 % while TST/NRTL 7.4 %. Due to their importance in the dehydration process, especially in the simulation of the regenerator, the infinite dilution activity coefficients of water in its mixture with TEG have been examined. The results presented in Figure 7.9*d* indicate that UMR-PRU predicts infinite dilution coefficient values that agree fairly well with the data of Bestani and Shing[70]. On the other hand, TST/NRTL describes very accurately the data of Parrish et al.[71], which have been included in the correlation of the TST/NRTL model parameters[72]. According to Bestani and Shing[70], the difference of their experimental data with those of Parrish et al.[71] is approximately 15 %, which is higher than the experimental uncertainty, but an application of a correction factor to the data of Parrish et al.[71] leads to a difference of 2 – 3 %, which is within the limits of the experimental uncertainty. This difference is reflected on the absorbing ability of TEG and as it is shown in Chapter 8, TST/NRTL requires lower amount of TEG than UMR-PRU to obtain the required dehydration level.

Moreover, the performance of the models is evaluated in the prediction of the excess enthalpies of the TEG/water mixture. As it is apparent from Figure 7.9*e*, UMR-PRU predicts very well the experimental data (AARD equal to 2.7 %), while TST/NRTL systematically overestimates them (AARD equal to 44.1 %). This result indicates that the temperature dependency of the UMR-PRU IPs is better as compared to the one of TST/NRTL, although both models use linear dependency for the specific mixture.

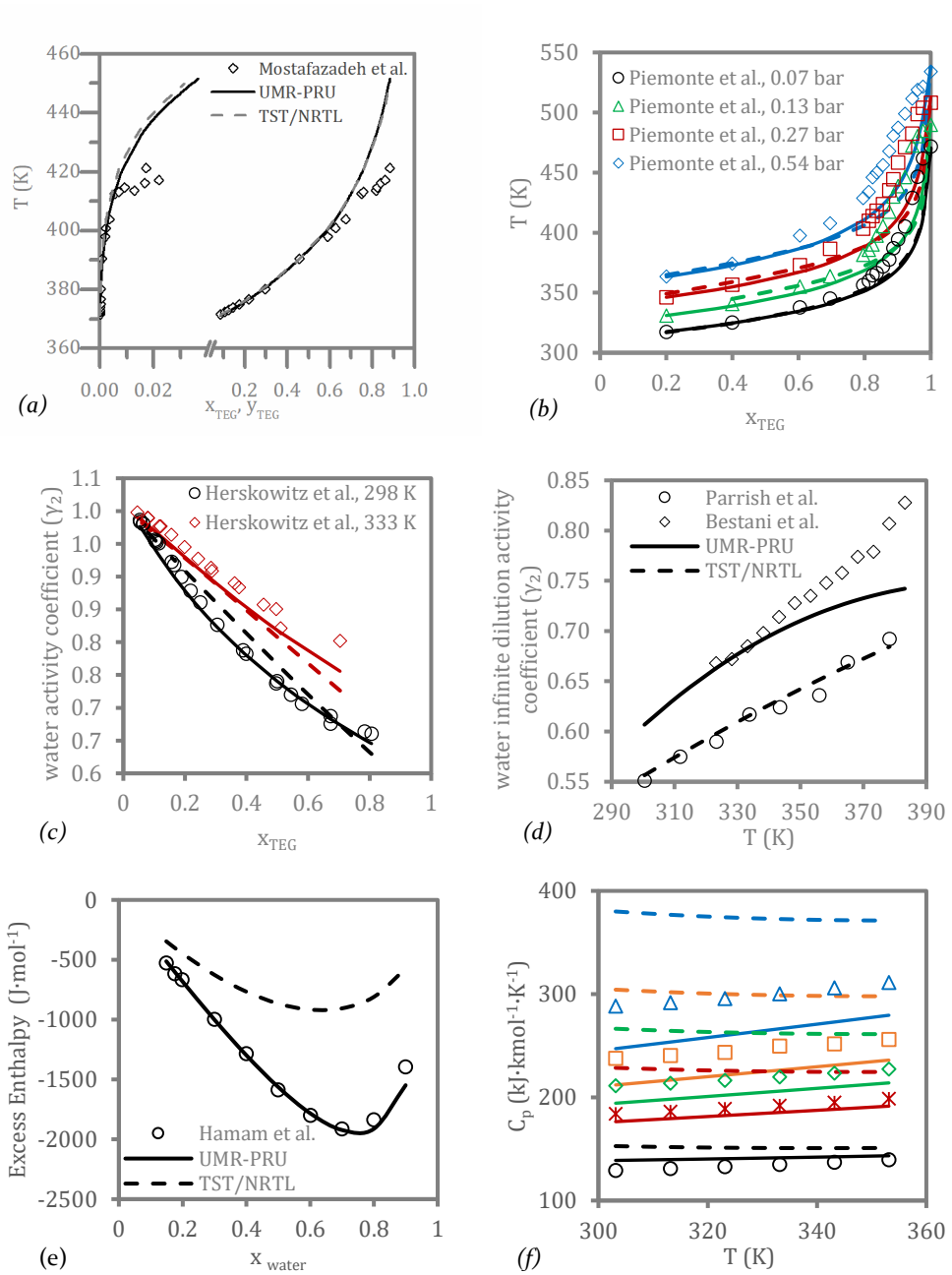

Figure 7.9: TEG/water mixture results with UMR-PRU (solid line) and TST/NRTL (dashed line). (a) VLE at 0.85 bar. (◇) Exp. data by Mostafazadeh et al.[33], (b) VLE at constant pressure. Exp. data by Piemonte et al.[66], (○) at 0.07 bar, (△) at 0.13 bar, (□) at 0.27 bar and (◇) at 0.54 bar. (c) Water activity coefficients. Experimental data by Herskowitz et al.[73] (○) at 297.6 K and (◇) at 332.6 K. (d). Water infinite dilution activity coefficients. Experimental data (○) by Parrish et al.[71] and (◇) by Bestani et al.[70], (e) Excess Enthalpies (◇) Experimental data by Hamam et al.[74] and (f) Heat capacity at constant pressure. Experimental data by Li et al.[16]. (○) x_{TEG} = 0.2, (✶) x_{TEG} = 0.4, (◇) x_{TEG} = 0.5, (□) x_{TEG} = 0.6 and (△) x_{TEG} = 0.8.

Finally, Figure 7.9*f* compares the predicted heat capacities with the experimental ones for the TEG/water mixture. Fairly good predictions are obtained with the UMR-PRU model for the examined mixtures especially at the lower TEG concentrations, while TST/NRTL model systematically overestimates the experimental values predicting also an opposite temperature dependency than the experimentally observed one. Overall, UMR-PRU yields an overall AARD equal to 7.3 % and TST/NRTL 19.8 %, while detailed results for various TEG/water compositions are presented in Table 7.4.

Table 7.4: Prediction results of aqueous TEG heat capacity with UMR-PRU and TST/NRTL. Experimental data by Li et al.[16]

	x_{TEG}					
	0.2	0.4	0.5	0.6	0.8	overall
UMR-PRU	5.2	3.7	6.7	9.2	12.0	7.3
TST/NRTL	12.9	18.5	20.4	21.9	25.4	19.8

In natural gas processing the Joule – Thomson (JT) valves are usually used to enhance NGL recovery, since hydrocarbons exhibit a positive Joule – Thomson coefficient. According to Satyro et al.[75], liquid TEG and water show a reverse behavior, i.e. negative JT coefficients, which result in temperature increase during expansion. Satyro et al.[75] experimentally measured the temperature in the outlet of a Joule – Thomson valve, after the rich TEG stream exiting the contactor. They studied pure water and TEG as well as their mixture and they showed that a temperature increase occurs in all cases. In this work, the predictions of TST/NRTL and UMR-PRU model in the conditions tested by Satyro et al.[75] are compared with the experimental data and the respective results are tabulated in Table 7.5.

Table 7.5: Temperature effect of decompression valve with the UMR-PRU and TST/NRTL models. Experimental data by Satyro et al.[75]

Mixture	Inlet T (K)	P (bar)	ΔT [a] (K)		
			Exp.	UMR-PRU	TST/NRTL
Pure water	292.7	4.4	1.4	1.43	1.42
TEG 99 % pure	291.9	4.4	2.4	3.43	1.93
Aqueous TEG (1 % wt.)	292.8	4.4	2.1	3.41	1.92

[a] $\Delta T = T_{out}-T_{in}$, where *in* stands for the rich TEG stream exiting the contactor which is routed to the isenthalpic valve and *out* stands for the stream exiting the valve.

It is observed that both UMR-PRU and TST/NRTL predict positive JT coefficient in all cases, in accordance with the experimental data. Both models yield almost the same ΔT for pure water, while for pure and aqueous TEG TST/NRTL underestimates the temperature increase while UMR-PRU overestimates it.

7.3.2. Liquid – Liquid Equilibrium

As stated in the previous, in order to obtain better description of the difficult to model hydrocarbon/water equilibria, the UNIFAC interaction parameters are re-estimated. The detailed database used for this purpose is given in Appendix A, while the procedure followed is described in the following subsections. Furthermore, prediction results for the LLE of binary hydrocarbon/TEG mixtures are also presented based on the interaction parameters fitted to VLE data. The detailed results are tabulated in Table 7.6.

Table 7.6: LLE binary prediction results with the UMR-PRU and TST/NRTL models.

System	ref.	n_p	T range (K)	P range (bar)	$x_1^{(I)}$ range	$x_1^{(II)}$ range	$\%\Delta x_1^{(I)}$ [a]		$\%\Delta x_2^{(II)}$ [b]	
							UMR-PRU	TST/NRTL	UMR-PRU	TST/NRTL
Water (2) with										
nC3[b]	76	10	278.9 – 360.9	5.7 – 37.1	0.00020 – 0.00036	0.00011 – 0.00558	133.6	10.6	85.7	18.1
nC4	77-79	12	278.7 – 377.6	0.2 – 6.5	0.00006 – 0.00014	0.00010 – 0.00850	72.9	13.7	100.5	17.1
nC5	77, 80	10	273.2 – 423.3	0.1 – 5.8	0.00001 – 0.00002	0.00010 – 0.03220	103.9	31.7	42.5	46.8
nC6	4	9	298.2 – 473.2	0.2 – 35.2	3 e-5 – 0.00019	0.00044 – 0.10900	49.6	100.0	25.8	8.3
nC7	81-83	15	293.2 – 443.8	0.1 – 7.0	4 e-7 – 0.000018	0.00053 – 0.00266	67.7	100.0	32.2	41.8
nC8	84	9	298.2 – 498.2	0.1 – 36.7	1 e-7 – 0.000078	0.00052 – 0.19369	24.3	100.0	6.5	14.8
nC9	85-88	7	288.2 – 409.7	1.0	3 e-8 – 7.1 e-7	0.00008 – 0.00032	46.3	100.0	279.3	259.2
nC10	89-92	7	296.2 – 573.0	1,0 – 150.0	1.2 e-8 – 2 e-5	0.00028 – 0.51100	83.9	100.0	18.2	22.3
i-C4	59, 63	12	280.2 – 363.2	0.1 – 4.0	0.00010 – 0.00011	0.00009 – 0.00027	10.9	62.6	106.5	6.1
i-C5	77, 80, 93	8	273.1 – 333.1	1.0	0.00001 – 0.00002	0.00011 – 0.00234	48.4	10.6	11.7	15.5
cy-C6	4, 82, 89, 94-97	15	278.3 – 450.8	0.2 – 17.3	0.00001 – 0.00031	0.00016 – 0.08300	48.7	165.1	16.8	99.9
benzene	4	21	279.2 – 490.8	0.1 – 41.9	0.00040 – 0.00860	0.00167 – 0.25780	5.1	28.1	2.7	45.2
toluene	82, 91, 98	19	283.2 – 473.5	0.0 – 138.0	0.00011 – 0.00259	0.00169 – 0.15920	11.7	99.1	5.4	79.1

Table 7.6 (continued)

System	ref.	n_p	T range (K)	P range (bar)	x_1 range	y_1 range	$\%\Delta x_1^{(I)}$ [a]		$\%\Delta x_2^{(II)}$ [b]	
							UMR-PRU	TST/ NRTL	UMR-PRU	TST/ NRTL
Water (2) with										
ebenzene	86	4	310.9 - 479.5	0.0 - 4.9	0.0 – 0.6860	0.0043 - 0.1630	32.8	14.4	10.7	21.9
o-xylene	80, 86	6	273.1 - 479.5	1.0	2.4 E-5 – 0.9800	0.0001 - 0.1630	20.2	25.9	15.8	5.3
m-xylene	83, 85	21	278.2 - 473.3	1.0 - 20.1	1.7 E-5 – 0.5230	0.0065 - 0.2480	28.9	18.5	39.9	58.5
p-xylene	82, 88	17	288.2 - 448.2	0.0 - 11.7	2.9 E-5 – 0.9941	0.0002 - 0.1020	19.4	20.2	17.3	55.1
TEG (2) with										
nC7	99, 100	12	309.4 - 409.6	1.0	0.0112 – 0.0195	0.0004 - 0.0135	23.1	91.4	63.9	728.4
benzene	101	5	279.6 - 287.6	0.1	0.6342 – 0.6732	0.0706 - 0.1095	17.6	25.8	16.6	44.6
toluene	101, 102	17	279.0 - 345.4	-	0.3084 – 0.4850	0.0107 - 0.0866	5.1	7.9	62.7	19.4

[a] *% Δx is defined as:* $\%\Delta X = 100 \cdot \frac{abs(X_i^{exp} - X_i^{calc})}{X_i^{exp}}$, *where X stands for liquid phase solubility (x_i) of the component i, or the vapor phase composition, y_i. (I): polar phase and (II): HC-rich phase.*

[b] The deviation of the water solubility in vapor phase ($\%\Delta y_2$) is 13.1 for UMR-PRU and 5.0 for TST/NRTL.

7.3.2.a. *Hydrocarbons/water*

The IPs between water with HCs groups, have been fitted to LLE data of water/ hydrocarbon binary mixtures of the database presented in Appendix A using the same objective function as in eq. 7.3, but in this case X stands for the solubility of water in the hydrocarbon-rich phase or for the solubility of hydrocarbon in the aqueous phase. The CH_2 – H_2O IP is fitted to binary data of n-pentane, n-hexane, n-heptane and n-octane with water, while for the other mixtures the results presented in Table 7.6 are actually predictions.

Figure 7.10 presents a comparison between the predicted and the experimental mutual solubilities for six representative binary water/hydrocarbon mixtures. In the case of water/propane mixture, water vapor phase compositions are also included. The UMR-PRU model gives very good description of the LLE behavior of the water/hydrocarbon mixtures, with the higher errors encountered for propane and n-butane. This is rational, since they are quite smaller compared to the HCs used for the parameter fitting and thus different behavior is expected. Taking into consideration the well – known challenge of modelling the water/HCs LLE due to their high immiscibility and the asymmetry of the solubilities in each phase, the results presented here, using the group – contribution approach to describe a range of HCs from propane to n-decane, are considered very good. Additionally, using the same IPs obtained from normal alkanes, the UMR-PRU model is able to predict accurately the LLE of naphthenic HCs and branched alkanes with water. Furthermore, it captures well the minimum of the HC solubility with the temperature in the aqueous phase. On the other hand, TST/NRLT gives good results only for the relatively light hydrocarbons, propane and n-butane, while it yields poor ones for the higher molecular weight HCs, especially for the solubility of the HC in the aqueous phase. Apart from the quantitative results, TST/NRTL predicts an ascending behavior with the temperature for the HCs solubility in aqueous phase, which is rational given that it uses only linear temperature dependency in its IPs.

For the aromatic hydrocarbons, it is shown that UMR-PRU predicts very satisfactorily the LLE of xylenes which are important from the environmental aspect, using parameters fitted only to benzene/water mixture.

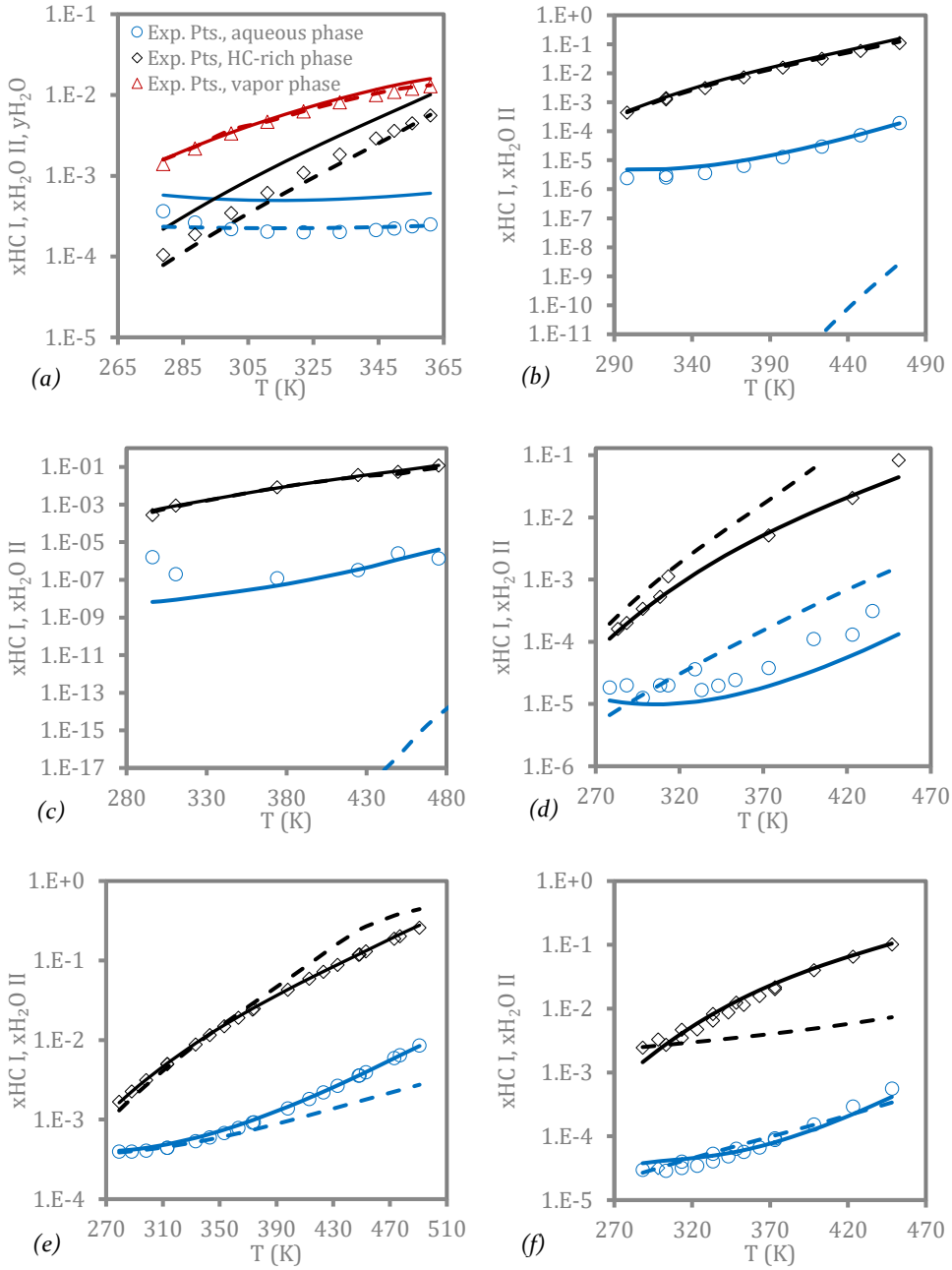

Figure 7.10: LLE prediction results of hydrocarbons with water with UMR-PRU (solid line) and TST/NRTL (dashed line). Blue circles denote experimental points in the aqueous phase (I), black diamonds in the HC-rich phase (II), and red triangles in the vapor phase. (a) Propane/H_2O. Exp. data by Kobayashi et al.[76], (b) n-hexane/H_2O. Exp. data by Tsonopoulos et al.[4], (c) n-decane/H_2O. Exp. data by Revellame et al.[92], Ng et al.[91] and Economou et al.[90], (d). cyclohexane/H_2O. Exp. data by Burd et al.[89], Guseva et al.[95], Pereda et al.[96], Marche et al.[82], Pierotti et al.[97], Goldman et al.[94] and Tsonopoulos et al.[4], (e) Benzene/H_2O. Exp. data by Tsonopoulos et al.[4] and (f) p-xylene/H_2O. Experimental data by Chen et al.[103] and Jou et al.[98].

7.3.2.b. *Hydrocarbons/TEG*

As shown in Table 7.6 and Figure 7.1l, UMR-PRU is able to predict quite satisfactorily the LLE of hydrocarbon/TEG mixtures using the IPs fitted only to VLE data. For the n-heptane/TEG mixture, Figure 7.1l*a*, UMR-PRU gives satisfactory predictions in both phases while TST/NRTL fails. For the benzene/TEG mixture, Figure 7.1l*b*, UMR-PRU yields slightly better results than TST/NRTL, while for the toluene/TEG, Figure 7.1l*c*, both models yield satisfactory results.

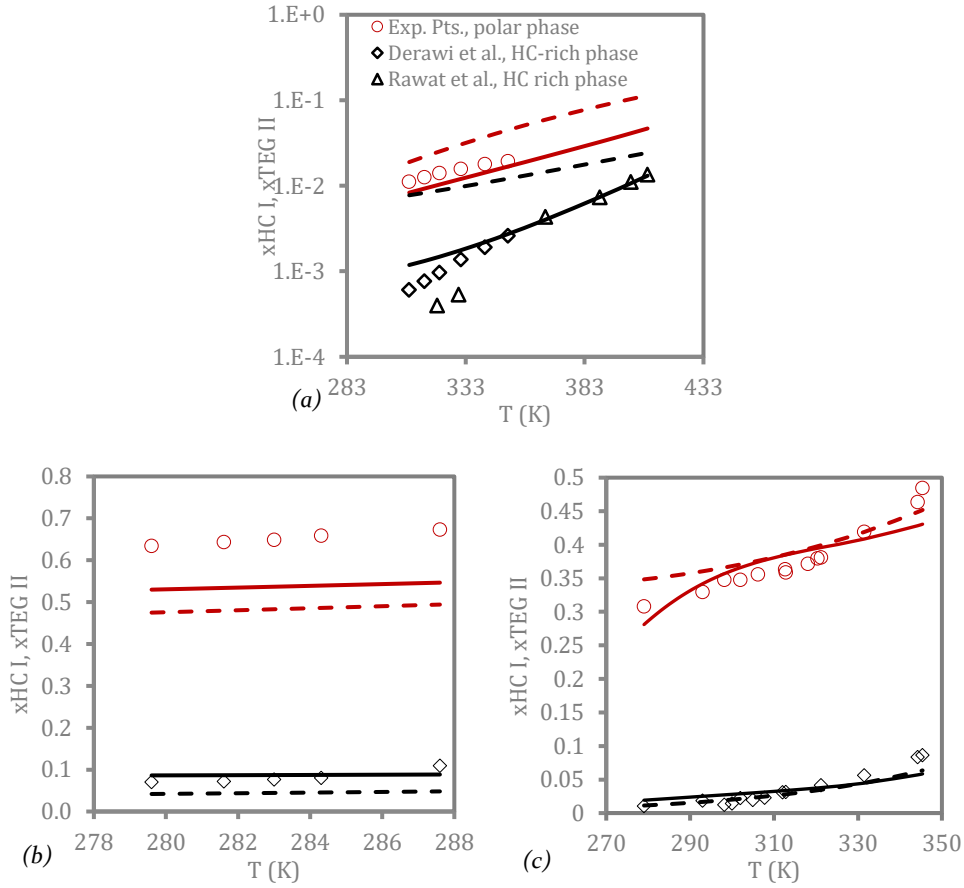

Figure 7.1l: LLE prediction results of hydrocarbons with TEG with UMR-PRU (solid line) and TST/NRTL (dashed line). Red circles denote experimental points in the polar phase (I) and black colour (triangles and diamonds) in the HC-rich phase (II). (a) n-heptane/TEG. Exp. data by Derawi et al.[99] and Rawat et al.[100]. (b) Benzene/TEG. Exp. data by Folas et al.[101]. (c) Toluene/TEG. Exp. data by Folas et al.[101] and Hughes et al.[102].

7.4. Multicomponent Mixtures

A severe test for the thermodynamic models is to predict the phase equilibria of multicomponent mixtures, starting from interaction parameters fitted only to binary phase equilibrium data. To this purpose, the performance of the model is tested on ternary mixtures comprised of natural gas components, water and methanol or glycols. Furthermore, due to the importance of the aromatic components content in the exiting streams of the dehydration process, their distribution with TEG and water is also studied. Finally, typical results of phase envelopes of natural gas mixtures saturated with water are presented.

7.4.1. Ternary mixtures

Experimental data for multicomponent mixtures are rather rare and they generally do not cover many concentrations, or they are reported only for a single phase. Yet, the performance of UMR-PRU in the VLE prediction of ternary mixtures is tabulated in Table 7.7, along with the prediction of TST/NRTL. Overall, the results from the two models are comparable. For the TEG/water/toluene mixture, Figure 7.12, both models predict accurately the BPT as well as the TEG composition in the vapor phase, while UMR-PRU yields better prediction of the water solubility in the vapor phase. For the CO_2/TEG/water mixture, Figure 7.13, UMR-PRU underpredicts the effect of water on the VLE behavior of the mixture while TST/NRTL overpredicts it.

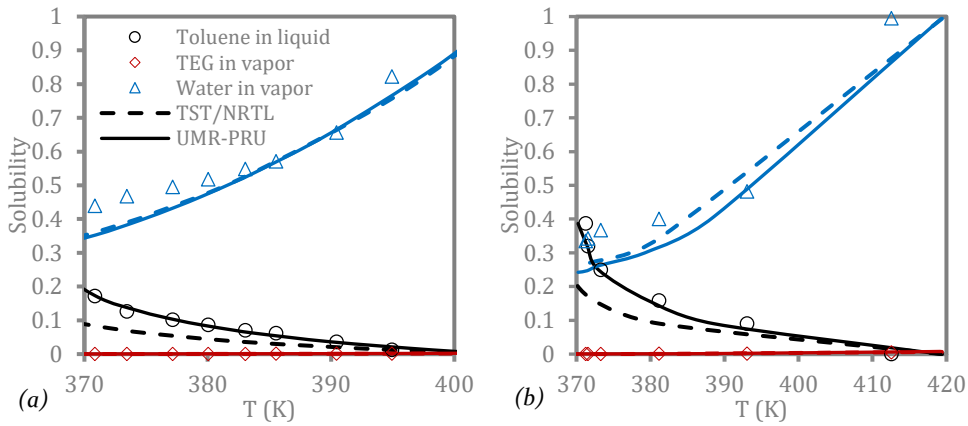

Figure 7.12: VLE bubble point temperature prediction results for the TEG/water/toluene mixture with UMR-PRU (solid line) and TST/NRTL (dashed line). Experimental data by Mostafazadeh et al.[33]. Black circles denote experimental solubility data of toluene in liquid phase, red diamonds the solubility of TEG in vapor phase and blue triangles the water solubility in vapor phase; (a), (b) indicate different tielines.

Table 7.7: VLE ternary mixtures prediction results with UMR-PRU and TST/NRTL.

System	ref.	n_p	T range (K)	P range (bar)	$1000 \cdot \Delta x_1$ [a.b]		$1000 \cdot \Delta x_2$		$1000 \cdot \Delta y_2$	
					UMR-PRU	TST/NRTL	UMR-PRU	TST/NRTL	UMR-PRU	TST/NRTL
CO_2/TEG/H_2O	104	30	297.1 – 322.1	25.2 - 80.3	28.6	28.6	-	-	-	-
CH_4/benzene/TEG	105	5	348.1 – 398.2	6.9 - 107.5	1.1	0.9	0.3	0.3	0.1	0.1
CH_4/toluene/TEG	105	4	348.2 – 398.2	6.9 - 22.5	0.2	0.8	1.6	1.6	0.6	0.4
CH_4/ebenzene/TEG	105	2	348.2	6.5 - 17.4	0.2	0.3	0.03	0.03	0.06	0.02
					$\%\Delta T$ [c]		$\%\Delta y_1$		$\%\Delta y_2$	
					UMR-PRU	TST/NRTL	UMR-PRU	TST/NRTL	UMR-PRU	TST/NRTL
TEG/H_2O/toluene[d]	33	17			0.2	1.6	0.03	0.03	6.1	10.7

[a] The indexes (1), (2) and (3) correspond to the order of the compound in the specific mixture.

[b] $1000 \cdot \Delta X = 1000 \cdot abs(X_i^{exp} - X_i^{calc})$, where X stands for the liquid phase composition of component i, x_i, or the vapor phase solubility of component i, y_i.

[c] $\%\Delta T = 100 \cdot \frac{abs(T_i^{exp} - T_i^{calc})}{T_i^{exp}}$, where T stands for the bubble point temperature.

[d] For the specific mixture, bubble point temperature prediction has been performed.

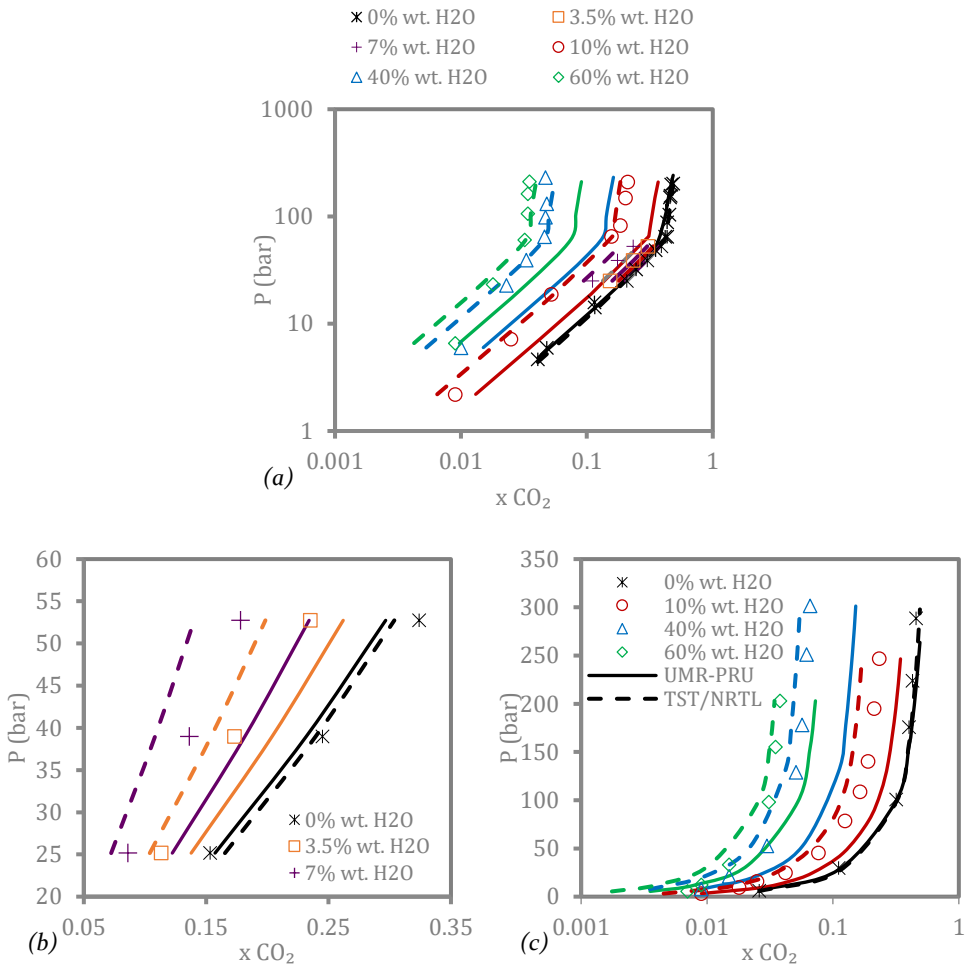

Figure 7.13: VLE prediction results for the CO_2/TEG/water mixture with UMR-PRU (solid line) and TST/NRTL (dashed line). (✶) 0 % wt. water, (□) 3.5 % wt. water, (+) 7 % wt. water, (○) 10 % wt. water, (△) 40 % wt. water and (◇) 60 % wt. water. (a) Experimental data at 297.04 K by Kaminishi et al.[106], at 298.15 K by Wise et al.[69] and Jou et al.[49]. (b) Experimental data by Kaminishi et al.[106] at 322.04 K. (c). Experimental data by Wise et al.[69] at 343.15 K.

Figure 7.14 compares the predicted partition coefficients in ternary mixtures containing methane, an aromatic hydrocarbon and TEG with the corresponding experimental data. Excellent predictions are obtained by both models for the distribution of methane and the aromatic compounds.

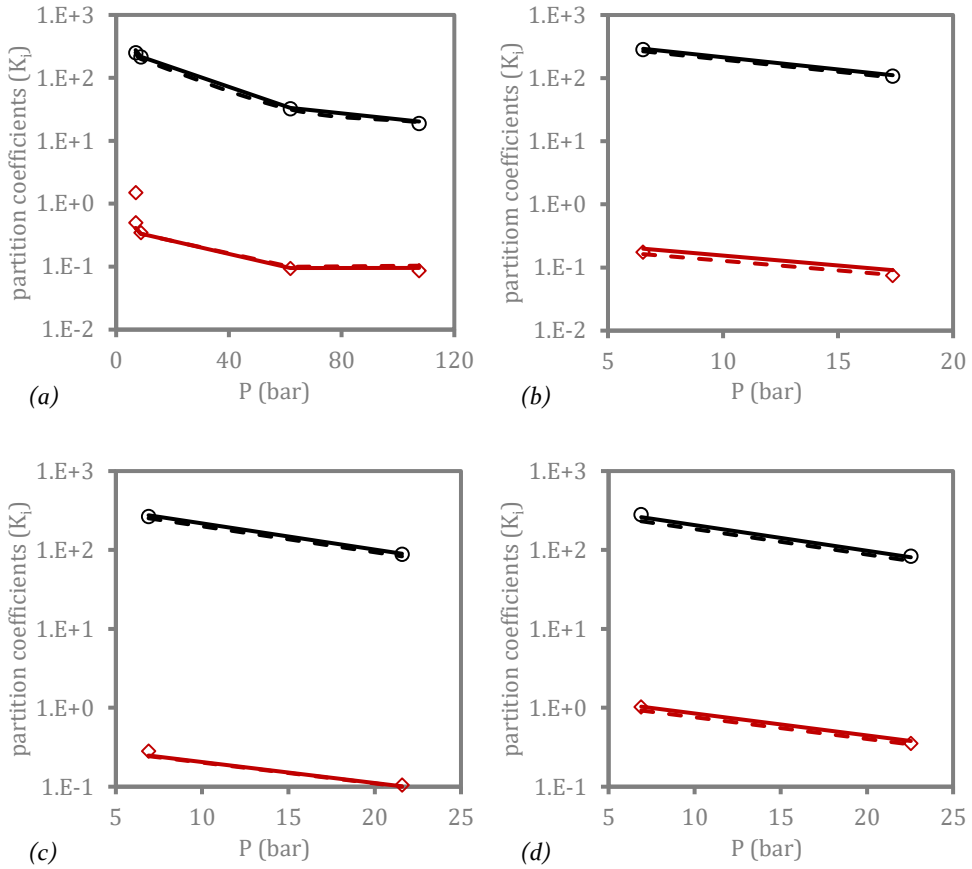

Figure 7.14: VLE prediction results for ternary mixtures containing methane, an aromatic hydrocarbon and TEG with UMR-PRU (solid line) and TST/NRTL (dashed line). Black circles denote experimental partition coefficients of methane and red diamonds partition coefficients of the respective aromatic hydrocarbon. Experimental data by Ng et al.[105]; (a) methane/benzene/TEG at 348.15 K, (b) methane/ethylbenzene/TEG at 348.15 K, (c) methane/toluene/TEG at 348.15 K and (d) methane/toluene/TEG at 398.15 K.

7.4.2. Multicomponent mixtures containing BTEX components

For environmental purposes the control of the emissions of certain hydrocarbons is very important. During the process of natural gas dehydration, the most important ones are the aromatic compounds which have significantly higher solubility in water and glycols compared for example to paraffins, as discussed in Section 3.3.2. Similarly, glycols present significantly higher solubility in aromatic compounds due to the donor – acceptor interactions encountered at the free electrons of the π-valence. Among them, the most important ones are benzene and its derivatives, namely toluene, ethylbenzene and several xylenes, which in industrial practice are commonly referred as BTEX, as taken from their initials. To this purpose, the UMR-PRU model is evaluated in the prediction of multicomponent aqueous mixtures of methane and TEG with BTEX compounds. The available experimental data of Ng et al.[107] are close to the conditions encountered in the flash drum, the contactor and the regenerator of a typical TEG dehydration process. Representative prediction results with UMR-PRU and TST/NRTL are presented in Figure 7.15. Both models predict very accurately the distributions of the BTEX components, as it is proved by the proximity of the points to the diagonal line. As for the methane and TEG distribution, both models yield accurate results with the UMR-PRU to be slightly superior than TST/NRTL.

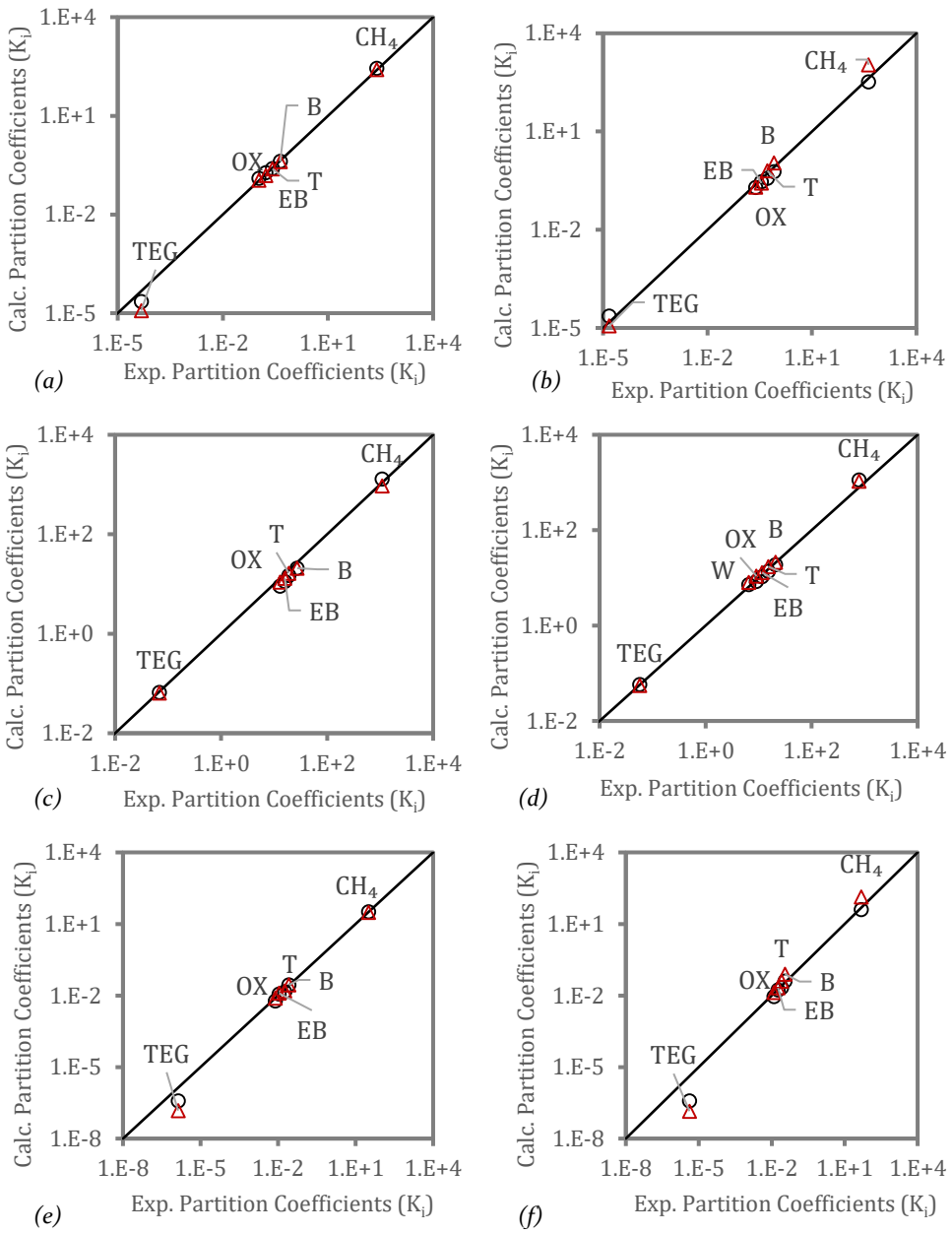

Figure 7.15: VLE prediction results for mixtures containing methane, BTEX, water and TEG at different conditions relative to dehydration process. Experimental data by Ng et al.[107]. Modelling results (○) with UMR-PRU (in black) and (△) with TST/NRTL (in red); (a) Flash drum conditions on dry basis, at 348.1 K and 6.89 bar, (b) Flash tank conditions with 5 % wt. water, at 348.1 K and 6.89 bar, (c) Regenerator conditions on dry basis, at 477.6 K and 1.38 bar, (d) Regenerator conditions with 1 % wt. water, at 477.6 K and 1.62 bar, (e) Contactor conditions on dry basis, at 298.1 K and 68.95 bar and (f) Contactor conditions with 1 % wt. water, at 298.1 K and 68.95 bar.

7.4.3. Phase envelope of wet natural gases

Since UMR-PRU and TST/NRTL are compared in the simulation of a natural gas TEG dehydration unit, it is rational to examine their performance on some representative natural gas mixtures both in dry and wet base. A wider database is examined with UMR-PRU in Chapter 9 and the detailed results are reported there. Nevertheless, the relative performance of the two models is illustrated in Figure 7.16.

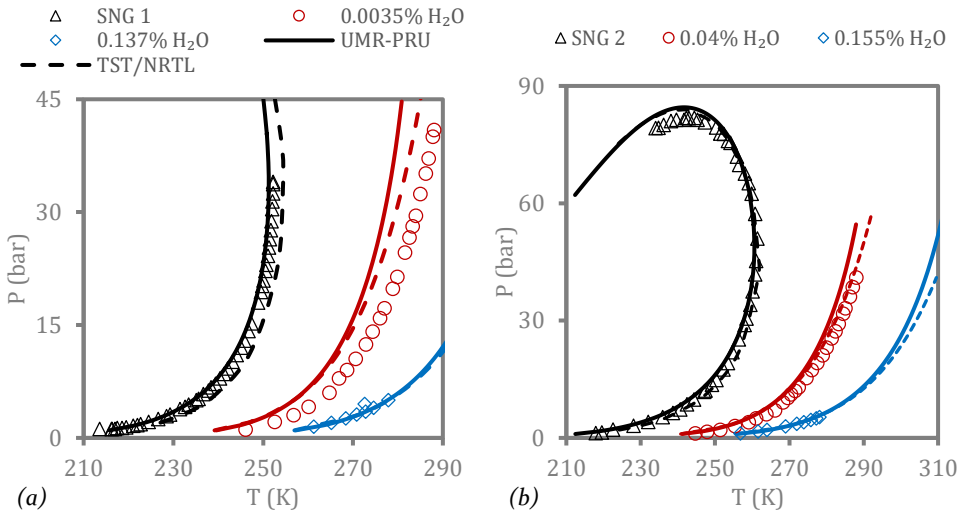

Figure 7.16: Dew point prediction on dry and wet basis with UMR-PRU (solid line) and TST/NRTL (dashed line). (a) Exp. data by Avila et al.[108]. Composition (molar) on dry basis: N_2: 0.31, CO_2: 0.20, CH_4: 90.42, C2: 8.04, C3: 0.80, iC4: 0.08, nC4: 0.12, iC5: 0.01, nC5: 0.01, nC6: 0.005 and nC7: 0.001 and (b) Exp. data by Jarne et al.[109]. Composition (molar) on dry basis: N_2: 0.77, CO_2: 1.70, CH_4: 84.45, C2: 8.68, C3: 3.3, iC4: 0.29, nC4: 0.59, iC5: 0.08, nC5: 0.09 and nC6: 0.05.

It is shown that very good results are obtained with both models in the dew point prediction of dry and wet synthetic natural gas mixtures. TST/NRTL overpredicts the cricondentherm temperature on dry basis. That leads to higher cricondentherm prediction compared to that of UMR-PRU in the wet gases, which is actually closer to the experimental data.

7.5. Conclusions

The UMR-PRU model has been successfully extended to the modelling of natural gas components with water and polar chemicals, namely methanol, MEG and TEG, which are encountered in several steps of the natural gas value chain.

Satisfactory correlation results have been obtained in all cases. Special interest presents the TEG solubility in methane vapor phase, which is of utmost importance for the accurate calculation of TEG loss during the dehydration process. Also, for the LLE in binary mixtures of hydrocarbons with water, UMR-PRU is able to accurately describe the mutual solubilities. The obtained results are comparable with those of TST/NRTL which is proposed by Hysys for application in the simulation of dehydration processes, for the mixtures with water and TEG. Instead, for the mixtures with methanol and MEG, UMR-PRU presents superior results, possibly due to the lack of specifically fitted parameters in the case of TST/NRTL.

The performance of the models is further evaluated in the prediction of multicomponent mixtures, with overall satisfactory results. The mixtures tested include light hydrocarbons with water and TEG. The models also showed very good results in the distribution of BTEX in conditions relevant to those which occur at TEG dehydration. Finally, quite satisfactory results are obtained for the dew point lines of synthetic NG mixtures. Therefore, the UMR-PRU is an accurate model for application in mixtures of natural gas components with polar chemicals and can be further used for natural gas process simulation purposes.

List of Symbols

Latin Characters

a-e	constants for the DIPPR-101 equation for vapor pressure calculation
c_p	specific heat capacity of a component ($kJ \cdot kmol^{-1} \cdot K^{-1}$)
H	molar enthalpy ($J \cdot kmol^{-1}$)
K_i	partition coefficient of a component *i* between the two phases in equilibrium
n	number of moles (mol)
n_p	number of datapoints
P	pressure (bar)
S	model fitting objective function to be minimized (eq. 7.3)
T	absolute temperature (K)
x_i	liquid mol fraction of component *i*
y_i	vapor mol fraction of component *i*

Greek Characters

ω	acentric factor

Superscripts and Subscripts

b	boiling
c	critical
calc	calculated
exp	experimental
I, II	phases at equilibrium
i, j	molecule in a mixture
p	points
∞	infinite

References

(1) Kontogeorgis G.M., Folas G.K., *Thermodynamic models for industrial applications: from classical and advanced mixing rules to association theories*. John Wiley & Sons: 2009.
(2) Magnussen T., Rasmussen P., Fredenslund A., UNIFAC parameter table for prediction of liquid-liquid equilibriums. *Industrial & Engineering Chemistry Process Design and Development* **1981,** *20*, (2), 331-339.
(3) Hansen H.K., Rasmussen P., Fredenslund A., Schiller M., Gmehling J., Vapor-liquid equilibria by UNIFAC group contribution. 5. Revision and extension. *Industrial & engineering chemistry research* **1991,** *30*, (10), 2352-2355.
(4) Tsonopoulos C., Wilson G., High-temperature mutual solubilities of hydrocarbons and water. Part I: Benzene, cyclohexane and n-hexane. *AIChE Journal* **1983,** *29*, (6), 990-999.
(5) Soave G., Equilibrium constants from a modified Redlich-Kwong equation of state. *Chemical Engineering Science* **1972,** *27*, (6), 1197-1203.
(6) Louli V., Pappa G., Boukouvalas C., Skouras S., Solbraa E., Christensen K.O., Voutsas E., Measurement and prediction of dew point curves of natural gas mixtures. *Fluid Phase Equilibria* **2012,** *334*, 1-9.
(7) Prausnitz J.M., Lichtenthaler R.N., de Azevedo E.G., *Molecular thermodynamics of fluid-phase equilibria*. Pearson Education: 1998.
(8) Boukouvalas C., Spiliotis N., Coutsikos P., Tzouvaras N., Tassios D., Prediction of vapor-liquid equilibrium with the LCVM model: a linear combination of the Vidal and Michelsen mixing rules coupled with the original UNIFAC and the t-mPR equation of state. *Fluid Phase Equilibria* **1994,** *92*, 75-106.
(9) Le Guennec Y., Privat R., Jaubert J.-N., Development of the translated-consistent tc-PR and tc-RK cubic equations of state for a safe and accurate prediction of volumetric, energetic and saturation properties of pure compounds in the sub- and super-critical domains. *Fluid Phase Equilibria* **2016,** *429*, 301-312.
(10) Derawi S.O., Michelsen M.L., Kontogeorgis G.M., Stenby E.H., Application of the CPA equation of state to glycol/hydrocarbons liquid–liquid equilibria. *Fluid Phase Equilibria* **2003,** *209*, (2), 163-184.
(11) Wise H., Puck T.T., Failey C.F., The Studies in Vapor–Liquid Equilibria. II. The Binary System Triethylene Glycol–Water. *The Journal of Physical Chemistry* **1950,** *54*, (5), 734-741.
(12) Steele W.V., Chirico R.D., Knipmeyer S.E., Nguyen A., Measurements of Vapor Pressure, Heat Capacity, and Density along the Saturation Line for ε-Caprolactam, Pyrazine, 1,2-Propanediol, Triethylene Glycol, Phenyl Acetylene, and Diphenyl Acetylene. *Journal of Chemical & Engineering Data* **2002,** *47*, (4), 689-699.
(13) Stull D.R., Vapor Pressure of Pure Substances. Organic and Inorganic Compounds. *Industrial & Engineering Chemistry* **1947,** *39*, (4), 517-540.
(14) NIST Thermophysical Properties of Fluid Systems, http://webbook.nist.gov/chemistry/fluid/, accessed on 01/09/2017.
(15) Stephens M.A., Tamplin W.S., Saturated liquid specific heats of ethylene glycol homologs. *Journal of Chemical and Engineering Data* **1979,** *24*, (2), 81-82.
(16) Li C.-K., Soriano A.N., Li M.-H., Heat capacities of the mixed-solvents desiccants (glycols+water+salts). *Thermochimica Acta* **2009,** *487*, (1), 26-32.
(17) Kertes, *IUPAC Solubility Data Series, Pergamon Press: Oxford*. 1979.

(18) Bamberger A., Sieder G., Maurer G., High-pressure (vapor+liquid) equilibrium in binary mixtures of (carbon dioxide+water or acetic acid) at temperatures from 313 to 353 K. *The Journal of Supercritical Fluids* **2000,** *17*, (2), 97-110.
(19) King M.B., Mubarak A., Kim J.D., Bott T.R., The mutual solubilities of water with supercritical and liquid carbon dioxides. *The Journal of Supercritical Fluids* **1992,** *5*, (4), 296-302.
(20) Muller G., Bender E., Maurer G., Vapor-liquid-equilibrium in the ternary-system ammonia-carbon dioxide-water at high water contents in the range 373-K to 473-K. *Berichte Der Bunsen-Gesellschaft-Physical Chemistry Chemical Physics* **1988,** *92*, (2), 148-160.
(21) Takenouchi S., Kennedy G.C., The binary system H_2O-CO_2 at high temperatures and pressures. *American Journal of Science* **1964,** *262*, (9), 1055-1074.
(22) Valtz A., Chapoy A., Coquelet C., Paricaud P., Richon D., Vapour–liquid equilibria in the carbon dioxide–water system, measurement and modelling from 278.2 to 318.2 K. *Fluid Phase Equilibria* **2004,** *226*, 333-344.
(23) Wiebe R., Gaddy V.L., The Solubility of Carbon Dioxide in Water at Various Temperatures from 12 to 40° and at Pressures to 500 Atmospheres. Critical Phenomena*. *Journal of the American Chemical Society* **1940,** *62*, (4), 815-817.
(24) Chapoy A., Mohammadi A.H., Tohidi B., Richon D., Estimation of water content for methane+ water and methane+ ethane+ n-butane+ water systems using a new sampling device. *Journal of Chemical & Engineering Data* **2005,** *50*, (4), 1157-1161.
(25) Frost M., Karakatsani E., von Solms N., Richon D., Kontogeorgis G.M., Vapor–Liquid Equilibrium of Methane with Water and Methanol. Measurements and Modeling. *Journal of Chemical & Engineering Data* **2013,** *59*, (4), 961-967.
(26) Kim Y.S., Ryu S.K., Yang S.O., Lee C.S., Liquid Water–Hydrate Equilibrium Measurements and Unified Predictions of Hydrate-Containing Phase Equilibria for Methane, Ethane, Propane, and Their Mixtures. *Industrial & engineering chemistry research* **2003,** *42*, (11), 2409-2414.
(27) Lekvam K., Bishnoi P.R., Dissolution of methane in water at low temperatures and intermediate pressures. *Fluid Phase Equilibria* **1997,** *131*, (1–2), 297-309.
(28) O'Sullivan T.D., Smith N.O., Solubility and partial molar volume of nitrogen and methane in water and in aqueous sodium chloride from 50 to 125. deg. and 100 to 600 atm. *The Journal of Physical Chemistry* **1970,** *74*, (7), 1460-1466.
(29) Sultanov R., Skripka V., Namiot A.Y., Phase equilibrium and critical effect of water-methane system under increased temperature and pressure. *Zhurnal Fizicheskoi Khimii* **1972,** *46*, (8), 2160.
(30) Yarym-Agaev N., Sinyavskaya R., Koliushko I., Phase equilibrium in the binary systems water-methane and methanol-methane under high pressure. *Zh. Prikl. Khim* **1985,** *58*, 165-168.
(31) Mohammadi A., Chapoy A., Tohidi B., Richon D., Measurements and thermodynamic modeling of vapor-liquid equilibria in ethane-water systems from 274.26 to 343.08 K. *Industrial & engineering chemistry research* **2004,** *43*, (17), 5418-5424.
(32) Gonzalez C., Van Ness H.C., Excess thermodynamic functions for ternary systems. 9. Total-pressure data and GE for water/ethylene glycol/ethanol at 50°C. *Journal of Chemical & Engineering Data* **1983,** *28*, (4), 410-412.

(33) Mostafazadeh A.K., Rahimpour M.R., Shariati A., Vapor–Liquid Equilibria of Water + Triethylene Glycol (TEG) and Water + TEG + Toluene at 85 kPa. *Journal of Chemical & Engineering Data* **2009,** *54*, (3), 876-881.
(34) Ohgaki K., Katayama T., Isothermal vapor-liquid equilibrium data for binary systems containing carbon dioxide at high pressures: methanol-carbon dioxide, n-hexane-carbon dioxide, and benzene-carbon dioxide systems. *Journal of Chemical and Engineering Data* **1976,** *21*, (1), 53-55.
(35) Gmelin T., *Handbuch BD. C* **1970,** *14*, 568.
(36) Brunner E., Hültenschmidt W., Schlichthärle G., Fluid mixtures at high pressures IV. Isothermal phase equilibria in binary mixtures consisting of (methanol+ hydrogen or nitrogen or methane or carbon monoxide or carbon dioxide). *The Journal of Chemical Thermodynamics* **1987,** *19*, (3), 273-291.
(37) Hong J.H., Malone P.V., Jett M.D., Kobayashi R., The measurement and interpretation of the fluid-phase equilibria of a normal fluid in a hydrogen bonding solvent: the methane - methanol system. *Fluid Phase Equilibria* **1987,** *38*, (1–2), 83-96.
(38) Nourozieh H., Kariznovi M., Abedi J., Phase equilibrium measurements and thermodynamic modeling of methane alcohol systems at ambient temperature. *The Journal of Chemical Thermodynamics* **2012,** *54*, (0), 165-170.
(39) Ukai T., Kodama D., Miyazaki J., Kato M., Solubility of methane in alcohols and saturated density at 280.15 K. *Journal of Chemical & Engineering Data* **2002,** *47*, (5), 1320-1323.
(40) Lam D.H., Luks K.D., Multiphase equilibrium behavior of the mixture ethane + methanol + 1-decanol. *Journal of Chemical & Engineering Data* **1991,** *36*, (3), 307-311.
(41) Ma Y.H., Kohn J.P., Multiphase and Volumetric Equilibria of the Ethane-Methanol System at Temperatures between -40 C. and 100 C. *Journal of Chemical & Engineering Data* **1964,** *9*, (1), 3-5.
(42) Nourozieh H., Kariznovi M., Abedi J., Vapor–liquid and liquid–liquid equilibrium properties of ethane + methanol system at ambient temperature. *Fluid Phase Equilibria* **2011,** *303*, (1), 31-34.
(43) Zeck S., Knapp H., Vapor-liquid and vapor-liquid-liquid phase equilibria for binary and ternary systems for nitrogen, ethane and methanol: Experiment and data reduction. *Fluid Phase Equilibria* **1986,** *25*, (3), 303-322.
(44) Zheng D.-Q., Ma W.-D., Wei R., Guo T.-M., Solubility study of methane, carbon dioxide and nitrogen in ethylene glycol at elevated temperatures and pressures. *Fluid Phase Equilibria* **1999,** *155*, (2), 277-286.
(45) Gui X., Tang Z., Fei W., Solubility of CO_2 in alcohols, glycols, ethers, and ketones at high pressures from (288.15 to 318.15) K. *Journal of Chemical & Engineering Data* **2011,** *56*, (5), 2420-2429.
(46) Jou F.-Y., Deshmukh R., Otto F., Mather A., Vapor - liquid equilibria of H_2S and CO_2 and ethylene glycol at elevated pressures. *Chemical engineering communications* **1990,** *87*, (1), 223-231.
(47) Serpa F.S., Vidal R.S., Filho J.o.H.A., Nascimento J.F.d., Ciambelli J.o.R., Figueiredo C.M., Salazar-Banda G.R., Santos A.F., Fortuny M.,Franceschi E., Solubility of carbon dioxide in ethane-1, 2-diol–water mixtures. *Journal of Chemical & Engineering Data* **2013,** *58*, (12), 3464-3469.
(48) Jou F.Y., Otto F.D., Mather A.E., Solubility of methane in glycols at elevated pressures. *The Canadian Journal of Chemical Engineering* **1994,** *72*, (1), 130-133.

(49) Jou F.Y., Deshmukh R.D., Otto F.D., Mather A.E., Vapor - liquid equilibria for acid gases and lower alkanes in triethylene glycol. *Fluid Phase Equilibria* **1987,** *36*, (0), 121-140.
(50) Wilson L., Wilding W., Wilson G., In *Vapor-Liquid Equilibrium Measurements on Four Binary Mixtures*, presented on AIChE Symp. Ser, **1989**
(51) Rowley R., Hoffma G., In *Vapor-Liquid Equilibrium Measurements on Mixtures Important to Industrial Design: Triethylene Glycol+ n-hexane, Triethylene Glycol+ Cyclohexane and Furfural+ Isoprene*, presented on AIChE Symp. Ser, **1990**
(52) Gupta S.K., Rawat B.S., Goswami A.N., Nanoti S.M.,Krishna R., Isobaric vapour-liquid equilibria of the systems: Benzene-triethylene glycol, toluene-triethylene glycol and benzene-N-methylpyrrolidone. *Fluid Phase Equilibria* **1989,** *46*, (1), 95-102.
(53) Hong J.H., Kobayashi R., Vapor-liquid equilibrium studies for the carbon dioxide-methanol system. *Fluid Phase Equilibria* **1988,** *41*, (3), 269-276.
(54) Wiebe R.,Gaddy V.L., The Solubility in Water of Carbon Dioxide at 50, 75 and 100°, at Pressures to 700 Atmospheres. *Journal of the American Chemical Society* **1939,** *61*, (2), 315-318.
(55) Wiebe R., Gaddy V.L., Vapor Phase Composition of Carbon Dioxide-Water Mixtures at Various Temperatures and at Pressures to 700 Atmospheres. *Journal of the American Chemical Society* **1941,** *63*, (2), 475-477.
(56) Afzal W., Liu X., Prausnitz J.M., Solubilities of some gases in four immidazolium-based ionic liquids. *The Journal of Chemical Thermodynamics* **2013,** *63*, 88-94.
(57) Kaminishi G.-I., Takano S., Yokoyama C., Takahashi S., Takeuchi K., Concentration of triethylene glycol, diethylene glycol and ethylene glycol in supercritical carbon dioxide up to 16 MPa at 313. 15 and 333. 15K. *Fluid Phase Equilibria* **1989,** *52*, 365-372.
(58) Sage B.H., Lacey W.N., Properties of light HC's, H_2S and CO_2, Part I. *American Petroleum Institute* **1955**.
(59) Yarrison M., Cox K.R.,Chapman W.G., Measurement and Modeling of the Solubility of Water in Supercritical Methane and Ethane from 310 to 477 K and Pressures from 3.4 to 110 MPa. *Industrial & engineering chemistry research* **2006,** *45*, (20), 6770-6777.
(60) Jerinić D., Schmidt J., Fischer K.,Friedel L., Measurement of the triethylene glycol solubility in supercritical methane at pressures up to 9 MPa. *Fluid Phase Equilibria* **2008,** *264*, (1–2), 253-258.
(61) Arya A., Maribo-Mogensen B., Tsivintzelis I., Kontogeorgis G.M., Process Design of Industrial Triethylene Glycol Processes Using the Cubic-Plus-Association (CPA) Equation of State. *Ind. & engineering chemistry research* **2014,** *53*, (29), 11766 - 11778.
(62) Folas G.K., Froyna E.W., Lovland J., Kontogeorgis G.M., Solbraa E., Data and prediction of water content of high pressure nitrogen, methane and natural gas. *Fluid Phase Equilibria* **2007,** *252*, (1–2), 162-174.
(63) Rigby M., Prausnitz J.M., Solubility of water in compressed nitrogen, argon, and methane. *The Journal of Physical Chemistry* **1968,** *72*, (1), 330-334.
(64) Althaus K. Messung und Berechung von Wassergehalten kohlenwasserst-offhaltiger Gasgemische. Universität Fridereciana zu Karlsruhe (Technische Hochschule) genehmigte, *1999*.

(65) Song K.Y., Yarrison M., Chapman W., Experimental low temperature water content in gaseous methane, liquid ethane, and liquid propane in equilibrium with hydrate at cryogenic conditions. *Fluid Phase Equilibria* **2004,** *224*, (2), 271-277.
(66) Piemonte V., Maschietti M., Gironi F., A Triethylene Glycol–Water System: A study of the TEG regeneration processes in natural gas dehydration plants. *Energy Sources, Part A: Recovery, Utilization, and Environmental Effects* **2012,** *34*, (5), 456-464.
(67) Joung S.N., Yoo C.W., Shin H.Y., Kim S.Y., Yoo K.-P., Lee C.S., Huh W.S., Measurements and correlation of high-pressure VLE of binary CO_2–alcohol systems (methanol, ethanol, 2-methoxyethanol and 2-ethoxyethanol). *Fluid Phase Equilibria* **2001,** *185*, (1–2), 219-230.
(68) Leu A.-D., Chung S.Y.-K., Robinson D.B., The equilibrium phase properties of (carbon dioxide+ methanol). *The Journal of Chemical Thermodynamics* **1991,** *23*, (10), 979-985.
(69) Wise M., Chapoy A., Carbon dioxide solubility in Triethylene Glycol and aqueous solutions. *Fluid Phase Equilibria* **2016,** *419*, 39-49.
(70) Bestani B., Shing K.S., Infinite-dilution activity coefficients of water in TEG, PEG, glycerol and their mixtures in the temperature range 50 to 140 °C. *Fluid Phase Equil.* **1989,** *50*, (1-2), 209.
(71) Parrish W.R., K.W. W., M.E. B., In *Phase behavior of the triethylene glycol–water system and dehydration/regeneration design for extremely low dew point requirements*, presented on 65th Annual GPA Convention, San Antonio, **1986**
(72) Twu C.H., Tassone V., Sim W.D., Watanasiri S., Advanced equation of state method for modeling TEG–water for glycol gas dehydration. *Fluid Phase Equilibria* **2005,** *228–229*, (0), 213-221.
(73) Herskowitz M., Gottlieb M., Vapor-liquid equilibrium in aqueous solutions of various glycols and polyethylene glycols. 1. Triethylene glycol. *Journal of Chemical & Engineering Data* **1984,** *29*, (2), 173-175.
(74) Hamam S.E.M., Benson G.C., Kumaran M.K., Excess enthalpies of (water + diethylene glycol) and (water + triethylene glycol). *The Journal of Chemical Thermodynamics* **1985,** *17*, (10), 973-976.
(75) Satyro M.A., Schoeggl F., Yarranton H.W., Temperature change from isenthalpic expansion of aqueous triethylene glycol mixtures for natural gas dehydration. *Fluid Phase Equilibria* **2011,** *305*, (1), 62-67.
(76) Kobayashi R., Katz D., Vapor-Liquid Equilibria For Binary Hydrocarbon-Water Systems. *Industrial & Engineering Chemistry* **1953,** *45*, (2), 440-446.
(77) Black C.J., G. G.; Taylor, H. S., The Solubility of Water in Hydrocarbons. *J. Chem. Phys* **1948,** *16*.
(78) Mokraoui S., Coquelet C., Valtz A., Hegel P.E., Richon D., New Solubility Data of Hydrocarbons in Water and Modeling Concerning Vapor–Liquid–Liquid Binary Systems. *Industrial & engineering chemistry research* **2007,** *46*, (26), 9257-9262.
(79) Reamer H., Sage B.,Lacey W., Phase Equilibria in Hydrocarbon Systems. n-Butane-Water System in the Two-Phase Region. *Industrial & Engineering Chemistry* **1952,** *44*, (3), 609-615.
(80) Polak J., Lu B.C.-Y., Mutual solubilities of hydrocarbons and water at 0 and 25 C. *Canadian Journal of Chemistry* **1973,** *51*, (24), 4018-4023.

(81) Englin B., Plate A., Tugolukov V., Pryanishnikova M., Solubility of water in individual hydrocarbons. *Chemistry and Technology of Fuels and Oils* **1965,** *1*, (9), 722-726.
(82) Marche C., Ferronato C.,Jose J., Solubilities of n-Alkanes (C6 to C8) in Water from 30 °C to 180 °C. *Journal of Chemical & Engineering Data* **2003,** *48*, (4), 967-971.
(83) Nelson H., de Ligny C., Determination of the solubilities of some n-alkanes in water at different temperatures by gas chromatography. *Recl. Trav. Chim. Pays-Bas* **1968,** *87*.
(84) Heidman J., Tsonopoulos C., Brady C., Wilson G., High-temperature mutual solubilities of hydrocarbons and water. Part II: Ethylbenzene, ethylcyclohexane, and n-octane. *AIChE Journal* **1985,** *31*, (3), 376-384.
(85) Benkovski V., Nauruzov M., Bogoslovskaya T., Tr Inst Khim Nefti Prir Solei. *Akad Nauk Kaz SSR* **1970,** *2*, 25.
(86) Jönsson J.Å., Vejrosta J., Novák J., Air/water partition coefficients for normal alkanes (n-pentane to n-nonane). *Fluid Phase Equilibria* **1982,** *9*, (3), 279-286.
(87) McAuliffe C., Solubility in water of C1–C9 hydrocarbons. *Nature* **1963,** *200*, (4911), 1092-1093.
(88) Price L.C., Aqueous solubility of petroleum as applied to its origin and primary migration. *Am. Assoc. Pet. Geol. Bull.* **1976,** *60*, (2), 213-244.
(89) Burd S.D.B., W. G., Vapor-liquid equilibria of some C6 hydrocarbons with water. *Proc. Am. Pet. Inst. Div. Refin.* **1968,** *48*.
(90) Economou I., Heidman J., Tsonopoulos C., Wilson G., Mutual solubilities of hydrocarbons and water: III. 1-hexene, 1-octene, C10-C12 hydrocarbons. *AIChE Journal* **1997,** *43*, (2), 535-546.
(91) Ng H.-J., Chen C.-J., *Mutual Solubility in Water-hydrocarbon Systems: GPA Project 895, RR-150*; Gas Processors Association: 1995.
(92) Revellame E.D., Holmes W.E., Hernandez R., French W.T., Lerma L., Forks A., Ashe T., Estévez L.A., Experimental measurement and modeling of the Type 3 ternary system containing (decane+ water+ triacetin). *The Journal of Chemical Thermodynamics* **2013,** *67*, 21-27.
(93) Pavlova S.P., S. Yu., Serafimov L. A., Kofman L. S., *Prom-st Sint. Kauch* **1966,** *3*.
(94) Goldman S., The determination and statistical mechanical interpretation of the solubility of water in benzene, carbon tetrachloride, and cyclohexane. *Canadian Journal of Chemistry* **1974,** *52*, (9), 1668-1680.
(95) Guseva A., Parnov E., Solubility of cyclohexane in water. *Zhurnal Fizicheskoi Khimii* **1963,** *37*, (12), 2763-2763.
(96) Pereda S., Awan J.A., Mohammadi A.H., Valtz A., Coquelet C., Brignole E.A., Richon D., Solubility of hydrocarbons in water: Experimental measurements and modeling using a group contribution with association equation of state (GCA-EoS). *Fluid Phase Equilibria* **2009,** *275*, (1), 52-59.
(97) Pierotti R., Liabastre A., Structure and Properties of Water Solutions US Nat. *Tech. Inform. Serv., PB Rep* **1972**, (21163).
(98) Jou F.-Y., Mather A.E., Liquid–Liquid Equilibria for Binary Mixtures of Water + Benzene, Water + Toluene, and Water + p-Xylene from 273 K to 458 K. *Journal of Chemical & Engineering Data* **2003,** *48*, (3), 750-752.

(99) Derawi S.O., Kontogeorgis G.M., Stenby E.H., Haugum T.,Fredheim A.O., Liquid-liquid equilibria for glycols+ hydrocarbons: data and correlation. *Journal of Chemical & Engineering Data* **2002,** *47*, (2), 169-173.
(100) Rawat B.S., Prasad G., Liquid-Liquid Equilibria for benzene - n-heptane systems with triethylene glycol, tetraethylene glycol, and sulfolane containing water at elevated temperatures. *Journal of Chemical and Engineering Data* **1980,** *25*, (3), 227-230.
(101) Folas G.K., Kontogeorgis G.M., Michelsen M.L., Stenby E.H., Solbraa E., Liquid–Liquid Equilibria for Binary and Ternary Systems Containing Glycols, Aromatic Hydrocarbons, and Water: Experimental Measurements and Modeling with the CPA EoS. *Journal of Chemical & Engineering Data* **2006,** *51*, (3), 977-983.
(102) Hughes M.A., Haoran Y., Liquid-liquid equilibria for separation of toluene from heptane by benzyl alcohol tri (ethylene glycol) mixtures. *Journal of Chemical and Engineering Data* **1990,** *35*, (4), 467-471.
(103) Chen H.,Wagner J., Mutual solubilities of alkylbenzene+ water systems at temperatures from 303 to 373 K: ethylbenzene, p-xylene, 1, 3, 5-trimethylbenzene, and butylbenzene. *Journal of Chemical and Engineering Data* **1994,** *39*, (4), 679-684.
(104) Takahashi S., Song K.Y., Kobayashi R., Experimental vapor-liquid equilibriums in the carbon dioxide-diethylene glycol-water and carbon dioxide-triethylene glycol-water systems at feasible absorption temperatures and pressures. *Journal of Chemical & Engineering Data* **1984,** *29*, (1), 23-28.
(105) Ng H.-J., Chen C.-J., Robinson D.B., *The solubility of selected aromatic hydrocarbons in triethylene glycol, RR-131*; Gas Processing Association: Tulsa, Oklahoma, 1991.
(106) Kaminishi G.-I., Arai Y., Saito S., Maeda S., Vapor-liquid equilibria for binary and ternary systems containing carbon dioxide. *J. Chem. Eng. Jpn.* **1968,** *1*, (2), 109-116.
(107) Ng H.-J., Chen C.-J., Razzaghi M., Vapor-liquid equilibria of selected aromatic hydrocarbons in triethylene glycol. *Fluid Phase Equilibria* **1993,** *82*, (0), 207-214.
(108) Avila S., Blanco S.T., Velasco I., Rauzy E., Otín S., Thermodynamic Properties of Synthetic Natural Gases. 1. Dew-Point Curves of Synthetic Natural Gases and Their Mixtures with Water and Methanol. Measurement and Correlation. *Industrial & engineering chemistry research* **2002,** *41*, (15), 3714-3721.
(109) Jarne C., Avila S., Blanco S.T., Rauzy E., Otín S.,Velasco I., Thermodynamic Properties of Synthetic Natural Gases. 5. Dew Point Curves of Synthetic Natural Gases and Their Mixtures with Water and with Water and Methanol: Measurement and Correlation. *Industrial & engineering chemistry research* **2003,** *43*, (1), 209-217.

Chapter 8: Simulation of a natural gas TEG dehydration unit

In the previous chapter, UMR-PRU has been extended to the modelling of natural gas components with water and polar chemicals, yielding very good results in the correlation and prediction of the phase equilibria of binary and multicomponent mixtures. In this Chapter, it is implemented in commercial software through the CAPE Open protocol in order to simulate a typical natural gas dehydration unit. The obtained results are compared with those of TST/NRTL, which is proposed by Hysys for use in the simulation of the dehydration process.

8.1. Introduction

As it has been stated in Chapter 2, natural gas is saturated with water at reservoir conditions, while depending on the field it can also contain other impurities such as sour compounds, carbon dioxide (CO_2) and hydrogen sulfide (H_2S). Those trace components can be diluted in the free – water phase creating corrosive conditions which could be harmful for equipment and the final product. Water should be removed from the gas stream to avoid operating faults and to ensure product quality.

In the majority of natural gas offshore plants, dehydration by absorption using a liquid desiccant, usually TEG, occurs. The latter is preferred over other glycols, since it combines good absorption properties with low volatility, rendering its application more viable from an economic and environmental aspect[1]. To comply with the demand for lower water content as well as the environmental legislation regarding e.g. the amount of hydrocarbons lost in the vapor phase or the glycol content in the dry natural gas product, many studies are available in the literature. Most of them focus on the effect of the operating conditions e.g. reboiler temperature, stripping gas rate, TEG circulation rate and are based on empirical correlations for the TEG and water distributions[2-8]. Another parameter of interest for the design and operation of dehydration plants is the solubility of aromatics in TEG[9-11], which is higher compared to that of paraffins, with typical concentrations ranging approximately from 5 – 10 % for benzene to 20 – 30 % for ethylbenzene and xylenes. Furthermore, the BTEX distribution in TEG streams is important due to environmental regulations since they remain in the process and they end in the regenerator. Finally, BTEX are usually exhausted to the atmosphere, so adequate prediction and control of their emissions is necessary, since due to the high temperatures involved and their affinity with TEG, large amounts of BTEX are emitted annually causing serious environmental concerns even in small plants. Furthermore, BTEX distribution is of interest also to the naphtha reforming in oil refineries[12]. For that reason, accurate thermodynamic modelling of BTEX compounds is necessary for the oil & gas industry in order to comply with the environmental legislation.[13]

8.2. Literature Review

In a series of papers[3, 14-16] Bahadori proposed several numerical correlations for various parameters that are of interest during natural gas dehydration with TEG, which can be easily implemented in non-commercial simulating software. Specifically, the light hydrocarbon loss in TEG streams has been estimated with an overall 3.3 % AARD in a range of conditions close to those which occur in the dehydration process[16]. According to Bahadori[15] the solubility of CO_2 and H_2S in TEG has been also modelled using a 16 - parameter correlation and it yields a 2 – 3 % AARD as compared to the average 14 % obtained by using a cubic EoS, such as Peng – Robinson. Bahadori et al.[3] also suggested an easy – to – use correlation for the water dew point depression as a function of the contactor temperature. The proposed correlation has been applied to lean TEG purity ranging from 90 % - 99.99 % wt. and resulted to a 0.5 % AARD compared to literature data. Based on their previous work, Bahadori et al.[4] proposed also an empirical

correlation for sizing the absorbers of a TEG dehydration system. Moreover, they correlated the water removing efficiency of a contactor as a function of TEG purity and TEG circulation rate for varying operating temperatures. Their proposed correlations have been evaluated against the reported Gas Processing Association (GPA) data for the contactor conditions, with satisfactory results. Gandhidasan[5] has proposed empirical correlations for the parametric analysis of a TEG dehydration plant, with which the lean TEG circulation rate, the column inner diameter and the number of trays required to obtain certain dehydration levels can be easily estimated. He concluded that the wet gas temperature has almost no effect on the required number of trays but it severely affects the TEG circulation rate, while when operating at higher temperatures the increase of the number of trays can result in lower TEG circulation rate. Furthermore, the increase of operating pressure results in a decrease of the TEG circulation rate as well as of the inner contactor diameter. Ghiasi et al.[6] developed a method to determine the TEG purity in terms of stripping gas flow rate and reboiler temperature. To this purpose, they used a multilayer preceptor and a least squares support vector machine resulting in TEG purity predictions with good accuracy as compared to the experimental data. Ahmadi et al.[17] employed particle swarm optimization to specify the optimum values of the interconnection weights throughout feed – forward neural network to predict equilibrium water dew point temperature of a natural gas stream with a TEG solution at different concentrations. Their modeling results confirmed the integrity and showed the ability of the suggested hybrid model for the estimation of water dew point with adequate precision compared to the experimental data existing in the open literature. Jacob[7] developed a Hysys simulation to optimize the natural gas dehydration process. His analysis has focused on the number of stages of the contactor, the effect of the reboiler temperature and the stripping gas required for the design of a TEG dehydration plant, although no reference is given to the thermodynamic properties package used. Neagu et al.[18] simulated a basic glycol dehydration unit in Honeywell UniSim® (Unisim) using the PR EoS. In their work, they compared a base operation without any glycol enrichment with one where stripping gas is used. They, also, conducted a preliminary economic evaluation and they resulted that, as expected, the process involving stripping gas is a more effective way to increase the lean TEG purity, despite its increased cost. Holoboff and Khoshkbarchi[10] compared the Hysys simulation software and the GRI-GLYCcalc simulation tools to predict benzene emissions from glycol dehydration systems. They concluded that Hysys with the optimized parameters of the Glycol Package predicts more accurately the dry gas water content, while Hysys-PR is generally better in predicting the methane equilibrium in flash tank conditions. They have also concluded that Hysys Glycol package yields a reasonable match of the TEG circulation rate. Overall, Hysys exhibits better performance as a simulator tool compared with the GRI-GLYCcalc software, especially since the latter does not enable rigorous calculations for the regenerator. Nassar et al.[19] investigated the solubility of hydrocarbons in several physical solvents used as dehydrating agents with the PROSIM software and they concluded that it matches the experimental data very accurately in a range of temperature and pressure similar to the typical absorber conditions. They also concluded that TEG is a good dehydration agent and its use with low circulation rate can reduce the emission of volatile organic compounds into the atmosphere. Hernandez – Valencia et al.[20] have also employed PROSIM for the TEG dehydration

simulation by using the number of contactor trays, stripping gas rate and reboiler temperature as independent variables. They concluded that an increase in the number of absorber trays decreases the glycol circulation rate, while the use of a three – stage absorber yields a typical TEG circulation rate as the one encountered in most plants. Additionally they have demonstrated that the reboiler temperature of the regenerator affects the water content by changing the glycol purity. They also showed that the increase of the reboiler temperature results in higher TEG purity, but the effect of stripping gas, even in small amounts, is more pronounced. Finally, they concluded that the increase of CO_2 concentration results in a small increase of water content for the same TEG circulation rate.

Darwish et al.[9] exploited the effect of the implemented thermodynamic model for the simulation of a typical TEG dehydration plant in Aspen plus with emphasis given in VOCs emissions in the regenerator. They examined two classic EoS, the PR and SRK combined with different mixing rules. They have employed both EoS with the classical vdW1f mixing rules and the Boston – Mathias expression for the alpha function of the attractive term, with a predictive mixing rule based on the Huron – Vidal (HV), with the modified Huron – Vidal mixing rule (MHV2) and with the Wong – Sandler (WS) mixing rule. They also examined the predictive SRK model commonly known as PSRK. For all cases, the default interaction parameters existing in Aspen plus database were utilized. They concluded that no EoS has an overall advantage, while the use of the same mixing rules yield similar results with both examined EoS. PSRK and MHV2 mixing rules yield the more rational results in terms of volatile organic compounds (VOCs) emissions while they predict a quite accurate dehydration rate.

King et al.[21] convicted a parametric analysis with emphasis given in the water content in the dry gas, the TEG loss and the BTEX emissions, using the PR EoS. Then, they examined alternative configurations of the TEG recycling process with emphasis given in the minimization of BTEX compounds emissions. Their study first concluded to an optimum TEG flowrate to balance the dry gas water content, TEG loss and BTEX emissions. Then, this optimum rate has been used to explore the recycle configuration. They showed that the different configurations do not improve the water content or substantially decrease the BTEX emissions. Instead, the modification of the process requires significant increase in the capital and operational costs. Rouzbahani et al.[8] investigated the optimization of a DEG dehydration unit in Aspen plus and they have concluded that the most accurate thermodynamic models to be used for that purpose are cubic EoSs combined with the MHV2 mixing rules. Among them, SRK combined with modified UNIFAC-Lyngby yields the more accurate results. They showed that VOCs emission is extremely sensitive to an increase in the purity or molar flowrate of DEG. As for the process optimization, they concluded that a 10 % increase in solvent molar flow rate can reduce the dry gas water content up to 6 % without a significant rise in the total energy consumption and VOCs emission from the dehydration unit.

Despite the promising results obtained in most of the abovementioned works, no reference has been made to the behavior of the examined models, in the phase equilibria prediction of the involved binary mixtures. Based on their previous results in terms of the appropriate selection of thermodynamic models[22], Amouei

Torkmahalleh et al.[23] used a combination of models, namely PR with the MHV2 mixing rules and PSRK, to perform a sensitivity analysis in the BTEX and CO_2 emissions of an existing dehydration plant in Abu Dhabi. They showed that the combination of two different thermodynamic models results in consistent responses among the unit operations and that by manipulating several operating parameters the BTEX emissions can be reduced by 40 %. Nevertheless, the decrease in the emissions results in an increase of the moisture in the gas.

Arya et al.[24] evaluated the performance of the CPA EoS as incorporated in a process simulator through the CAPE-Open protocol. They have satisfactorily correlated various binary mixtures and predicted multicomponent ones, showing that CPA EoS can be accurately used for the design of a dehydration system. In the same context, dos Santos et al.[25] validated CPA EoS by incorporating the model in the PETROX-Petrobras simulator. They investigated the CPA prediction in binary mixtures of hydrocarbons with alcohols (methanol, ethanol) and glycols (MEG, TEG) and they obtained satisfactory results. Finally, they evaluated the proposed model in an industrial application, in terms of modelling a TEG absorber, as well as a typical dehydration process. They validated their results through comparison with those obtained with the proposed models for use with the dehydration process in two commercial simulators; that is Twu – Sim – Tassone for Aspen and SRKM for PRO II. They showed that the results obtained by implementing CPA on PETROX are similar to those obtained by Aspen Plus and PRO II, concluding thus that their model is as reliable as the currently available thermodynamic packages proposed for glycol applications. A thorough literature review, up to 2017, concerning natural gas dehydration processes has been conducted by Zong – Yang et al.[26].

8.3. Process description

The typical glycol dehydration unit comprises of two columns, as it is illustrated in Figure 8.1. The first one is the absorber (Contactor) where the actual dehydration occurs, while the second is a still column which is used to regenerate the glycol (Regenerator). After an inlet scrubber, which ensures that only saturated with water gas enters the absorber, the wet gas stream enters at its bottom. The lean (in water) glycol enters on the top of the Contactor, counter – current to the gas flow. Glycol – gas contact occurs on tray or packing, but the lack of space in offshore units justifies the use of the more expensive structured packing. At the top of the absorber leaves the dry gas stream, while at its bottom, exits the rich (in water) glycol. The rich glycol exiting the absorber flows to a reflux condenser at the top of the still column and then it enters a flash tank where most of the volatile components are vaporized. The typical operating pressure of the flash tank ranges between 3 to 7 bar. [1]

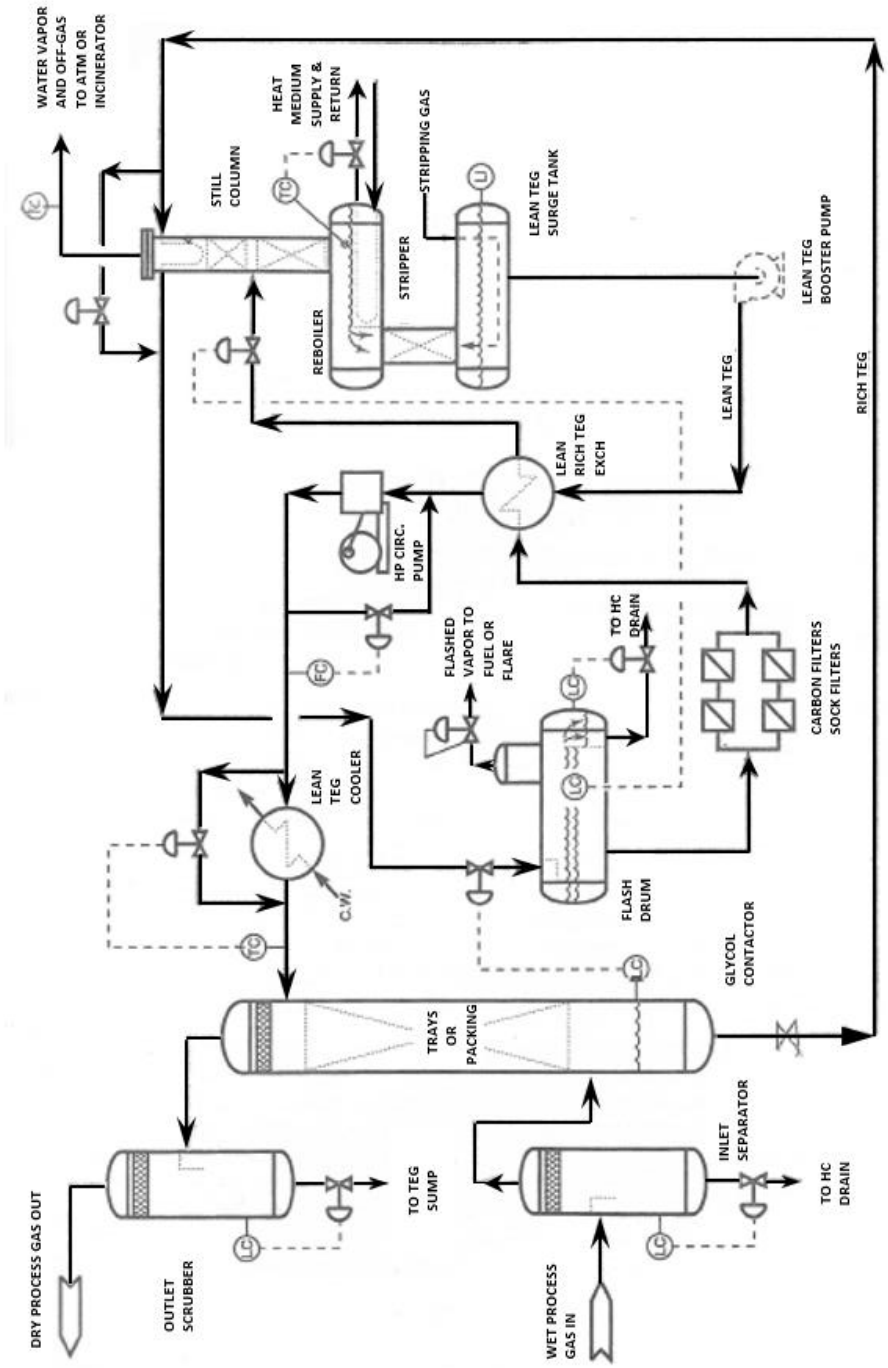

Figure 8.1: Typical TEG dehydration unit[1]

Apart from the light hydrocarbons removal, the flash tank also separates any liquid hydrocarbons from the glycol, preventing thus the fouling and foaming in the reboiler of the Regenerator. Furthermore, an amount of sour compounds is removed which reacts to some degree with glycols. This degassing of the sour compounds acts auxiliary to mitigate corrosion in the regenerator and it is more efficient if the glycol is first preheated. After the flash tank, the rich glycol passes through the glycol filters where the solid remnants and other impurities, such as salts, are removed from the glycol stream to ensure that liquid only enters the still column. According to Campbell[1] good filtration is critical for satisfactory performance, because it can improve dehydration efficiency while it minimizes foaming which is a major cause of glycol loss. He also recommends the use of a carbon purifier after the filter to increase the performance. The rich glycol then enters in the bottom of the still column, where water is separated from the glycol through distillation. Typically, the regenerator is designed to operate at prevailing atmospheric pressure, while the reboiler operating temperature is dictated by the decomposition temperature of the used glycol.

Table 8.1: Glycol decomposition temperature and corresponding lean glycol concentration calculated through Campbell's correlations[1].

Glycol	Decomposition Temperature (K)	Lean glycol[a] concentration (% wt.)	Equilibrium water[b] dew point (K)
MEG	438.15	96.0	276.15
DEG	437.15	97.1	276.15
TEG	479.15	98.7	265.15
TeEG	511.15	>99	255.15

[a] Equilibrium concentration at decomposition temperature and 1.013 bar
[b] Calculated at the respective lean glycol concentration

Table 8.1 presents the temperatures at which significant glycol decomposition starts to occur in the presence of air. Although the decomposition temperature should increase with the increase of molecular weight, DEG deviates from the rest of the glycols and it actually decomposes at temperature similar to that of MEG. That occurs due to the fact that DEG pyrolyzes in contact with the carbon steel. Industrial practice has showed that at typical units, in oxygen – free environment, the reboiler can operate at temperatures very close to the decomposition one. Thus, the maximum concentration of the lean glycol is dictated by its equilibrium composition at the reboiler pressure. If higher concentration is required in the lean glycol in order to achieve the required dry gas water content, then further increase of the glycol content must be incorporated to the unit. Several methodologies have been suggested, which actually lower the partial pressure of water in the glycol solution either by the introduction of a stripping gas or by lowering the operating pressure. The most common solution used in the natural gas industry is that of stripping gas, since gas is readily available. The process alternatives are briefly presented in Section 8.3.1.[1]

After achieving the required purity, the lean glycol should reach the contactor conditions by passing through the glycol pumps and the glycol/glycol heat exchangers.

Actually, it is a basic heat exchanger, the efficiency of which has a direct effect on the reboiler heat load. The rich glycol usually has a temperature 5 - 13 K higher compared to that of the inlet wet gas due to the condenser duty, while the lean glycol a temperature close to its decomposition one, e.g. about 479 K in the case of TEG. The exchanger is designed so as the exiting lean TEG temperature does not exceed the range of 333 – 338 K, while in most cases a 15 – 20 K approach is desirable. In most cases, the necessary cooling of lean glycol in the glycol/glycol heat exchanger is not adequate to meet the Contactor specifications and thus further cooling is required, in the glycol cooler.[1]

8.3.1. Glycol purity enhancing alternatives

The lean glycol purity is enhanced either by the introduction of a stripping gas or by lowering the regenerator operating pressure. Three popular alternatives of stripping gas use are discussed in the following.

8.3.1.a. *Typical stripping gas system*

Any inert gas is suitable to be used as a stripping agent. In industrial practice, a cut-off of the produced dry natural gas can be used for this purpose. Pure methane or the gases exiting the flash tank and the regenerator can also be used. An attractive alternative is the use of CO_2, especially if the unit is combined with CCS technologies.

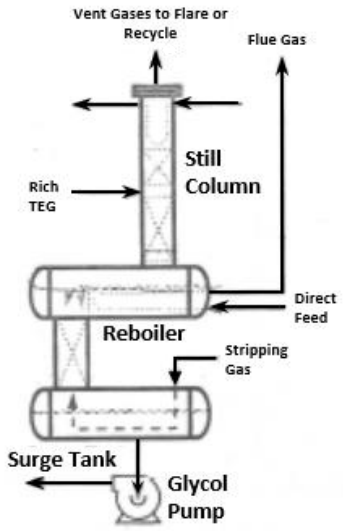

Figure 8.2: Typical stripping gas unit structure.[1]

The stripping gas can be introduced either directly into the reboiler of the stripping column, or after it passes through a packed stripping column between the reboiler and the surge tank, as shown in Figure 8.2. Theoretically, its introduction to an initial stripping column should increase the efficiency leading thus to lower stripping gas rates.

8.3.1.b. *DRIZO process*

Another alternative, with the additional advantage of handling the BTEX components leading to reduced emissions is the so-called DRIZO® process, illustrated schematically in Figure 8.3*a*.

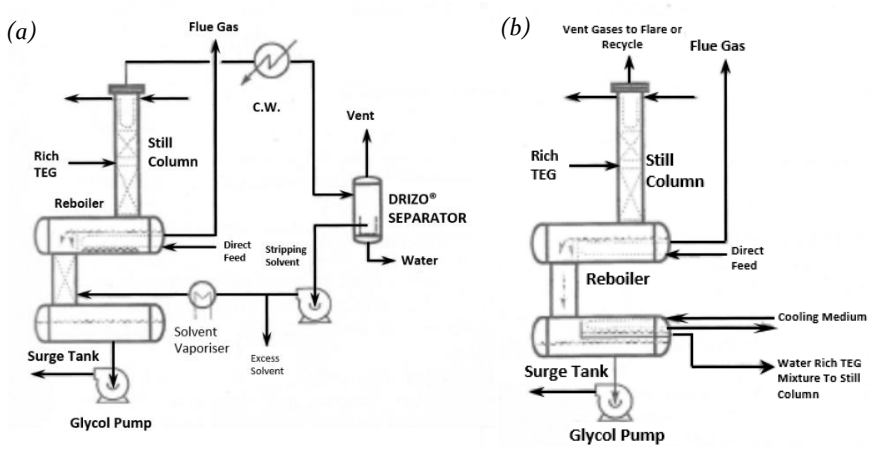

Figure 8.3: Alternative methods of glycol enrichment: (a) the DRIZO® process, (b) the coldfinger® process

In this process, the stripping gas loop is closed, while a material as iso-octane is used as the stripping agent. The latter vaporizes at reboiler temperature but it can be condensed and separated from the water in a three – phase separator. After the separation, the stripping agent is routed back to the regenerator to close the stripping loop. This process modification has the additional advantage of providing high stripping gas rates with little or no venting of hydrocarbons and can thus achieve glycol concentrations higher than 99.99 % wt. Furthermore, the aromatic hydrocarbons from the still column overhead are recovered and condensed.

8.3.1.c. *COLDFINGER® process*

A third alternative is the COLDFINGER® process, which achieves the glycol enrichment by passing a cooling medium through a cool finger inserted in the surge tank vapor space (Figure 8.3*b*). The cooling medium is usually the rich glycol resulting thus in the condensation of a TEG/water mixture, which is rich in water. The mixture is drawn out of the surge tank by the use of a trough below the coldfinger and is recycled back to the regenerator. The water partial pressure in the surge tank is thus lowered which leads to increased glycol concentration. This procedure can result to lean TEG concentrations of the order of 99.5 – 99.9 % wt. without the use of stripping gas. Nevertheless, a small amount of gas is introduced to the surge tank to balance the pressure.

8.4. Incorporation of the UMR-PRU in process simulators

One of the main strengths of modern commercial process simulators is their flexibility and ability to make different kinds of thermodynamic calculations. Since 2001, the CO-LaN (CAPE–Open Laboratories Network) organization has promoted the creation of the CAPE–Open standards[27], where a set of free – to – use non-proprietary rules and interfaces are defined, that allow CAPE (Computer – Aided Process Engineering) applications or components to interoperate. As such, the UMR-PRU model, which is not available as a built-in model in commercial process simulators such as Hysys, is implemented instead of the thermodynamic models available as built-in in the process simulators. Most commercial simulator tools nowadays are compatible with the CAPE Open standard maintained by the co-LAN consortium, which enables the communication between an external property package and a simulator.

The CAPE–Open standard[27] defines different properties which can be interfaced from the simulator. The properties currently supported by the UMR-PRU property package are presented in Table 8.2. In this work, the UMR-PRU model is implemented through the CAPE–Open 1.1 protocol to the Aspen HYSYS© and Honeywell UniSim© process simulators.

Table 8.2: Compound specific properties and properties calculated through the CAPE OPEN standard.

Property	Unit
Input Property	
Molecular weight (MW)	kg·kmol^{-1}
Critical temperature (T_c)	K
Critical pressure (P_c)	bar
Acentric factor (ω)	(-)
Mathias-Copeman parameters (c_1, c_2, c_3)	(-)
Normal boiling point	K
Liquid density at 298.15 K	mol·m^{-3}
Ideal gas Gibbs Energy of formation at 298.15 K	J·mol^{-1}
Ideal gas Enthalpy of formation at 298.15 K	J·mol^{-1}
UNIFAC group IDs	(-)
relative van der Waals volume of group i (R_i)	(-)
relative van der Waals surface area of group i (Q_i)	(-)
UNIFAC group interaction parameters	
Calculated Properties	
Compressibility factor (Z_c)	(-)
Fugacity coefficient and its derivatives under constant pressure, temperature and composition	(-)
Natural logarithm of fugacity coefficients	(-)
Fraction of a fluid in a given phase	(-)
Partition coefficient between the phases (k-factor)	(-)

Table 8.2 (continued)

Molar volume and its derivatives under constant pressure, temperature and composition	$m^3 \cdot mol^{-1}$
Heat capacity at constant pressure	$J \cdot mol^{-1} \cdot K^{-1}$
Enthalpy	$J \cdot mol^{-1}$
Entropy	$J \cdot mol^{-1}$
Gibbs free energy	$J \cdot mol^{-1}$
Molar mass of mixture	$kg \cdot kmol^{-1}$

8.5. Simulation Results

The phase equilibrium and derivative property calculations of pure components and multicomponent mixtures prove that UMR-PRU is a quite accurate thermodynamic model to describe natural gas mixtures with water and polar chemicals. In fact, the predictions of the model in such terms are similar with those of the model proposed by Hysys for use in the simulation of such processes. Therefore, in the following, the UMR-PRU model is validated in the simulation of a natural gas dehydration unit by absorption, using TEG as the liquid desiccant. To this purpose, it is implemented through the CAPE–Open 1.1 protocol to Hysys and Unisim process simulators. Since there are no available real field data, the model is validated against the predictions of the TST/NRTL model in Hysys. Two cases have been considered: *Case I* is a simple absorber, and *Case II* simulates a simplified offshore dehydration unit.

8.5.1. *Case I*: the simple absorber

A dehydration unit has a number of variables that affect its efficiency, such as the lean TEG purity, TEG circulation rate, number of trays in the absorber and the regenerator, as well as the operating conditions. As a first step, a simple absorber is considered, where the feed and operating conditions are fixed, approximately at 40 bar and 305 K. The schematic diagram of the absorber, consisting of three ideal trays, is presented in Figure 8.4. The wet gas feed enters at the bottom of the absorber (contactor) and the solvent that is lean (in water) TEG, enters at the top and flows countercurrent to the gas. The dry gas product exits at the top of the contactor, while the rich (in water) TEG leaves at the bottom of the column. The composition of the wet gas used as feed to the absorber and of the lean TEG used as solvent is taken from the work of dos Santos et al.[25] and contains hydrocarbons up to n-hexane.

Table 8.3 summarizes the simulation results obtained with UMR-PRU implemented in Hysys and Unisim and those obtained by TST/NRTL with Hysys. Also, Figure 8.5 presents a graphical comparison of the predicted molar compositions of the components in dry gas and rich TEG streams. The first observation is that, as expected, identical results are obtained with UMR-PRU in Hysys and Unisim.

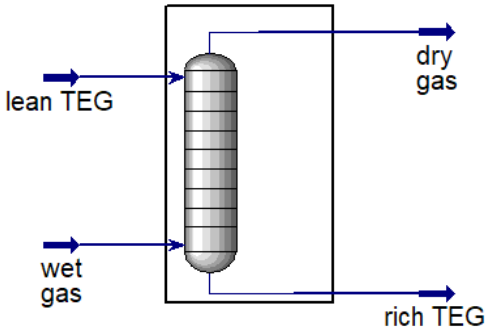

Figure 8.4: Process flowchart of Case I, as constructed in the Hysys environment.

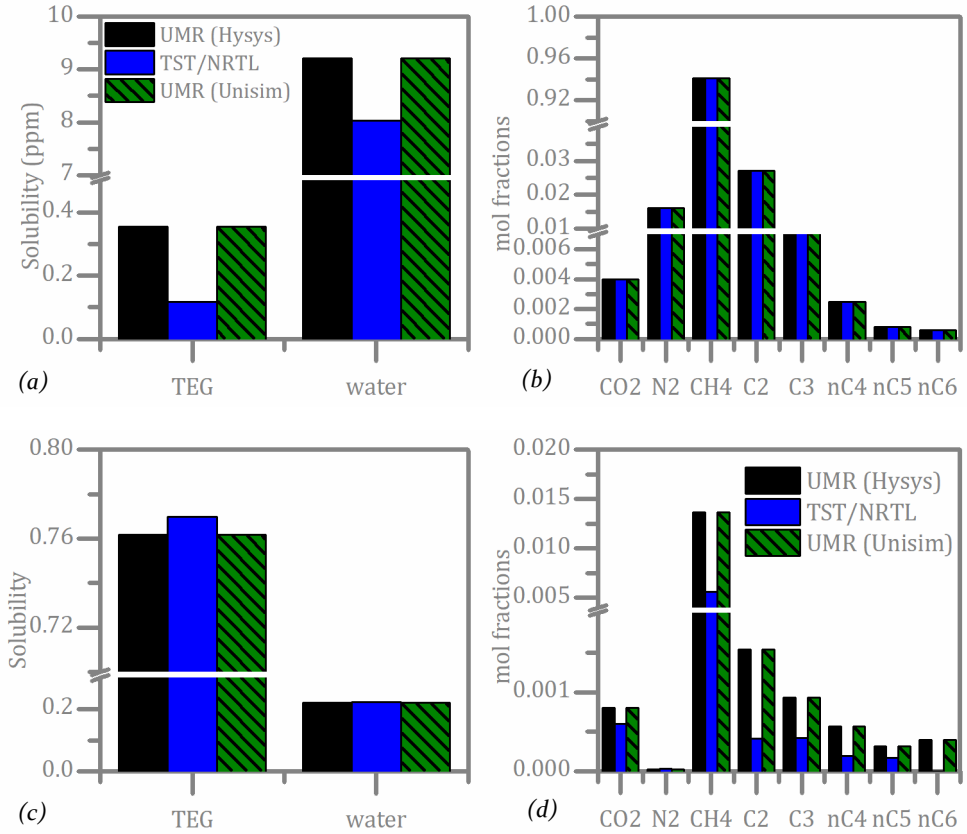

Figure 8.5: Simulation results for Case I with UMR-PRU implemented in Hysys and Unisim and TST/NRTL. UMR-PRU in Hysys is given with solid black fill, TST/NRTL is given in solid blue fill and UMR-PRU in Unisim is given with stripped patterned black color in green background; (a) TEG and water composition in the dry gas, (b) Natural gas components composition in the dry gas, (c) TEG and water composition in the Rich TEG stream and (d) Natural gas components composition in the Rich TEG stream.

Table 8.3: Simulation Results for Case I with UMR-PRU model in two different simulators (Hysys, Unisim) and TST/NRTL model in Hysys

	Lean TEG			Wet gas		
	UMR-PRU		TST/NRTL	UMR-PRU		TST/NRTL
	Hysys	Unisim		Hysys	Unisim	
Molar flow (kmol/h)						
CO_2	0.0	0.0	0.0	69.3	69.3	69.3
Nitrogen	0.0	0.0	0.0	277.3	277.3	277.3
Methane	0.0	0.0	0.0	16292.0	16292.0	16292.0
Ethane	0.0	0.0	0.0	468.0	468.0	468.0
Propane	0.0	0.0	0.0	133.5	133.5	133.5
n-Butane	0.0	0.0	0.0	43.3	43.3	43.3
n-Pentane	0.0	0.0	0.0	13.9	13.9	13.9
n-Hexane	0.0	0.0	0.0	10.4	10.4	10.4
TEG	84.6	84.6	84.6	0.0	0.0	0.0
H_2O	0.4	0.4	0.4	24.3	24.3	24.3
total flow (kmol/h)	85.0	85.0	85.0	17332.0	17332.0	17332.0
T (K)	314.0	314.0	314.0	303.0	303.0	303.0
P (bar)	41.0	41.0	41.0	34.0	34.0	34.0
Enthalpy ($kJ \cdot kmol^{-1}$)	793.0	793.0	810.0	76.0	76.0	76.0
	Rich TEG			Dry gas		
	UMR-PRU		TST/NRTL	UMR-PRU		TST/NRTL
	Hysys	Unisim		Hysys	Unisim	
Molar flow (kmol/h)						
CO_2	0.089	0.089	0.066	69.2	69.2	69.3
Nitrogen	0.003	0.003	0.004	277.3	277.3	277.3
Methane	1.519	1.519	0.619	16290.5	16290.5	16291.4
Ethane	0.171	0.171	0.045	467.8	467.8	467.9
Propane	0.103	0.103	0.046	133.4	133.4	133.4
n-Butane	0.063	0.063	0.021	43.3	43.3	43.3
n-Pentane	0.035	0.035	0.019	13.8	13.8	13.8
n-Hexane	0.044	0.044	0.00002	10.4	10.4	10.4
TEG	84.6	84.6	84.6	0.006	0.006	0.002
H_2O	24.5	24.5	24.5	0.159	0.159	0.139
total flow (kmol/h)	111.1	111.1	109.9	17305.8	17305.8	17307.0
T (K)	303.9	303.9	303.8	304.5	304.5	304.5
P (bar)	34.47	34.47	34.47	34.47	34.47	34.47
Enthalpy ($kJ \cdot kmol^{-1}$)	673	673	694	76	76	76

For the same purity and lean TEG circulation rate, UMR-PRU yields about 9 ppm (molar) of water in the dry gas, while TST/NRTL yields 8 ppm. This difference is actually due to the slight difference of the models' prediction in the methane/water binary, as it is depicted in Figure 7.5*a*. TST/NRTL yields also lower concentration of TEG in the dry gas than UMR-PRU. This behavior is attributed to the fact that TST/NRTL underpredicts the vapor phase solubility of water (Figure 7.7*a*) and TEG (Figure 7.8*b*) in their mixtures with methane, which is the major natural gas component, while UMR-PRU gives results that are in better agreement with the experimental data. UMR-PRU and TST/NRTL predict similarly the natural gas components distribution in the dry gas and rich TEG streams. In the rich TEG stream, instead, TST/NRTL predicts lower solubility of the HCs compared to UMR-PRU. This difference is higher in the case of n-hexane, which is the heavier component of the specific gas. This behavior is attributed to the difference in the HCs distribution in the polar phase of the binary mixtures. As presented in Figure 7.10, TST/NRTL systematically underpredicts the HC solubility in the aqueous phase with the exception of cyclohexane, while the opposite is valid for the distribution of n-heptane in TEG (Figure 7.11). It seems that despite the higher TEG content of the rich TEG stream examined here, the dominating factor is the solubility of HCs in water. Finally, both models calculate similar energy values for the gaseous streams, while this is not the case for the TEG-rich ones. This difference is attributed to the different heat capacities (c_p) of the TEG/water mixture predicted with the two models. As it has been shown in Section 7.2, at the specific operating conditions, UMR-PRU predicts this property better than TST/NRTL, which systematically overpredicts the experimental data. Furthermore, the simulation results for the absorber are in good agreement with the simulations of dos Santos et al.[25], where the CPA EoS has been evaluated.

8.5.2. *Case II*: Simplified TEG dehydration unit

The process flowsheet, as simulated in Hysys, is presented in Figure 8.6. Of course, many variables affect the dehydration operation, such as the number of stages in the columns, the lean TEG circulation rate and its purity, the selected operating conditions, the sort of the configuration used to increase the lean TEG purity such as stripping gas or vacuum etc. To examine the behavior of the models initially typical values of the operating variables are used, which are kept constant during the simulations. The input composition of the saturated wet gas feed (Table 8.4) is taken by the work of dos Santos et al.[25] and is typical for units operating in Brazil. The contactor is simulated by an absorber unit sub-flowsheet, consisting of three ideal trays. The contactor operates essentially isothermally at high pressure and low temperature conditions, at about 56 bar and 303 K. Since the mass of water and TEG is small as compared to the gas flow, the inlet wet gas controls the absorber temperature[1]. The specified parameters for the contactor are presented in Table 8.5. The dry gas exits at the top of the contactor, with a concentration in water approximately 30 ppm molar. At the bottom of the contactor exits the rich TEG.

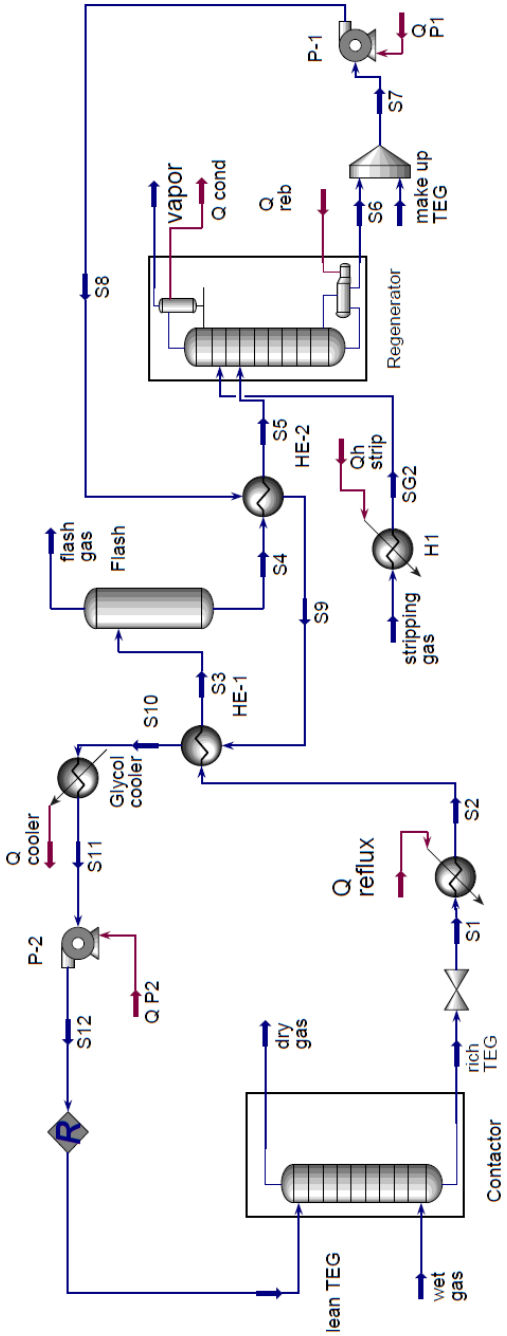

Figure 8.6: Process flowchart of Case II, as constructed in the Hysys environment.

Table 8.4: Simulation results in Hysys for the streams connected to the Contactor of Case II with UMR-PRU and TST/NRTL.

	Lean TEG		Wet gas	
	UMR-PRU	TST/NRTL	UMR-PRU	TST/NRTL
molar flow (kmol/h)				
CO_2	0.012	0.013	26.5127	26.5127
Methane	0.006	0.007	1711.96	1711.96
Ethane	0.00353	0.00263	124.503	124.503
Propane	0.00023	0.00012	33.2332	33.2332
n-Butane	0.0002	0.00003	4.6422	4.6422
n-Pentane	0.0002	0.00005	1.379	1.379
n-Hexane	0.0004	0.00001	1.0489	1.0489
H_2O	1.67	1.64	0.75	0.75
TEG	32.57	33.16	0	0
total flow (kmol/h)	34.26	34.82	1904.03	1904.03
Temperature (K)	328.83	328.40	299.82	299.82
Pressure (bar)	51.65	51.65	51.65	51.65
Enthalpy ($kJ \cdot mol^{-1}$)	765	781	82	82
Entropy ($J \cdot mol^{-1}K^{-1}$)	171	136	149	152
Heat Flow (kW)	7283	7553	43290	43307
	Rich TEG		Dry gas	
	UMR-PRU	TST/NRTL	UMR-PRU	TST/NRTL
molar flow (kmol/h)				
CO_2	0.166	0.156	26.359	26.370
Methane	0.747	0.600	1711.220	1711.367
Ethane	0.202	0.137	124.305	124.368
Propane	0.106	0.076	33.128	33.158
n-Butane	0.026	0.012	4.616	4.630
n-Pentane	0.013	0.008	1.366	1.371
n-Hexane	0.016	0.002	1.034	1.047
H_2O	2.365	2.331	0.055	0.055
TEG	32.571	33.157	0.0008	0.0003
total flow (kmol/h)	36.21	36.48	1902.08	1902.37
Temperature (K)	299.74	299.82	303.01	304.73
Pressure (bar)	50.66	50.66	50.66	50.66
Enthalpy ($kJ \cdot mol^{-1}$)	742	766	82	82
Entropy ($J \cdot mol^{-1}K^{-1}$)	141.92	97.41	149.20	152.98
Heat Flow (kW)	7283.32	7553.19	43112.35	43095.78

Table 8.5: Specifications for the columns used in Case II.

	Contactor	Regenerator
Column type	Absorber	Distillation Column
Ideal trays	3	3
Reboiler	-	1
Condenser	-	1
Efficiency	1	1
Degrees of freedom	0	2
Condenser temperature (K)	-	373.15
Reboiler temperature (K)	-	477.15
Feed	Lean TEG (1)[a] Wet gas (3)	SG2 (3)[b] S4 (3)

[a] numbers in parenthesis denote the stage (counting from the top) where the feed is inserted to the column.
[b] The labeling of the inlet streams refers to the names indicated in Figure 8.6.

The regenerator is usually a stripper, but for simulation purposes a distillation column is used. It operates at atmospheric or close to atmospheric pressure and high temperature, due to the high TEG boiling point, c.a. 540 K[28]. The rich TEG stream from the contactor is decompressed to 5.1 bar, before it enters the glycol/glycol Heat Exchangers (HE-1, HE-2). In the real process, the Rich TEG stream passes through the top of the regenerator, condensing the vapor stream, while it is preheated. For simulation purposes, a heater is added after the decompression valve and before the HE-1, where its energy duty is set equal to the condenser duty at the top of the regenerator. Furthermore, the glycol filters are omitted and their effect is added as a pressure drop equal to 100 kPa in each Glycol/Glycol Heat Exchanger. The preheated rich TEG (S3) exiting HE-1 is routed to an isothermal flash to exhaust the diluted hydrocarbons, which can be either mixed with other streams for HC recovery or it is sent to the flair. The liquid outlet stream (S4) enters the HE-2, and then, after its pre-heat from the lean TEG stream (S8), it enters at the bottom of the Regenerator. Stripping gas (SG) is used to increase the TEG purity, which for simplicity reasons, is considered to enter the regenerator directly, at the bottom tray, along with the rich TEG inlet. The operating conditions of the regenerator are determined by the glycol decomposition temperature, which for TEG is approximately 479.15 K. In industrial practice, at the regenerator where no air is present, no noticeable decomposition is observed for temperatures close to the decomposition one and as such the lean glycol composition is determined by the bubble point composition at the regenerator pressure. In order to increase the purity of lean TEG, a decrease of the partial pressure of the glycol solution is required which in the specific simulation is achieved by the introduction of a stripping gas. A make–up stream is added to account for the TEG loss in the process. Finally, the pressure increase is achieved through glycol pumps P-1 and P-2, in order to reach the contactor conditions.

The specification to be met in the simulations is the water content of the dry gas, which is set to approximately 30 ppm molar. The independent variable that is used to control

the lean TEG purity and thus the required level of dehydration is the stripping gas flow, while all the other parameters are kept constant. The detailed simulation results are given in Table 8.4 and Table 8.6 - Table 8.7, while the results regarding some important variables are summarized in Table 8.8.

Table 8.6: Simulation Results in Hysys for the streams connected to the Regenerator of Case II with UMR-PRU and TST/NRTL.

	S5		SG2	
	UMR-PRU	TST/NRTL	UMR-PRU	TST/NRTL
Molar flow (kmol/h)				
CO_2	0.046	0.051	1.636	1.764
Methane	0.036	0.031	6.545	7.055
Ethane	0.029	0.018	0.818	0.882
Propane	0.026	0.019	0	0
n-Butane	0.010	0.003	0	0
n-Pentane	0.007	0.004	0	0
n-Hexane	0.010	0.001	0	0
H_2O	2.36	2.33	0	0
TEG	32.57	33.16	0	0
total flow (kmol/h)	35.09	35.61	9.00	9.70
Temperature (K)	403.15	403.15	353.15	353.15
Pressure (bar)	2.15	2.15	1.70	1.70
Enthalpy ($kJ \cdot mol^{-1}$)	731	739	132	132
Entropy ($J \cdot mol^{-1}K^{-1}$)	233	221	185	191
Heat Flow (kW)	7121	7309	329	355
	Vapor		S6	
	UMR-PRU	TST/NRTL	UMR-PRU	TST/NRTL
Molar flow (kmol/h)				
CO_2	1.67	1.80	0.0124	0.0131
Methane	6.58	7.08	0.0062	0.0071
Ethane	0.844	0.898	0.0035	0.0026
Propane	0.026	0.018	0.0002	0.0001
n-Butane	0.010	0.003	0.00016	0.00003
n-Pentane	0.006	0.004	0.00017	0.00005
n-Hexane	0.009	0.001	0.00040	0.00001
H_2O	0.69	0.69	1.67	1.64
TEG	0.005	0.004	32.57	33.15
total flow (kmol/h)	9.83	10.50	34.26	34.813
Temperature (K)	373.15	373.15	477.56	477.55
Pressure (bar)	1.23	1.23	1.27	1.27
Enthalpy ($kJ \cdot mol^{-1}$)	139	139	713	713
Entropy ($J \cdot mol^{-1}K^{-1}$)	189	197	301	301
Heat Flow (kW)	380	405	6790	7032

Table 8.7: Simulation Results in Hysys for the streams connected to the flash tank for Case II with UMR-PRU and TST/NRTL.

	S3		S4		vapor	
	UMR-PRU	TST/NRTL	UMR-PRU	TST/NRTL	UMR-PRU	TST/NRTL
Molar flow (kmol/h)						
CO_2	0.166	0.156	0.046	0.047	0.120	0.105
Methane	0.747	0.600	0.036	0.037	0.711	0.570
Ethane	0.202	0.137	0.029	0.030	0.173	0.119
Propane	0.106	0.076	0.026	0.027	0.080	0.057
n-Butane	0.026	0.012	0.010	0.010	0.016	0.008
n-Pentane	0.013	0.008	0.007	0.007	0.006	0.004
n-Hexane	0.016	0.002	0.010	0.010	0.006	0.001
H_2O	2.36	2.33	2.36	2.49	0.007	0.005
TEG	32.57	33.16	32.57	33.71	0.00005	0.00002
total flow (kmol/h)	36.21	36.48	35.09	36.37	27.44	20.82
Vapor fraction	0.03	0.02	0.00	0.00	1.00	1.00
T (K)	348.15	348.15	348.15	348.15	348.15	348.15
P (bar)	3.15	3.15	3.15	3.15	3.15	3.15
Enthalpy ($kJ \cdot mol^{-1}$)	729	747	748	748	113	116
Entropy ($J \cdot mol^{-1} K^{-1}$)	186	160	186	186	179	188
Heat flow (kW)	7330	7566	7295	7554	35	28

Table 8.8: Simulation results in Hysys for Case II, with UMR-PRU and TST/NRTL.

	UMR-PRU	TST/NRTL
dry gas water content (ppm)	29.1	29.1
purity lean TEG (% wt.)	99.4	99.4
lean TEG ($kmol \cdot h^{-1}$)	34.3	34.8
TEG circulation rate (kg TEG/kg absorbed water)	1.2	1.2
total TEG loss (kmol/h)	0.006	0.004
% TEG loss of the total in the regenerator[a]	86.4	90.6
Stripping gas rate ($kmol \cdot h^{-1}$)	9.0	9.7

[a] $\% \text{ TEG loss in Regenerator} = 100 \cdot \text{abs}\left(\frac{\text{moles TEG in vapor}}{\text{moles TEG in dry gas+moles TEG in flash gas+moles TEG in vapor}}\right)$

UMR-PRU and TST/NRTL calculate similar TEG circulating rate and purity of lean TEG. TST/NRTL requires slightly higher stripping gas rate as compared to UMR-PRU, which leads to a slightly higher lean TEG flow. On the other hand, the calculated TEG circulation rate per kg of absorbed water is almost the same for the two models. As it is illustrated in Figure 8.7, the composition of the obtained dry gas is also similar for all components except for TEG where TST/NRTL yields lower concentration than UMR-PRU, which is attributed to the difference of the models in the description of the VLE of methane/TEG binary.

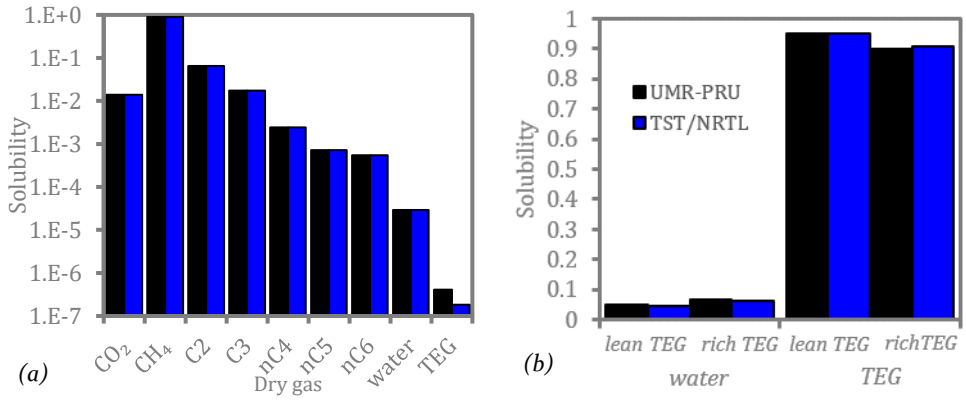

Figure 8.7: Simulation results for the Contactor of Case II with UMR-PRU (solid black fill) and TST/NRTL (solid blue fill). (a) NG Component distribution in the dry gas stream and (b) TEG and water distribution in the Rich and Lean TEG streams.

The composition of the vapor and reflux streams of the regenerator are presented in Figure 8.8. It is shown that both models yield similar results concerning the compounds of interest, which are the light gases, TEG and water. Additionally, they give similar vapor rate, with that of UMR-PRU to be a little higher. This corresponds to slightly higher hydrocarbon loss in the case of UMR-PRU, which consists mostly of the lighter compounds. The models differ, also, in the calculated composition of hydrocarbons heavier than butane in the vapor phase, as well as in n-hexane in the reflux polar phase. The latter is due to the significantly low solubility of n-hexane in water predicted by TST/NRTL, as shown in Section 7.3.2.

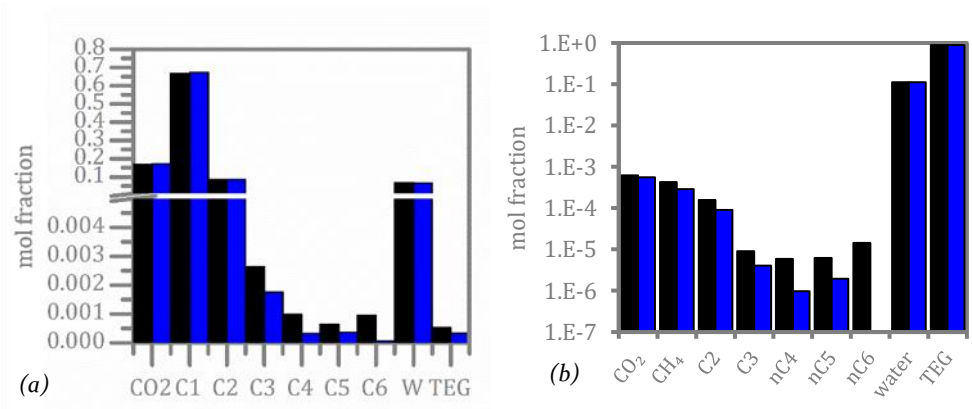

Figure 8.8: Simulation results for the Regenerator of Case II with UMR-PRU (solid black fill) and TST/NRTL (solid blue fill). (a) Vapor stream and (b) Reflux stream.

It is interesting to note that the low solubility of the heavier hydrocarbons with the TST/NRTL in the gaseous streams examined here is the outcome of the low solubility predicted by the model in the rich TEG stream, which is essentially the input to the column. Moreover, similar reflux rate is required to achieve the TEG regeneration, which is 0.021 kmol/h for the UMR-PRU and 0.018 kmol/h for TST/NRTL.

Finally, in Table 8.9, the energy requirements of the dehydration process are compared. It is shown that TST/NRTL systematically yields higher duties compared to UMR-PRU, which is due to the high overestimation of the heat capacity values for the TEG/water (Section 7.2). Although this is systematic for all equipment, the difference is more apparent in the reboiler. Of course, part of the increased duty is also due to the slightly higher stripping gas rate calculated with TST/NRTL. In the temperature range of the regenerator, i.e. 373 – 477 K, UMR-PRU predicts fairly well the c_p, so it is expected that the UMR-PRU results should better meet the actual process data.

Table 8.9: Simulation Results in Hysys concerning the Energy Requirements of Case II, with UMR-PRU and TST/NRTL.

	Duties (kW)	
	UMR-PRU	TST/NRTL
HE 1	127.0	194.6
HE 2	174.0	228.9
Glycol Cooler	201.9	209.1
Reboiler	283.8	332.5
Condenser	3.4	3.7

Another aspect of interest from the engineering point of view is the TEG loss encountered in the process. UMR-PRU predicts a higher TEG loss compared to TST/NRTL. This is rational considering that UMR-PRU yields higher TEG solubility in the vapor phase compared to TST/NRTL, as it has been shown in Figure 7.8. It should be noted that UMR-PRU predictions are in better agreement with the available experimental data, indicating that the TEG loss calculated with the UMR-PRU model is more accurate than the one calculated with TST/NRTL.

8.6. Sensitivity Analysis

In the previous, it has been shown that UMR-PRU is a reliable model for the simulation of natural gas dehydration with TEG. In this section, a sensitivity analysis of several of the independent operating parameters is presented. The examined parameters are:

- the stripping gas rate
- the reboiler temperature at the regenerator
- the regenerator pressure
- the temperature of the feed to the regenerator
- the flash tank temperature
- the contactor temperature
- the contactor pressure

In order to proceed with the sensitivity analysis, all the parameters, apart from the examined one are kept to the value of the base case, which is actually *Case II*, with the only exception in the case of varying the regenerator pressure. In the latter, no stripping gas is used, as suggested by the methodology.

8.6.1. Effect of the stripping gas rate

Figure 8.9 demonstrates the effect of stripping gas rate in some parameters of interest. As expected, due to the lowering of the partial pressure of water, the increase of stripping gas rate results in increased lean TEG purity (Figure 8.9*a*) and as such in lower water content in the produced dry gas (Figure 8.9*b*). That comes with the cost of increased TEG loss (Figure 8.9*c*) and increased reboiler duty (Figure 8.9*d*).

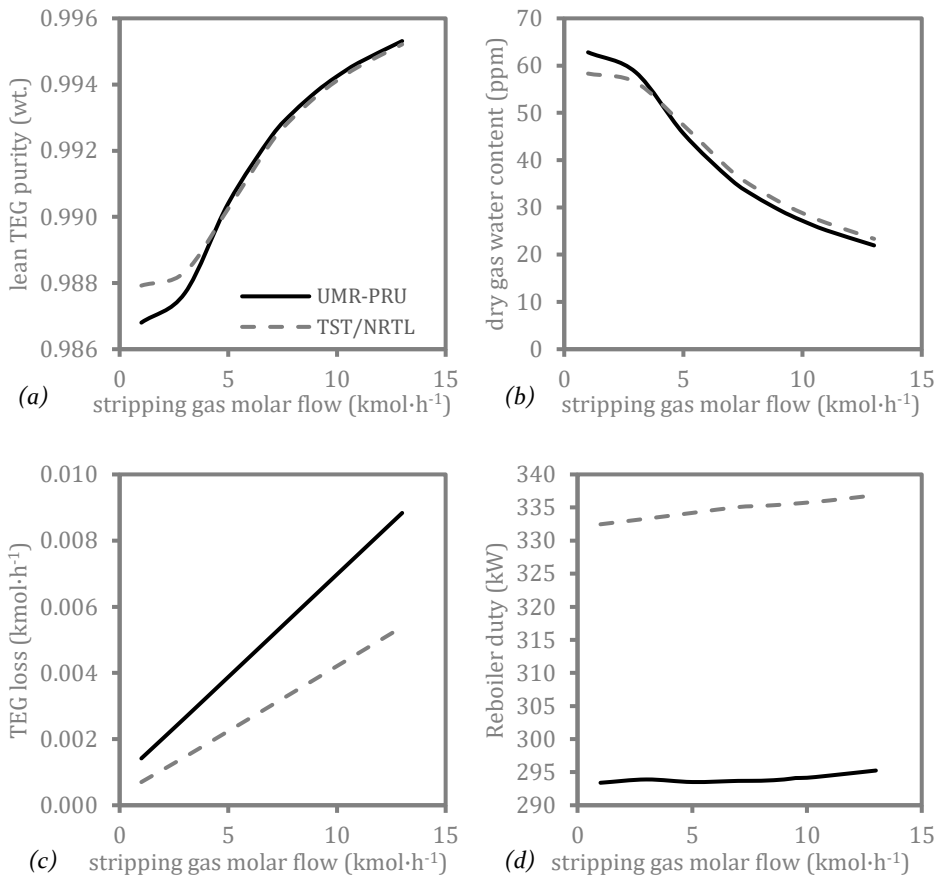

Figure 8.9: Effect of stripping gas rate in (a) lean TEG purity, (b) dry gas water content, (c) TEG loss and (d) Reboiler duty.

It is of interest to note that for stripping gas rates higher than approximately 4 kmol/h, UMR-PRU and TST/NRTL show the same response. Instead, in the limiting end where there is almost no stripping gas, the models differ in the obtained purity and therefore in the dry gas water content. This behavior reflects the difference in the VLE of TEG/water mixture between UMR-PRU and TST/NRTL. The difference in the TEG heat capacity predicted with UMR-PRU and TST/NRTL is systematically depicted in the calculated duty, as it has been also shown for the base case.

8.6.2. Effect of the reboiler temperature

Due to the limitation of the TEG degradation temperature, the reboiler of the still column cannot operate close to the boiling point, but the temperature is controlled to be close to the degradation one.[1] To this end, the effect of this temperature is examined, in a narrow range close to this limiting value.

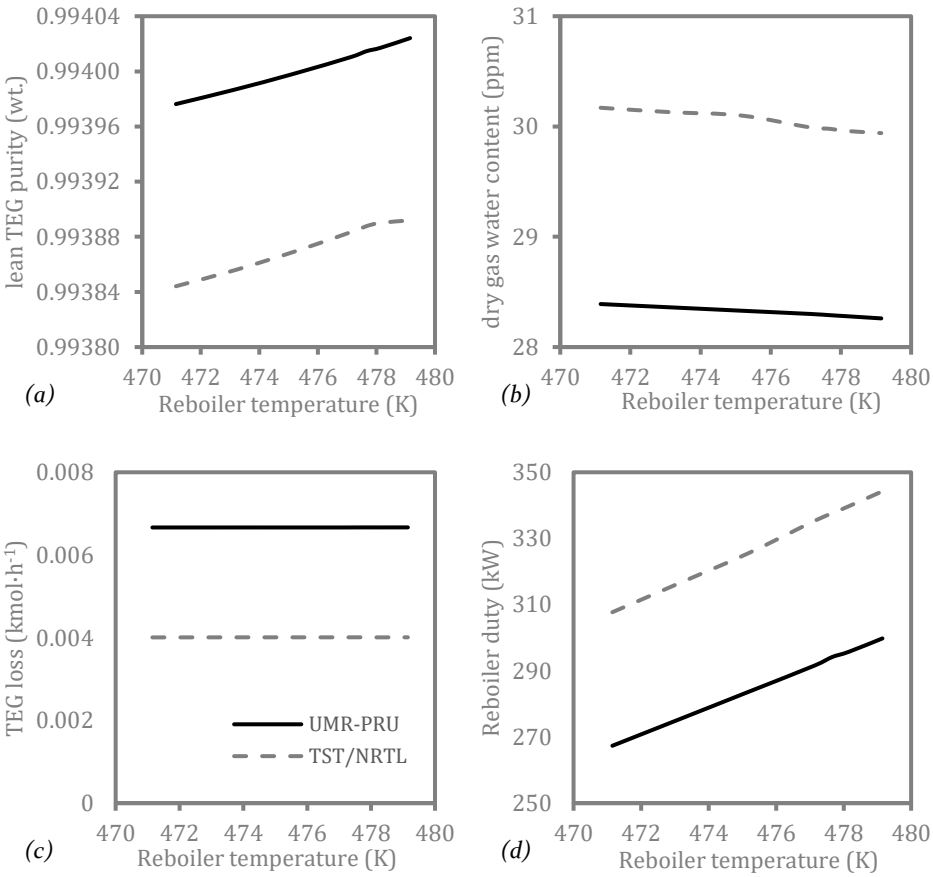

Figure 8.10: Effect of the reboiler operating temperature in (a) lean TEG purity, (b) dry gas water content, (c) TEG loss and (d) Reboiler duty.

As it is demonstrated in Figure 8.10, the increase of the reboiler temperature leads, as expected, in higher lean TEG purity and therefore lower dry gas water content. The variation of the reboiler temperature does not affect the calculated TEG loss. The reboiler duty increases accordingly to the reboiler temperature.

8.6.3. Effect of the Regenerator pressure

In this case, no stripping gas is added in the regenerator, while the operation of the column occurs basically at vacuum conditions. Figure 8.11 shows that with the increase of pressure, the lean TEG purity decreases and therefore the water content increases. A steep slope is observed for the reboiler duty at the limiting low pressures, as well as for the TEG loss. For pressure above 0.2 bar the TEG loss is basically stable while the reboiler duty shows a decreasing, but rather slight, trend.

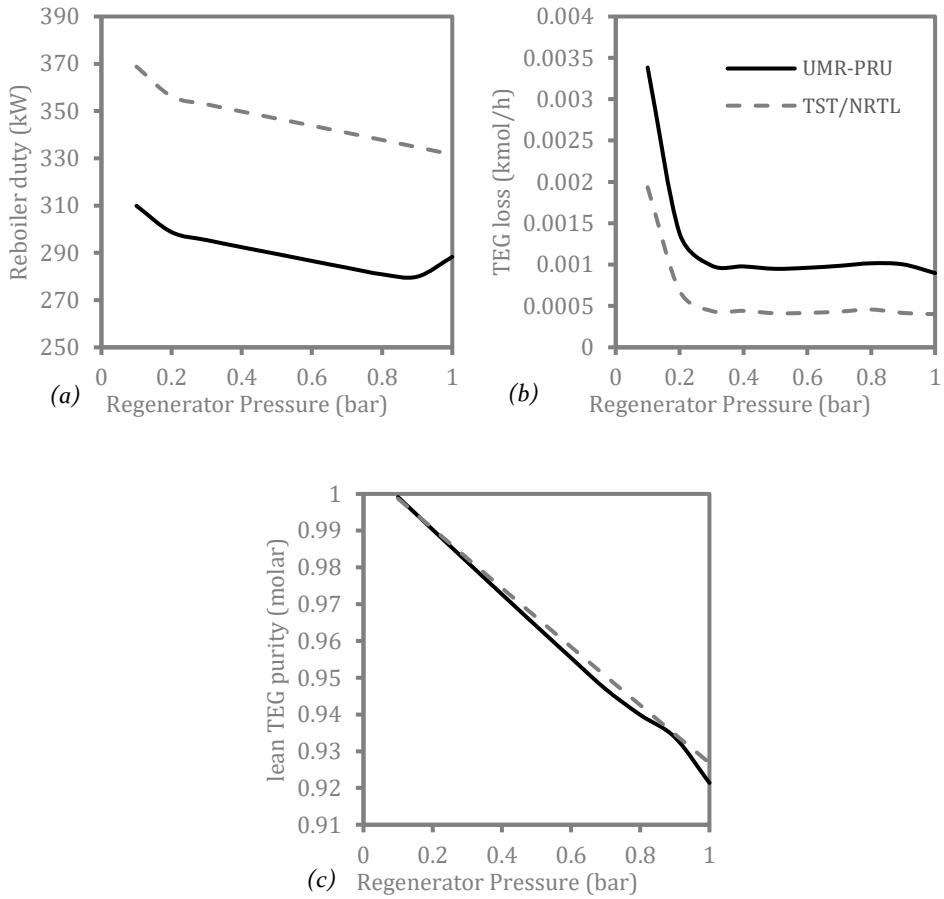

Figure 8.11: Effect of the regenerator pressure in (a) Reboiler duty, (b) TEG loss and (c) lean TEG purity

8.6.4. Effect of the feed temperature in the regenerator

One of the parameters to affect the efficiency or the energy requirements of the distillation unit operation is the feed temperature.

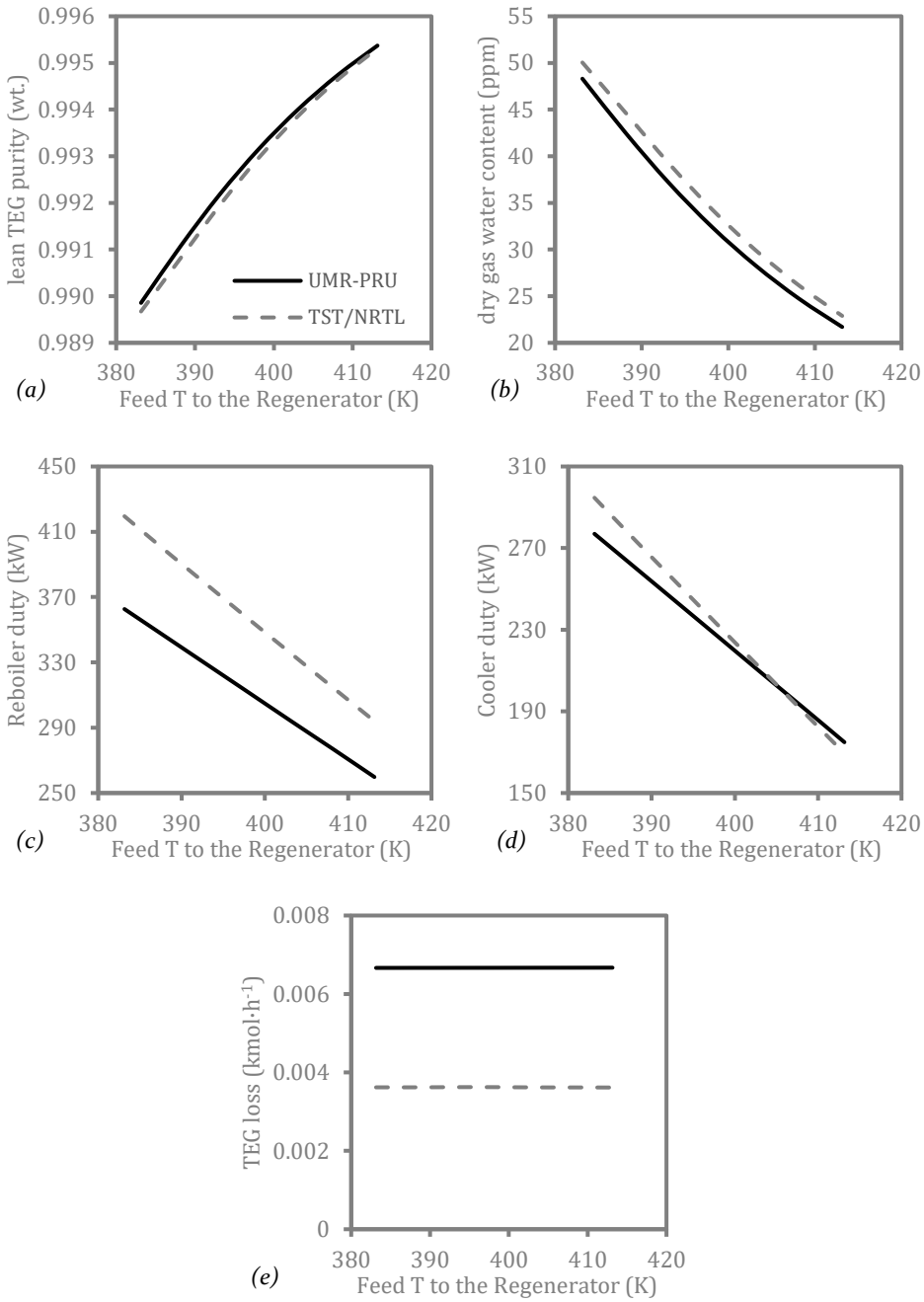

Figure 8.12: Effect of the temperature of the feed stream to the regenerator (S5) in (a) lean TEG purity, (b) dry gas water content, (c) reboiler duty, (d) cooler duty and (e) TEG loss.

It is shown that the increase of the temperature of the feed stream (S5) leads to increased lean TEG purity (Figure 8.12*a*) and therefore in decrease of the dry gas water content (Figure 8.12*b*). The interesting observation is that this decrease in dry gas water content is accompanied by significant decrease of the reboiler (Figure 8.12*c*) and cooler duties (Figure 8.12*d*) with no change in the TEG loss (Figure 8.12*e*). Both models show an about 30 % decrease in the reboiler duty and about 40 % in the cooler duty if the extreme ends are taken into consideration.

8.6.5. Effect of the flash tank temperature

Another parameter of interest which can affect the efficiency of the dehydration process is the operating temperature of the flash tank, which is defined by the exit temperature of the first heat exchanger. Figure 8.13 demonstrates that the increase of the flash tank temperature leads to increased lean TEG purity and therefore to reduced dry gas water content. The latter results also in a slight increase of TEG and hydrocarbon loss in the flash gas stream. Although this increase does not seem significant, and the trend seems rather constant, it should be taken into consideration that this may lead in increased BTEX loss from the vapor stream exiting the flash since BTEX solubility increases with temperature. Nevertheless, according to Braek et al.[29] this can be applied as a method to reduce the total BTEX emissions exiting the regenerator, especially if the flash gas is recycled or used as the stripping agent. In the specific simulation, the effect of the flash tank temperature with respect to the BTEX solubility is not considered, since there are no aromatic components in the treated wet gas. The reboiler duty is almost constant with a slight decreasing slope.

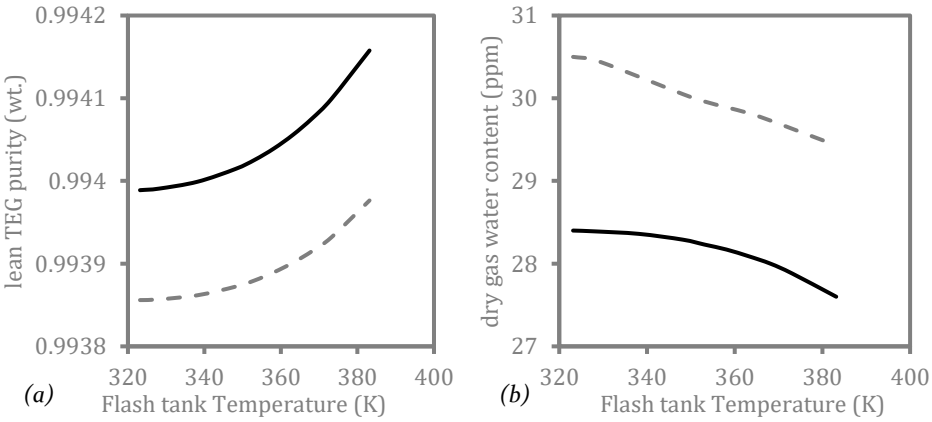

Figure 8.13: Effect of the flash tank temperature on (a) lean TEG purity, (b) dry gas water content, (c) TEG loss, (d) flash gas hydrocarbon content and (e) reboiler duty.

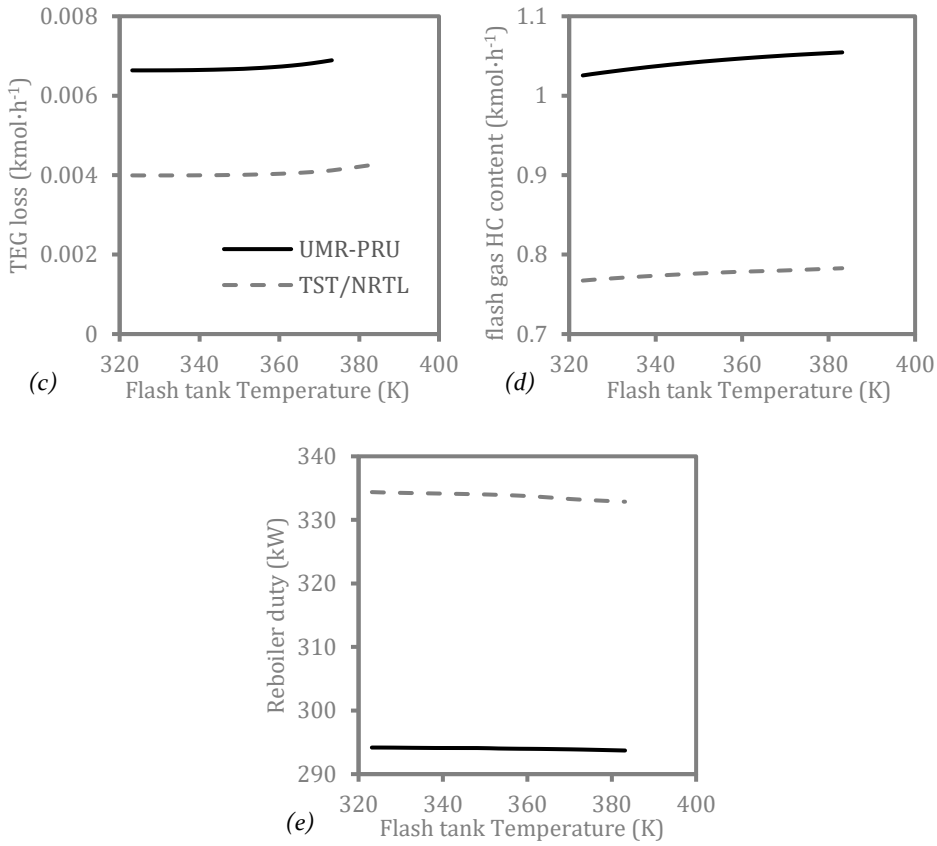

Figure 8.13 (continued)

8.6.6. Effect of the contactor temperature

The contactor operating temperature is actually defined by the wet gas temperature.[1] The lowest temperature which can be used is limited by the hydrate formation temperature at the specific conditions and water content. Using the hydrates unit operation of Hysys which is actually based on the van der Waals and Platteeuw[30] theory, the highest hydrate formation temperature is about 282 K. Thus, the effect of contactor temperature is examined for temperatures above 283 K.

Figure 8.14 shows that the increase in the contactor temperature results in increased TEG purity. It is of interest to note that in spite of the increase in lean TEG purity, Figure 8.14*b* shows an increasing trend in the dry gas water content. This is because the increase in the contactor temperature results in higher temperature in the dry gas stream and as such in higher solubility of water in the vapor phase. TST/NRTL calculates almost constant TEG loss, while UMR-PRU yields an increasing trend, due to the increase of the TEG solubility with the temperature. For the hydrocarbon loss in the rich TEG stream, UMR-PRU yields a decreasing trend (Figure 8.14) while

TST/NRTL presents a constant one. The required reboiler duty is almost unaffected by the change in the operating temperature of the contactor, while the cooler duty increases, as demonstrated in Figure 8.15.

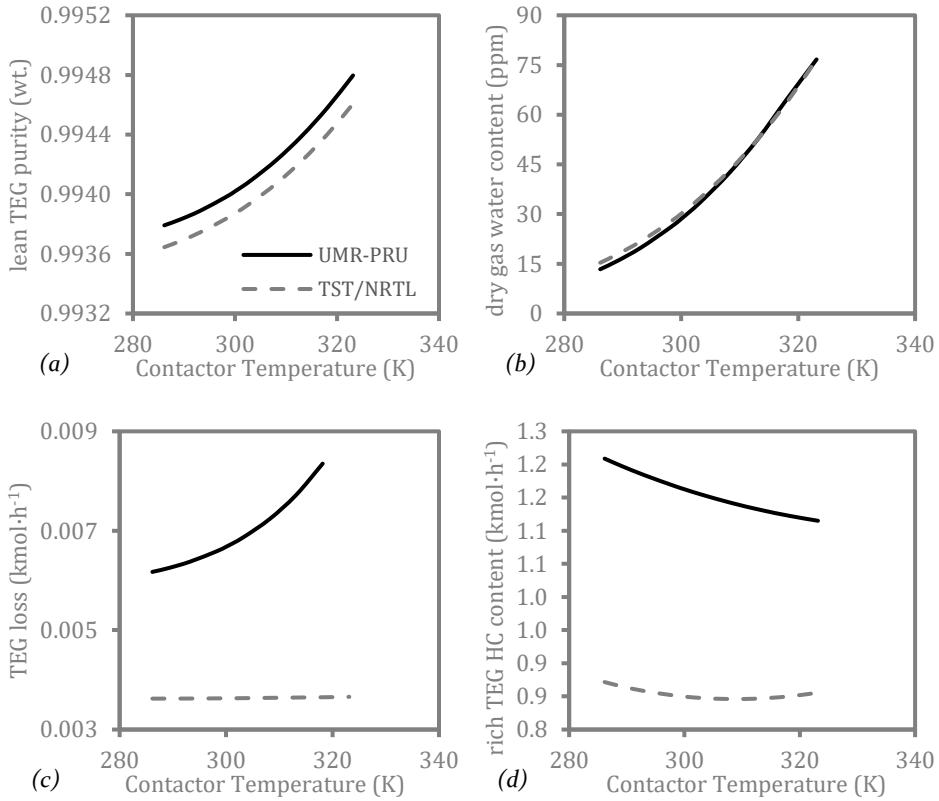

Figure 8.14: Effect of the contactor operating temperature at (a) lean TEG purity, (b) dry gas water content, (c) TEG loss and (d) rich TEG hydrocarbon content.

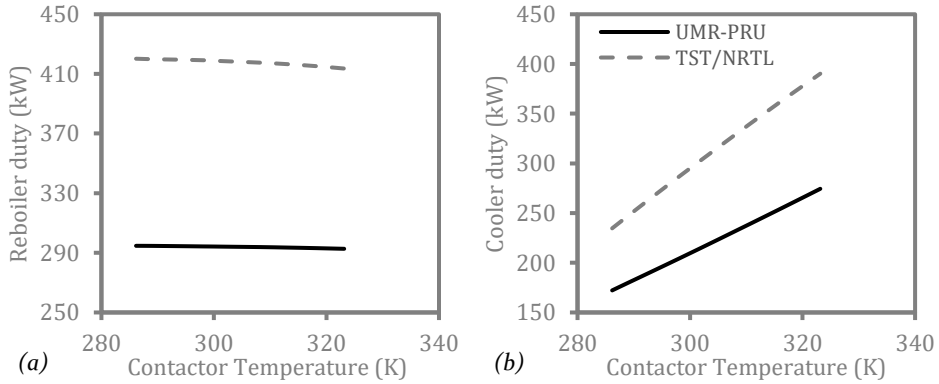

Figure 8.15: Effect of the contactor operating temperature at (a) reboiler duty and (b) cooler duty.

8.6.7. Effect of the contactor pressure

Finally, the effect of the contactor pressure is examined as illustrated in Figure 8.16. It is observed that the increase of pressure leads in increased TEG purity but like in the case of the variation of the contactor temperature it also leads to increased water content. UMR-PRU yields an increasing trend in the TEG loss while TST/NRTL predicts no change. Instead, both models coincide in the prediction of the hydrocarbon loss in both phases which is an increasing one.

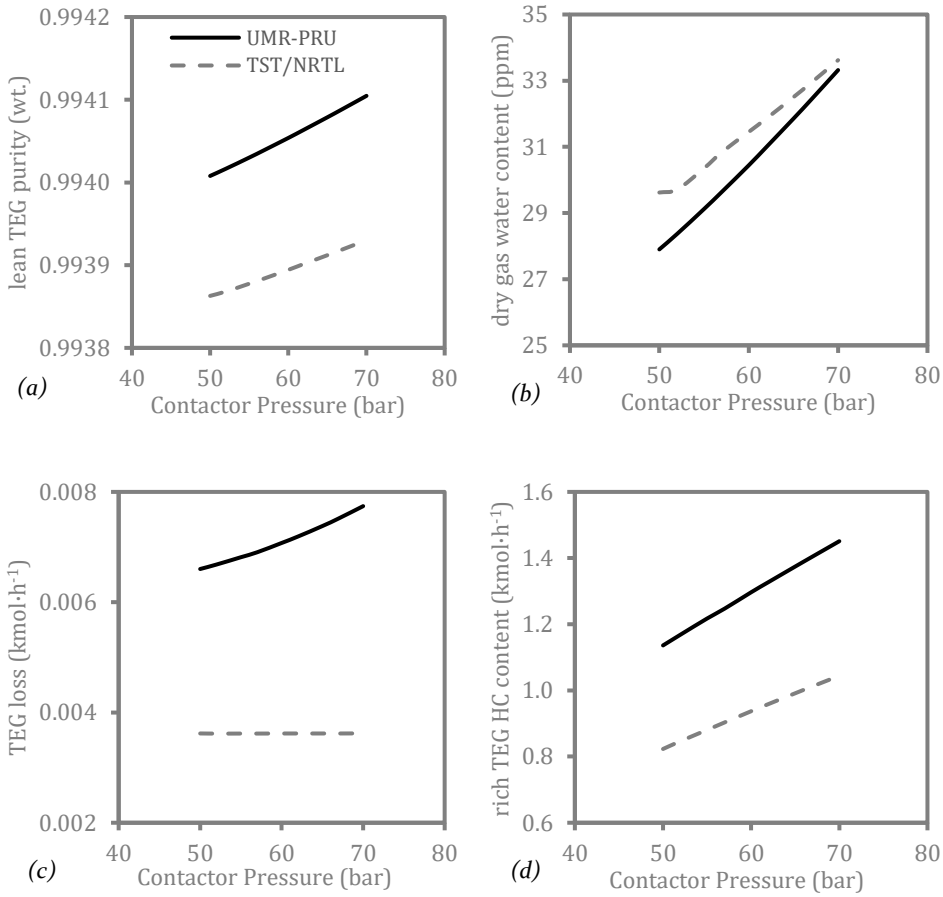

Figure 8.16: Effect of the contactor operating pressure at (a) lean TEG purity, (b) dry gas water content, (c) TEG loss and (d) rich TEG hydrocarbon content.

8.7. Process Optimization

Following the results of the sensitivity analysis, a preliminary study for the process optimization in terms of the required heat duties is conducted for the UMR-PRU model. According to the results shown in Figure 8.12 and Figure 8.13, the increase in the temperature of the rich TEG stream entering the Regenerator and the temperature of the flash tank result in lower dry gas water content while the required duty of the reboiler decreases. As such, they are used as the manipulated variables to lead in the process optimization. A specification of 30 ppm water in the dry gas is defined, which is met by utilizing the stripping gas rate as the independent variable. The optimized input parameters and their comparison with the base case are tabulated in Table 8.10.

Table 8.10: Operating parameters for base and optimized simulation

	base	optimized
Feed (S5) T (K)	403.15	410.15
Flash tank T (K)	348.15	363.15

Table 8.11 summarizes the results of base and optimized simulations. The first observation is that the required stripping gas rate is quite lower compared to the base conditions and actually by about 22 %. The obtained lean TEG purity is the same with the base case, while the dry gas water content is similar. The TEG loss is also lower compared to the base conditions, while the TEG circulation rate is similar with that of the base case.

Table 8.11: Simulation results for base and optimized conditions with UMR-PRU

	base	optimized
dry gas water content (ppm)	29.1	29.8
dry gas TEG content (ppm)	0.4	0.4
purity lean TEG (% wt.)	99.4	99.4
lean TEG (kmol·h^{-1})	34.3	35.5
TEG circulation rate (kg TEG/kg absorbed water)	1.19	1.18
total TEG loss (kmol·h^{-1})	0.006	0.005
% TEG loss of the total in the regenerator[a]	86.4	81.5
Stripping gas rate (kmol·h^{-1})	9.0	7.0

[a] $\% \text{ TEG loss in Regenerator} = 100 \cdot \text{abs}\left(\frac{\text{moles TEG in vapor}}{\text{moles TEG in dry gas+moles TEG in flash gas+moles TEG in vapor}}\right)$

The optimization was based on the minimization of the required duties, which are presented along with their relative deviations from the base case in Table 8.12. It is observed that the increase in the flash tank temperature results in an about 40 % increase in the duty of the first heat exchanger. Instead, the duty of the second heat exchanger decreases by about 9 %. For the reboiler of the still column, which consists the majority of the required duties of the whole process, a 5 % decrease is observed.

The duty of the cooler also decreases, due to the lower exit temperature of the lean TEG stream.

Table 8.12: Simulation results in Hysys concerning the Energy Requirements of the optimized simulation, with UMR-PRU and TST/NRTL and comparison with the base case scenario.

	Duties (kW)	
	base	optimized
HE 1	127	179
HE 2	174	158
Glycol Cooler	202	182
Reboiler	284	269
Condenser	3.4	3.6

8.8. Economic Evaluation

Following the optimization of the process in terms of energy requirements, a preliminary economic evaluation of the unit is conducted. To this purpose, the Aspen ICARUS® (Icarus) Economic evaluator is used with the parameters set as presented in Appendix B. The examined plant is based on *Case II* and has a relatively small capacity, about 360 SMcmy. In order to evaluate the results of Icarus, the required installation costs are calculated through correlations taken from the literature[18, 31].

The use of stainless steel is justified according to Campbell[1] in the parts that get in contact with the rich TEG stream and especially in the regenerator to avoid corrosion. Following the work of Neagu et al.[18] the fixed capital and operating cost of the unit are calculated without considering any detailed investment parameters.

8.8.1. Capital Cost

The main parts of the unit are considered for this calculation which are the Contactor, the flash tank, the Regenerator, the glycol cooler, the two glycol/glycol heat exchangers and the two pumps. The heater which precedes the heat exchanger is not taken into consideration for the cost estimation since it is an assumption made for simulation purposes rather than an actual unit. For the contactor, the cost is calculated separately for the vessel and the trays. The same is valid for the regenerator, where the cost of the reboiler is also calculated as that of a heat exchanger. The pumps are considered to be centrifugal, consisting of a mechanical part (rotor) and an electrical motor, while for the heat exchangers a counter – current shell and tube model is considered.

The preliminary analysis, focused on the calculation of the fixed capital cost *(c)*. This is based on an estimate of the equipment cost required for the process and other costs such as structural work, piping, automatic process control units etc. are estimated as a percentage of the equipment cost (C_e) based on a hand factor *(f)*, as presented in eq. 8.1,

$$C = \sum_{i}^{M} F \cdot C_e \qquad \text{eq. 8.1}$$

where M is the number of the major equipment items. The equipment cost is calculated through eq. 8.2, where S is a sizing factor.

$$C_e^{CS} = a + b \cdot S^n \qquad \text{eq. 8.2}$$

The parameters a, b and exponent n are taken from the work of Towler and Sinnott[31] for the year 2006 and they are presented along with the type of the required sizing parameter S for each type of equipment on Table 8.13. The exponent CS denotes that the cost is calculated for carbon steel.

To calculate the equipment cost for different materials, in this case stainless steel, where required, a correction material factor (f_m) equal to 1.3 is used as per eq. 8.3.

$$C_e = C_e^{CS} \cdot f_m \qquad \text{eq. 8.3}$$

The Chemical Engineering Plant Cost Index (CEPCI) from Chemical Engineering Magazine[32] is used to update the prices to those of 2017, according to eq. 8.4,

$$Cost\ in\ year\ A = Cost\ in\ year\ B \cdot \frac{Cost\ Index\ in\ year\ A}{Cost\ Index\ in\ year\ B} \qquad \text{eq. 8.4}$$

where cost in year A relates to year 2017, cost in year B relates to year 2006. The average cost index in 2017 is 567.5 while in 2006 equals 478.6. All monetary values are given in US dollars ($).

Table 8.13: Cost parameters for the calculation of the equipment costs for the major pieces of equipment (eq. 8.2) and the hand factor for eq. 8.1.

		S	*a*	*b*	*n*	*F*
Vessels	Vertical, carbon steel	shell mass (kg)	400	230	0.6	4
	condenser	area (m^2)	500	1100	1	
Trays	Sieve	diameter (m)	100	120	2	2.5
Heat Exchangers	U-tube, shell & tube	area (m^2)	10000	88	1	3.5
	thermosiphon reboiler	area (m^2)	13000	95	1	
Pumps	Single – stage centrifugal	flow ($l \cdot s^{-1}$)	3300	48	1.2	4
	Explosion-proof motor	Power (kW)	920	600	0.7	

It is interesting to note that the equipment cost calculated through Icarus is higher by about 1.5 % at optimised conditions, while it decrases by about 0.8 % if the correlations are used. In both cases, the difference is relative small and it is actually shown that the change of the opertaing conditions does not affect the equipment cost. This

observation is more apparent if the fixed capital cost is considered, where the difference between base and optimized conditions is about 0.6 % with both ways of calculation.

There is a significant difference for the equipment cost calculated through Icarus and the generalized correlations, as presented in Table 8.14. Yet, this difference is not reflected in the fixed capital cost. The detailed results of the economic evaluation of the base (*Case II*) and optimized case are presented on Table 8.15.

Table 8.14: Total equipment and fixed capital costs calculated with UMR-PRU for base and optimized conditions based on Aspen Icarus and literature correlations.

	C_e (€)		C (€)		% ARD[a]	
	Icarus	Corr.	Icarus	Corr.	C_e	C
Base	165070	185810	738070	695970	13	-6
Opt.	167560	184330	742560	691180	10	-7

[a] $\% ARD = \frac{C_{corr} - C_{Icarus}}{C_{Icarus}} \cdot 100$, where C stands for equipment (C_e) or capital cost (C).

The next step is to compare the calculated fixed capital cost with actual data. Tannehill[33] provided a correlation of the capital cost of TEG dehydration plants, without including the gas sweetening costs, based on actual data of real plants. The graph is reproduced in Figure 8.17.

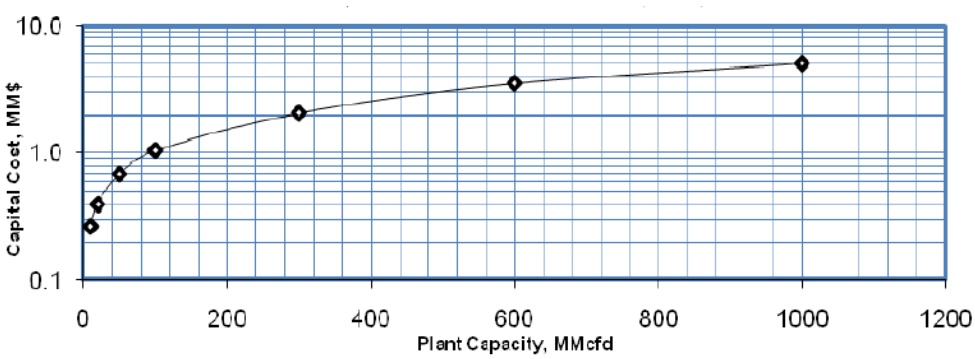

Figure 8.17: Capital cost of a TEG dehydration plant for year 2008 as a function of the capacity of the plant.[33]

The capacity of the examined unit is about 38 MMcfd which corresponds to a capital cost of 53300 € in year 2008. The latter is updated to late 2017 according to eq. 8.4 and equals 604400 €. This corresponds to an AAD about +23 % deviation from the optimized simulation using Icarus and a +14 %, if the literature correlations are utilized. According to Carroll[34] a 30 % uncertainty is expected in the graphs presented by Tannehill[35] and thus the calculated costs are acceptable.

Table 8.15: Economic evaluation results of base and optimized case[a] with UMR-PRU with Aspen Icarus software and based on empirical correlations

		Size parameter[b] (S)		Equipment Cost C_e (€)				Capital Cost C (€)			
				Icarus		Corr.		Icarus		Corr.	
		base	optimize	base	optimized	base	optimized	base	optimized	base	optimized
Conta-ctor	vessel (kg)	5534	5534			56044	56044			224175	224175
	trays (m)	1.5	1.5			1521	1521			3802	3802
	total			45000	47400	57564	57564	181800	183800	227977	227977
Regene-rator	vessel (kg)	1089	1089	16086	16086	21469	21469	126114	126114	85874	85874
	trays (m)	1.5	1.5			1521	1521			3802	3802
	reb. (m^2)	11.47	10.3	10043	10043	19303	19174	61413	61413	67558	67024
	total			26129	26129	42292	42163	187526	187526	157234	156700
Flash		1361	1361	15464	15464	24466	24466	93941	95363	97862	97862
HE 1		18.67	8.25	9510	9065	15950	14695	54658	54036	55826	51430
HE 2		8.03	7.96	9065	9065	14668	14659	57413	57858	51340	51307
cooler		8.66	7.93	8621	9154	14743	14655	56258	57502	51603	51295
P -1	rotor ($l \cdot s^{-1}$)	1.24	1.26			4606	4606			18424	18429
	motor (kW)	0.52	0.55			1778	1778			4443	4500
	total			3999	3999	6384	6384	29773	29773	22867	22929
P-2	rotor ($l \cdot s^{-1}$)	1.24	1.26			4606	4606			18424	18429
	motor (kW)	9.16	9.73			5136	5136			12840	13256
	total			47282	47282	9742	9742	76699	76699	31264	31685
	total			165070	167559	185810	184329	738069	742557	695972	691184

[a]Plant capacity: 360 MScmy, [b] The size parameter of eq. 8.2 as defined in Table 8.13

8.8.2. Operating cost

Next, the operating cost is estimated by considering the major units which are the reboiler of the still column, the glycol cooler and the glycol pumps. For the first two units, the operating cost is calculated in terms of heating/cooling utilities, that is high – pressure steam for the reboiler and cooling water for the cooler, while for the pumps the electricity cost is considered. The costing parameters for each derivative are taken from literature and are presented on Table 8.16, along with the calculated costs.

Table 8.16: Operating cost for base and optimized process with UMR-PRU.

	Reduced cost		Operating cost (k€/yr)		
	Value	unit	base	Opt.	% ARD[a]
HP steam	26.7[36]	€/tn	132.3	121.4	-8.2
Cool. H_2O	0.07[37]	€/tn	21.4	18.8	-12.2
Electricity	0.06[38]	€/kW	55.8	55.8	0.0
total			209.5	196.0	-6.4

[a] $\%ARD = \frac{C_{opt}-C_{base}}{C_{base}} \cdot 100$, where C stands for the operating cost.

The cost is calculated through eq. 8.5, where the required rate is obtained directly from Hysys and is presented on Table 8.17.

$$C_{oper} = rate \cdot C_{oper}^{red} \qquad \text{eq. 8.5}$$

where C_{oper} denotes the operating cost in annual base, exponent *red* denotes the reduced value of the operating cost and *rate* the determined need for utilities or electricity as calculated by Hysys.

Table 8.17: Calculated required rates in terms of utilities and electricity by Hysys for base and optimized process with UMR-PRU.

	UMR-PRU	
	base	opt.
HP steam (kg/h)	619	568
Cool. water (kg/h)	35850	31472
Electricity (kW)	106	106

As expected, the optimized simulation results in reduced operating cost by about 6 %. If the total cost values are considered they correspond to a saving of about 15000 $ annually. This difference seems rather small for an industrial procedure, but since the considered capacity is relatively small (360 SMcmy), this corresponds to 7 % of the annual operating cost, which is a cost reduction of about 37 €/SMcm of treated wet gas.

8.9. Conclusions

The UMR-PRU model is evaluated in the simulation of a natural gas dehydration unit using TEG as absorbent. To obtain this, the model is implemented into Hysys and Unisim through the CAPE Open 1.1 protocol and is then evaluated in the simulation of the dehydration process. The obtained results are compared with the ones of the TST/NRTL model, which is proposed by Hysys for application in such processes.

In *Case I* that represents a simple absorber, UMR-PRU yields the same level of dehydration as TST/NRTL. In *Case II* that represents a simplified offshore dehydration process, it is shown that UMR-PRU and TST/NRTL calculate similar stripping gas rate, TEG purity and circulation rate to achieve the same dehydration level in the dry gas. The two models differ in the calculated TEG loss, where UMR-PRU is considered to be closer to the real case than TST/NRTL. UMR-PRU also predicts lower duties in the reboiler, condenser and heat exchangers compared to TST/NRTL, which is considered more realistic due to the better prediction of the TEG/water heat capacities.

Furthermore, a sensitivity analysis of several operating parameters, such as stripping gas rate, operating temperature and pressure of the columns, is conducted and is concluded that both models yield similar trends while the relative comparisons predicted in *Case II*, are consistent with the change of the operating parameters. Based on the observations of the sensitivity analysis, an optimization of the operating parameters of the process in terms of the operating cost took place, which led to the increase of the operating temperature of the flash tank and the feed to the regenerator.

Then, a preliminary economic evaluation of the base and optimized process has been conducted. The capital cost has been estimated based on Aspen Icarus software and on literature correlations and is in good accordance with literature values. It is shown that the change in the operating parameters does not actually affect the capital cost. Instead, the optimized simulation results in a reduction operating cost by about 6 %, which is corresponding to a saving of about 37 €/SMcm of treated wet gas.

Based on the abovementioned results, it is concluded that the UMR-PRU model can be used to accurately simulate natural gas TEG dehydration units.

List of Symbols

Latin Characters

a, b, n	generalized equipment cost parameters (eq. 8.2)
C	cost ($)
c_1, c_2, c_3	Mathias – Copeman parameters
F	hand factor
f_m	correction material factor (eq. 8.3)
MW	molecular weight (kg·kmol^{-1})
P	pressure (bar)
Q_i	relative van der Waals surface area of group i
R_i	relative van der Waals volume of group i
S	sizing factor (eq. 8.2)
T	absolute temperature (K)
Z	compressibility factor

Greek Characters

ω	acentric factor

Superscripts and Subscripts

c	critical property
CS	carbon steel
e	equipment
m	material
$oper$	operating
opt	optimized
red	reduced property

References

(1) Campbell J.M., Maddox R.N., *Gas conditioning and processing*. Campbell Petroleum Series: 1970, *Vol. 2*.
(2) Bahadori A., Estimation of Hydrate Inhibitor Loss in Hydrocarbon Liquid Phase. *Petroleum Science and Technology* **2009,** *27*, (9), 943-951.
(3) Bahadori A., Vuthaluru H.B., Rapid estimation of equilibrium water dew point of natural gas in TEG dehydration systems. *Journal of Natural Gas Science and Engineering* **2009,** *1*, (3), 68-71.
(4) Bahadori A., Vuthaluru H.B., Simple methodology for sizing of absorbers for TEG (triethylene glycol) gas dehydration systems. *Energy* **2009,** *34*, (11), 1910-1916.
(5) Gandhidasan P., Parametric Analysis of Natural Gas Dehydration by a Triethylene Glycol Solution. *Energy Sources* **2003,** *25*, (3), 189-201.
(6) Ghiasi M.M., Bahadori A., Zendehboudi S.,Chatzis I., Rigorous models to optimise stripping gas rate in natural gas dehydration units. *Fuel* **2015,** *140*, (0), 421-428.
(7) Jacob N.C.G., Optimization of Triethylene Glycol (Teg) Dehydration in a natural gas processing plant. *Int J Res Eng Res Eng Technol* **2014,** *3*, (6), 346-350.
(8) Nemati Rouzbahani A., Bahmani M., Shariati J., Tohidian T., Rahimpour M.R., Simulation, optimization, and sensitivity analysis of a natural gas dehydration unit. *Journal of Natural Gas Science and Engineering* **2014,** *21*, (0), 159-169.
(9) Darwish N.A., Al-Mehaideb R.A., Braek A.M., Hughes R., Computer simulation of BTEX emission in natural gas dehydration using PR and RKS equations of state with different predictive mixing rules. *Environmental Modelling & Software* **2004,** *19*, (10), 957-965.
(10) Holoboff J., Khoshkbarchi M., In *Prediction of BTEX emissions and water content in TEG dehydration units*, presented on GPA Convention, March 9th, **2009**
(11) Saidi M., Parhoudeh M., Rahimpour M.R., Mitigation of BTEX emission from gas dehydration unit by application of Drizo process: A case study in Farashband gas processing plant; Iran. *Journal of Natural Gas Science and Engineering* **2014,** *19*, (Supplement C), 32-45.
(12) Rawat B.S., Prasad G., Liquid-Liquid Equilibria for benzene - n-heptane systems with triethylene glycol, tetraethylene glycol, and sulfolane containing water at elevated temperatures. *Journal of Chemical and Engineering Data* **1980,** *25*, (3), 227-230.
(13) Ziaee M., ZareNezhad B., Accurate Prediction of the Phase Behavior of BTEX and Alkane Hydrocarbons in the Presence of Tri-Ethylene Glycol (TEG) Solvent Considering Hydrogen Bonding Association and Solvation Effects. *Petroleum Science and Technology* **2017**, 1-7.
(14) Bahadori A., New numerical model for solubility of light alkanes in triethylene glycol. *Korean Journal of Chemical Engineering* **2007,** *24*, (3), 418-425.
(15) Bahadori A., New model predicts solubility in glycols. *Oil and Gas Journal* **2007,** *105*, (8), 50.
(16) Bahadori A., New model calculates solubility of light alkanes in triethylene glycol. *Petroleum Chemistry* **2009,** *49*, (2), 171-179.
(17) Ahmadi M.A., Soleimani R., Bahadori A., A computational intelligence scheme for prediction equilibrium water dew point of natural gas in TEG dehydration systems. *Fuel* **2014,** *137*, (0), 145-154.

(18) Neagu M., Cursaru D.L., Technical and economic evaluations of the triethylene glycol regeneration processes in natural gas dehydration plants. *Journal of Natural Gas Science and Engineering* **2017,** *37*, 327-340.
(19) Nassar V.L., Bullin J.A., Lyddon L.G., Solubility of Hydrocarbons in Physical Solvents. *Bryan Research and Engineering, Inc. Technical Papers* **2000**.
(20) Hernandez-Valencia V.N., Hlavinka M.W., Bullin J., In *Design glycol units for maximum efficiency*, presented on Proceedings of the Seventy-First GPA Annual Convention., Tulsa, OK, **1992**
(21) Kong Z.Y., Mahmoud A., Liu S., Sunarso J., A Parametric Study of Different Recycling Configurations for the Natural Gas Dehydration Process Via Absorption Using Triethylene Glycol. *Process Integration and Optimization for Sustainability* **2018**.
(22) Amouei Torkmahalleh M., Magazova G., Magazova A., Hassani Rad S.J., Simulation of environmental impact of an existing natural gas dehydration plant using a combination of thermodynamic models. *Process Safety and Environmental Protection* **2016,** *104*, 38-47.
(23) Amouei Torkmahalleh M., Assanova Z., Baimaganbetova M., Zinetullina A., *A study to reduce atmospheric emissions of an existing natural gas dehydration plant using multiple thermodynamic models*. 2018.
(24) Arya A., Maribo-Mogensen B., Tsivintzelis I., Kontogeorgis G.M., Process Design of Industrial Triethylene Glycol Processes Using the Cubic-Plus-Association (CPA) Equation of State. *Industrial & engineering chemistry research* **2014,** *53*, (29), 11766-11778.
(25) dos Santos L.C., Abunahman S.S., Tavares F.W., Ruiz Ahón V.R.,Kontogeorgis G.M., Cubic Plus Association Equation of State for Flow Assurance Projects. *Industrial & engineering chemistry research* **2015,** *54*, (26), 6812-6824.
(26) Kong Z.Y., Mahmoud A., Liu S., Sunarso J., *Revamping existing glycol technologies in natural gas dehydration to improve the purity and absorption efficiency: Available methods and recent developments*. 2018, *Vol. 56*.
(27) Breil M.P., Kontogeorgis G.M., Von Solms N., Stenby E.H., CAPE-OPEN: An international standard for process simulation. *Chemical Engineering* **2007,** *114*, (13), 52.
(28) NIST Thermophysical Properties of Fluid Systems, http://webbook.nist.gov/chemistry/fluid/, accessed on 01/09/2017.
(29) Braek A.M., Almehaideb R.A., Darwish N.,Hughes R., Optimization of Process Parameters for Glycol Unit to Mitigate the Emission of BTEX/VOCs. *Process Safety and Environmental Protection* **2001,** *79*, (4), 218-232.
(30) Waals J.v.d., Platteeuw J., Clathrate solutions. *Advances in chemical physics* **1958**, 1-57.
(31) Towler G., Sinnott R.K., *Chemical engineering design: principles, practice and economics of plant and process design*. Elsevier: 2012.
(32) Chemical Engineering Magazine, http://www.chemengonline.com/pci-home, accessed on 01/06/2018.
(33) Tannehill C., In *Budget Estimate Capital Cost Curves for Gas Conditioning and Processing - Updated*, presented on GPA Annual Convention, Atlanta Georgia (Mar 2009). S, **2009**
(34) Carroll J., *Natural Gas Hydrates: A Guide for Engineers*. Gulf Professional Publishing, Elsevier: USA, 2003.

(35) Tannehill C., In *Budget Estimate Capital Cost Curves for Gas Conditioning and Processing*, presented on GPA Annual Convention, Atlanta Georgia (Mar 2000). S, **2000**
(36) Turton R., Bailie R.C., Whiting W.B.,Shaeiwitz J.A., *Analysis, synthesis and design of chemical processes*. Pearson Education: 2008.
(37) Peters M.S., Timmerhaus K.D., West R.E., Timmerhaus K.,West R., *Plant design and economics for chemical engineers*. 4th ed., McGraw-Hill New York: 1968, *Vol. 4*.
(38) Peters M.S., Timmerhaus K.D.,West R.E., *Σχεδιασμός και οικονομική μελέτη εγκαταστάσεων για μηχανικούς (in greek)*. Τζιόλας: 2006, *Vol. 5*.

Chapter 9: Impact of the advanced mixing rules and explicit calculation of association at natural gas mixtures with hydrogen bonding compounds

In the previous chapters, UMR-PRU has been successfully extended in the modelling of natural gas mixtures with polar components encountered during natural gas processing and transportation. In this chapter, the effect of different theories in the modelling of polar and actually hydrogen bonding components is investigated. To this purpose, an equation of state is selected, namely Peng – Robinson and is combined with classic (vdW1f) and advanced (UMR-PRU) mixing rules. Furthermore, a model directly accounting for the hydrogen bonding interactions is considered, namely CPA-PR. To fairly examine the performance of the models, a specific database of binary mixtures is used for fitting their interaction parameters. The models are then evaluated on an equal basis in the prediction of multicomponent mixtures containing natural gas components and water, methanol, or MEG.

9.1. Introduction

As it has been stated in the previous chapters, water is one of the impurities encountered in natural gas coming from reservoir. To prevent hydrate formation, a certain amount of hydrate inhibitor, such as methanol or MEG, is injected into the flow in order to shift the hydrate formation curve outside the pipeline operating conditions. Additionally, a dehydration process typically precedes the further processing of natural gas and its distribution in onshore pipelines. Thus, the availability of a sufficient thermodynamic framework that is able to accurately predict the phase equilibria of mixtures containing hydrocarbons and polar compounds, such as water, methanol and MEG, is vital for the simulation of such operations in order to ensure product quality, safe and economic production and transportation, as well as to comply with the environmental legislation.[1]

In the following, the effect of advanced mixing rules and explicit accounting for the association on a cubic equation of state is examined. To this purpose, the Peng – Robinson EoS is selected and is coupled with: *(a)* the conventional van der Waals one fluid mixing rules[2], *(b)* the universal mixing rules leading to the so-called UMR-PRU[3] model, and *(c)* the associating term of Wertheim[4, 5] leading to CPA-PR EoS[6]. Initially, the VLE of two ternary systems, methane/water/methanol and methane/water/MEG is examined, while next, the dew point curves of synthetic natural gases (SNG) mixtures with water and methanol are investigated. In order to ensure a fair comparison between the models, their interaction parameters are fitted to the same database of binary phase equilibrium experimental data.

9.2. Literature review

Much work has been conducted in the literature concerning the modelling of these challenging mixtures such as those involving hydrogen bonding compounds. The difficulty of the modelling is enhanced when non-polar and asymmetric components are involved, such as those comprising the natural gas. In order to evaluate the performance of the models, accurate experimental data are necessary. Relatively recently, an increasing number of studies concerning the phase equilibrium of common natural gas components with alcohols or glycols and water have been published in the literature, involving new measurements or evaluation of existing ones. Frost et al.[7] evaluated some of the existing VLE data of the methane/water/methanol ternary mixture and its respective binaries and conducted new experimental measurements. Folas et al.[8] measured new experimental data for the binary methane/ MEG and the ternary methane/MEG/water with emphasis given to the water solubility measurements in the vapor phase. They used CPA and SRK, combined with both the conventional vdwlf mixing rules[2] and the Huron Vidal[9] ones, and concluded that both models, the latter with Huron – Vidal mixing rules (SRK-HV), perform satisfactorily for the prediction of MEG and water solubility in the vapor phase. According to the authors, CPA has an advantage over the other models.

In another communication, Folas et al.[10] applied the CPA and the SRK-HV to predict the multiphase equilibria of ternary, MEG/water/aromatic HCs, and quaternary mixtures, water/methane/toluene/MEG. Chapoy et al.[11, 12] focused on the hydrate forming conditions of natural gas mixtures; to that end, they evaluated the existing phase equilibrium data and measured the solubility of methane and water near hydrate forming conditions. Li and Englezos[13] employed the SAFT EoS to predict the phase equilibria of nine hydrocarbon/water/alcohol ternary systems, among them the methane/water/methanol and methane/water/MEG, using binary interaction parameters fitted to the respective binaries. Overall, a satisfactory agreement between the model predictions and experimental data has been found, except for the methane/water/methanol mixture.

Unfortunately, only very few experimental data are available in the open literature concerning phase equilibrium of natural gas mixtures with water, methanol or MEG and, consequently, the performance of the thermodynamic models is ambiguous. In a series of publications, Avila et al.[14-17] and Jarne et al.[18] measured dew points of synthetic natural gas mixtures with water and methanol and modelled them with a model based on the excess function equation of state. Also, Yan et al.[19] modelled, among others the dew points of two SNGs mixtures measured by Jarne et al.[18] with the CPA EoS.

9.3. Investigation of the associating schemes of CPA-PR

9.3.1. Associating schemes for MEG and glycols

The pure component parameters of CPA-PR for the associating compounds are fitted to vapor pressure and liquid density data. Since there is a multiplicity of roots, the obtained parameters are evaluated in the prediction of the LLE of binary mixtures. For water and methanol there is no such need, since this work has been already conducted by Voutsas et al.[6]. Instead, an appropriate associating scheme should be established for MEG. Following the work of Derawi et al.[20] the 2B and 4C associating schemes are investigated. Although if all the oxygen and hydrogen atoms in MEG are considered, more than six associating sites should be expected, the steric hindrance does not permit the formation of intermolecular hydrogen bonds and thus less association sites are assigned. The examined parameters are presented in Table 5.5 for both schemes, along with the obtained deviations from DIPPR. It is observed that very low deviations are obtained in both cases, with the 4C scheme to result in better prediction of the vapor pressure with an overall deviation equal to 0.8 %, while the 2B to a 1.5 % one. In the case of liquid density, both considerations yield similar deviation of about 1.6 %. The parameters are further evaluated in the prediction of the LLE of n-heptane/MEG mixture. The results are illustrated in Figure 9.1, where the superiority of the 4C associating scheme is apparent.

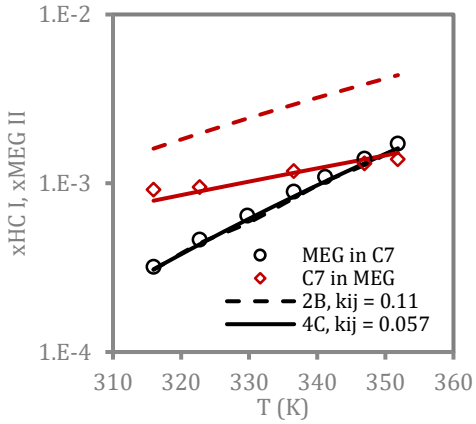

Figure 9.1: LLE prediction of the n-heptane/MEG mixture with CPA-PR using the 2B and 4C associating scheme. Experimental data by Derawi et al.[20]

It is observed that the 2B scheme is able to accurately predict the solubility in only the HC-rich phase, while the 4C scheme shows superior results in both phases, with the use of a small k_{ij} value. The latter is apparent in terms of deviations, which for the HC-rich phase is 6.9 % for 2B and 5.7 % for the 4C scheme. In the polar phase thought, the 2B scheme yields a deviation equal to 146.5 % while the 4C a 6.2 % one. From the above, the superiority of the 4C scheme approach is apparent and thus it is used for further study. According to Derawi et al.[20], the scheme used for MEG is appropriate for all glycols, since the number of sites may increase but steric hindrance is also more pronounced.

9.3.2. Selection of associating scheme for CO_2

Another molecule of interest from the aspect of the associating sites is that of CO_2. This molecule, due to its symmetric structure, has zero dipole moment, but it has quadrupole one. In combination with its small size, which contradicts with the longer hydrocarbon molecules which accompany it in a natural gas mixture, its modelling through a thermodynamic model is rather challenging. Despite the fact that CO_2 does not normally self-associate, it has been shown in the literature[21, 22] that the assigning of the 4C scheme or its consideration as a solvating compound considerably improves the performance of the models, especially when dealing with other associating compounds. Actually, to be able to accurately correlate the CO_2/water and CO_2/methanol binaries a second interaction parameter is required for the cross-association energy of the components, the lack of which leads to poor results.

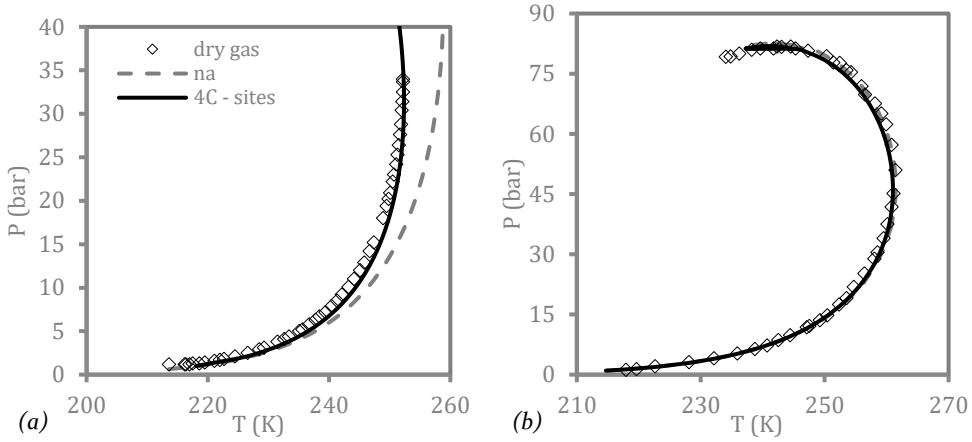

Figure 9.2: Dew point prediction results with CPA-PR for two SNGs, with the CO_2 assigned as a 4C-sites component (solid black line) and as inert one (gray dashed line). Diamonds denote experimental data by Jarne et al.[18] SNG composition (% molar): (a) N_2: 1.56, CO_2: 15.91 , CH_4: 69.11, C2: 2.62 , C3:0.42 , iC4: 0.11 , nC4: 0.10, iC5: 0.03, nC5: 0.02, nC6: 0.11 and (b) N_2: 0.77, CO_2: 1.70, CH_4: 84.45, C2: 8.68, C3: 3.3, iC4: 0.29, nC4: 0.59, iC5: 0.08, nC5: 0.09 and nC6: 0.05.

It is apparent that for the dry SNGs, the consideration of CO_2 as an associating or inert component does not severely affect the dew point predictions of typical SNG composition (Figure 9.2*b*). Instead, when the mixture has high CO_2 concentration, the 4C-sites approach yields substantially improved prediction results, even at low pressure (Figure 9.2*a*).

9.4. Binary phase equilibrium results

To examine the influence of the different models on an equal basis, it is necessary to fit their interaction parameters on the same database of experimental data. To make the observations more reliable, a small range of pressure is selected, which is of interest for the prediction of the multicomponent mixtures. Temperature specific interaction parameters are obtained for each model using the objective function of eq. 7.3. The database used for the correlation is given in Table 9.1 and the respective parameters for UMR-PRU in Table 9.2 while for PR and CPA-PR in Table 9.3. For the hydrocarbon components with methane and methanol the lowest available isotherm has been selected for the fitting of the parameters. Since ternary VLE data for the system methane/water/methanol are also available at 313 K, a different set of parameters has been also fitted to isothermal binary VLE data at that temperature, aiming to the better representation of the corresponding binary mixtures. These parameters are presented in Table 9.4. In the dew point prediction of synthetic natural gases, the parameters obtained in the lower temperature are utilized.

Table 9.1: Database of experimental data used for fitting the EoS parameters

Mixture	Ref.	Type	range			
			T (K)	P (bar)	$100 \cdot x_1$	$100 \cdot y_2$
Water (2) with						
N_2	[23]	VLE	298.15	25.3 - 810.6	0.03 - 0.44	0.02 - 0.14
CO_2	[24, 25]	VLE	288.26	5.0 - 202.7	0.40 - 3.01	0.07 - 0.15
CH_4	[11, 26, 27]	VLE	298.15	23.0 - 166.0	0.02 - 0.27	0.06 - 0.25
	[11, 27]	VLE	313.15	10.3 - 180.0	0.02 - 0.23	0.09 - 0.30
nC2	[11]	VLE	293.31	3.8 - 36.3	0.01 - 0.10	–
nC3	[28]	VLLE	278.90 - 360.93	5.7 - 37.1	0.02 -0.03	0.01 - 0.56
nC4	[29]	LLE	310.90 - 410.90	–	0.01 - 0.03	0.05 - 1.30
nC5	[30]	LLE	273.15 - 298.15	–	1.0 E-3 - 1.4 E-4	0.01 - 0.04
nC6	[31]	LLE	298.15 - 473.15	0.2 - 35.2	2 E-4 - 0.02	0.04 - 10.9
meOH	[32]	VLE	298.14	0.1 - 0.2	4.44 - 100.00	0.00 - 72.23
	[33]	VLE	313.05	0.2 - 0.3	20.95 - 95.10	1.75 - 35.65
MEG	[34]	VLE	298.03	0.0 - 0.03	10.18 - 83.27	–
Methanol (2) with						
N_2	[23]	VLE	273.15 - 198.15	49.0 - 245.0	1.09 - 5.05	–
CO_2	[35]	VLE	298.15	7.9 - 59.5	5.96 - 90.02	0.69 - 2.39
CH_4	[27]	VLE	298.15	25.0 - 125.0	2.28 - 9.44	0.44 - 0.81
	[27]	VLE	313.15	25.0 - 125.0	2.28 - 9.20	0.72 - 1.52
nC2	[36, 37]	VLE	298.15	10.1 - 31.4	3.70 - 17.55	0.86 - 1.780
nC3	[38]	VLE	313.10	3.5 - 13.8	2.52 - 75.20	2.80 - 12.20
nC5	[39]	VLE	372.70	4.5 - 7.5	1.20 - 95.60	20.5- 77.60
nC6	[40]	VLE	298.15	0.3 - 0.4	5.00 - 95.00	42.0 - 50.0
MEG (2) with						
CH_4	[41]	VLE	298.15	1.4 - 203.5	0.02 - 1.82	–

Table 9.2: Binary group interaction parameters of UMR-PRU determined in this study.

n	*m*	A_{nm}	A_{mn}
N_2	H_2O	525.91	860.03
N_2	CH_3OH	525.38	169.00
CO_2	H_2O	847.95	211.80
CO_2	CH_3OH	433.06	-87.21
CH_4	H_2O	1490.20	630.03
CH_4	CH_3OH	869.91	-17.52
CH_4	MEG	1018.36	293.13
C_2H_6	H_2O	1085.31	545.71
C_2H_6	CH_3OH	167.53	162.89
CH_3OH	H_2O	-110.48	124.14
MEG	H_2O	-170.19	69.89

Table 9.3: Binary interaction parameters for PR and CPA-PR.

	PR			CPA-PR		
	Water	Methanol	MEG	Water	Methanol	MEG
N_2	-0.6255	-0.1390	-	-0.1596	0.0588	-
CO_2	-0.1207	0.0451	-	k_{ij} = -0.0900 l_{ij} = 0.398031	k_{ij} = -0.0979 l_{ij} = 0.6537	-
CH_4	-0.2950	-0.0303	0.0458	0.0352	0.0641	0.2021
nC2	-0.1896	0.0293	-	0.0567	0.0771	-
nC3	0.4800	0.0600	-	0.1350	0.0693	-
iC4	0.4800	0.0690	-	0.0910	0.0606	-
nC4	0.4800	0.0690	-	0.0910	0.0606	-
iC5	0.4800	0.0600	-	0.0300	0.0519	-
nC5	0.4800	0.0600	-	0.0300	0.0519	-
nC6	0.4800	0.0510	-	0.0400	0.0432	-
nC7	0.4800	0.0800	-	-0.0089	0.0345	-
H_2O	0.0000	-0.0925	-0.0603	0.0000	-0.0900	-0.0400
MeOH	-0.0925	0.0000	-	-0.0900	0.0000	-
MEG	-0.0603	-	0.0000	-0.0400	-	0.0000

Table 9.4: Binary interaction parameters for PR, UMR-PRU and CPA-PR regressed from experimental data at 313 K.

		PR	UMR-PRU		CPA-PR
n	*m*		A_{nm}	A_{mn}	
CH_4	H_2O	-0.2520	1423.20	712.03	0.0832
CH_4	CH_3OH	-0.0168	946.14	-22.68	0.0651
CH_3OH	H_2O	-0.0815	-172.00	269.03	-0.0600

Correlation results for the binary mixtures are presented in Table 9.5, while Figure 9.3 shows representative results for methane with water and methane with methanol and MEG. It is observed that the three models can successfully correlate the liquid phase in all cases.

Table 9.5: VLE correlation results with PR, UMR-PRU and CPA-PR.

Mixture	n_p [a]	T – range (K)	% AARD[b] in P			% AARD[b] in y_2		
			PR	UMR-PRU	CPA-PR	PR	UMR-PRU	CPA-PR
Water (2) with								
N_2	8	298.15	1.23	2.74	2.22	–	–	–
CO_2	8	288.26	30.04	12.21	16.03	473.94	4.39	8.76
CH_4	14	298.15	4.02	6.14	3.78	81.67	38.22	41.00
	9	313.15	2.71	2.70	2.63	119.98	4.69	9.77
nC2	5	293.31	0.64	0.73	0.89	–	–	–
MeOH	14	298.14	1.69	1.16	0.89	4.15	1.81	4.18
	10	313.05	0.91	1.29	1.24	4.35	2.43	6.25
MEG	7	298.03	2.26	2.67	2.40	–	–	–
Methanol (2) with								
N_2	9	273.15-298.15	6.04	1.56	2.01	–	–	–
CO_2	8	298.15	5.20	0.94	2.64	6.66	4.99	21.04
CH_4	5	298.15	1.94	2.08	2.15	77.98	19.17	4.07
	5	313.15	2.36	1.54	2.63	51.34	8.78	9.59
C2	6	298.15	6.79	8.21	8.04	8.77	21.48	13.09
MEG (2) with								
CH_4	7	298.15	1.75	1.55	1.89	268.80	20.28	34.45

[a] n_p: number of experimental data points.

[b] $\%AARD = \frac{100}{n_p}\sum_{i=1}^{n_p}\frac{abs(X_i^{exp}-X_i^{calc})}{X_i^{exp}}$, where X: bubble point pressure (P) or vapor phase composition of component i (y_i)

Knowledge of water solubility in the methane-rich vapor phase is of utmost importance for the determination of the water content in wet natural gas mixtures and the corresponding amount of glycol required to achieve the final water dew point specification by glycol dehydration. As shown in Figure 9.3 *a* and *b*, UMR-PRU and CPA-PR yield very accurate water solubility predictions, while PR significantly overestimates them. For methane/methanol (Figure 9.3 *c* and *d*), CPA-PR better predicts the methanol solubility in vapor phase compared to UMR-PRU at 298 K, while similar results are obtained by the two models at 313 K. PR, as is in the case of methane with water, again, it significantly overestimates the solubility of methanol in the vapor phase. Similar results are obtained by UMR-PRU and CPA-PR for the solubility of MEG in vapor phase (Figure 9.3*e*), while again PR overestimates them. Finally, all three models yield very good correlation of the liquid and the vapor phase of methanol/water and MEG/water mixtures. It should be noted that very satisfactory predictions are obtained with UMR-PRU by utilizing the existing UNIFAC interaction parameters. However, in order to have a fair comparison in ternary VLE predictions with the other models, the parameters determined in this work for both binaries (Table 9.2) will be next used for UMR-PRU.

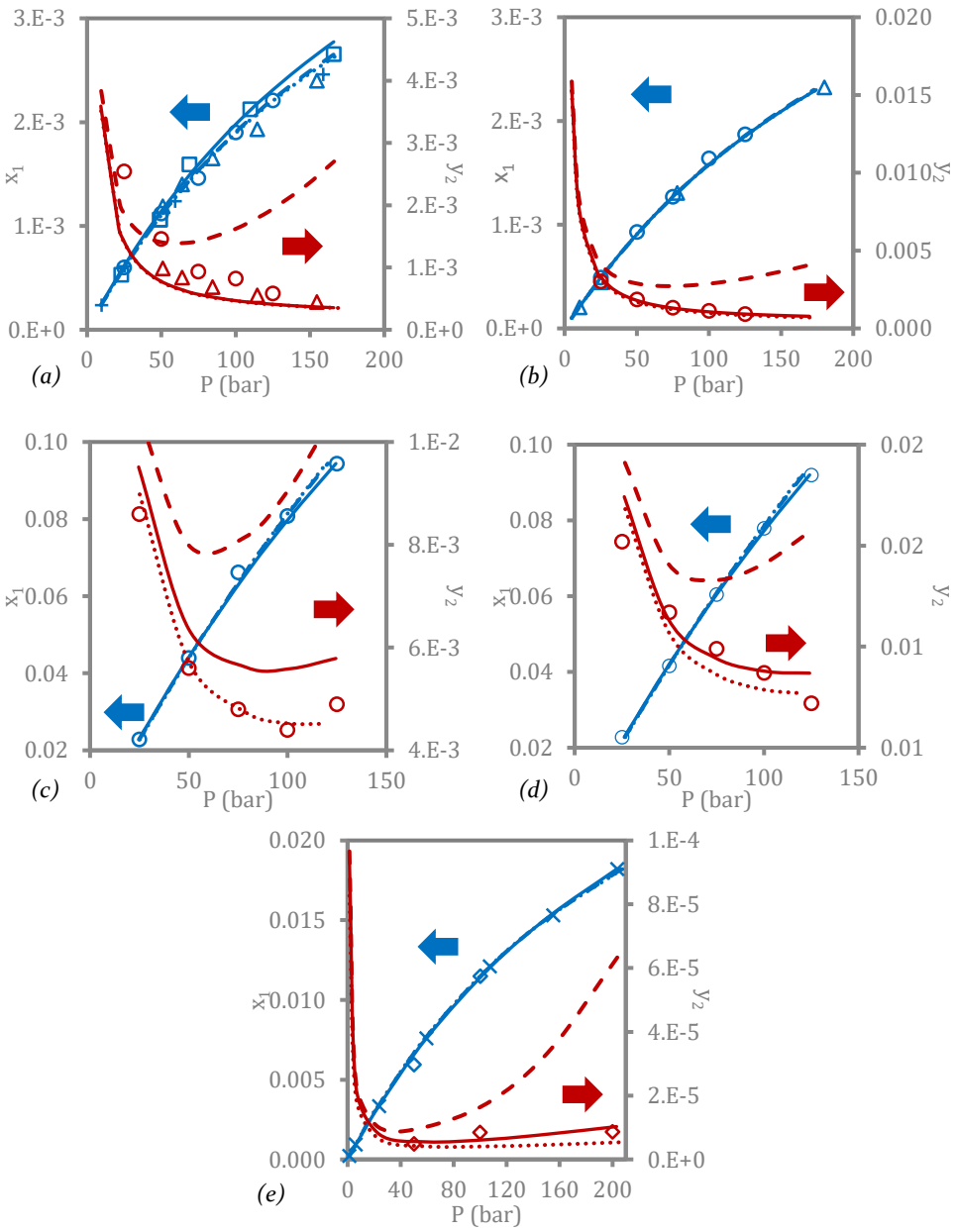

Figure 9.3: VLE correlation results with PR (dashed line), UMR-PRU (solid line) and CPA-PR (dotted line) for: (a) methane (1)/water (2) at 298.15 K, (b) methane (1)/water (2) at 313.15 K, (c) methane (1)/methanol (2) at 298.15 K, (d) methane (1)/methanol (2) at 313.15 K, and (e) methane (1)/MEG (2) at 298.15 K. Triangles denote data by Frost et al.[7], circles by Yarym – Agaev et al.[27], crosses by Chapoy et al.[11], squares by Kim et al.[26], ex (x) by Jou et al.[41] and diamonds by Folas et al.[1]. Blue colour for the liquid phase and red for the vapor one.

Representative results for CO_2/water, n-pentane/methanol and n-hexane/water binary mixtures are presented in Figure 9.4. For CO_2/water (Figure 9.4*a*), UMR-PRU and CPA-PR describe accurately both the liquid and the vapor phase, while PR fails to predict the solubility of water in the CO_2-rich vapor phase. For the n-pentane/ methanol mixture (Figure 9.4*b*), UMR-PRU predicts very well the VLE data using the existing UNIFAC interaction parameters, CPA-PR correlates satisfactorily the same data, while PR cannot even correlate well the data. For the n-hexane/water LLE, as illustrated in Figure 9.4*c*, PR highly underestimates the solubility of hydrocarbon in the aqueous phase despite of the use of a very high value for the binary interaction parameter, k_{ij} = 0.48. UMR-PRU gives improved results over PR using the existing UNIFAC interaction parameters, while the best results are obtained by CPA-PR. The fact that the latter cannot capture the minimum in the water solubility is attributed to the use of only one temperature – independent k_{ij} value for the whole examined range.

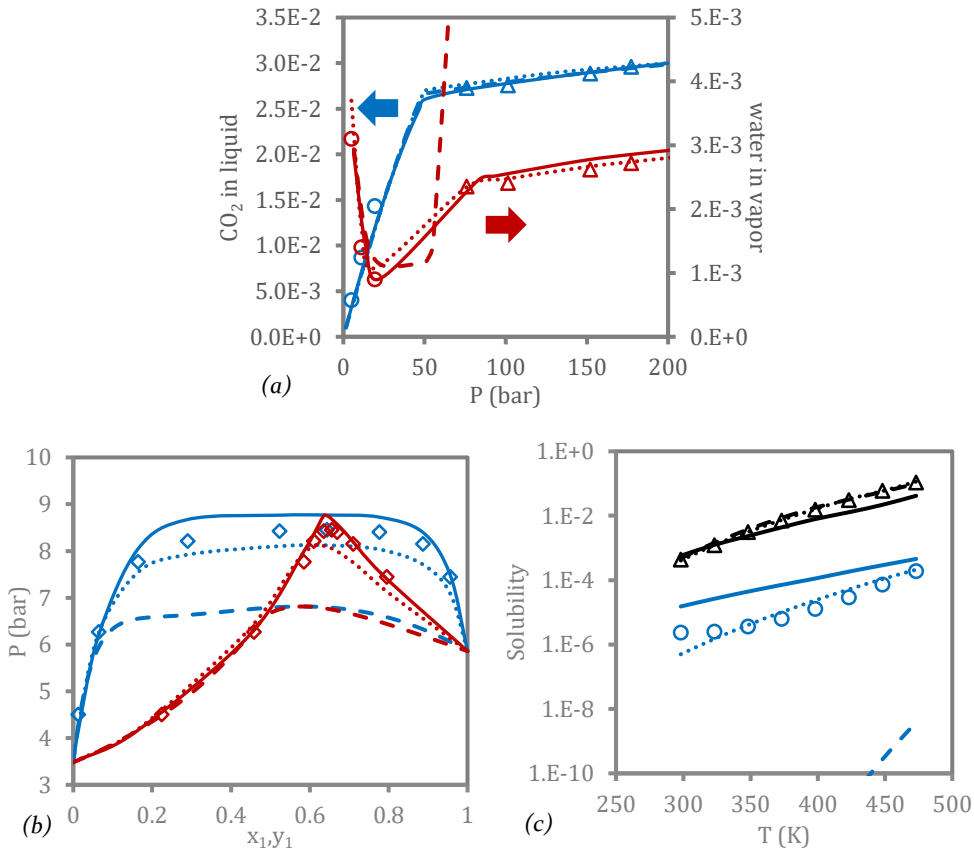

Figure 9.4: Binary VLE and LLE results with PR (dashed line), UMR-PRU (solid line) and CPA-PR (dotted line) for the mixtures (a) CO_2 (1)/water (2) at 288 K, (b) n-pentane (1)/methanol (2) at 372.7 K and (c) n-hexane (1)/water (2). Circles denote experimental data by Valtz et al.[25], triangles by King et al.[24], diamonds by Wilsak et al.[39]; blue colour for liquid phase and red for the vapor one. For (c) experimental are by Tsonopoulos et al.[31]; blue colour for aqueous phase and black for the HC-rich one.

9.5. Multicomponent mixtures prediction results

The next step taken for the evaluation of the models is the prediction of multicomponent mixtures. To that end two ternary mixtures are considered, comprising from methane, which is the major natural gas component, water and methanol or MEG, as well as a selection of SNGs and their mixtures with water and methanol.

9.5.1. Ternary Mixtures

The detailed ternary VLE prediction results are reported in Table 9.6, while typical ones are shown graphically in Figure 9.5. For the methane/water/methanol mixture, the experimental data show that the increase of methanol concentration in feed results to an increase of methane solubility in the liquid phase, a decrease of methane and water solubility in the vapor phase and an increase of the methanol solubility in vapor phase. As for the effect of temperature, the experimental data show that the increase of temperature leads to a slight decrease of the methane solubility in the liquid phase, an increase of methanol and water solubility in the vapor phase and a decrease of methane solubility in the vapor phase.

All three models predict qualitatively correct the experimental trends. Quantitatively, PR and UMR-PRU overestimate the solubility of methane in the liquid phase, where CPA-PR has an apparent advantage over the other two models. The better performance of CPA-PR is attributed to the better description of the intermolecular forces developed in the liquid phase due to that it explicitly takes into account hydrogen bonding interactions. For the methanol solubility in vapor phase, CPA-PR gives the best predictions followed by UMR-PRU, while PR significantly overestimates them. Finally, for the water solubility in the vapor phase UMR-PRU and CPA-PR give similar results while PR yields poor predictions, especially at 313 K. It is of interest to note, that the performance of the rather *simpler* models is improved at lower water concentrations, which leads to the conclusion that the better description of the water hydrogen bonding interactions in the case of CPA-PR is the dominating factor for the improved results. Yet, the application of advanced mixing rules substantially improves the performance of PR EoS, especially at middle concentrations where the mixing effects are more pronounced.

For the methane/water/MEG mixture (Figure 9.6) all models give similar predictions for the methane solubility in the liquid phase. For the vapor phase, UMR-PRU and CPA-PR give similar results for the solubility of water, while for the solubility of MEG, CPA-PR gives better predictions than UMR-PRU for the lower pressures. On the other hand, PR gives poor vapor phase solubility predictions.

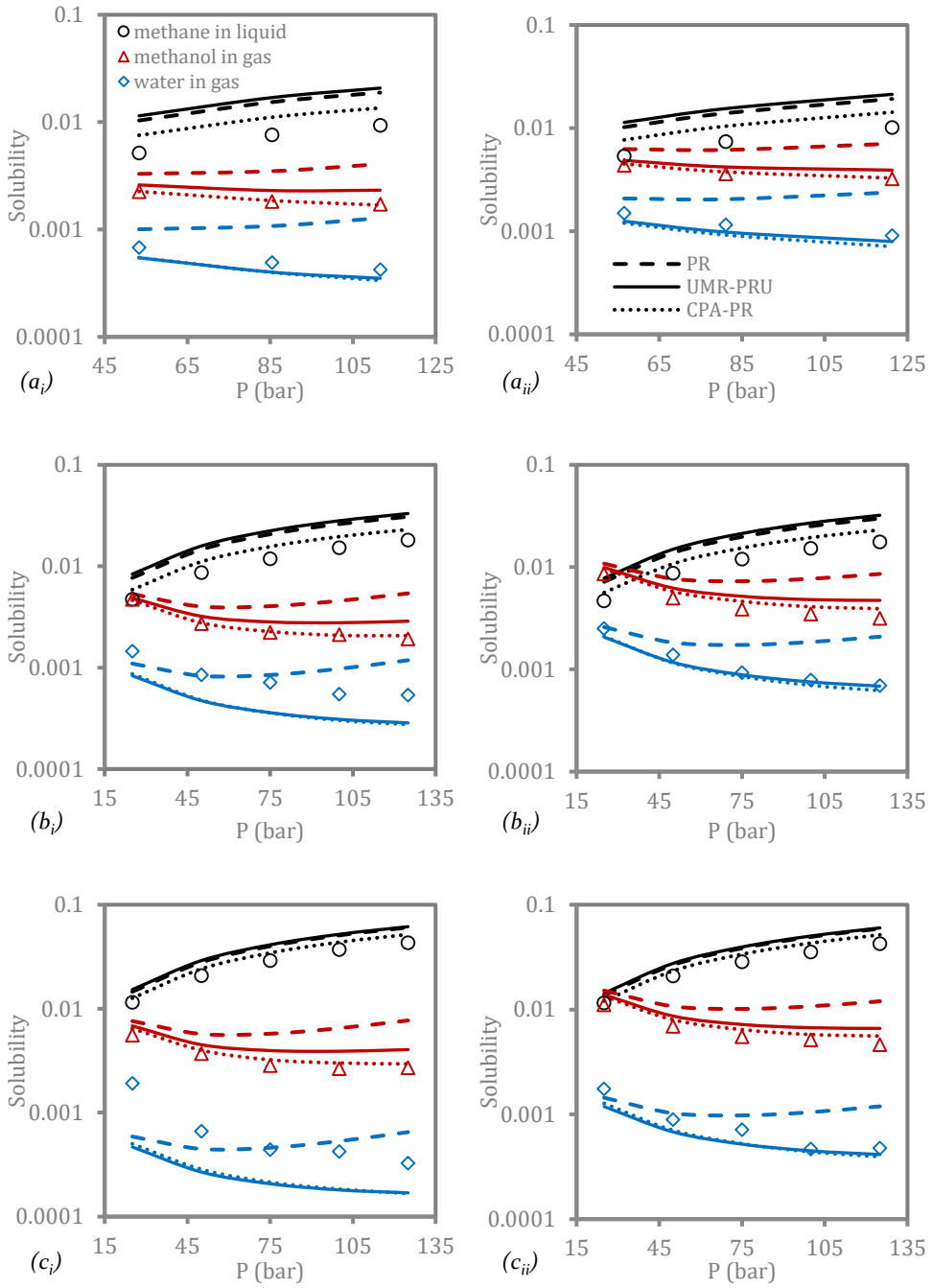

Figure 9.5: VLE prediction results for the ternary mixture methane/methanol/water at (i) 298.15 K and (ii) 313.15 K, for three concentrations (% wt.) of methanol in feed: (a) 42.7 %, (b) 50.2 % and (c) 75.6 %, with PR (dashed line), UMR-PRU (solid line) and CPA-PR (dotted line). Experimental data by Sinyavskaya et al.[42] and Frost et al.[7]. Black circles denote the solubility of methane in liquid phase, red triangles the solubility of methanol in vapor phase, and blue diamonds the solubility of water in vapor phase.

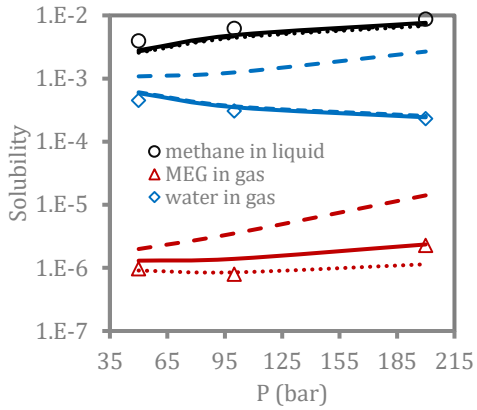

Figure 9.6: VLE prediction results for the ternary mixture methane/MEG/water at 298.15 K (44.6 % wt. MEG in feed) with: PR (dashed line), UMR-PRU (solid line) and CPA-PR (dotted line). Experimental data by Folas et al.[1]. Black circles denote methane solubility in liquid phase, red triangles MEG solubility in vapor phase and blue diamonds water solubility in vapor phase.

Table 9.6: VLE prediction results for the ternary methane (1) / hydrate inhibitor (2) / water (3) with PR, UMR-PRU and *CPA-PR*.

% wt. inhibitor	ref	%AARD[a] in x_1			%AARD[a] in y_2			%AARD[a] in y_3		
		PR	UMR-PRU	CPA-PR	PR	UMR-PRU	CPA-PR	PR	UMR-PRU	CPA-PR
Methane/methanol/water at 298.15 K										
26.5	42	97.8	127.1	44.4	82.6	20.1	5.9	89.2	27.0	28.0
42.7	7	101.4	122.1	45.6	91.6	25.8	1.6	123.1	18.3	19.6
50.2	42	69.0	82.7	27.6	87.7	25.8	3.1	48.9	45.4	45.5
75.6	42	35.2	39.4	16.4	104.5	36.0	11.8	46.1	58.7	57.5
26.5	42	97.8	127.1	44.4	82.6	20.1	5.9	89.2	27.0	28.0
Overall		73.0	89.6	32.2	91.6	27.0	6	71.7	39.5	39.7
Methane/methanol/water at 313.15 K										
26.5	42	84.9	114.6	39.5	80.9	19.6	9.6	104.9	5.2	9.3
42.7	7	89.8	110.5	41.9	77.6	16.3	2.8	92.7	14.7	20.7
50.2	42	62.4	75.2	26.2	92	32.4	12.7	91.6	8.7	12.7
75.6	42	31.9	35.6	15.5	88.6	30.6	16.9	68.8	20.1	19.7
Overall		64.7	81.0	29.6	85.5	25.7	12.8	89.1	11.9	15.0
Methane/MEG/water at 298.15 K										
44.6	1	28.4	25.4	32.0	225	55.0	6.9	225.1	22.8	26.9

[a] $\%\,AARD = 100 \cdot \frac{abs(X_i^{exp} - X_i^{calc})}{X_i^{exp}}$, *where X stands for the solubility of component i in the liquid (x) or vapor phase (y)*

9.5.2. Dew point prediction of SNG mixtures

After the evaluation of the models in the prediction of the ternary mixtures, where the better prediction of CPA-PR is apparent, the models are evaluated in the prediction of dew points of synthetic natural gases. To investigate the influence of water and methanol on the phase equilibrium of natural gases, seven SNGs that differ in their dry basis composition are studied. The compositions of the dry gases are presented in Table 9.7.

Table 9.7: Composition of the Dry Synthetic Natural Gas Mixtures (% molar).

	SNG1[17]	SNG2[14]	SNG3[14]	SNG4[14]	SNG5[14]	SNG6[18]	SNG7[18]
N_2	0.313	0.67	0.48	0.862	0.41	1.559	0.772
CO_2	0.202	-	-	-	-	25.908	1.7
CH_4	90.4183	89.9584	88.7634	86.4838	96.4654	69.114	84.446
C2	8.038	8.22	8.54	9.832	2.51	2.62	8.683
C3	0.801	0.9	1.68	2.388	0.213	0.423	3.297
iC4	0.081	0.11	0.22	0.183	0.184	0.105	0.293
nC4	0.123	0.13	0.29	0.231	0.197	0.104	0.589
iC5	0.01	0.0084	0.0182	0.0139	0.0096	0.034	0.084
nC5	0.0079	0.0032	0.0084	0.0063	0.01	0.023	0.086
nC6	0.0047	-	-	-	0.001	0.11	0.05
nC7	0.0011	-	-	-	-	-	-

9.5.2.a. *Interaction parameters between natural gas components, water and methanol*

For the dry natural gas components, UMR-PRU model is applied in a fully predictive way using the interaction parameters suggested by Louli et al.[43]. Also, following the results of the same publication.[43], zero interaction parameters are implemented to PR and CPA-PR among the dry natural gas components for all SNGs, except from SNG 6 which contains high amount of CO_2. For this particular mixture, binary interaction parameters between the CO_2 and the other natural gas components are required in order to obtain satisfactory description of the dew points of the dry gas[44]. For PR those interaction parameters have been obtained from Hysys vs 8.8 database. Finally, CPA-PR using the 4C association scheme for CO_2, predicts well the phase envelope of the dry gas with zero interaction parameters between CO_2 and the other dry NG components (Figure 9.2*b*). Only the CO_2/n-hexane interaction parameter has been slightly adjusted (k_{ij} = 0.1) in order to obtain similar dry gas dew point predictions with PR and UMR-PRU. The deviations in dew point temperature at given pressure of the dry synthetic natural gases are presented in Table 9.8.

Table 9.8: Dew point temperature prediction of SNGs and their mixtures with water and methanol, with PR, UMR-PRU and CPA-PR.

Gas	Ref.	n_p	T (K)	P (bar)	AAD in DPT[a] (K)		
					PR	UMR-PRU	CPA-PR
SNG 1 (dry)	[15]	17	205.8-229.1	2.5-69.7	4.11	1.86	1.55
0.003 % H_2O	[17]	15	230.5-264.2	2.9-71.1	18.19	10.18	9.64
0.009 % H_2O	[17]	15	236.3-273.9	1.8-71.1	14.58	6.19	5.79
0.010 % H_2O + 0.07 % meOH	[15]	15	238.7-278.6	2.1-71.1	9.36	2.95	1.40
0.009 % H_2O + 0.17 % meOH	[15]	15	240.9-283.9	1.7-72.1	6.54	2.60	0.64
SNG 2 (dry)	[16]	15	200.3-226.9	5.4-66.7	1.49	1.07	1.02
0.002 % H_2O	[14]	15	225.8-258.5	2.3-73.2	15.70	9.26	8.47
0.006 % H_2O + 0.12 % meOH	[16]	15	242.3-277.1	3.1-71.7	6.51	2.63	1.86
0.027 % H_2O + 0.10 % meOH	[16]	17	242-282.6	1.4-34.9	4.30	1.52	1.61
SNG 3 (dry)	[16]	19	202.9-237.7	2.9-71.2	1.61	1.64	0.67
0.006 % H_2O	[14]	15	237.0-270.2	2.6-71.8	14.95	7.64	7.03
0.01 % H_2O + 0.06 % meOH	[16]	14	241.9-276.2	3.2-63.4	8.21	2.49	0.96
SNG 4 (dry)	[16]	22	199.9-240.8	2.3-77.7	2.20	1.34	1.25
0.003 % H_2O	[14]	15	228.7-263.8	2.3-70.0	20.89	9.22	8.20
0.006 % H_2O	[14]	15	231.1-270.1	2.2-71.6	14.85	7.23	6.35
0.003 % H_2O + 0.16 % meOH	[16]	15	236.4-277.6	1.7-71.9	7.87	3.27	1.46
0.004 % H_2O + 0.22 % meOH	[16]	15	243.3-284.1	2.2-72.2	7.00	3.64	0.81
SNG 5 (dry)	[16]	14	203.4-218.9	4.7-58.4	1.96	1.33	0.80
0.002 % H_2O	[14]	15	224.3-258.7	2.1-68.4	18.25	9.68	9.61
0.010 % H_2O + 0.15 % meOH	[16]	15	244.7-283.3	2.6-70.9	6.11	1.72	0.63
0.006 % H_2O + 0.31 % meOH	[16]	17	246.3-283.2	2.1-35	1.56	1.59	2.24
SNG 6 (dry)	[18]	48	213.6-252.2	1.2- 34.0	0.66	0.79	1.49
0.035 % H_2O	[18]	23	246.1-288.1	1.1-40.9	9.75	6.68	6.63
0.173 % H_2O	[18]	8	261.3-277.9	1.5-5.0	0.74	0.77	0.85
0.023 % H_2O + 0.45 % meOH	[18]	13	248.1-288.6	1.1-20.5	2.27	1.56	1.62
0.042 % H_2O + 0.34 % meOH	[18]	16	249-288.2	1.2-20.7	2.64	1.62	1.92
SNG 7 (dry)	[18]	47	217.9-261.4	1.2-81.8	2.40	2.65	1.67
0.040 % H_2O	[18]	26	244.7-288.0	1.1-41.0	6.39	3.14	3.35
0.155 % H_2O	[18]	9	256.9-278.1	1.1-5.3	1.15	0.50	1.26
0.048 % H_2O + 0.44 % meOH	[18]	21	247.6-288.2	1.1-20.2	1.13	1.79	1.67
0.088 % H_2O + 0.24 % meOH	[18]	17	248.7-288.1	1.1-20.6	1.92	3.34	2.95
Overall							
dry SNGs		182			1.89	1.59	1.84
SNGs with H_2O		171			12.68	6.65	6.34
SNGs with H_2O and meOH		205			4.85	2.34	1.55

[a]AAD is defined as: $\Delta T = \left|T^{exp} - T^{calc}\right|$, where T stands for the dew point temperature at defined pressure, exponent *exp* for the experimental and *calc* for the calculated with the models.

Apart from the interaction parameters already examined, the rest are determined as follows:

PR and CPA-PR

The parameters between the light natural gas components (nitrogen, CO_2 and ethane) with water and methanol are determined by fitting binary VLE data, following the procedure discussed in Section 9.4. The interaction parameters between the heavier alkanes (n-butane up to n-heptane) and water, have been fitted to the HC-rich phase of the corresponding alkane/water LLE data. For the alkanes, n-propane up to n-heptane, with methanol, the interaction parameters have been obtained from the Hysys database for PR. For CPA-PR, a linear correlation of the binary interaction parameter with the number of carbon atoms (CN) of the alkane has been developed, based on the interaction parameters determined by fitting the VLE data for propane/methanol, n-pentane/methanol and n-hexane/methanol as in eq. 9.1,

$$k_{ij} = -0.0087 \cdot CN + 0.0954 \qquad \text{eq. 9.1}$$

where CN stands for the carbon number of the alkane. Finally, for the iso-paraffins with methanol the same interactions as those for the respective normal alkanes are considered both for PR and CPA-PR. All the required interaction parameters are reported in Table 9.3.

UMR-PRU

Due to the group contribution character of the UMR-PRU model, the parameters for water and methanol with the "CH_2" main group, which is used to describe all alkanes, have been taken from the existing UNIFAC tables[45] as suggested by Voutsas et al.[3]. The interaction parameters between the light gases (N_2, CO_2 and C_2H_6) with water and methanol, which are not included in the standard UNIFAC tables, have been determined in this work, and they are reported in Table 9.2.

9.5.2.b. *Prediction Results*

Table 9.8 presents the deviations obtained with the three models in dew point temperature at given pressure, for SNG mixtures containing water and methanol. Typical results are illustrated graphically in Figure 9.7. All models underestimate the water effect on dew point temperature for the very low water content but their performance improves for higher water contents. Note that, as discussed by Jarne et al.[18], experimental errors are encountered for the low water content measurements. and thus the uncertainty is high. All models yield the best predictions at the low – pressure region. At higher pressures, however, where associating effects become more pronounced due to higher density, the results by all models worsen. PR strongly underestimates the water and methanol effect on the dew point, yielding a more ideal behavior than that experimentally observed in all cases. On the other hand, the advanced mixing rules employed in UMR-PRU improve substantially the dew point predictions of PR. The best overall results are obtained with CPA-PR, indicating again the necessity of taking explicitly into account hydrogen bonding interactions.

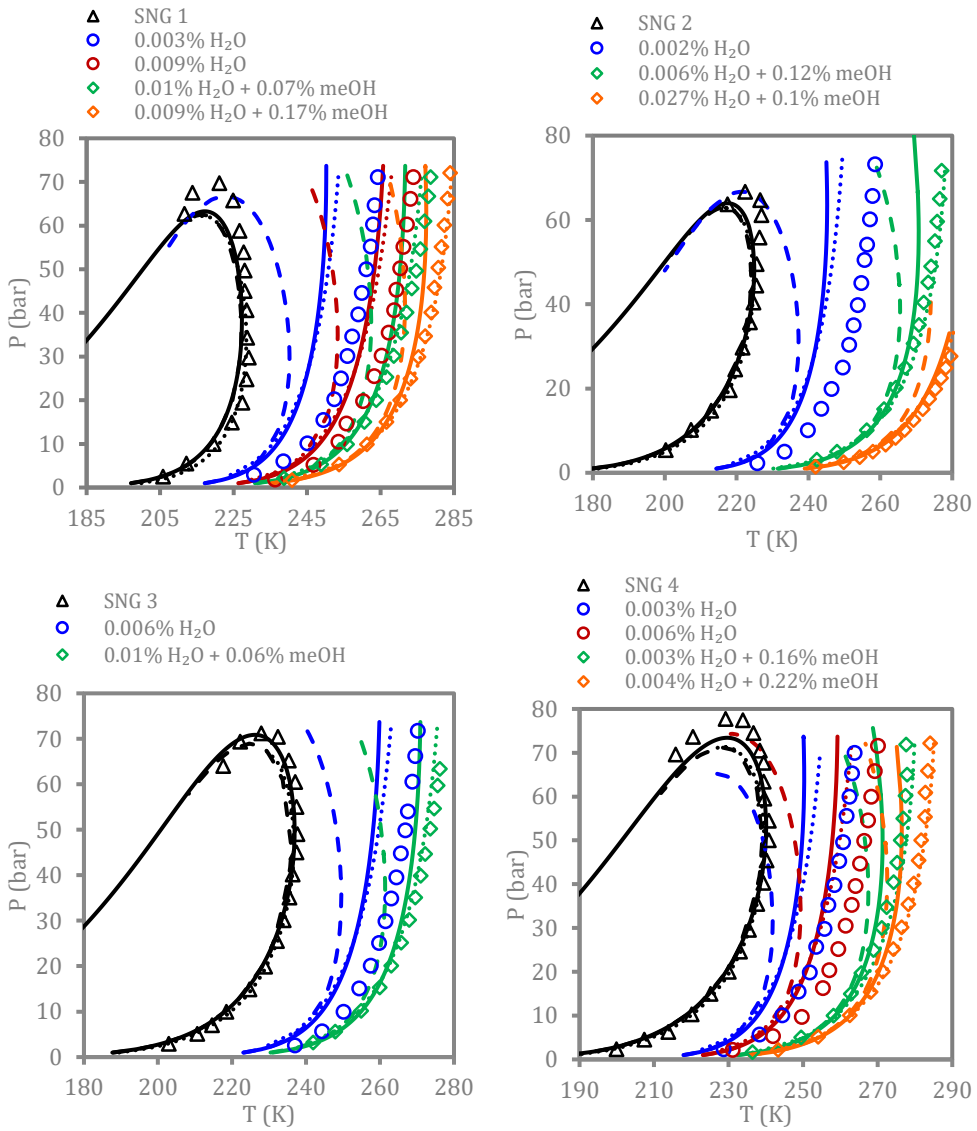

Figure 9.7: Dew point prediction results of synthetic natural gases and their mixtures with water and methanol, with PR (dashed line), UMR-PRU (solid line) and CPA-PR (dotted line). Experimental data by Avila et al.[14-17] and Jarne et al.[18].

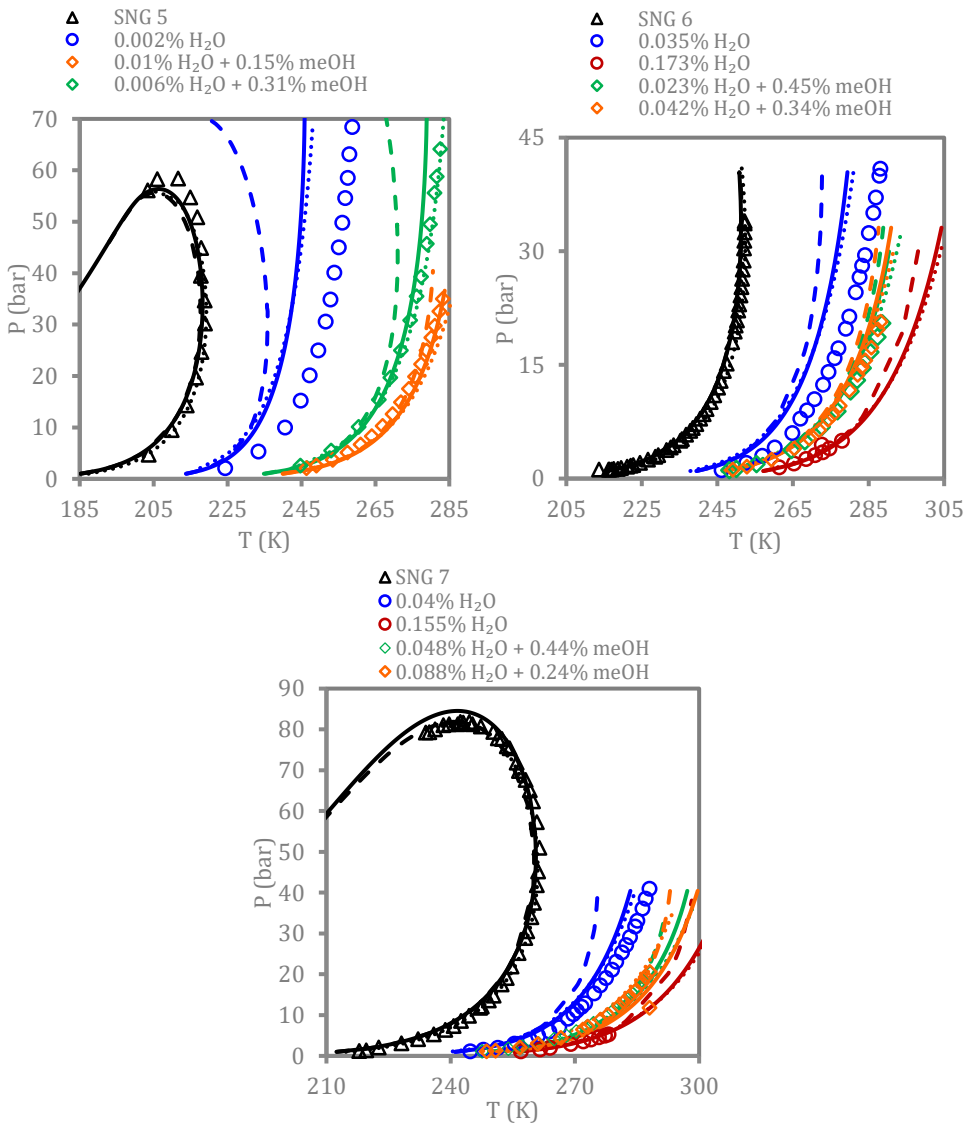

Figure 9.7 (continued)

9.6. Conclusions

Three versions of the Peng – Robinson equation of state are evaluated in the prediction of the VLE of ternary and multicomponent natural gas mixtures that contain water, methanol and MEG. It is shown that both UMR-PRU and CPA-PR provide significant improvement over the Peng – Robinson EoS combined with van der Waals one fluid mixing rules in the prediction of multicomponent phase equilibrium. For the methane/methanol/water mixture, CPA-PR has an advantage over UMR-PRU in the prediction of the solubility of methane in the liquid phase, while for the methane/ MEG/water mixture UMR-PRU and CPA-PR give similar results. Furthermore, UMR-PRU and CPA-PR are able to predict satisfactorily the dew points of natural gas mixtures with water and/or methanol, yielding much better results than Peng – Robinson, with CPA-PR to give the best overall results. These observations suggest that the selection of advanced mixing rules for the attractive and co-volume parameters, as well as the direct implementation of an associating term are essential in order to obtain accurate phase equilibrium description of complex mixtures containing natural gas components, water and hydrogen bonging chemicals such as methanol and MEG, with a cubic equation of state.

List of Symbols

Latin Characters

A_{nm}, B_{nm}, C_{nm}	UNIFAC binary interaction parameter between groups n and m
k_{ij}, l_{ij}	binary interaction parameters
n, m	UNIFAC groups
n_p	number of datapoints
P	pressure (bar)
T	absolute temperature (K)
x_i	liquid mol fraction of component i
y_i	vapor mol fraction of component i

Superscripts and Subscripts

calc	calculated
exp	experimental
i, j	molecule in a mixture
n, m	UNIFAC groups
p	points

References

(1) Folas G.K., Berg O.J., Solbraa E., Fredheim A.O., Kontogeorgis G.M., Michelsen M.L., Stenby E.H., High-pressure vapor–liquid equilibria of systems containing ethylene glycol, water and methane: Experimental measurements and modeling. *Fluid Phase Equilibria* **2007,** *251*, (1), 52-58.
(2) van der Waals J.D., *Over de Continuiteit van den Gas-en Vloeistoftoestand*. Sijthoff: 1873, *Vol. 1*.
(3) Voutsas E., Magoulas K., Tassios D., Universal Mixing Rule for Cubic Equations of State Applicable to Symmetric and Asymmetric Systems: Results with the Peng–Robinson Equation of State. *Industrial & engineering chemistry research* **2004,** *43*, (19), 6238-6246.
(4) Wertheim M., Fluids with highly directional attractive forces. II. Thermodynamic perturbation theory and integral equations. *Journal of statistical physics* **1984,** *35*, (1-2), 35-47.
(5) Wertheim M., Fluids with highly directional attractive forces. I. Statistical thermodynamics. *Journal of statistical physics* **1984,** *35*, (1-2), 19-34.
(6) Voutsas E., Perakis C., Pappa G., Tassios D., An evaluation of the performance of the Cubic-Plus-Association equation of state in mixtures of non-polar, polar and associating compounds: Towards a single model for non-polymeric systems. *Fluid Phase Equilibria* **2007,** *261*, (1–2), 343-350.
(7) Frost M., Karakatsani E., von Solms N., Richon D., Kontogeorgis G.M., Vapor–Liquid Equilibrium of Methane with Water and Methanol. Measurements and Modeling. *Journal of Chemical & Engineering Data* **2013,** *59*, (4), 961-967.
(8) Fonseca J.M.S., Dohrn R., Peper S., High-pressure fluid-phase equilibria: Experimental methods and systems investigated (2005–2008). *Fluid Phase Equilibria* **2011,** *300*, (1–2), 1-69.
(9) Huron M.-J., Vidal J., New mixing rules in simple equations of state for representing vapour-liquid equilibria of strongly non-ideal mixtures. *Fluid Phase Equilibria* **1979,** *3*, (4), 255-271.
(10) Folas G.K., Kontogeorgis G.M., Michelsen M.L., Stenby E.H., Vapor–liquid, liquid–liquid and vapor–liquid–liquid equilibrium of binary and multicomponent systems with MEG: Modeling with the CPA EoS and an EoS/GE model. *Fluid Phase Equilibria* **2006,** *249*, (1-2), 67-74.
(11) Chapoy A., Mohammadi A.H., Richon D., Tohidi B., Gas solubility measurement and modeling for methane–water and methane–ethane–n-butane–water systems at low temperature conditions. *Fluid Phase Equilibria* **2004,** *220*, (1), 111-119.
(12) Chapoy A., Mohammadi A.H., Tohidi B., Richon D., Estimation of water content for methane+ water and methane+ ethane+ n-butane+ water systems using a new sampling device. *Journal of Chemical & Engineering Data* **2005,** *50*, (4), 1157-1161.
(13) Li X.-S., Englezos P., Vapor–liquid equilibrium of systems containing alcohols, water, carbon dioxide and hydrocarbons using SAFT. *Fluid Phase Equilibria* **2004,** *224*, (1), 111-118.
(14) Avila S., Blanco S.a.T., Velasco I., Rauzy E., Otín S., Thermodynamic properties of synthetic natural gases: Part 4. Dew point curves of synthetic natural gases and their mixtures with water: measurement and correlation. *Fluid Phase Equilibria* **2002,** *202*, (2), 399-412.

(15) Avila S., Blanco S.T., Velasco I., Rauzy E., Otín S., Thermodynamic Properties of Synthetic Natural Gases. 1. Dew-Point Curves of Synthetic Natural Gases and Their Mixtures with Water and Methanol. Measurement and Correlation. *Industrial & engineering chemistry research* **2002,** *41*, (15), 3714-3721.
(16) Avila S., Blanco S.T., Velasco I., Rauzy E., Otín S., Thermodynamic Properties of Synthetic Natural Gases. 2. Dew Point Curves of Synthetic Natural Gases and Their Mixtures with Water and Methanol. Measurement and Correlation. *Energy & Fuels* **2002,** *16*, (4), 928-934.
(17) Avila S., Blanco S.T., Velasco I., Rauzy E., Otín S., Thermodynamic properties of synthetic natural gases. Part 3. Dew point curves of synthetic natural gases and their mixtures with water. Measurement and correlation. *Energy & Fuels* **2003,** *17*, (2), 338-343.
(18) Jarne C., Avila S., Blanco S.T., Rauzy E., Otín S., Velasco I., Thermodynamic Properties of Synthetic Natural Gases. 5. Dew Point Curves of Synthetic Natural Gases and Their Mixtures with Water and with Water and Methanol: Measurement and Correlation. *Industrial & engineering chemistry research* **2003,** *43*, (1), 209-217.
(19) Yan W., Kontogeorgis G.M., Stenby E.H., Application of the CPA equation of state to reservoir fluids in presence of water and polar chemicals. *Fluid Phase Equilibria* **2009,** *276*, (1), 75-85.
(20) Derawi S.O., Michelsen M.L., Kontogeorgis G.M., Stenby E.H., Application of the CPA equation of state to glycol/hydrocarbons liquid–liquid equilibria. *Fluid Phase Equilibria* **2003,** *209*, (2), 163-184.
(21) Pappa G.D., Perakis C., Tsimpanogiannis I.N., Voutsas E.C., Thermodynamic modeling of the vapor–liquid equilibrium of the CO_2/H_2O mixture. *Fluid Phase Equilibria* **2009,** *284*, (1), 56-63.
(22) Perakis C.A., Voutsas E.C., Magoulas K.G., Tassios D.P., Thermodynamic modeling of the water+ acetic acid+ CO_2 system: The importance of the number of association sites of water and of the nonassociation contribution for the CPA and SAFT-type models. *Industrial & engineering chemistry research* **2007,** *46*, (3), 932-938.
(23) Kertes, *IUPAC Solubility Data Series, Pergamon Press: Oxford*. 1979.
(24) King M.B., Mubarak A., Kim J.D., Bott T.R., The mutual solubilities of water with supercritical and liquid carbon dioxides. *The Journal of Supercritical Fluids* **1992,** *5*, (4), 296-302.
(25) Valtz A., Chapoy A., Coquelet C., Paricaud P., Richon D., Vapour–liquid equilibria in the carbon dioxide–water system, measurement and modelling from 278.2 to 318.2 K. *Fluid Phase Equilibria* **2004,** *226*, 333-344.
(26) Kim Y.S., Ryu S.K., Yang S.O., Lee C.S., Liquid Water–Hydrate Equilibrium Measurements and Unified Predictions of Hydrate-Containing Phase Equilibria for Methane, Ethane, Propane, and Their Mixtures. *Industrial & engineering chemistry research* **2003,** *42*, (11), 2409-2414.
(27) Yarym-Agaev N., Sinyavskaya R., Koliushko I., Phase equilibrium in the binary systems water-methane and methanol-methane under high pressure. *Zh. Prikl. Khim* **1985,** *58*, 165-168.
(28) Kobayashi R., Katz D., Vapor-Liquid Equilibria For Binary Hydrocarbon-Water Systems. *Industrial & Engineering Chemistry* **1953,** *45*, (2), 440-446.

(29) Reamer H., Sage B., Lacey W., Phase Equilibria in Hydrocarbon Systems. n-Butane-Water System in the Two-Phase Region. *Industrial & Engineering Chemistry* **1952,** *44*, (3), 609-615.
(30) Sørensen J.M., Arlt W., *Liquid-liquid Equilibrium Data Collection: Binary Systems*. Dechema: 1979, *Vol. V*.
(31) Tsonopoulos C., Wilson G., High-temperature mutual solubilities of hydrocarbons and water. Part I: Benzene, cyclohexane and n-hexane. *AIChE Journal* **1983,** *29*, (6), 990-999.
(32) Koner Z., Phutela R., Fenby D., Determination of the equilibrium constants of water-methanol deuterium exchange reactions from vapour pressure measurements. *Australian Journal of Chemistry* **1980,** *33*, (1), 9-13.
(33) Ratcliff G.A., Chao K.C., Prediction of thermodynamic properties of polar mixtures by a group solution model. *The Canadian Journal of Chemical Engineering* **1969,** *47*, (2), 148-153.
(34) Mokbel I., Porcedda S., Guetachew T., Marongiu B.,Jose J., Static measurements of the total vapor pressure of ethane-1, 2-diol+ water mixtures at temperatures from 258 K to 363 K. *ELDATA International Electronic Journal of Physico-Chemical Reference Data* **1999,** *5*, 79-84.
(35) Ohgaki K., Katayama T., Isothermal vapor-liquid equilibrium data for binary systems containing carbon dioxide at high pressures: methanol-carbon dioxide, n-hexane-carbon dioxide, and benzene-carbon dioxide systems. *Journal of Chemical and Engineering Data* **1976,** *21*, (1), 53-55.
(36) Ma Y.H., Kohn J.P., Multiphase and Volumetric Equilibria of the Ethane-Methanol System at Temperatures between -40 C. and 100 C. *Journal of Chemical & Engineering Data* **1964,** *9*, (1), 3-5.
(37) Ohgaki K., Sano F., Katayama T., Isothermal vapor-liquid equilibrium data for binary systems containing ethane at high pressures. *Journal of Chemical and Engineering Data* **1976,** *21*, (1), 55-58.
(38) Galivel-Solastiouk F., Laugier S., Richon D., Vapor-liquid equilibrium data for the propane-methanol and propane-methanol-carbon dioxide system. *Fluid Phase Equilibria* **1986,** *28*, (1), 73-85.
(39) Wilsak R.A., Campbell S.W., Thodos G., Vapor-liquid equilibrium measurements for the n-pentane-methanol system at 372.7, 397.7 and 422.6 K. *Fluid Phase Equilibria* **1987,** *33*, (1–2), 157-171.
(40) Iguchi A., Vapor-liquid equilibriums at 25 C for binary systems between alcohols and hydrocarbons. *Kagaku Sochi* **1978,** *20*, 66-68.
(41) Jou F.Y., Otto F.D., Mather A.E., Solubility of methane in glycols at elevated pressures. *The Canadian Journal of Chemical Engineering* **1994,** *72*, (1), 130-133.
(42) Sinyavskaya R., Yarym-Agaev N., Koliushko I., Levinton L.Y., British Gas Corp. L., Phase equilibria in the methane– water– methanol system at high pressures. *Gazovaya Prom* **1984,** *1*, 39.
(43) Louli V., Pappa G., Boukouvalas C., Skouras S., Solbraa E., Christensen K.O., Voutsas E., Measurement and prediction of dew point curves of natural gas mixtures. *Fluid Phase Equilibria* **2012,** *334*, 1-9.
(44) Nasrifar K., Bolland O., Prediction of thermodynamic properties of natural gas mixtures using 10 equations of state including a new cubic two-constant equation of state. *Journal of Petroleum Science and Engineering* **2006,** *51*, (3-4), 253-266.

(45) Hansen H.K., Rasmussen P., Fredenslund A., Schiller M., Gmehling J., Vapor-liquid equilibria by UNIFAC group contribution. 5. Revision and extension. *Industrial & engineering chemistry research* **1991,** *30*, (10), 2352-2355.

Chapter 10: Development of a new group – contribution EoS for the modelling of hydrogen bonding mixtures

Following the investigation of the effect of advanced mixings rules and the implementation of a term, based on Wertheim's first order perturbation theory, which explicitly accounts for the hydrogen bonding interactions, a new group – contribution model is developed. This model is based on the Peng – Robinson EoS while it includes the Wertheim's associating term with the same considerations as is in the CPA-PR EoS, but for the extension to mixtures, the Universal Mixing Rules are applied for the physical term. The model is first evaluated on two ternary mixtures, as in Chapter 9 and then it is fully extended to describe natural gas mixtures with water and polar chemicals.

10.1. Introduction

Previously it is has been proved that the incorporation of Wertheim's first order perturbation term in a classic EoS, in this case PR, substantially improves the prediction of mixtures containing associating components. One of the most attractive characteristics of such an EoS, as CPA-PR in this case, is that when non-associating components are not encountered the model reverts to the cubic EoS and is fully applicable without the need for further parametrization. In complex mixtures, such as those presenting high degrees of asymmetry, this becomes rather a disadvantage since the classic cubic EoS fail to accurately predict their properties. The application of advanced mixing rules, instead of the vdW1f ones, significantly improves the cubic EoS prediction in complex systems as showed for example by Louli et al.[1] and Novak et al.[2]. Furthermore, in Chapter 9 it is shown that the use of advanced mixing rules also yields improved prediction results for associating mixtures.

Based on the above considerations, it is assumed that the combination of the two approaches should yield better prediction results for associating mixtures, or at least improved results for the non-associating compounds. This is of interest since in an industrial application, such as in the simulation of a natural gas topside platform, several unit operations take place with a huge diversity in the conditions and the compositions of the mixtures. For example, the gas coming from the reservoir is first separated in a three – phase flash where the model should be able to predict well the interactions in the aqueous phase but also to handle the heavy compounds which consist the oil phase. Then the sweetening and dehydration operations follow, where associating components along with natural gas ones are encountered. Finally, after sufficient handling of the impurities, the hydrocarbon dew point is controlled to meet the pipeline specifications. A more precise description of the properties of the mixture, as that obtained through the application of an accurate thermodynamic model, can lead to increased profit margins. Although most simulators give the opportunity to use different thermodynamic models for different unit operations or parts of the process, this requires a good knowledge of the advantages and limitations of those models; as well, it can cause a discontinuity between each unit which may lead to robustness issues. To this end, a new, group – contribution, model is developed, the so-called UMR-CPAPRU, which combines the Wertheim's association term[3, 4] in PR EoS with the application of the UMR advanced mixing rules. Another attractive characteristic of the proposed model is its group – contribution nature, which permits the prediction of phase equilibria of various mixtures based on interaction parameters fitted to selected binaries.

10.2. Model development

The model is developed in the context of CPA-PR, as a combination of a physical and associating term (eq. 10.1).

$$P = P^{Phys} + P^{Assoc} \qquad \text{eq. 10.1}$$

Soave's expression is employed for the temperature dependency of the attractive term, as in eq. 10.2 - eq. 10.6. This is justified so that a continued description of vapor pressure is obtained in both *sub*- and *super*- critical regions. Furthermore, this permits the model to revert to UMR-PRU for non-associating components.

$$P^{phys} = \frac{RT}{v-b} - \frac{a_c \mathrm{a}(T)}{v(v+b)+b(v-b)} \qquad \text{eq. 10.2}$$

$$\mathrm{a}(T) = \left(1 + m(1 - T_r^{0.5})\right)^2 \qquad \text{eq. 10.3}$$

$$m = 0.37464 + 1.54226\omega - 0.26992\omega^2 \qquad \text{eq. 10.4}$$

$$a_c = 0.45724 \frac{(RT_c)^2}{P_c} \qquad \text{eq. 10.5}$$

$$b = 0.07780 \frac{RT_c}{P_c} \qquad \text{eq. 10.6}$$

where T_c, P_c, ω are the critical properties and the acentric factor, T the system temperature, P the pressure, v the molecular volume and R the ideal gas constant.

The contribution of the associating term with respect to pressure is expressed from eq. 10.7 and eq. 10.8,

$$P^{Assoc} = \frac{z^{Assoc} RT}{v} \qquad \text{eq. 10.7}$$

$$Z^{Assoc} = -\frac{1}{2}\left(1 + \rho \frac{\partial lng}{\partial \rho}\right) \sum_i \sum_{Ai} x_i \, [d(Ai)](1 - X_{Ai}) \qquad \text{eq. 10.8}$$

where $\rho = 1/v$ the molar density, g the radial distribution function, x_i is the analytical molar fraction of the component i in the mixture and $d(A_i)$ is the number of association sites of type A in molecule i.

X^{A_i} in eq. 10.8 is the mol fraction of the molecule i not bonded at site A, which is calculated by eq. 10.9.

$$X_{Ai} = \left(1 + \rho \sum_i \sum_{Bj} xj \, X^{Bj} \Delta^{AiBj}\right)^{-1} \qquad \text{eq. 10.9}$$

The associating strength $\Delta^{A_i B_j}$ between the associating sites A and B in the components i and j respectively, is calculated by eq. 10.10,

$$\Delta^{A_iB_j} = g\left[exp\left(\frac{\varepsilon^{A_iB_j}}{RT}\right) - 1\right] b\beta^{A_iB_j} \qquad \text{eq. 10.10}$$

where b is the co-volume parameter of the EoS, $\varepsilon^{A_iB_j}$ the association energy and $\beta^{A_iB_j}$ the associating volume between the associating sites A and B in components i and j.

The radial distribution function, g, is the same with that of CPA and is defined analogically to the SAFT formulation as that of a hard – sphere fluid, through the Carnahan – Starling EoS[5] as in eq. 10.11,

$$g = \frac{(1 - y/2)}{(1 - y)^3} \qquad \text{eq. 10.11}$$

where $y = \frac{b\rho}{4}$ is the reduced packing factor.

As it is obvious from the above, for the pure components the model reverts to CPA-PR, where the Soave's alpha function, eq. 10.3, is used to determine the temperature dependency of the attractive term energy parameter. The association is considered as molecular – specific, as is for CPA-PR, rather than assigning associating sites to specific groups.

For the extension to mixtures, it is well known that the associating term is explicitly calculated and only combining rules for the associating components are required, as it is expressed through eq. 10.12.

$$\varepsilon^{A_iB_j} = \frac{\varepsilon^{A_iB_i} + \varepsilon^{A_jB_j}}{2}$$

$$\beta^{A_iB_j} = \sqrt{\beta^{A_iB_i}\beta^{A_jB_j}} \qquad \text{eq. 10.12}$$

The same is not valid for the physical part of the EoS. In its conventional form, CPA-PR, uses the classic vdW1f mixing rules, as is the case for PR. As it has been shown in previous work[6], the use of advanced mixing rules to PR improves the model performance both in polar and non-polar mixtures. Taking this under consideration, for the extension to mixtures the Universal Mixing Rules (UMR), proposed by Voutsas et al.[7], are applied for the physical part of the EoS, as it is expressed by eq. 10.13 and eq. 10.14. As such, additional interaction parameters are required and actually the UNIFAC interaction ones, as is in the case of UMR-PRU.

$$\frac{\mathrm{a}}{bRT} = \frac{1}{-0.53}\frac{G_{AC}^{E,SG} + G_{AC}^{E,res}}{RT} + \sum_{\mathrm{i}} x_i \frac{\mathrm{a_i}}{b_i RT} \qquad \text{eq. 10.13}$$

$$b = \sum_i \sum_j x_i x_j\, b_{ij} \;\text{ with }\; b_{ij} = \left(\frac{b_i^{1/2} + b_j^{1/2}}{2}\right)^2 \qquad \text{eq. 10.14}$$

It has to be noted that the application of the UMR, implicitly affects the associating term, through the incorporation of different combining rules for the co-volume parameter (eq. 10.14).

The Staverman – Guggenheim term of the combinatorial part ($G_{AC}^{E,SG}$) and the residual part ($G_{AC}^{E,res}$) of the excess Gibbs energy (G^E) respectively, are calculated from eq. 10.15 to eq. 10.19.

$$\frac{G_{AC}^{E,SG}}{RT} = 5\sum_{i=1}^{NC} x_i q_i \, ln\frac{\theta_i}{\varphi_i}, \qquad \frac{G_{AC}^{E,res}}{RT} = \sum_{i=1}^{NC} x_i \nu_k^i \left(ln\Gamma_k - ln\Gamma_k^i\right) \qquad \text{eq. 10.15}$$

$$ln\Gamma_k = Q_k\left[1 - ln\left(\sum_m \theta_m \Psi_{mk}\right) - \sum_m \frac{\theta_m \Psi_{mk}}{\sum_n \theta_n \Psi_{nm}}\right] \qquad \text{eq. 10.16}$$

For compound i: $\varphi_i = \frac{x_i R_i}{\sum_j x_j R_j}, \quad \theta_i = \frac{x_i Q_i}{\sum_j x_j Q_j}$ eq. 10.17

$$r_i = \sum_{k=1}^{NG} \nu_k^i R_k, \quad q_i = \sum_{k=1}^{NG} \nu_k^i Q_k \qquad \text{eq. 10.18}$$

For group m: $\theta_m = \frac{X_m Q_m}{\sum_n X_n Q_n}, \; X_m = \frac{\sum_j \nu_m^j x_j}{\sum_j \sum_n \nu_n^j x_j}$ eq. 10.19

where m, n, k are referred to UNIFAC groups, NC is the number of components in the mixture, NG the number of the UNIFAC groups comprising a component, ν_k^i is the number of group k in molecule i, x_i the mol fraction of compound i, R_k the van der Waals volume parameter of group k, Q_k the surface parameter of group k, φ_i the volume fraction of component i and θ_i the surface fraction of component i.

The interaction parameter Ψ_{mk} between groups m and k is a function of temperature, and it is calculated by eq. 10.20.

$$\Psi_{mk} = exp\left[-\frac{A_{mk} + B_{mk}(T - 298.15) + C_{mk}(T - 298.15)^2}{T}\right] \qquad \text{eq. 10.20}$$

When only non-associating compounds are present in the mixture, the model reverts to the UMR-PRU model.

10.3. Pure Component Parameters

Following the work of Perakis et al.[8] three pure component parameters T_c', P_c' and ω_c' are required for the non-associating components and two extra parameters, the associating energy, ε^{AB}, and associating volume, β^{AB}, are required for the associating ones, rendering a total of five adjustable parameters. The associating schemes assigned for CPA-PR are used for the compounds examined here as previously discussed in

Section 5.4.1.b. The pure components parameters need to be re-estimated though, due to the change in the expression of the alpha function of the attractive term from Boston – Mathias[9] to that of Soave[10].

Following the typical procedure for such systems, the pure component parameters have been fitted to vapor pressure and liquid density data generated from the DIPPR correlations. The T_r step used for the fitting of the parameters is 0.01 with the exception of MEG for which it is 0.02, so that a similar number of points is used in the correlation.

Although the assumption of CO_2 as an associating component, yields improved results[11, 12], in this work it is considered as inert, since the quadrupole moment is implicitly taken into consideration through the UNIFAC interaction parameters of the mixing rule. Furthermore, this is required in order to avoid the need of re-estimation of the interaction parameters between CO_2 and the non-polar groups. For the non-associating components, the fitted parameters of PR-fit EoS are incorporated as in Table 10.1. As it is apparent very similar results as for the deviation in vapor pressure and liquid density are obtained with the ones proposed in the original CPA-PR (Table 5.5). Actually, the observed deviations are systematically lower for all examined components both for vapor pressure and liquid density. Additionally, the association energy parameter is within the limits of the energy of the hydrogen bond which has been calculated from spectroscopic data (Table 10.1). Of course, as expected, the obtained parameters result in an overestimation of the critical point of the compound (Figure 10.1).

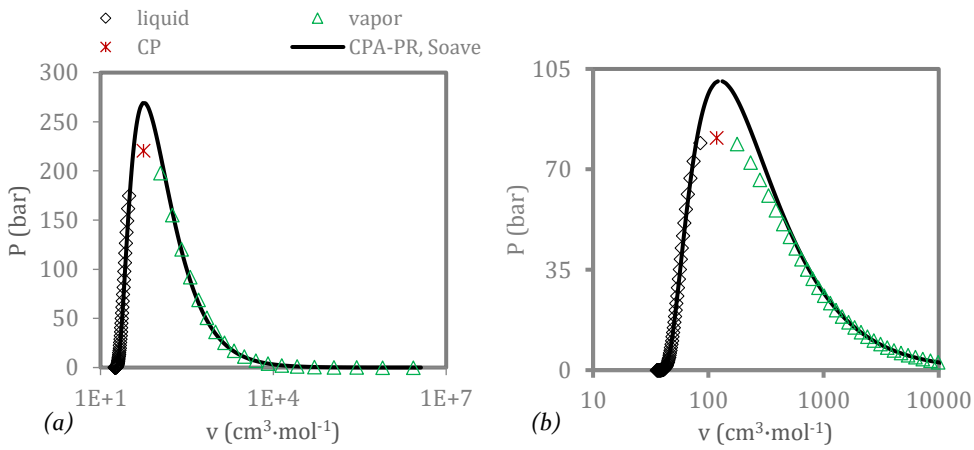

Figure 10.1: Phase diagram of pure components calculated with the parameters determined in this study with UMR-CPAPRU. Experimental vapor pressure data are taken from DIPPR[13] while the density ones are from NIST[14] (a) water and (b) methanol.

Table 10.1: Pure component parameters for UMR-CPAPRU EoS. The deviation refers to that from DIPPR correlation.

Compound	Ref.	T_r range (K)	T_c' (K)	P_c' (bar)	ω'	$\varepsilon^{A_iB_j}/R$ (K)	$\beta^{A_iB_j}$	Exp HB	%AARD [a] in P^s	%AARD [a] in v_l
N_2	Chapter 5	0.53 - 0.99	125.49	32.74	0.0449	–	–	–	0.4	7.3
CO_2	Chapter 5	0.72 - 0.98	304.78	74.63	0.2154	–	–	–	0.3	3.8
CH_4	[18]	0.53 - 0.99	190.80	45.80	0.0092	–	–	–	0.4	7.8
C_2H_6	[18]	0.41 - 0.99	306.10	48.70	0.0937	–	–	–	2.1	6.3
C3	[19]	0.33 - 0.98	371.00	42.50	0.1524	–	–	–	2.2	4.1
iC4	Chapter 5	0.45 - 0.99	405.12	36.17	0.2244	–	–	–	5.8	7.8
nC4	[18]	0.32 - 0.99	425.40	38.10	0.2106	–	–	–	2.9	4.4
iC5	Chapter 5	0.45 - 0.99	458.57	33.70	0.2498	–	–	–	2.7	6.3
nC5	[19]	0.40 - 0.99	470.54	34.59	0.2786	–	–	–	1.7	3.3
nC6	[19]	0.40 - 0.99	508.20	31.10	0.3244	–	–	–	3.2	3.7
nC7	[19]	0.51 - 0.95	542.50	28.70	0.3745	–	–	–	0.9	2.2
water	This work	0.43 - 0.99	302.51	134.85	0.2236	1811.91	0.1090	1813[15]	0.4	0.7
meOH	This work	0.55 - 0.98	368.58	74.83	0.0399	2763.66	0.0185	2630[16]	0.8	0.6
etOH	This work	0.50 - 0.99	411.97	55.85	0.0476	3039.88	0.0049	3007[17]	0.4	0.6
MEG	This work	0.45 - 0.97	569.64	70.27	0.1521	2279.91	0.0144	–	0.8	1.6

[a] $\%\,AARD = \frac{100}{n_p} \cdot \sum_i^{n_p} \frac{abs(X_i^{calc} - X_i^{exp})}{X_i^{exp}}$, where X stands for P^s or v_l and n_p for the number of experimental data points

10.4. Evaluation of the UMR-CPAPRU model in two ternary mixtures and their respective binaries

The first step of the evaluation of the model is the explicit comparison of its performance in the modelling of binary mixtures followed by the prediction of the thermodynamic behavior of multicomponent ones. In the same context with Chapter 9, two ternary mixtures of interest to the gas industry are investigated. That is the methane/methanol/water and methane/MEG/water at two different isotherms, 298.15 K and 313.15 K. Table 10.2 presents the specific parameters fitted to the same database of experimental data at constant temperature, in order to have the optimum behavior in each isotherm. The database is the same as the one used for the evaluation of PR, UMR-PRU and CPA-PR (Table 9.1).

Table 10.2: Temperature – specific interaction parameters for UMR-CPAPRU for the isotherms of 298.15 K and 313.15 K.

		298.15 K	
n	*m*	A_{nm}	A_{mn}
CH_4	H_2O	-126.27	448.55
CH_4	CH_3OH	19.33	146.44
CH_3OH	H_2O	-225.60	58.35
CH_4	MEG	-95.57	553.21
MEG	H_2O	-436.39	600.48
		313.15 K	
n	*m*	A_{nm}	A_{mn}
CH_4	H_2O	-52.27	405.55
CH_4	CH_3OH	56.54	120.89
CH_3OH	H_2O	-184.07	5.66

The detailed VLE correlation results are presented in Table 10.3 along with the respective results with UMR-PRU and CPA-PR. Some representative VLE correlation results are illustrated in Figure 10.2 and Figure 10.3. UMR-CPAPRU correlates satisfactorily the binary mixtures yielding equivalent or even improved results compared to UMR-PRU and CPA-PR. The latter is more apparent in the vapor phase, which has not been included in the objective function for the fitting of the IPs.

Table 10.3: VLE correlation results per isotherm for the mixtures of interest with UMR-PRU, CPA-PR and UMR-CPAPRU.

T (K)	Ref	n_p	UMR-PRU		CPA-PR		UMR-CPAPRU	
			%AARD [a] in P	AAD[b] in y_1	%AARD [a] in P	AAD [b] in y_1	%AARD [a] in P	AAD[b] in y_1
Methanol/Water								
298.14	20	24	1.25	0.59	0.91	0.63	1.66	0.76
313.05	21	10	1.29	0.35	1.24	0.70	1.29	0.71
overall		*34*	*1.27*	*0.48*	*1.05*	*0.66*	*1.50*	*0.74*
Methane/MEG								
298.15	22	7	1.55	-	1.89	-	1.92	-
Methane/Methanol								
298.15	23	5	2.08	0.08	2.15	0.04	1.90	0.03
313.15	23	5	1.54	0.09	2.63	0.10	2.14	0.10
overall		*10*	*1.81*	*0.09*	*2.39*	*0.06*	*2.02*	*0.07*
Methane/Water								
298.15	23	5	5.54	0.05	1.74	0.05	3.40	0.06
298.15	24	5	5.90	-	7.55	-	5.87	-
298.13	25	4	7.19	-	7.78	-	5.75	-
298.31	26	6	8.23	0.01	7.90	0.01	8.23	0.02
313.15	23	5	1.96	0.01	2.10	0.01	2.15	0.02
313.11	25	4	4.49	0.03	5.42	0.03	5.18	0.03
overall		*25*	*5.62*	*0.02*	*5.42*	*0.03*	*5.18*	*0.03*
MEG/water								
298.11	27	9	3.69	-	2.16	-	1.52	-

[a] $\%\,AARD = 100 \cdot \frac{abs(P^{exp} - P^{calc})}{P^{exp}}$, *where P stands for bubble point pressure*

[b] $AAD = 100 \cdot abs(y_1^{exp} - y_1^{calc})$, where y_1 stands for vapor phase solubility of component 1.

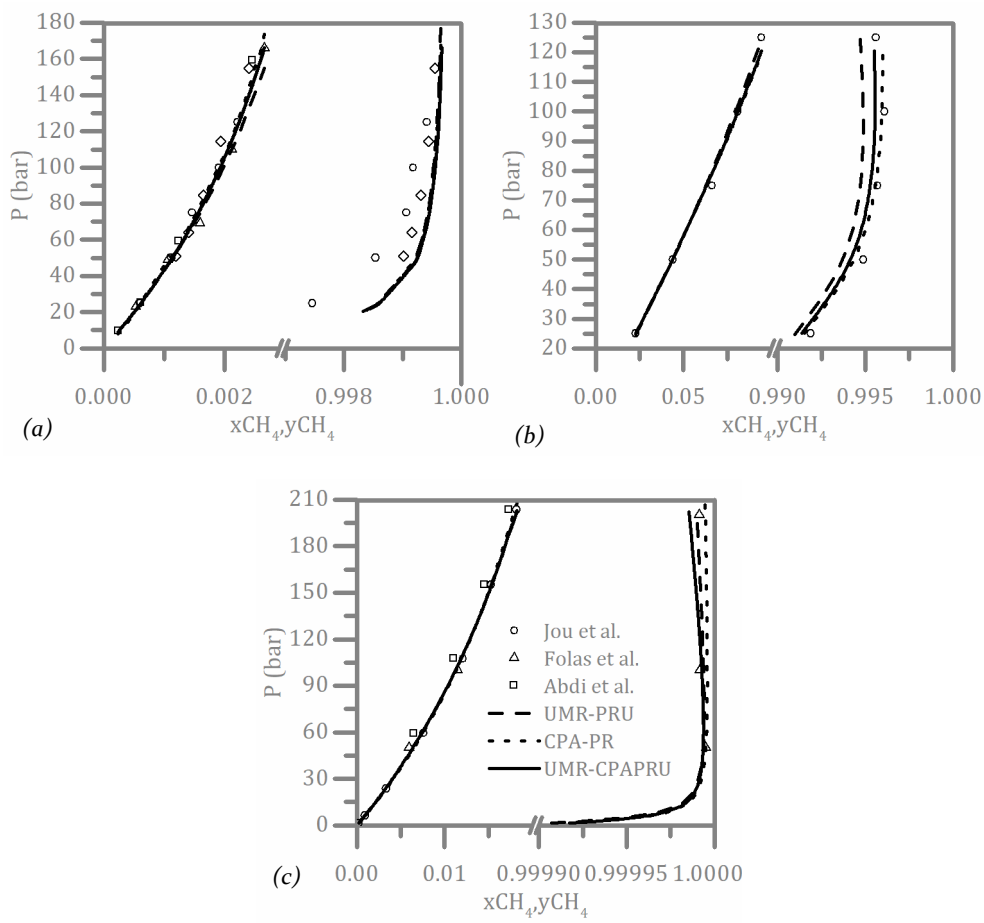

Figure 10.2: VLE correlation results at 298.15 K with UMR-PRU (dashed line), CPA-PR (dotted line) and UMR-CPAPRU (solid line). (a) methane/water, (b) methane/methanol and (c) methane/MEG. In (a) and (b) circles denote experimental data by Yarym – Agaev et al.[23], triangles by Kim et al.[24], squares by Chapoy et al.[28] and triangles by Frost et al.[26]. In (c) circles denote exp. data by Jou et al.[22], triangles by Folas et al.[29] and squares by Abdi et al.[30].

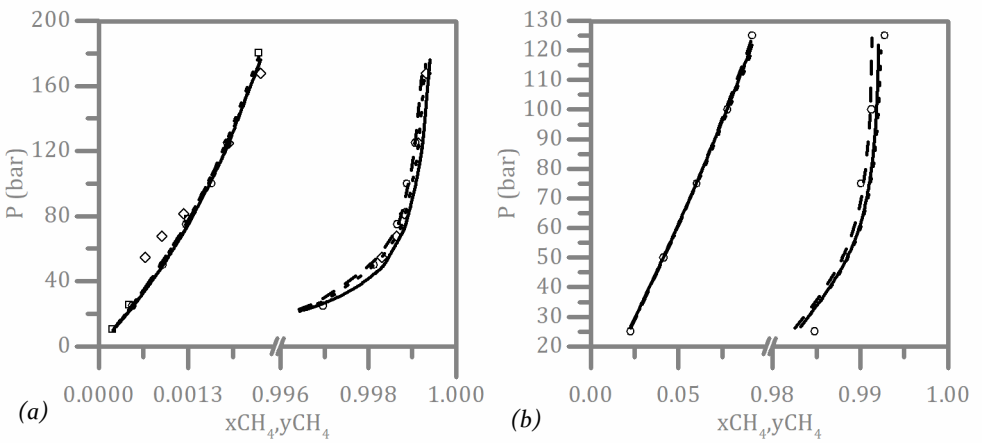

Figure 10.3: VLE correlation results at 313.15 K with UMR-PRU (dashed line), CPA-PR (dotted line) and UMR-CPAPRU (solid line). (a) methane/water, (b) methane/methanol and (d) methane/MEG. Circles denote experimental data by Yarym – Agaev et al.[23], squares by Chapoy et al.[28] and diamonds by Frost et al.[26].

The model is further evaluated in the prediction of two ternary mixtures of interest to natural gas processing, that is methane/methanol/water and methane/MEG/water. The results are presented in tabulated form in Table 10.4. The first observation is that the addition of the direct contribution for the associating effects between the components substantially improves the prediction of the methane solubility in liquid phase, where the hydrogen bonding effects are more pronounced. Actually, the model yields better prediction results compared to CPA-PR EoS proving thus that the mixing rules play quite an important role in the multicomponent mixtures prediction. In the vapor phase, the results are similar with those of the other two models.

Table 10.4: VLE ternary prediction results for mixtures containing methane (1), hydrate inhibitor (2) and water (3) with UMR-PRU, CPA-PR and UMR-CPAPRU.

Inhibitor	n_p	T (K)	P (bar)	% AARD[a] in x_1			% AARD[a] in y_2			% AARD[a] in y_3		
				UMR-PRU	CPA-PR	UMR-CPAPRU	UMR-PRU	CPA-PR	UMR-CPAPRU	UMR-PRU	CPA-PR	UMR-CPAPRU
CH_3OH	18	298.15	25 - 125	89.58	32.18	28.92	27.04	6.02	10.78	39.45	39.65	43.84
	18	313.15	25 - 125	81.04	29.55	18.33	25.65	12.75	13.55	11.91	15.02	24.16
MEG	9	298.15	50 - 200	19.73	20.80	19.97	41.55	16.21	35.54	19.44	22.25	20.22

[a] *% AARD is defined as:* $\%AARD = 100 \cdot \frac{abs(X_i^{exp} - X_i^{calc})}{X_i^{exp}}$, *where X stands for the solubility of component i in the liquid (x) or vapor phase (y)*

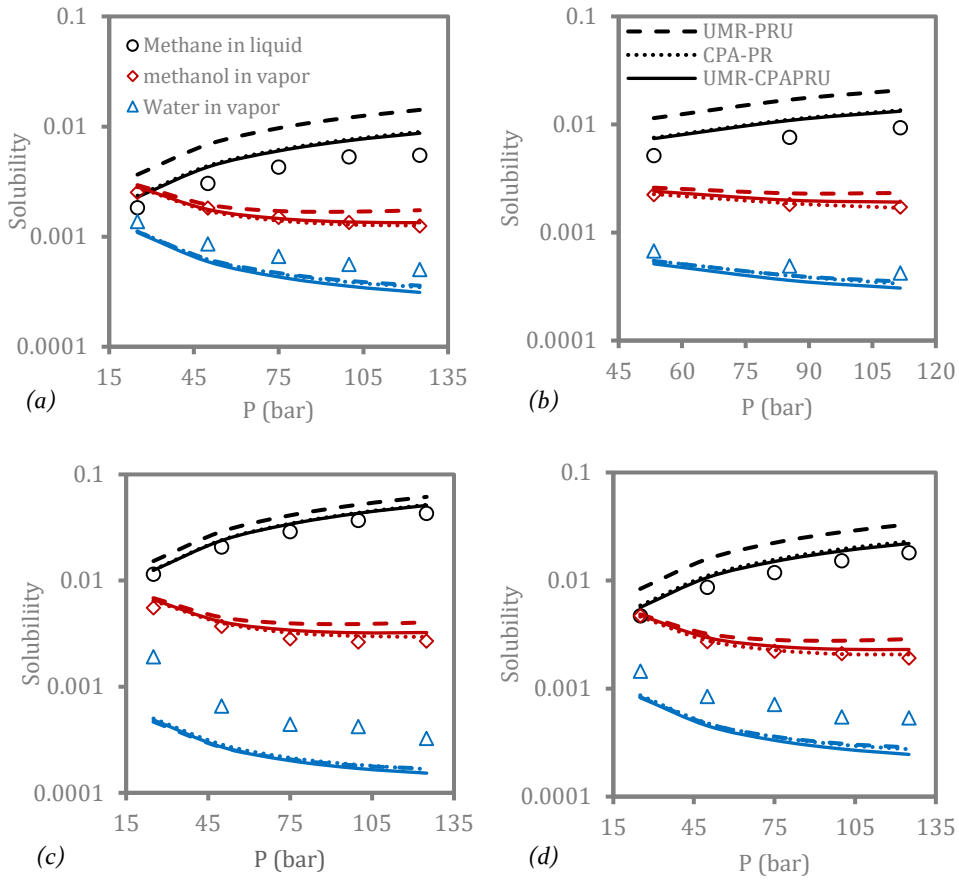

Figure 10.4: VLE prediction results for the methane/methanol/water mixture at 298.15 K with different concentrations of methanol in feed (% wt.) with UMR-PRU (dashed line), CPA-PR (dotted line) and UMR-CPAPRU (solid line). (a) 26 % methanol in liquid, (b) 42 % methanol in liquid, (c) 50 % methanol in liquid and (d) 75 % methanol in liquid. Exp. data by Sinyavskaya et al.[31] and Frost et al.[26]. Black circles denote methane solubility in liquid, red diamonds methanol in the vapor phase and blue triangles water in the vapor phase.

The performance of the models is better illustrated in Figure 10.4. It is apparent that the addition of the associating term improves the performance of the UMR-PRU in the prediction of the ternary mixture. The observed performance is similar with the one presented in the binary mixtures, e.g. for the solubility of methanol or water in the vapor phase. The improvement is more apparent in the prediction of the methane solubility in liquid phase. Due to the importance of this parameter in the NG industry, e.g. causing HC loss, a more subtle analysis of the effect of the percentage of the methanol in its solubility is presented in Figure 10.5.

As it has been discussed in Chapter 3 the hydrogen bonding effects is associating mixtures is not analogous to the concentration. As such, the advanced mixing rules help in better predicting the solubility of methane in polar phase with increasing methanol content, which can be attributed to the better prediction of the components distribution in the mixture.

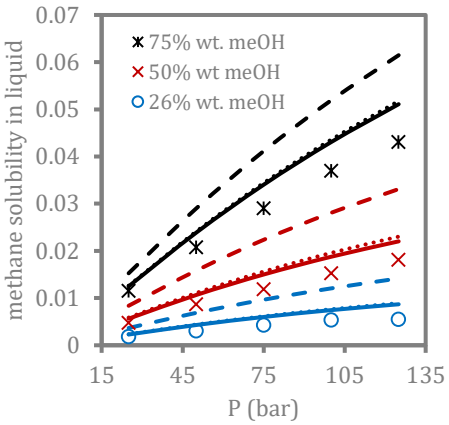

Figure 10.5: VLE prediction results for the methane solubility in liquid phase of the methane/ methanol/water mixture at 298.15 K, at different methanol concentrations in feed (% wt.) with UMR-PRU (dashed line), CPA-PR (dotted line) and UMR-CPAPRU (solid line). Exp. data by Sinyavskaya et al.[31]. Blue circles denote 26 % methanol, red ex (x) 50 % methanol and black stars 75 % methanol in feed.

The good predictive behavior of the model is more apparent in Figure 10.6 at the temperature of 313.15 K. Here, the effect of mixing rules is more pronounced, since the associating forces are less important due to the higher temperature.

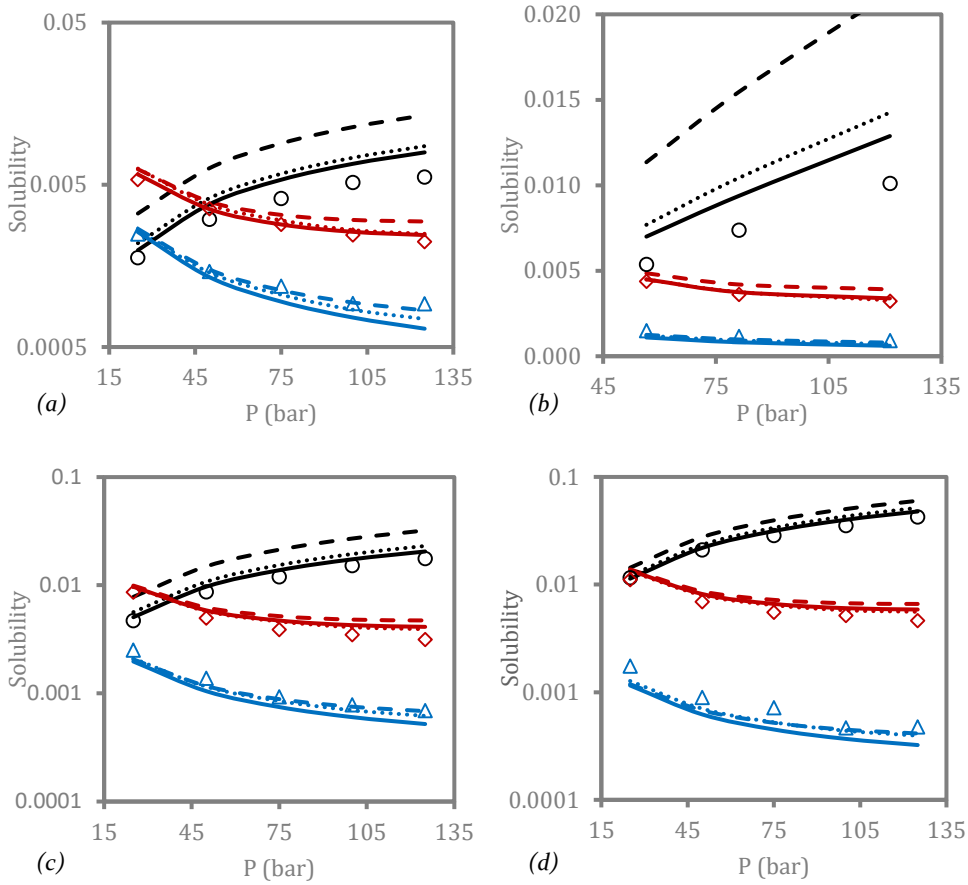

Figure 10.6: VLE prediction results for the methane/methanol/water mixture at 313.15 K with different concentrations of methanol in feed (% wt.) with UMR-PRU (dashed line), CPA-PR (dotted line) and UMR-CPAPRU (solid line). (a) 26 % methanol in liquid, (b) 42 % methanol in liquid, (c) 50 % methanol in liquid and (d) 75 % methanol in liquid. Exp. data by Sinyavskaya et al.[31] and Frost et al.[26]. Black circles denote methane solubility in liquid, red diamonds methanol in the vapor phase and blue triangles water in the vapor phase.

Figure 10.7*a* shows that improved results over the UMR-PRU and CPA-PR are obtained with the new model for the methane solubility in the polar phase of the methane/ MEG/water ternary at the data of Folas et al.[29] with about 27 % molar MEG in feed. The water solubility in vapor phase is similarly predicted with all models, while for MEG in vapor phase CPA-PR predicts lower solubility. The performance of the model has been also tested against newly available experimental data which differ significantly in the MEG content and it is shown that good prediction is observed for both phases.

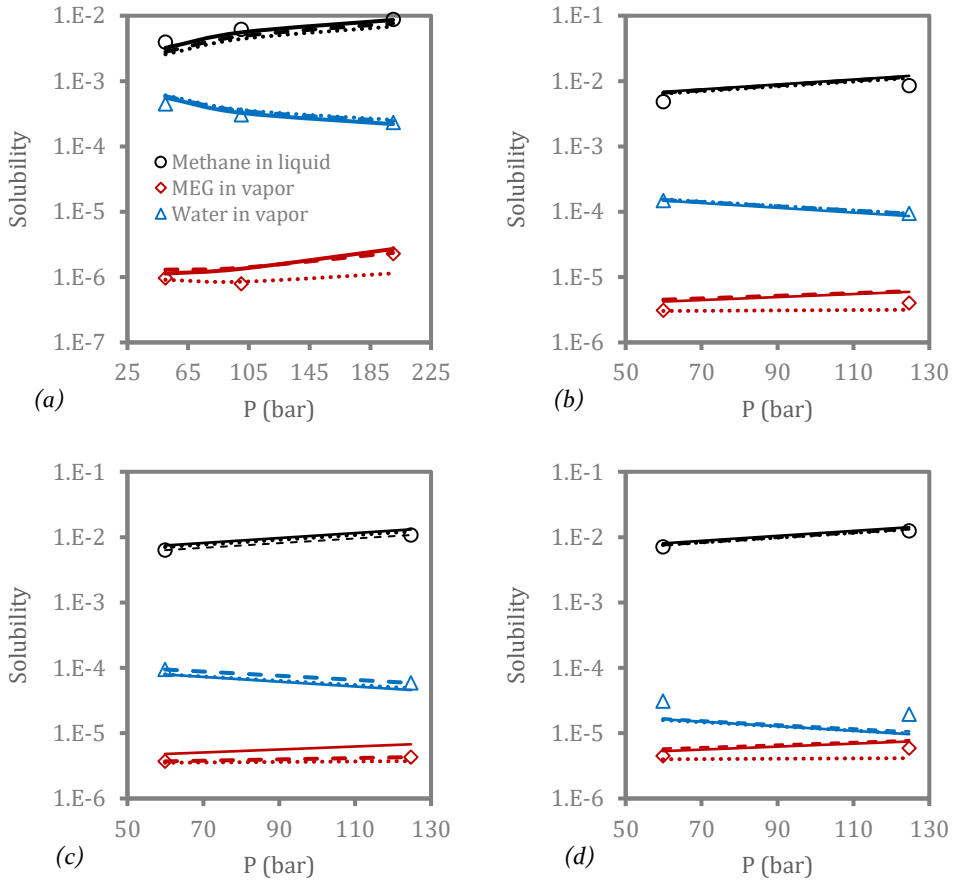

Figure 10.7: VLE prediction results for the methane/MEG/water mixture at 298.15 K. with UMR-PRU (dashed line), CPA-PR (dotted line) and UMR-CPAPRU (solid line) at different concentrations of MEG in the feed (% molar). Blue circles denote methane solubility in liquid phase, red diamonds MEG solubility in vapor phase and blue triangles water solubility in vapor phase. (a) 19 % MEG, Experimental data by Folas et al.[29], (b) 46 %, (c) 47 % and (d) 56 %. Exp. data by Kruger et al.[32].

10.5. Development of a group-contribution EoS for associating mixtures

In order to develop UMR-CPAPRU as a group – contribution model, the UNIFAC interaction parameters for the pairs of groups encountered at the associating compounds should be re-estimated. The parameters are fitted to binary VLE data, using the objective function of eq. 7.3, where *X* stands for the bubble point pressure. The fitting of the interaction parameters of the groups comprising the hydrocarbons, namely CH_2, ACH, $ACCH_3$, with water, have been performed in binary LLE data and therefore *X* stands for the component solubility in the indicated phase. The database used for the fitting of the model IPs is given in Appendix C. On the other hand, for the non-associating compounds, the UNIFAC interaction parameters are those of UMR-PRU. The UMR-PRU interaction parameters table used are given in Appendix D.

The obtained IPs following the temperature dependency of eq. 5.19 are presented in Table 10.5. The overall VLE correlation results are given in Table 10.6. It is apparent that UMR-CPAPRU systematically improves the description of the mixtures, especially in the liquid phase compared to UMR-PRU. Only in the case of CO_2/water higher deviations are obtained, which are attributed to the characterization of CO_2 as a non-associating component. The latter is more pronounced in the high-pressure areas. In some cases, such as in MEG/water or ethane/methanol slightly higher deviations are obtained for the vapor phase compared to UMR-PRU. Nevertheless, they are accompanied with better description of the solubility in the liquid phase.

Table 10.5: Binary interaction parameters for the UMR-CPAPRU model.

n	*m*	A_{nm} (K)	B_{nm} (-)	C_{nm} (K^{-1})	A_{mn} (K)	B_{mn} (-)	C_{mn} (K^{-1})
H_2O	N_2	375.03	1.6093	-0.007570	98.92	6.4493	-0.009140
H_2O	CO_2	-134.74	0.9181	-0.011314	39.01	1.8180	-0.012960
H_2O	CH_4	591.80	1.2384	-0.001460	-200.97	1.2853	-0.007200
H_2O	C_2H_6	187.19	1.2643	-0.000110	75.87	0.6388	-0.006380
H_2O	CH_2	861.67	7.4712	-0.015720	-349.97	-2.0491	0
H_2O	ACH	-445.61	-0.6209	0.001125	442.06	-0.4041	-0.010560
H_2O	ACCH	-143.74	1.1636	-0.008650	228.78	-0.0917	-0.008800
H_2O	CH_3OH	136.21	-1.7805	0.000470	-260.36	1.1292	-0.000170
H_2O	etOH	-327.19	0.6783	-0.001580	349.59	-2.4685	0.003013
H_2O	MEG	215.63	0.6410	0.003353	-333.90	-0.5157	-0.006040
N_2	CH_3OH	13.27	-0.1784	0.002093	329.12	0.3627	-0.005710
CO_2	CH_3OH	-105.93	-1.0346	-0.001049	176.29	0.5964	-0.004570
CH_4	CH_3OH	-40.84	1.0010	0.002986	216.90	-1.0384	0.002502
C_2H_6	CH_3OH	-129.90	-1.1711	0	343.75	2.3921	0
CH_2	CH_3OH	-34.04	-0.3036	0.000544	143.71	0.53687	-0.000920
ACH	CH_3OH	84.78	0.2964	-0.00031	-111.30	-0.4209	-0.000003
ACCH	CH_3OH	210.04	-2.0740	0	-69.35	3.1709	0
N_2	MEG	-181.28	18.6784	0	600.93	-3.5128	0
CH_4	MEG	-51.47	-0.2313	0.009044	491.90	1.4198	-0.021290
C_2H_6	MEG	6.59	-0.7615	0	322.04	0.9744	0

Table 10.6: VLE binary correlation results with the UMR-CPAPRU model. Comparison with UMR-PRU is given

System	n_p	T range (K)	P range (bar)	% AARD[a] in P		100·AAD[b] in y_1	
				UMR-PRU	UMR-CPAPRU	UMR-PRU	UMR-CPAPRU
Water (2) with							
N_2	31	283.15 - 513.15	5 - 1013.3	3.78	5.3	–	–
CO_2	87	278.22 - 598.15	3.3 - 1500.0	13.9	17.59	1.75	1.29
CH_4	221	274.19 - 603.20	1.0 - 1029.7	10.3	9.15	0.94	0.63
C_2H_6	64	274.26- 444.26	3.7 - 137.9	7.81	6.10	–	–
meOH	158	298.14 - 523.15	0.0- 84.0	3.73	1.86	1.43	0.73
MEG	169	298.03 - 395.15	0.0 - 1.5	3.17	2.28	0.73	0.94
etOH	368	273.15 - 623.15	0.0 - 189.7	8.6	2.37	2.87	2.52
Methanol (2) with							
N_2	45	213.15 - 343.15	1.0 - 1000	11.27	9.04	0.23	0.23
CO_2	151	230.01 - 477.6	4.4 - 165	8.17	3.58	1.47	1.11
CH_4	126	273.15 - 373.15	10.5 - 1066	20.99	6.42	0.44	0.17
C_2H_6	37	273.15 - 373.15	9.6 - 60.8	8.12	8.78	2.06	3.01
C3	80	310.7 - 474.3	0.3 - 86.6	14.37	7.11	2.32	1.26

Table 10.6 (continued)

System	n_p	T range (K)	P range (bar)	% AARD[a] in P		100·AAD[b] in y_1	
				UMR-PRU	UMR-CPAPRU	UMR-PRU	UMR-CPAPRU
Methanol (2) with							
nC5	57	303.15 - 422.6	0.2 - 25.3	6.94	2.64	1.81	1.95
nC6	34	298.15 - 318.15	0.3 - 0.84	11.14	2.45	8.15	3.97
benzene	166	288.15 - 493.11	0.1 - 7.6	6.11	2.22	1.81	1.48
toluene	63	313.15 - 383.72	0.1 - 1.0	5.41	1.92	5.22	1.89
MEG (2) with							
N_2	31	323.15 - 398.15	15.7 - 396	9.39	10.08	–	–
CH_4	79	298.15 - 423.15	1.1 - 396.2	7.72	7.28	–	–
C_2H_6	34	298.15 - 398.15	0.8 - 203.4	3.19	7.56	–	–

[a] $\% AARD = 100 \cdot \frac{abs(P^{exp} - P^{calc})}{P^{exp}}$, where P stands for bubble point pressure

[b] $100 \cdot AAD = 100 \cdot abs(y_1^{exp} - y_1^{calc})$, where y_1 is the vapor phase composition

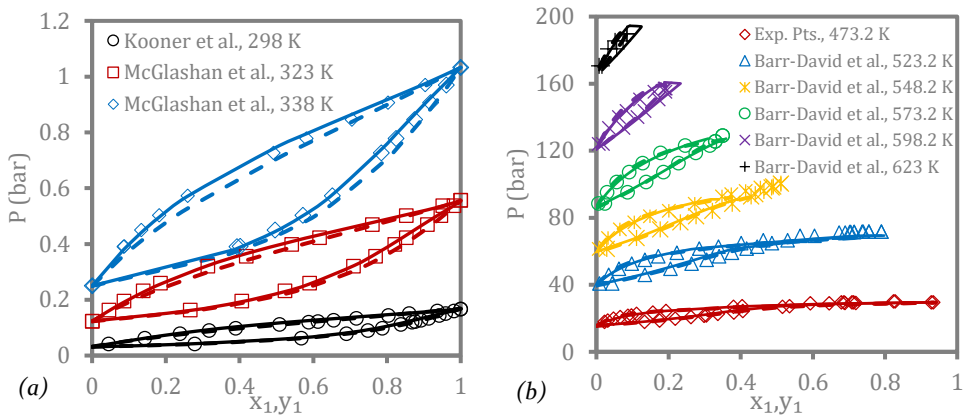

Figure 10.8: VLE correlation results with UMR-CPAPRU (solid line). Prediction with UMR-PRU model using the UNIFAC VLE 2 coeff. parameters is also presented (dashed line). (a) methanol/water. Black circles denote exp. data by Koner et al.[20] at 298 K, red squares at 323 K by McGlashan et al.[33] and blue diamonds at 338 K by McGlashan et al.[33] and (b) ethanol/water. Red diamonds denote exp. data by Niesen et al.[34] and Barr – David et al.[35] at 373 K, blue diamonds at 523.2 K, yellow stars at 548.2 K, green circles at 573.2 K, purple ex at 598.2 K and black cross at 623.2 K. Exp. data by Barr – David et al.[35]

Very satisfactory correlation results are obtained for alcohols with water at a wide range of temperatures. As indicated by Figure 10.8*b* for ethanol/water mixture very good results are obtained even at the proximity to the critical temperature. The correlation of the model is good both at low and high pressure.

Apart from the very good results in terms of deviations, UMR-CPAPRU correlates satisfactorily the homoazeotrope encountered at the hydrocarbon/methanol mixtures, showing good agreement at both the azeotrope pressure and composition. That is illustrated in Figure 10.9 which demonstrates some representative results of the VLE of binary mixtures of CO_2 and hydrocarbons with methanol. Also, good description of the dependence of the pressure and composition with temperature is observed. On the other hand, UMR-PRU qualitatively predicts the behavior of the mixtures, but it systematically overpredicts somehow the bubble point pressure. Furthermore, at the higher presented isotherm of benzene/methanol mixture (Figure 10.9*b*) at low methanol concentrations UMR-PRU predicts an heteroazeotrope formation which is not experimentally observed, as it is indicated by the formation of a maximum in the bubble point pressure.

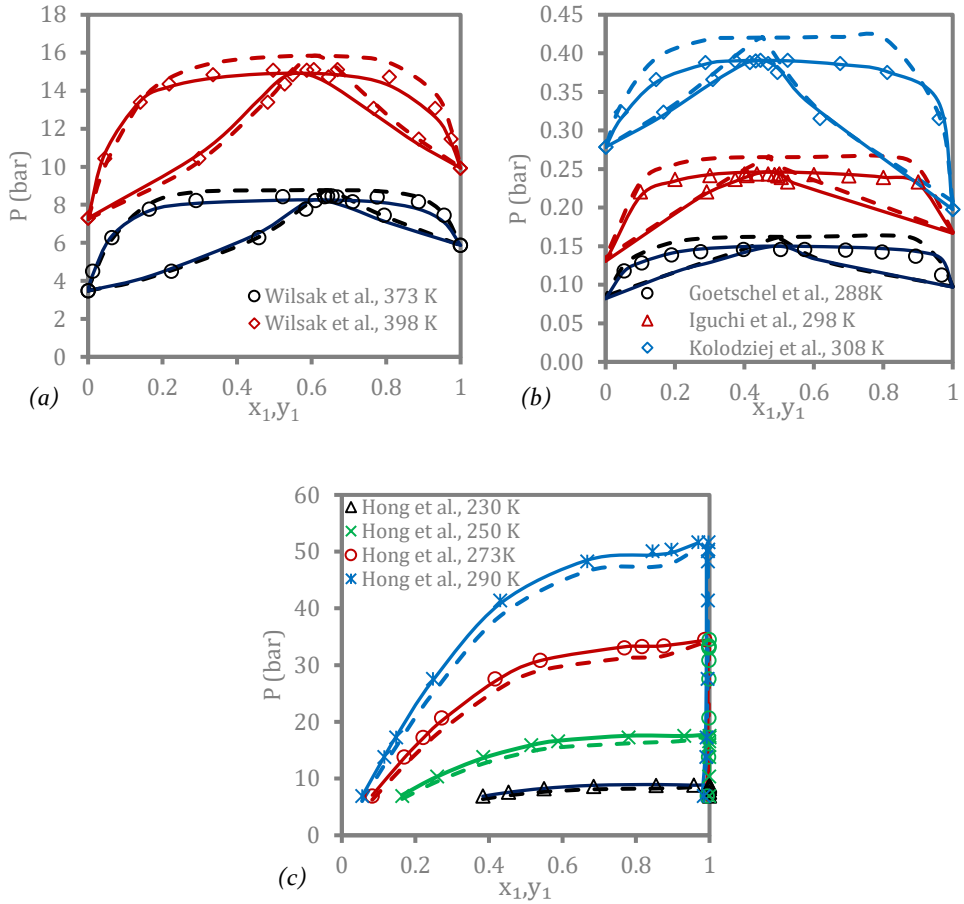

Figure 10.9: VLE correlation results with UMR-CPAPRU model (solid line). Prediction with UMR-PRU (dashed line) is also presented. (a) n-pentane/methanol. Experimental data by Wilsak et al.[36] black circles denote 373 K, red diamonds 398 K, (b) benzene/methanol. Black circles denote exp. data by Goetschel et al.[37] at 288 K, red triangles by Iguchi et al.[38] at 298 K and blue diamonds by Kolodziej et al.[39] at 308 K. and (c) CO_2/methanol. Experimental data by Hong et al.[40], Black triangles denote 230 K, green ex 250 K, red circles 273 K and blue stars 290 K.

Table 10.7: LLE results with the UMR-PRU and the UMR-CPAPRU.

System	n_p	T range (K)	P range (bar)	%AARD[a] in x_1^I		%AARD[a] in x_2^{II}	
				UMR-PRU	UMR-CPAPRU	UMR-PRU	UMR-CPAPRU
Water (2) with							
nC3[b]	10	278.87 - 360.93	5.7 - 37.1	133.60	38.44	85.71	31.62
nC4	12	278.65 - 510.95	2.8 - 120.7	69.27	32.79	102.06	59.29
nC5	15	273.15 - 625.19	0.3 - 283.7	103.86	38.99	42.48	12.15
nC6	9	298.15 - 473.15	0.2 - 35.2	49.60	12.08	25.75	15.56
nC7	15	293.15 - 443.75	0.1 – 7.0	67.69	44.28	32.21	57.20
nC8	9	298.15 - 498.15	0.1 - 36.7	24.34	38.66	6.54	37.79
nC9	7	288.15 - 409.72	1.0	46.27	47.93	279.33	161.62
nC10	9	296.15 – 593.00	1.0 – 200.0	83.90	137.64	18.21	34.44
cyC6	17	278.26 - 482.17	0.2 - 17.2	48.71	66.09	16.75	36.02
iC4	12	280.15 - 363.19	3.5 - 16.4	10.90	34.42	106.47	53.68
iC5	8	273.10 - 333.12	1.0	48.42	25.30	11.65	17.19
benzene	21	279.15 - 490.8	0.1 - 41.9	5.11	28.26	2.68	10.13
toluene	19	283.15 - 473.51	0.0 - 137.9	11.69	16.78	5.42	53.51
methanol (2) with							
nC6	8	298.15 - 323.15	1.0	283.72	267.75	564.61	566.11
nC7	8	298.15 - 333.15	–	0.79	1.22	7.30	8.55
nC8	8	298.15 - 333.15	–	90.47	6.15	97.46	17.88
nC9	8	298.15 - 333.15	–	90.99	4.00	98.09	17.17
nC10	8	298.15 - 333.15	–	9.98	8.02	17.89	18.06

[a] *% ΔX is defined as:* $\%\Delta X = 100 \cdot \frac{abs(X_i^{exp} - X_i^{calc})}{X_i^{exp}}$, *where X stands for liquid phase solubility (x_i) of the component i, or the vapor phase composition, y_i. (I) denotes the polar phase and (II) the HC-rich phase.*

[b] The deviation of the water solubility in vapor phase (% Δy_2) is 13.1 for UMR-PRU and 5.3 for UMR-CPAPRU.

Table 10.7 presents the LLE results with UMR-CPAPRU and UMR-PRU. The interaction parameters for alkanes with water of UMR-CPAPRU have been fitted only to the n-hexane/water binary. Exceptions are n-decane, cyclohexane and aromatic compounds where higher deviations as compared to UMR-PRU are encountered. The situation with cyclohexane can be handled by adding a specific methyl group for the *cyclo-* compounds[41], while for the case of aromatic hydrocarbons solvating effects should be considered due to the π-valence of the aromatic ring. The latter is of importance for the accurate description of the LLE of aromatic/water mixtures, as it is shown by Folas et al.[42]. Some representative results of hydrocarbons with water are illustrated in Table 10.7.

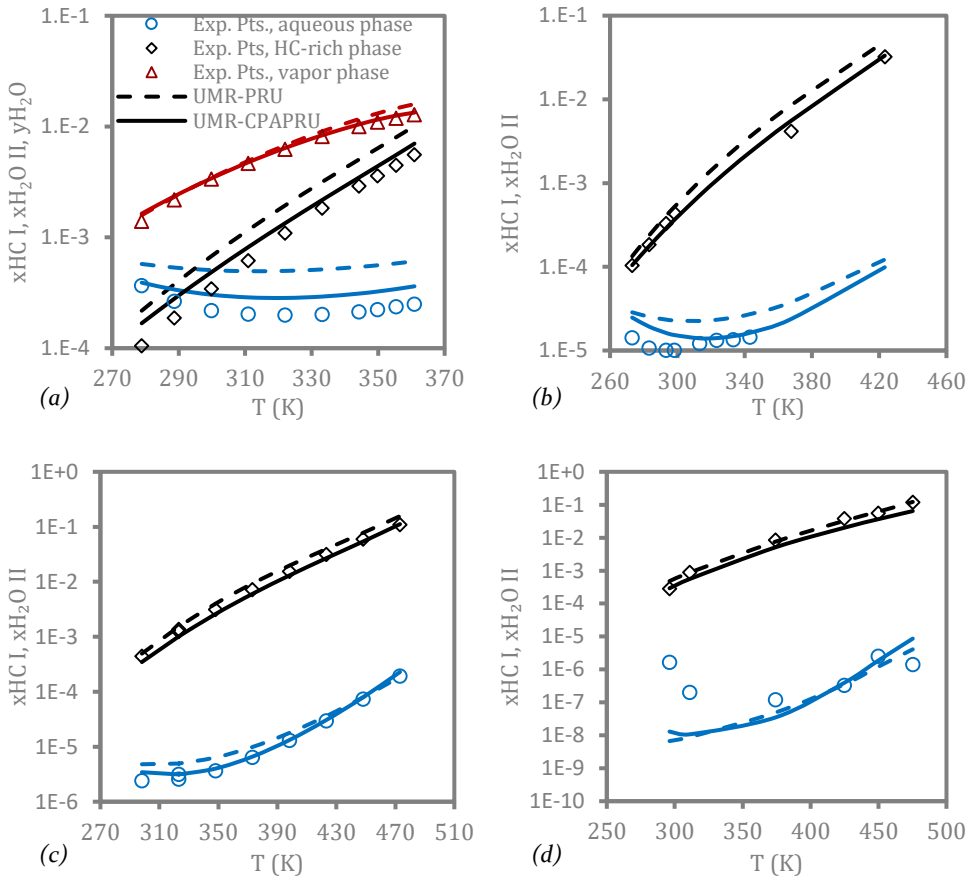

Figure 10.10: LLE prediction results of HCs with water with the UMR-CPAPRU and the UMR-PRU. Blue circles denote HC solubility in aqueous phase, black diamonds water solubility in HC-rich phase and red diamonds water solubility in vapor phase. (a) propane/water, exp. data by Kobayashi et al.[43]. (b) n-pentane/water, exp. data by Black et al.[44] , Polak et al.[45] (c) n-hexane/water, exp. data by Tsonopoulos et al.[46], (d) n-decane/water, exp. data by Revellame et al.[47], Ng et al.[48] and Economou et al.[49], (e) cyclohexane/water, exp. data by Burd et al.[50], Guseva et al.[51], Pereda et al.[52], Marche et al.[53], Pierotti et al.[54], Goldman et al.[55] and Tsonopoulos et al.[46], (f) i-pentane/water, exp data by Black et al. [76], Polak et al. [79] and Pavlova et al. [93], (g) benzene/water, exp. data by Tsonopoulos et al.[46] and (h) toluene/water, exp data by Marche et al.[53], Ng et al.[48] and Jou et al.[56]
.

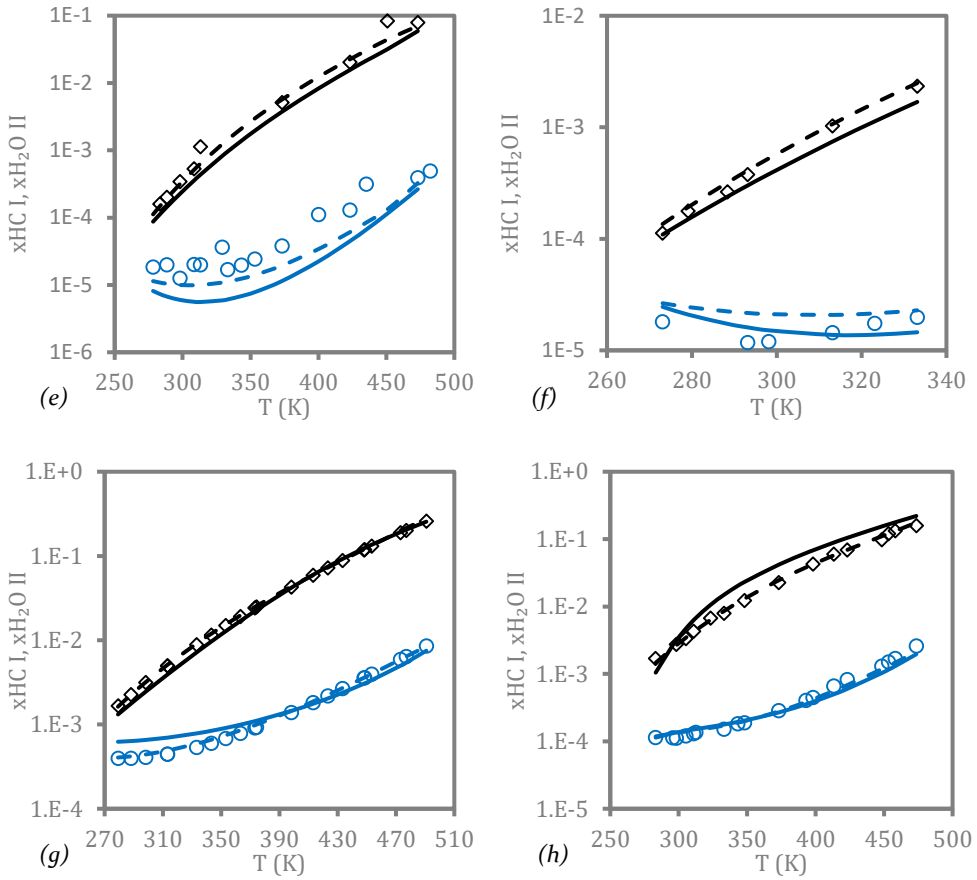

Figure 10.10 (continued)

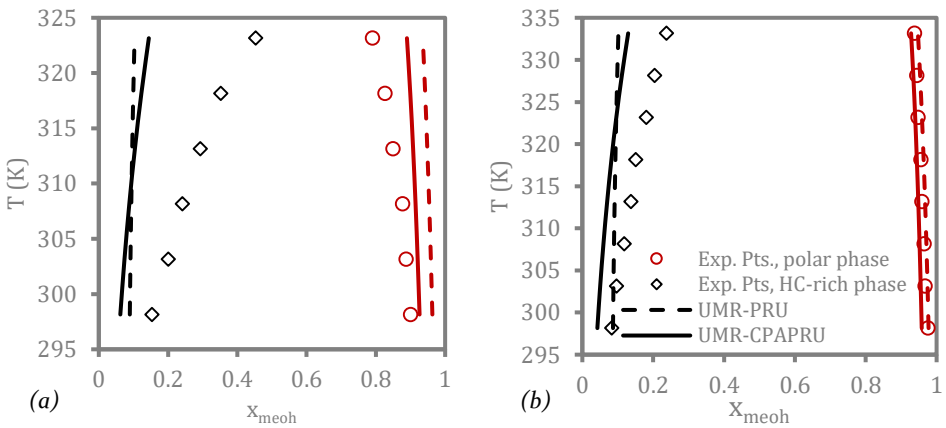

Figure 10.11: LLE prediction results of HCs with methanol with UMR-CPAPRU (solid line) and UMR-PRU (dashed line). red circles denote the polar phase while black diamonds the HC-rich one. (a) n-hexane/methanol, exp. data by Higashiuchi et al.[57] and (b) n-heptane/methanol, exp. data by Higashiuchi et al.[58].

10.6. Prediction results

The model is then evaluated in the prediction of multicomponent mixtures. In the first part, ternary mixtures of methanol and water with a hydrocarbon are considered, while in the second the dew point curves of natural gas and their mixtures with water and methanol.

10.6.1. Ternary mixtures prediction results

The LLE of three ternary mixtures is examined, namely propane/water/methanol, n-butane/water/methanol and benzene/water/methanol. The prediction results for propane/water/methanol are illustrated in Figure 10.12 where it is shown that UMR-CPAPRU has an advantage over UMR-PRU in the prediction of methanol partition coefficients in both examined temperatures.

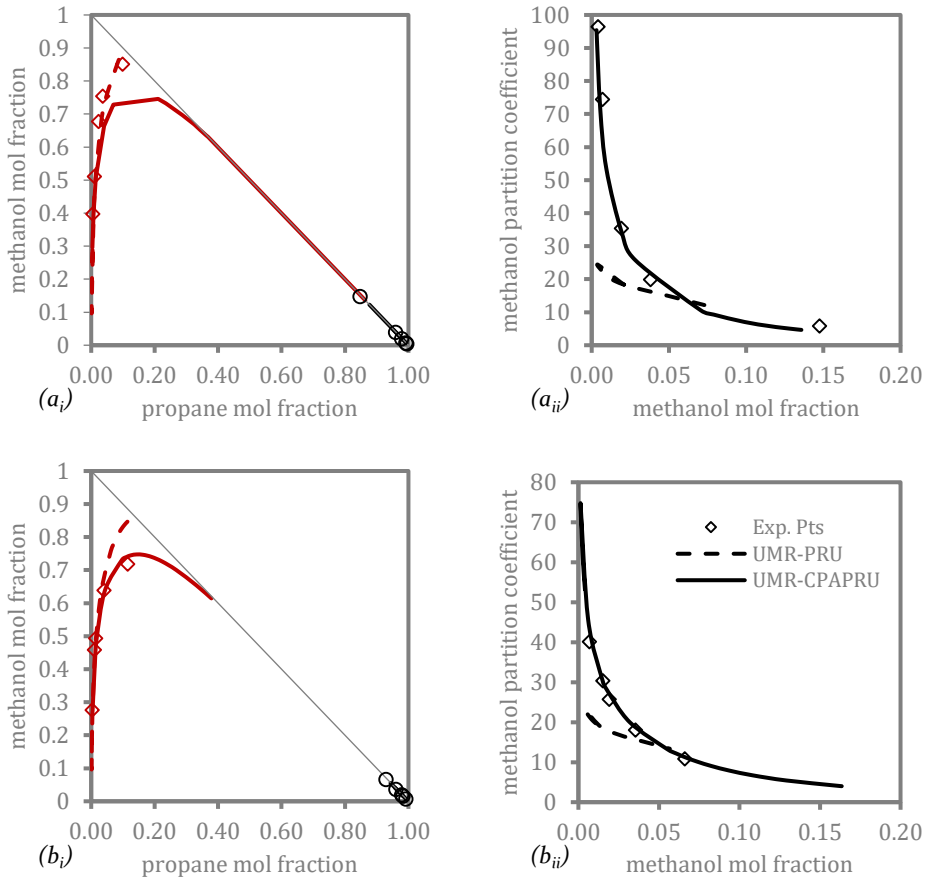

Figure 10.12: LLE prediction results for the propane/water/methanol mixture with UMR-PRU (dashed line) and UMR-CPAPRU (solid line) at (a) 273.15 K and (b) 293.15 K. Red colour indicates the polar phase while black the HC-rich one. (i) solubility and (ii) methanol partition coefficient. Exp. data by Noda et al.[59]

At 293 K, UMR-CPAPRU captures very well the solubilities in both phases. Instead, at 273 K UMR-PRU better predicts the experimental data. It is of interest to note that the relative prediction of the models is similar, that is, UMR-PRU predicts a rather less ideal solution compared to UMR-CPAPRU.

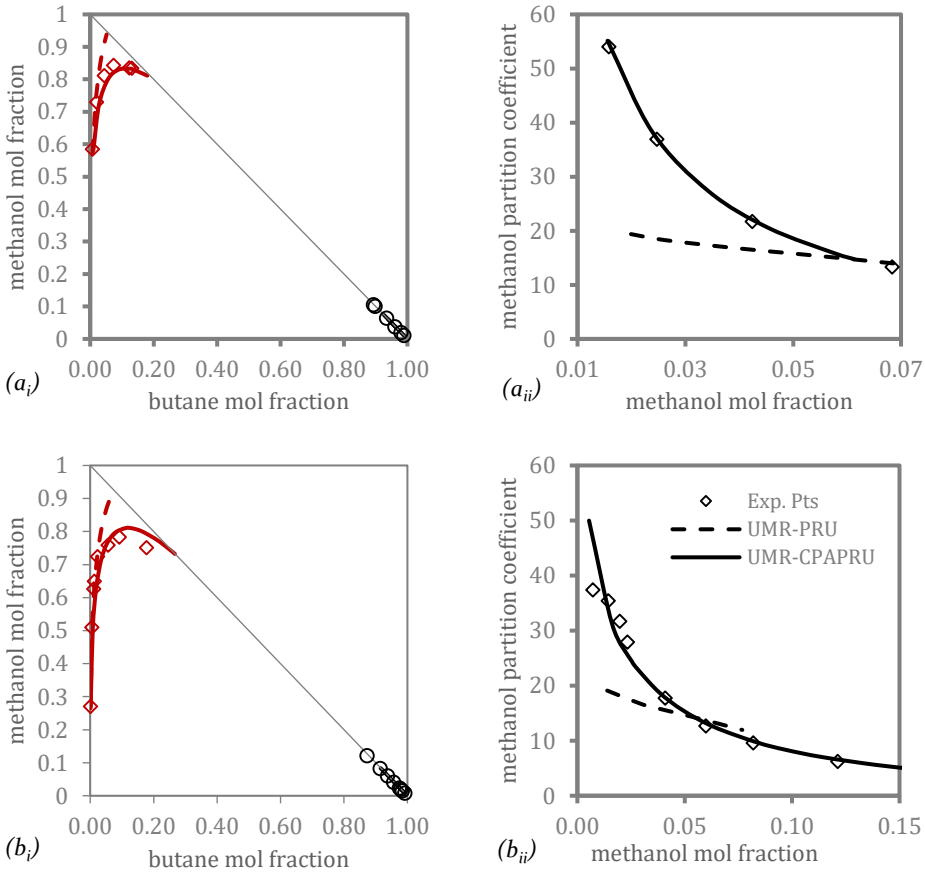

Figure 10.13: LLE prediction results for the n-butane/water/methanol mixture with UMR-PRU (dashed line) and UMR-CPAPRU (solid line) at (a) 273.15 K and (b) 293.15 K. Red colour indicates the polar phase while black the HC-rich one. (i) solubility and (ii) methanol partition coefficient. Exp. data by Noda et al.[59]

For the n-butane/water/methanol mixture (Figure 10.13) it is observed that UMR-CPAPRU better predicts the solubilities and methanol partition coefficient in both examined temperatures.

In the case of benzene/water/methanol mixture (Figure 10.14) similar relative performance of the models is observed. UMR-PRU overestimates the solubilities in both phases, while UMR-CPAPRU underestimates it. If the methanol partition coefficients are examined, it is observed that for higher methanol content, UMR-CPAPRU yields quite accurate results. Instead, for low methanol content, opposite prediction compared to the experimental one is obtained. Furthermore, it fails to

predict the turning slope of the partition coefficient for low methanol concentrations. This performance, can be attributed to the rather worse performance of the model in the benzene/water binary as compared to the mixtures with alkanes.

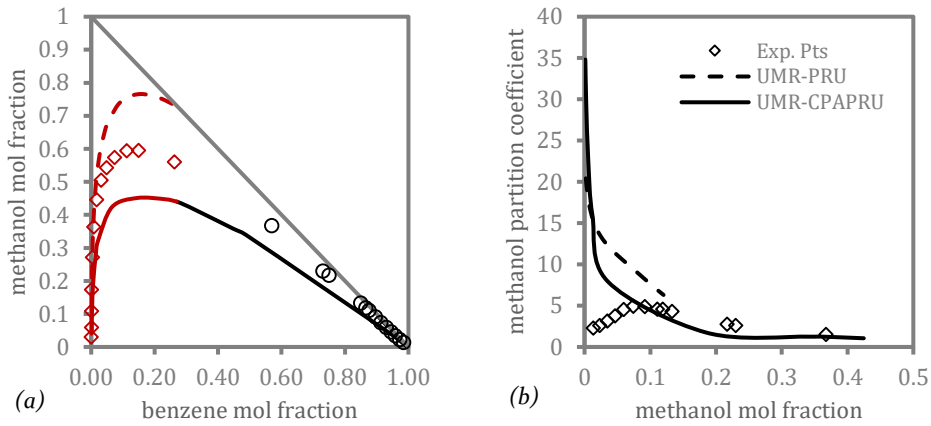

Figure 10.14: LLE prediction results for benzene/water/methanol mixture at 303.15 K with UMR-PRU (dashed line) and UMR-CPAPRU (solid line). Red colour indicates the polar phase while black the HC-rich one. (a) solubility and (b) methanol partition coefficient. Exp. data by Udovenko et al.[60]

10.6.2. Dew point prediction of SNG mixtures

In this section the performance of UMR-CPAPRU is evaluated in the prediction of the dew points of SNG mixtures with water and methanol. The database used for the evaluation is shown on Table 9.7, while the detailed results are presented in Table 10.8. For UMR-PRU, the temperature dependent parameters of Table 5.4 are used, while for CPA-PR the ones of Section 9.5.2.a. For the dry gases, UMR-CPAPRU reverts to UMR-PRfit and the required interaction parameters are those presented in Appendix D. It is observed that the addition of Wertheim's term improves the dew point predictions of SNG mixtures containing water and methanol. The new model performs similarly or in some cases better as compared to CPA-PR, as it is illustrated in Figure 10.15. Note that PR-fit yields worse dew point predictions for the dry gases than the other models. As such, the improvement of this behavior is expected to lead to even better results in the dew point prediction of natural gases in the presence of water and methanol.

Table 10.8: Dew point temperature (DPT) predictions of SNGs and their mixtures with water and methanol, with UMR-CPAPRU, UMR-PRU and CPA-PR.

Gas	Ref.	n_p	T (K)	P (bar)	AAD in T[a] (K)		
					UMR-CPAPRU	UMR-PRU	CPA-PR
SNG 1 (dry)	61	17	205.8 - 229.1	2.5 - 69.7	1.76	1.86	1.55
0.003 % H_2O	62	15	230.5 - 264.2	2.9 - 71.1	9.99	10.20	9.64
0.009 % H_2O	62	15	236.3 - 273.9	1.8 - 71.1	5.90	6.19	5.79
0.010 % H_2O + 0.07 % meOH	61	15	238.7 - 278.6	2.1 - 71.1	1.23	2.96	1.40
0.009 % H_2O + 0.17 % meOH	61	15	240.9 - 283.9	1.7 - 72.1	0.44	2.60	0.64
SNG 2 (dry)	63	15	200.3 - 226.9	5.4 - 66.7	1.42	1.07	1.02
0.002 % H_2O	64	15	225.8 - 258.5	2.3 - 73.2	8.91	9.26	8.47
0.006 % H_2O + 0.12 % meOH	63	15	242.3 - 277.1	3.1 - 71.7	0.77	2.64	1.86
0.027 % H_2O + 0.10 % meOH	63	17	242.0 - 282.6	1.4 - 34.9	0.97	1.51	1.61
SNG 3 (dry)	63	19	202.9 - 237.7	2.9 - 71.2	2.92	1.64	0.67
0.006 % H_2O	64	15	237.0 - 270.2	2.6 - 71.8	7.35	7.65	7.03
0.010 % H_2O + 0.06 % meOH	63	14	241.9 - 276.2	3.2 - 63.4	1.07	2.49	0.96
SNG 4 (dry)	63	22	199.9 - 240.8	2.3 - 77.7	1.43	1.34	1.25
0.003 % H_2O	64	15	228.7 - 263.8	2.3 - 70.0	8.69	9.23	8.20
0.006 % H_2O	64	15	231.1 - 270.1	2.2 - 71.6	6.66	7.24	6.35
0.003 % H_2O + 0.16 % meOH	63	15	236.4 - 277.6	1.7 - 71.9	0.68	3.28	1.46
0.004 % H_2O + 0.22 % meOH	63	15	243.3 - 284.1	2.2 - 72.2	0.35	3.66	0.81
SNG 5 (dry)	63	14	203.4 - 218.9	4.7 - 58.4	0.93	1.33	0.80
0.002 % H_2O	64	15	224.3 - 258.7	2.1 - 68.4	10.21	9.69	9.61
0.010 % H_2O + 0.15 % meOH	63	15	244.7 - 283.3	2.6 - 70.9	0.50	1.73	0.63
0.006 % H_2O + 0.31 % meOH	63	17	246.3 - 283.2	2.1 - 35	1.88	1.58	2.24
SNG 6 (dry)	65	48	213.6 - 252.2	1.2 - 34.0	1.78	0.79	1.49
0.035 % H_2O	65	23	246.1 - 288.1	1.1 - 40.9	6.11	6.69	6.63
0.173 % H_2O	65	8	261.3 - 277.9	1.5 - 5.0	0.61	0.74	0.85
0.023 % H_2O + 0.45 % meOH	65	13	248.1 - 288.6	1.1 - 20.5	1.46	1.61	1.62
0.042 % H_2O + 0.34 % meOH	65	16	249.0 - 288.2	1.2 -20.7	1.54	1.62	1.92
SNG 7 (dry)	65	47	217.9 - 261.4	1.2 - 81.8	1.71	7.65	1.67
0.040 % H_2O	65	26	244.7 - 288.0	1.1 - 41.0	3.08	3.16	3.35
0.155 % H_2O	65	9	256.9 - 278.1	1.1 - 5.3	0.91	0.51	1.26
0.048 % H_2O + 0.44 % meOH	65	21	247.6 -288.2	1.1 - 20.2	1.60	1.77	1.67
0.088 % H_2O + 0.24 % meOH	65	17	248.7 -288.1	1.1 - 20.6	3.47	3.30	2.95
Overall							
dry SNG's[b]		182			1.02	1.47	0.76
SNGs with H_2O		171			6.43	6.66	6.34
SNGs with H_2O and meOH		205			1.26	2.34	1.55

[a] AAD= $\left|T^{exp} - T^{calc}\right|$, exp: experimental, calc: calculated

[b] total rejected points at dry gases; UMR-CPAPRU: 29, UMR-PRU: 12 and CPA-PR: 19.

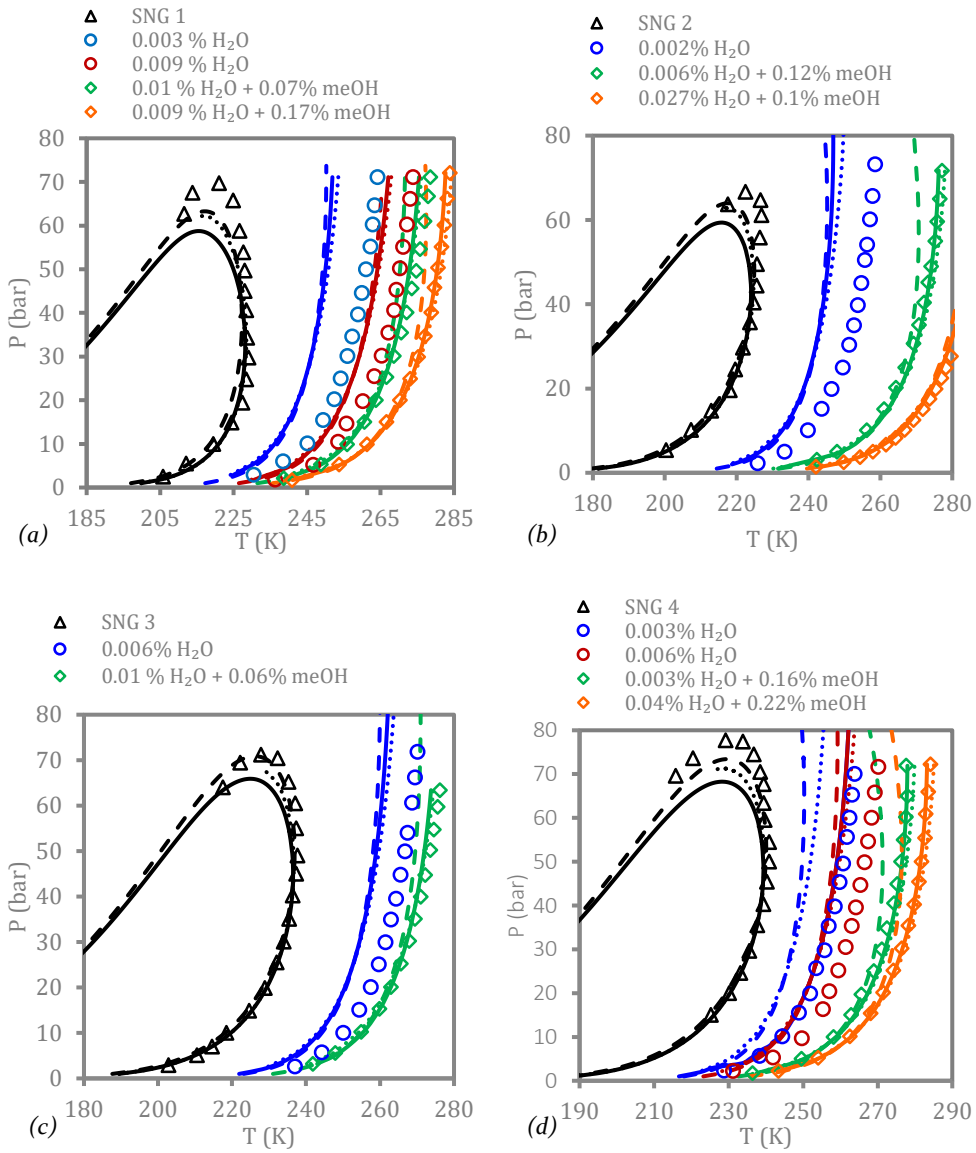

Figure 10.15: Dew point prediction results of synthetic natural gases and their mixtures with water and methanol, with UMR-CPAPRU (solid line), UMR-PRU (dashed line) and CPA-PR (dotted line). Experimental data by Avila et al.[61-64] and Jarne et al.[65]

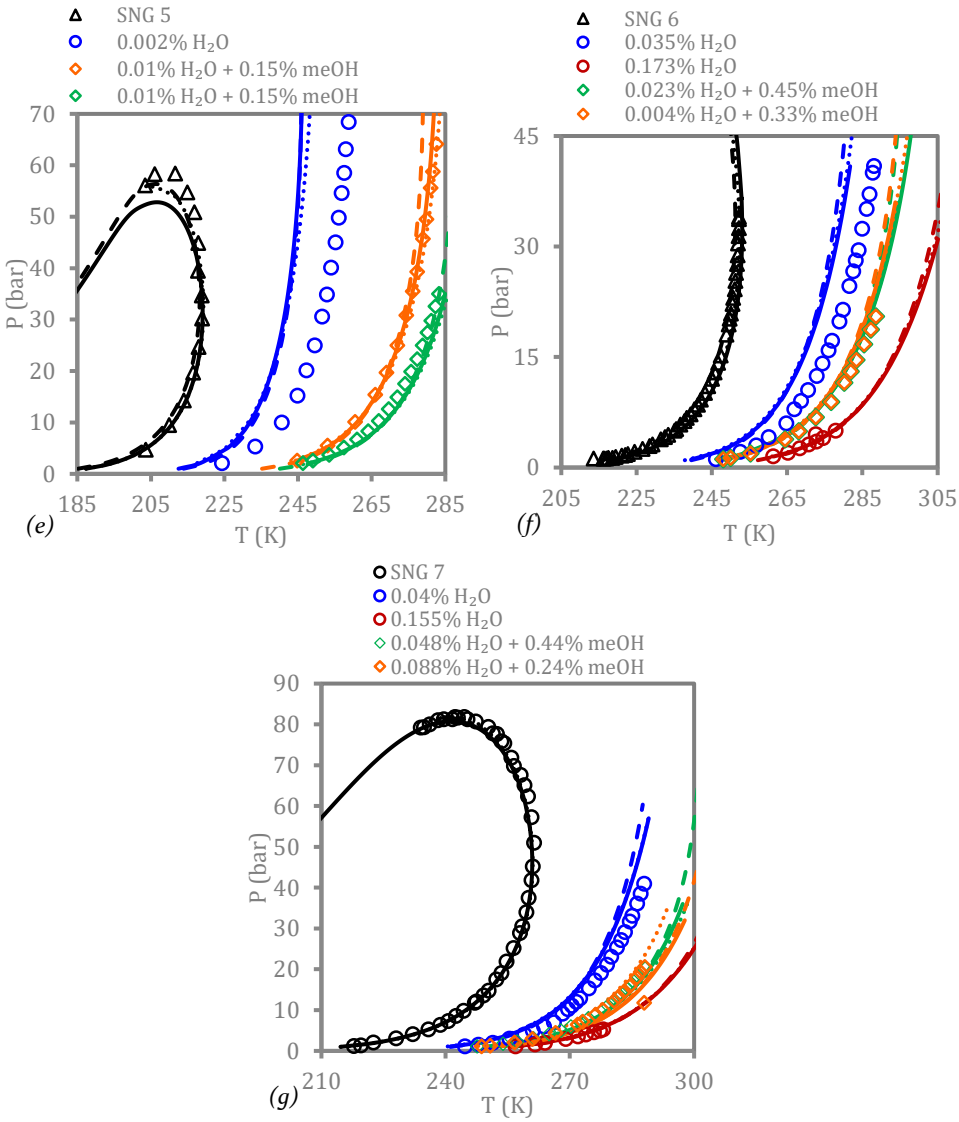

Figure 10.15 (continued)

10.7. Conclusions

To improve the description of natural gas mixtures with hydrogen bonding components, a new group – contribution model is introduced which combines the advantages of EoS/G^E models with the elegance of the perturbation theory. It is first validated in the prediction of two ternary mixtures consisting of methane, which is the major natural gas component, water and a hydrate inhibitor (methanol or MEG). By correlating the same database of binary VLE data, the new model yields improved results compared to UMR-PRU and CPA-PR, especially in the methane solubility in liquid phase, where the associating effects are more pronounced. Additionally, the use of advanced mixing rules gives a higher flexibility to the model, e.g. for the same deviation in bubble point pressure, different prediction of the vapor phase solubility can occur based on different IPs. Instead, CPA-PR has a unique k_{ij} value and thus its performance in both phases is a subject to change only from the pure component parameters. Of course, the group – contribution approach improves the predictive performance of the model, which can be applied to various mixtures using IPs fitted only to selected binaries. This is the major advantage over CPA-PR, which requires mixture – specific IPs, in order to yield satisfactory results.

Since the model performs satisfactorily by improving the behavior of UMR-PRU and CPA-PR in the examined ternary mixtures, its IP database is extended to the groups of interest to NG industry. Unfortunately, the original UMR-PRU model IPs cannot be used for the groups comprising the associating components since they implicitly include the associating contribution in the residual part. Very satisfactory correlation results are obtained in the VLE of binary mixtures, with an overall AARD in bubble point pressure of 2099 experimental points equal to 5.43 % for UMR-CPAPRU over 8.83 % for UMR-PRU. In terms of AARD in the solubility in vapor phase both models yield an average value of about 15 %. The new model correlates very well the homoazeotrope formation in the VLE of hydrocarbons with methanol yielding substantial improvement over the UMR-PRU predictions.

Also, it yields better results in the LLE of water/hydrocarbons, based on IPs fitted only to n-hexane. In terms of AARD, in the polar phase UMR-CPAPRU yields about 41 % in 163 examined points over the 50 % of UMR-PRU. In the HC-rich phase, again UMR-CPAPRU improves the performance of UMR-PRU yielding an average % AARD equal to 41 over 46 of the latter. The model better performs also in the prediction of the vapor phase solubility in the propane/water mixture. For the LLE of hydrocarbon/methanol mixture, using IPs fitted only to VLE data, UMR-CPAPRU shows improved performance over UMR-PRU, with an average AARD in 40 points, equal to 14 % in the polar phase over 23 % of UMR-PRU and 31 % in the HC-rich phase over 39 % of the latter. In the prediction of the LLE of ternary mixtures UMR-CPAPRU yields better qualitative and quantitative results compared to UMR-PRU in terms of solubility and partition coefficients. Finally, the new model improves the performance of UMR-PRU in the dew point prediction of SNG mixtures with water and methanol.

Overall, the UMR-CPAPRU is a valuable tool to describe accurately the phase equilibria of natural gas mixtures with associating compounds.

List of Symbols

Latin Characters

a	attractive term parameter of a cubic EoS (bar·cm^6·mol^{-2})
a_c	constant term of the attractive parameter of a cubic EoS
$a(T)$	term that express the temperature dependency of the attractive parameter of a cubic EoS
A_{nm}, B_{nm}, C_{nm}	UNIFAC binary interaction parameter between groups n and m
b	co-volume parameter of a cubic EoS (cm^3·mol^{-1})
d_{A_i}	number of associating sites of type A in molecule i
g	radial distribution function
G	molar Gibbs free energy (J·mol^{-1})
m	Soave parameter for the expression of the temperature dependency of the attractive term of an EoS
NC	total number of components in a mixture
NG	total number of groups in a component
n_p	number of datapoints
P	pressure (bar)
P^s	vapor pressure (bar)
q_i	relative van der Waals surface area of component i
Q_i	relative van der Waals surface area of group i
R	universal ideal gas constant (83.14 bar·cm^3·mol^{-1}·K^{-1})
r_i	relative van der Waals volume of component i
R_i	relative van der Waals volume of group i
T	absolute temperature (K)
v	molar volume (cm^3·mol^{-1})
v_l	saturated liquid volume (cm^3·mol^{-1})
ν_k^i	the number of group k in molecule i,
X_{A_i}	the fraction of moles of molecule i not bonded at site A (eq. 10.9eq. 5.39)

x_i	liquid mol fraction of component *i*
y	the reduced packing factor ($y = b\rho/4$)
y_i	vapor mol fraction of component *i*
z	compressibility factor

Greek Characters

β^{AiBj}	association volume parameter between site *A* of component *i* and site *B* of component *j*
$\Gamma_n^{(i)}$	activity of an isolated UNIFAC group *n* in a solution consisting only of molecules of type *i*
Δ^{AiBj}	associating strength between the sites of types *A* and *B* of components *i* and *j* (eq. 10.10)
ε^{AiBj}	association energy parameter between site *A* of component *i* and site *B* of component *j* ($bar \cdot cm^3 \cdot mol^{-1}$)
θ_i	UNIFAC surface fraction of component *i*
ρ	molar density ($mol \cdot m^{-3}$)
φ_i	UNIFAC volume fraction of component *i*
Ψ_{mk}	binary interaction parameter between the UNIFAC groups *m*, *k* for the UMR-PRU model
ω	acentric factor

Superscripts and Subscripts

Assoc	association
c	critical property
I, II	phases at equilibrium
i, j	component in a mixture
k,m,n	UNIFAC groups
l	liquid
p	points
Phys	physical

r reduced property

res residual term of the G^E calculated through UNIFAC

s saturation

SG Staverman-Guggenheim contribution of the combinatorial term of UNIFAC

‘ states that the property is not the experimentally measured one

References

(1) Louli V., Boukouvalas C., Voutsas E., Magoulas K., Tassios D., Application of the UMR-PRU model to multicomponent systems: Prediction of the phase behavior of synthetic natural gas and oil systems. *Fluid Phase Equilibria* **2007,** *261*, (1–2), 351-358.
(2) Novak N., Louli V., Skouras S., Voutsas E., Prediction of dew points and liquid dropouts of gas condensate mixtures. *Fluid Phase Equilibria* **2018,** *457*, (Supplement C), 62-73.
(3) Wertheim M., Fluids with highly directional attractive forces. II. Thermodynamic perturbation theory and integral equations. *Journal of statistical physics* **1984,** *35*, (1-2), 35-47.
(4) Wertheim M., Fluids with highly directional attractive forces. I. Statistical thermodynamics. *Journal of statistical physics* **1984,** *35*, (1-2), 19-34.
(5) Carnahan F.N., Starling K.E., Equation of State for Nonattracting Rigid Spheres. *J. Chem. Phys.* **1969,** *51*, 635.
(6) Louli V., Pappa G., Boukouvalas C., Skouras S., Solbraa E., Christensen K.O., Voutsas E., Measurement and prediction of dew point curves of natural gas mixtures. *Fluid Phase Equilibria* **2012,** *334*, 1-9.
(7) Voutsas E., Magoulas K., Tassios D., Universal Mixing Rule for Cubic Equations of State Applicable to Symmetric and Asymmetric Systems: Results with the Peng –Robinson Equation of State. *Industrial & engineering chemistry research* **2004,** *43*, (19), 6238-6246.
(8) Perakis C., Voutsas E., Magoulas K., Tassios D., Thermodynamic modeling of the vapor–liquid equilibrium of the water/ethanol/CO_2 system. *Fluid Phase Equilibria* **2006,** *243*, (1–2), 142-150.
(9) Boston J., Mathias P., In presented on Second International Conference on Phase Equilib. Fluid Properties Chem. Process Ind., Berlin, March 17–21, **1980**
(10) Soave G., Equilibrium constants from a modified Redlich-Kwong equation of state. *Chemical Engineering Science* **1972,** *27*, (6), 1197-1203.
(11) Pappa G.D., Perakis C., Tsimpanogiannis I.N., Voutsas E.C., Thermodynamic modeling of the vapor–liquid equilibrium of the CO_2/H_2O mixture. *Fluid Phase Equilibria* **2009,** *284*, (1), 56-63.
(12) Perakis C.A., Voutsas E.C., Magoulas K.G.,Tassios D.P., Thermodynamic modeling of the water+ acetic acid+ CO_2 system: The importance of the number of association sites of water and of the nonassociation contribution for the CPA and SAFT-type models. *Industrial & engineering chemistry research* **2007,** *46*, (3), 932-938.
(13) Daubert T.E., Danner R.P., Sibul H., Stebbins C., *Physical and thermodynamic properties of pure chemicals: data compilation*. Hemisphere: New York, 1989.

(14) NIST Thermophysical Properties of Fluid Systems, http://webbook.nist.gov/chemistry/fluid/, accessed on 01/09/2017.
(15) Koh C.A., Tanaka H., Walsh J.M., Gubbins K.E., Zollweg J.A., Thermodynamic and structural properties of methanol-water mixtures: experiment, theory, and molecular simulation. *Fluid Phase Equilibria* **1993,** *83*, 51-58.
(16) Nath A., Bender E., On the thermodynamics of associated solutions. I. An analytical method for determining the enthalpy and entropy of association and equilibrium constant for pure liquid substances. *Fluid Phase Equilibria* **1981,** *7*, (3), 275-287.
(17) Pimentel G.C., McClellan A.L., The hydrogen bond. **1960**.
(18) Voutsas E.C., Pappa G.D., Magoulas K., Tassios D.P., Vapor liquid equilibrium modeling of alkane systems with Equations of State: "Simplicity versus complexity". *Fluid Phase Equilibria* **2006,** *240*, (2), 127-139.
(19) Voutsas E., Perakis C., Pappa G., Tassios D., An evaluation of the performance of the Cubic-Plus-Association equation of state in mixtures of non-polar, polar and associating compounds: Towards a single model for non-polymeric systems. *Fluid Phase Equilibria* **2007,** *261*, (1–2), 343-350.
(20) Koner Z., Phutela R., Fenby D., Determination of the equilibrium constants of water-methanol deuterium exchange reactions from vapour pressure measurements. *Australian Journal of Chemistry* **1980,** *33*, (1), 9-13.
(21) Ratcliff G.A., Chao K.C., Prediction of thermodynamic properties of polar mixtures by a group solution model. *The Canadian Journal of Chemical Engineering* **1969,** *47*, (2), 148-153.
(22) Jou F.Y., Otto F.D., Mather A.E., Solubility of methane in glycols at elevated pressures. *The Canadian Journal of Chemical Engineering* **1994,** *72*, (1), 130-133.
(23) Yarym-Agaev N., Sinyavskaya R., Koliushko I., Phase equilibrium in the binary systems water-methane and methanol-methane under high pressure. *Zh. Prikl. Khim* **1985,** *58*, 165-168.
(24) Kim Y.S., Ryu S.K., Yang S.O., Lee C.S., Liquid Water–Hydrate Equilibrium Measurements and Unified Predictions of Hydrate-Containing Phase Equilibria for Methane, Ethane, Propane, and Their Mixtures. *Industrial & engineering chemistry research* **2003,** *42*, (11), 2409-2414.
(25) Chapoy A., Coquelet C., Richon D., Corrigendum to "Revised solubility data and modeling of water in the gas phase of the methane/water binary system at temperatures from 283.08 to 318.12 K and pressures up to 34.5 MPa": [Fluid Phase Equilibria 214 (200 3) 101–117]. *Fluid Phase Equilibria* **2005,** *230*, (1–2), 210-214.
(26) Frost M., Karakatsani E., von Solms N., Richon D., Kontogeorgis G.M., Vapor–Liquid Equilibrium of Methane with Water and Methanol. Measurements and Modeling. *Journal of Chemical & Engineering Data* **2013,** *59*, (4), 961-967.
(27) Mokbel I., Porcedda S., Guetachew T., Marongiu B., Jose J., Static measurements of the total vapor pressure of ethane-1, 2-diol+ water mixtures at temperatures from 258 K to 363 K. *ELDATA International Electronic Journal of Physico-Chemical Reference Data* **1999,** *5*, 79-84.
(28) Chapoy A., Mohammadi A.H., Tohidi B., Richon D., Estimation of water content for methane+ water and methane+ ethane+ n-butane+ water systems using a new sampling device. *Journal of Chemical & Engineering Data* **2005,** *50*, (4), 1157-1161.

(29) Folas G.K., Berg O.J., Solbraa E., Fredheim A.O., Kontogeorgis G.M., Michelsen M.L., Stenby E.H., High-pressure vapor–liquid equilibria of systems containing ethylene glycol, water and methane: Experimental measurements and modeling. *Fluid Phase Equilibria* **2007,** *251*, (1), 52-58.
(30) Abdi M.A., Hussain A., Hawboldt K., Beronich E., Experimental Study of Solubility of Natural Gas Components in Aqueous Solutions of Ethylene Glycol at Low-Temperature and High-Pressure Conditions. *Journal of Chemical & Engineering Data* **2007,** *52*, (5), 1741-1746.
(31) Sinyavskaya R., Yarym-Agaev N., Koliushko I., Levinton L.Y., British Gas Corp. L., Phase equilibria in the methane– water– methanol system at high pressures. *Gazovaya Prom* **1984,** *1*, 39.
(32) Kruger F.J., Danielsen M.V., Kontogeorgis G.M., Solbraa E., von Solms N., Ternary Vapor–Liquid Equilibrium Measurements and Modeling of Ethylene Glycol (1) + Water (2) + Methane (3) Systems at 6 and 12.5 MPa. *Journal of Chemical & Engineering Data* **2018,** *63*, (5), 1789-1796.
(33) McGlashan M.L., Williamson A.G., Isothermal liquid-vapor equilibriums for system methanol-water. *Journal of Chemical & Engineering Data* **1976,** *21*, (2), 196-199.
(34) Niesen V., Palavra A., Kidnay A.J., Yesavage V.F., An apparatus for vapor-liquid equilibrium at elevated temperatures and pressures and selected results for the water-ethanol and methanol-ethanol systems. *Fluid Phase Equilibria* **1986,** *31*, (3), 283-298.
(35) Barr-David F., Dodge B.F., Vapor-Liquid Equilibrium at High Pressures. The Systems Ethanol-Water and 2-Propanol-Water. *Journal of Chemical & Engineering Data* **1959,** *4*, (2), 107-121.
(36) Wilsak R.A., Campbell S.W., Thodos G., Vapor-liquid equilibrium measurements for the n-pentane-methanol system at 372.7, 397.7 and 422.6 K. *Fluid Phase Equilibria* **1987,** *33*, (1–2), 157-171.
(37) Goetschel B., Z. W., Calculation of partial pressures in the methanol + benzene system by measuring the total pressure. *Univ. Rostock, Math.-Naturwiss. Reihe* **1969,** *18*, 927.
(38) Iguchi A., Vapor-liquid equilibriums at 25 C for binary systems between alcohols and hydrocarbons. *Kagaku Sochi* **1978,** *20*, 66-68.
(39) Kolodziej E.J.G., R. A., presented on National AJChE Meeting, New Orleans, **1981**
(40) Hong J.H., Kobayashi R., Vapor-liquid equilibrium studies for the carbon dioxide-methanol system. *Fluid Phase Equilibria* **1988,** *41*, (3), 269-276.
(41) Koulocheris V., Louli V., Panteli E., Skouras S., Voutsas E., Modelling of elemental mercury solubility in natural gas components. *Fuel* **2018,** *233*, 558-564.
(42) Folas G.K., Kontogeorgis G.M., Michelsen M.L., Stenby E.H., Solbraa E., Liquid –Liquid Equilibria for Binary and Ternary Systems Containing Glycols, Aromatic Hydrocarbons, and Water: Experimental Measurements and Modeling with the CPA EoS. *Journal of Chemical & Engineering Data* **2006,** *51*, (3), 977-983.
(43) Kobayashi R., Katz D., Vapor-Liquid Equilibria For Binary Hydrocarbon-Water Systems. *Industrial & Engineering Chemistry* **1953,** *45*, (2), 440-446.
(44) Black C.J., G. G., Taylor, H. S., The Solubility of Water in Hydrocarbons. *J. Chem. Phys* **1948,** *16*.
(45) Polak J., Lu B.C.-Y., Mutual solubilities of hydrocarbons and water at 0 and 25 C. *Canadian Journal of Chemistry* **1973,** *51*, (24), 4018-4023.

(46) Tsonopoulos C., Wilson G., High-temperature mutual solubilities of hydrocarbons and water. Part I: Benzene, cyclohexane and n-hexane. *AIChE Journal* **1983,** *29*, (6), 990-999.
(47) Revellame E.D., Holmes W.E., Hernandez R., French W.T., Lerma L., Forks A., Ashe T., Estévez L.A., Experimental measurement and modeling of the Type 3 ternary system containing (decane+water+triacetin). *The Journal of Chemical Thermodynamics* **2013,** *67*, 21-27.
(48) Ng H.-J., Chen C.-J., *Mutual Solubility in Water-hydrocarbon Systems: GPA Project 895, RR-150*; Gas Processors Association: 1995.
(49) Economou I., Heidman J., Tsonopoulos C., Wilson G., Mutual solubilities of hydrocarbons and water: III. 1-hexene, 1-octene, C10-C12 hydrocarbons. *AIChE Journal* **1997,** *43*, (2), 535-546.
(50) Burd S.D.B., W. G., Vapor-liquid equilibria of some C6 hydrocarbons with water. *Proc. Am. Pet. Inst. Div. Refin.* **1968,** *48*.
(51) Guseva A., Parnov E., Solubility of cyclohexane in water. *Zhurnal Fizicheskoi Khimii* **1963,** *37*, (12), 2763-2763.
(52) Pereda S., Awan J.A., Mohammadi A.H., Valtz A., Coquelet C., Brignole E.A., Richon D., Solubility of hydrocarbons in water: Experimental measurements and modeling using a group contribution with association equation of state (GCA-EoS). *Fluid Phase Equilibria* **2009,** *275*, (1), 52-59.
(53) Marche C., Ferronato C., Jose J., Solubilities of n-Alkanes (C6 to C8) in Water from 30 °C to 180 °C. *Journal of Chemical & Engineering Data* **2003,** *48*, (4), 967-971.
(54) Pierotti R., Liabastre A., Structure and Properties of Water Solutions US Nat. *Tech. Inform. Serv., PB Rep* **1972**, (21163).
(55) Goldman S., The determination and statistical mechanical interpretation of the solubility of water in benzene, carbon tetrachloride, and cyclohexane. *Canadian Journal of Chemistry* **1974,** *52*, (9), 1668-1680.
(56) Jou F.-Y., Mather A.E., Liquid–Liquid Equilibria for Binary Mixtures of Water + Benzene, Water + Toluene, and Water + p-Xylene from 273 K to 458 K. *Journal of Chemical & Engineering Data* **2003,** *48*, (3), 750-752.
(57) Higashiuchi H., Sakuragi Y., Iwai Y., Arai Y., Nagatani M., Measurement and correlation of liquid-liquid equilibria of binary and ternary systems containing methanol and hydrocarbons. *Fluid Phase Equilibria* **1987,** *36*, (0), 35-47.
(58) Higashiuchi H., Sakuragi Y., Arai Y., Nagatani M., Measurement and correlation of liquid-liquid equilibria of methanol-alkane-aromatic compound ternary systems. *Fluid Phase Equilibria* **1990,** *58*, (1), 147-157.
(59) Noda K., Sato K., Nagatsuka K., Ishida K., Ternary liquid-liquid equilibria for the systems of aqueous methanol solutions and propane or n-butane. *Journal of chemical engineering of Japan* **1975,** *8*, (6), 492-493.
(60) Udovenko V.V., Frid T.B., *Zh. Fiz. Khim.* **1948,** *22*, 1135.
(61) Avila S., Blanco S.T., Velasco I., Rauzy E., Otín S., Thermodynamic Properties of Synthetic Natural Gases. 1. Dew-Point Curves of Synthetic Natural Gases and Their Mixtures with Water and Methanol. Measurement and Correlation. *Industrial & engineering chemistry research* **2002,** *41*, (15), 3714-3721.
(62) Avila S., Blanco S.T., Velasco I., Rauzy E., Otín S., Thermodynamic properties of synthetic natural gases. Part 3. Dew point curves of synthetic natural gases and their

mixtures with water. Measurement and correlation. *Energy & Fuels* **2003,** *17*, (2), 338-343.
(63) Avila S., Blanco S.T., Velasco I., Rauzy E., Otín S., Thermodynamic Properties of Synthetic Natural Gases. 2. Dew Point Curves of Synthetic Natural Gases and Their Mixtures with Water and Methanol. Measurement and Correlation. *Energy & Fuels* **2002,** *16*, (4), 928-934.
(64) Avila S., Blanco S.T., Velasco I., Rauzy E., Otín S., Thermodynamic properties of synthetic natural gases: Part 4. Dew point curves of synthetic natural gases and their mixtures with water: measurement and correlation. *Fluid Phase Equilibria* **2002,** *202*, (2), 399-412.
(65) Jarne C., Avila S., Blanco S.T., Rauzy E., Otín S.,Velasco I., Thermodynamic Properties of Synthetic Natural Gases. 5. Dew Point Curves of Synthetic Natural Gases and Their Mixtures with Water and with Water and Methanol: Measurement and Correlation. *Industrial & engineering chemistry research* **2003,** *43*, (1), 209-217.

Chapter 11: Concluding remarks

This Chapter summarizes the obtained results and discusses suggestions for further study.

11.1. Conclusions

In the first part of this work, new vapor – liquid experimental data for the CO_2/CH_4 binary mixture have been measured at the mean temperatures of 293.13 K, 298.14 K and 303.15 K in order to improve the data situation for the CO_2/CH_4 mixture at temperatures of interest to various CCS and NG applications. The measured data are of high accuracy, with a maximum uncertainty of 3 mK in temperature, 0.02 bar in pressure and 0.0008 in composition. Emphasis is given to the critical region of the mixtures by estimating the critical point through a scaling law, after several measurements in its proximity. As expected, an increased uncertainty is observed in that region, namely 0.1 bar in critical pressure and 0.0009 in the critical composition of the mixture. Yet, the obtained results are very good and of increased accuracy compared to other literature data. Apart from the uncertainty analysis the obtained data show a very good agreement with other literature data at 293 K. Moreover, the new experimental data have been correlated with four thermodynamic models; the cubic equation of state SRK and PR combined with the classic vdW1f mixing rules, PC-SAFT and UMR-PRU. Very satisfactory correlation results are obtained for all models away from the critical point. UMR-PRU yields the lower deviations in both phases as well as in the prediction of the critical point of the mixture, while PR, SRK and PC-SAFT yield similar predictions of the critical point.

The UMR-PRU model is then extended in the modelling of mixtures that contain polar compounds of interest to the gas industry, namely water, methanol, MEG and TEG. The required interaction parameters are obtained by fitting vapor – liquid equilibrium data, with satisfactory results in all cases. In the special case of hydrocarbons with water, the UNIFAC interaction parameters are re-estimated by fitting the aqueous and HC-rich phases of LLE solubility data. Emphasis is given in the TEG solubility in methane vapor phase, which is of interest for the accurate calculation of TEG loss during the dehydration process. The obtained results are comparable with those of TST/NRTL which is proposed by Hysys for the simulation of dehydration processes, for the mixtures with water and TEG. Instead, for the mixtures with methanol and MEG, UMR-PRU presents superior results compared to TST/NRTL. The performance of the models is further evaluated in the prediction of multicomponent mixtures, with overall satisfactory results. The models also showed very good results in the distribution of BTEX in conditions relevant to those which occur at TEG dehydration. Finally, similar and quite satisfactory results are obtained for the dew point lines of synthetic SNG mixtures. Therefore, the UMR-PRU model yields very good results for mixtures of natural gas components with strongly polar compounds.

UMR-PRU is also evaluated in the simulation of natural gas dehydration unit using TEG as absorbent. The model is first validated in the prediction of a single absorber by its implementation in two simulators, Hysys and Unisim through the CAPE-Open 1.1 protocol. Identical results are obtained as expected in both simulators and similar with the ones of TST/NRTL in Hysys. Then, a simplified offshore dehydration process is simulated and it is shown that UMR-PRU and TST/NRTL calculate similar stripping

gas rate, TEG purity and circulation rate to achieve the same dehydration level in the dry gas. The two models differ in the calculated TEG loss, where UMR-PRU is considered to be closer to the real case than TST/NRTL due to its better performance in the VLE of the methane/TEG binary. UMR-PRU also predicts lower heat duties in the reboiler, condenser and heat exchangers compared to TST/NRTL, which is considered more realistic due to the better prediction of the aqueous TEG heat capacities.

Following a sensitivity analysis of several operating parameters, e.g. stripping gas rate, operating temperature and pressure of the columns etc., an optimization of the operating parameters of the process in terms of the operating cost was performed, as well as a preliminary economic evaluation of the base and optimized process. For a plant of a relative small capacity (360 SMcmy), the optimized parameters do not actually affect the capital cost, either calculated through Icarus or literature correlations. Instead, when the operating cost is considered, the optimized conditions lead to a saving of about 37 €/SMcm of treated wet gas. Based on the abovementioned results, it is concluded that the UMR-PRU model can be used to accurately simulate natural gas TEG dehydration units.

Whilst UMR-PRU does not take explicitly into account the hydrogen bonding interactions, it has been proven to perform quite well in phase equilibrium of mixtures involving associating compounds. This gives birth to the question of what is more important in the modelling of hydrogen bonding mixtures: is it necessary to use complex expressions which directly take into account hydrogen bonding, or a rather simpler model such as an EoS combined with advanced mixing rules is adequate? To answer this, three versions of the Peng – Robinson equation of state have been considered and were evaluated in the modelling of natural gas mixtures with water, methanol and MEG. The EoS used are, the PR with conventional vdW1f mixing rules, the UMR-PRU and CPA-PR which directly accounts for the association based on Wertheim's first order perturbation theory. To obtain a fair comparison among the models, temperature – specific IPs have been fitted to the same database of experimental data. The application of advanced mixing rules (UMR-PRU) and the direct incorporation of the associating term (CPA-PR) substantially improve the predictions in multicomponent mixtures. The advantage of CPA-PR is more apparent in the prediction of the liquid phase of multicomponent mixtures. Furthermore, UMR-PRU and CPA-PR are able to predict satisfactorily the dew points of natural gas mixtures with water and/or methanol, yielding much better results compared to those of Peng – Robinson. CPA-PR yields the best overall results, proving thus the necessity of the direct calculation of the hydrogen bonding interactions. These observations suggest that the selection of advanced mixing rules for the attractive and co-volume parameters, as well as the direct implementation of the associating term are essential in order to obtain accurate phase equilibrium description of complex mixtures containing natural gas components, water and hydrogen bonging chemicals such as methanol and MEG, with an equation of state.

Therefore, a new model is introduced which combines the assets of advanced mixing rules with the direct calculation of hydrogen bonding. The new model is first evaluated in the prediction of two ternary mixtures consisting of methane, which is the major natural gas component, water and a hydrate inhibitor (methanol or MEG) and the obtained results are compared with those of the "*parent models*" UMR-PRU and CPA-PR. By correlating the same database of binary VLE data, the new model yields improved results. UMR-CPAPRU is further extended in the modelling of natural gas components with associating compounds. It is shown that the model correlates satisfactorily the binary mixtures in a wide range of temperature and pressure, yielding improved prediction over UMR-PRU in the hydrocarbon/water LLE as well as in the azeotrope prediction of the hydrocarbon/methanol mixtures. Then, the model is evaluated in the prediction of the LLE of ternary mixtures, where it yields better qualitative and quantitative results compared to UMR-PRU. Finally, UMR-CPAPRU yields improved results over UMR-PRU in the dew point prediction of SNG mixtures with water and methanol. Overall, the proposed model is a valuable tool to acquire good prediction results for natural gas mixtures with associating compounds.

11.2. Future work

As it has always been in scientific research, one work cannot include all the possible scenarios, but rather acts as a step for the next researcher. In this essence, several questions are left unanswered and new ones have been generated.

With regards to the UMR-PRU model, new UNIFAC groups can be also added to extend the applicability of the model to other processes. Such groups can be for example the "DEG" one. This can lead to further analysis, e.g. regarding the applicability of selected glycols. Also, in order to improve the prediction results in the branched alkanes and cycloalkanes, specific groups can be assigned so that the interaction parameters take into consideration the different compounds behavior. It is also shown that the Mathias – Copeman alpha function although performs well for the vapor pressure, does not improve the volumetric properties, especially of the associating components. An addition of a volume translation can be considered to improve the volumetric properties of the mixtures.

Regarding the simulation results, the gas examined in this work does not consist of any aromatic compounds. Nevertheless, the BTEX distribution is one of the most important parameters environmentally–wise when dealing with the dehydration process. To that end, a simulation with a feed gas containing such compounds can be considered and the obtained results can be compared with literature data. The most interesting application would be to examine the performance of the model against field data. To the best of our knowledge such data are not available in the open literature. As such, an interesting aspect is first to obtain field data and then use them to evaluate the prediction of the models. This will also give an insight regarding the performance of the models in a predictive way in terms of glycol or HC loss as well as of the required costs.

Finally, regarding the proposed model, UMR-CPAPRU, several thoughts consist an interesting base for further analysis. Apart from the good phase equilibrium results other properties of the associating components should also be examined. Such an example is the heat capacity which as previously stated is crucial in the estimation of the required duty of processes. Additionally, the examination of solvation for aromatic compounds should also be examined. Other associating components, such as other glycols, can be added to extend the applicability of the model to other applications. In this essence, the model should be also introduced in a process simulator, in order to study the overall effect in a simulation of a more complex model over the results obtained with simpler models, in this case the EoS/G^E. Another scenario would be to consider the association effects as group based, e.g. one *–OH* group with specific association parameters, rather than molecularly–based. That will improve the predictive nature of the model, since the parameters determined for one *–OH* group can be applied to more than one associating components.

Appendix A

Experimental points database used for the fitting of UMR-PRU IPs.

Table A.1: Database of experimental binary VLE data used for the regression of UNIFAC group IPs for UMR-PRU.

Component	Ref.	n_p	Type	Year	T range (K)	P range (bar)	x_1 range	y_2 range
Water (2) with								
CO_2	1	11	Isothermal (TPx)	2004	278.22 - 298.28	4.96 - 34.91	0.00314 - 0.01772	0.0007 - 0.0065
	2	15	Isothermal (TPxy)	1992	288.15 - 313.15	50.70 - 202.70	0.02142 - 0.03013	0.0013 - 0.0058
	3	15	Isothermal (TPx)	1941	323.15 - 348.15	25.30 - 709.30	0.00545 - 0.03082	–
	4	6	Isothermal (TPx)	1940	304.19	25.30 - 506.60	0.01127 - 0.03014	–
	5	18	Isothermal (TPxy)	2000	333.15 - 353.15	40.50 - 141.10	0.00800 - 0.02080	0.0047 - 0.0143
	6	88	Isothermal (TPxy)	1964	383.15 - 598.15	100.00 - 1499.98	0.00400 - 0.25000	0.0420 - 0.9200
	7	12	Isothermal (TPxy)	1988	373.13	3.25 - 23.07	0.00045 - 0.00414	0.0450 - 0.2880
N_2	8	34	Isothermal (TPx)	1979	298.15 - 513.15	25.33 - 1013.25	0.00018 - 0.00508	–
methane	9	29	Isothermal (TPxy)	1970	323.15 - 588.71	13.789 - 616.06	0.00017 - 0.00676	0.1678 - 0.9990
	10	18	Isothermal (TPx)	1997	283.37 - 283.37	5.67 - 90.82	0.00026 - 0.00200	–
	11	11	Isothermal (TPxy)	1972	423.2 - 523.2	98.10 - 980.70	0.00100 - 0.01510	0.0600 - 0.0900
	12	22	Isothermal (TPxy)	2013	283.89 - 323.56	47.80 - 194.90	0.00060 - 0.00261	0.0004 - 0.0017
	13	16	Isothermal (TPx)	2003	283.2 - 313.11	9.73 - 179.98	0.00020 - 0.00246	–
	14	9	Isothermal (TPx)	2003	298.15	23.00 – 166.00	0.00053 - 0.00265	–
	15	15	Isothermal (TPxy)	1985	298.15 - 338.15	25.00 - 125.00	0.00041 - 0.00221	0.0026 - 0.0023
ethane	16	43	Isothermal (TPx)	2004	274.26 - 343.08	3.73 - 49.52	0.00009 - 0.00097	–
	8	15	Isothermal (TPx)	1979	377.59 - 444.26	7.80 - 137.89	0.00005 - 0.00168	–
	14	6	Isothermal (TPx)	2003	298.15	14.00 - 39.00	0.00039 - 0.00113	–
MEG	17	23	Isothermal (TPx)	1983	323.15	0.00 - 0.12	0.00000 - 1.00000	–
TEG	18	18	Isobaric (TPxy)	2009	371.55 - 421.25	0.85	0.08500 - 0.88300	0.9829 – 0.9999

Table A.1 (continued)

Component	Ref.	n_p	Type	Year	T range (K)	P range (bar)	x_1 range	y_2 range
methanol (2) with								
N_2	8	21	Isothermal (TPx)	1979	273.15 - 343.15	49.00 – 295.00	0.0109 - 0.0687	–
CO_2	19	28	Isothermal (TPx)	1970	213.15 - 247.15	1.01 - 15.20	0.0246 - 0.6220	–
	20	17	Isothermal (TPxy)	1976	298.15 - 313.15	5.77 - 80.58	0.0285 - 0.9002	0.0690 - 0.0637
CH_4	21	49	Isothermal (TPxy)	1987	273.15 - 330	13.79 - 413.69	0.0095 - 0.2575	0.0009 - 0.0626
	22	9	Isothermal (TPx)	2002	280.15	21.12 - 114.08	0.0170 - 0.0880	–
	23	8	Isothermal (TPx)	2012	294.20 - 294.80	10.50 - 79.90	0.0110 - 0.0750	–
	15	15	Isothermal (TPxy)	1985	298.15 - 338.15	25.00 – 125.00	0.0221 - 0.0944	0.0039 - 0.0457
	12	9	Isothermal (TPxy)	2013	298.87 - 298.87	52.4 - 180.10	0.0413 - 0.1348	0.0037 - 0.0054
	24	15	Isothermal (TPxy)	1987	298.15 - 373.15	54.50 - 592.00	0.0374 - 0.5648	0.0047- 0.3058
C_2H_6	25	43	Isothermal (TPx)	1986	240.00 - 298.14	4.01 - 41.95	0.0199 - 1.0000	–
	26	41	Isothermal (TPx)	1991	263.15 - 309.18	18.25 - 67.69	0.3476 - 0.9415	–
	27	24	Isothermal (TPxy)	1964	273.15 - 373.15	10.13 - 60.80	0.0027 - 0.3210	0.0220 – 1.0000
	28	5	Isothermal (TPxy)	1998	298.15 - 298.15	9.63 - 39.4	0.0530 - 0.3440	0.0050 - 0.0410
	29	5	Isothermal (TPxy)	1976	298.15 - 298.15	10.94 - 41.25	0.0403 - 0.3511	0.0078 - 0.0178

Table A.1 (continued)

Component	Ref.	n_p	Type	Year	T range (K)	P range (bar)	x_1 range	y_2 range
MEG (2) with								
N_2	30	31	Isothermal (TPx)	1979	323.15 - 398.15	15.70 - 396.00	0.00150 - 0.01900	–
CO_2	31	39	Isothermal (TPx)	1994	298.15 - 398.15	0.29 - 202.90	0.00069 - 0.13880	–
	30	30	Isothermal (TPx)	1999	323.15 - 398.15	8.94 - 384.00	0.00490 - 0.17240	–
	32	52	Isothermal (TPx)	2011	288.15 - 318.15	0.94 - 57.90	0.00230 - 0.09540	–
	33	10	Isothermal (TPx)	2013	303.00 - 333.00	1.05 - 5.05	0.00120 - 0.00890	–
	34	4	Isothermal (TPx)	2013	298.4 - 298.9	0.39 - 1.36	0.00090 - 0.00330	–
CH_4	35	34	Isothermal (TPx)	1994	298.15 - 398.15	1.05 - 203.50	0.00016 - 0.02240	–
	30	31	Isothermal (TPx)	1999	323.15 - 398.15	2.00 - 396.20	0.00030 - 0.04210	–
C_2H_6	36	34	Isothermal (TPx)	1994	298.15 - 398.15	0.00 - 203.40	0.00033 - 0.03080	–

Table A.1 (continued)

Component	Ref.	n_p	Type	Year	T range (K)	P range (bar)	x_1 range	y_2 range
TEG (2) with								
CO_2	37	40	Isothermal (TPx)	1987	298.15 - 398.15	1.05 - 202.50	0.0046 - 0.4848	–
methane	37	51	Isothermal (TPx)	1987	298.15 - 398.15	1.10 - 202.00	0.0006 - 0.0840	–
	38	16	Isothermal (TPx)	1989	273.15 - 298.14	34.4 - 173.00	0.0153 - 0.0598	–
ethane	37	59	Isothermal (TPx)	1987	298.15 - 398.15	1.10 - 204.80	0.0016 - 0.1482	–
propane	38	40	Isothermal (TPx)	1987	298.15 - 398.15	0.22 - 64.50	0.0007 - 0.1043	–
n-hexane	39	16	Isothermal (TPxy)	1980	473	0.10 - 18.14	0.0000 - 1.0000	0.0 - 1.0
cyclohexane	39	18	Isothermal (TPxy)	1980	473	0.10 - 13.77	0.0000 - 1.0000	0.0 - 1.0
benzene	40	11	Isobaric (TPxy)	1989	354.65 - 428.75	1.01	0.0680 - 0.8849	0.0001 – 0.0100
toluene	40	11	Isobaric (TPxy)	1989	385.22 - 442.51	1.01	0.0815 - 0.9353	0.0006 – 0.0200

Table A.2: Database of experimental binary LLE data used for the regression of UNIFAC group IPs for UMR-PRU.

Component	Ref.	n_p	Type	Year	T range (K)	P range (bar)	x_1 aqueous phase (I)	x_2 HC–rich phase (II)
water (2) with								
n-pentane	41	4	TPx_1^I	2007	313.19 - 343.15	–	1.2 E-5 - 1.5 E-5	–
	42	4	$TPx_1^I x_2^{II}$	2004	273.15 - 298.15	–	1.0 E-5 - 1.4 E-5	1.0 E-4 – 4.4 E-4
	43	2	TPx_1^I	1982	311.47 - 423.34	–	–	0.0004 - 0.032
n-hexane	44	8	$TPx_1^I x_2^{II}$	1983	298.15 - 473.15	0.23 - 35.18	0.0004 - 0.1090	3.0 E-6 - 1.9 E-4
n-heptane	45	4	$Tx_1^I x_2^{II}$	1965	293.15 - 323.15	–	4.3 E-7 - 6.1 E-7	5.3 E-4 -2.7 E-3
	46	2	TPx_1^I	1968	308.15 - 318.15	–	3.5 E-7 - 4.8 E-7	–
	47	8	TPx_1^I	2003	305.85 - 443.75	7	4.7 E-7 - 1.8 E-5	–
n-octane	48	10	$TPx_1^I x_2^{II}$	1985	298.15 - 523.15	0.05 - 56.99	1.0 E-7 - 2.3 E-4	5.2 E-4 - 0.3232
Benzene	44	21	$Tx_1^I x_2^{II}$	1983	279.15 - 490.80	–	0.0004 - 0.0061	0.0017 - 0.2578
toluene	49	11	$TPx_1^I x_2^{II}$	2003	283.15 - 458.15	0.03 – 17.00	0.0001 - 0.0017	0.0017 - 0.1328
	50	1	$Tx_1^I x_2^{II}$	1995	310.9	–	1.2 E-5	0.0039
	51	2	TPx_2^{II}	1986	448.31 - 473.51	14.25 - 23.76	0.0013 - 0.0026	0.0098 - 0.1592
	47	1	TPx_1^I	2006	323.15	1.01	–	0.0068

Literature Cited

(1) Valtz A., Chapoy A., Coquelet C., Paricaud P., Richon D., Vapour–liquid equilibria in the carbon dioxide–water system, measurement and modelling from 278.2 to 318.2 K. *Fluid Phase Equilibria* **2004,** *226*, 333-344.
(2) King M.B., Mubarak A., Kim J.D., Bott T.R., The mutual solubilities of water with supercritical and liquid carbon dioxides. *The Journal of Supercritical Fluids* **1992,** *5*, (4), 296-302.
(3) Wiebe R., Gaddy V.L., Vapor Phase Composition of Carbon Dioxide-Water Mixtures at Various Temperatures and at Pressures to 700 Atmospheres. *Journal of the American Chemical Society* **1941,** *63*, (2), 475-477.
(4) Wiebe R., Gaddy V.L., The Solubility of Carbon Dioxide in Water at Various Temperatures from 12 to 40° and at Pressures to 500 Atmospheres. Critical Phenomena*. *Journal of the American Chemical Society* **1940,** *62*, (4), 815-817.
(5) Bamberger A., Sieder G., Maurer G., High-pressure (vapor+liquid) equilibrium in binary mixtures of (carbon dioxide+water or acetic acid) at temperatures from 313 to 353 K. *The Journal of Supercritical Fluids* **2000,** *17*, (2), 97-110.
(6) Takenouchi S., Kennedy G.C., The binary system H2O-CO2 at high temperatures and pressures. *American Journal of Science* **1964,** *262*, (9), 1055-1074.
(7) Muller G., Bender E., Maurer G., Vapor-liquid-equilibrium in the ternary-system ammonia-carbon dioxide-water at high water contents in the range 373-K to 473-K. *Berichte Der Bunsen-Gesellschaft-Physical Chemistry Chemical Physics* **1988,** *92*, (2), 148-160.
(8) Kertes, *IUPAC Solubility Data Series, Pergamon Press: Oxford*. 1979.
(9) O'Sullivan T.D., Smith N.O., Solubility and partial molar volume of nitrogen and methane in water and in aqueous sodium chloride from 50 to 125. deg. and 100 to 600 atm. *The Journal of Physical Chemistry* **1970,** *74*, (7), 1460-1466.
(10) Lekvam K., Bishnoi P.R., Dissolution of methane in water at low temperatures and intermediate pressures. *Fluid Phase Equilibria* **1997,** *131*, (1–2), 297-309.
(11) Sultanov R., Skripka V., Namiot A.Y., Phase equilibrium and critical effect of water-methane system under increased temperature and pressure. *Zhurnal Fizicheskoi Khimii* **1972,** *46*, (8), 2160.
(12) Frost M., Karakatsani E., von Solms N., Richon D., Kontogeorgis G.M., Vapor–Liquid Equilibrium of Methane with Water and Methanol. Measurements and Modeling. *Journal of Chemical & Engineering Data* **2013,** *59*, (4), 961-967.
(13) Chapoy A., Mohammadi A.H., Tohidi B., Richon D., Estimation of water content for methane+ water and methane+ ethane+ n-butane+ water systems using a new sampling device. *Journal of Chemical & Engineering Data* **2005,** *50*, (4), 1157-1161.
(14) Kim Y.S., Ryu S.K., Yang S.O., Lee C.S., Liquid Water–Hydrate Equilibrium Measurements and Unified Predictions of Hydrate-Containing Phase Equilibria for Methane, Ethane, Propane, and Their Mixtures. *Industrial & engineering chemistry research* **2003,** *42*, (11), 2409-2414.
(15) Yarym-Agaev N., Sinyavskaya R., Koliushko I., Phase equilibrium in the binary systems water-methane and methanol-methane under high pressure. *Zh. Prikl. Khim* **1985,** *58*, 165-168.
(16) Mohammadi A.H., Chapoy A., Tohidi B., Richon D., Measurements and thermodynamic modeling of vapor-liquid equilibria in ethane-water systems from

274.26 to 343.08 K. *Industrial & engineering chemistry research* **2004,** *43*, (17), 5418-5424.
(17) Gonzalez C., Van Ness H.C., Excess thermodynamic functions for ternary systems. 9. Total-pressure data and GE for water/ethylene glycol/ethanol at 50.degree.C. *Journal of Chemical & Engineering Data* **1983,** *28*, (4), 410-412.
(18) Mostafazadeh A.K., Rahimpour M.R., Shariati A., Vapor–Liquid Equilibria of Water + Triethylene Glycol (TEG) and Water + TEG + Toluene at 85 kPa. *Journal of Chemical & Engineering Data* **2009,** *54*, (3), 876-881.
(19) Gmelin T., *Handbuch BD. C* **1970,** *14*, 568.
(20) Ohgaki K., Katayama T., Isothermal vapor-liquid equilibrium data for binary systems containing carbon dioxide at high pressures: methanol-carbon dioxide, n-hexane-carbon dioxide, and benzene-carbon dioxide systems. *Journal of Chemical and Engineering Data* **1976,** *21*, (1), 53-55.
(21) Hong J.H., Malone P.V., Jett M.D., Kobayashi R., The measurement and interpretation of the fluid-phase equilibria of a normal fluid in a hydrogen bonding solvent: the methane - methanol system. *Fluid Phase Equilibria* **1987,** *38*, (1-2), 83-96.
(22) Ukai T., Kodama D., Miyazaki J., Kato M., Solubility of methane in alcohols and saturated density at 280.15 K. *Journal of Chemical & Engineering Data* **2002,** *47*, (5), 1320-1323.
(23) Nourozieh H., Kariznovi M., Abedi J., Phase equilibrium measurements and thermodynamic modeling of methane alcohol systems at ambient temperature. *The Journal of Chemical Thermodynamics* **2012,** *54*, (0), 165-170.
(24) Brunner E., Hültenschmidt W., Schlichthärle G., Fluid mixtures at high pressures IV. Isothermal phase equilibria in binary mixtures consisting of (methanol+ hydrogen or nitrogen or methane or carbon monoxide or carbon dioxide). *The Journal of Chemical Thermodynamics* **1987,** *19*, (3), 273-291.
(25) Zeck S., Knapp H., Vapor-liquid and vapor-liquid-liquid phase equilibria for binary and ternary systems for nitrogen, ethane and methanol: Experiment and data reduction. *Fluid Phase Equilibria* **1986,** *25*, (3), 303-322.
(26) Lam D.H., Luks K.D., Multiphase equilibrium behavior of the mixture ethane + methanol + 1-decanol. *Journal of Chemical & Engineering Data* **1991,** *36*, (3), 307-311.
(27) Ma Y.H., Kohn J.P., Multiphase and Volumetric Equilibria of the Ethane-Methanol System at Temperatures between -40 C. and 100 C. *Journal of Chemical & Engineering Data* **1964,** *9*, (1), 3-5.
(28) Ishihara K., Tanaka H., Kato M., Phase equilibrium properties of ethane+ methanol system at 298.15 K. *Fluid Phase Equilibria* **1998,** *144*, (1), 131-136.
(29) Ohgaki K., Sano F., Katayama T., Isothermal vapor-liquid equilibrium data for binary systems containing ethane at high pressures. *Journal of Chemical and Engineering Data* **1976,** *21*, (1), 55-58.
(30) Zheng D.-Q., Ma W.-D., Wei R., Guo T.-M., Solubility study of methane, carbon dioxide and nitrogen in ethylene glycol at elevated temperatures and pressures. *Fluid Phase Equilibria* **1999,** *155*, (2), 277-286.
(31) Jou F.-Y., Deshmukh R., Otto F., Mather A., Vapor - liquid equilibria of H_2S and CO_2 and ethylene glycol at elevated pressures. *Chemical engineering communications* **1990,** *87*, (1), 223-231.

(32) Gui X., Tang Z., Fei W., Solubility of CO_2 in alcohols, glycols, ethers, and ketones at high pressures from (288.15 to 318.15) K. *Journal of Chemical & Engineering Data* **2011,** *56*, (5), 2420-2429.
(33) Serpa F.S., Vidal R.S., Filho J.o.H.A., Nascimento J.F.d., Ciambelli J.o.R., Figueiredo C.M., Salazar-Banda G.R., Santos A.F., Fortuny M., Franceschi E., Solubility of carbon dioxide in ethane-1, 2-diol–water mixtures. *Journal of Chemical & Engineering Data* **2013,** *58*, (12), 3464-3469.
(34) Afzal W., Liu X., Prausnitz J.M., Solubilities of some gases in four immidazolium-based ionic liquids. *The Journal of Chemical Thermodynamics* **2013,** *63*, 88-94.
(35) Jou F.Y., Otto F.D., Mather A.E., Solubility of methane in glycols at elevated pressures. *The Canadian Journal of Chemical Engineering* **1994,** *72*, (1), 130-133.
(36) Jou F.-Y., Schmidt K.A.G., Mather A.E., Vapor–liquid equilibrium in the system ethane + ethylene glycol. *Fluid Phase Equilibria* **2006,** *240*, (2), 220-223.
(37) Jou F.Y., Deshmukh R.D., Otto F.D., Mather A.E., Vapor - liquid equilibria for acid gases and lower alkanes in triethylene glycol. *Fluid Phase Equilibria* **1987,** *36*, (0), 121-140.
(38) Wilson L., Wilding W., Wilson G., In *Vapor-Liquid Equilibrium Measurements on Four Binary Mixtures*, presented on AIChE Symp. Ser, **1989**
(39) Rowley R., Hoffma G., In *Vapor-Liquid Equilibrium Measurements on Mixtures Important to Industrial Design: Triethylene Glycol+ n-hexane, Triethylene Glycol+ Cyclohexane and Furfural+ Isoprene*, presented on AIChE Symp. Ser, **1990**
(40) Gupta S.K., Rawat B.S., Goswami A.N., Nanoti S.M., Krishna R., Isobaric vapour—liquid equilibria of the systems: Benzene-triethylene glycol, toluene-triethylene glycol and benzene-N-methylpyrrolidone. *Fluid Phase Equilibria* **1989,** *46*, (1), 95-102.
(41) Mokraoui S., Coquelet C., Valtz A., Hegel P.E., Richon D., New Solubility Data of Hydrocarbons in Water and Modeling Concerning Vapor–Liquid–Liquid Binary Systems. *Industrial & engineering chemistry research* **2007,** *46*, (26), 9257-9262.
(42) Mączyński A., Wiśniewska-Gocłowska B., Goral M., Recommended liquid–liquid equilibrium data. Part 1. Binary alkane–water systems. *Journal of Physical and Chemical Reference Data* **2004,** *33*, (2), 549-577.
(43) Gillespie P.C., Wilson G.M., *Vapour–Liquid and Liquid–Liquid Equilibria: Water–Methane, Water–Carbon Dioxide, Water–Hydrogen Sulphide, Water–n Pentane, Water–Methane–n-Pentane., RR-48*; Gas Processing Association: Tulsa, OK, 1982.
(44) Tsonopoulos C., Wilson G., High-temperature mutual solubilities of hydrocarbons and water. Part I: Benzene, cyclohexane and n-hexane. *AIChE Journal* **1983,** *29*, (6), 990-999.
(45) Englin B., Plate A., Tugolukov V., Pryanishnikova M., Solubility of water in individual hydrocarbons. *Chemistry and Technology of Fuels and Oils* **1965,** *1*, (9), 722-726.
(46) Nelson H., de Ligny C., Determination of the solubilities of some n-alkanes in water at different temperatures by gas chromatography. *Recl. Trav. Chim. Pays-Bas* **1968,** *87*.
(47) Marche C., Ferronato C., Jose J., Solubilities of n-Alkanes (C6 to C8) in Water from 30 °C to 180 °C. *Journal of Chemical & Engineering Data* **2003,** *48*, (4), 967-971.
(48) Heidman J., Tsonopoulos C., Brady C., Wilson G., High-temperature mutual solubilities of hydrocarbons and water. Part II: Ethylbenzene, ethylcyclohexane, and n-octane. *AIChE Journal* **1985,** *31*, (3), 376-384.

(49) Jou F.-Y., Mather A.E., Liquid–Liquid Equilibria for Binary Mixtures of Water + Benzene, Water + Toluene, and Water + p-Xylene from 273 K to 458 K. *Journal of Chemical & Engineering Data* **2003,** *48*, (3), 750-752.
(50) Ng H.-J., Chen C.-J., *Mutual Solubility in Water-hydrocarbon Systems: GPA Project 895, RR-150*; Gas Processors Association: 1995.
(51) Anderson F.E., Prausnitz J.M., Mutual solubilities and vapor pressures for binary and ternary aqueous systems containing benzene, toluene, m-xylene, thiophene and pyridine in the region 100–200° C. *Fluid Phase Equilibria* **1986,** *32*, (1), 63-76.

Appendix B

Parameters of Aspen Icarus used for the economic evaluation of a natural gas TEG dehydration plant

Table B.1: Cashflow parameters as used in the Aspen Icarus software for the economic evaluation of a natural gas TEG dehydration plant

ITEM	Units	Value
TW (Number of Weeks per Period)	Weeks/period	52
T (Number of Periods for Analysis)	Period	20
DTEPC (Duration of EPC Phase)	Period	0.365385
DT (Duration of EPC Phase and Startup)	Period	0.75
WORKP (Working Capital Percentage)	Percent/period	5
OPCHG (Operating Charges)	Percent/period	25
PLANTOVH (Plant Overhead)	Percent/period	50
CAPT (Total Project Cost)	Cost	5.21E+06
RAWT (Total Raw Material Cost)	Cost/period	23527.8
PRODT (Total Product Sales)	Cost/period	0
OPMT (Total Operating Labor and Maintenance Cost)	Cost/period	612200
UTILT (Total Utilities Cost)	Cost/period	188526
ROR (Desired Rate of Return/Interest Rate)	Percent/period	20
AF (ROR Annuity Factor)		5
TAXR (Tax Rate)	Percent/period	40
IF (ROR Interest Factor)		1.2
ECONLIFE (Economic Life of Project)	Period	5
SALVAL (Salvage Value (Percent of Initial Capital Cost))	Percent	20
DEPMETH (Depreciation Method)		Straight Line
DEPMETHN (Depreciation Method Id)		1
ESCAP (Project Capital Escalation)	Percent/period	5
ESPROD (Products Escalation)	Percent/period	5
ESRAW (Raw Material Escalation)	Percent/period	3.5
ESLAB (Operating and Maintenance Labor Escalation)	Percent/period	3
ESUT (Utilities Escalation)	Percent/period	3
START (Start Period for Plant Startup)	Period	1
PODE (Desired Payout Period (excluding EPC and Startup Phases))	Period	
POD (Desired Payout Period)	Period	
DESRET (Desired Return on Project for Sales Forecasting)	Percent/Period	10.5
END (End Period for Economic Life of Project)	Period	5
GA (G and A Expenses)	Percent/Period	8
DTEP (Duration of EP Phase before Start of Construction)	Period	0.173077
OP (Total Operating Labor Cost)	Cost/period	600000
MT (Total Maintenance Cost)	Cost/period	12200

Table B.2: Summary of the project parameters used for the evaluation of the capital cost and the time period in Aspen Icarus Software.

ITEM	Units	Value
Capital Cost Evaluation Basis		
Date		14MAY18
Country		EU
Units of Measure		METRIC
System Cost Base Date		1Q 14
Project Type		Grass roots/Clear field
Design code		DIN
Plant Location		Rotterdam
Time Difference Between System Cost Base Date and Start Date for Engineering	Days	1007
Time period		
Period Description		Year
Operating Hours per Period	Hours/period	8000
Number of Weeks per Period	Weeks/period	52
Number of Periods for Analysis	Period	20

Table B.3: Equipment type used for the mapping and costing of the equipment cost in Aspen Icarus software.

Unit	Component Type
Glycol cooler	DHE TEMA EXCH
HE-1	DHE TEMA EXCH
HE-2	DHE TEMA EXCH
P-1	DCP CENTRIF
P-2	DCP CENTRIF
Flash	DVT CYLINDER
Contactor	
Main Tower	DTW TRAYED
Regenerator	
Condenser	EHE JACKETED
Reboiler	DRB THERMOSIPH
Main Tower	DTW TRAYED

Table B.4: Summary of the utility types and rate used by Aspen Icarus software for the estimation of the operating cost

Utility	Fluid	Item	Rate	Units
Electricity		DCP CENTRIF	0.75	kWh
Electricity		DCP CENTRIF	11	kWh
Cooling Water	Water	EHE JACKETED	0.282597	m^3/h
Cooling Water	Water	DHE TEMA EXCH	16.189165	m^3/h
Steam @690KPA	LP Steam	DHE TEMA EXCH	0.011051	ton/h
Steam @690KPA	LP Steam	DHE TEMA EXCH	0.006355	ton/h
Steam @2760KPA	HP Steam	DRB THERMOSIPH	0.659334	ton/h

Appendix C

Experimental points database used for the fitting of UMR-CPAPRU IPs.

Table C.1: Database of experimental binary VLEdata used for the regression of UNIFAC group IPs for UMR-CPAPRU.

Component	Ref.	n_p	Type	Year	T range (K)	P range (bar)	x_1 range	y_2 range
Water (2) with								
CO_2	1	11	Isothermal (TPx)	2004	278.22 - 298.28	4.96 - 34.91	0.00314 - 0.01772	0.0007 - 0.0065
	2	7	Isothermal (TPxy)	1992	288.15 - 313.15	50.70 - 126.70	0.02142 - 0.02757	0.0013 - 0.0047
	3	6	Isothermal (TPx)	1941	323.15 - 348.15	25.30 - 101.33	0.00545 - 0.00206	–
	4	3	Isothermal (TPx)	1940	304.19	25.30 - 101.30	0.01127 - 0.02368	–
	5	18	Isothermal (TPxy)	2000	333.15 - 353.15	40.50 - 141.10	0.00800 - 0.02080	0.0047 - 0.0143
	6	12	Isothermal (TPxy)	1988	373.13	3.25 - 23.07	0.00045 - 0.00414	0.0450 - 0.2880
methane	7	29	Isothermal (TPxy)	1970	323.15 - 588.71	13.789 - 616.06	0.00017 - 0.00676	0.1678 - 0.9990
	8	18	Isothermal (TPx)	1997	283.37 - 283.37	5.67 - 90.82	0.00026 - 0.00200	–
	9	11	Isothermal (TPxy)	1972	423.2 - 523.2	98.10 - 980.70	0.00100 - 0.01510	0.0600 - 0.0900
	10	22	Isothermal (TPxy)	2013	283.89 - 323.56	47.80 - 194.90	0.00060 - 0.00261	0.0004 - 0.0017
	11	16	Isothermal (TPx)	2003	283.2 - 313.11	9.73 - 179.98	0.00020 - 0.00246	–
	12	9	Isothermal (TPx)	2003	298.15	23.00 – 166.00	0.00053 - 0.00265	–
	13	15	Isothermal (TPxy)	1985	298.15 - 338.15	25.00 - 125.00	0.00041 - 0.00221	0.0026 - 0.0023
	14	4	Isobaric (TPx)	1997	273.10 – 288.15	34.50	0.00120 – 0.01520	
	15	15	Isothermal (TPxy)	2012	298.21 – 303.28	52.46 – 123.45	0.00098 – 0.00203	0.0003 - 0.0008
	16	8	Isothermal (TPx)	2009	298.77 – 314.28	9.93 – 99.81	0.00021 – 0.00160	–
	17	12	Isothermal (TPx)	2010	313.15 – 323.15	1.12 – 6.38	0.00001 – 0.00023	–
	18	29	Isothermal (TPx)	2003	313.35 - 373.29	0.07 - 92.60	0.00000 - 0.00154	–
	19	6	Isothermal (TPxy)	1988	298.14 – 313.71	30.00 – 80.00	0.00051 - 0.00162	0.0004 – 0.0045
	20	3	Isothermal (TPx)	1998	344	200.00 – 750.00	0.00218 - 0.00466	–
	21	14	Isothermal (TPx)	1997	324.15 - 375.15	56.00 – 580.00	0.00089 - 0.00411	–

Table C.1 (continued)

Component	Ref.	n_p	Type	Year	T range (K)	P range (bar)	x_1 range	y_2 range
Water (2) with								
N_2	22	34	Isothermal (TPx)	1979	298.15 - 513.15	25.33 - 1013.25	0.0002 - 0.0051	–
ethane	23	43	Isothermal (TPx)	2004	274.26 - 343.08	3.73 - 49.52	9.0 E-5 - 9.7 E-5	–
	22	15	Isothermal (TPx)	1979	377.59 - 444.26	7.80 - 137.89	5.0 E-5 - 0.0017	–
	12	6	Isothermal (TPx)	2003	298.15	14.00 - 39.00	0.0004 - 0.0011	–
methanol	24	14	Isothermal (TPxy)	1980	298.14	0.04 - 0.17	0.0444 - 1.0	0.0 - 0.7223
	25	39	Isothermal (TPxy)	1976	308.15 - 338.13	0.06 - 1.03	0.0 - 1.0	0.0 - 1.0
	26	10	Isothermal (TPxy)	1969	313.05	0.17 - 0.34	0.2095 - 0.9510	0.0175 - 0.3565
	27	33	Isothermal (TPxy)	1989	318.14 - 333.13	0.10 - 0.85	0.0 - 1.0	0.0 - 1.0
	28	9	Isothermal (TPxy)	1995	353.15	0.64 - 1.75	0.0500 - 0.9430	0.0330 - 0.7150
	29	53	Isothermal (TPxy)	1952	373.15 - 523.15	1.04 - 84.05	0.0022 - 0.9690	0.0180 - 0.9808
MEG	30	23	Isothermal (TPx)	1983	323.15	0.00 - 0.12	0.0 - 1.0	–
	31	15	Isothermal (TPx)	1999	298.03 - 303.06	0.00 - 0.04	0.0 - 1.0	–
	32	24	Isothermal (TPx)	1984	332.98	0.00 - 0.20	0.0 - 1.0	–
	33	26	Isothermal (TPx)	1983	338.23 - 350.83	0.02 - 0.43	0.0 - 0.9450	–
	34	39	Isothermal (TPxy)	1993	343.10 - 363.20	0.06 - 0.70	0.0 - 0.8605	0.9105 - 1.0
	35	42	Isothermal (TPxy)	1996	371.15 - 395.15	0.04 - 1.50	0.0300 - 0.994	0.1910 - 0.9990

Table C.1 (continued)

Component	Ref.	n_p	Type	Year	T range (K)	P range (bar)	x_1 range	y_2 range
Water (2) with								
ethanol	36	57	Isothermal (TPx)	1960	273.15 - 293.14	0.00 - 0.06	0.0020 - 1.0	–
	37	11	Isothermal (TPxy)	1995	298.15	0.05 - 0.08	0.0630 - 0.9730	0.0290 - 0.6350
	38	95	Isothermal (TPxy)	1978	303.14 - 363.13	0.04 - 1.59	0.0043 - 0.9815	0.0181 - 0.9588
	39	28	Isothermal (TPxy)	2006	313.15	0.07 - 0.18	0.0 - 1.0	0.0000 - 1.0000
	40	13	Isothermal (TPxy)	1972	328.14	0.23 - 0.37	0.0510 - 0.9540	0.0480 - 0.6640
	41	36	Isothermal (TPxy)	1995	333.15	0.32 - 0.47	0.0742 - 0.9583	0.0438 - 0.5870
	42	12	Isothermal (TPxy)	2013	353.15	0.47 - 1.11	0.0 - 1.0	0.0000 - 1.0000
	43	48	Isothermal (TPxy)	2013	381.4 - 423.7	1.56 - 9.88	0.0137 - 0.9991	0.0006 - 0.8900
	44	10	Isothermal (TPxy)	1986	473.15	17.93 - 30.13	0.0230 - 0.9340	0.0710 - 0.8660
	45	7	Isothermal (TPxy)	1959	473.15	21.71 - 29.47	0.0970 - 0.6860	0.2870 - 0.6950
methanol (2) with								
N_2	22	21	Isothermal (TPx)	1979	273.15 - 343.15	49.00 - 295.00	0.0109 - 0.0687	–
	46	24	Isothermal (TPxy)	2002	298.15 - 318.15	6.70 - 101.90	0.0010 - 0.0221	0.0037 - 0.0799

Table C.1 (continued)

Component	Ref.	n_p	Type	Year	T range (K)	P range (bar)	x_1 range	y_2 range
methanol (2) with								
CO_2	47	64	Isothermal (TPxy)	1988	230.01 - 329.99	6.90 - 106.46	0.0245 - 0.9865	0.0002 - 0.1241
	48	6	Isothermal (TPxy)	2002	298.15	13.00 - 54.40	0.0946 - 0.5399	0.0098 – 0.0176
	49	45	Isothermal (TPxy)	2001	313.15 - 342.8	6.00 - 123.90	0.0247 - 0.9350	0.0143 - 0.2280
	50	36	Isothermal (TPxy)	1991	323.2 - 477.6	4.39 - 165.00	0.0087 - 0.8500	0.0223 - 0.8717
CH_4	51	49	Isothermal (TPxy)	1987	273.15 - 330	13.79 - 413.69	0.0095 - 0.2575	0.0009 - 0.0626
	52	9	Isothermal (TPx)	2002	280.15	21.12 - 114.08	0.0170 - 0.0880	–
	53	8	Isothermal (TPx)	2012	294.50	10.50 - 79.90	0.0110 - 0.0750	–
	13	15	Isothermal (TPxy)	1985	298.15 - 338.15	25.00 - 125.00	0.0221 - 0.0944	0.0039 - 0.0457
	10	9	Isothermal (TPxy)	2013	298.87 - 298.87	52.4 - 180.10	0.0413 - 0.1348	0.0037 - 0.0054
	54	15	Isothermal (TPxy)	1987	298.15 - 373.15	54.50 - 592.00	0.0374 - 0.5648	0.0047 - 0.3058
C_2H_6	55	24	Isothermal (TPxy)	1964	273.15 - 373.15	10.13 - 60.80	0.0027 - 0.3210	0.0220 - 1.0

Table C.1 (continued)

Component	Ref.	n_p	Type	Year	T range (K)	P range (bar)	x_1 range	y_2 range
methanol (2) with								
propane	56	9	Isothermal (TPxy)	2004	327.95	3.50 - 19.00	0.0192 - 0.7414	0.0434 - 0.2499
	57	39	Isothermal (TPxy)	1992	310.70 - 474.30	0.32 - 86.63	0.0000 - 0.9840	0.0200 - 1.0000
	58	32	Isothermal (TPxy)	1986	313.10 - 373.10	3.50 - 42.80	0.0153 - 1.0	0.0000 - 0.4630
nC5	59	24	Isothermal (TPx)	1991	303.15	0.22 - 1.00	0.0 - 1.0	–
	60	33	Isothermal (TPxy)	1987	372.70 - 422.60	3.47 - 25.28	0.0 - 1.0	0.0000 - 1.0000
nC6	61	7	Isothermal (TPxy)	1978	298.15	0.33 - 0.35	0.0500 - 0.9500	0.4980 - 0.5760
	62	14	Isothermal (TPx)	1985	313.15	0.35 - 0.69	0.0 - 1.0	–
	63	13	Isothermal (TPxy)	1931	318.15	0.44 - 0.84	0.0718 - 1.0	0.0000 - 0.5261
benzene	64	11	Isothermal (TPx)	1969	288.15	0.11 - 0.15	0.0530 - 0.9680	–
	61	9	Isothermal (TPxy)	1978	298.14	0.22 - 0.24	0.1000 - 0.9000	0.4760 - 0.7090
	65	10	Isothermal (TPxy)	1981	308.19	0.20 - 0.39	0.0 - 1.0	0.0000 - 1.0000
	66	33	Isothermal (TPxy)	1994	318.15	0.30 - 0.60	0.0 - 1.0	0.0000 - 1.0000
	67	5	Isothermal (TPxy)	1952	328.15	0.66 - 0.90	0.4012 - 0.9595	0.3518 - 0.6056

Table C.1 (continued)

Component	Ref.	n_p	Type	Year	T range (K)	P range (bar)	x_1 range	y_2 range
methanol (2) with								
benzene	68	22	Isothermal (TPx)	1926	333.12 - 353.12	0.53 - 2.17	0.0 - 1.0	–
	69	16	Isothermal (TPxy)	1957	363.12 - 373.07	2.49 - 4.18	0.0935 - 0.9074	0.1624 - 0.5423
	70	60	Isothermal (TPxy)	1968	393.12 - 493.11	4.87 - 57.64	0.0479 - 0.9767	0.1068 - 0.9477
toluene	71	15	Isothermal (TPx)	2004	313.15	0.08 - 0.37	0.0 - 1.0	–
	72	11	Isothermal (TPxy)	1988	318.14	0.23 - 0.47	0.0400 - 0.9750	0.5800 - 0.9350
	73	37	Isobaric (TPxy)	1972	336.63 - 383.72	1.01	0.0 - 1.0	0.0 - 1.0
MEG (2) with								
N_2	74	31	Isothermal (TPx)	1979	323.15 - 398.15	15.70 - 396.00	0.0015 - 0.0190	–
CH_4	75	34	Isothermal (TPx)	1994	298.15 - 398.15	1.05 - 203.50	0.0001 - 0.0224	–
	74	31	Isothermal (TPx)	1999	323.15 - 398.15	2.00 - 396.20	0.0003 - 0.0421	–
C_2H_6	76	34	Isothermal (TPx)	1994	298.15 - 398.15	0.00 - 203.40	0.0003 - 0.0308	–

Table C.2: Database of experimental binary LLE data used for the regression of UNIFAC group IPs for UMR-CPAPRU.

Component	Ref.	n_p	Type	Year	T range (K)	P range (bar)	x_1 aqueous phase (I)	x_2 HC–rich phase (II)
water (2) with								
n-pentane	77	4	TPx_1^I	2007	313.19 - 343.15	–	1.2 E-5 – 1.5 E-5	–
Benzene	78	21	$Tx_1^I x_2^{II}$	1983	279.15 - 490.80	–	0.0004 - 0.0061	0.0017 - 0.2578
toluene	79	11	$TPx_1^I x_2^{II}$	2003	283.15 - 458.15	0.03 - 17.00	0.0001 - 0.0017	0.0017 - 0.1328
	80	1	$Tx_1^I x_2^{II}$	1995	310.90	–	1.2 E-5	0.0039
	81	2	TPx_2^{II}	1986	448.31 - 473.51	14.25 - 23.76	0.0013 - 0.0026	0.0098 - 0.1592
	82	1	TPx_1^I	2006	323.15	1.01	–	0.00675

Literature Cited

(1) Valtz A., Chapoy A., Coquelet C., Paricaud P., Richon D., Vapour–liquid equilibria in the carbon dioxide–water system, measurement and modelling from 278.2 to 318.2 K. *Fluid Phase Equilibria* **2004,** *226*, 333-344.
(2) King M.B., Mubarak A., Kim J.D., Bott T.R., The mutual solubilities of water with supercritical and liquid carbon dioxides. *The Journal of Supercritical Fluids* **1992,** *5*, (4), 296-302.
(3) Wiebe R., Gaddy V.L., Vapor Phase Composition of Carbon Dioxide-Water Mixtures at Various Temperatures and at Pressures to 700 Atmospheres. *Journal of the American Chemical Society* **1941,** *63*, (2), 475-477.
(4) Wiebe R., Gaddy V.L., The Solubility of Carbon Dioxide in Water at Various Temperatures from 12 to 40° and at Pressures to 500 Atmospheres. Critical Phenomena*. *Journal of the American Chemical Society* **1940,** *62*, (4), 815-817.
(5) Bamberger A., Sieder G., Maurer G., High-pressure (vapor+liquid) equilibrium in binary mixtures of (carbon dioxide+water or acetic acid) at temperatures from 313 to 353 K. *The Journal of Supercritical Fluids* **2000,** *17*, (2), 97-110.
(6) Muller G., Bender E., Maurer G., Vapor-liquid-equilibrium in the ternary-system ammonia-carbon dioxide-water at high water contents in the range 373-K to 473-K. *Berichte Der Bunsen-Gesellschaft-Physical Chemistry Chemical Physics* **1988,** *92*, (2), 148-160.
(7) O'Sullivan T.D., Smith N.O., Solubility and partial molar volume of nitrogen and methane in water and in aqueous sodium chloride from 50 to 125. deg. and 100 to 600 atm. *The Journal of Physical Chemistry* **1970,** *74*, (7), 1460-1466.
(8) Lekvam K., Bishnoi P.R., Dissolution of methane in water at low temperatures and intermediate pressures. *Fluid Phase Equilibria* **1997,** *131*, (1-2), 297-309.
(9) Sultanov R., Skripka V., Namiot A.Y., Phase equilibrium and critical effect of water-methane system under increased temperature and pressure. *Zhurnal Fizicheskoi Khimii* **1972,** *46*, (8), 2160.
(10) Frost M., Karakatsani E., von Solms N., Richon D., Kontogeorgis G.M., Vapor–Liquid Equilibrium of Methane with Water and Methanol. Measurements and Modeling. *Journal of Chemical & Engineering Data* **2013,** *59*, (4), 961-967.
(11) Chapoy A., Mohammadi A.H., Tohidi B., Richon D., Estimation of water content for methane+ water and methane+ ethane+ n-butane+ water systems using a new sampling device. *Journal of Chemical & Engineering Data* **2005,** *50*, (4), 1157-1161.
(12) Kim Y.S., Ryu S.K., Yang S.O., Lee C.S., Liquid Water–Hydrate Equilibrium Measurements and Unified Predictions of Hydrate-Containing Phase Equilibria for Methane, Ethane, Propane, and Their Mixtures. *Industrial & engineering chemistry research* **2003,** *42*, (11), 2409-2414.
(13) Yarym-Agaev N., Sinyavskaya R., Koliushko I., Phase equilibrium in the binary systems water-methane and methanol-methane under high pressure. *Zh. Prikl. Khim* **1985,** *58*, 165-168.
(14) Song K.Y., Feneyrou G., Fleyfel F., Martin R., Lievois J.,Kobayashi R., Solubility measurements of methane and ethane in water at and near hydrate conditions. *Fluid Phase Equilibria* **1997,** *128*, (1), 249-259.

(15) Fonseca J.M.S., von Solms N., Development and testing of a new apparatus for the measurement of high-pressure low-temperature phase equilibria. *Fluid Phase Equilibria* **2012,** *329*, 55-62.
(16) Awan J.A., Thomsen K., Coquelet C., Fosbøl P.L., Richon D., Vapor– liquid equilibrium measurements and modeling of the propyl mercaptan+ methane+ water system. *Journal of Chemical & Engineering Data* **2009,** *55*, (2), 842-846.
(17) Siqueira Campos C.E.P., Penello J.R., Pellegrini Pessoa F.L., Cohen Uller A.M., Experimental Measurement and Thermodynamic Modeling for the Solubility of Methane in Water and Hexadecane. *Journal of Chemical & Engineering Data* **2010,** *55*, (7), 2576-2580.
(18) Kiepe J., Horstmann S., Fischer K., Gmehling J., Experimental determination and prediction of gas solubility data for methane+ water solutions containing different monovalent electrolytes. *Industrial & engineering chemistry research* **2003,** *42*, (21), 5392-5398.
(19) Yokoyama C., Wakana S., Kaminishi G., Takahashi S., Vapor-liquid equilibria in the methane-diethylene glycol-water system at 298.15 and 323.15 K. *Journal of Chemical and Engineering Data* **1988,** *33*, (3), 274-276.
(20) Dhima A., de Hemptinne J.-C., Moracchini G., Solubility of light hydrocarbons and their mixtures in pure water under high pressure. *Fluid Phase Equilibria* **1998,** *145*, (1), 129-150.
(21) Gao J., Zheng D.-Q., Guo T.-M., Solubilities of methane, nitrogen, carbon dioxide, and a natural gas mixture in aqueous sodium bicarbonate solutions under high pressure and elevated temperature. *Journal of Chemical & Engineering Data* **1997,** *42*, (1), 69-73.
(22) Kertes, *IUPAC Solubility Data Series, Pergamon Press: Oxford*. 1979.
(23) Mohammadi A.H., Chapoy A., Tohidi B.,Richon D., Measurements and thermodynamic modeling of vapor-liquid equilibria in ethane-water systems from 274.26 to 343.08 K. *Industrial & engineering chemistry research* **2004,** *43*, (17), 5418-5424.
(24) Koner Z., Phutela R., Fenby D., Determination of the equilibrium constants of water-methanol deuterium exchange reactions from vapour pressure measurements. *Australian Journal of Chemistry* **1980,** *33*, (1), 9-13.
(25) McGlashan M.L., Williamson A.G., Isothermal liquid-vapor equilibriums for system methanol-water. *Journal of Chemical & Engineering Data* **1976,** *21*, (2), 196-199.
(26) Ratcliff G.A., Chao K.C., Prediction of thermodynamic properties of polar mixtures by a group solution model. *The Canadian Journal of Chemical Engineering* **1969,** *47*, (2), 148-153.
(27) Fu J.W., Hu, Y., Studies on vapor-liquid and liquid-liquid-vapor equilibria for the ternary system methanol-methyl methacrylate - water (I) three binary systems. *Huagong Xuebao* **1989**, (1), 1-13.
(28) Zonghong B., Mingjian L., Jianpin Y., Nianci W., Measurement and correlation of moderate pressure vapor-liquid equilibrium data for methanol-water binary system. *Journal of Chemical Industry and Engineering (China)* **1995,** *2*, 015.
(29) Griswold J., Wong S.Y., *Chem. Eng. Prog. Symp. Ser.* **1952,** *48*, 18.
(30) Gonzalez C., Van Ness H.C., Excess thermodynamic functions for ternary systems. 9. Total-pressure data and GE for water/ethylene glycol/ethanol at 50.degree.C. *Journal of Chemical & Engineering Data* **1983,** *28*, (4), 410-412.

(31) Mokbel I., Porcedda S., Guetachew T., Marongiu B., Jose J., Static measurements of the total vapor pressure of ethane-1, 2-diol+ water mixtures at temperatures from 258 K to 363 K. *ELDATA International Electronic Journal of Physico-Chemical Reference Data* **1999,** *5*, 79-84.
(32) Villamanan M.A., Gonzalez C., Van Ness H.C., Excess thermodynamic properties for water/ethylene glycol. *Journal of Chemical and Engineering Data* **1984,** *29*, (4), 427-429.
(33) Nath A., Bender E., Isothermal vapor-liquid equilibriums of binary and ternary mixtures containing alcohol, alkanolamine, and water with a new static device. *Journal of Chemical and Engineering Data* **1983,** *28*, (4), 370-375.
(34) Chiavone-Filho O., Proust P., Rasmussen P., Vapor-liquid equilibria for glycol ether+ water systems. *Journal of Chemical and Engineering Data* **1993,** *38*, (1), 128-131.
(35) Lancia A., Musmarra D., Pepe F., Vapor-liquid equilibria for mixtures of ethylene glycol, propylene glycol, and water between 98. DEG. and 122. DEG. C. *Journal of chemical engineering of Japan* **1996,** *29*, (3), 449-455.
(36) Garbarenko V., Stabnikov V., On the vapor–liquid phase equilibrium in the system ethanol–water. *Izvestiya Vysshikh Uchebnykh Zavedenii Pishchevaya Tecknologiya* **1960,** *4*, 112-120.
(37) Yamamoto H., Terano T., Nishi Y., Tokunaga J., Vapor-liquid equilibria for methanol+ ethanol+ calcium chloride,+ ammonium iodide, and+ sodium iodide at 298.15 K. *Journal of Chemical and Engineering Data* **1995,** *40*, (2), 472-477.
(38) Pemberton R.C., Mash C.J., Thermodynamic properties of aqueous non-electrolyte mixtures II. Vapour pressures and excess Gibbs energies for water + ethanol at 303.15 to 363.15 K determined by an accurate static method. *The Journal of Chemical Thermodynamics* **1978,** *10*, (9), 867-888.
(39) Vu D.T., Lira C.T., Asthana N.S., Kolah A.K., Miller D.J., Vapor– liquid equilibria in the systems ethyl lactate+ ethanol and ethyl lactate+ water. *Journal of Chemical & Engineering Data* **2006,** *51*, (4), 1220-1225.
(40) Mertl I., Liquid-vapour equilibrium. IL. Phase equilibria in the ternary system ethyl acetate-ethanol-water. *Collection of czechoslovak chemical communications* **1972,** *37*, (2), 366-374.
(41) Kurihara K., Minoura T., Takeda K., Kojima K., Isothermal Vapor-Liquid Equilibria for Methanol + Ethanol + Water, Methanol + Water, and Ethanol + Water. *J. Chem. Eng. Data* **1995,** *40*, 679-684.
(42) Arango I.C., Villa A.L., Isothermal vapor–liquid and vapor–liquid–liquid equilibrium for the ternary system ethanol+ water+ diethyl carbonate and constituent binary systems at different temperatures. *Fluid Phase Equilibria* **2013,** *339*, 31-39.
(43) Cristino A.F., Rosa S., Morgado P., Galindo A., Filipe E.J.M., Palavra A.M.F., Nieto de Castro C.A., High-temperature vapour–liquid equilibrium for the water–alcohol systems and modeling with SAFT-VR: 1. Water–ethanol. *Fluid Phase Equilibria* **2013,** *341*, 48-53.
(44) Niesen V., Palavra A., Kidnay A.J., Yesavage V.F., An apparatus for vapor-liquid equilibrium at elevated temperatures and pressures and selected results for the water-ethanol and methanol-ethanol systems. *Fluid Phase Equilibria* **1986,** *31*, (3), 283-298.

(45) Barr-David F., Dodge B.F., Vapor-Liquid Equilibrium at High Pressures. The Systems Ethanol-Water and 2-Propanol-Water. *Journal of Chemical & Engineering Data* **1959,** *4*, (2), 107-121.
(46) Laursen T., Andersen S.I., High-pressure vapor-liquid equilibrium for nitrogen+ methanol. *Journal of Chemical & Engineering Data* **2002,** *47*, (5), 1173-1174.
(47) Hong J.H., Kobayashi R., Vapor-liquid equilibrium studies for the carbon dioxide-methanol system. *Fluid Phase Equilibria* **1988,** *41*, (3), 269-276.
(48) Laursen T., Rasmussen P., Andersen S.I., VLE and VLLE measurements of dimethyl ether containing systems. *Journal of Chemical & Engineering Data* **2002,** *47*, (2), 198-202.
(49) Joung S.N., Yoo C.W., Shin H.Y., Kim S.Y., Yoo K.-P., Lee C.S., Huh W.S., Measurements and correlation of high-pressure VLE of binary CO2–alcohol systems (methanol, ethanol, 2-methoxyethanol and 2-ethoxyethanol). *Fluid Phase Equilibria* **2001,** *185*, (1–2), 219-230.
(50) Leu A.-D., Chung S.Y.-K., Robinson D.B., The equilibrium phase properties of (carbon dioxide+ methanol). *The Journal of Chemical Thermodynamics* **1991,** *23*, (10), 979-985.
(51) Hong J.H., Malone P.V., Jett M.D., Kobayashi R., The measurement and interpretation of the fluid-phase equilibria of a normal fluid in a hydrogen bonding solvent: the methane - methanol system. *Fluid Phase Equilibria* **1987,** *38*, (1–2), 83-96.
(52) Ukai T., Kodama D., Miyazaki J., Kato M., Solubility of methane in alcohols and saturated density at 280.15 K. *Journal of Chemical & Engineering Data* **2002,** *47*, (5), 1320-1323.
(53) Nourozieh H., Kariznovi M., Abedi J., Phase equilibrium measurements and thermodynamic modeling of methane alcohol systems at ambient temperature. *The Journal of Chemical Thermodynamics* **2012,** *54*, (0), 165-170.
(54) Brunner E., Hültenschmidt W., Schlichthärle G., Fluid mixtures at high pressures IV. Isothermal phase equilibria in binary mixtures consisting of (methanol+ hydrogen or nitrogen or methane or carbon monoxide or carbon dioxide). *The Journal of Chemical Thermodynamics* **1987,** *19*, (3), 273-291.
(55) Ma Y.H., Kohn J.P., Multiphase and Volumetric Equilibria of the Ethane-Methanol System at Temperatures between -40 C. and 100 C. *Journal of Chemical & Engineering Data* **1964,** *9*, (1), 3-5.
(56) Joung S.N., Shin H.Y., Kim H.S., Yoo K.-P., High-Pressure Vapor– Liquid Equilibrium Data and Modeling of Propane+ Methanol and Propane+ Ethanol Systems. *Journal of Chemical & Engineering Data* **2004,** *49*, (3), 426-429.
(57) Lev A.D., Robinson D.B., Chung S.Y.K., Chen C.J., The equilibrium phase properties of the propane-methanol and n-Butane-methanol binary systems. *The Canadian Journal of Chemical Engineering* **1992,** *70*, (2), 330-334.
(58) Galivel-Solastiouk F., Laugier S., Richon D., Vapor-liquid equilibrium data for the propane-methanol and propane-methanol-carbon dioxide system. *Fluid Phase Equilibria* **1986,** *28*, (1), 73-85.
(59) Thomas S., Bhethanabotla V.R., Campbell S.W., Total pressure measurements for n-pentane-methanol-2-butanol at 303.15 K. *Journal of Chemical and Engineering Data* **1991,** *36*, (4), 374-378.

(60) Wilsak R.A., Campbell S.W., Thodos G., Vapor-liquid equilibrium measurements for the n-pentane-methanol system at 372.7, 397.7 and 422.6 K. *Fluid Phase Equilibria* **1987,** *33*, (1–2), 157-171.
(61) Iguchi A., Vapor-liquid equilibriums at 25 C for binary systems between alcohols and hydrocarbons. *Kagaku Sochi* **1978,** *20*, 66-68.
(62) Choi J.-S., Park D.-W., Rhim J.-N., Isothermal phase equilibria for the ternary system (methanol (1)-n-hexane (2)-n-heptane (3)). *Korean Chemical Engineering Research* **1985,** *23*, (2), 89-89.
(63) Ferguson J.B., The System Methyl Alcohol-n-Hexane at 45 Degrees. *The Journal of Physical Chemistry* **1931,** *36*, (4), 1123-1128.
(64) Goetschel B., Z. W., Calculation of partial pressures in the methanol + benzene system by measuring the total pressure. *Univ. Rostock, Math.-Naturwiss. Reihe* **1969,** *18*, 927.
(65) Kolodziej E.J.G., R. A. , In presented on National AJChE Meeting, New Orleans, **1981**
(66) Toghiani H., Toghiani R.K., Viswanath D.S., Vapor-liquid equilibria for the methanol-benzene and methanol-thiophene systems. *Journal of Chemical and Engineering Data* **1994,** *39*, (1), 63-67.
(67) Scatchard G., Ticknor L.B., Vapor-Liquid Equilibrium. IX. The Methanol-Carbon Tetrachloride-Benzene System1. *Journal of the American Chemical Society* **1952,** *74*, (15), 3724-3729.
(68) Schmidt G.C., Binäre Gemische. *Zeitschrift für Physikalische Chemie* **1926,** *121*, (1), 221-253.
(69) Jost W., Roeck H., Schröder W., Sieg L., Wagner H.G., Apparatur zur Messung von Dampf-Flüssigkeits-Gleichgewichten bei Überdruck. *Z. Phys. Chem.(Frankfurt am Main)* **1957,** *10*, 133.
(70) Butcher K., Medani M., Thermodynamic properties of methanol–benzene mixtures at elevated temperatures. *Journal of Applied Chemistry* **1968,** *18*, (4), 100-107.
(71) Goral M., Skrzecz A., Bok A., Mączyński A.,Oracz P., Recommended vapor–liquid equilibrium data. Part 3. Binary alkanol–aromatic hydrocarbon systems. *Journal of Physical and Chemical Reference Data* **2004,** *33*, (3), 959-997.
(72) Nagata I., Isothermal (vapour+ liquid) equilibria of (methanol+ toluene) and of (methanol+ acetonitrile+ toluene). *The Journal of Chemical Thermodynamics* **1988,** *20*, (4), 467-471.
(73) Ishikawa T., Vapor-liquid equilibria of 1, 2-dichloromethane-methyl butyl ketone and methanol-toluene binary systems at 760 mm of Hg. *Kagaku Kogaku* **1972,** *36*, 566-569.
(74) Zheng D.-Q., Ma W.-D., Wei R., Guo T.-M., Solubility study of methane, carbon dioxide and nitrogen in ethylene glycol at elevated temperatures and pressures. *Fluid Phase Equilibria* **1999,** *155*, (2), 277-286.
(75) Jou F.Y., Otto F.D.,Mather A.E., Solubility of methane in glycols at elevated pressures. *The Canadian Journal of Chemical Engineering* **1994,** *72*, (1), 130-133.
(76) Jou F.-Y., Schmidt K.A.G., Mather A.E., Vapor–liquid equilibrium in the system ethane + ethylene glycol. *Fluid Phase Equilibria* **2006,** *240*, (2), 220-223.

(77) Mokraoui S., Coquelet C., Valtz A., Hegel P.E., Richon D., New Solubility Data of Hydrocarbons in Water and Modeling Concerning Vapor–Liquid–Liquid Binary Systems. *Industrial & engineering chemistry research* **2007,** *46*, (26), 9257-9262.
(78) Tsonopoulos C., Wilson G., High-temperature mutual solubilities of hydrocarbons and water. Part I: Benzene, cyclohexane and n-hexane. *AIChE Journal* **1983,** *29*, (6), 990-999.
(79) Jou F.-Y., Mather A.E., Liquid–Liquid Equilibria for Binary Mixtures of Water + Benzene, Water + Toluene, and Water + p-Xylene from 273 K to 458 K. *Journal of Chemical & Engineering Data* **2003,** *48*, (3), 750-752.
(80) Ng H.-J., Chen C.-J., *Mutual Solubility in Water-hydrocarbon Systems: GPA Project 895, RR-150*; Gas Processors Association: 1995.
(81) Anderson F.E., Prausnitz J.M., Mutual solubilities and vapor pressures for binary and ternary aqueous systems containing benzene, toluene, m-xylene, thiophene and pyridine in the region 100–200° C. *Fluid Phase Equilibria* **1986,** *32*, (1), 63-76.
(82) Marche C., Ferronato C., Jose J., Solubilities of n-Alkanes (C6 to C8) in Water from 30 °C to 180 °C. *Journal of Chemical & Engineering Data* **2003,** *48*, (4), 967-971.

Appendix D

UNIFAC Group interaction parameters for the UMR-PR-fit.

Table D.1: UNIFAC group interaction parameters for the UMR-PR-fit model following the temperature dependency of eq. 5.19, used for the interactions between the non-associating components for UMR-CPAPRU.

n	*m*	A_{nm} (K)	B_{nm} (-)	C_{nm} (K^{-1})	A_{mn} (K)	B_{mn} (-)	C_{mn} (K^{-1})
CO_2	CH_2	38.44	-1.8130	0.003247	101.56	0.1006	0.006430
CO_2	ACH	16.20	-2.2538	0.001050	94.49	1.5570	0.007850
CO_2	ACCH	-102.70	-3.0502	0.012000	274.36	15.5931	0.012930
CO_2	C_2H_6	92.20	-0.6847	0.	110.50	-0.3805	0.
N_2	CH_4	-141.07	-0.8494	0.	192.06	0.7909	0.
N_2	C_2H_6	-157.17	-0.9411	0.	308.97	1.0030	0.
N_2	CO_2	-128.17	-1.6650	0.	366.62	1.5300	0.
N_2	CH_2	157.35	-0.3614	0.000036	3.00	-0.1919	-0.000287
N_2	ACH	-104.18	1.8010	-0.006569	37.23	-1.2050	-0.001061
N_2	ACCH	-240.46	-3.6140	0.015020	122.55	0.5598	-0.003968
CH_4	CO_2	85.80	-0.1959	0.	126.21	-0.4439	0.
CH_4	C_2H_6	110.50	0.2497	0.	-56.01	-0.1798	0.
CH_4	CH_2	101.56	2.7666	0.001441	-252.68	-1.4066	-0.000282
CH_4	ACH	94.49	1.6950	0.000509	-63.53	-1.3050	0.002178
CH_4	ACCH	274.36	-3.1420	0.010180	-88.33	1.3930	-0.008429
C_2H_6	CH_2	157.35	-1.1031	0.000052	-142.16	0.3059	0.001857
C_2H_6	ACH	-104.18	-0.5662	0.	171.39	-0.7241	0.
C_2H_6	ACCH	-240.46	2.6500	-0.000086	674.59	2.5318	0.051615

Appendix E

Calculation of the fugacity coefficient with the UMR-CPAPRU model

The fugacity coefficient φ_i of a component i in a mixture is given by the fundamental relationship.

$$RTln\varphi_i = \left(\frac{\partial A^r}{\partial n_i}\right)_{T,V,n_j} - RTlnZ \qquad \text{eq. E.1}$$

where A^r is the residual Helmholtz energy for the mixture, R the ideal gas constant, T the temperature, V the total volume of the system, n the quantity of material of component i or j, and Z the compressibility factor, defined as per eq. E.2.

$$Z = \frac{PV}{nRT} \qquad \text{eq. E.2}$$

The UMR-CPAPRU model combines the PR EoS with first order perturbation theory of Wertheim, using the application of the Universal Mixing Rules for the extension to mixtures. As such, the residual Helmholtz energy can be expressed as a summation of the physical and the association contributions, as per eq. E.3.

$$A^r = A^r_{ph} + A^r_{assoc} \qquad \text{eq. E.3}$$

By combining eq. E.1 with eq. E.3, we get the following:

$$RTln\varphi_i = \left(\frac{\partial A^r_{phys}}{\partial n_i}\right)_{T,V,n_j} + \left(\frac{\partial A^r_{assoc}}{\partial n_i}\right)_{T,V,n_j} - RTlnZ \qquad \text{eq. E.4}$$

In eq. E.4 the derivative of the residual Helmholtz energy with respect to the quantity of material is the association contribution to the chemical potential (μ_i^{assoc}) of component i, as per eq. E.5.

$$\mu_i^{assoc} = \left(\frac{\partial A^r_{assoc}}{\partial n_i}\right)_{T,V,n_j} \qquad \text{eq. E.5}$$

Therefore, after the appropriate substitution for the expression of the physical part of the EoS, the following expression is derived for the fugacity coefficient of UMR-CPAPRU model.

$$ln\varphi_i = \left(\frac{B_i}{B} - 1\right) \cdot (Z^{phys} - 1) - ln(Z - B) - \frac{D_iB - DB_i}{2B\sqrt{2}} ln\left(\frac{Z + \left(1 + \sqrt{2}\right)B}{Z - \left(1 + \sqrt{2}\right)B}\right) + \frac{\mu_i^{assoc}}{RT} \qquad \text{eq. E.6}$$

where:

$$\mathrm{D} = n^2 abRT \qquad \text{eq. E.7}$$

$$\mathrm{D}_i = \mathrm{B}\left(\frac{a_i}{b_i} - \frac{RT\,ln\gamma_i}{0.53} + \frac{D}{B^2}B_i\right) \qquad \text{eq. E.8}$$

$$B = \sum_i \sum_j x_i x_j b_{ij} \qquad \text{eq. E.9}$$

$$B_i = 2\sum_j x_j b_{ij} - B \qquad \text{eq. E.10}$$

Appendix F

Publications – Communications

F.1. Paper I

Journal:	Fluid Phase Equilibria
Volume:	433
Year:	2017
Pages:	135 - 148
Title:	Modelling of phase equilibrium of natural gas mixtures containing associating compounds
Authors:	Eirini G. Petropoulou, Georgia D. Pappa, Epaminondas C. Voutsas

Abstract

The effect of mixing rules and the incorporation of an association term in a cubic equation of state (EoS), on the modelling of phase equilibria of natural gas mixtures in the presence of hydrogen bonding compounds, is investigated. To this purpose, the Peng-Robinson equation of state coupled with the van der Waals one-fluid mixing rules, the UMR-PRU group contribution EoS and the CPA-PR EoS, are evaluated in the prediction of phase equilibrium in ternary and multicomponent mixtures containing natural gas components, water and methanol or monoethylene glycol. It is concluded that UMR-PRU and CPA-PR give significantly improved results over the classical Peng-Robinson EoS, indicating that the use of advanced mixing rules and the explicit implementation of an association term in a cubic EoS is important for modelling the phase equilibrium of natural gas mixtures containing associating compounds.

F.2. Paper II

Journal:	Fluid Phase Equilibria
Volume:	462
Year:	2018
Pages:	44 - 58
Title:	Vapor – liquid equilibrium of the carbon dioxide/methane mixture at three isotherms
Authors:	Eirini G. Petropoulou, Epaminondas C. Voutsas, Snorre-Foss Westman, Anders Austegard, Jacob H.G. Stang, Sigurd W. Løvseth

Abstract

Experimental vapor – liquid equilibrium data for the CO_2/CH_4 mixture have been measured at 293.13 K, 298.14 K and 303.15 K, with emphasis on the mixture critical area. The maximum estimated standard uncertainties are 3 mK in temperature, 2 kPa in pressure and 0.0008 in mol fraction. The scaling law of statistical thermodynamics has been fitted to the critical region data of each isotherm and very good estimation of the critical point is achieved with a maximum uncertainty of 10 kPa in critical pressure and 0.0009 in critical molar composition. The measurements have been validated against experimental data taken from the literature, where available, and against the prediction of the GERG-2008 model. The Soave-Redlich-Kwong (SRK) and Peng-Robinson (PR) Equations of State using the classic van der Waals one fluid mixing rules, the perturbed chain statistical association fluid theory (PC-SAFT) and the Universal Mixing Rule – Peng Robinson (UMR-PRU) model have been fitted to the data of each isotherm with very satisfactory results. UMR-PRU yields the lowest deviation, especially concerning the critical point area, with an overall absolute average deviation (AAD) of 0.18% in bubble point pressure and 0.43% in CO2 mol fraction of the vapor phase. In the critical points, UMR-PRU results in an average % AAD equal to 1.55 in critical pressure and 0.99 in the critical point composition.

F.3. Paper III

Journal:	Industrial & Engineering Chemistry Research
Volume:	57
Year:	2018
Pages:	8584-8604
Title:	Thermodynamic Modeling and Simulation of Natural Gas Dehydration Using Triethylene Glycol with the UMR-PRU Model
Authors:	Eirini G. Petropoulou, Epaminondas C. Voutsas

Abstract

Dehydration of natural gas (NG) by absorption is a common industrial procedure implemented in order to avoid flow blockage and equipment breakdown. Despite the widespread use of dehydration units, few experimental data are available in the literature and most engineering practices are based on empirical correlations for the design and the determination of the optimum operational parameters. In this paper, an accurate thermodynamic model for NG mixtures, the UMR-PRU, is further extended to mixtures containing triethylene glycol (TEG) and is then used to simulate a typical NG dehydration unit using TEG by incorporating it in commercial simulators through the CAPE-OPEN standard. The results are compared with those obtained by the recommended by Aspen Hysys, TST/NRTL model. The two models calculate similar lean TEG purity, TEG circulation rate, and stripping gas rate in order to obtain the same level of dehydration, ca. 30 ppm water in the dry gas, while some differences are observed in the component distribution in the vapor and liquid phases. In addition, different reboiler duties are calculated by the two models, with those of UMR-PRU to be considered more realistic due to better prediction of the heat capacities of aqueous TEG mixtures.

F.4. Contribution in a peer-reviewed book chapter

Book:	*Natural Gas Processing from Midstream to Downstream*
Editor:	N. Elbashir, M. El-Halwagi, I. Economou, K. Hall
Chapter:	3
Year:	2019 (*in press*)
Pages:	57 - 88
Ch. Title:	Thermodynamic Modeling of Natural Gas and Gas Condensate Mixtures
Authors:	Epaminondas Voutsas, Nefeli Novak, Vasiliki Louli, Georgia Pappa, Eirini Petropoulou, Christos Boukouvalas, Eleni Panteli, Efstathios Skouras

Abstract

Natural gas is one of the major combustion fuels used worldwide with the largest increase in world primary energy consumption. Abundant natural gas resources and robust production contribute to the strong competitive position of natural gas among other resources. Natural gas is a key fuel in the electric power sector and the industrial sector because of its fuel efficiency. It burns cleaner than coal or petroleum products, and as more governments begin implementing national or regional plans to reduce carbon dioxide emissions, they may encourage the use of natural gas to displace more carbon-intensive coal and liquid fuels.

The effective exploitation of natural gas resources, as well as the modeling and simulation of midstream and downstream natural gas processing, requires the accurate knowledge of the phase equilibrium and other thermodynamic properties of natural gas mixtures, which involve hydrocarbons ranging from methane up to high molecular weight ones, water and other components, such as nitrogen, carbon dioxide, hydrogen sulfide, hydrate inhibitors etc.. The availability of thermodynamic models capable of accurately predicting the phase behavior of the multicomponent mixtures encountered in such processes, with little input information, is very important for the oil and gas industry, offering both time saving and process cost reduction.

Although the gas industry traditionally uses classical cubic equations of state (EoS), such as Peng-Robinson (PR) or Soave-Redlich-Kwong (SRK), for process simulation in order to avoid operational/safety problems and to determine process parameters that fulfill product specifications, more advanced models that overcome the weaknesses of cubic EoSs and give more accurate results can be also successfully applied. One such completely predictive model is the Universal Mixing Rules – Peng Robinson UNIFAC (UMR-PRU) that is a cubic equation of state– based model coupled with advanced mixing rules, the so-called Universal Mixing Rules (UMR). Another popular non-cubic equation of state based on a perturbation theory for chain molecules, is the perturbed-chain statistical associating fluid theory (PC-SAFT).

In this chapter, phase equilibrium calculations, like dew point curve and liquid dropouts, which are two key parameters in natural gas processing, are presented using PR, UMR-PRU, and PC-SAFT. It is shown that the use of advanced mixing rules, like those used in the UMR-PRU model, can overcome the inefficiencies of the classical van der Waals one one-fluid mixing rules that are usually coupled with cubic EoS, and can lead to satisfactory prediction of the hydrocarbon mixtures' behaviour. Moreover, UMR-PRU predictions are comparable to those of the more complex PC-SAFT EoS. Finally, through the CAPE-OPEN standards (Computer-Aided Process Engineering), UMR-PRU can be incorporated in most process simulators, thus offering thus the possibility to fully simulate a natural gas treatment process. A case study is presented, which deals with a topside offshore operation that processes a well-fluid to produce rich gas and stabilized condensate.

F.5. Communications in National and International Scientific Conferences

10th Concawe Symposium
February 25-26, 2013, Brussels, Belgium (poster presentation)
Petropoulou E., Voutsas E.
Dew Point Prediction of Natural Gas Mixtures

27th European Symposium of Applied Thermodynamics,
July 6-9th 2014, Eindhoven, the Netherlands (poster presentation)
E. Petropoulou, E. Voutsas
Phase Equilibrium in Aqueous Hydrocarbon mixtures with Hydrate Inhibitors,

11th Concawe Symposium
23-24 February 2015, Brussels, Belgium (poster presentation)
E. Petropoulou, E. Voutsas
Thermodynamic Modelling to Enhance Natural Gas Quality

28th ESAT
June 11th – 14th 2015, Athens, Greece (oral presentation)
E. G. Petropoulou, E. C. Voutsas
Thermodynamic Modelling of Industrially Important Associating Mixtures

29th European Symposium of Applied Thermodynamics
May 18-21th 2017, Bucharest, Romania (poster presentation)
E. Petropoulou, G.D. Pappa, K. Magoulas, E. Voutsas
Simulation of a Natural Gas Dehydration Process with the UMR-PRU model

29th European Symposium of Applied Thermodynamics,
May 18-21th 2017, Bucharest, Romania (poster presentation)
N. Novak, E. Petropoulou, A. Plakia. K. Pittas, V. Louli, G. Pappa, C. Boukouvalas, E. Voutsas
Prediction of Dew point and Liquid Dropout of Natural Gas and Gas Condensates

11th National Scientific Conference of Chemical Engineering
May 25-27 2017, Thessaloniki, Greece
N. Novak, E. Petropoulou, K. Pittas, A. Plakia. V. Louli, G. Pappa, C. Boukouvalas, E. Voutsas
Thermodynamic modelling and simulation of natural gas processes

30th European Symposium of Applied Thermodynamics, June 10-13th 2018
June 10-13th 2018, Prague, Czech Republic (oral presentation)
E. Petropoulou, E. Voutsas
Extension of the UMR-PRU model to natural gas mixtures containing glycols and application to natural gas dehydration process